NZ-SPECIFIC PSEUDO-SPECTRAL ACCELERATION GROUND MOTION PREDICTION EQUATIONS BASED ON FOREIGN MODELS

Brendon A. Bradley

Research report 2010-03

Department of Civil Engineering
University of Canterbury
Christchurch
New Zealand

22 September 2010

ABSTRACT

Ground motion prediction equations (GMPEs) for geometric-mean pseudo-spectral acceleration amplitudes from New Zealand (NZ) earthquakes are developed. A database of 2437 three-component ground motion records is developed by applying stringent quality criteria to the historically recorded events in NZ. Despite the large number of records, the database is deficient in empirical records from large magnitude events recorded at close distances to the fault rupture plane. As a result, the basis for the NZ-specific GMPE development is to examine the applicability of foreign GMPEs for similar tectonic regions and then modify the most applicable GMPEs based on both theoretical and statistically significant empirically-driven arguments.

For active shallow crustal events, five different GMPEs are considered. It was found that the McVerry *et al.* (2006) model, which is the current model upon which seismic design guidelines and site-specific seismic hazard analyses in NZ are based, provided the worst fit to the NZ database, and that the Chiou *et al.* (2010) (C10) modification of the Chiou and Youngs (2008) model was the most applicable. Discrepancies between the C10 model and the NZ database that were empirically identified and theoretically justified were used to modify the C10 model for: (i) small magnitude scaling; (ii) scaling of short period ground motion from normal faulting events in volcanic crust; (iii) scaling of ground motions on very hard rock sites; (iv) anelastic attenuation in the NZ crust; and (v) consideration of the increased anelastic attenuation in the Taupo Volcanic Zone (TVZ).

For subduction slab events, initially three models were considered. It was found that all of the models had some significant biases with respect to applicability for NZ. The Zhao et al. (2006) (Z06) model was selected because of the rigorous database upon which it was developed and modified by: (i) NZ-specific scaling at small magnitudes; (ii) path scaling at large distances; (iii) consideration of the increased TVZ attenuation; and (iv) revision of the standard deviation model. Based on these modifications the developed model showed no bias of the inter- and intra-event residuals as a function of various predictor variables. The standard deviation of the residuals using the revised standard deviation model also indicated that the model has an adequate precision.

Three GMPEs were considered for subduction interface events. The Zhao *et al.* (2006) (Z06) model was the best performing model with only bias exhibited in the site response model, and possible over-prediction of large magnitude events. The Z06 interface model was modified to account for site response and magnitude scaling using the same functional forms as those of the developed active shallow crustal and subduction slab models. The developed model showed no bias of the inter- and intra-event residuals as a function of various predictor variables.

The developed GMPEs include specific features as evident in the NZ database; consistent scaling for parameters not well constrained by the NZ database; and pseudo-spectral amplitudes for vibration periods from 0.01 to 10 seconds. Hence, these models represent a significant advance in the state-of-the art for empirical ground motion prediction in NZ.

Table of Contents

1. INTRODUCTION

The assessment of seismic hazards in burdened by uncertainties related to uncertainties in our understanding of the physics of earthquake nucleation, rupture propagation, seismic wave propagation, and seismic site effects. From an engineering viewpoint such physical processes are generally separated into: (i) the prediction of the location, size, and likelihood of earthquake ruptures; and (ii) the prediction of ground motions (or ground motion intensity measures) at a specific site, given the occurrence of a specific earthquake event at a specific location. Because both earthquake rupture and ground motion prediction are highly uncertain, they are typically represented quantitatively in a probabilistic form (Bommer and Abrahamson 2006, Field et al. 2008, Stirling 2007) and convoluted using methods such as probabilistic seismic hazard analysis (PSHA) (Cornell 1968, Field et al. 2003).

Ground motion prediction can generally be approached from an empirical or theoretical/physical perspective . Both of these approaches have their own benefits and limitations. Empirical ground motion prediction equations (GMPEs) are typically developed via regression of empirical ground motion recording from past events. Therefore the first limitation of the empirical approach is the representativeness of the ground motions used to develop the empirical model (i.e. the number of ground motion records and their distribution in terms of causal earthquake size, tectonic type, focal mechanism, as well as site type, and source-to-site distance). The second limitation of the empirical approach (which results from an insufficient number of records) is the consequences of the assumed functional form of the empirical model (Petersen et al. 2008).

Historically, a significant number of empirical GMPEs have been developed using a wide variety of distinct or partially overlapping ground motion databases, and functional forms, which unsurprisingly have yielded GMPEs providing significantly different predictions for the same future earthquake scenarios. More recently, there has been somewhat of a paradigm shift away from the idea of regionalisation of ground motion prediction toward the idea that ground motions from similar tectonic regions should exhibit similar characteristics (Douglas 2004, Douglas 2007). Along this line of though one should attempt to develop GMPEs based on a large database of ground motions, potentially from different geographical regions, rather than use a small database from a single region. Such an approach was taken during the Next Generation Attenuation (NGA) project (Power et al. 2008), which used a world-wide database of ground motions for active shallow crustal earthquakes.

Several studies (e.g. Atkinson 2008, Scasserra et al. 2009, Stafford et al. 2008) have examined the applicability of the NGA equations for other active shallow crustal tectonic regions. Such an examination is particularly useful in cases where the target region of interest does not have sufficient strong ground motion recordings to develop an empirical GMPE in a robust manner. This is critically important as it has been shown frequently that GMPEs developed from weak motions provide little inference regarding the character of strong ground motions.

In this study the applicable of several empirical GMPEs are examined for use in future ground motion prediction in New Zealand. Such an appraisal of foreign GMPEs is novel in that NZ is a tectonically active region with earthquakes of active shallow crustal, subduction slab, and subduction interface tectonic types. For each of these three tectonic regions the currently adopted, NZ-specific, McVerry et al. (2006) model is considered in addition to foreign GMPEs to demonstrate whether such

foreign models can provide an improved ground motion prediction than that at present.

2. NZ STRONG MOTION DATABASE

2.1. Quality criteria to determine the present NZ database

Initially a database of strong ground motions recordings in NZ over the period 1966-2009 compiled by Zhao and Gerstenberger (2010) was adopted. As with all strong ground motion data obtained over a period of several decades, the strong motion recordings in NZ have a wide range of quality which is principally dependent on: (i) the type of seismometer; (ii) the quality of the inversion to determine the event location and depth, seismic moment and other ground motion metadata; (iii) the number of ground motion records from a single event (to adequately obtain inter-event residuals); and (iv) the size of the ground motion (affecting the signal to noise ratio), among others. The following paragraphs explain how this initial database was scrutinized to arrive at a smaller final database of higher overall data quality.

The first criterion examined was the quality of the event inversion. Accurate location of the earthquake is important, not just to determine source-to-site distances for the strong motion records, but also in the determination of the tectonic nature of the event based on its location relative to the known plate boundaries (elaborated upon below). Locations and depths determined from the International Seismological Centre (ISC) (Engdahl et al. 1998) or a relocated NZ catalogue (Eberhart-Phillips et al. 2010) were deemed to be of 'high quality', while those of the standard GeoNet catalogue (http://www.geonet.org.nz/) were deemed to be of 'lower quality' (i.e. the majority of such locations, until recently, are based on restricted depths). The estimate of moment magnitude was also considered to be 'high quality' if M_w estimates were available for an event either from the Global Centroid Moment Tensor (CMT) catalogue (Ekström 2010) or from regional moment tensor solutions (Ristau 2008). M_w inferences obtained from estimated M_L values (Haines 1981, Zhao and Gerstenberger 2010) were deemed to be of 'lower quality'. Thus earthquake events (and their associated ground motions) were deemed to be of: 'high quality' (Quality 1) if the location and depth were 'high quality' and the M_w estimate was 'high quality; 'medium quality' (Quality 2) if either the location and depth *or* M_w was high quality; and 'low quality' (Quality 3) if both the location and depth as well as the M_w estimate were of 'lower quality'.

The second criterion examined was the number of ground motion records that were obtained from a given event. This is directly important for determining inter-event residuals in the ground motion analysis, but also it indirectly provides a way of removing ground motions which were recorded on poorer quality seismometers (i.e. film records etc.), because when such seismometers were the norm, they were sparsely located and hence only larger events (which are of particular significance) could trigger a significant number of seismometers. Thus, based on the data available it was determined that events which contained only one or two ground motions in quality 1 were re-classified as quality 1a. Events of quality 2 which contained less than ten ground motions (i.e. a stricter criteria) were similarly re-classified as quality 2a.

Table 1 illustrates the number of events and recorded ground motions according to the aforementioned quality of the metadata. It can be seen, for example, that while quality 1 events represent only 43% of the total number of events in the initial database, they account for 70% of the strong motion recordings. Figure 1 illustrates the magnitude-distance distribution of the strong motion recordings for the different

data qualities. It can be seen that the quality 1a and 2a data do not contain any significant $M_w - R_{rup}$ pairs that are not well covered by the quality 1 and 2 datasets and therefore these were removed from consideration of the final database. Examination of Figure 1 would also suggest that quality 2 data do not represent any significant $M_w - R_{rup}$ pairs that are not covered by quality 1 data. However, closer examination reveals that the majority of quality 2 data are for subduction slab events, where as quality 1 data have very little slab events. Such slab events (which typically have depths greater than 50 km) have more accurate locations than shallow crustal events (Zhao and Gerstenberger 2010). As a result, the final NZ strong motion database used in this study used both quality 1 and 2 data. Table 1 illustrates that the final database had a total of 213 events and 2437 ground motion records (for active shallow crustal, subduction interface, and subduction slab events).

Table 1: Number of events and recorded ground motions in NZ assigned according to quality of metadata.

Quality	Number of events, N_{eq}	Number of ground motion records, N_{record}
Initial	438	3410
1	187	2388
1a	39	35
2	26	467
2a	121	303
3	65	217
Final	213	2437
McVerry *et al.* (2006)	49[2]	435[2]

[1]The final NZ database uses quality 1 and 2 data as well as the M_w - R_{rup} filter.
[2]These are the numbers having response spectral data; N_{eq} = 51, and N_{record} = 535 events had PGA data.

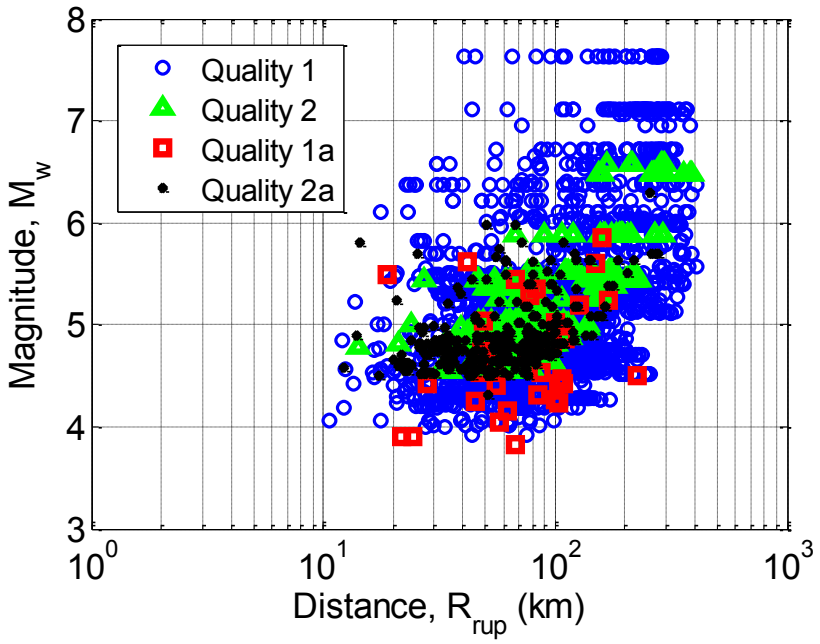

Figure 1: Magnitude distance distribution of the recorded strong motions in NZ based on data quality criteria.

2.2. Comparison of NZ and NGA databases

Figure 2 illustrates a comparison between the aforementioned NZ strong motion database used in this study with that of the NGA database (Chiou et al. 2008). It can be seen that the NZ database is deficient in recorded ground motions in the large-magnitude small-distance range compared to the NGA database. Conversely, a significant number of ground motions of smaller magnitude ($M_w < 5$) are included in the NZ database, as compared to the NGA database.

The selected NZ database, as summarised in Table 1, was based on data quality alone. For the purposes of using the database to test the validity of strong ground motion prediction equations it is prudent to remove ground motions which may be deemed as not of engineering significance. On this basis a magnitude distance ($M_w - R_{rup}$) filter is used as shown in Figure 2. The $M_w - R_{rup}$ filter values were chosen to remove records with *PGA* values approximately less than 0.001g (i.e. 0.1%g), which were deemed to be of no engineering significance. It is noted that this $M_w - R_{rup}$ filter is relatively consistent with the distribution of recorded motions used in the NGA database. It is important to note that the use of a $M_w - R_{rup}$ filter does not lead to bias in ground motion prediction residual analysis in the same way that removing ground motions based explicitly on their amplitudes (which may be deemed to be have low signal-to-noise ratios) does.

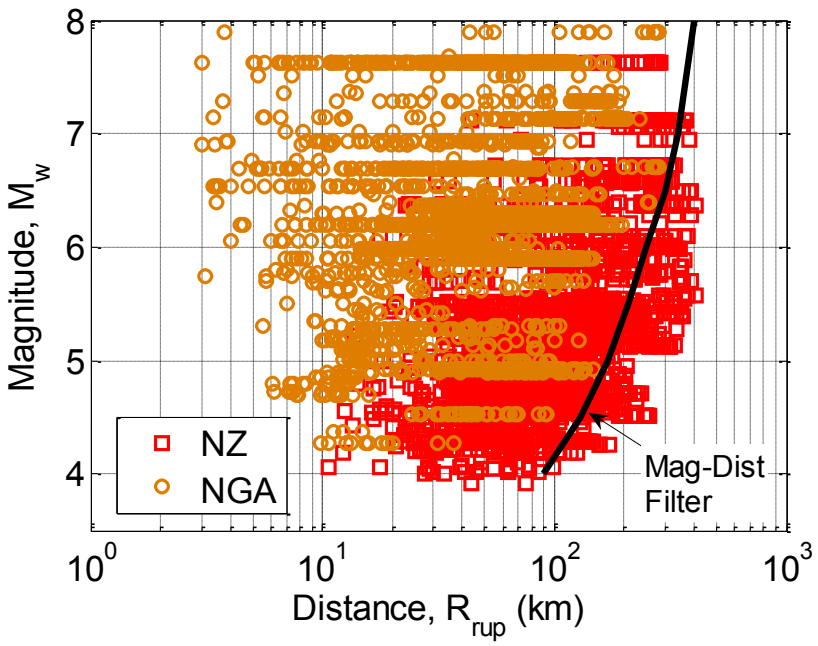

Figure 2: Comparison of the NZ and NGA database, as well as the magnitude-distance filter used to remove ground motions deemed not of engineering significance.

2.3. Determination of ground motion metadata

As previously mentioned the moment magnitude of events in the strong motion database had either M_W estimates directly from CMT solutions, or otherwise were obtained based on local magnitude, M_L, estimates. All of the major events with M_L estimates (>5.0) have been converted to M_W on a case-by-case basis (Dowrick and Rhoades 1998), while the remaining (predominantly $M_L < 5$) events were converted to

an equivalent M_W value using the conversion of Zhao and Gerstenberger (2010):

$$M_w = 1.05M_L - 0.00495h - 0.365 \quad (1)$$

where h is focal depth in km. As can be seen from Table 1 the majority of the final database used in this study (which comprised Quality 1 and 2 data), had M_w estimates from CMT solutions (i.e. Quality 1 data). The majority of the Quality 2 data (which primarily do not have M_w estimates), are from subduction slab events (because such events produce 'weak' low frequency ground motion, making CMT solutions based on teleseismic body waves more difficult). It can be appreciated from Equation (1) that the converted M_w values are smaller than the estimated M_L. For example, for an $M_L = 5$ event at focal depths of 50 and 100 km the difference, $M_w - M_L$, is -0.36 and -0.61, respectively.

Empirical GMPE's for active shallow crustal earthquakes often include style-of-faulting as a predictor variable. For those events with CMT solutions, the focal mechanism was used to determine the style of faulting factor for each GMPE considered, while events without CMT solutions were assigned focal mechanisms based on the regional tectonic setting (e.g. Stirling et al. 2002). The Chiou and Youngs (2008) and Chiou *et al.* (2010) GMPEs examined also make use of fault dip as a predictor variable. For those events with unknown dips, following Chiou and Youngs (2008), the following values were assigned: SS $\delta = 90°$; RV $\delta = 40°$; NM $\delta = 55°$.

The tectonic type of an earthquake event (e.g. active shallow crustal, subduction interface, subduction slab) is also known to significantly influence the character of ground motions (Morikawa and Sasatani 2004, Zhao et al. 1997, Zhao et al. 2006). In the NZ database the classification of the tectonic type of an event was based on the location (primarily focal depth), focal mechanism, and the known subducting slab boundary. An event with a small distance, and one nodal plane parallel to, the subducting slab boundary (i.e. a reverse focal mechanism) was classified as a subduction interface event. Events located near the slab boundary with normal focal mechanism were classified as subduction slab events, as were events (of any focal mechanism) with focal depths greater than 50 km (i.e. below the interface contact zone). Figure 3 illustrates the distribution of events throughout NZ as a function of their focal depth, while Table 2 provides the number of ground motions from subduction interface, subduction slab, and active shallow crustal events of various focal mechanism. It can be seen that the majority of the events in the database are from subduction slab events (62%), while active shallow crustal, and subduction interface events comprise notable smaller proportions or 26% and 12%, respectively. A large proportion of the crustal events in the database are from reverse events (42%), while there are the least number of events from normal faulting (17%). Note that while there are no normal-oblique crustal events in the database, many of the Subduction slab events have normal oblique focal mechanism.

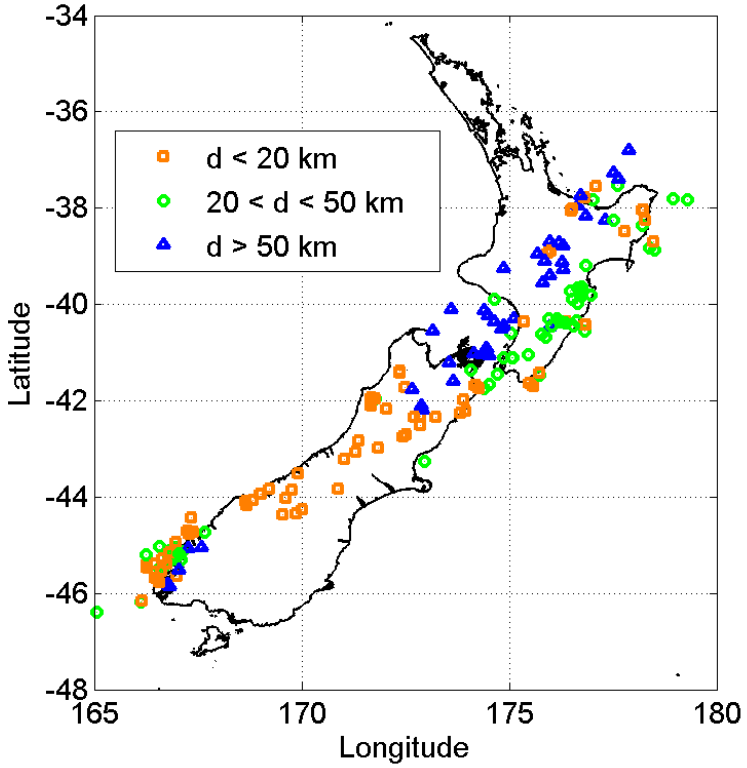

Figure 3: Spatial and depth distribution of events in the final NZ database

Table 2: Number of records, N_{record}, classified according to tectonic type and focal mechanism.

Crustal				Subduction Interface	Subduction Slab
Reverse	Strike-slip	Normal	Reverse Oblique		
271	139	106	125	296	1500

The majority of events in the NZ database do not have finite fault models and hence only hypocentral distance, R_{hyp}, and epicentral distance, R_{epi}, are available. The empirical ground motion prediction equations that are subsequently examined require the closest distance to the fault plane, R_{rup}, and the closest distance to the surface projection of the fault plane, R_{jb}. To obtain these finite fault source-to-site distances, the Monte Carlo approach of Chiou and Youngs (2006) was adopted. Following Chiou and Youngs (2006), only the median values obtained from this analysis were used in the subsequent examination of the applicability of empirical GMPE's. However, sensitivity studies revealed that the results obtained were not sensitive to the percentile of the Monte Carlo simulated relationships used. This is because of the aforementioned fact that the NZ database lacks ground motion records in the large magnitude small distance range, and hence the approximations $R_{rup} \approx R_{hyp}$ and $R_{jb} \approx R_{epi}$ are generally adequate.

The Chiou and Youngs (2008) and Chiou *et al.* (2010) GMPE's also use the depth to the top of the rupture plane, Z_{TOR}, as a predictor variable. For those events without finite fault models, the down-dip width of the fault was estimated from Wells and Coppersmith (1994). Assuming that the focal depth is at half the down-dip width, Z_{TOR} can be computed from:

$$Z_{TOR} = h - \frac{W}{2} sin(\delta) \quad (2)$$

where h is the focal depth, W is the down-dip width, and δ is the fault plane dip.

All sites where ground motion seismometers are located are classified using a discrete classification as provided by the NZ loadings standard (NZS 1170.5 2004), and outlined in Table 3. The GeoNet DELTA website (http://magma.geonet.org.nz/delta/app) provides details of the geotechnical characteristics of each site and the corresponding site class.

Table 3: NZ Site class definitions (NZS 1170.5 2004).

Class	Definition (abbreviated)
A – Strong rock	σ[1] > 50 MPa; $V_{s,30}$[2] > 1500 m/s; not underlain by materials with σ < 18 MPa or V_s > 600 m/s
B – Rock	$1 < \sigma < 50$ MPa; $V_{s,30}$ > 360 m/s; not underlain by materials with σ < 0.8 MPa or V_s < 300 m/s; a surface layer of no more than 3 m depth of highly weathered or completely-weathered rock or soil
C – Shallow soil	Not class A, B and E; T_1 < 0.6 s; soil depth less than Table 3.2 in NZS1170.5 (2004)
D – Deep or soft soil	Not class A, B and E; T_1 < 0.6 s; soil depths greater than Table 3.2 in NZS1170.5 (2004); underlain by < 10 m soil with q[4] < 12.5 kPa or N[5] < 6.
E – Very soft soil	Sites with: > 10 m of soil with q[4] < 12.5 kPa, N[5] < 6, and $V_{s,30}$ < 150 m/s, or > 10 m of soil with properties q[4] < 12.5 kPa, N[5] < 6, or $V_{s,30}$ < 150 m/s.

[1] σ = unconfined compressive strength of rock. [2] $V_{s,30}$ = average shear wave velocity over the upper 30 m. [3] T_1 = low amplitude natural vibration period. [4] q = undrained shear strength. [5] N = SPT blowcount.

2.4. Limitations of ground motion prediction equations based on NZ data

The *PGA* and pseudo-response spectral acceleration, S_a, prediction equation of McVerry *et al.* (2006) (herein McV06 for brevity) represents the most recent attempt to develop an empirical GMPE based on NZ strong motion data (supplemented with overseas strong motion data having large magnitude and small source-to-site distances). While this equation has only recently been published in the public domain, it was in fact developed much earlier (McVerry et al. 2000). Based on strong ground motions in the period 1966-1995, the McV06 GMPE used a total of 49 earthquakes and 435 records (from NZ) for developing a response spectra prediction equation (51 earthquakes and 535 records were used to develop PGA prediction equation). An additional 66 records from 17 foreign crustal events with moment magnitudes of 5.2 – 7.4, and source-to-site distances less than 10 km were also added to constrain the model where NZ data were deemed insufficient.

Comparison of the above metadata used by McV06, with the NZ strong motion database from 1973-2009 complied here (i.e. 213 events and 2852 records as per Table 1) illustrates that the empirical database has increased significantly in the past 15 years, primarily as a result of the GeoNet project (http://www.geonet.org.nz). Furthermore, over the period 1973-1995 (McV06 used data from 1966-1995), the NZ strong motion database used in this study contains 34 events and 323 earthquakes. Hence, in addition to the present database having a larger total number of events and records, more rigorous constraints have been enforced when determining the quality of data to be included.

The four-fold increase in the number of events, and six-fold increase in the number of ground motion records in the present database, relative to that used in McV06, may initially be considered to justify the development of a new empirical GMPE using NZ data. However, the database adopted in the current study, as depicted in Figure 2, lacks a significant number of strong motion recordings from moderate to large magnitude events at small-to-moderate source-to-site distances. This deficiency is even more clearly elucidated by plotting the number of strong motion recordings which exceed various values of some (geometric mean) ground motion intensity measure. Figure 4 illustrates such a plot for geometric mean peak ground acceleration, where the database has been separated into the three different tectonic classes: active shallow crustal, subduction interface, and subduction slab events. It can be seen that there are only a total of 66 ground motion records which have PGA values above 0.1g (28 crustal, 11 interface, and 27 slab). Furthermore, the maximum PGA values recorded are 0.39g, 0.31g, and 0.28g for crustal, interface, and slab events, respectively.

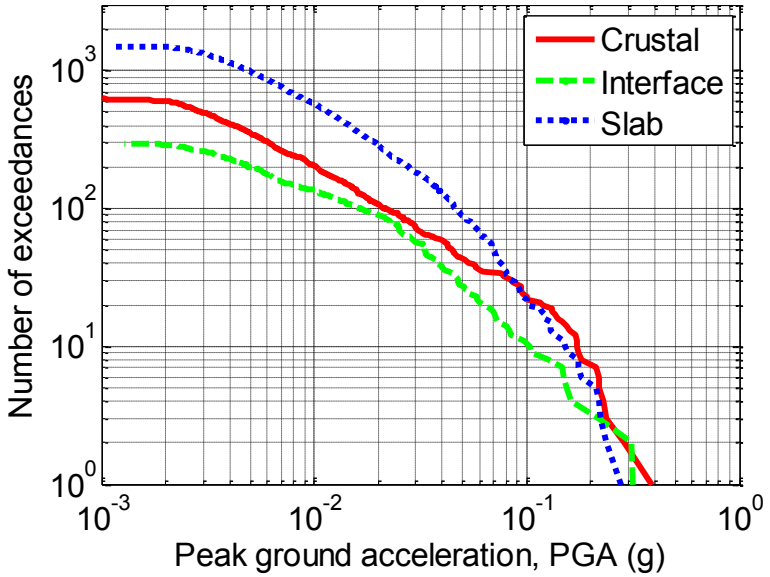

Figure 4: Number of PGA observations exceeding specific values for NZ ground motions.

The lack of observed intense strong motion records is problematic, because much of NZ is considered to be of high seismicity. For comparison, the loadings standard (NZS 1170.5 2004) design PGA values in major city centres such as Christchurch and Wellington are 0.22g and 0.4g for the 10% in 50 year exceedance probability, and 0.4g and 0.72g for the 2% in 50 year exceedance probability, respectively. That is, the 2% in 50 year design PGA values in both cities are larger than those ever recorded at any location in the country. This therefore highlights the robustness (or lack thereof) of empirical ground motion prediction equations which are developed from NZ data alone for use in forecasting seismic hazard in New Zealand.

Finally, it is noted that the McV06 model provides spectral amplitudes for vibration periods up to 3 seconds. This vibration period is below the constant displacement plateau region for large magnitude events, which is a critical region in the displacement response spectra needed in emerging displacement-based seismic design procedures. Ideally, such contemporary GMPE's will be applicable for

vibration periods beyond this corner period so they can be faithfully used in such seismic design procedures.

3. METHODOLOGY FOR CONSIDERATION OF FOREIGN RESPONSE SPECTRA PREDICTION EQUATIONS

Based on the identified limitations of using solely NZ data to develop empirical GMPEs directly, an alternative postulate is made that strong ground motion phenomena in other tectonically similar regions of the world should be similar to that in New Zealand. Consequently, empirical GMPE's developed for such regions should also be applicable for estimating strong ground motion intensity measures in NZ. On this basis, the following sections examine foreign GMPE's developed in other regions of the world with abundant ground motion observations, and their applicability to NZ using the aforementioned NZ strong motion database.

3.1. Methodology for comparison

There are various means by which the applicability of foreign ground motion prediction equations may be ascertained, including: (i) qualitative comparison of the predictor variable (i.e. M_w, R_{rup}) scaling; (ii) Analysis of variance of the empirical data binned by M_w and R_{rup} (e.g. Douglas 2004); (iii) Overall goodness of fit of the model to the data (e.g. Scherbaum et al. 2004, Stafford et al. 2008); and (iv) goodness of fit as a function of predictor variables (e.g. Scasserra et al. 2009).

Each of the above means for comparison have their own limitations. For example, Stafford *et al.* (2008) compared the inter- and intra- event residuals of empirical data to foreign GMPEs in a overall sense, in that they only examined the distribution of these residuals, and did not inspect the marginal distributions of the residuals with predictor variables such as magnitude, distance etc. Such marginal distributions can clearly identify the inapplicability of some GMPEs which is not obvious by examination of the total distribution of residuals alone. While the fourth aforementioned approach may be considered the most rigorous for comparison of the applicability of foreign GMPEs (and will be utilized in herein), it still has the limitation that applicability can only be examined for the empirical data which is available. Thus, with regard to the present NZ database, such an approach cannot ascertain the applicability of foreign GMPEs for large M_w NZ events recorded at small R_{rup} distances, because there are no such observations in the NZ database. To account for this limitation, consideration is also given to the qualitative scaling of the various GMPEs (i.e. approach (i) above), relative to the empirical database upon which each GMPE was constructed.

The empirical ground motion predictions considered here all have the common mathematical form of a particular type of mixed-effects model (Lindstrom and Bates 1990):

$$ln y_{i,j} = f\left(\boldsymbol{\theta}_{ij}\middle|\boldsymbol{\beta}\right) + \eta_i \tau + \varepsilon_{i,j}\sigma \tag{3}$$

where $y_{i,j}$ is the j^{th} observed ground motion intensity measure (e.g. spectral acceleration for a given vibration period) from the i^{th} event; $f\left(\boldsymbol{\theta}_{ij}\middle|\boldsymbol{\beta}\right)$ is the predicted median value of the intensity measure, which is a function of a vector of predictor variables $\boldsymbol{\theta}_{ij}$ (e.g. M_w, R_{rup} etc.), and model coefficients, $\boldsymbol{\beta}$; η_i is the (normalised) inter-event residual, common to all j recordings from the i^{th} event; $\varepsilon_{i,j}$ is the (normalised) intra-event residual for the j^{th} recording from the i^{th} event; and τ and σ represent the standard deviations of the inter- and intra-event errors respectively.

Note that τ and σ are potentially functions of the predictor variables also, e.g. $\tau = \tau(\boldsymbol{\theta}_{ij}|\boldsymbol{\beta})$, but the concise notation in Equation (3) is used for brevity.

Both η_i and $\varepsilon_{i,j}$ are assumed to be drawn from a normal distribution with zero mean and unit variance. Under these assumptions the log-likelihood of a set of observed data, $\boldsymbol{y}$, given the model parameters is:

$$lnL(\boldsymbol{y}|\boldsymbol{\beta},\tau,\sigma) = \sum_{i}^{N_i}\sum_{j}^{N_{j,i}} ln\left[\frac{1}{\sigma}\phi\left(\frac{lny_{i,j} - \{f(\boldsymbol{\theta}_{ij}|\boldsymbol{\beta}) + \eta_i\tau\}}{\sigma}\right)\right] \quad (4)$$

where N_i is the number of events; $N_{j,i}$ is the number of recordings for event *i*; and the inter-event residual for event *i*, η_i, may be calculated from:

$$\eta_i = \frac{1}{\tau}\frac{\sigma^2}{N_{j,i}\sigma^2 + \tau^2}\sum_{j}^{N_{j,i}}\left(lny_{i,j} - f(\boldsymbol{\theta}_{ij}|\boldsymbol{\beta})\right) \quad (5)$$

It can be appreciated from Equation (5) that for events with a large number of recordings (i.e. such that the quotient approaches $1/\tau N_{j,i}$), that the inter-event residual approaches the average normalised total residual from the $N_{j,i}$ records. Once the inter-event residual, η_i, has been obtained the intra-event residual can be computed from rearranging Equation (3):

$$\varepsilon_{i,j} = \frac{lny_{i,j} - \{f(\boldsymbol{\theta}_{ij}|\boldsymbol{\beta}) + \eta_i\tau\}}{\sigma} \quad (6)$$

Hence, using Equations (5) and (6), it is possible to determine the normalised inter- and intra-event residuals of a specific intensity measure from a given ground motion recording using a particular ground motion prediction equation. Because both η_i and $\varepsilon_{i,j}$ are defined to have standard normal distributions, then the statistics of the observed residuals can be used to assess the accuracy and precision of a given ground motion prediction equation, and hence its potential applicability, to the target region under consideration.

3.2. Predictor variable compatibility

A critical step in the comparison between different empirical GMPE's, and interpretation of the applicability of foreign GMPE's is ensuring (as best as possible) compatibility between the metadata of recordings in the strong motion database and the predictor variables of the GMPE's. The subsections below address this issue for the different predictor variables of concern.

3.2.1. Magnitude and source-to-site distance

All the foreign GMPE's considered in this study use M_w as the predictor variable for earthquake magnitude. As every event in the NZ database has an associated M_w estimate (either explicitly or implicitly obtained as previous discussed) then there are no compatibility problems for magnitude. In a similar vein, all of the strong motion records in the NZ database have associated source-to-site distances in terms of both R_{jb} and $R_{rup.}$ As all the foreign GMPEs use one of these two source-to-site distance metrics then there is also no compatibility issues for source-to-site distance.

3.2.2. Focal mechanism

For the different active shallow crustal GMPE's considered, focal mechanisms are assigned based on the rake angle as shown in Figure 5. It can be seen that for an event of a given rake angle the corresponding focal mechanism is not always the same for different GMPE's. Only the McV06 GMPE makes a distinction between reverse (RV) and reverse-oblique (OR) focal mechanisms, while Zhao *et al.* (2006) (Z06) considers only reverse or 'other' focal mechanisms. The three other crustal GMPEs considered in this study, Boore and Atkinson (2008) (BA08), Chiou and Youngs (2008) (CY08), and Chiou *et al.* (2010) (C10) are also shown. The events in the NZ database for which focal mechanism solutions are available have been assigned one of five possible focal mechanisms based on the *P*-,*T*-, and *N*- axes of the moment tensor analysis (J. Ristau, Pers. Comm.). Boore and Atkinson (2008) have also shown that while moment tensor analysis has some benefits over using rake angle alone, practically speaking it gives similar results.

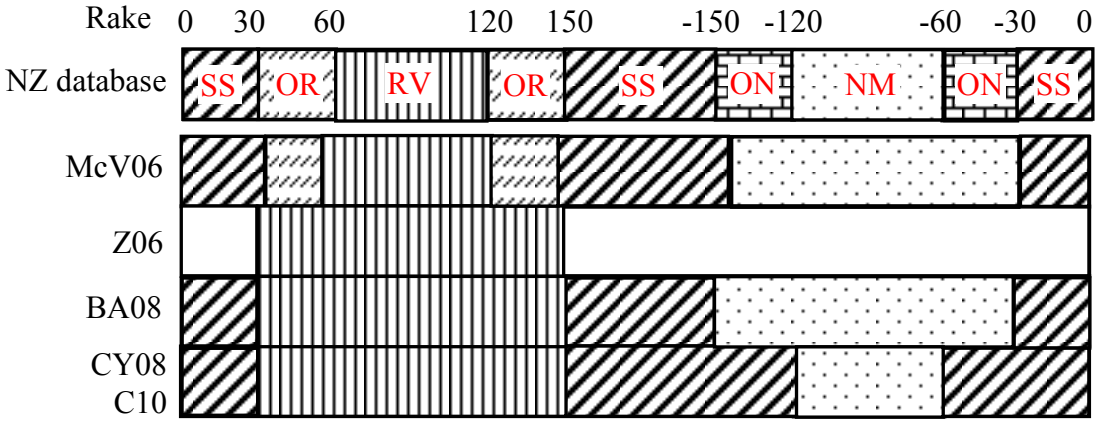

Figure 5: Compatibility between focal mechanism classifications of different GMPE's with the NZ database classification. SS = strike-slip; OR = Reverse-oblique; RV = Reverse; ON = Normal-oblique; NM = Normal.

3.2.3. Site classification

The discrepancy between the site classification scheme used in different GMPEs represents the predictor variable in this study which requires the most compatibility consideration. As has been previously mentioned, NZ sites are represented using an alphabet-based discrete classification (Table 3). Some of the foreign GMPEs examined here also use a discrete site classification, with different criteria, while others use continuous parameters (e.g. the average shear wave velocity in the top 30m, $V_{s,30}$), and formulations to represent site effects.

Table 4 presents the compatibility matrix used to convert the NZ site classes into predictor variables required by the foreign GMPEs. The compatibility was largely achieved by comparing the definitions of the NZ site class (i.e. Table 3) with the definitions of the site classification used by the foreign GMPEs. It can be seen that there are some small discrepancies between the definition of these site classes (e.g. the NZ site class C/D boundary is based on a site period of $T = 0.6s$, while for Z06 it is $T = 0.4s$, also the $V_{s,30}$ values are marginally offset). However, it is important to remember that as long as the site class compatibility is applied in accordance with these definitions, that any significant departures can be identified and rectified based on the observed statistics of the intra-event residuals as a function of

site class. In addition to V_{s30}, the CY08 and C10 models also require the basin depth to the 1km/s shear wave velocity horizon, $Z_{1.0}$. Because such site-specific basin depths are not available in NZ, then the relationship proposed by CY08 is adopted:

$$Z_{1.0} = exp\left[28.5 - 0.4775ln\left(V_{s,30}^{8} + 378.7^{8}\right)\right] \quad (7)$$

where $Z_{1.0}$ is in units of meters (m).

When examining the inter- and intra- event residuals obtained from the NZ database for each of the considered GMPEs, those records from all five site classes are considered. This is done so to enable a GMPE to be examined for all possible site classes considered in the NZ loadings standard (NZS 1170.5 2004). Despite this decision, it is noted that in the opinion of the author it is inappropriate to account for site response effects for site class E sites (and even many site class D sites) simply using such site response factors because highly nonlinear responses are expected for strong ground shaking, and therefore site-specific seismic site response analyses should be used if higher accuracy and precision is desired.

Table 4: Compatibility matrix adopted to convert NZ site classes into those predictor variables required for the considered foreign GMPEs.

NZS 1170.5 (2004)		Z06[1]			AB03[2]		BA08[3], CY08[4], C10[5]
Class	Desc.	Class	V_{s30} (m/s)	T_1 (s)	NEHRP	V_{s30} (m/s)	V_{s30} (m/s)
A	Strong rock	Hard rock	>1100	-	A	>1500	1800
B	Rock	SCI	600-1100	< 0.2	B	760-1500	800
C	Shallow Soil	SCII	300-600	0.2-0.4	C	360-760	450
D	Deep or soft soil	SCIII	200-300	0.4-0.6	D	180-360	250
E	Very soft soil	SCIV	<200	> 0.6	E	<180	200

[1]Zhao et al. (2006); [2]Atkinson and Boore (2003); [3]Boore and Atkinson (2008); [4]Chiou and Youngs (2008); [5]Chiou et al. (2010).

4. APPLICABILITY OF FOREIGN PREDICTION EQUATIONS FOR ACTIVE SHALLOW CRUSTAL EARTHQUAKES

4.1. Foreign crustal ground motion prediction equations considered

There are numerous GMPEs for active shallow crustal earthquakes. The five different GMPEs considered in this study are: McV06, Z06, BA08, CY08, C10. As previously mentioned, McV06 is the most recent NZ-specific model developed, and hence forms a useful benchmark on the applicability of other GMPEs, and whether there is in fact any benefit to be gained in using foreign GMPEs for ground motion prediction in NZ. The Z06 model is considered, both because it was developed using an extensive database of recordings from Japan, and also because previous research has suggested that the strong motion characteristics in NZ and Japan are similar (Zhao et al. 1997). The BA08 and CY08 models were considered as relatively simple and relatively complex, models produced from the Next Generation Attenuation (NGA) project, which utilized arguably the most comprehensive active shallow crustal strong motion database available. Finally, a Chiou et al. (2010)-based (C10) model was also considered, as it has been recently found that the CY08 model was not representative of strong motion observations for small-to-moderate magnitude events in California, (an observation which may also carry-over to NZ strong motion observations). Details of how the C10 model was obtained from the interpolation of results of Chiou *et al.* (2010) is given in the appendix.

4.2. Qualitative comparison of GMPEs considered

Before examining the statistics of the inter- and intra-event residuals of the NZ database using each of the GMPEs considered, it is insightful to examine the scaling of the GMPEs as a function of several predictor variables. Such insight is useful in the interpretation of the observed inter- and intra-event residuals, and as previously mentioned, in understanding the limitations of the models, particularly those associated with model extrapolation.

This section presents only sufficient results to convey the general predictor variable scaling characteristics of each of the models. More elaborate results are given in the appendices.

4.2.1. Magnitude scaling of median

Figure 6 illustrates the magnitude scaling of the median of the five GMPEs considered for both Sa(0.0) (i.e. PGA) and Sa(2.0). Figure 6a illustrates that all of the GMPEs predict similar Sa(0.0) values for $M_w = 6.5$, but that the scaling to small and large magnitudes is significantly different. This observation is primarily the result of databases used in developing empirical GMPEs typically having few large magnitude events (because of a lack of recordings), and few small magnitude events (because of a combination of their perceived unimportance in seismic hazard, and poor metadata quality). It can be seen that the scaling with magnitude of the McV06 model is significantly less 'concave from below' than the other models, and in fact for Sa(0.0), the scaling is linear (McVerry et al. 2006). As a consequence, the predicted Sa values of the McV06 model at small M_w are significantly larger (more than a factor of two at $M_w = 4.5$) than any of the other GMPEs considered. It is also pertinent to note that the small M_w scaling of using C10 produces notably smaller Sa(0.0) amplitudes (and

short period amplitudes in general) than the CY08 model.

At large magnitudes it can be seen that with the exception of the Z06 model, the other models exhibit similar scaling. The difference in the large magnitude scaling of Z06 is very significant, with the predicted amplitudes for Sa(0.0) being a factor of approximately 1.5 larger than the other considered models. Examination of the Z06 model and ground motion database (Zhao et al. 2006), reveals firstly that the largest well recorded crustal Japanese event has a $M_w < 7$ and that overseas ground motion records from events up to M_w~7.5 were used to supplement the Z06 Japanese ground motion database. Secondly, the quadratic magnitude scaling in the Z06 model was developed based on the observed residuals of a simpler linear magnitude scaling model, rather than in the initial mixed-effects model formulation. In fact,the Z06 model also exhibits linear magnitude scaling for Sa(0.0) (i.e. the quadratic M_w coefficient is zero), and the observed non-linear trend in Figure 6a results from the near-source saturation terms. Because of the fact that the near-source large magnitude overseas data used by Zhao *et al.* (2006) is significantly less comprehensive than the near-source large-magnitude NGA database then it is likely that the scaling in the Z06 model in this region is less constrained than the BA08, CY08 (and C10) NGA models. Hence, it is argued that the large magnitude scaling of the Z06 model is an artefact of the functional form adopted and not well constrained by data. Clearly, this artefact is important given that such large events are often critical in seismic hazard studies of high seismicity regions.

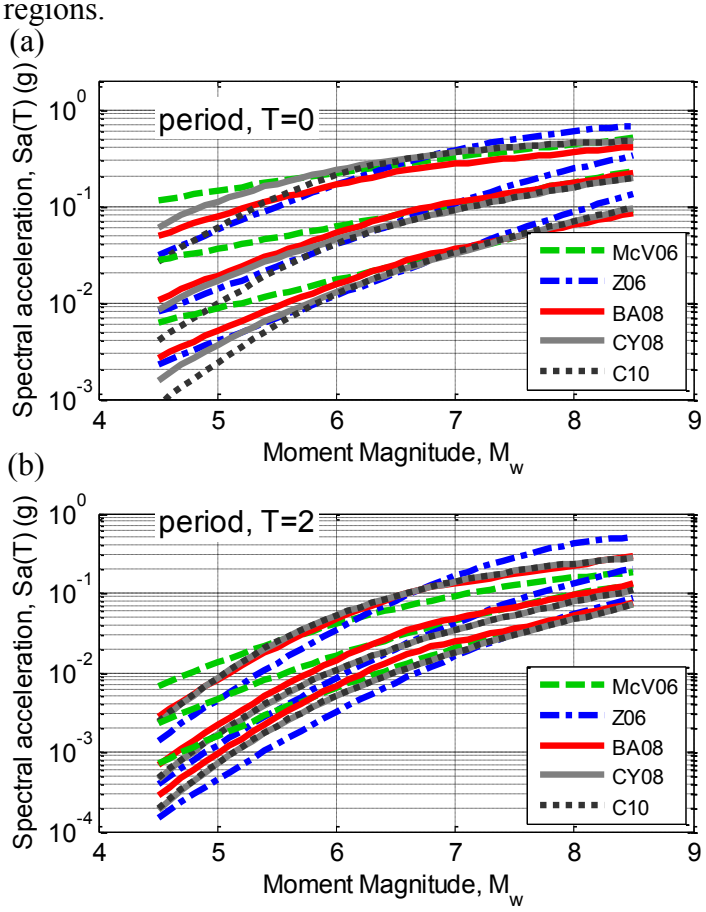

Figure 6: Magnitude scaling of the considered active shallow crustal GMPEs for three source-to-site distances of 10, 50, and 120 km: (a) Sa(0.0); and (b) Sa(2.0). (predictions for site class C sites).

4.2.2. Path scaling of median

Figure 7 illustrates the path scaling of the median of the five GMPEs considered for both Sa(0.0) (i.e. PGA) and Sa(2.0). In general, the path scaling of GMPEs can be separated into: (i) near-source scaling considering the finite dimension of the fault source; (ii) geometric spreading at moderate to large distances; and (iii) anelastic attenuation at large distances. While all five models consider these three aspects of path scaling, the functional forms adopted to do so are often different.

The near-source scaling of the five models at short periods is similar, with the relatively smaller near-source saturation of the BA08 model being the only notable observation. At long periods, all models other than McV06 exhibit similar scaling. The discrepancy of the McV06 model is due to the small geometric spreading coefficients for Sa(2.0) at moderate to large distances as discussed below.

The path scaling of the five different models at moderate to large distances (i.e. beyond where finite fault effects are significant), differ drastically in terms of complexity. The Z06 model uses a constant geometric spreading slope of -1 (the theoretical value for the geometric spreading of direct arrival Fourier spectra amplitudes); while the BA08 model uses a constant slope of -0.8. The McV06 model uses a magnitude and period dependent geometric spreading term, with larger coefficients for smaller magnitudes and short periods. This wide variation of geometric spreading of the McV06 model can be clearly seen, for example, in Figure 7b (a very small coefficient of -0.23 for the $M_w = 7.5$ event) and in Figure 7a (a coefficient of -0.73 for the $M_w = 6$ event). The CY08 and C10 models consider geometric spreading at moderate to large distances in two parts. At large distances the geometric spreading coefficient is -0.5 (i.e. $y_{i,j} \propto 1/\sqrt{R_{rup}}$), and at moderate distances the geometric spreading rate transitions from the near source coefficient of -2.1 to -0.5. The transition source-to-site distance is $R_{rup} = c_{RB} = 50$km. These effects of the CY08/C10 path scaling are partially obscured by anelastic attenuation effects for Sa(0.0) in Figure 7a, but can be clearly seen for Sa(2.0) in Figure 7b (in which the effects of anelastic attenuation are small).

All of the models consider anelatic attenuation using the same functional form (i.e. $lny_{i,j} \propto \gamma R_{rup}$), but with significantly different values for the anelastic attenuation coefficient(s), γ. The McV06 model has the largest anelastic attenuation at short periods (e.g. Sa(0.0)), followed by the BA08 model, while the Z06, CY08, and C10 models are similar. At longer periods (e.g. Sa(2.0)) the McV06 model also the largest anelastic attenuation, followed by the Z06 model, while the BA08, CY08, and C10 models are similar.

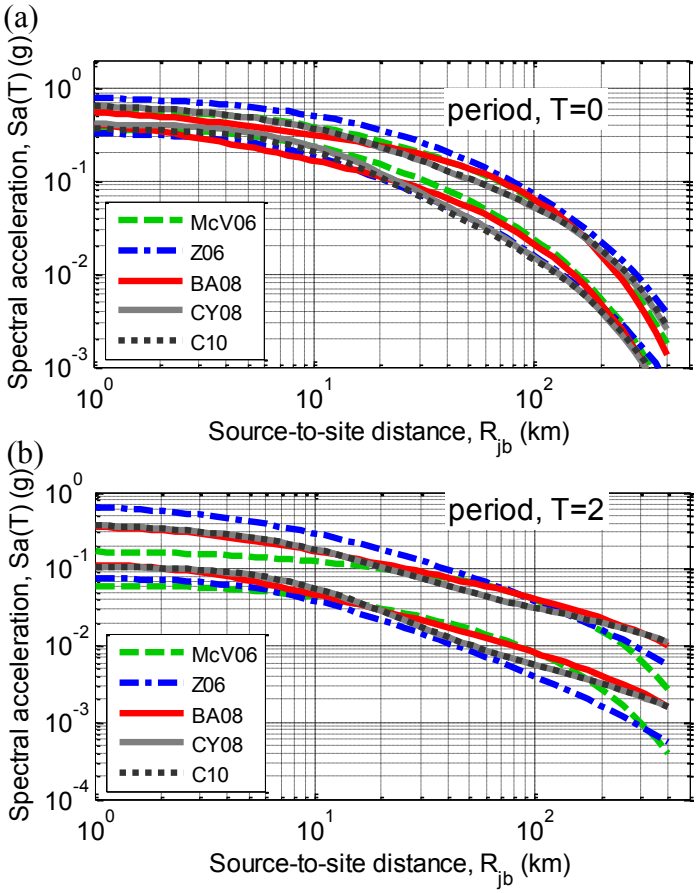

Figure 7: Path scaling of the considered active shallow crustal GMPEs for two magnitudes of 6 and 7.5: (a) Sa(0.0); and (b) Sa(2.0) (predictions for site class C sites).

4.2.3. Median response spectra (vibration period scaling)

Figure 8 illustrates the median response spectra predicted by the five considered GMPEs for magnitudes 5.5 and 7.5 and distances of 10 and 50 km. For $M_w = 5.5$ it can be seen that the McV06 model generally predicts higher spectral amplitudes (particularly at short periods), as a result of the previously discussed small magnitude scaling. Similarly, for M_w =7.5 the Z06 model predicts higher spectral amplitudes as a result of the Z06 large magnitude scaling. Other observations include: the larger amplitudes of long period (T > 2 seconds) ground motion for the BA08 model relative to the remaining equations; and the unsmoothed nature of the McV06 model.

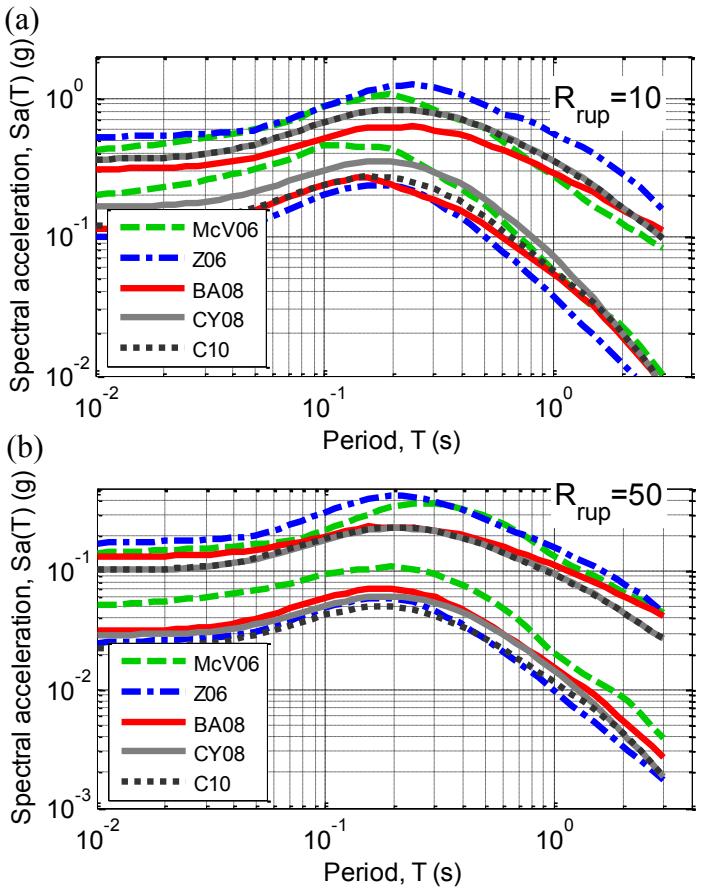

Figure 8: Median response spectra of the considered active shallow crustal GMPEs for two magnitudes of 5.5 and 7.5: (a) R_{rup}=10km; and (b) R_{rup}=50km (predictions for site class C sites).

4.2.4. Magnitude and period dependence of model standard deviations

Figure 9 illustrates the scaling of the inter-event standard deviation of the models as a function of vibration period and magnitude. Figure 9c and Figure 9d illustrate that only the CY08 and C10 models have magnitude-dependent inter-event residuals, and that the dependence reduces with increasing vibration period. for large magnitudes it can be seen that the BA08, CY08 and C10 inter-event standard deviation generally increases with vibration period, T, while the Z06 model is relatively constant with T, and the McV06 model varies rather erratically with period.

Figure 10 illustrates the dependence of the intra-event residuals with magnitude and distance. Similar to the inter-event residuals it can be seen that the Z06 and BA08 models are independent of magnitude, and that the CY08 and C10 magnitude dependence decreases with vibration period. In contrast, the intra-event standard deviation of the McV06 model exhibits magnitude dependence, but strangely the magnitude dependent coefficient is not always negative (e.g. for Sa(0.2) and Sa(2.0)) as is common in most GMPEs with magnitude dependent standard deviations (e.g. CY08 and C10). This observation as well as the observed scaling of the McV06 intra-event standard deviation provide further evidence of the insufficient number of recordings used in developing this model. It is also noted that the Z06 model has a significantly larger intra-event standard deviation than the BA08 and CY08/C10 models (for M_w>6).

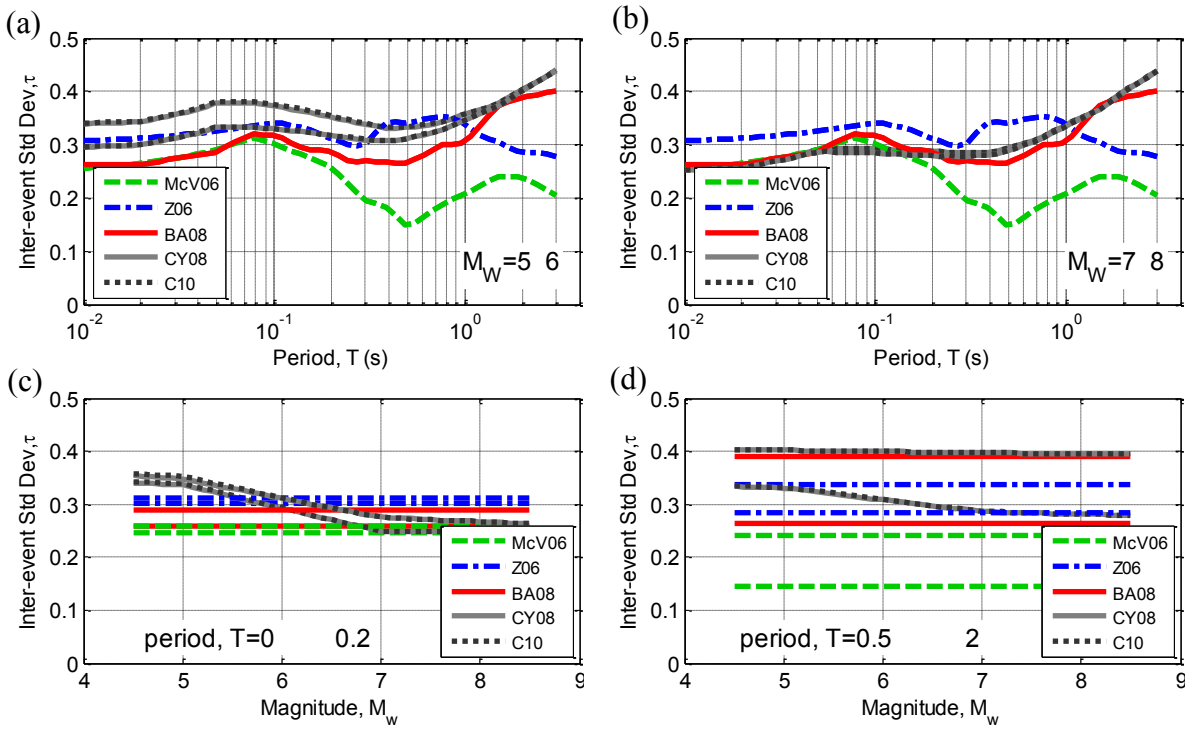

Figure 9: Inter-event standard deviation scaling of active shallow crustal ground motion prediction equations with period and magnitude.

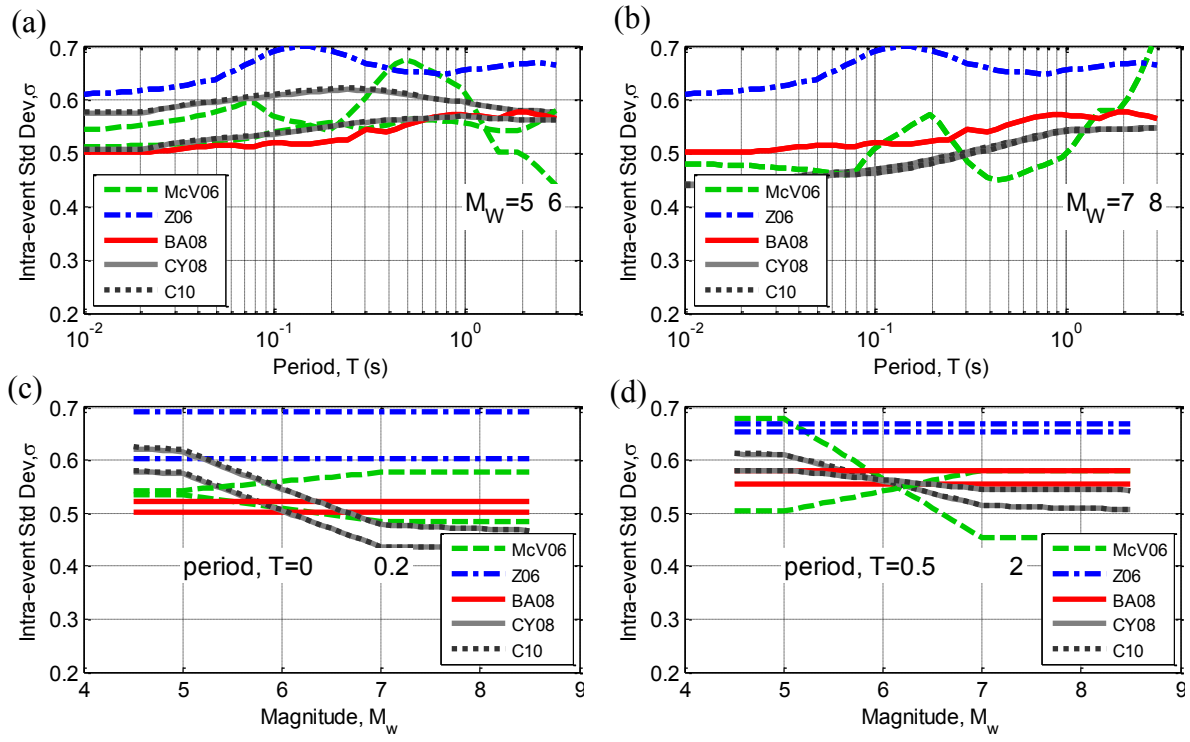

Figure 10: Intra-event standard deviation scaling of active shallow crustal ground motion prediction equations with period and magnitude.

4.3. Observed inter- and intra-event residuals from the NZ database

Now that insight has been obtained as to some of the general predictor variable scaling features of the considered GMPEs it is possible to thoroughly examine the statistics of the observed inter- and intra-event residuals of the NZ database for each

of the considered models. This section presents only sufficient results (typically for a single vibration period) to convey the general observations of the inter- and intra-event residuals as a function of predictor variables for each of the models. More elaborate results for vibration periods of 0.0, 0.2, 0.5, 1.0, and 5.0 seconds (or 3.0 seconds if the model was not applicable for 5.0 seconds) are given in the appendices.

In the examination of the cumulative distribution of the residuals, the Kolmogorov-Smirnov goodness-of-fit test (Ang and Tang 2007) is used to identify statistically significant departures from the residuals having a standard normal distribution. Furthermore, in order to illustrate the key trends in the observed residuals as a function of the predictor variables, non-parametric regression (Wasserman 2006) of the mean is used. The optimal bandwidth to use in the non-parametric bandwidth to use in the non-parametric regression was determined using the approach of Ruppert *et al*. (1995). In addition to this non-parametric mean, the 98% confidence interval of the mean is also computed from the Student's *t*-distribution (as a result of η_i and $\varepsilon_{i,j}$ having normal distributions) (Ang and Tang 2007). The non-parametric mean and its confidence interval are shown in subsequent figures with solid and dashed lines, respectively, and can be used to identify statistically significant biases in the prediction models. The high level of confidence used is based on the desire to only identify high significance biases.

4.3.1. McVerry et al. (2006), McV06.

Figure 11 illustrates the observed inter- and intra-event residuals for Sa(0.5) from the NZ database using the McV06 model. It is immediately obvious that the McV06 model significantly over predicts ground motions from $M_w < 6$ events, as seen by the negative trend in the inter-event residuals in Figure 11a and its dependence as a function of M_w in Figure 11c. This can be understood based on the magnitude scaling of the McV06 model presented in Figure 6. The significant over-prediction for small M_w events also effects the intra-event residuals because of the manner in which error is partitioned between the inter- and intra-event terms (i.e. Equation (5)). There is also an observed bias in the intra-event residuals as a function of source-to-site distance (Figure 11e).

Figure 11g illustrates that there is some variation in the mean inter-event residual as a function of focal mechanism, indicating some bias in the focal mechanism factors. There is no observed bias with respect to source depth as evident in Figure 11f (although the significant magnitude scaling problem makes this inconclusive).

Figure 11i illustrates that there is a variation in the mean intra-event residual as a function of site class, with site classes A and E in particular being over- and under-predicted, respectively. This can be explained by noting that the McV06 model uses the same site class factor for site classes A and B and site classes D and E, respectively. Clearly the assumption that these site classes, on average, have the same site effects is not valid.

Converse to the poor performance of the McV06 model with respect to the aforementioned predictor variables, it can be seen that there is no trend of the intra-event residuals with respect to the normalised path distance through the Taupo Volcanic Zone (TVZ) (only records with $R_{rup} > 70$km for which anelastic attenuation is important are shown). This confirms the importance of the increased anelastic attenuation in the TVZ (Cousins et al. 1999, Haines 1981, McVerry et al. 2006).

4.3.2. Zhao et al. (2006), Z06

Figure 12 illustrates the observed inter- and intra-event residuals for Sa(0.0) from the NZ database using the Z06 model. While there is a systematic over-prediction of the ground motions, as evident from the negative mean value of the inter-event residuals in Figure 12a and Figure 12c, it can be seen that there is significantly less bias with magnitude in the Z06 model compared to the McV06 model. Figure 12e illustrates that there are marginally apparent biases in the near-source distance scaling and also in the large-distance scaling.

Figure 12f illustrates that there is bias in the scaling with depth, but this bias was only apparent for Sa(0.0) and not significant for other vibration periods.

Figure 12g illustrates that there is a significant over-prediction of normal events using the Z06 model. This is a result of the fact that the Z06 model considers only 'reverse' and 'other' focal mechanisms, and not for the typically lower ground motions from normal faulting events considered in the other four models examined (likely due to the fact that only 24 out of the 1481, or 1.6%, of the records from crustal events in the Z06 database were normal faulting events (Zhao et al. 2006)).

Figure 12h illustrates that there is a significant negative trend in the intra-event residuals as a function of the normalised TVZ distance, indicating the importance of TVZ anelastic attenuation which is not accounted by Z06 (or any of the other foreign models considered here).

Figure 12i illustrates that the Z06 model provides a relatively good prediction of site class effects with no significant biases for Sa(0.0). For short period amplitudes (i.e. Sa(0.2), Sa(0.5), and Sa(1.0)) there was however a statistically significant over-prediction of the amplitudes of site class A motions, which can be attributed to the fact that the Z06 Hard rock site class is defined for $V_{s,30}$ > 1100 m/s, while it is $V_{s,30}$ > 1500 m/s for NZ site class A (i.e. Table 4).

Finally, it is noted that the over-prediction of site class A amplitudes, neglection of TVZ effects, over-prediction of normal events, and over-prediction at large-distances leads to the resulting observed negative inter-event residuals for several of the large magnitude (M_w > 6) events in the NZ database, which were predominantly normal events near the TVZ and recorded at class A sites. Thus, the observed inter-event residuals for these M_w > 6 events are not related to errors in the Z06 magnitude scaling. This same result is also true for the BA08, CY08, and C10 models examined subsequently. Conversely, no significant over-prediction of these large events is observed using the McV06 model because it accounts for TVZ distance, and also over-predicts site class A motions.

4.3.3. Boore and Atkinson (2008), BA08.

Figure 13 illustrates the observed inter- and intra-event residuals for Sa(0.0) from the NZ database using the BA08 model. Similar to the Z06 model it can be seen that there is a systematic over-prediction of the ground motions for small magnitudes, and a slight over-prediction for larger magnitudes (M_w>5.5), partially the result of the aforementioned neglection of TVZ effects, and an over-prediction of site class A amplitudes from normal faulting events. Figure 13e illustrates that there is also an apparent bias in the near-source distance scaling ($20 < R_{rup} < 90$km).

Figure 13f illustrates that there is a dependence of the inter-event residuals with source depth, because such an effect is not accounted for based on the R_{jb} distance measure.

Figure 13g illustrates that there is a significant difference between the mean

inter-event residuals as a function of focal mechanism. Normal events, in particular, are consistently over-predicted for short period amplitudes (i.e. $T < 0.5$ seconds) as illustrated for several vibration periods in the appendix.

Similar to the Z06 model, Figure 13h illustrates bias of the BA08 model with respect to normalised TVZ distance.

Figure 13i illustrates the intra-event residuals as a function of site class. It can be seen that there is a good prediction for site classes B, C, and D, but an over-prediction for site classes A and E. This over-prediction only occurs for short periods (i.e. $T < 0.5$ seconds), with no bias across all site classes for longer vibration periods.

4.3.4. Chiou and Youngs (2008),CY08.

Figure 14 illustrates the observed inter- and intra-event residuals for Sa(0.0) from the NZ database using the CY08 model. Similar to the BA08 model it can be seen that there is a consistent over-prediction of small magnitude ground motions, and large magnitude ground motions due to aforementioned neglection of TVZ effects, and over-prediction from normal events and site class A amplitudes. It can also be seen that there is a statistically significant bias at long distances for short period ground motion amplitudes, suggesting the anelastic attenuation is insufficient.

Figure 13f illustrates that there is a dependence of the intra-event residuals as a function of source depth for Sa(0.0), as well as several other vibration periods (see appendix).

Similar to the BA08 model, Figure 13g illustrates that there is a consistent over-prediction of normal faulting events at short periods.

Figure 13i illustrates that the CY08 site response model provides a good prediction for site classes B, C and D, but there is an over-prediction for site classes A and E at short periods. The over-prediction for site class A can be explained from the fact that the CY08 site amplification factor is unity for $V_{s,30} >$1130m/s, while NZ site class A have shear wave velocities greater than 1500 m/s (Table 3).

4.3.5. Chiou et al. (2010)-based model, C10.

Figure 15 illustrates the observed inter- and intra-event residuals for Sa(0.0) from the NZ database using the C10 model. It can be seen that based on the distributions of the inter- and intra-event residuals alone (i.e. Figure 15a and Figure 15b) that the C10 model is unbiased (i.e. this is the approach of Stafford *et al*. (2008) and Scherbaum *et al*. (2004)). As can be appreciated from Figure 6a the C10 model predicts lower ground motions for small magnitude events than the CY08 model. This is clearly apparent in the inter-event residuals as a function of magnitude shown in Figure 15c with negligible bias for M_w<6. Similar to the BA08 and CY08 models there is an observed bias in large distance scaling at short periods, suggesting insufficient anelastic attenuation effects.

Unlike the CY08 model, Figure 15f illustrates that there is no significant bias of the intra-event residuals for source depths less than 20km. It is noted that the source depth scaling of the CY08 and C10 models is identical, therefore demonstrating the difficulty in examining biases in multidimensional data and models, using uni-dimensional marginal trends.

Figure 15g illustrates that the C10 model over-predicts the amplitude of normal faulting events for Sa(0.0), and similar to the BA08 and CY08 models, this over-prediction only occurs for short periods (see appendix for residuals at other periods).

Figure 15h illustrates the bias in ground motion amplitudes as a function of

normalized TVZ distance, which is not accounted for in the C10 model.

Similar to the CY08 model, Figure 15i illustrates that the C10 model (which has the same site response formulation as the CY08 model) provides a good prediction for class B, C, D sites. Furthermore, it can be seen that the prediction for class E sites is unbiased for both Sa(0.0) and other vibration periods (see appendix). There is also a minor reduction in the bias for site class A sites due to the improved M_w scaling.

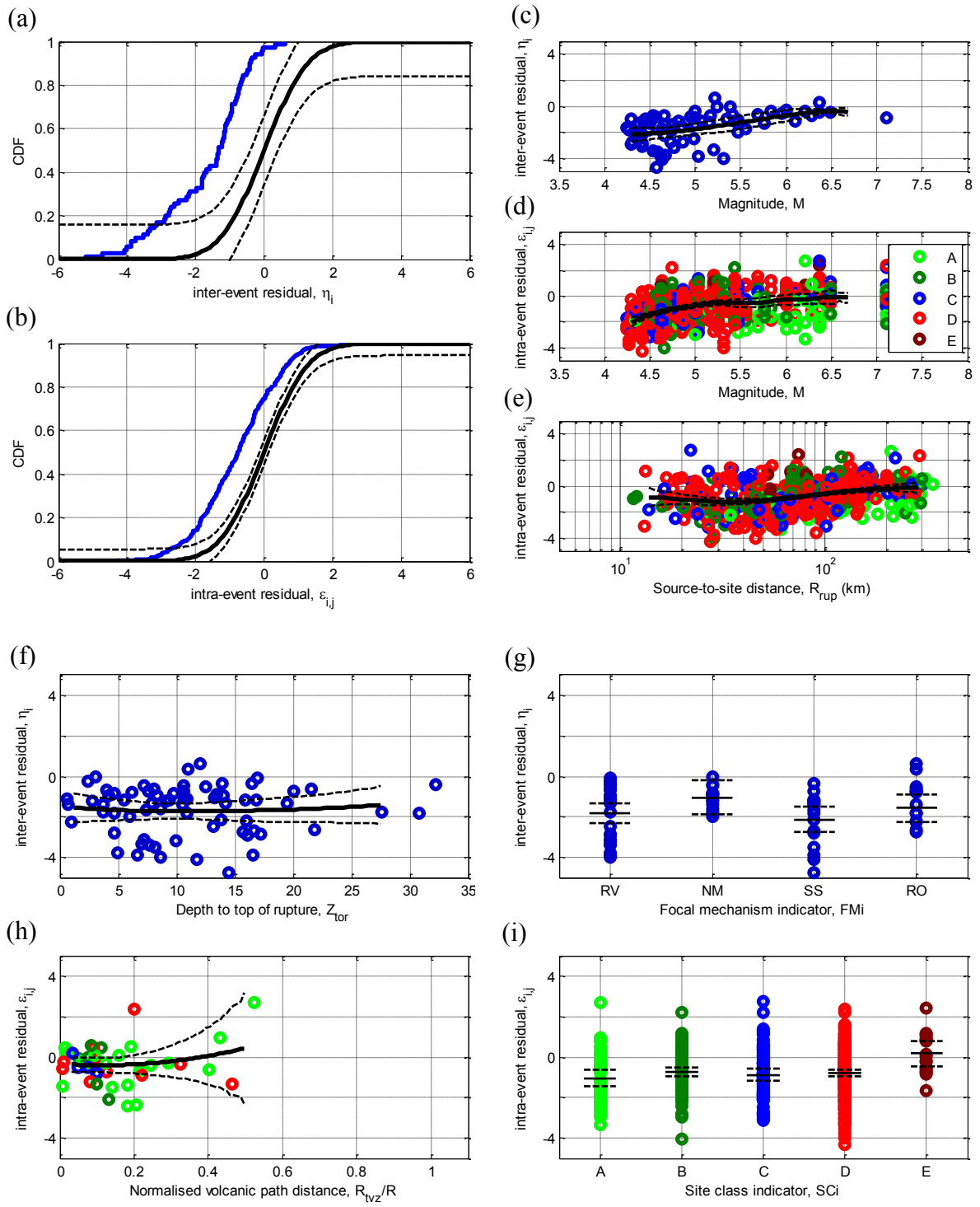

Figure 11: Residuals for Sa(0.5) using the McV06 model: (a)&(b) distribution of inter- and intra-event residuals; (c)&(d) inter- and intra-event residuals as a function of magnitude; (e) intra-event residuals as a function of distance; (f)&(g) inter-event residuals as a function of depth and focal mechanism; (h)&(i) intra-event residuals as a function of normalised volcanic path distance and site class.

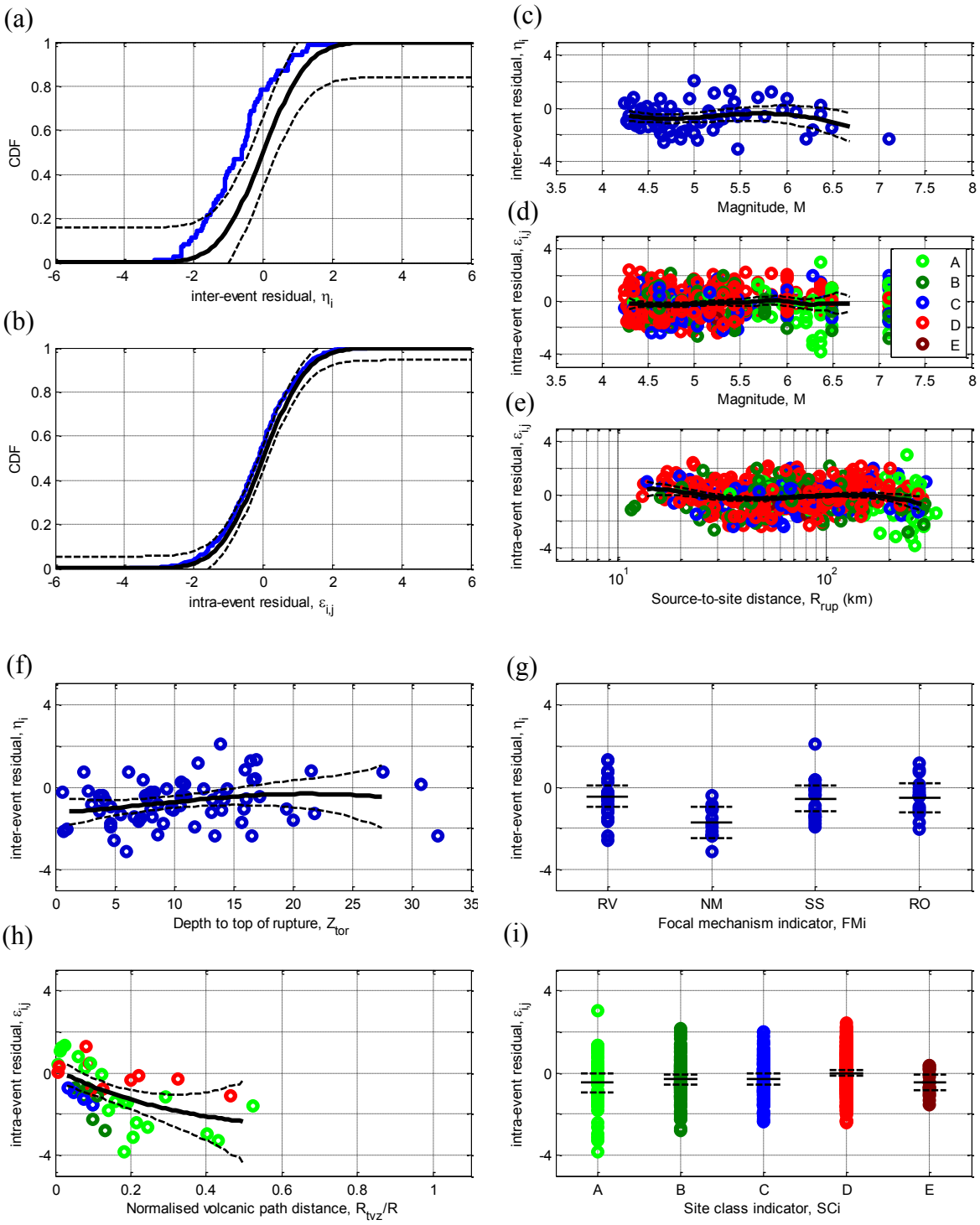

Figure 12: Residuals for Sa(0.0) using the Z06 model: (a)&(b) distribution of inter- and intra-event residuals; (c)&(d) inter- and intra-event residuals as a function of magnitude; (e) intra-event residuals as a function of distance; (f)&(g) inter-event residuals as a function of depth and focal mechanism; (h)&(i) intra-event residuals as a function of normalised volcanic path distance and site class.

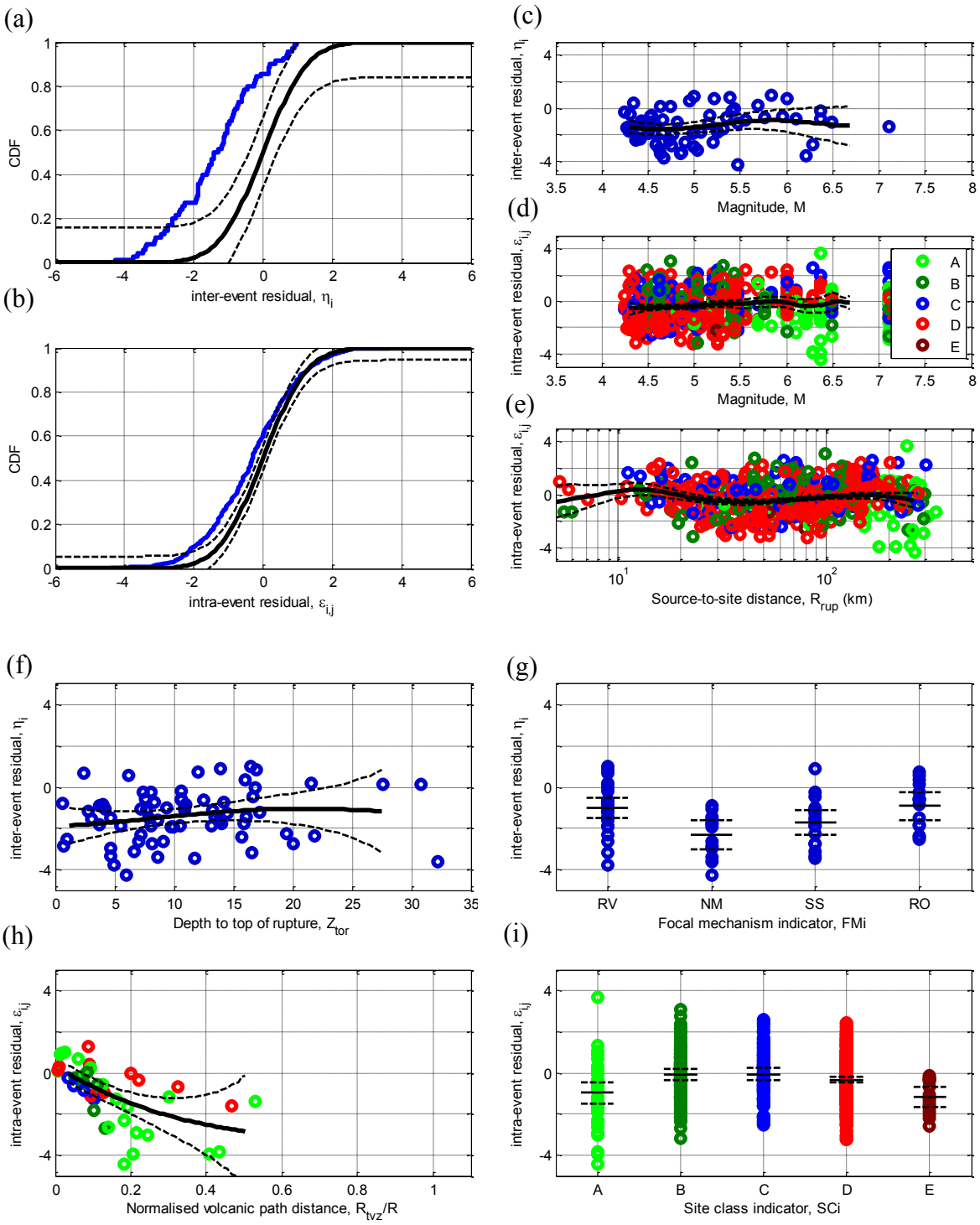

Figure 13: Residuals for Sa(0.0) using the BA08 model: (a)&(b) distribution of inter- and intra-event residuals; (c)&(d) inter- and intra-event residuals as a function of magnitude; (e) intra-event residuals as a function of distance; (f)&(g) inter-event residuals as a function of depth and focal mechanism; (h)&(i) intra-event residuals as a function of normalised volcanic path distance and site class.

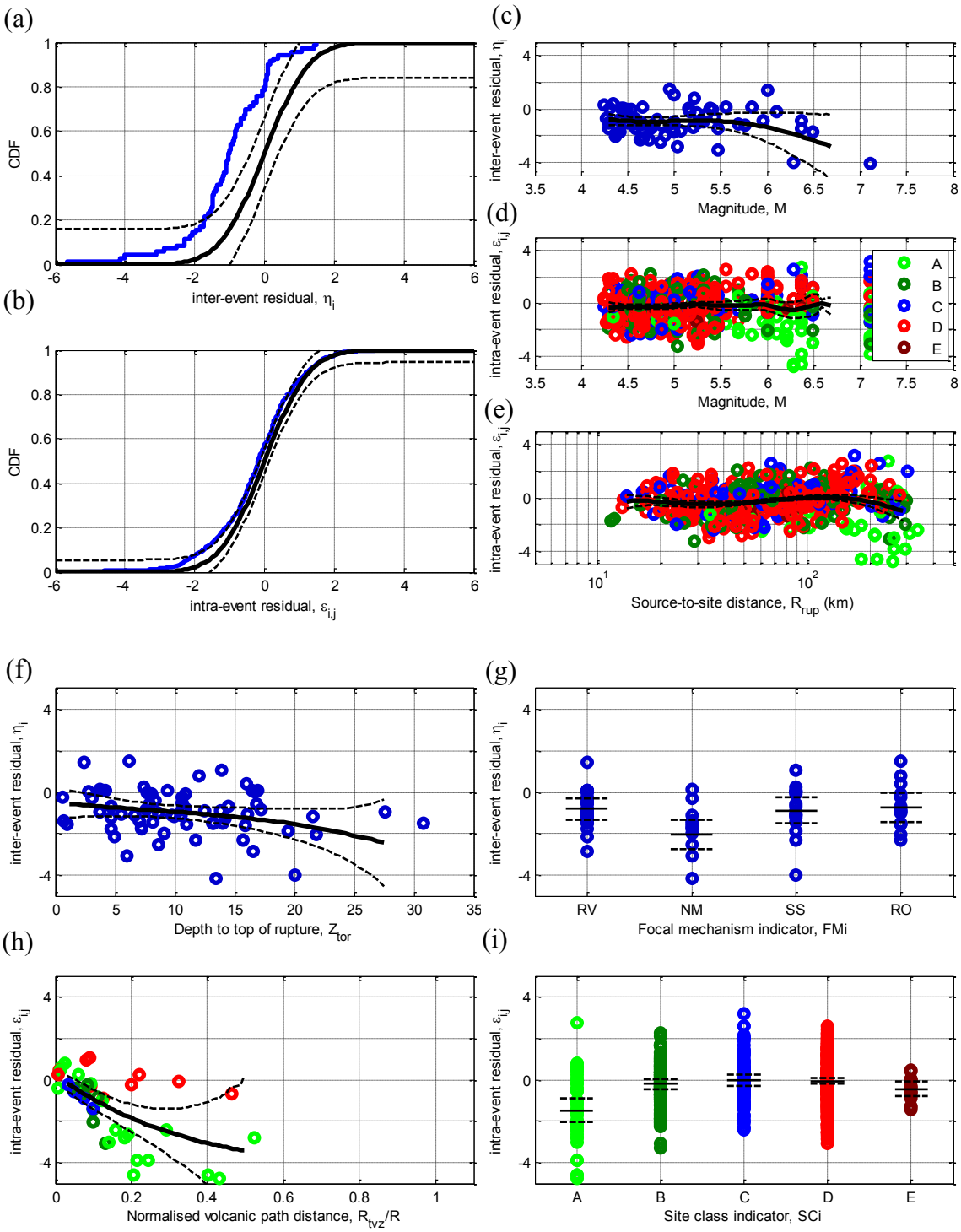

Figure 14: Residuals for Sa(0.0) using the CY08 model: (a)&(b) distribution of inter- and intra-event residuals; (c)&(d) inter- and intra-event residuals as a function of magnitude; (e) intra-event residuals as a function of distance; (f)&(g) inter-event residuals as a function of depth and focal mechanism; (h)&(i) intra-event residuals as a function of normalised volcanic path distance and site class.

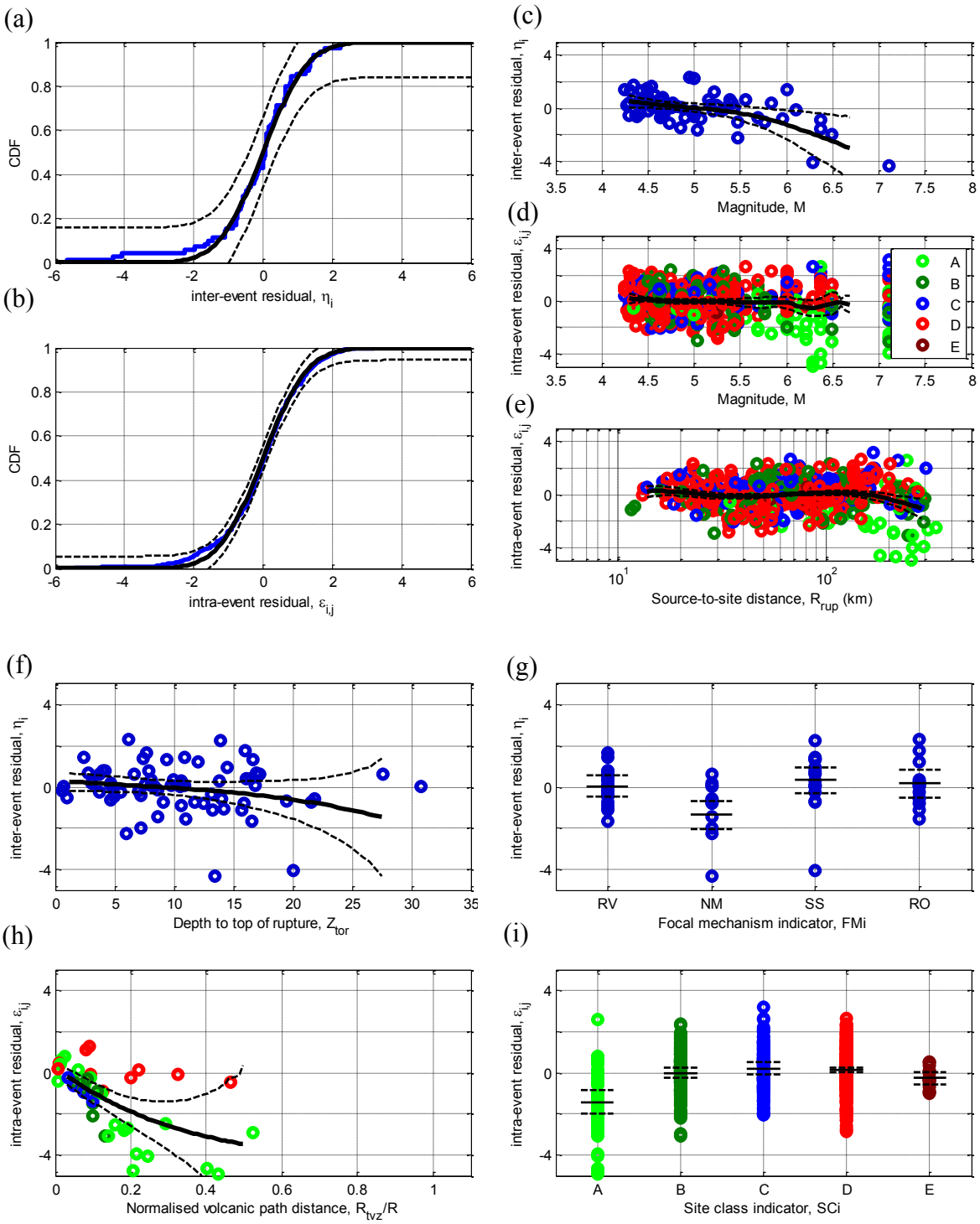

Figure 15: Residuals for Sa(0.0) using the C10 model: (a)&(b) distribution of inter- and intra-event residuals; (c)&(d) inter- and intra-event residuals as a function of magnitude; (e) intra-event residuals as a function of distance; (f)&(g) inter-event residuals as a function of depth and focal mechanism; (h)&(i) intra-event residuals as a function of normalised volcanic path distance and site class.

5. NZ-SPECIFIC SHALLOW ACTIVE SHALLOW CRUSTAL MODEL

The five active shallow crustal GMPEs considered in this study span a range of applicability for NZ strong motion prediction based on the observed inter- and intra-event residuals examined in the previous section. While it was relatively clear that the most recent NZ-specific model, McV06, has the most significant bias with respect to the NZ empirical data, the determination of the 'best' of the remaining four foreign models is a non-trivial task. Most importantly, the results of the previous section demonstrate that none of the four foreign models are directly applicable to NZ in their present form, and therefore whichever model is selected will require modification.

5.1. "Base-model" adopted

In the examination of the observed inter- and intra-event residuals it is important to bear in mind that the NZ strong motion database lacks large magnitude events recorded at near source distances (Figure 2). Recall from Figure 4 that there are only 28 records from active shallow crustal events with PGA values above 0.1g with the largest being 0.39g. Given the apparent high seismicity of NZ it can be concluded that the trends in the observed inter- and intra-event residuals of the various models cannot be used to identify a superior GMPE for large magnitude, near-source ground motion scenarios, which often dominate seismic hazard analyses. Notwithstanding this comment it is also important to have an accurate and precise prediction of ground motions for other earthquake scenarios. For example, while smaller magnitude events on average produce lower ground motions, their increased frequency of occurrence means that they are still important contributors toward the seismic hazard at a given site.

Based on the above argument it is necessary to examine the rigour of the Z06, BA08, CY08 and C10 models for large magnitude, near-source ground motions. Firstly, it is noted that the C10 model is essentially an extension of the CY08 model to be more consistent for short period spectral amplitudes at small-to-moderate magnitudes, therefore in the discussion below reference is made only to CY08, although both are implied. The Z06 model is based on Japanese recordings, but a lack of near-source records in the Japanese database led Zhao *et al.* (2006) to include 196 motions from the western USA and Iran. On the other hand, the BA08, CY08 models are both developed from the NGA database (Chiou et al. 2008), which contains global recordings from active shallow crustal earthquakes. Furthermore, the BA08 and CY08 models were developed specifically for active shallow crustal events, while the Z06 model was developed for crustal, interface, and slab tectonic types. The relatively simple functional form in the Z06 model may therefore lead to a bias in the model for a single tectonic type. Hence because of the less rigorous database used by Z06 with respect to large magnitude, near-source records, and the fact that the Z06 model does not demonstrate notably better inter- and intra-event residual trends than the BA08, CY08 models, then the Z06 model was not selected for further consideration.

The BA08, and CY08 models can be considered as equally representative models for large magnitude, near-source events. Therefore, the hierarchy of these two models for applicability to NZ strong motion prediction is a function of their performance as indicated by the observed residual analysis presented in the previous

section. Furthermore, because it was previously noted that the residual analysis demonstrated that none of the models could be used without modification, then those models with a sounder theoretical basis or various scaling features which are functionally the least dependent will lead to a more rational modification for NZ-specific conditions.

Both the BA08 and CY08 models illustrated: (i) an over-prediction of normal faulting events at short periods; (ii) an over-prediction of site class A spectral amplitudes; and (iii) neglection of the increased anelastic attenuation in the TVZ. The BA08 model in addition exhibited bias for small magnitudes, path scaling bias over 20-90km and bias with source depth. On the other hand, the C10-version of the CY08 model did not exhibit bias for small magnitudes, moderate path distances, or source depth; but did illustrate bias at long distances for short vibration periods due to insufficient anelastic attenuation.

The modifications required to correct the aforementioned observed biases in the BA08 model for NZ-specific application would require significant modification because the BA08 formulation is such that the required modifications would influence other aspects of the model prediction. On the other hand, the necessary modifications to the CY08 model can be achieved without significantly modifying the 'base' model (as is evident from the C10 modification to achieve the correct small magnitude scaling). Furthermore, the changes required for the CY08 model can be justified based on physical arguments regarding the differences of the CY08 model development and NZ-specific details. Such physical justification for modifications is desirable because of the aforementioned lack of empirical NZ data, and the strong correlation between the observed biases in site class A amplitudes, normal faulting events, TVZ and non-TVZ anelastic attenuation. Hence, based on the above arguments the CY08 model is adopted as the 'base' model for modification.

5.2. Modifications of base-model to develop a NZ-specific active shallow crustal model

Five main modifications are required in order to rectify the observed predictor variable dependence of the inter- and intra-event residuals of the CY08/C10 model: (i) NZ-specific scaling for small magnitudes, which may be different than that for central or southern California (Chiou et al. 2010); (ii) normal faulting factor for short periods; (iii) site class A effects; (iv) anelastic attenuation in the NZ crust; and (v) consideration of the increased TVZ attenuation.

The five modifications of the CY08/C10 model noted above were done so using subsets of the NZ database in order to separate these effects as much as possible. Below, justification is provided for the functional and/or parametric modification for each of these five points, and the resulting features of the NZ-specific (B10) active shallow crustal model are examined.

5.2.1. Modification for NZ-specific small magnitude scaling

It was observed that the CY08 and BA08 NGA models over-predicted the amplitude of short-period spectral amplitudes for small-to-moderate magnitude (SMM) events (i.e. $M_w<5.5$). Atkinson and Morrison (2009) (using the BA08 model) and Chiou *et al.* (2010) (using the CY08 model) also observed an over prediction of ground motions in California using these models for SMM events. This is despite the fact that California is the region for which these NGA equations are considered most applicable. Atkinson and Morrison (2009) and Chiou *et al.* (2010) noted that the

NGA database has comparatively little ground motion recordings from such SMM events (as can be further seen in comparison of the NGA and NZ data in Figure 2). The limitation on the applicability of the NGA equations based on the magnitude range of their database is further highlighted by the findings of Bommer *et al.* (2007), who found that not only should empirical GMPEs not be extrapolated below the magnitude range of their empirical database, but also that their applicability at the limits of the magnitude range are questionable. Cotton et al (2008) also made a similar observation when examining European GMPEs relative to KiK-Net data.

One benefit of the CY08 model is that the functional form of magnitude scaling is such that the small magnitude scaling can be modified without influencing the scaling (and predicted amplitudes) for large magnitude events. This was specifically the approach taken by Chiou *et al.* (2010) for Central and Southern California. The intention here is to use the same logic as Chiou *et al.* (2010) for modifying the small magnitude scaling of the CY08 model based on the observed residuals from the NZ database, which can be achieved by modifying CY08 coefficients c_3 and c_m.

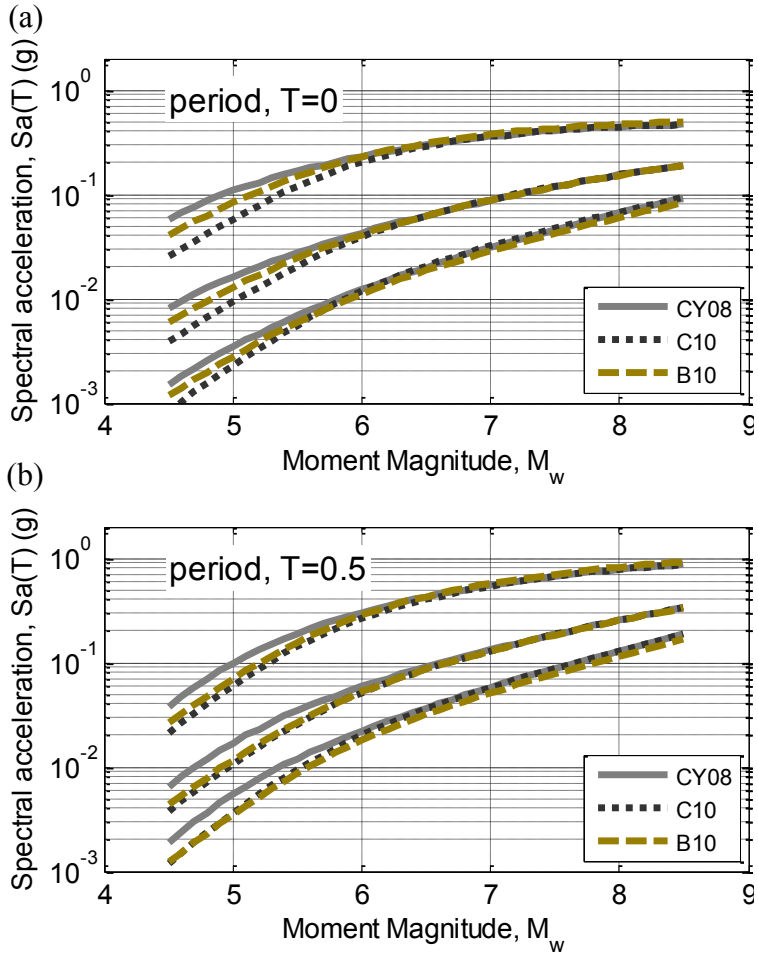

Figure 16: Magnitude scaling of the median B10 active shallow crustal model compared with the CY08 and C10 models for path distances of 10, 50 and 120 km: (a) Sa(0.0); and (b) Sa(0.5) (predictions for site class C and strike-slip focal mechanism).

Figure 16 provides a comparison between the magnitude scaling of the B10, CY08 and C10 models. It can be seen that at short vibration periods (i.e. Figure 16a) the B10 model exhibits smaller spectral acceleration ordinates for $M_w < 6$ than the

CY08 model (consistent with the observed negative residuals of the CY08 model in Figure 14c). Furthermore, at these short vibration periods the amplitudes predicted by the B10 model are larger than those predicted by the C10 model. As can be seen from Figure 17, the discrepancy between the magnitude scaling of the B10 and C10 models decreases with increasing period.

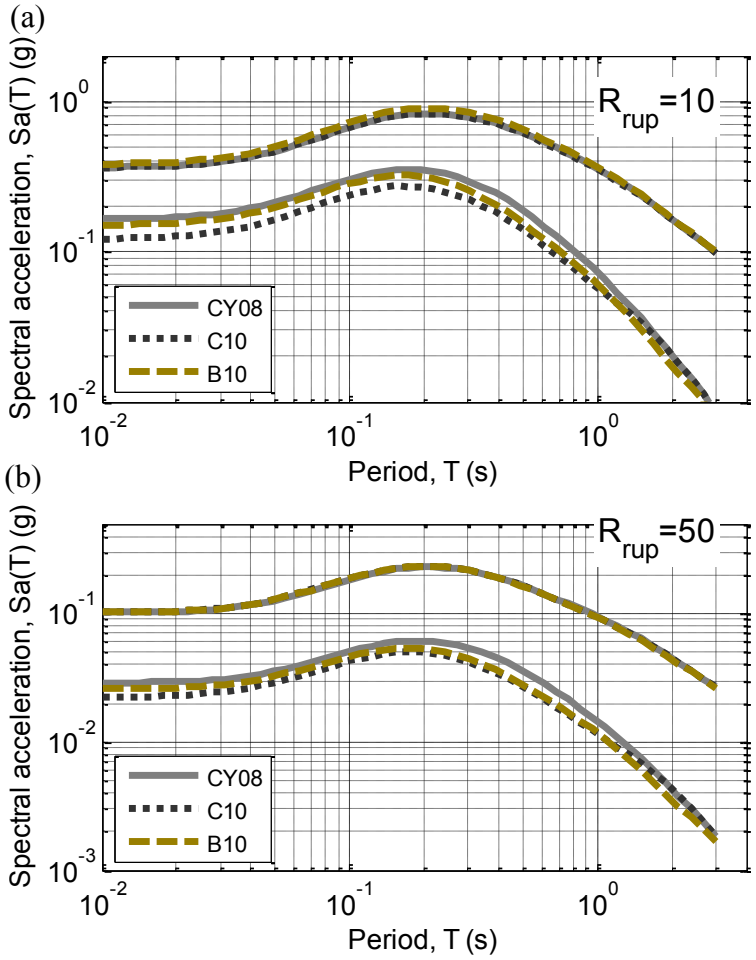

Figure 17: Vibration period scaling of the median B10 active shallow crustal model compared with the CY08 and C10 models for magnitudes of 5.5 and 7.5: (a) R_{rup} = 10km; and (b) R_{rup} = 50km (predictions for site class C and strike-slip focal mechanism).

5.2.2. Modification of normal faulting events

It was observed that at short vibration periods the CY08 and C10 model significantly over-predicted the spectral amplitudes from normal faulting events (e.g. Figure 14g and Figure 15g). The NZ database compiled in this study contains 106 recordings from normal crustal events (out of 641 crustal recordings, i.e. 16.5%). On the other hand, the NGA database has only 87 normal crustal recordings from 13 events (i.e. 2.5% of the NGA database (Chiou et al. 2008)). This small proportion of recordings from normal events has also been noted by Scasserra *et al.* (2009). It is also important to note that the normal faulting events in New Zealand occur in the Taupo Volcanic Zone (TVZ), which has potentially different geologic properties than the other normal faulting active shallow crustal tectonic types in the NGA database. The fact that the CY08/C10 models only over-predict normal faulting events at short periods may suggest that the stress-drop from normal faulting events in volcanic

regions is lower than that in non-volcanic regions, although more detailed studies are suggested to confirm such a speculation.

Figure 18 illustrates the predicted response spectra from the B10 model for a $M_w = 7$ event of various focal mechanisms. The predicted response spectral amplitudes for this scenario are essentially identical to the CY08 model for all focal mechanism except for normal faulting. Therefore, for comparison the CY08 normal faulting prediction is also shown upon which it can be seen that for vibration periods less than 0.5 seconds, the B10 model predicts smaller spectral amplitudes. For vibration periods larger than 0.5 seconds there was no significant bias in the intra-event residuals for normal events using the CY08 models, and hence the B10 model utilized the same normal faulting factor as the CY08 model.

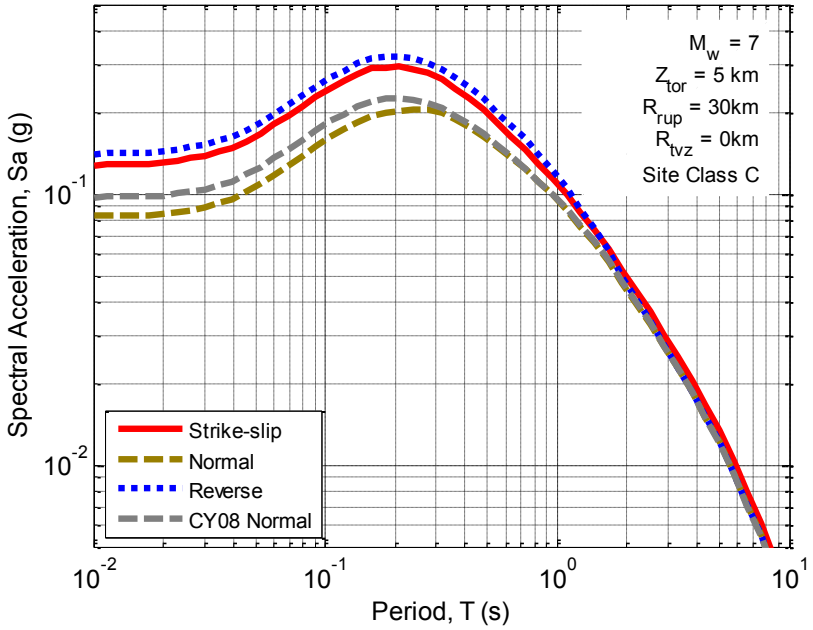

Figure 18: Effects of style-of-faulting on response spectra obtained from the B10 active shallow crustal model. For this scenario the prediction is essentially identical to that predicted from CY08 with the exception of normal faulting events, which are shown for comparison.

Figure 19 illustrates, as a function of vibration period, the predicted spectral amplitudes from normal and reverse events as a ratio of that predicted for strike-slip events. It can be seen that the CY08, BA08 and McV06 models all predict a similar ratio of between normal and strike-slip events (although the McV06 ratio was pre-set and not determined based on empirical data). For periods less than 0.5 seconds it can be seen that, as previously discussed, the B10 model predicts smaller normal faulting events than that of the CY08 and BA08 models.

Another important observation from Figure 19 is that there is still quite significant uncertainty as to the effect of style-of-faulting in GMPEs, with the normal/strike-slip ratio increasing for vibration periods greater than 0.5 seconds in the CY08 model (and the B10 model), but decreasing for the BA08 model. Similarly the BA08 model predicts a reverse/strike-slip spectral amplitude ratio of 1.0 for short periods, compared with ratios greater than 1.1 for all of the other models considered.

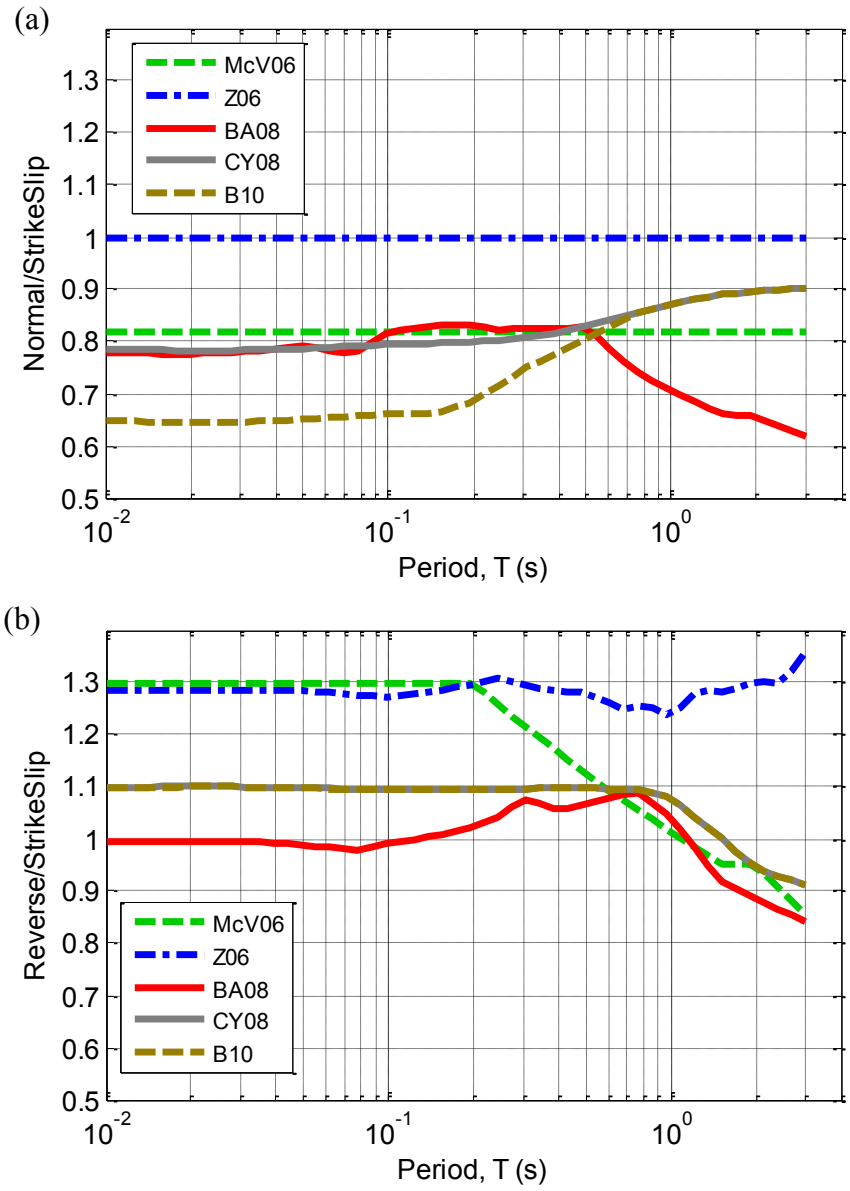

Figure 19: Predicted ratios between: (a) normal and strike slip events; and (b) reverse and strike-slip events as a function of vibration periods for the different active shallow crustal models considered.

5.2.3. Modification of class A site response

It was observed that the CY08/C10 models over-predicted the amplitudes of short period spectral ordinates for class A sites but were unbiased for longer period spectral ordinates. This under-prediction can be attributed to the fact that the CY08 model uses a reference shear-wave velocity of 1130 m/s, Sa_{1130}, and that the site response amplification for $V_{s,30}$ >1130 m/s is equal to 1.0. Chiou and Youngs (2008) adopted 1130 m/s as a reference value because very few of the NGA data had $V_{s,30}$ values in excess of this. For NZ conditions, however, there are numerous strong motion records on site class A, defined as having $V_{s,30}$ >1500 m/s (with a value of $V_{s,30}$ =1800 m/s used as the average value as given in Table 4). Based on this difference in shear wave velocities, theory dictates that (Fourier) spectral amplitudes will be over-predicted for short periods (high frequencies) with the over-prediction

decreasing with increasing vibration period. This expected bias from theoretical considerations is clearly observed in the (response spectra) residuals of the NZ database using the CY08/C10 models.

Because the CY08 site response model is based on nonlinear site response analyses (Chiou and Youngs 2008), it is desired to modify the site response model as little as possible. An obvious modification is to remove the constraint that the site response amplification for $V_{s,30}$ >1130 m/s is unity, and allow the amplification to have a value less than one for very stiff sites. This modification would lead to a similar reduction in the amplitude of spectral ordinates across all vibration periods (which is the case using the BA08 model), because the linear scaling of spectral amplitudes with $V_{s,30}$ is relatively constant with period (Chiou and Youngs 2008). To avoid this, Abrahamson and Silva (2008) (AS08) use an additional parameter, V_1, which is a function of period to provide a $V_{s,30}$ value above which the amplification is constant. The value of V_1 increases with decreasing vibration period in the Abrahamson and Silva (2008) model. This functional form allows a significant reduction in short period spectral amplitudes for $V_{s,30}$ =1800 m/s (compared with Sa_{1130}) which decreases with increasing vibration period. The functional form adopted for V_1 is:

$$V_1 = \begin{cases} 1800 & T = 0 \\ min[max(1130\{T/0.75\}^{-0.11}, 1130), 1800] & otherwise \end{cases} \quad (8)$$

It can be seen that Equation (8) gives a value of $V_1 = 1130$ for $T > 0.75s$ and $V_1 = 1800$ for $T < 0.01s$ (including $T = 0$). Figure 20 illustrates the variation of V_1 with period as given by Equation (8) in comparison to that of AS08. It can be seen that while both models exhibit a reduction of V_1 for increasing period, that the AS08 model has a limiting value of 1500 m/s and a stronger dependence with period beyond 0.5 seconds. Abrahamson and Silva (2008) note that the functional form for V_1 was not determined from regression but from equivalent-linear site response analyses conducted by Walling *et al.* (2008). However, Walling *et al.* (2008) considered only sites up to $V_{s,30}$ values of 900 m/s, so it is not clear how the V_1 formulation was obtained.

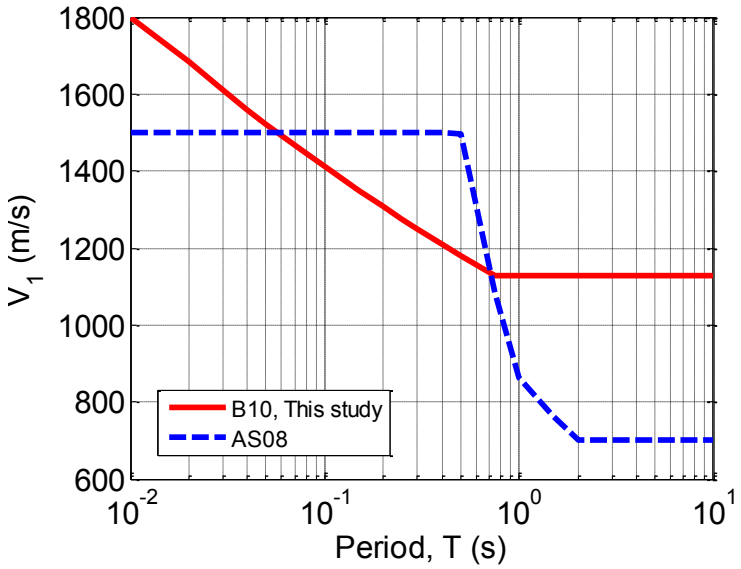

Figure 20: Comparison of the variation of the parameter V_1, which defines the shear-wave velocity above which the amplification is constant, with period for the Abrahamson and Silva (2008) (AS08) model and that developed in this study.

Figure 21 illustrates the site response amplification factors for the B10 model. The amplification factors are composed of linear and non-linear site response components. It can be seen that the influence of the non-linear site response component leads to a larger reduction in short period spectral amplitudes compared with those at longer periods. Of particular note is the amplification for $V_{s,30} > 1130$ m/s, which for $Sa(0.0)$ reduces to approximately 0.8 at $V_{s,30} = 1800$ m/s, and for Sa(0.5) to approximately 0.96 for $V_{s,30} > 1180$ m/s. The details of the mathematical formulation for the inclusion of V_1 into the CY08 site effects model is presented in a subsequent section.

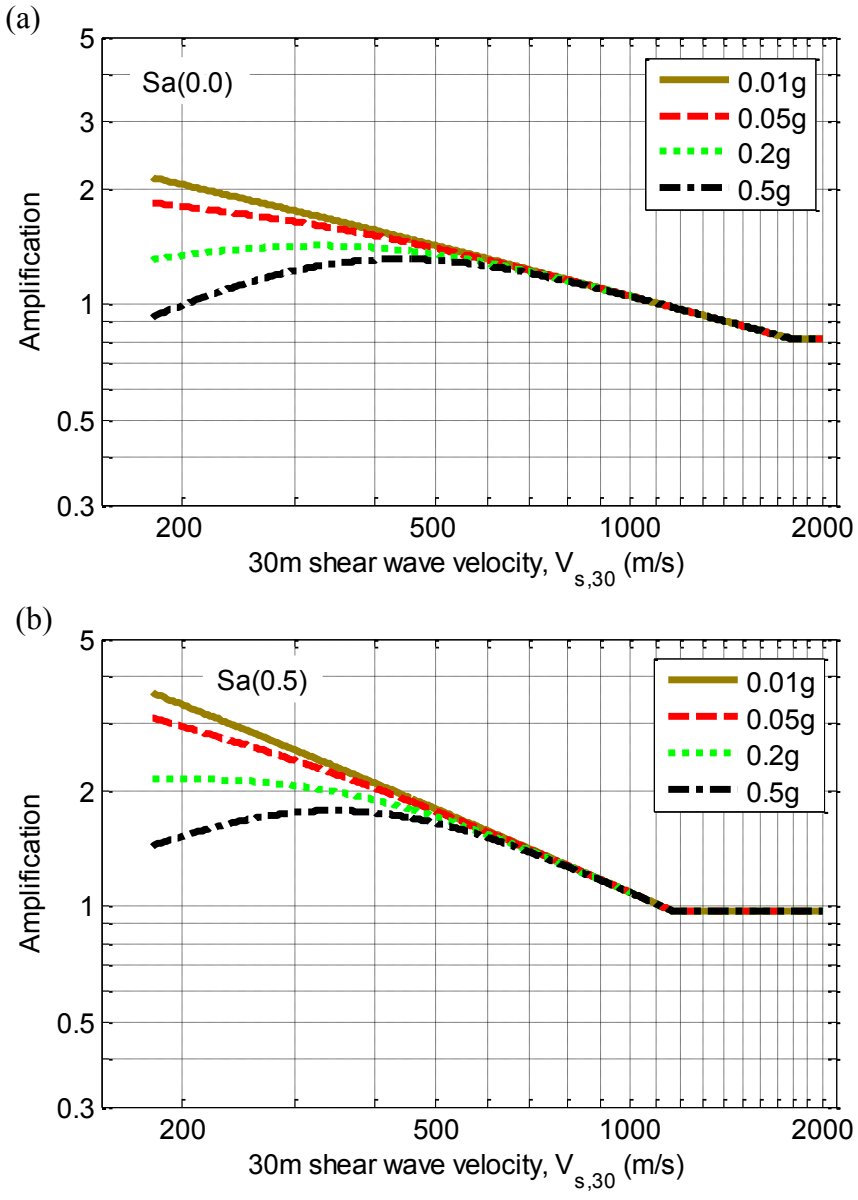

Figure 21: Site response amplification factors in the B10 active shallow crustal model as a function of shear wave velocity and reference spectral amplitude: (a) Sa(0.0); and (b) Sa(0.5). Note in particular the effect of V_1 on the amplification for $V_{s,30} > 1130$ m/s.

Figure 22 illustrates the predicted response spectra of the B10 model for various site classes for two different rupture scenarios. Generally, it can be seen that for softer soil sites (i.e. from site class A to site class C) there is an amplification of long

period spectral amplitudes. On the other hand, the amplification at short periods is dependent on the intensity of ground motion, with amplification in Figure 22a and a de-amplification for several vibration periods in Figure 22b.

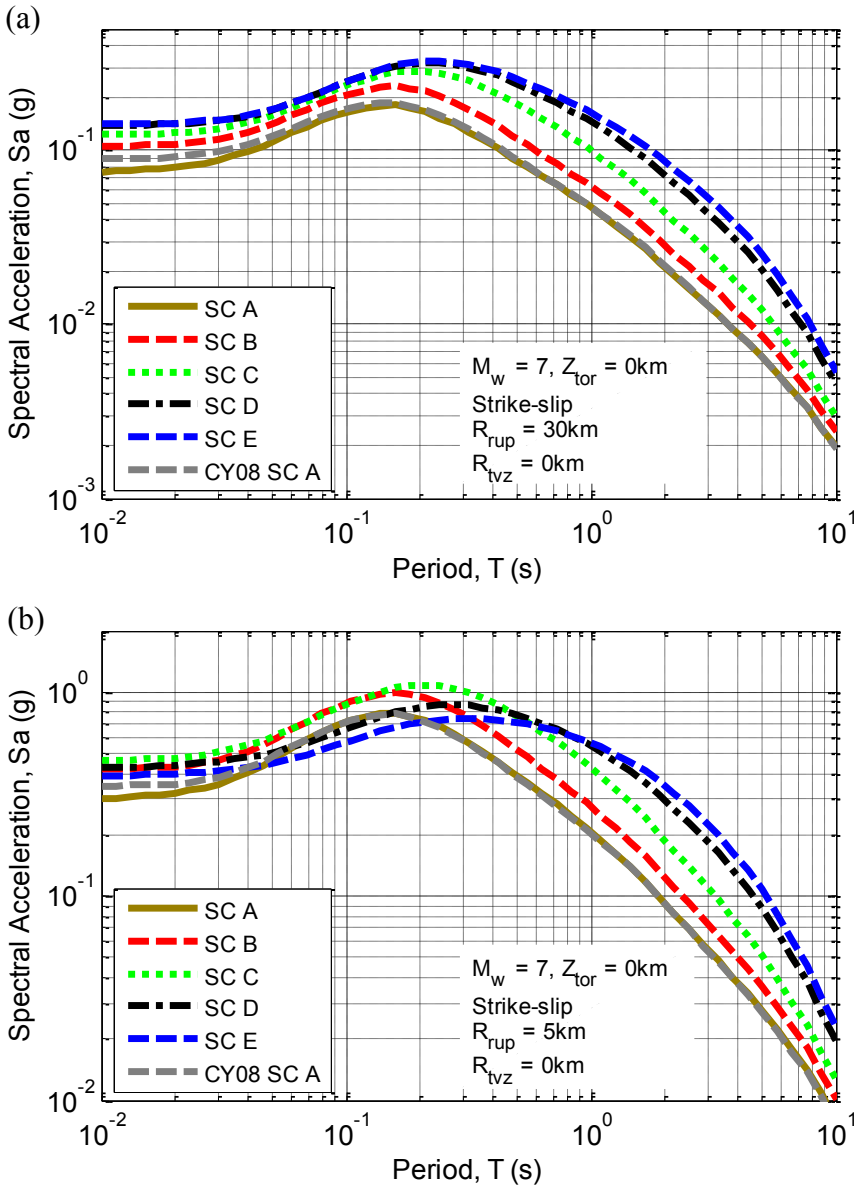

Figure 22: Effect of site class on the predicted response spectra for a M_w 7 event at distances of: (a) 30km; and (b) 5 km.

5.2.4. Modification of anelastic attenuation

The observed bias in short period residuals at large distances for the CY08 and C10 models (i.e. Figure 14 and Figure 15), can be attributed to both the differences in the anelastic attenuation of the NZ and western US crust (for which the CY08/C10 model was developed), and also the influence of the increased anelastic attenuation in the TVZ. In order to avoid this correlation of physical mechanisms which is inherent in some of the NZ database, only those motions for which the TVZ distance was zero were considered in determining the 'general' anelastic attenuation coefficients.

The same functional form for anelastic attenuation used by C10 is adopted here, in which the anelastic attenuation is a function of both period and source magnitude:

$$lny \propto \left\{ c_{\gamma 1} + \frac{c_{\gamma 2}}{cosh\left[max\left(\boldsymbol{M} - c_{\gamma 3}, 0\right)\right]} \right\} R_{RUP} \tag{9}$$

where $c_{\gamma 1}$, $c_{\gamma 2}$, and $c_{\gamma 3}$ are the empirical parameters. Based on exploratory analysis of the NZ database, and the desire to only modify empirical parameters where the NZ database suggests statistically significant biases exist it was found that only parameters $c_{\gamma 1}$ and $c_{\gamma 2}$ required modification.

Figure 23 illustrates the final anelastic attenuation coefficients of the B10 model as a function of vibration period for two different magnitudes. It can be seen that the anelastic attenuation for all periods is larger than the corresponding C10 model which is consistent with the negative residuals observed from the NZ database at large distances (e.g. Figure 15). For comparison the anelastic attenuation from the McV06 and Z06 model are also shown, as is the anelastic attenuation for the TVZ (discussed subsequently). It is noted that the anelastic attenuation as a function of period in the Z06 model is relatively similar to that C10, despite not being a smooth function of vibration period. The McV06 model on the other hand has an anelastic attenuation coefficient which has significantly less period dependence than that for the C10, Z06 or B10 model developed here.

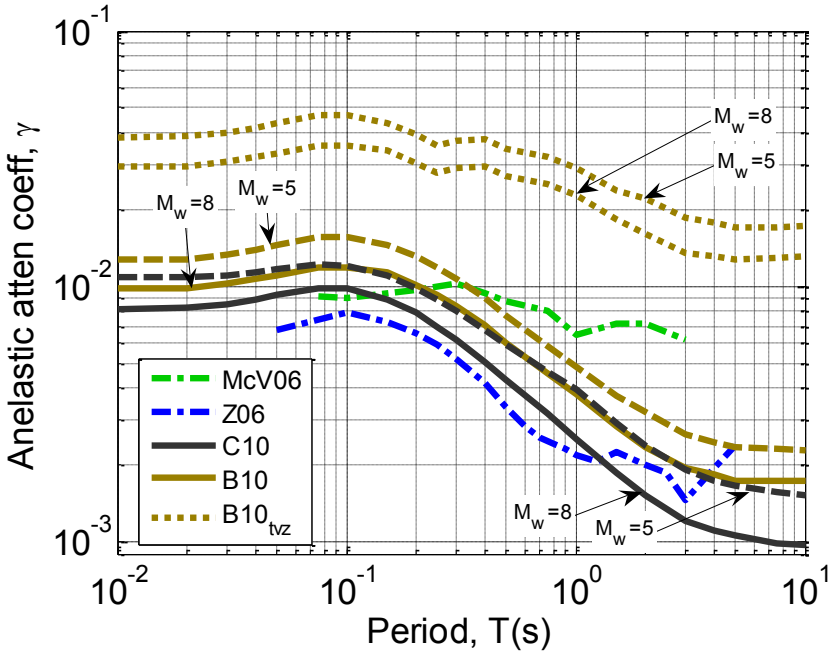

Figure 23: Anelastic attenuation for the B10 active shallow crustal model and comparison with the other candidate GMPEs considered here.

Figure 24 illustrates the effect of the larger anelastic attenuation in the B10 model as compared with the CY08 and C10 models. It can be seen that the influence of this difference in anelastic attenuation is only significant for source-to-site distances of 100 km or greater.

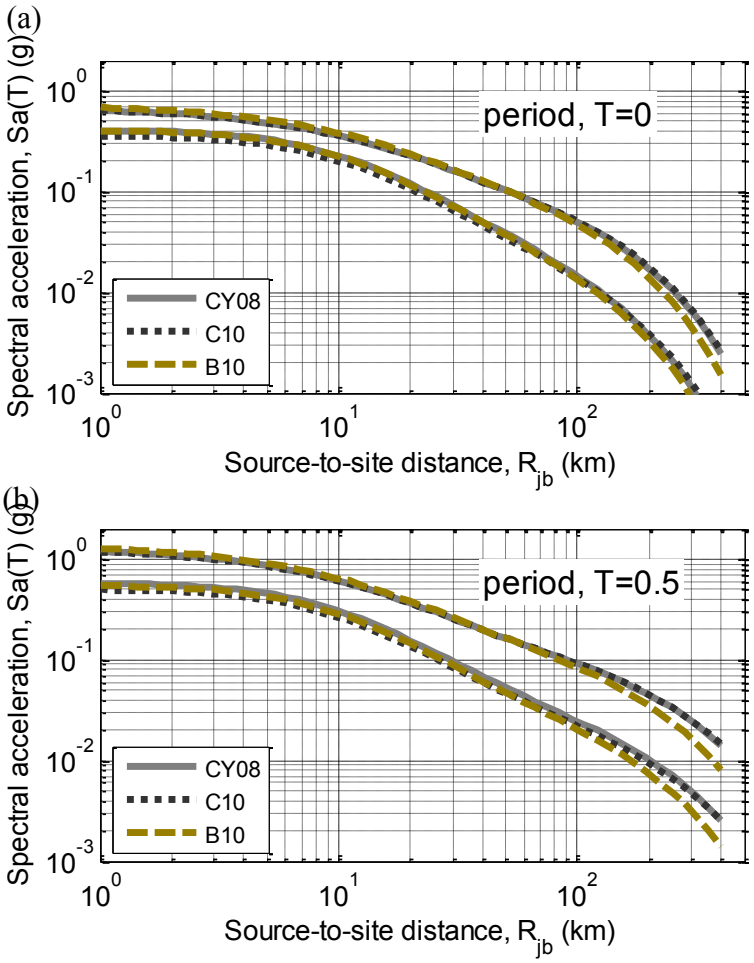

Figure 24: Illustration of the effect of anelastic attenuation in the B10 active shallow crustal model compared with the CY08 and C10 models.

5.2.5. Consideration of TVZ path distance

Finally, once all of the other modifications of the base model had been made, those ground motions for which some portion of the path distance was through the TVZ were used to determine how to include TVZ attenuation in the developed model. In order to determine the functional form for the TVZ attenuation previous studies which have considered heterogeneous anelastic attenuation were examined. As previously mentioned, the McV06 model considers TVZ-specific anelastic attenuation, which combined with the 'general' anelastic attenuation gives the following anelastic attenuation model (McVerry et al. 2006):

$$lny \propto C_5 r + C_{46} r_{vol} \;\Rightarrow\; lny \propto C_5 r \left[1 + \frac{C_{46}}{C_5}\frac{r_{vol}}{r}\right] \qquad (10)$$

where r and r_{vol} are the total and volcanic path distances, and C_5 and C_{46} are the coefficients for 'general' and TVZ-specific anelastic attenuation, respectively. The right-hand expression illustrates how this relationship can be re-expressed as a function of the normalised volcanic path distance, r_{vol}/r. In a similar vein, Dhakal *et al*. (2010) developed prediction equations for pseudo-spectral velocity accounting for the heterogeneous structure of the fore-arc and back-arc regions using Northern Japanese recordings. There model had the following anelastic attenuation term (Dhakal et al. 2010):

$$lny \propto b_1 r_1 + b_2 r_2 \;\Rightarrow\; lny \propto b_1 r \left[1 + \left(\frac{b_2}{b_1} - 1\right)\frac{r_2}{r}\right] \tag{11}$$

where r_1 and r_2 are the fore-arc and back-arc source-to-site distances, respectively (so $r = r_1 + r_2$ is the total source-to-site distance), and b_1 and b_2 are the anelastic attenuation coefficients for the fore-arc and back-arc regions, respectively. Similar to Equation (10), the right-hand side of Equation (11) illustrates how this relationship can be re-expressed as a function of the normalised back-arc path distance (the back-arc anelastic attenuation is larger than in the fore-arc, similar to the TVZ and 'general' anelastic attenuation in NZ).

Hence for both Equations (10) and (11) the anelastic attenuation can be expressed as the 'general' anelastic attenuation multiplied by a factor which contains the normalised volcanic path distance and the ratio of the TVZ to 'general' anelastic attenuation. Hence, the functional form of the anelastic attenuation including TVZ attenuation in the B10 active shallow crustal model is:

$$lny \propto \left\{c_{\gamma 1} + \frac{c_{\gamma 2}}{cosh\left[max\left(\boldsymbol{M} - c_{\gamma 3}, 0\right)\right]}\right\}\left(1 + c_{TVZ}\frac{R_{TVZ}}{R_{RUP}}\right)R_{RUP} \tag{12}$$

where $R_{TVZ_{ij}}$ is the path distance through the TVZ, and c_{TVZ} is an empirical coefficient representing the ratio of the TVZ to 'general' anelastic attenuation.

Figure 23 illustrates the TVZ anelastic attenuation as a function of period for the B10 model (equal to the 'general' anelastic attenuation multiplied by c_{TVZ}). It can be seen that the TVZ anelastic attenuation is notably larger than that for the remainder of the NZ crust, with c_{TVZ} having a values ranging from 2.0 at $T = 0.1$s to 6.3 at $T = 5$s. Figure 25a and Figure 25b demonstrate the effect of TVZ anelastic attenuation for Sa(0.0) and Sa(2.0). Both the B10 and McV06 models are shown for three different values for the normalized TVZ path distance, $R_{TVZ}/R_{RUP} = 0$, 0.5 and 1.0. It can be seen that for both short and long periods the influence of TVZ attenuation is significant. Comparison of the B10 and McV06 models demonstrates that the scaling with normalised TVZ path distance is relatively similar for both models, with the TVZ anelastic attenuation in the B10 model being slightly less than the McV06 model.

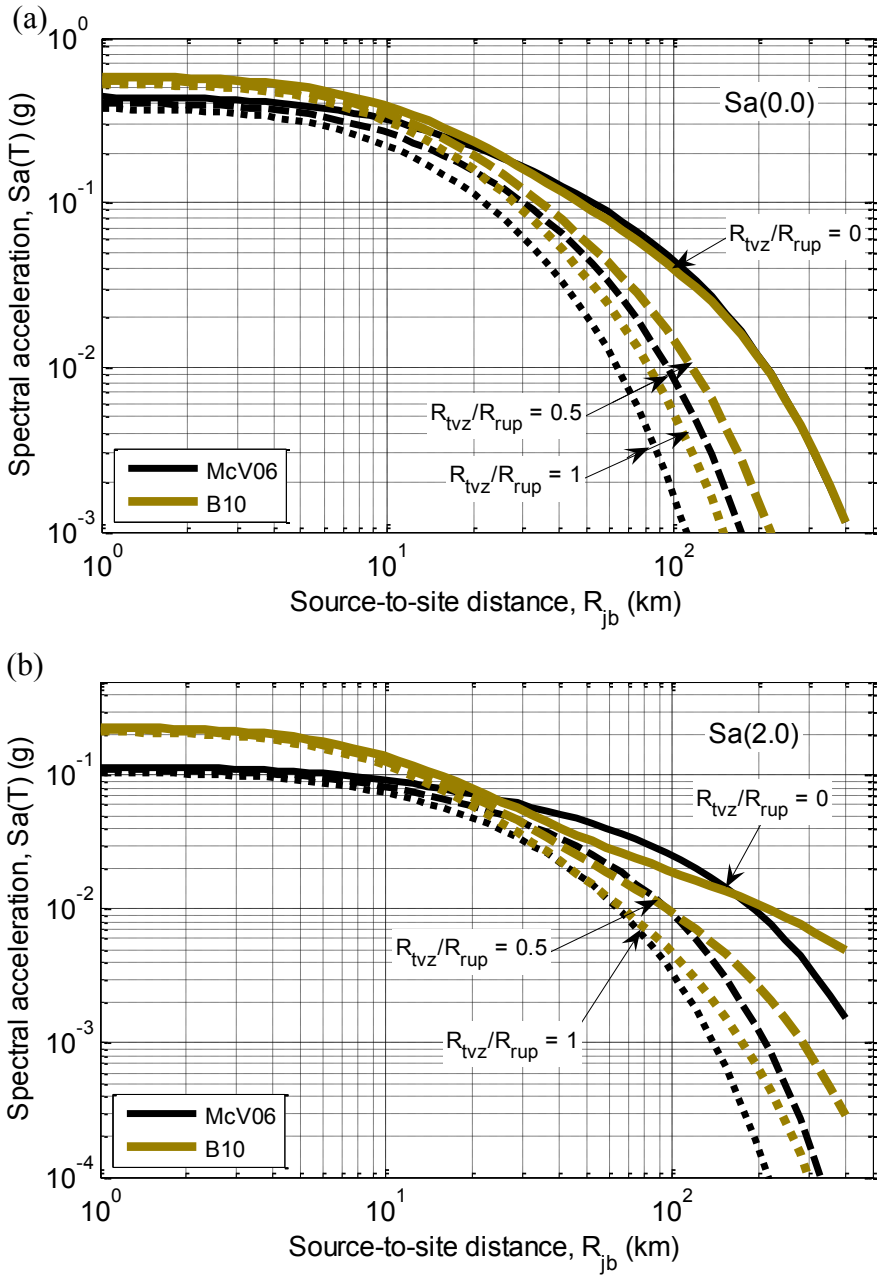

Figure 25: Illustration of the increased anelastic attenuation in the TVZ region using the B10 and McV06 models.

The anelastic attenuation coefficients shown in Figure 23 can be related to the seismological quality factor, Q_s, by:

$$Q_s = \frac{\pi f}{\gamma \beta_s} \tag{13}$$

where γ is the anelastic attenuation coefficient; f is frequency; and β_s is the shear wave velocity of the crust. Hence, based on a linear fit of the anelastic attenuation coefficient as a function of frequency (in log-log space) over the period range 0.1-2 seconds (i.e. f = 0.5-10 Hz), the quality factor for the NZ crust and the TVZ region can be determined. The obtained expressions are:

$$Q_s{}^{NZ} = 180 f^{0.45} \quad ; \quad Q_s{}^{NZ,TVZ} = 36 f^{0.67} \tag{14}$$

Figure 26 illustrates the obtained functional relationships for Q_s v.s. frequency compared with those obtained for Western and Eastern North America (Campbell 2003), and the fore-arc and back-arc regions in Japan (Dhakal et al. 2010). It can be seen that the quality factor for the active shallow regions of WNA and NZ is very similar (as can also be seen from Figure 23). The stable shallow crustal ENA region has a higher quality factor (lower anelastic attenuation), while the fore-arc and back-arc regions in Japan have higher and lower quality factors (i.e. lower and higher anelastic attenuation) than NZ and WNA. Finally it can be seen that the TVZ has a lower quality factor (i.e. higher anelastic attenuation) than all of these other regions.

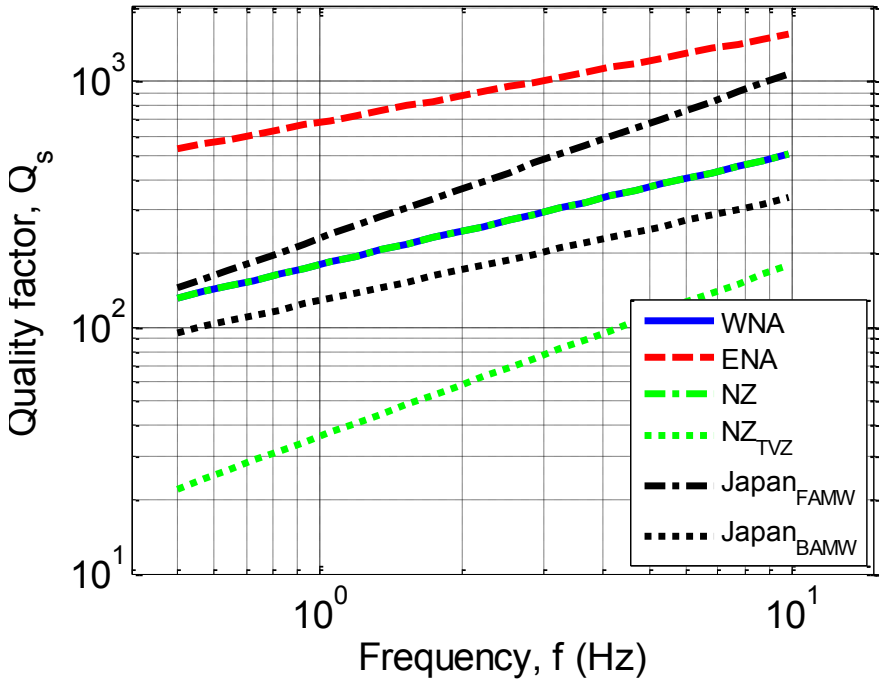

Figure 26: Obtained values of Q_s for NZ and the TVZ crust compared with those obtained for Western and Eastern North America and the fore-arc and back-arc regions in Japan.

5.2.6. Other modifications

In addition to the aforementioned modifications to the CY08 model to develop the NZ-specific B10 active shallow crustal model, several other changes are worthy of note. CY08, and the B10 model developed here, both consider the depth to the top of the fault rupture plane, Z_{TOR}, as an important parameter in characteristing spectral amplitudes at short periods. The linear scaling of spectral amplitudes with Z_{TOR} in the CY08 model was based on the observed residuals of the ground motion database used, which contained no events with depths greater than 15 km (and only 10 events out of 125 with depths greater than 10 km) (Chiou and Youngs 2008). The NZ database, on the other hand, contains events with depths up to 32 km, and in particular six events with depths greater than 20 km. When developing the B10 model based on modifying the CY08 model it was found that the linear scaling of spectral amplitudes with Z_{TOR} produced over-estimates of these 'deeper' events (observed as systematically negative inter-event residuals). In order to account for this an additional parameter, c_8, was introduced to bound the maximum value of Z_{TOR} considered in the model. The value of c_8 was found to be vibration period dependent with values ranging from 10 km at short periods to 20 km at longer periods. Further

research is needed to examine this 'depth-saturation' in detail.

The examination of, and discussion around, the inter- and intra-event residuals has to date focused on the biases in the mean value of these residuals. It is however recognized that the standard deviation of the residuals is of equal importance in understanding the applicability of a GMPE. The applicability of the CY08 standard deviation formulation was also examined and is presented in a subsequent section. It was found that the inter- and intra-event residuals obtained from the B10 model using the NZ database do not systematically reject the hypothesis that the CY08 standard deviation model is correct, and therefore it was adopted for the B10 model.

In addition to considering pseudo-spectral amplitudes from mainshock earthquakes the CY08 model considers aftershock earthquakes and also the intensity measure, peak ground velocity (PGV). The examination of the applicability of the CY08 PGV GMPE is beyond the scope of this work and is not discussed further. Aftershock ground motions are also not included in the present work, because of the limited number of NZ events against which to test the difference between mainshock and aftershock ground motions predicted in the CY08 model. It is also noted that one of the main reasons that the CY08 model considered aftershock ground motions was to provide additional constraint for their site response model (Chiou and Youngs 2006).

5.3. Functional form and parameters of the Bradley (2010) active shallow crustal model

The developed, NZ-specific, Bradley (2010), (B10) active shallow crustal model is based on the CY08 and C10 models with the aforementioned modifications. The complete B10 active shallow crustal median model formulation is given by:

$$\begin{aligned} ln(y_{ref}) = {} & c_1 + [c_{1a}F_{RV} + c_{1b}F_{NM} + c_7(min\{Z_{TOR}, c_8\} - 4)] \\ & + c_2(\boldsymbol{M} - 6) + \frac{c_2 - c_3}{c_n} ln\left(1 + e^{c_n(c_M - \boldsymbol{M})}\right) \\ & + c_4 ln[R_{RUP} + c_5 cosh\{c_6 max(\boldsymbol{M} - c_{HM}, 0)\}] \\ & + (c_{4a} - c_4) ln\left(\sqrt{R_{RUP}^2 + c_{RB}^2}\right) \\ & + \left\{c_{\gamma 1} + \frac{c_{\gamma 2}}{cosh\left[max\left(\boldsymbol{M} - c_{\gamma 3}, 0\right)\right]}\right\}\left(1 + c_{TVZ}\frac{R_{TVZ}}{R_{RUP}}\right)R_{RUP} \\ & + c_9 F_{HW} tanh\left(\frac{R_X cos^2\delta}{c_{9a}}\right)\left\{1 - \frac{\sqrt{R_{JB}^2 + Z_{TOR}^2}}{R_{RUP} + 0.001}\right\} \end{aligned} \quad (15)$$

and

$$\begin{aligned} ln(y) = {} & ln\left(y_{ref}\right) + \phi_1 log\left(\frac{min(V_{s30}, V_1)}{1130}\right) + b.ln\left(\frac{y_{ref} + \phi_4}{\phi_4}\right) \\ & + \phi_5\left(1 - \frac{1}{cosh[\phi_6 max(0, Z_{1.0} - \phi_7)]}\right) + \frac{\phi_8}{cosh[0.15.max(0, Z_{1.0} - 15)]} \end{aligned} \quad (16)$$

where

$$V_1 = min\left(1130.max\left\{\left(\frac{T}{0.75}\right)^{-0.11}, 1\right\}, 1800\right) \quad (17)$$

$$b = \phi_2\left\{e^{\phi_3(min(V_{s30},1130)-360)} - e^{\phi_3(1130-360)}\right\} \quad (18)$$

The predictor variables are:

$\boldsymbol{M}$	Moment magnitude
R_{RUP}	Closest distance to the fault rupture plane (km)
R_{JB}	Joyner-Boore distance to the fault rupture plane (km)
R_X	Distance (km) from the surface projection of the updip edge of the fault plane, measured perpendicular to the fault strike (positive in the downdip direction).
R_{TVZ}	Distance of wave propagation through the Taupo Volcanic Zone (TVZ) (km)
F_{HW}	Hanging wall flag: 1 for $R_X \geq 0$ and 0 for $R_X < 0$
δ	Fault dip angle
Z_{TOR}	Depth to top of the fault rupture plane.
F_{RV}	Reverse faulting flag: 1 for rake angles $30^0 \leq \lambda \leq 150^0$; 0 otherwise
F_{NM}	Normal faulting flag: 1 for rake angles $-120^0 \leq \lambda \leq -60^0$; 0 otherwise
V_{s30}	Average shear wave velocity for the top 30m of the site (m/s)
$Z_{1.0}$	Depth to shear wave velocity of 1.0 km/s (m)

The period-independent parameters for the B10 active shallow crustal median model are given in Table 5, while the period-dependent parameters are given in Table 6 and Table 7. It is worthy of note that only parameters c_1, c_{1b}, c_3, c_M, c_8, $c_{\gamma 1}$, $c_{\gamma 2}$ and c_{TVZ} in the B10 model differ from those in the CY08 model.

Table 5: Period-independent coefficients for the reference model, $\boldsymbol{ln(y_{ref})}$ (Equation (15))

c_2	c_4	c_{4a}	c_{RB}	c_{HM}	$c_{\gamma 3}$
1.06	-2.1	-0.5	50	3	4

Table 6: Period-dependent coefficients for the reference model, $ln(y_{ref})$ (Equation (15))[1]

Vibration Period (s)	c_1	c_{1a}	c_{1b}	c_3	c_n	c_M	c_5	c_6	c_7	c_8	c_9	c_{9a}	$c_{\gamma 1}$	$c_{\gamma 2}$	c_{TVZ}
pga	-1.1985	0.1	-0.455	1.50000	2.996	5.85	6.16	0.4893	0.0512	10.0	0.79	1.5005	-0.0096	-0.0048	2.0
0.01	-1.1958	0.1	-0.455	1.50299	2.996	5.81711	6.16	0.4893	0.0512	10.0	0.79	1.5005	-0.0096	-0.00481	2.0
0.02	-1.1756	0.1	-0.455	1.50845	3.292	5.80023	6.158	0.4892	0.0512	10.0	0.8129	1.5028	-0.0097	-0.00486	2.0
0.03	-1.0909	0.1	-0.455	1.51549	3.514	5.78659	6.155	0.489	0.0511	10.0	0.8439	1.5071	-0.0101	-0.00503	2.0
0.04	-0.9793	0.1	-0.455	1.52380	3.563	5.77472	6.1508	0.4888	0.0508	10.0	0.874	1.5138	-0.0105	-0.00526	2.0
0.05	-0.8549	0.1	-0.455	1.53319	3.547	5.76402	6.1441	0.4884	0.0504	10.0	0.8996	1.523	-0.0109	-0.00549	2.0
0.075	-0.6008	0.1	-0.454	1.56053	3.448	5.74056	6.12	0.4872	0.0495	10.0	0.9442	1.5597	-0.0117	-0.00588	2.0
0.1	-0.47	0.1	-0.453	1.59241	3.312	5.72017	6.085	0.4854	0.0489	10.0	0.9677	1.6104	-0.0117	-0.00591	2.0
0.15	-0.4139	0.1	-0.45	1.6664	3.044	5.68493	5.9871	0.4808	0.0479	10.0	0.966	1.7549	-0.0111	-0.0054	2.0
0.2	-0.5237	0.1	-0.4149	1.75021	2.831	5.65435	5.8699	0.4755	0.0471	10.0	0.9334	1.9157	-0.01	-0.00479	2.0
0.25	-0.6678	0.1	-0.3582	1.84052	2.658	5.62686	5.7547	0.4706	0.0464	10.5	0.8946	2.0709	-0.0091	-0.00427	2.0
0.3	-0.8277	0.0999	-0.3113	1.9348	2.505	5.60162	5.6527	0.4665	0.0458	11.0	0.859	2.2005	-0.0082	-0.00384	2.5
0.4	-1.1284	0.0997	-0.2646	2.12764	2.261	5.55602	5.4997	0.4607	0.0445	12.0	0.8019	2.3886	-0.0069	-0.00317	3.2
0.5	-1.3926	0.0991	-0.2272	2.31684	2.087	5.51513	5.4029	0.4571	0.0429	13.0	0.7578	2.5	-0.0059	-0.00272	3.5
0.75	-1.8664	0.0936	-0.162	2.73064	1.812	5.38632	5.29	0.4531	0.0387	14.0	0.6788	2.6224	-0.0045	-0.00209	4.5
1.0	-2.1935	0.0766	-0.14	3.03000	1.648	5.31	5.248	0.4517	0.035	15.0	0.6196	2.669	-0.0037	-0.00175	5.0
1.5	-2.6883	0.0022	-0.1184	3.43384	1.511	5.29995	5.2194	0.4507	0.028	16.0	0.5101	2.6985	-0.0028	-0.00142	5.4
2.0	-3.104	-0.0591	-0.11	3.67464	1.47	5.3273	5.2099	0.4504	0.0213	18.0	0.3917	2.7085	-0.0023	-0.00143	5.8
3.0	-3.7085	-0.0931	-0.104	3.64933	1.456	5.4385	5.204	0.4501	0.0106	19.0	0.1244	2.7145	-0.0019	-0.00115	6.0
4.0	-4.1486	-0.0982	-0.102	3.60999	1.465	5.5977	5.202	0.4501	0.0041	19.75	0.0086	2.7164	-0.0018	-0.00104	6.15
5.0	-4.4881	-0.0994	-0.101	3.50	1.478	5.7276	5.201	0.45	0.001	20.0	0.0	2.7172	-0.0017	-0.00099	6.3
7.5	-5.0891	-0.0999	-0.101	3.45	1.498	5.9891	5.2	0.45	0.0	20.0	0.0	2.7177	-0.0017	-0.00094	6.425
10.0	-5.553	-0.1	-0.1	3.45	1.502	6.193	5.2	0.45	0.0	20.0	0.0	2.718	-0.0017	-0.00091	6.55

[1]The units for *pga* and *psa* are g's.

Table 7: Period-dependent coefficients for the site response model, $ln(y)$ (Equation (16))

Vibration Period (s)	ϕ_1	ϕ_2	ϕ_3	ϕ_4	ϕ_5	ϕ_6	ϕ_7	ϕ_8
pga	-0.4417	-0.1417	-0.007010	0.102151	0.2289	0.014996	580.0	0.0700
0.01	-0.4417	-0.1417	-0.007010	0.102151	0.2289	0.014996	580.0	0.0700
0.02	-0.434	-0.1364	-0.007279	0.108360	0.2289	0.014996	580.0	0.0699
0.03	-0.4177	-0.1403	-0.007354	0.119888	0.2289	0.014996	580.0	0.0701
0.04	-0.4000	-0.1591	-0.006977	0.133641	0.2289	0.014996	579.9	0.0702
0.05	-0.3903	-0.1862	-0.006467	0.148927	0.229	0.014996	579.9	0.0701
0.075	-0.404	-0.2538	-0.005734	0.190596	0.2292	0.014996	579.6	0.0686
0.1	-0.4423	-0.2943	-0.005604	0.230662	0.2297	0.014996	579.2	0.0646
0.15	-0.5162	-0.3113	-0.005845	0.266468	0.2326	0.014988	577.2	0.0494
0.2	-0.5697	-0.2927	-0.006141	0.255253	0.2386	0.014964	573.9	-0.0019
0.25	-0.6109	-0.2662	-0.006439	0.231541	0.2497	0.014881	568.5	-0.0479
0.3	-0.6444	-0.2405	-0.006704	0.207277	0.2674	0.014639	560.5	-0.0756
0.4	-0.6931	-0.1975	-0.007125	0.165464	0.312	0.013493	540.0	-0.0960
0.5	-0.7246	-0.1633	-0.007435	0.133828	0.361	0.011133	512.9	-0.0998
0.75	-0.7708	-0.1028	-0.008120	0.085153	0.4353	0.006739	441.9	-0.0765
1.0	-0.7990	-0.0699	-0.008444	0.058595	0.4629	0.005749	391.8	-0.0412
1.5	-0.8382	-0.0425	-0.007707	0.031787	0.4756	0.005544	348.1	0.0140
2.0	-0.8663	-0.0302	-0.004792	0.019716	0.4785	0.005521	332.5	0.0544
3.0	-0.9032	-0.0129	-0.001828	0.009643	0.4796	0.005517	324.1	0.1232
4.0	-0.9231	-0.0016	-0.001523	0.005379	0.4799	0.005517	321.7	0.1859
5.0	-0.9222	0.0000	-0.001440	0.003223	0.4799	0.005517	320.9	0.2295
7.5	-0.8346	0.0000	-0.001369	0.001134	0.4800	0.005517	320.3	0.2660
10.0	-0.7332	0.0000	-0.001361	0.000515	0.4800	0.005517	320.1	0.2682

The inter-event, τ, intra-event, σ, and total, σ_T, standard deviation models are given by:

$$\tau = \tau_1 + \frac{\tau_2 - \tau_1}{2}[min\{max(\boldsymbol{M}, 5), 7\} - 5] \tag{19}$$

$$\sigma = \left[\sigma_1 + \frac{\sigma_2 - \sigma_1}{2}(min\{max(\boldsymbol{M}, 5), 7\} - 5)\right] \times \sqrt{\sigma_3(1 - F_{measured}) + 0.7F_{measured} + (1 + NL_0)^2} \tag{20}$$

$$\sigma_T = \sqrt{(1 + NL_0)^2\tau^2 + \sigma^2} \tag{21}$$

with

$$NL_0 = \left(b\frac{y_{ref}}{y_{ref} + \phi_4}\right) \tag{22}$$

where $F_{measured}$ is 1 if V_{s30} is measured directly, and 0 if inferred from geology. The parameters for the standard deviation model are given in Table 8. As the adopted standard deviation model in B10 active shallow crustal model is identical to that of CY08 (because the observed residuals to follow do not suggest otherwise), further details regarding the mathematically basis of this formulation can be found in Chiou and Youngs (2008).

Table 8: Period-dependent coefficients for the standard deviation model (Equations (19)-(21))

Vibration Period (s)	τ_1	τ_2	σ_1	σ_2	σ_3
pga	0.3437	0.2637	0.4458	0.3459	0.8000
0.01	0.3437	0.2637	0.4458	0.3459	0.8000
0.02	0.3471	0.2671	0.4458	0.3459	0.8000
0.03	0.3603	0.2803	0.4535	0.3537	0.8000
0.04	0.3718	0.2918	0.4589	0.3592	0.8000
0.05	0.3848	0.3048	0.4630	0.3635	0.8000
0.075	0.3878	0.3129	0.4702	0.3713	0.8000
0.1	0.3835	0.3152	0.4747	0.3769	0.8000
0.15	0.3719	0.3128	0.4798	0.3847	0.8000
0.2	0.3601	0.3076	0.4816	0.3902	0.8000
0.25	0.3522	0.3047	0.4815	0.3946	0.7999
0.3	0.3438	0.3005	0.4801	0.3981	0.7997
0.4	0.3351	0.2984	0.4758	0.4036	0.7988
0.5	0.3353	0.3036	0.4710	0.4079	0.7966
0.75	0.3429	0.3205	0.4621	0.4157	0.7792
1.0	0.3577	0.3419	0.4581	0.4213	0.7504
1.5	0.3769	0.3703	0.4493	0.4213	0.7136
2.0	0.4023	0.4023	0.4459	0.4213	0.7035
3.0	0.4406	0.4406	0.4433	0.4213	0.7006
4.0	0.4784	0.4784	0.4424	0.4213	0.7001
5.0	0.5074	0.5074	0.442	0.4213	0.7000
7.5	0.5328	0.5328	0.4416	0.4213	0.7000
10.0	0.5542	0.5542	0.4414	0.4213	0.7000

5.4. Observed inter- and intra-event residuals of Bradley (2010) active shallow crustal model

This section presents the inter- and intra-event residuals obtained from applying the B10 active shallow crustal model to the NZ database. Similar to previous discussions only the inter- and intra-event residuals for vibration periods of 0.0 and 0.5 are presented here. Results for other vibration periods can be found in the appendix.

Figure 27 illustrates the observed inter- and intra-event residuals for Sa(0.0) from the NZ database using the B10 model. It can be seen that based on the distributions of the inter- and intra-event residuals alone (i.e. Figure 27a and Figure 27b) that the B10 model is unbiased. Examination of the magnitude-dependence of the intra-event residuals also reveals no bias, in contrast to the bias in the CY08 or C10 models (i.e. Figure 14c and Figure 15c), as a result of the small magnitude scaling; normal faulting factor; site class A; and anelastic attenuation scaling modifications previously discussed. That is, the unbiased prediction for the larger magnitude events in the NZ database (compared with the C10 model in Figure 15c) has been obtained without modifying the large magnitude scaling of the B10 model, but via other modifications based on theoretical considerations and utilizing a significantly larger portion of the NZ database. It can also be seen in Figure 27d and Figure 27e that there is no significant bias in the intra-event residuals obtained from the B10 model with either magnitude or path distance.

Figure 27f illustrates that there is no significant bias observed for the inter-event residuals as a function of Z_{TOR}. It is noted that for Sa(0.0) the parameter, c_8, which limits the maximum considered Z_{TOR} value in the model has a value of 10 km (i.e. for

all events with $Z_{TOR} > 10$km, the B10 model essentially uses $Z_{TOR} = 10$ km), and therefore it can be appreciated that given the strong scaling of Sa(0.0) with Z_{TOR} the lack of this c_8 parameter would lead to a significant over-prediction of these 'deep-events'.

Figure 27g illustrates that there is no significant bias of the inter-event residuals as a function of focal mechanism. In particular, the significant over-prediction of normal faulting events by all of the foreign GMPEs considered is not apparent.

Figure 27h illustrates that the inclusion of the normalised TVZ distance in the B10 model leads to no significant dependence on the intra-event residuals as a function of normalised TVZ distance.

Finally, Figure 27i illustrates the observed intra-event residuals as a function of site class. It is noted that despite the modified formulation of the B10 site response model, which affects the prediction of site class A spectral amplitudes, there is still a slight over-prediction of site class A Sa(0.0) amplitudes. However, the mean value of the inter-event residual of approximately -0.4 for the B10 model compared with the mean value of approximately -1.5 for the CY08 and C10 models (i.e. Figure 14i and Figure 15i), indicates that the bias has been notably reduced (as can be seen from Figure 27 the bias is only just statistically significant). Rather than modify the site response model further to remove this observed bias (in what must be remembered is relatively sparse data), it was preferred to retain the theoretical basis of the original CY08 site response model. This observed bias was only statistically significant for short vibration periods (i.e. Sa(0.0) and Sa(0.2)). It can also be seen in Figure 27i that there is a slight over-prediction of Sa(0.0) at site class E sites. This over-prediction was only apparent at short vibration periods (i.e. Sa(0.0) and Sa(0.2)), and as previously mentioned it is argued that for such soft soil sites, site-specific response analysis should be performed.

Figure 28 illustrates the observed inter- and intra-event residuals for Sa(0.5) from the NZ database using the B10 model. Similar to the results for Sa(0.0), it can be seen in Figure 28a and Figure 28b that the inter- and intra-event residuals cannot be rejected as different from the standard normal distribution. It can also be seen that the inter- and intra-event residuals are unbiased with respect to magnitude and path distance (Figure 28c-Figure 28e).

Similar to the results for Sa(0.0), Figure 28f and Figure 28g illustrate that the inter-event residuals obtained using the B10 model show no bias with respect to either source depth (Z_{TOR}) or focal mechanism, respectively. In particular, there is no bias for 'deep' (c_8=13 km for Sa(0.5)), or normal faulting events.

Figure 28h and Figure 28i illustrate that the intra-event residuals are unbiased as a function of both normalised TVZ path distance and site class, respectively. In particular, the biases for site class A and E noted for Sa(0.0) are not evident for Sa(0.5).

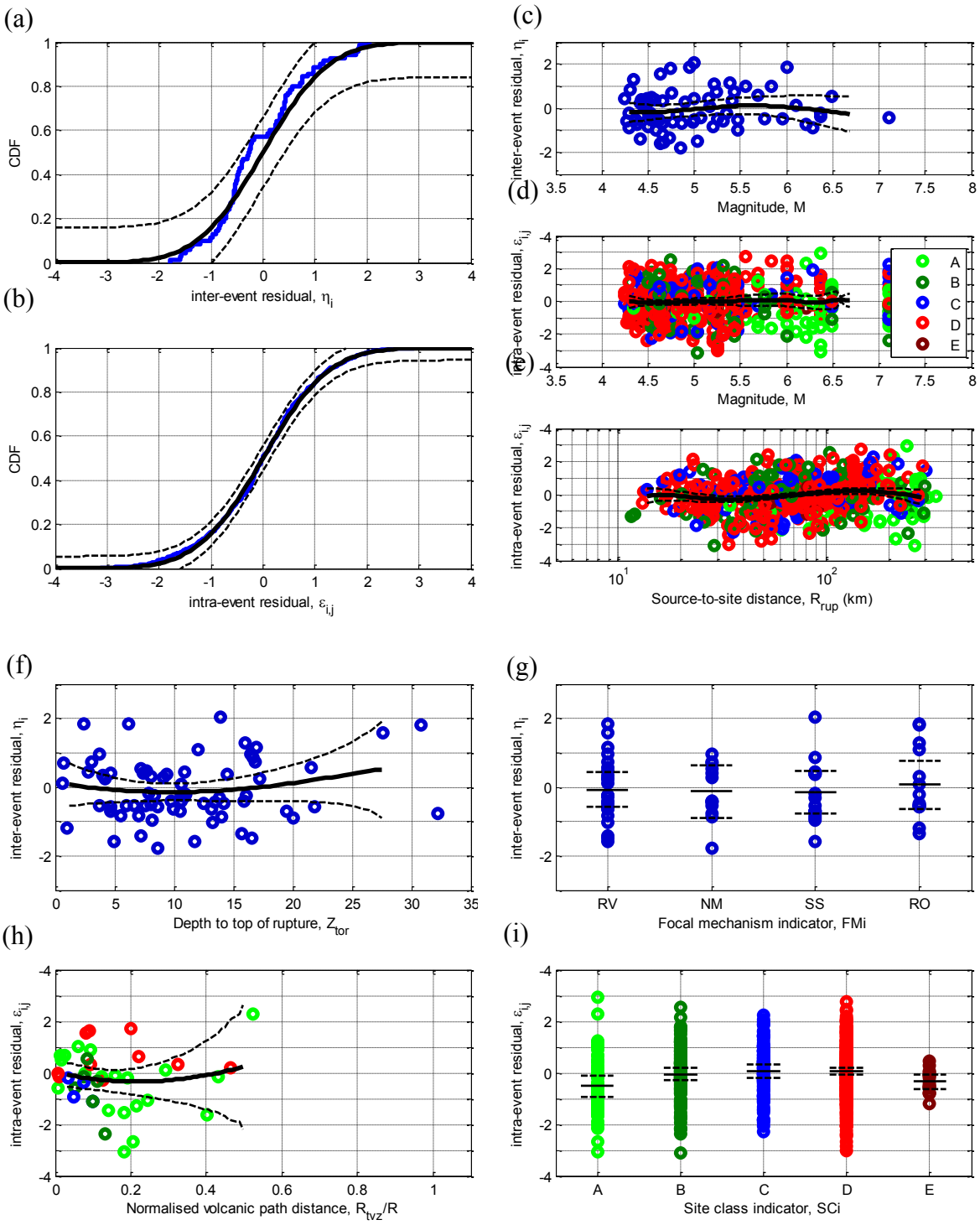

Figure 27: Residuals for Sa(0.0) using the B10 active shallow crustal model: (a)&(b) distribution of inter- and intra-event residuals; (c)&(d) inter- and intra-event residuals as a function of magnitude; (e) intra-event residuals as a function of distance; (f)&(g) inter-event residuals as a function of depth and focal mechanism; (h)&(i) intra-event residuals as a function of normalised volcanic path distance and site class.

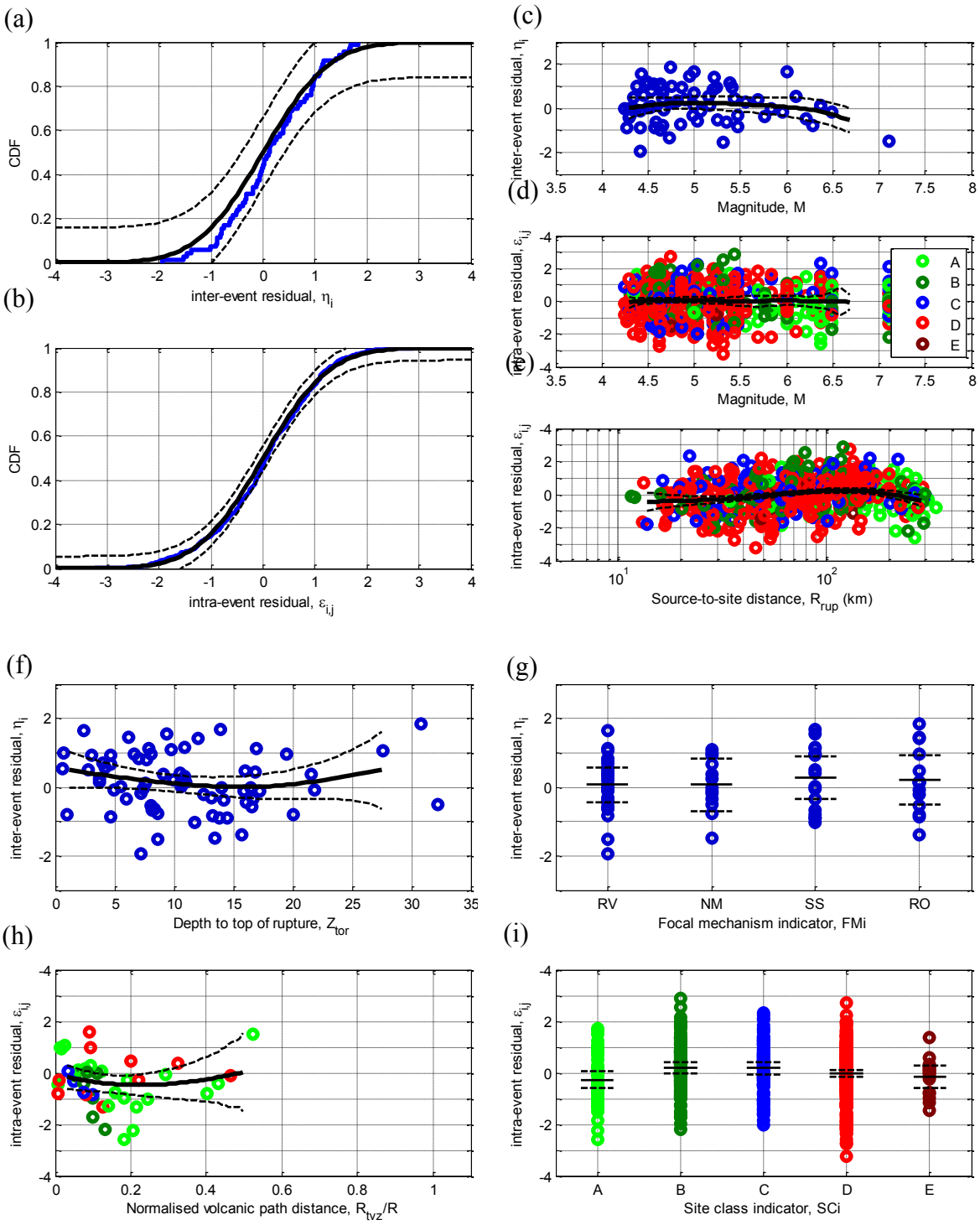

Figure 28: Residuals for Sa(0.5) using the B10 active shallow crustal model: (a)&(b) distribution of inter- and intra-event residuals; (c)&(d) inter- and intra-event residuals as a function of magnitude; (e) intra-event residuals as a function of distance; (f)&(g) inter-event residuals as a function of depth and focal mechanism; (h)&(i) intra-event residuals as a function of normalised volcanic path distance and site class.

5.5. Standard deviation of the inter- and intra-event residuals

The median of a GMPE represents only one aspect of the predicted distribution of spectral amplitudes that such GMPEs provide. The other component of equal importance, but often not treated in such a way, is the standard deviation of the model (which given the lognormal assumption is sufficient to characterise the entire distribution). Therefore, in addition to examining the inter- and intra-event residuals for bias (i.e. that based on the mean), it is also important to examine the precision of the residuals (i.e. that based on the standard deviation).

With the limited number of earthquakes and ground motion recordings in the NZ database it is difficult to make any strong statistically significant statements regarding the standard deviation of the observed residuals. Therefore when examining the results to follow emphasis was given to the identification of systematic trends in the residual standard deviations which were apparent over multiple vibration periods considered. The two key features of the standard deviation model for consideration are: (i) the size of the inter- and intra-event standard deviations; and (ii) the magnitude dependence of the standard deviation of the inter- and intra-event residuals. Both of these are fundamentally important and have a strong influence on any seismic hazard analysis that is conducted using empirical GMPEs (e.g. Musson 2010). Magnitude-dependence of standard deviations, in particular, is still an unresolved issue as indicated by the different homoskedastic and heteroskedastic models developed as part of the NGA project (Abrahamson et al. 2008).

Figure 27a and Figure 27b illustrated that the distribution (i.e. the median and standard deviation) of the normalised inter- and intra-event residuals for Sa(0.0) was not statistically different from the standard normal distribution (Figure 28a and Figure 28b illustrated the same trend for Sa(0.5), and other vibration periods can be found in the appendix). This observation suggests that the size of the inter- and intra-event standard deviations of the B10 model (which adopts the CY08 standard deviation model) is approximately correct. Further insight can however be obtained from examining the standard deviation of the observed residuals as a function of predictor variables such as magnitude. Figure 29 illustrates that the standard deviations of both the inter- and intra-event residuals for Sa(0.0) using the B10 model are not statistically different from (the theoretical value of) one for a range of magnitudes. The effect of the limited size of the NZ database on inferring statistically significant trends in the standard deviation can be clearly seen in Figure 29, particularly for the inter-event residuals. As magnitude dependent (heteroskedastic) standard deviation models generally illustrate a reduction in standard deviation with increasing magnitude (including the B10 model), then it would be expected that if such magnitude dependence is not apparent in the NZ database, there would be a positive trend of increasing standard deviation in the residuals with increasing magnitude. Figure 29a illustrates that while the point estimate of the standard deviation of the intra-event residuals increases with magnitude, that this increase is not statistically significant (as can be seen from the confidence interval always including the theoretical value of 1.0). Furthermore, for the intra-event residuals it can be seen that the point estimate of the standard deviation in fact decreases with increasing magnitude, although again this is not statistically significant.

The standard deviations of the residuals for other vibration periods are presented in the appendix. In summary, for the active shallow crustal events and recordings in the NZ database, there is no evidence to suggest that the size or magnitude dependence of the B10 standard deviation model (i.e. the CY08 standard

deviation model) produces significant imprecision in the estimated inter- and intra-event residuals.

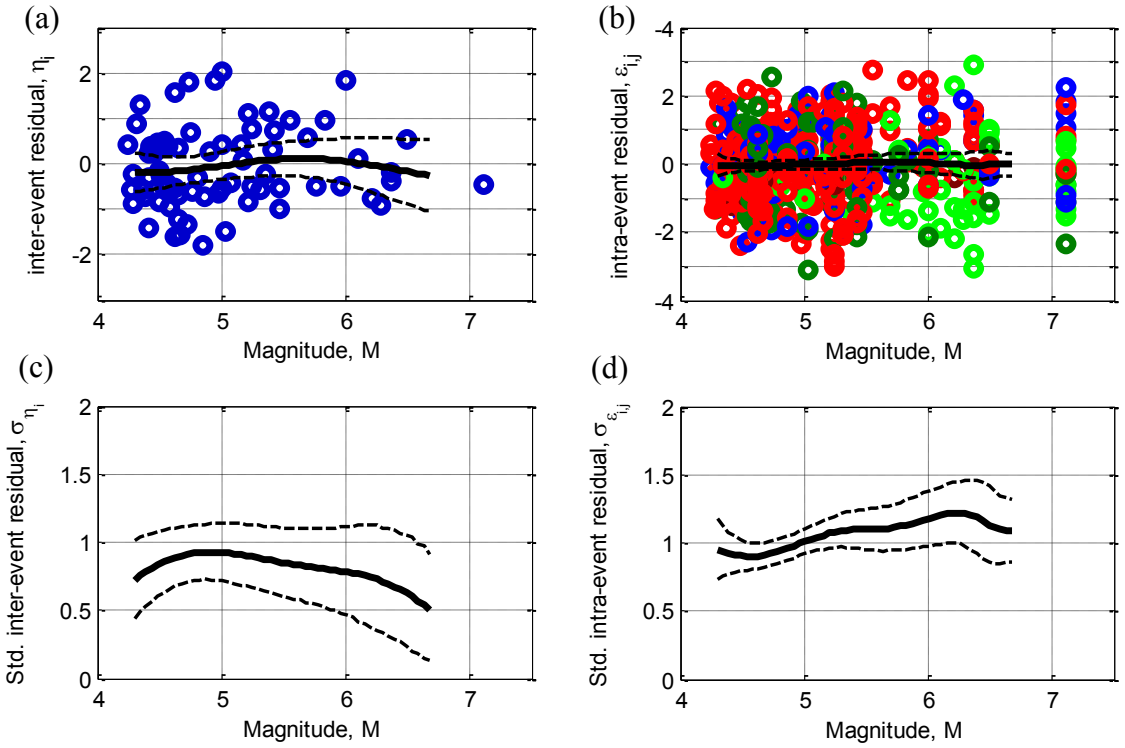

Figure 29: Inter- and intra-event residuals and their standard deviation as a function of magnitude for Sa(0.0) using the B10 active shallow crustal model.

6. APPLICABILITY OF FOREIGN PREDICTION EQUATIONS FOR SUBDUCTION SLAB EARTHQUAKES

6.1. Foreign subduction slab ground motion prediction equations considered

The applicability of three different GMPEs for subduction slab events were examined. Firstly, the McVerry *et al.* (2006) (McV06) was considered, as it represents the present model used for NZ-specific seismic hazard studies when subduction slab events are of importance. Secondly, the Japanese-based model of Zhao *et al.* (2006) (Z06) was considered because of its extensive empirical database, and also because of the similarity of ground motions in Japan and New Zealand noted by previous researchers (Zhao et al. 1997). Finally, the Atkinson and Boore (2003) (AB03) GMPE based on world-wide empirical data was also considered.

6.2. Qualitative comparison of GMPEs considered

Before examining the statistics of the inter- and intra-event residuals of the NZ database using each of the GMPEs considered, it is insightful to examine the scaling of the GMPEs as a function of several predictor variables. As with previous sections of this work, only sufficient results to convey the general predictor variable scaling of each of the models are given here. Additional results for other vibration periods may be found in the appendices.

6.2.1. Magnitude scaling of median

Figure 6 illustrates the magnitude scaling of the median of the three GMPEs considered for both Sa(0.0) (i.e. PGA) and Sa(2.0). It can be seen that all of the GMPEs predict similar Sa(0.0) and Sa(2.0) amplitudes for $M_w = 7.0$, but that the scaling to small and large magnitudes is significantly different. This is primarily a result of the differences in the empirical databases used in the development of each of these models. It can be seen that the McV06 and Z06 models scale similarly to small magnitudes for Sa(0.0), but the gradient for the McV06 model is smaller than the Z06 model for Sa(2.0). On the other hand, the small magnitude scaling of the AB03 model is significantly more pronounced than the other two models for both Sa(0.0) and Sa(2.0). At large magnitudes (i.e. $M_w > 7.5$) the three different models display significantly different scaling. The AB03 model exhibits complete magnitude saturation at $M_w = 8.0$, while the reduction in magnitude scaling for the McV06 is less pronounced. The Z06 model has the most significant scaling at large magnitudes, and in fact, for Sa(0.0) the Z06 model magnitude scaling is concave from above (i.e. the quadratic magnitude term is positive (2006)), leading to median predicted PGA values of approximately 2.0g at $R_{RUP} = 50$km from a $M_w = 8.5$ event.

The discrepancy between the three models at large magnitudes is concerning, given the importance of such events in seismic hazard studies, and the lack of large magnitude events in the NZ database with which the applicability of such large magnitude scaling for NZ can be scrutinized. The Z06 model utilized an empirical database with three subduction slab events above $M_w = 7$. However, these three events were not well-recorded (relative to other events in the Z06 database). Furthermore, the records from such events were recorded at large path distances

which Zhao (2010) has illustrated that the Z06 model over-predicts. Hence, it is concluded that the large magnitude scaling of the Z06 model (particularly the positive magnitude squared dependence at short periods) is inappropriate. As previously mentioned, the McV06 model used a very small empirical database with only 20 subduction slab events and a maximum magnitude of $M_w = 6.69$. The AB03 model used an empirical database with only four events above $M_w = 7$, with the best recorded event contributing 14 records.

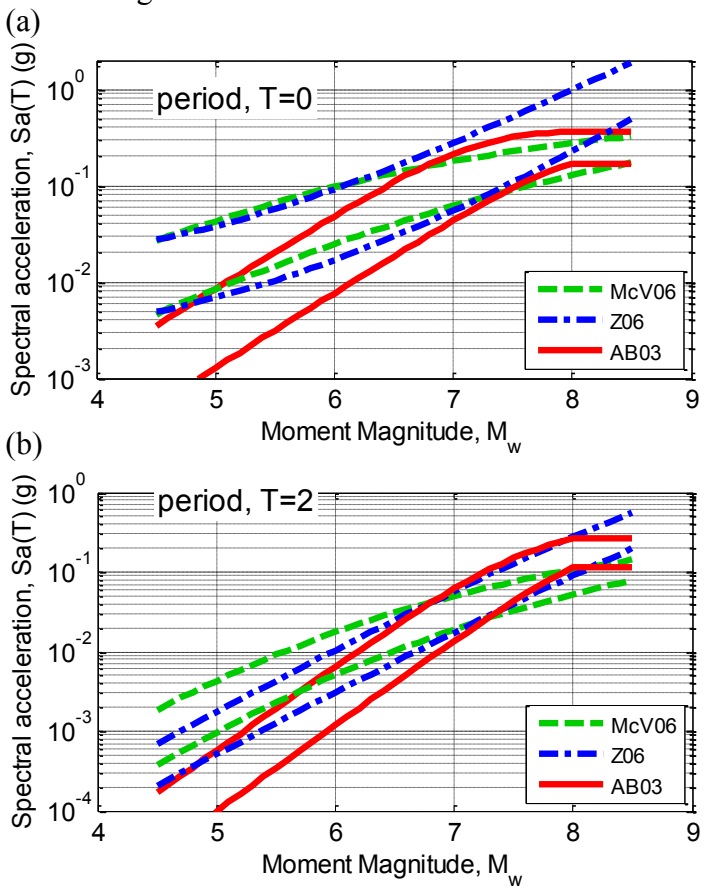

Figure 30: Magnitude scaling of the considered subduction slab GMPEs for two source-to-site distances of 50 and 120 km: (a) Sa(0.0); and (b) Sa(2.0) (predictions for site class C and 40km focal depth).

6.2.2. Path scaling of median

Figure 31 illustrates the path scaling of the median of the three subduction slab GMPEs considered for both Sa(0.0) and Sa(2.0). In general, the path scaling of GMPEs can be separated into: (i) near-source scaling considering the finite dimension of the fault source; (ii) geometric spreading at moderate to large distances; and (iii) anelastic attenuation at large distances. The different functional forms adopted for each of these three aspects of path scaling for the considered models are discussed below.

Figure 31a illustrates that the McV06 model exhibits the most pronounced near-source saturation, followed by the AB03 model and then the Z06 model. The lack of near-source saturation for the Z06 model coupled with the aforementioned pronounced large magnitude scaling leads to very large ground motions at near source distances (e.g. from Figure 31a a median PGA of 0.8g at 40km from a M_w = 7.5 event).

The path scaling of the three different models at moderate to large distances (i.e. beyond where finite fault effects are significant), are relatively similar, but have varying values for the geometric spreading coefficient. The McV06 model has a geometric spreading coefficient ranging from approximately -2.5 at short periods to -2.0 at long periods. The Z06 model has an effective geometric spreading coefficient which ranges from -1.5 at short periods to -1.1 at long periods. Finally, the AB03 model has a geometric spreading coefficient which is independent of vibration period, but very weakly dependent on magnitude and has a value of -1.7 for M_w = 7.

At long distances, both the Z06 and the AB03 model include an anelastic attenuation term, but the McV06 model does not (although an anelastic attenuation term for TVZ attenuation is considered). This absence of anelastic attenuation in the McV06 model is clearly evident in the lack of reduction in Sa(0.0) amplitudes at large distances in Figure 31a. The magnitude of anelastic attenuation coefficient in the AB03 model, which ranges from 0.002 at short periods to 0.00045 at long periods is notably lower than the Z06 model (similar to the B10 crustal model) values of 0.0056 at short periods to 0.0015 at long periods.

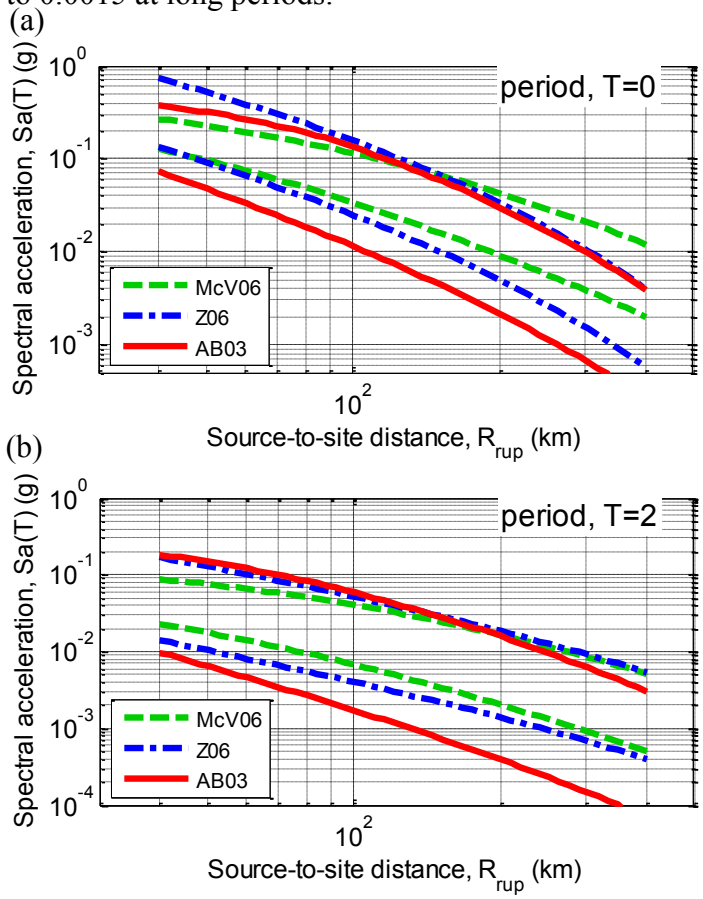

Figure 31: Path scaling of the considered subduction slab GMPEs for two magnitudes of 6 and 7.5: (a) Sa(0.0); and (b) Sa(2.0) (predictions for site class C and 40km focal depth).

6.2.3. Median response spectra (vibration period scaling)

Figure 32 illustrates the median response spectra predicted by the three considered GMPEs for magnitudes 5.5 and 7.5 and distances of 50 and 150 km. For both magnitudes and path distances considered it can be seen that the shape of the predicted AB03 spectra is significantly 'flatter' than that for the McV06 and Z06 models. It can also be seen that the AB03 spectra for $M_w = 5.5$ are lower than the

Z06 and McV06 predictions as a result of the aforementioned magnitude scaling. Similarly, for M_w =7.5 the Z06 model predicts higher spectral amplitudes as a result of the Z06 large magnitude scaling. One final observation is the unsmoothed nature of the McV06 predicted spectral amplitudes with period.

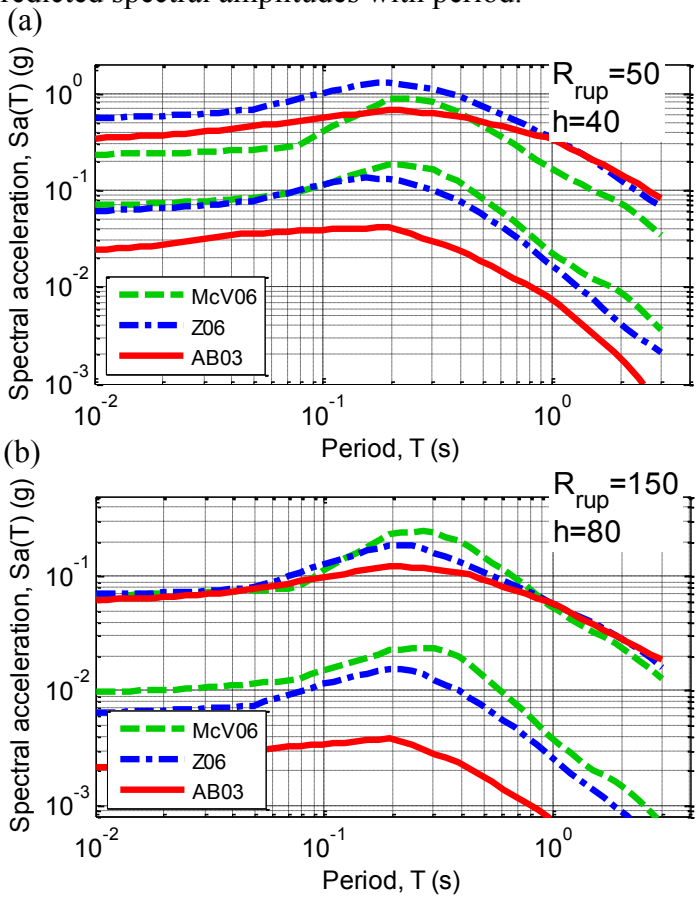

Figure 32: Median response spectra of the considered subduction slab GMPEs for two magnitudes of 5.5 and 7.5: (a) R_{rup}=50km, h=40km; and (b) R_{rup}=150km, h=80km (predictions for site class C sites).

6.2.4. Magnitude and period dependence of model standard deviations

Figure 33 illustrates the inter-event standard deviation of the models. None of the three models consider magnitude dependent inter-event standard deviation. It can be seen that the Z06 model has the largest inter-event standard deviation for all vibration periods, while the AB03 model has generally the lowest standard deviation for periods less than 0.2 seconds, and the McV06 model for periods greater than 0.2 seconds.

Figure 34 illustrates the dependence of the intra-event residuals with magnitude and distance. Similar to the inter-event residuals it can be seen that the Z06 and AB03 models are independent of magnitude. In contrast, the intra-event standard deviation of the McV06 model exhibits magnitude dependence, but strangely the magnitude dependent coefficient is not always negative (e.g. for Sa(0.2) and Sa(2.0)) as is common in most GMPEs with magnitude dependent standard deviations. This observation as well as the observed scaling of the McV06 intra-event standard deviation are a possible repercussion of the small number of recordings used in developing the McV06 model. The Z06 model has the largest intra-event standard deviation which is approximately 0.05 units larger than the AB03 model at short

periods.

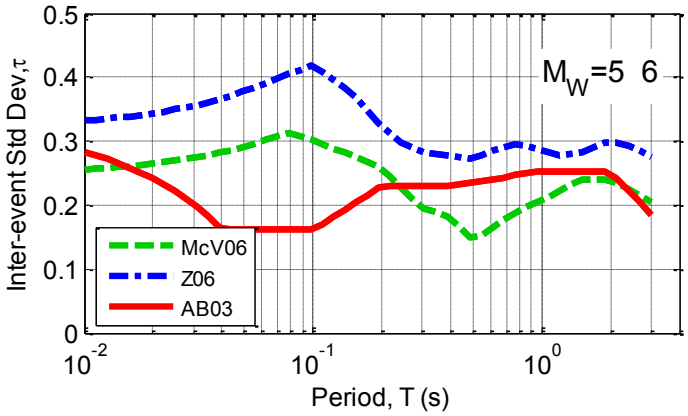

Figure 33: Inter-event standard deviation of subduction slab ground motion prediction equations.

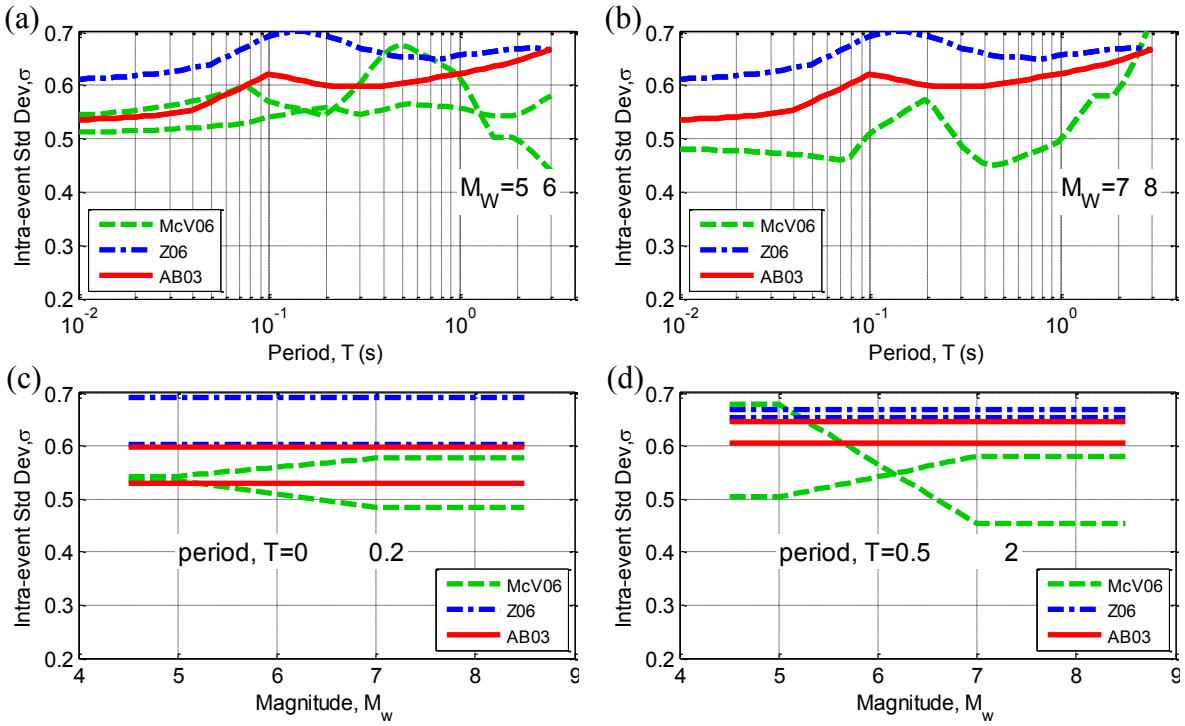

Figure 34: Intra-event standard deviation scaling of subduction slab ground motion prediction equations with period and magnitude.

6.3. Observed inter- and intra-event residuals from the NZ database

Now that insight has been obtained as to some of the general predictor variable scaling features of the considered slab GMPEs, it is possible to thoroughly examine the statistics of the observed inter- and intra-event residuals of the NZ database for each of the considered models. This section presents only sufficient results (typically for a single vibration period) to convey the general observations of the inter- and intra-event residuals as a function of predictor variables for each of the models. More elaborate results for vibration periods of 0.0, 0.2, 0.5, 1.0, and 5.0 seconds (or 3.0 seconds if the model was not applicable for 5.0 seconds) are given in the appendices.

In the examination of the cumulative distribution of the residuals, the Kolmogorov-Smirnov goodness-of-fit test (Ang and Tang 2007) is used to identify

statistically significant departures from the residuals having a standard normal distribution. Furthermore, in order to illustrate the key trends in the observed residuals as a function of the predictor variables, non-parametric regression (Wasserman 2006) of the mean is used. In addition to this non-parametric mean, the 98% confidence interval of the mean is also computed from the Student's *t*-distribution (as a result of η_i and $\varepsilon_{i,j}$ having normal distributions) (Ang and Tang 2007). The non-parametric mean and its confidence interval are shown in subsequent figures with solid and dashed lines, respectively, and can be used to identify statistically significant biases in the prediction models. The high level of confidence used is based on the desire to only identify high significance biases.

Finally, it is noted that there are 1500 ground motion records from subduction slab events in the NZ database in comparison to the 641 and 296 records from crustal and subduction interface events, respectively. Hence, the inter- and intra-event residuals for subduction slab events provide more robust evidence on the applicability (or lack thereof) of the three GMPEs considered, than is possible for the active shallow crustal GMPEs previously examined.

6.3.1. McVerry et al. (2006), McV06.

Figure 35 illustrates the observed inter- and intra-event residuals for Sa(1.0) from the NZ database using the McV06 model. Similar to the observations for crustal events it is immediately obvious that the McV06 model significantly over-predicts ground motions from $M_w < 6$ events (Figure 35a and Figure 35c). Figure 35e also illustrates that there is some bias of the intra-event residuals as a function of source to site distance (recall in the discussion pertaining to Figure 31 that the geometric spreading coefficient for the McV06 was significantly larger than the Z06 and AB03 models).

Figure 35f illustrates that there is a trend in the inter-event residuals as a function of source depth, but this observed trend is likely influenced by the poor magnitude scaling of the McV06 model.

Figure 35g illustrates that similar to the observations for crustal events, the McV06 model over- and under-predicts ground motions for site class A and E sites, respectively. This is because the McV06 model considers the response of sites A and B and sites D and E to be equal (McVerry et al. 2006).

Figure 35h provides an insightful result that despite the McV06 model considering the anelastic attenuation in the TVZ, there is still bias observed in the intra-event residuals as a function of the normalised-TVZ path distance. This observation may be the result of the fact that the McV06 model does not consider anelastic attenuation for the non-TVZ portion of the propagation path.

6.3.2. Zhao et al. (2006), Z06.

Figure 36 illustrates the observed inter- and intra-event residuals for Sa(1.0) from the NZ database using the Z06 model. Similar to the McV06 model, it can be seen that the Z06 model over-predicts ground motions from events with $M_w < 5$, although the over-prediction is not as pronounced as the McV06 model. Figure 36e also illustrates that there is an under-prediction of ground motions recorded at large source-to-site distances caused by a reduction in the apparent rate of attenuation. Zhao (2010) attributed this reduction in large distance attenuation to constructive interference of waves propagating through the mantle and those propagating a significantly larger distance within the subduction slab itself.

It is not immediately clear on inspection of Figure 36a, but Figure 36b illustrates that the standard deviation of the intra-event residuals is less and that for a standard normal distribution. This observation is more pronounced at short vibration periods (see appendix). This is the result of the Z06 model having a relatively large standard deviation in comparison with the McV06 and AB03 models, which based on the NZ database appears to be too large.

Figure 36f illustrates that there is negligible dependence of the inter-event residuals as a function of source depth. Figure 36g illustrates that while the mean of the intra-event residuals for site classes C and E are statistically different from zero, that the bias is still relatively minor in relation to the McV06 model site class predictions (Figure 35g). Finally, Figure 36h illustrates that there is a dependence of the intra-event residuals as a function of the normalised TVZ distances resulting from the lack of a TVZ-specific term in the Z06 model.

6.3.3. Atkinson and Boore (2003), AB03.

Figure 37 illustrates the observed inter- and intra-event residuals for Sa(1.0) from the NZ database using the AB03 model. It can be seen immediately in Figure 37a and Figure 37c that the AB03 model significantly under-predicts spectral amplitudes from ground motions in the NZ database. This can be interpreted from the magnitude scaling of the AB03 model illustrated in Figure 30. Figure 37e also illustrates that there is a strong dependence of the intra-event residuals as a function of path distance.

Figure 37f-Figure 37h illustrate the dependence of the residuals on source depth, site class, and normalised TVZ distance, respectively. While it appears that there is little dependence of the AB03 model with respect to these predictor variables it is difficult to robustly state this given the significant dependence of the residuals with magnitude and distance.

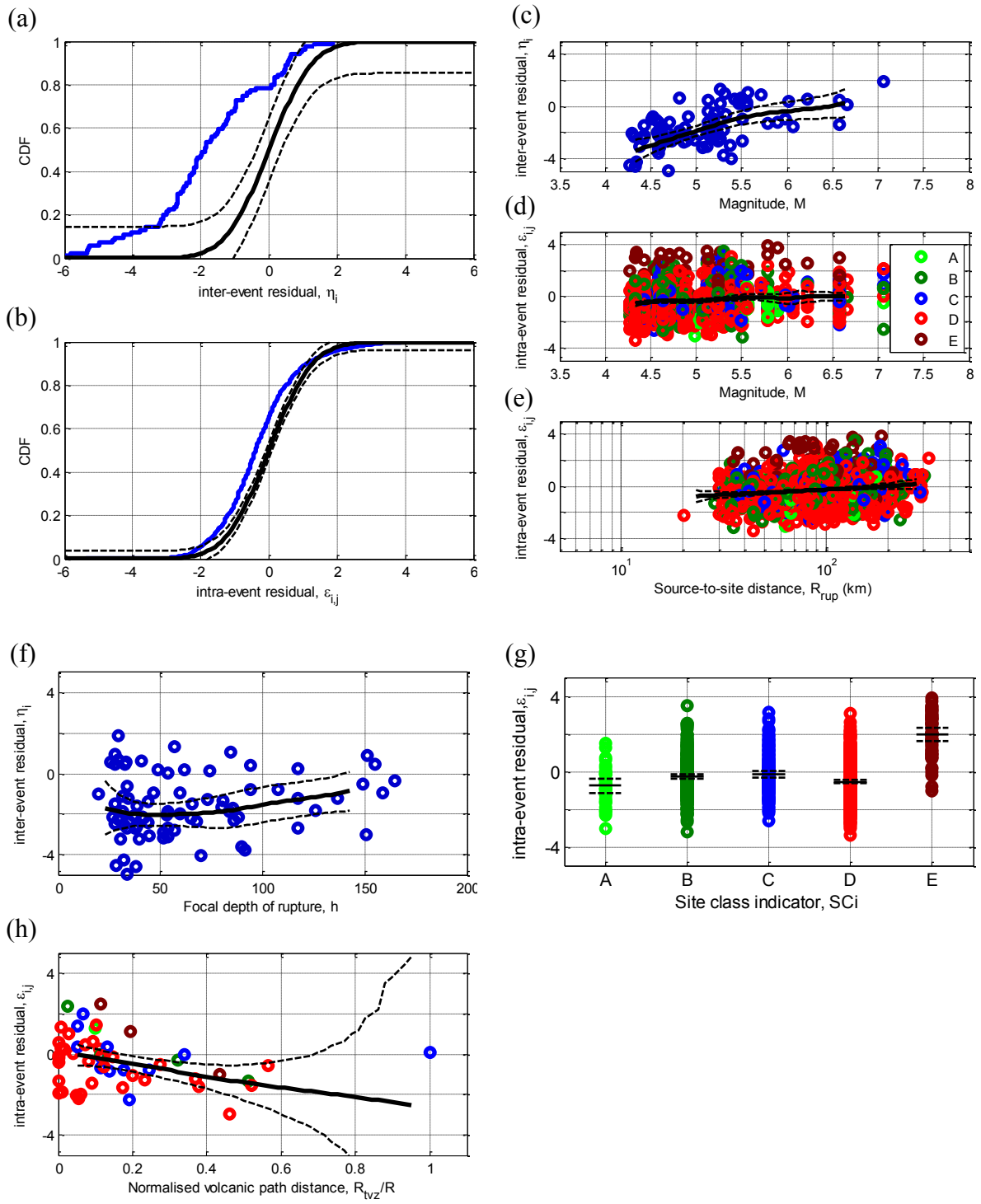

Figure 35: Residuals for Sa(1.0) using the McV06 model: (a)&(b) distribution of inter- and intra-event residuals; (c)&(d) inter- and intra-event residuals as a function of magnitude; (e) intra-event residuals as a function of distance; (f) inter-event residuals as a function of depth; (g)&(h) intra-event residuals as a function of site class and normalised volcanic path distance.

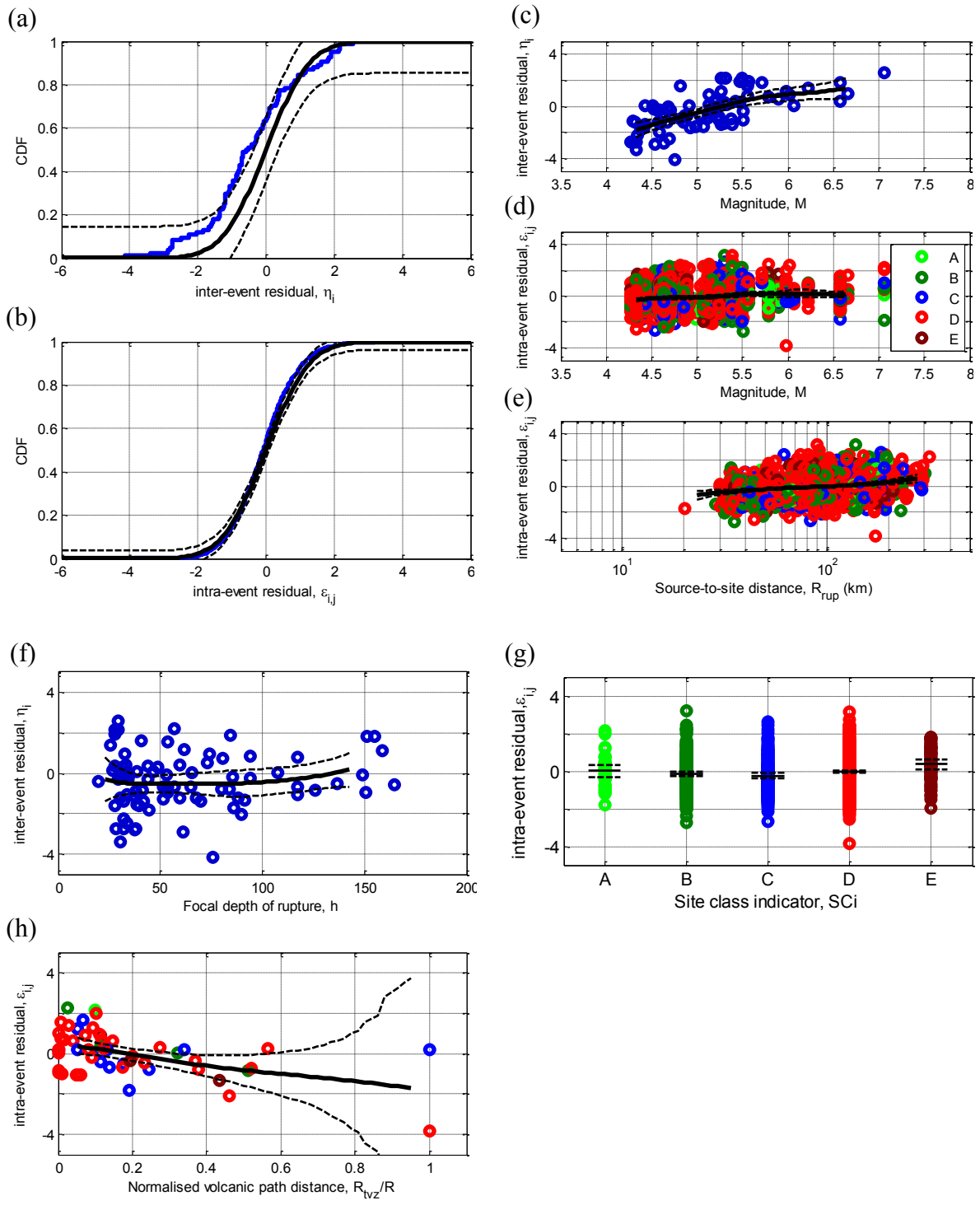

Figure 36: Residuals for Sa(1.0) using the Z06 model: (a)&(b) distribution of inter- and intra-event residuals; (c)&(d) inter- and intra-event residuals as a function of magnitude; (e) intra-event residuals as a function of distance; (f) inter-event residuals as a function of depth; (g)&(h) intra-event residuals as a function of site class and normalised volcanic path distance.

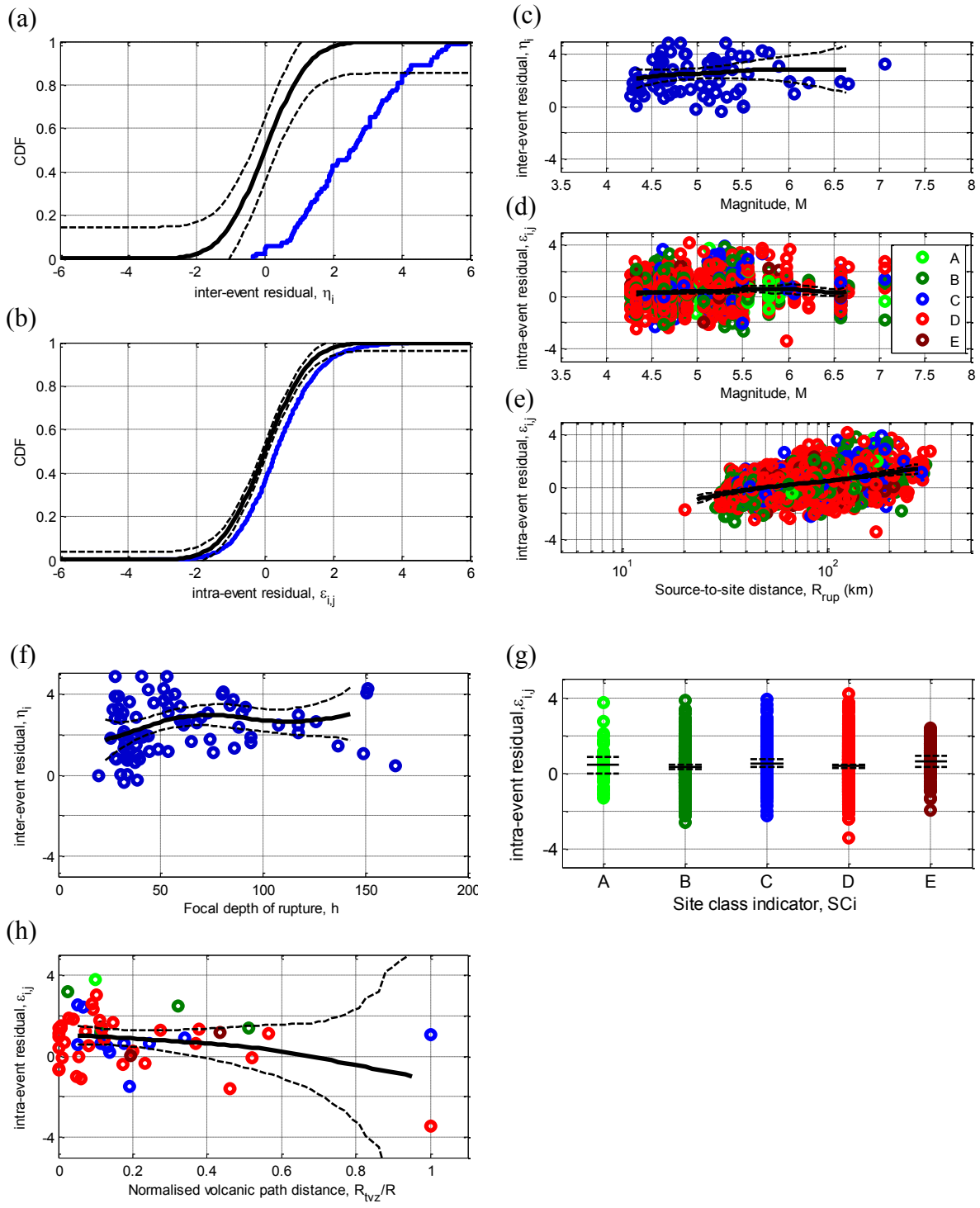

Figure 37: Residuals for Sa(1.0) using the AB03 model: (a)&(b) distribution of inter- and intra-event residuals; (c)&(d) inter- and intra-event residuals as a function of magnitude; (e) intra-event residuals as a function of distance; (f) inter-event residuals as a function of depth; (g)&(h) intra-event residuals as a function of site class and normalised volcanic path distance.

7. NZ-SPECIFIC SUBDUCTION SLAB MODEL

The three subduction slab GMPEs considered span a range of applicability to NZ strong motion prediction based on the observed inter- and intra-event residuals examined in the previous section. It was relatively clear that the AB03 provided the poorest prediction as evident from the obtained inter- and intra-event residual dependence on various predictor variables. However, both the McV06 and Z06 models also demonstrated several deficiencies in predictor variable scaling compared with empirical data. Hence clearly the status-quo of using the McV06 model for ground motion prediction from subduction slab events can be improved, but the best way to achieve such an improvement is not obvious.

7.1. "Base-model" adopted

In the examination of the observed inter- and intra-event residuals it is important to bear in mind that while the subduction slab database contained significantly more ground motion records than for shallow crustal events (1500 compared to 641), there is still a paucity of high spectral amplitude records originating from large magnitude events. Recall that the maximum PGA recorded from subduction slab events was 0.28g (Figure 4), and that there are only four events with $M_w > 6.5$ and only one event $M_w > 7$.

Hence, based on the above argument it is necessary to consider the rigour of the McV06 and Z06 models for large amplitude ground motions (which are recorded from large magnitude events at relatively near-source distances). The McV06 subduction slab model is based solely on NZ ground motion data from 1966-1995. As previously noted the McV06 database was significantly smaller than the database developed in this study. Conversely, the Z06 database contains 1725 records from subduction slab events. In particular, the Z06 database contains four relatively well recorded events with $M_w > 7$. For this reason the Z06 model is selected as the base model to modify for NZ-specific application.

7.2. Modifications of base-model to develop a NZ-specific subduction slab model

Based on theoretical considerations and empirical observations from Figure 36 (and the additional figures in the appendix) four modifications are required in order to rectify the observed predictor variable dependence of the inter- and intra-event residuals of the Z06 model: (i) NZ-specific scaling for small magnitudes; (ii) scaling of the Z06 model at large distances; and (iii) consideration of the increased TVZ attenuation; (iv) possible revision of the standard deviation model.

In addition to the four modifications above one further modification is made on practical grounds. It is advantageous that NZ-specific GMPEs for different tectonic regions require the same information at the site of interest. Because of the success of the CY08-based site response model in the B10 active shallow crustal model, and the fact that this site response model offers the benefit of: (i) continuous site variables accounting for both near surface velocity and depth of sediments; and (ii) linear and non-linear site response, it is also desired to adopt the same site response model for the NZ-specific subduction slab model.

These five modifications of the Z06 model noted above are done so using

subsets of the NZ database in order to separate these effects as much as possible. Below, justification is provided for the functional and/or parametric modification for each of these five points, and the resulting features of the NZ-specific (B10) slab model are examined.

7.2.1. Modification for NZ-specific small magnitude scaling

It was observed that the Z06 model over-predicted the amplitude of short-period spectral amplitudes for small-to-moderate magnitude (SMM) events (i.e. $M_w < 5.5$). This observation can be appreciated from the fact that the Z06 strong motion database used only ground motions from events of $M_w > 5$, and that the applicability of GMPEs near their magnitude limits are questionable (Bommer et al. 2007). The Z06 model uses a quadratic magnitude scaling functional form, which for hard rock site conditions is given by (Zhao et al. 2006):

$$lny^{Z06} \propto [S_s + C_{HR} + a\boldsymbol{M}] + [P_s(\boldsymbol{M} - M_c) + Q_s(\boldsymbol{M} - M_c)^2 + W_s] \tag{23}$$

The quadratic magnitude scaling in the Z06 model, in particular, was developed subsequent to the development of a model with linear magnitude scaling (Zhao et al. 2006). This subsequent inclusion of quadratic magnitude scaling was clearly ill-conditioned based on the observation that the quadratic magnitude scaling coefficient is positive for several vibration periods (e.g. Figure 30). The observations from Figure 36 (and those in the appendix for other vibration periods) clearly demonstrate that a quadratic magnitude scaling functional form is insufficient to capture the observed magnitude scaling of the empirical NZ data.

To account for the observed complexity in magnitude scaling of the empirical observations the same functional form of magnitude scaling used in the B10 active shallow crustal model is adopted for the B10 subduction slab model:

$$lny^{B10,crustal} \propto c_1 + c_2(\boldsymbol{M} - 6) + \frac{c_2 - c_3}{c_n} ln\left(1 + e^{c_n(c_M - \boldsymbol{M})}\right) \tag{24}$$

Because it is expected that the response spectral amplitudes from subduction slab and active shallow crustal events will be different, then the value of the parameter c_1 in Equation (24) was initially set such that the prediction of the original Z06 model and the modified model had the same prediction for $\boldsymbol{M} = 6.5$ and 'rock' conditions (i.e. $lny_{i,j}^{CY08}[\boldsymbol{M} = 6.5] = lny^{Z06}[\boldsymbol{M} = 6.5]$ for CY08 reference site $V_{s,1130}$ and Z06 site class A). This 'pivot' magnitude was selected to be the same as the 'corner' magnitude, M_c, of the Z06 model so that the magnitude squared terms have no effect (as previously mentioned they are ill-conditioned), and also because there is a large number of events around a magnitude of 6.5 in the Z06 ground motion database (so the regression equation is expected to be well representative of the empirical data).

Figure 38 provides a comparison between the magnitude scaling of the developed B10 subduction slab model with the Z06 and McV06 models. It can be seen that the B10 model exhibits smaller spectral acceleration ordinates for $M_w < 6$ than the Z06 and McV06 models (consistent with the observed negative residuals of the Z06 and McV06 models in Figure 36 and Figure 35, respectively). Furthermore, it can be seen that the B10 and Z06 models are very similar for $M_w = 6.5$ because this was used as the pivot magnitude. The only reason for the difference between the B10 and Z06 models at $M_w = 6.5$ is that Figure 38 is for site class C site conditions, while the constraint that the B10 and Z06 models be equal was enforced for the Z06 site

class A and the B10 reference site class of $V_{s,1130}$ (i.e. the B10 slab model uses a different site response formulation than the Z06 model as discussed subsequently).

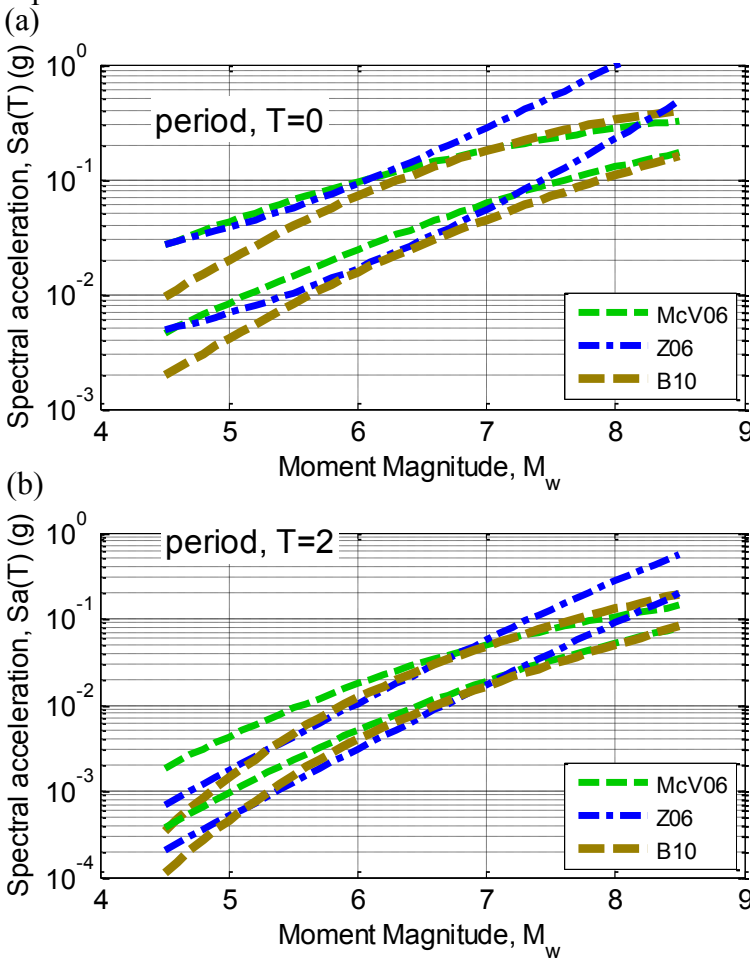

Figure 38: Magnitude scaling of the median B10 subduction slab model compared with the Z06 and McV06 models for path distances of 50 and 120 km: (a) Sa(0.0); and (b) Sa(2.0) (predictions for site class C, focal depth 40km).

7.2.2. Consideration of TVZ attenuation

It has been previously shown for active shallow crustal events that the increased anelastic attenuation through the TVZ has a pronounced effect on response spectral amplitudes. As a result, the same functional form developed for spectral amplitudes from active shallow crustal events was adopted for subduction slab events. The functional form of the anelastic-portion of path scaling for the B10 subduction slab model is therefore:

$$lny \propto c_\gamma \left(1 + c_{TVZ}\frac{R_{TVZ}}{R_{RUP}}\right) R_{RUP} \qquad (25)$$

where c_γ is the anelastic attenuation coefficient with parameter values obtained directly from Z06 (i.e. $c_\gamma^{B10} = b^{Z06}$); R_{RUP} is the closest-distance from the site to the fault rupture plane; R_{TVZ} is the path distance through the TVZ; and c_{TVZ} is an empirical parameter representing the ratio of the TVZ and non-TVZ anelastic attenuations.

The adequacy of the Z06 anelastic attenuation coefficient adopted in the B10

model was examined based on the observed intra-event residuals. It was found that this coefficient lead to no significant bias. It was also found that the use of the c_{TVZ} values developed based on active shallow crustal empirical data was also adequate, and for consistency was therefore adopted without change.

7.2.3. Modification of the site response model

The Z06 model considers site response effects based on five discrete site classes (Zhao et al. 2006), with a formulation given by:

$$lny \propto C_{SCi} \tag{26}$$

where C_{SCi} is a period-dependent site factor for site class i. Thus the Z06 site response formulation is linear in that the ratio between the predicted spectral amplitudes between two site classes is constant and independent of the amplitude of the ground motion.

Development of the B10 active shallow crustal model demonstrated that the CY08-based site response model provided a good comparison with the empirical observations from active shallow crustal events in the NZ database. The CY08-based site response model is based on the (continuous) predictor variables: $V_{s,30}$ and $Z_{1.0}$. The CY08-based site response model also considers non-linear site effects which are a function of the spectral amplitude at a reference shear wave velocity of 1130 m/s, $V_{s,1130}$. Finally, the B10 active shallow crustal model modified the CY08-based site response model to account for the larger shear wave velocities for NZ site class A sites. Hence, because of the high fidelity of the CY08-based site response model relative to the Z06 model; its modification for NZ-specific site class A; and the benefit of consistency in site parameters required for active shallow crustal and subduction slab events, this site response model is adopted for the B10 subduction slab model. The effects of site class on predicted response spectra for subduction slab events are shown for two scenarios in Figure 39. Figure 39a and Figure 39b clearly illustrate the effect of non-linear site response which leads to a small amplification (or even de-amplification) of short period spectral ordinates, and a large amplification of longer period spectral ordinates.

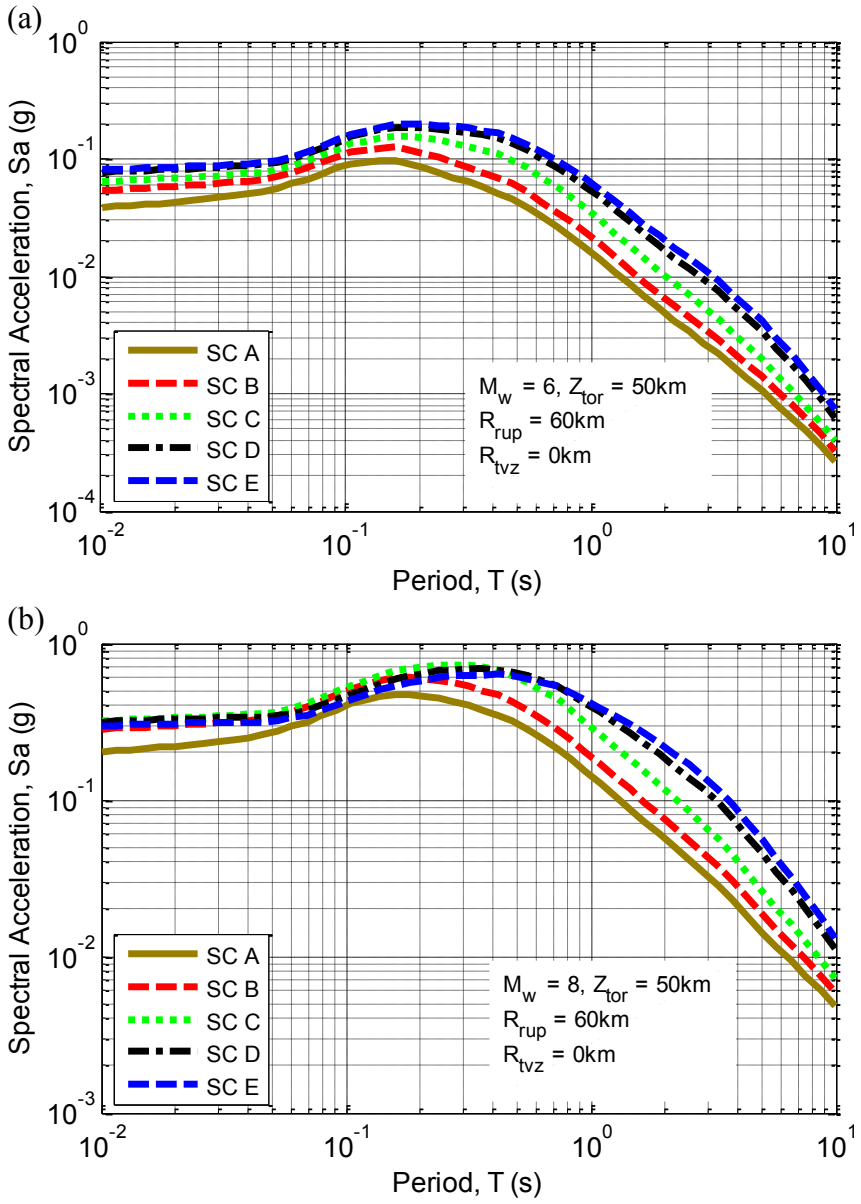

Figure 39: Effect of site class on the predicted response spectra for: (a) a M_w 6 event at distance of 60km; and (b) a M_w 8 event at distance of 60km (focal depth 50km in both cases).

7.2.4. Modification of path scaling at large distances

At all vibration periods considered it was observed that the Z06 model under-predicts spectral amplitudes from ground motions observed at large source to site distances (e.g. Figure 36e). The fact that this bias is observed for all vibration periods suggests that there is a problem in the large-distance geometric spreading attenuation, rather than anelastic attenuation (which would lead to larger biases for short vibration periods and negligible biases for longer vibration periods). Zhao (2010) also observed that spectral amplitudes from well-recorded Japanese subduction slab events exhibit a substantial (and almost complete) reduction in geometric spreading rate at large source to site distances. Zhao (2010) suggested that such observations were the result of the complex wave propagation paths (both direct waves travelling a significant distance through the low Q mantle, and indirect waves travelling along

strike and up dip of the high Q subduction slab itself).

To rectify the poor prediction of spectral amplitudes at large distances using a model with constant geometric spreading, Zhao (2010) proposed the use of a 'two-slope' model with the distance at which the geometric spreading coefficient changes being a function of depth. A similar two-slope model was considered to represent the observations in the NZ data, however it was found that the best transition distance varied for different earthquakes. Following the logic of Chiou and Youngs (2008), who made similar observations in the development of their active shallow crustal NGA GMPE, it was instead preferred to use a functional form which allows a smooth transition of geometric spreading rate with distance. The functional form for the geometric spreading adopted is:

$$lny \propto c_{GS_1} ln[R_{RUP} + c_5 exp(c_6 \boldsymbol{M})] + \left(\frac{c_{GS_2} - c_{GS_1}}{c_{GS_4}}\right) ln\left[\left(\frac{R_{RUP}}{c_{GS_3}}\right)^{c_{GS_4}} + 1\right] \quad (27)$$

where R_{RUP} is the source-to-site rupture distance; c_5 and c_6 are parameters for finite source effects (from Zhao et al. (2006)); c_{GS_1} is the geometric spreading at moderate path distances; c_{GS_2} is the geometric spreading at large path distances; c_{GS_3} is the transition distance between the moderate and large path distances; and c_{GS_4} controls the distance range over which the transition from the two geometric spreading rates occurs. Figure 40 illustrates schematically the effect of these four parameters on the geometric spreading. It is noted that Equation (27) is a generalised form of that adopted by Chiou and Youngs (2008) to provide a smooth transition for active shallow crustal events (CY08 used $c_{GS_4} = 2$ and also did not normalise the second term in Equation (27) by c_{GS_4}). The benefit of the formulation in Equation (27) is that the same geometric spreading functional form and empirical parameters of Z06 can be used for path scaling at moderate distances (i.e. the first term of Equation (27)) and the second term in Equation (27) can be simply added.

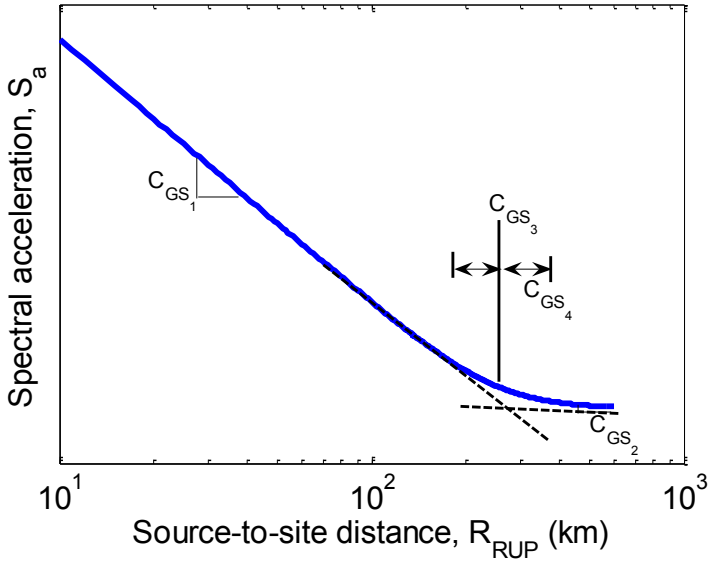

Figure 40: Schematic illustration of the effect of the four parameters in the geometric spreading functional form adopted for ground motion prediction from subduction slab events.

Based on three well-recorded Japanese events, Zhao (2010) suggested that the transition distance at which the geometric spreading rate changes is a function of source depth. However, using the NZ database it was not possible to validate this suggestion and instead a constant value of c_{GS_3} =180 km was adopted (this value is however near the mid-range of the values given in Zhao (2010)). The parameters c_{GS_2} and c_{GS_4} were found to be relatively insensitive to vibration period and therefore were considered independent of period with values $c_{GS_2} = 0$ and $c_{GS_4} = 3$. Note that while $c_{GS_2} = 0$ implies that there is no geometric spreading at large distances, this 'large distance' is well beyond the 400 km for which the NZ database has empirical observations, and hence is not of practical concern. The formulation of Equation (27) is considered as an empirical adjustment to adequately capture the observed reduction in attenuation at large path distances. Further studies are clearly warranted however to more clearly understand the wave propagation mechanisms causing these observations and to develop more theoretically-based functional forms for empirical GMPEs.

Figure 41 illustrates the path scaling of the B10 slab model in comparison to the Z06 and McV06 models. In Figure 41a it can be seen that for Sa(0.0) the Z06 model exhibits significantly more attenuation at large distances than the B10 and McV06 models. It is worth noting that the McV06 model does not exhibit a bias in the intra-event residuals at large distances for Sa(0.0) (see appendix). In Figure 41b it can be seen that the B10 model exhibits notably larger spectral ordinates at large path distances compared to the Z06 and McV06 models as a result of the additional geometric spreading terms in Equation (27).

As previously mentioned, the fact that the McV06 model does not consider anelastic attenuation effects is the reason for the similarity of the B10 and McV06 path scaling for Sa(T=0), but difference for Sa(T=2).

7.2.5. Modification of the standard deviation model

Figure 33 and Figure 34 illustrated that the Z06 model has larger inter- and intra-event standard deviations than either the AB03 or McV06 models. Figure 36a and Figure 36b also illustrated that the standard deviation of the Sa(1.0) inter- and intra-event residuals from the NZ database using the Z06 model have less variability than the standard normal distribution, indicating that the Z06 intra-event standard deviation is potentially too large (similar observations for other vibration periods are given in the appendix).

The Z06 model was developed using the same functional form for active shallow crustal, subduction interface, and subduction slab events (with the exception of a constant source term and additional geometric spreading for slab events (Zhao et al. 2006)). It is speculated that the use of this simple functional form of the Z06 model applied to these three different source types has lead to the large standard deviations in the Z06 model. Furthermore, the improved scaling of the median prediction (i.e. the aforementioned four modifications of the Z06 model) will also lead to a reduction in the observed variability in the empirical data.

Because of the success of the CY08 variance model for use in the B10 active shallow crustal model it was also examined whether this same variance model was applicable for characterising the ground motion variability from subduction slab events. The CY08 variance model is functionally more complex than the Z06 model in that it is both magnitude and intensity dependent (Chiou and Youngs 2008). The observed standard deviation of the inter- and intra-event residuals from the NZ

database using this variance model (presented in the next section) were found to not be statistically different than the standard normal distribution, and therefore the CY08 variance model was adopted for the B10 subduction slab model.

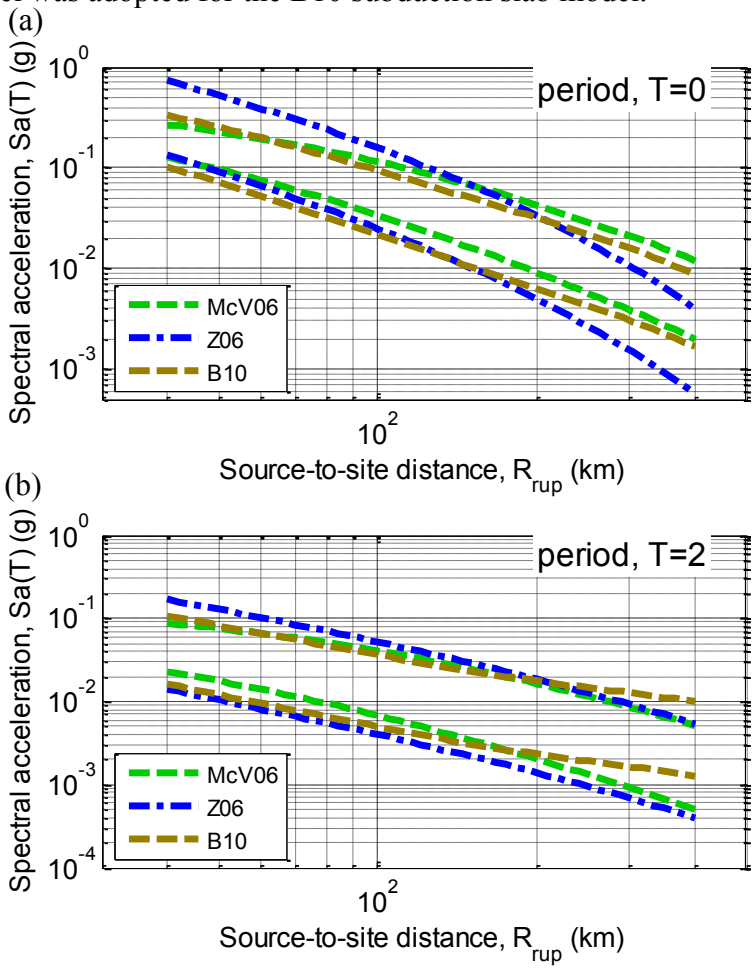

Figure 41: Path scaling of the median B10 subduction slab model compared with the Z06 and McV06 models for magnitudes of 6 and 7.5: (a) Sa(0.0); and (b) Sa(2.0) (predictions for site class C, focal depth 40km).

7.3. Functional form and parameters of the Bradley (2010) subduction slab model

The developed, NZ-specific subduction slab model (B10) is based on the Z06 subduction slab model with the aforementioned modifications. The complete B10 subduction slab median model formulation is given by:

$$\begin{aligned} ln(y_{ref}) &= c_1 + c_7 max(min\{h, 125\} - 15, 0) \\ &+ c_2(\boldsymbol{M} - 6) + \frac{c_2 - c_3}{c_n} ln\left(1 + e^{c_n(c_M - \boldsymbol{M})}\right) \\ &+ c_{GS_1} ln[R_{RUP} + c_5 exp(c_6 \boldsymbol{M})] + \left(\frac{c_{GS_2} - c_{GS_1}}{c_{GS_4}}\right) ln\left[\left(\frac{R_{RUP}}{c_{GS_3}}\right)^{c_{GS_4}} + 1\right] \\ &+ c_\gamma \left(1 + c_{TVZ} \frac{R_{TVZ}}{R_{RUP}}\right) R_{RUP} \end{aligned} \quad (28)$$

and

$$ln(y) = ln(y_{ref}) + \phi_1 log\left(\frac{min(V_{s30}, V_1)}{1130}\right) + b.ln\left(\frac{y_{ref} + \phi_4}{\phi_4}\right)$$
$$+\phi_5\left(1 - \frac{1}{cosh[\phi_6 max(0, Z_{1.0} - \phi_7)]}\right) + \frac{\phi_8}{cosh[0.15.max(0, Z_{1.0} - 15)]} \quad (29)$$

where

$$V_1 = min\left(1130.max\left\{\left(\frac{T}{0.75}\right)^{-0.11}, 1\right\}, 1800\right) \quad (30)$$

$$b = \phi_2\left\{e^{\phi_3(min(V_{s30},1130)-360)} - e^{\phi_3(1130-360)}\right\} \quad (31)$$

The predictor variables are:

$\boldsymbol{M}$	Moment magnitude
R_{RUP}	Closest distance to the fault rupture plane (km)
R_{TVZ}	Distance of wave propagation through the Taupo Volcanic Zone (TVZ) (km)
h	Focal depth of the fault rupture plane.
V_{s30}	Average shear wave velocity for the top 30m of the site (m/s)
$Z_{1.0}$	Depth to shear wave velocity of 1.0 km/s (m)

The period-independent parameters for the B10 median model are given in Table 9, while the period-dependent parameters are given in Table 10 and Table 11. It is worthy of note that only the parameters c_1 (constant term), and c_{GS_2}, c_{GS_3} c_{GS_4} (large distance attenuation) in the B10 slab model were constrained from the NZ database. Parameters c_5, c_6, c_7, c_γ (denoted as *c*, *d*, *e*, and *b* in Z06, respectively) and c_2, c_n, $\phi_1 - \phi_8$ were fixed at their values in the Z06 and CY08 models, respectively. Parameters c_3, c_M (small magnitude scaling) and c_{TVZ} (TVZ scaling) were taken to be the same as that for the B10 active shallow crustal model. The parameter c_{GS_1} was fixed to be the sum of the geometric spreading factors, *b* and S_{SL} in the Z06 model (noting that in the Z06 model $r_{i,j} \approx x_{i,j}$ at distances of concern for subduction slab events)

Table 9: Period-independent coefficients for the reference model, $\boldsymbol{ln(y_{ref})}$ (Equation (28))

c_2	c_{GS_2}	c_{GS_3}	c_{GS_4}
1.06	0.0	180.0	3.0

Table 10: Period-dependent coefficients for the reference model, $ln(y_{ref})$ (Equation (28))

Vibration Period (s)	c_1	c_3	c_n	c_M	c_5	c_6	c_7	c_{GS_1}	c_γ	c_{TVZ}
pga	3.0546	1.50000	2.996	5.85000	6.16	0.4893	0.0512	-1.5280	-0.0056	2.0
0.01	3.1444	1.50299	2.996	5.81711	6.16	0.4893	0.0512	-1.5326	-0.0059	2.0
0.02	3.2343	1.50845	3.292	5.80023	6.158	0.4892	0.0512	-1.5372	-0.0061	2.0
0.03	3.3241	1.51549	3.514	5.78659	6.155	0.489	0.0511	-1.5418	-0.0063	2.0
0.04	3.4140	1.52380	3.563	5.77472	6.1508	0.4888	0.0508	-1.5464	-0.0065	2.0
0.05	3.5038	1.53319	3.547	5.76402	6.1441	0.4884	0.0504	-1.5510	-0.0067	2.0
0.075	3.5406	1.56053	3.448	5.74056	6.12	0.4872	0.0495	-1.4855	-0.0073	2.0
0.1	3.5774	1.59241	3.312	5.72017	6.085	0.4854	0.0489	-1.4200	-0.0079	2.0
0.15	3.6641	1.6664	3.044	5.68493	5.9871	0.4808	0.0479	-1.4310	-0.0072	2.0
0.2	3.3248	1.75021	2.831	5.65435	5.8699	0.4755	0.0471	-1.3720	-0.0066	2.0
0.25	3.1109	1.84052	2.658	5.62686	5.7547	0.4706	0.0464	-1.3600	-0.0059	2.0
0.3	3.3394	1.9348	2.505	5.60162	5.6527	0.4665	0.0458	-1.4500	-0.0052	2.5
0.4	3.3939	2.12764	2.261	5.55602	5.4997	0.4607	0.0445	-1.5060	-0.0042	3.2
0.5	3.4002	2.31684	2.087	5.51513	5.4029	0.4571	0.0429	-1.5540	-0.0034	3.5
0.75	2.8696	2.73064	1.812	5.38632	5.29	0.4531	0.0387	-1.5560	-0.0025	4.5
1.0	2.2441	3.03000	1.648	5.31	5.248	0.4517	0.035	-1.5090	-0.0022	5.0
1.5	1.0895	3.43384	1.511	5.29995	5.2194	0.4507	0.028	-1.3790	-0.0022	5.4
2.0	0.1196	3.67464	1.47	5.3273	5.2099	0.4504	0.0213	-1.2480	-0.002	5.8
3.0	-0.3938	3.64933	1.456	5.4385	5.204	0.4501	0.0106	-1.2630	-0.0015	6.0
4.0	-1.1602	3.60999	1.465	5.5977	5.202	0.4501	0.0041	-1.1690	-0.0019	6.15
5.0	-1.6524	3.50	1.478	5.7276	5.201	0.45	0.001	-1.1200	-0.0024	6.3
7.5	-2.2504	3.45	1.498	5.9891	5.2	0.45	0.0	-1.0950	-0.0027	6.425
10.0	-2.5924	3.45	1.502	6.193	5.2	0.45	0.0	-1.0830	-0.0029	6.55

[1]The units for *pga* and *psa* are g's.

Table 11: Period-dependent coefficients for the site response model, $ln(y)$ (Equation (29))

Vibration Period (s)	ϕ_1	ϕ_2	ϕ_3	ϕ_4	ϕ_5	ϕ_6	ϕ_7	ϕ_8
pga	-0.4417	-0.1417	-0.007010	0.102151	0.2289	0.014996	580.0	0.0700
0.01	-0.4417	-0.1417	-0.007010	0.102151	0.2289	0.014996	580.0	0.0700
0.02	-0.434	-0.1364	-0.007279	0.108360	0.2289	0.014996	580.0	0.0699
0.03	-0.4177	-0.1403	-0.007354	0.119888	0.2289	0.014996	580.0	0.0701
0.04	-0.4000	-0.1591	-0.006977	0.133641	0.2289	0.014996	579.9	0.0702
0.05	-0.3903	-0.1862	-0.006467	0.148927	0.229	0.014996	579.9	0.0701
0.075	-0.404	-0.2538	-0.005734	0.190596	0.2292	0.014996	579.6	0.0686
0.1	-0.4423	-0.2943	-0.005604	0.230662	0.2297	0.014996	579.2	0.0646
0.15	-0.5162	-0.3113	-0.005845	0.266468	0.2326	0.014988	577.2	0.0494
0.2	-0.5697	-0.2927	-0.006141	0.255253	0.2386	0.014964	573.9	-0.0019
0.25	-0.6109	-0.2662	-0.006439	0.231541	0.2497	0.014881	568.5	-0.0479
0.3	-0.6444	-0.2405	-0.006704	0.207277	0.2674	0.014639	560.5	-0.0756
0.4	-0.6931	-0.1975	-0.007125	0.165464	0.312	0.013493	540.0	-0.0960
0.5	-0.7246	-0.1633	-0.007435	0.133828	0.361	0.011133	512.9	-0.0998
0.75	-0.7708	-0.1028	-0.008120	0.085153	0.4353	0.006739	441.9	-0.0765
1.0	-0.7990	-0.0699	-0.008444	0.058595	0.4629	0.005749	391.8	-0.0412
1.5	-0.8382	-0.0425	-0.007707	0.031787	0.4756	0.005544	348.1	0.0140
2.0	-0.8663	-0.0302	-0.004792	0.019716	0.4785	0.005521	332.5	0.0544
3.0	-0.9032	-0.0129	-0.001828	0.009643	0.4796	0.005517	324.1	0.1232
4.0	-0.9231	-0.0016	-0.001523	0.005379	0.4799	0.005517	321.7	0.1859
5.0	-0.9222	0.0000	-0.001440	0.003223	0.4799	0.005517	320.9	0.2295
7.5	-0.8346	0.0000	-0.001369	0.001134	0.4800	0.005517	320.3	0.2660
10.0	-0.7332	0.0000	-0.001361	0.000515	0.4800	0.005517	320.1	0.2682

The inter-event, τ, intra-event, σ, and total, σ_T, standard deviation models are given by:

$$\tau = \tau_1 + \frac{\tau_2 - \tau_1}{2}[min\{max(\boldsymbol{M}, 5), 7\} - 5] \tag{32}$$

$$\sigma = \left[\sigma_1 + \frac{\sigma_2 - \sigma_1}{2}(min\{max(\boldsymbol{M}, 5), 7\} - 5)\right] \times \sqrt{\sigma_3(1 - F_{measured}) + 0.7F_{measured} + (1 + NL_0)^2} \tag{33}$$

$$\sigma_T = \sqrt{(1 + NL_0)^2\tau^2 + \sigma^2} \tag{34}$$

with

$$NL_0 = \left(b\frac{y_{ref}}{y_{ref} + \phi_4}\right) \tag{35}$$

where $F_{measured}$ is 1 if V_{s30} is measured directly, and 0 if inferred from geology. The parameters for the standard deviation model are given in Table 12. As the adopted standard deviation model is identical to that of CY08 (because the observed residuals to follow do not suggest otherwise), further details regarding the mathematically basis of this formulation can be found in Chiou and Youngs (2008).

Table 12: Period-dependent coefficients for the standard deviation model (Equations (32)-(34)).

Vibration Period (s)	τ_1	τ_2	σ_1	σ_2	σ_3
pga	0.3437	0.2637	0.4458	0.3459	0.8000
0.01	0.3437	0.2637	0.4458	0.3459	0.8000
0.02	0.3471	0.2671	0.4458	0.3459	0.8000
0.03	0.3603	0.2803	0.4535	0.3537	0.8000
0.04	0.3718	0.2918	0.4589	0.3592	0.8000
0.05	0.3848	0.3048	0.4630	0.3635	0.8000
0.075	0.3878	0.3129	0.4702	0.3713	0.8000
0.1	0.3835	0.3152	0.4747	0.3769	0.8000
0.15	0.3719	0.3128	0.4798	0.3847	0.8000
0.2	0.3601	0.3076	0.4816	0.3902	0.8000
0.25	0.3522	0.3047	0.4815	0.3946	0.7999
0.3	0.3438	0.3005	0.4801	0.3981	0.7997
0.4	0.3351	0.2984	0.4758	0.4036	0.7988
0.5	0.3353	0.3036	0.4710	0.4079	0.7966
0.75	0.3429	0.3205	0.4621	0.4157	0.7792
1.0	0.3577	0.3419	0.4581	0.4213	0.7504
1.5	0.3769	0.3703	0.4493	0.4213	0.7136
2.0	0.4023	0.4023	0.4459	0.4213	0.7035
3.0	0.4406	0.4406	0.4433	0.4213	0.7006
4.0	0.4784	0.4784	0.4424	0.4213	0.7001
5.0	0.5074	0.5074	0.442	0.4213	0.7000
7.5	0.5328	0.5328	0.4416	0.4213	0.7000
10.0	0.5542	0.5542	0.4414	0.4213	0.7000

7.4. Observed inter- and intra-event residuals of Bradley (2010) subduction slab model

This section presents the inter- and intra-event residuals obtained from applying the B10 subduction slab model to the NZ database. Similar to previous discussions only the inter- and intra-event residuals for vibration periods of 0.0 and 1.0 are presented here. Results for other vibration periods can be found in the appendix.

Figure 42 illustrates the observed inter- and intra-event residuals for Sa(0.0) from the NZ database using the B10 model. It can be seen that based on the distributions of the inter- and intra-event residuals alone (i.e. Figure 42a and Figure 42b) that the B10 slab model is unbiased. Examination of the magnitude-dependence of the intra-event residuals also reveals no bias, compared to the bias in the Z06 model (i.e. Figure 36c), as a result of the modifications of the small magnitude scaling previously discussed. Figure 42d and Figure 42e also illustrate that there is no significant bias in the intra-event residuals obtained from the B10 slab model as a function of either magnitude or path distance. Thus, the bias with path distance in the inter-event residuals obtained using the Z06 model (i.e. Figure 36e) has been eliminated via the reduction in the geometric spreading rate at large path distances.

Figure 42f illustrates that there is no significant bias observed for the inter-event residuals as a function of source depth, h. This is to be expected, given that the same depth scaling as the Z06 model is adopted in the B10 slab model, which also did not exhibit bias (i.e. Figure 36f).

Figure 42g illustrates the observed intra-event residuals as a function of site class. It can be seen that there is a slight under-prediction at class B and C sites and a slight over-prediction of site class D Sa(0.0) values, but no bias for site class A, and E

Sa(0.0) amplitudes.

Figure 42h illustrates that the inclusion of the normalised TVZ distance in the B10 subduction slab model leads to no significant dependence on the intra-event residuals as a function of normalised TVZ distance. In contrast such a bias was observed in the Z06 model (i.e. Figure 36h) which does not explicitly consider TVZ distance as a predictor variable.

Figure 43 illustrates the observed inter- and intra-event residuals for Sa(1.0) from the NZ database using the B10 subduction slab model. Similar to the results for Sa(0.0), it can be seen in Figure 43a that the inter-event residuals cannot be rejected as different from the standard normal distribution. On the other hand, Figure 43b illustrates that while the mean intra-event residual is not statistically different from zero, that the distribution of intra-event residuals is statistically different from the standard normal distribution. This suggests for Sa(1.0) that the magnitude of the intra-event standard deviation of the B10 subduction slab model is too large. The statistical significance of this observation is not overwhelming (as evident by the empirical distribution of the intra-event residuals only just intersecting the KS confidence bounds), and it was not observed over the majority of vibration periods examined (see appendix for further details).

Similar to the results for Sa(0.0), Figure 43f illustrates that the inter-event residuals obtained using the B10 slab model show no bias with respect to source depth (h). Figure 43g illustrates that there is a minor under- and over-prediction for site class B and D Sa(1.0) amplitudes and no bias for site class A and C amplitudes. There is however a noticeable under-prediction of the amplitudes of site class E events. Closer examination of the empirical dataset from subduction slab events illustrated that a large portion of these site class E empirical records come from a few sites which exhibit pronounced site-specific near-surface responses (e.g. Fry et al. 2010, Figure 8). As was previously conveyed with reference to active shallow crustal events, empirical ground motion models will always be inadequate in accounting for such site-specific response of soft soil deposits and therefore it is recommended that seismic hazards at such sites are estimated via site-specific site response analysis. Notwithstanding the aforementioned comment, this model still provides predictions for site class E sites, but these predictions are intended to represent non-site specific amplitudes, and hence the bias observed (which is only apparent at Sa(1.0) and not at other vibration periods) is not used to modify the site response portion of the B10 slab model further.

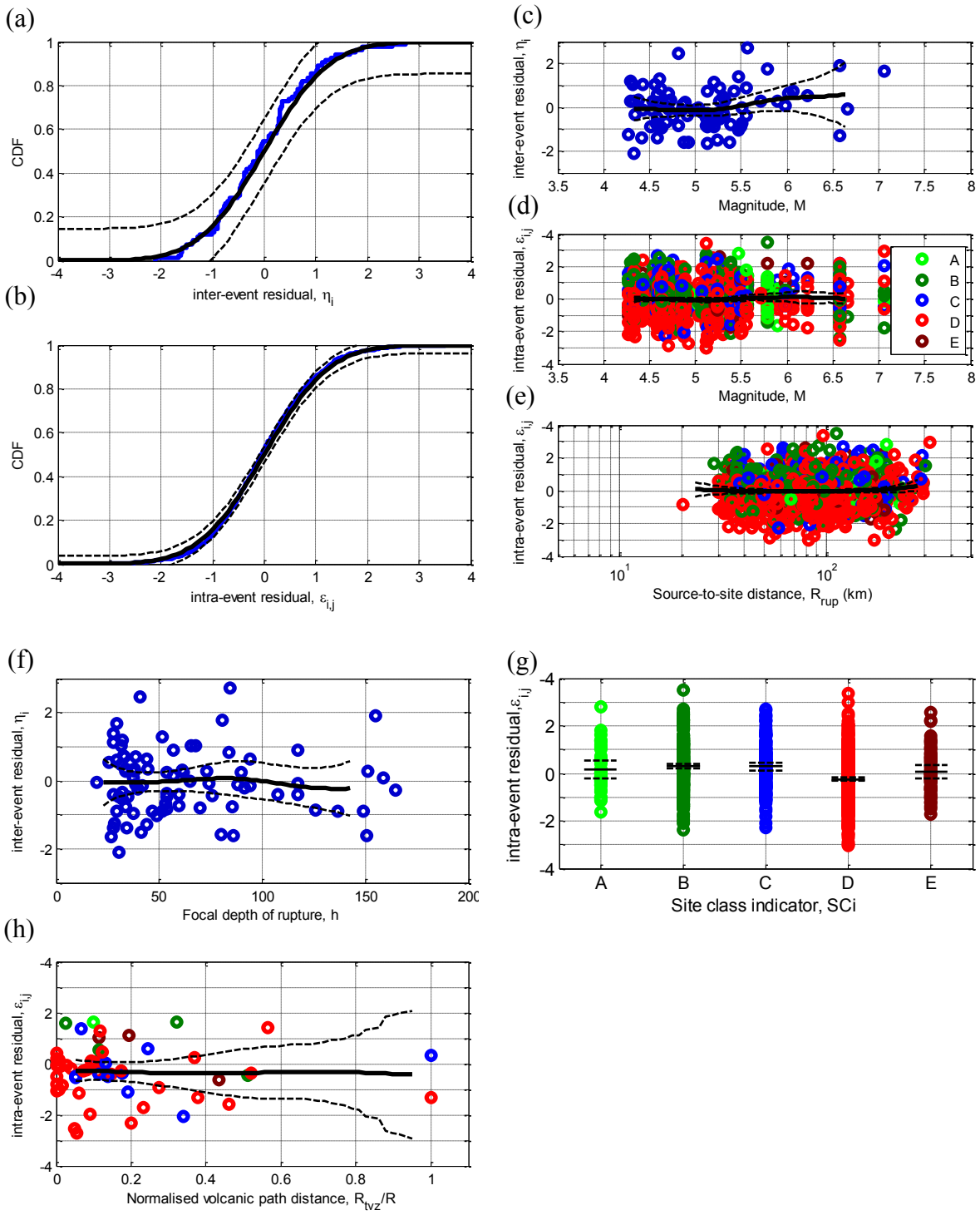

Figure 42: Residuals for Sa(0.0) using the B10 slab model: (a)&(b) distribution of inter- and intra-event residuals; (c)&(d) inter- and intra-event residuals as a function of magnitude; (e) intra-event residuals as a function of distance; (f) inter-event residuals as a function of depth; (g)&(h) intra-event residuals as a function of site class and normalised volcanic path distance.

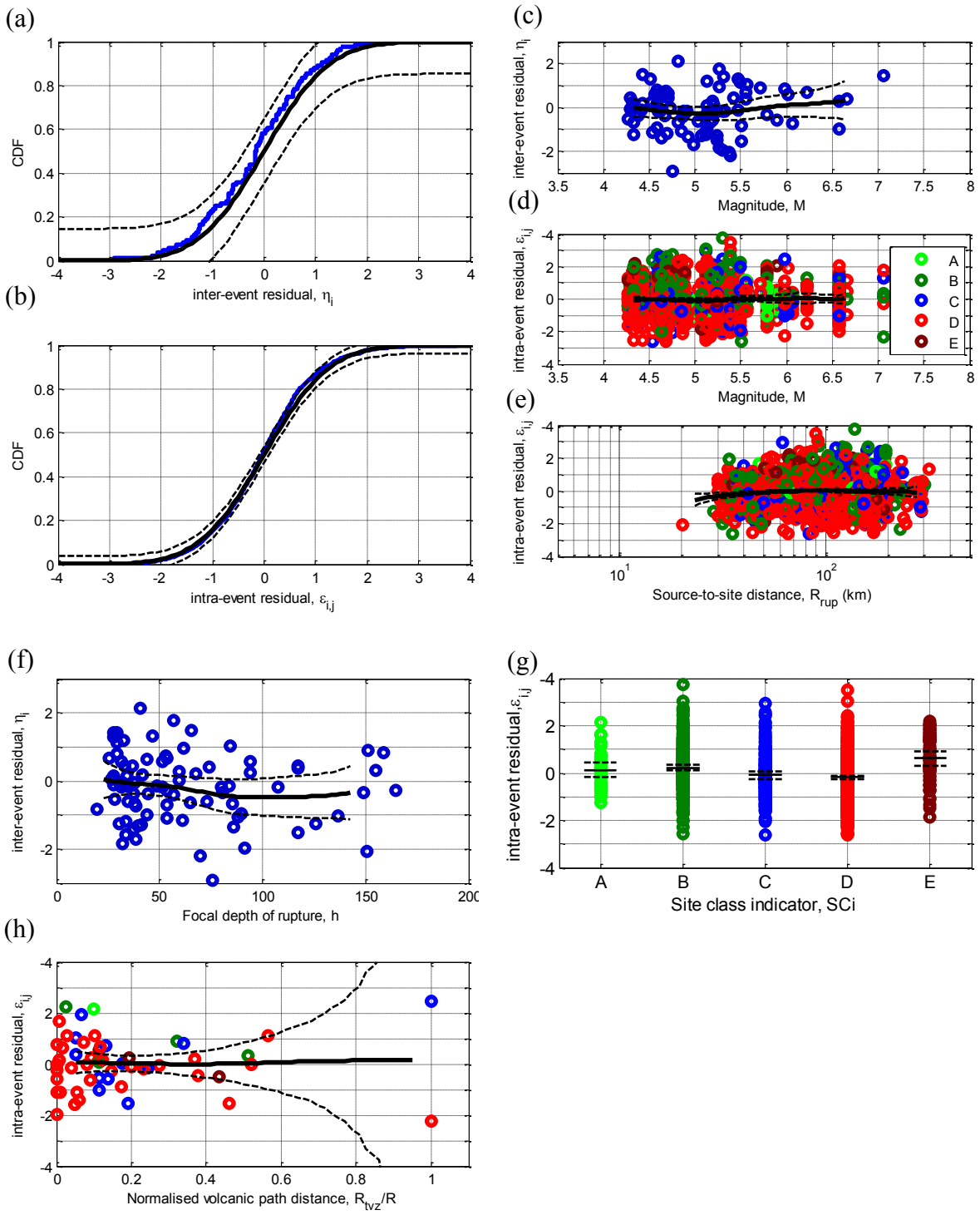

Figure 43: Residuals for Sa(1.0) using the B10 slab model: (a)&(b) distribution of inter- and intra-event residuals; (c)&(d) inter- and intra-event residuals as a function of magnitude; (e) intra-event residuals as a function of distance; (f) inter-event residuals as a function of depth; (g)&(h) intra-event residuals as a function of site class and normalised volcanic path distance.

7.5. Standard deviation of the inter- and intra-event residuals

As was noted with respect to the B10 active shallow crustal model, the median of a GMPE represents only one aspect of the predicted distribution of spectral amplitudes that such GMPEs provide. The other component of equal importance is the standard deviation of the model. Therefore, in addition to examining the inter- and intra-event residuals for bias (i.e. that based on the mean), it is also important to examine the precision of the residuals (i.e. that based on the standard deviation).

The NZ database comprises a relatively large number of subduction slab events and recordings compared to active shallow crustal recordings (i.e. Table 2), and therefore it is possible to make more meaningful inferences as to the precision of the B10 subduction slab model than was possible for the B10 active shallow crustal model. However, in examination of the standard deviation of the inter- and intra-event residuals emphasis was still given primarily to the identification of systematic trends which were apparent over multiple vibration periods considered. The two key features of the standard deviation model for consideration are: (i) the size of the inter- and intra-event standard deviations; and (ii) the magnitude dependence of the standard deviation of the inter- and intra-event residuals. Figure 42a and Figure 42b illustrated that the distribution (i.e. the median and standard deviation) of the normalised inter- and intra-event residuals for Sa(0.0) was not statistically different from the standard normal distribution (Figure 43a and Figure 43b illustrated a similar trend for Sa(1.0), and other vibration periods can be found in the appendix).

The aforementioned observations suggest that the size of the inter- and intra-event standard deviations of the B10 model is approximately correct. Further insight can however be obtained from examining the standard deviation of the observed residuals as a function of predictor variables such as magnitude. Figure 44 illustrates that the standard deviations of both the inter- and intra-event residuals for Sa(0.0) using the B10 subduction slab model are not statistically different from (the theoretical value of) one for a range of magnitudes. It can be seen that the confidence bounds on the standard deviation of the inter-event residuals for subduction slab events is notably less than those for active shallow crustal events (i.e. Figure 29), however there is still significant uncertainty in the point estimate of the standard deviation of the intra-event residuals for subduction slab events. As magnitude dependent (heteroskedastic) standard deviation models generally exhibit a reduction in standard deviation with increasing magnitude (including the B10 subduction slab model), then it would be expected that if such magnitude dependence is not apparent in the NZ database, there would be a positive trend of increasing standard deviation in the residuals with increasing magnitude. Figure 44a illustrates that while the point estimate of the standard deviation of the intra-event residuals increases slightly with magnitude, that this increase is not statistically significant (as can be seen from the confidence interval always including the theoretical value of 1.0).

The standard deviations of the residuals for other vibration periods are presented in the appendix. With the exception of Sa(5.0) which is poorly constrained by the empirical data, in summary the subduction slab events and recordings in the NZ database do not provide any evidence to suggest that the size or magnitude dependence of the B10 subduction slab standard deviation model produces significant imprecision in the estimated inter- and intra-event residuals.

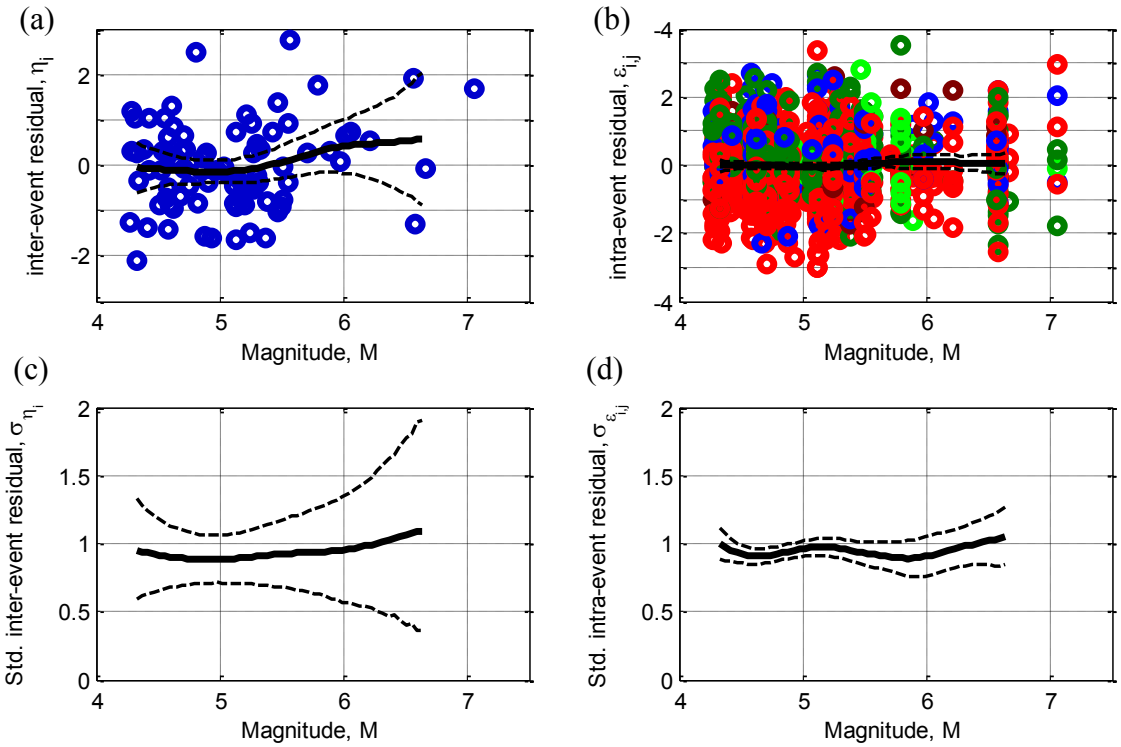

Figure 44: Inter- and intra-event residuals and their standard deviation as a function of magnitude for Sa(0.0) using the B10 slab model.

8. APPLICABILITY OF FOREIGN PREDICTION EQUATIONS FOR SUBDUCTION INTERFACE EARTHQUAKES

8.1. Foreign subduction interface ground motion prediction equations considered

The applicability of three different GMPEs for subduction interface events were examined. Firstly, the McVerry *et al.* (2006) (McV06) model was considered, as it represents the present model used for NZ-specific seismic hazard studies when subduction interface events are of importance. Secondly, the Japanese-based model of Zhao *et al.* (2006) (Z06) was considered because of its extensive empirical database, and also because of the similarity of ground motions in Japan and New Zealand noted by previous researchers (Zhao et al. 1997). Finally, the Atkinson and Boore (2003) (AB03) GMPE based on world-wide empirical data was also considered. The Youngs *et al.* (1997) model, which was also utilized in the most recent update of the USGS national seismic hazard maps (Petersen et al. 2008), was not considered because it does not provide a distinction between inter- and intra-event standard deviations making it impossible to partition total residuals into inter- and intra-event components.

8.2. Qualitative comparison of GMPEs considered

Before examining the statistics of the inter- and intra-event residuals of the NZ database, using each of the subduction interface GMPEs considered, it is insightful to examine the scaling of the GMPEs as a function of several predictor variables. As with similar previous sections, only sufficient results to convey the general predictor variable scaling of each of the models are given here. Additional results for other vibration periods may be found in the appendices.

8.2.1. Magnitude scaling of median

Figure 45 illustrates the magnitude scaling of the median of the three subduction interface GMPEs considered for both Sa(0.0) (i.e. PGA) and Sa(2.0). Similar to the observations for subduction interface events, it can be seen that at small magnitudes the AB03 model predicts significantly smaller spectral amplitudes than the McV06 and Z06 models. The McV06 model predicts the largest spectral amplitudes for small magnitude events. The Z06 model predicts only slightly smaller Sa(0.0) amplitudes than the McV06 model at small magnitudes, but significantly smaller Sa(2.0) amplitudes. At large magnitudes (i.e. $M_w > 7.5$) the three models also display significantly different magnitude scaling. The AB03 model exhibits complete magnitude saturation for Sa(0.0), while the reduction in magnitude scaling for the McV06 is less pronounced. Similar to the observations made for active shallow crustal and subduction slab events, the Z06 model exhibits a significantly less pronounced reduction in magnitude scaling at large magnitudes.

The discrepancy between the three models at large magnitudes is concerning, given the importance of such events in seismic hazard studies, and the lack of large-magnitude well-recorded subduction interface events in the NZ database with which the applicability of such large magnitude scaling for NZ can be scrutinized. The Z06 model utilized an empirical database with three well-recorded subduction interface events above $M_w = 7$, including the $M_w = 8.29$ 2003 Tokachi-Oki event (319

records), and its $M_w = 7.37$ aftershock (222 recordings). Conversely, the McV06 model was developed from an empirical database containing only 7 subduction interface events, none of which were well recorded. The AB03 contains 11 subduction interface events with $M_w > 7$, with the best recorded having 23 ground motion records.

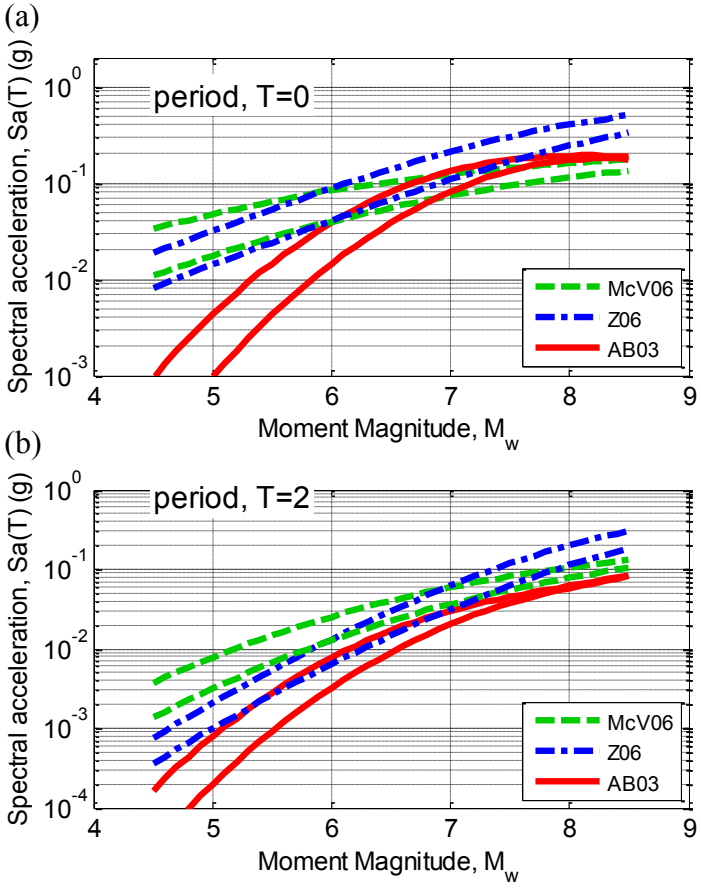

Figure 45: Magnitude scaling of the considered subduction interface GMPEs for two source-to-site distances of 15 and 25 km: (a) Sa(0.0); and (b) Sa(2.0) (predictions for site class C and focal depth 15km).

8.2.2. Path scaling of median

Figure 46 illustrates the path scaling of the median of the three subduction interface GMPEs considered for both Sa(0.0) and Sa(2.0). In general, the path scaling of GMPEs can be separated into: (i) near-source scaling considering the finite dimension of the fault source; (ii) geometric spreading at moderate to large distances; and (iii) anelastic attenuation at large distances. The different functional forms adopted for each of these three aspects of path scaling for the considered models are discussed below.

Figure 46a illustrates that the AB03 model exhibits the most pronounced near-source saturation for both Sa(0.0) and Sa(2.0), followed by the McV06 model and then the Z06 model. The less pronounced near-source saturation for the Z06 model coupled with the aforementioned large magnitude scaling leads to large ground motions at near source distances (e.g. from Figure 46a a median PGA of 0.4g at 15km from a M_w = 7.5 event, compared with approximately 0.2g predicted by the AB03 and McV06 models).

The path scaling of the three different models at moderate to large distances (i.e.

beyond where finite fault effects are significant), are relatively similar, with one notable exception being the very low attenuation of Sa(2.0) amplitudes from a $M_w = 7.5$ event predicted by the AB03 model (Figure 46b).

At large distances, both the Z06 and AB03 models include an anelastic attenuation term, but the McV06 model does not (although an anelastic attenuation term for TVZ attenuation is considered). This absence of anelastic attenuation in the McV06 model is evident in the lack of reduction in Sa(0.0) amplitudes at large distances in Figure 46a. The magnitude of the anelastic attenuation coefficient in the AB03 model, which ranges from 0.002 at short periods and tending to zero for periods greater than 2 seconds, is notably lower than the Z06 model values of 0.0056 at short periods to 0.0015 at long periods.

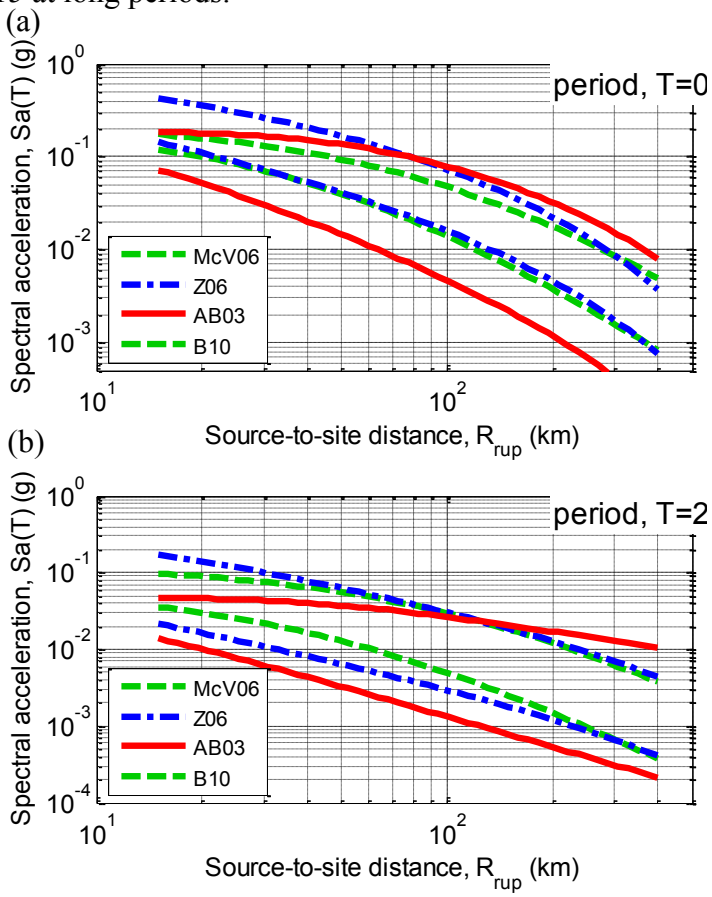

Figure 46: Path scaling of the considered subduction interface GMPEs for two magnitudes of 6 and 7.5: (a) Sa(0.0); and (b) Sa(2.0) (predictions for site class C and focal depth 15km).

8.2.3. Median response spectra (vibration period scaling)

Figure 47 illustrates the median response spectra predicted by the three considered GMPEs for magnitudes 5.5 and 7.5 and path distances of 25 and 100 km. For the magnitudes and path distances considered it can be seen that the shape of the predicted AB03 spectra is significantly 'flatter' than that for the McV06 and Z06 models. It can also be seen that the AB03 spectra for $M_w = 5.5$ are lower as a result of the aforementioned magnitude scaling. Similarly, for M_w =7.5 the Z06 model predicts higher spectral amplitudes as a result of the Z06 large magnitude scaling. One final observation is the unsmoothed nature of the McV06 predicted spectral amplitudes with period.

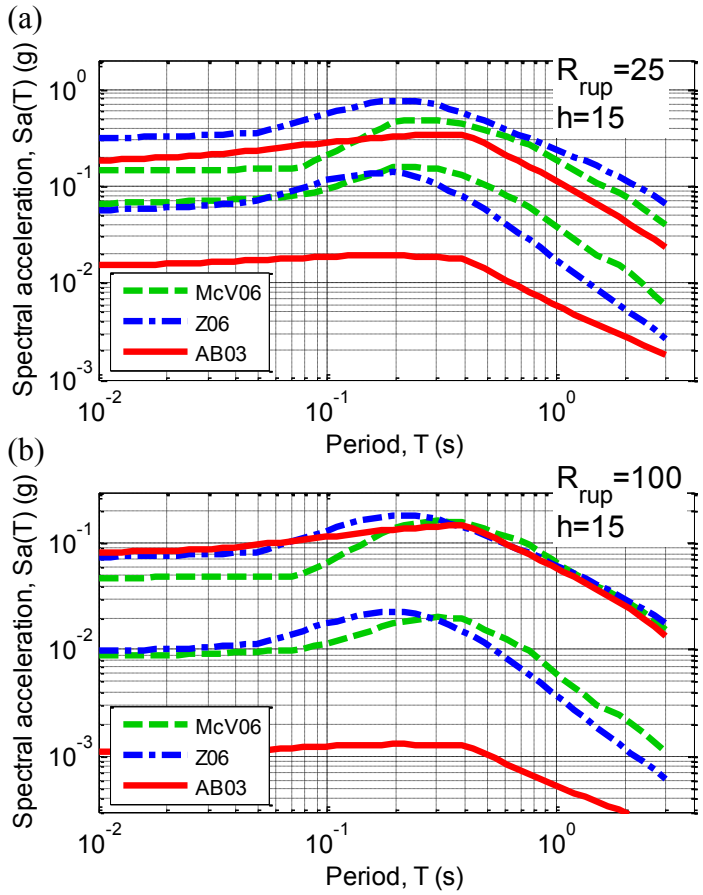

Figure 47: Median response spectra of the considered subduction interface GMPEs for two magnitudes of 5.5 and 7.5: (a) R_{rup}=25km, h =15 km; and (b) R_{rup}=100km, h =15km.

8.2.4. Magnitude and period dependence of model standard deviations

The McV06, Z06 and AB03 models use the same inter- and intra-event standard deviations for both subduction slab and subduction interface models. Hence, refer to section 6.2.4 for a discussion on the inter- and intra-event standard deviations of these models.

8.3. Observed inter- and intra-event residuals from the NZ database

Now that insight has been obtained as to some of the general predictor variable scaling features of the considered subduction interface GMPEs, it is possible to thoroughly examine the statistics of the observed inter- and intra-event residuals of the NZ database for each of the considered models. This section presents only sufficient results (for a single vibration period) to convey the general observations of the inter- and intra-event residuals as a function of predictor variables for each of the models. More elaborate results for vibration periods of 0.0, 0.2, 0.5, 1.0, and 5.0 seconds (or 3.0 seconds if the model was not applicable for 5.0 seconds) are given in the appendices. In particular, there are very few recording with non-zero propagation distances through the Taupo Volcanic Zone (TVZ) such that no statistically significant trends can be inferred. Hence, TVZ dependence is not discussed herein (see appendix for further details of residuals with TVZ distance).

In the examination of the cumulative distribution of the residuals, the Kolmogorov-Smirnov goodness-of-fit test (Ang and Tang 2007) is used to identify

statistically significant departures from the residuals having a standard normal distribution. Furthermore, in order to illustrate the key trends in the observed residuals as a function of the predictor variables, non-parametric regression (Wasserman 2006) of the mean is used. In addition to this non-parametric mean, the 98% confidence interval of the mean is also computed from the Student's *t*-distribution (as a result of η_i and $\varepsilon_{i,j}$ having normal distributions) (Ang and Tang 2007). The non-parametric mean and its confidence interval are shown in subsequent figures with solid and dashed lines, respectively, and can be used to identify statistically significant biases in the prediction models. The high level of confidence used is based on the desire to only identify high significance biases.

Finally, it is noted that there are only 296 ground motion records from subduction interface events in the NZ database in comparison to the 641 and 1500 records from crustal and subduction slab events, respectively. Hence, the inter- and intra-event residuals for subduction interface events provide the least robust evidence on the applicability (or lack thereof) of the three GMPEs considered relative to previous comparisons for active shallow crustal and subduction slab events. Nonetheless, it was still found that there was sufficient empirical data to establish a hierarchy of the three considered models.

8.3.1. McVerry et al. (2006), McV06.

Figure 48 illustrates the observed inter- and intra-event residuals for Sa(1.0) from the NZ database using the McV06 model. Similar to the observations for active shallow crustal and subduction slab events it is immediately apparent that the McV06 model significantly over-predicts ground motions from $M_w < 6$ events (Figure 48a and Figure 48c). This over-prediction is relatively minor at short vibration periods, but increases with increasing vibration period. Figure 48e also illustrates that there a dependence of the intra-event residuals as a function of source to site distance for distances less than 100km and vibration periods larger than 0.5 seconds.

Figure 48f illustrates that there is no apparent trend in the inter-event residuals as a function of source depth. Figure 48g illustrates that the McV06 model over-predicts spectral amplitudes for site class A and B sites and under-predicts spectral amplitudes for site class E sites.

8.3.2. Zhao et al. (2006), Z06.

Figure 49 illustrates the observed inter- and intra-event residuals for Sa(1.0) from the slab NZ database using the Z06 model. It can be seen in Figure 49c that there is essentially no bias of the inter-event residuals as a function of magnitude for all spectral periods considered. Figure 49a and Figure 49c illustrate that there is a constant bias in the inter-event residual, but this was only observed for Sa(1.0). One point of note, not apparent in Figure 49, is the large over-prediction of the 2009 $M_w = 7.63$ event (Fry et al. 2010), which had an inter-event residual of approximately -2 for periods of 0.0, 0.2, and 0.5. Figure 49e illustrates that there is also no observed bias in the intra-event residuals with source-to-site distance.

Figure 49b illustrates that the standard deviation of the intra-event residuals is less than that for a standard normal distribution as indicated by the empirical distribution intersecting the KS bounds. This is a possible result of the Z06 model having a relatively large standard deviation in comparison with the McV06 and AB03 models.

Figure 49f illustrates that there is negligible dependence of the inter-event

residuals as a function of source depth. Figure 49g illustrates that while there is all small bias in the site class B and D predictions for Sa(1.0) (as indicated mean of the intra-event residuals being statistically different from zero). At all vibration periods except for Sa(5.0) site class B motions were over-predicted, while site class C and D motions were also biased for Sa(0.5) and Sa(1.0), respectively.

8.3.3. Atkinson and Boore (2003), AB03.

Figure 50 illustrates the observed inter- and intra-event residuals for Sa(1.0) from the slab NZ database using the AB03 model. It can be seen immediately in Figure 50a and Figure 50c that the AB03 model significantly under-predicts spectral amplitudes from ground motions in the NZ database. This can be interpreted from the magnitude scaling of the AB03 model illustrated in Figure 45. Figure 50e also illustrates that there is a dependence of the intra-event residuals as a function of path distance (some of which may be caused by the poor magnitude scaling).

Figure 50f and Figure 50g illustrate the dependence of the residuals on source depth and site class, respectively. While it appears that there is little dependence of the AB03 model with respect to these predictor variables it is difficult to robustly state this given the significantly poor predictions with respect to magnitude and distance.

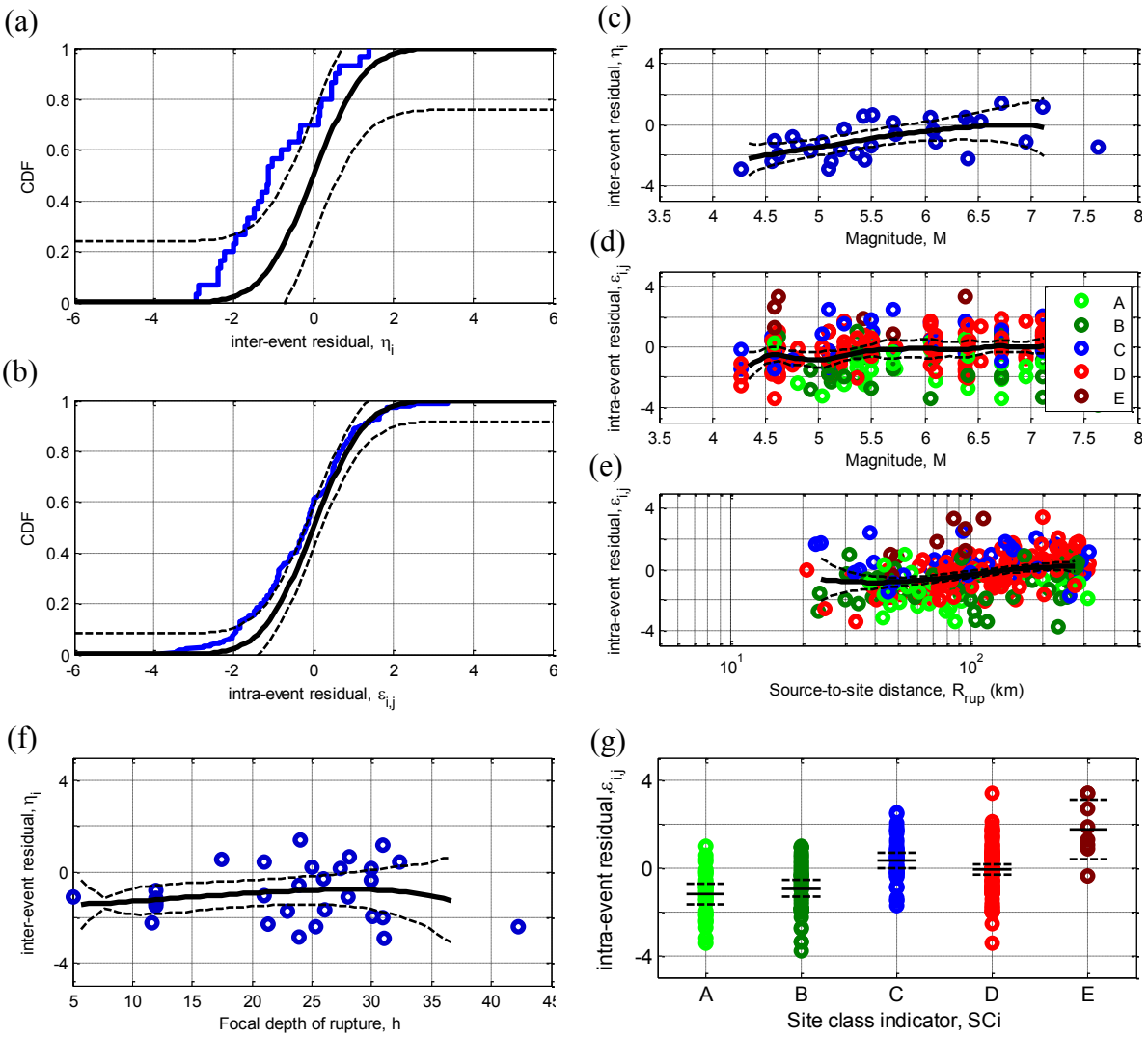

Figure 48: Residuals for Sa(1.0) using the McV06 model: (a)&(b) distribution of inter- and intra-event residuals; (c)&(d) inter- and intra-event residuals as a function of magnitude; (e) intra-event residuals as a function of distance; (f) inter-event residuals as a function of depth; and (g) intra-event residuals as a function of site class.

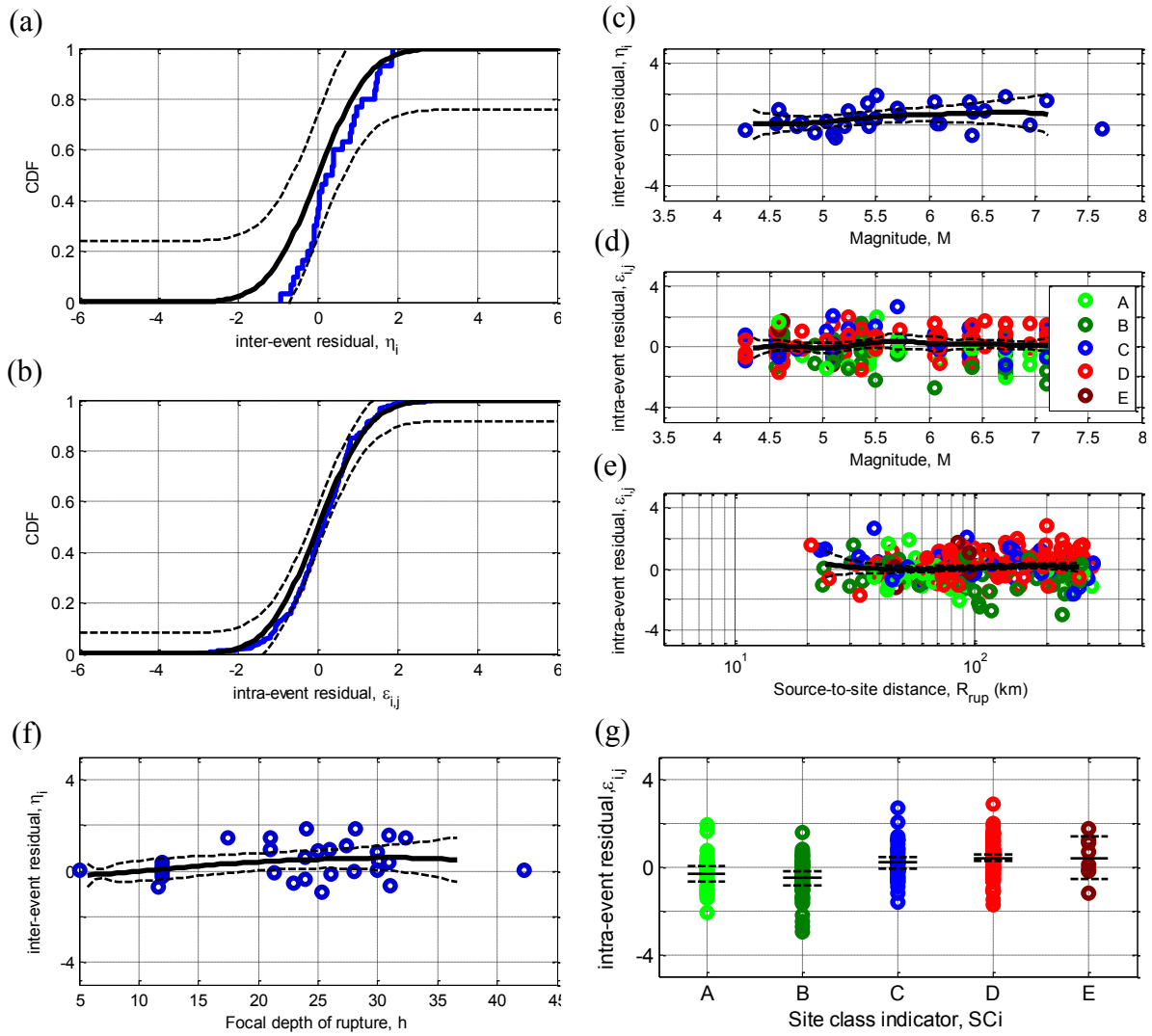

Figure 49: Residuals for Sa(1.0) using the Z06 model: (a)&(b) distribution of inter- and intra-event residuals; (c)&(d) inter- and intra-event residuals as a function of magnitude; (e) intra-event residuals as a function of distance; (f) inter-event residuals as a function of depth; and (g) intra-event residuals as a function of site class.

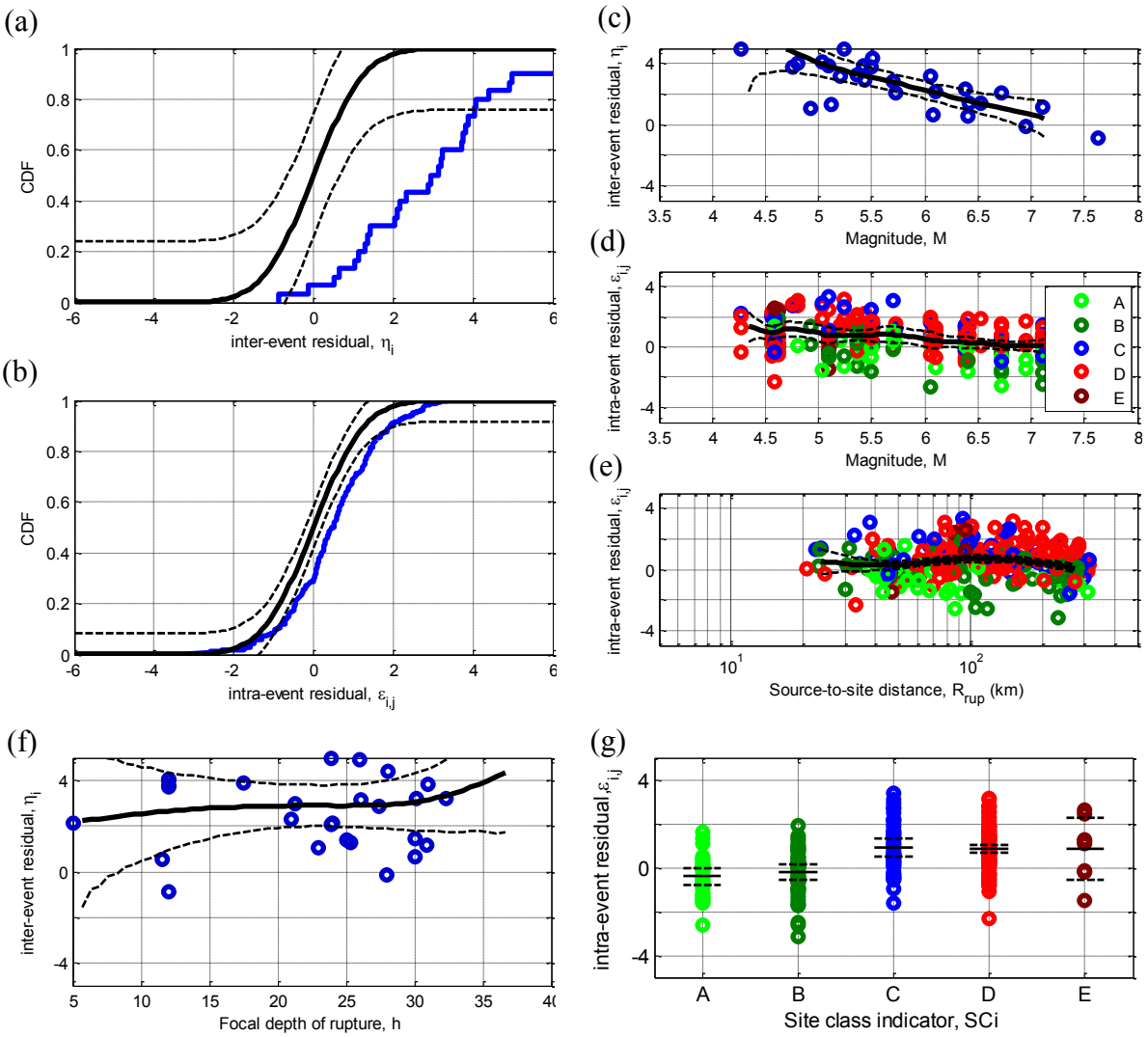

Figure 50: Residuals for Sa(1.0) using the AB03 model: (a)&(b) distribution of inter- and intra-event residuals; (c)&(d) inter- and intra-event residuals as a function of magnitude; (e) intra-event residuals as a function of distance; (f) inter-event residuals as a function of depth; and (g) intra-event residuals as a function of site class.

9. NZ-SPECIFIC SUBDUCTION INTERFACE MODEL

9.1. "Base-model" adopted

The three GMPEs considered for subduction interface events in NZ were shown in the previous section to vary in applicability based on the observed inter- and intra-event residuals. It was relatively clear that of these three models, the Z06 model was the most applicable to NZ in its present form with only bias observed for the site response model, and possible over-prediction of large magnitude events. Furthermore, of the three models considered, the Z06 model also arguably uses the most comprehensive ground motion database, an important consideration given the limited number of records in the NZ database upon which the trends in the inter- and intra-event residuals have been observed. Hence, the Z06 model was adopted as a starting point for further development of a NZ-specific subduction interface model.

9.2. Modifications of base-model to develop a NZ-specific subduction interface model

Based on theoretical considerations and empirical observations from Figure 36 (and the additional figures in the appendix) four modifications are required in order to rectify the observed predictor variable dependence of the inter- and intra-event residuals of the Z06 model: (i) NZ-specific magnitude scaling; (ii) consideration of the increased TVZ attenuation; (iii) site response model; and (iv) possible revision of the standard deviation model.

These four modifications of the Z06 model noted above were done so using subsets of the NZ database in order to separate these effects as much as possible. Below, justification is provided for the functional and/or parametric modification for each of these four points, and the resulting features of the NZ-specific subduction interface (B10) model are examined.

9.2.1. Modification for NZ magnitude scaling

It was observed that the Z06 model provided a generally good prediction of spectral amplitudes as a function of magnitude. On notable exception was the significant over-prediction of the recent $M_w = 7.63$ Dusky Sound earthquake (Fry et al. 2010). While this event represents only a single point on the plot of inter-event residuals versus magnitude, clearly the accurate prediction of such large magnitude events is paramount. The possibility that the Z06 model over-predicts such events is clearly a possibility given the poor performance of the Z06 model at large magnitudes for active shallow crustal and subduction slab events already examined previously in the present work. For this reason, preliminary analyses were conducted using the Chiou and Youngs (Chiou and Youngs 2008) magnitude scaling functional form which has been shown to be applicable for NZ active shallow crustal and subduction slab events.

The same logic as that used for subduction slab events in the previous section was used here to incorporate the CY08 magnitude scaling functional form (i.e. Equations (23) and (24) and the related text). Because it is expected that the response spectral amplitudes from subduction slab and active shallow crustal events will be different, then the value of the parameter c_1 in Equation (24) was initially set such that the prediction of the original Z06 subduction interface model and the modified

model had the same prediction for $\boldsymbol{M} = 6.3$ and 'rock' conditions (i.e. $lny_{i,j}^{CY08}[\boldsymbol{M} = 6.3] = lny^{Z06}[\boldsymbol{M} = 6.3]$ for CY08 reference site $V_{s,1130}$ and Z06 site class A). This 'pivot' magnitude was selected to be the same as the 'corner' magnitude, M_c, of the Z06 model so that the magnitude squared terms have no effect (as previously mentioned they are potentially ill-conditioned), and also because there is a large number of events around a magnitude of 6.3 in the Z06 ground motion database (so the regression equation is expected to be well representative of the empirical data).

Initially the parameters of the CY08 magnitude scaling functional form which were determined for the NZ active shallow crustal and NZ subduction slab events (as presented in previous sections) were utilized. However, it was found that the small magnitude scaling from these coefficients lead to an under-prediction of small magnitude interface events. The parameters c_3 and c_m were consequently modified to provide an unbiased prediction of these small magnitude events which are well constrained by empirical data (see subsequent section for inter- and intra-event residuals).

Figure 51 provides a comparison between the magnitude scaling of the B10, Z06 and McV06 subduction interface models. It can be seen that the B10 model exhibits smaller spectral acceleration ordinates for PGA compared to the Z06 model at all magnitudes, with an increasing difference for large magnitudes. Conversely, Figure 51b illustrates that the B10 and Z06 models are essentially identical for Sa(0.5). Further comparisons for Sa(0.2) and Sa(2.0) are given in the appendix.

9.2.2. Consideration of TVZ attenuation

It has been previously shown for active shallow crustal events that the increased anelastic attenuation through the TVZ has a pronounced effect on response spectral amplitudes. As a result, the same functional form developed for spectral amplitudes from active shallow crustal events, and shown to be also valid for subduction slab events was adopted for subduction interface events. The functional form of the anelastic-portion of path scaling for the B10 subduction interface model is therefore:

$$lny \propto c_\gamma \left(1 + c_{TVZ} \frac{R_{TVZ}}{R_{RUP}}\right) R_{RUP} \tag{36}$$

where c_γ is the anelastic attenuation coefficient with parameter values obtained directly from Z06 (i.e. $c_\gamma^{B10} = b^{Z06}$); R_{RUP} is the closest-distance from the site to the fault rupture plane; R_{TVZ} is the path distance through the TVZ; and c_{TVZ} is an empirical parameter representing the ratio of the TVZ and non-TVZ anelastic attenuations. The adequacy of the Z06 anelastic attenuation coefficient adopted in the B10 model was examined based on the observed intra-event residuals. It was found that this coefficient lead to no significant bias in the residuals at large path distances.

Although there is insufficient empirical data from subduction interface events for validating the applicability of the c_{TVZ} values, given they were found to be appropriate for spectral amplitudes from active shallow crustal and subduction slab events they were deemed applicable for subduction interface events also.

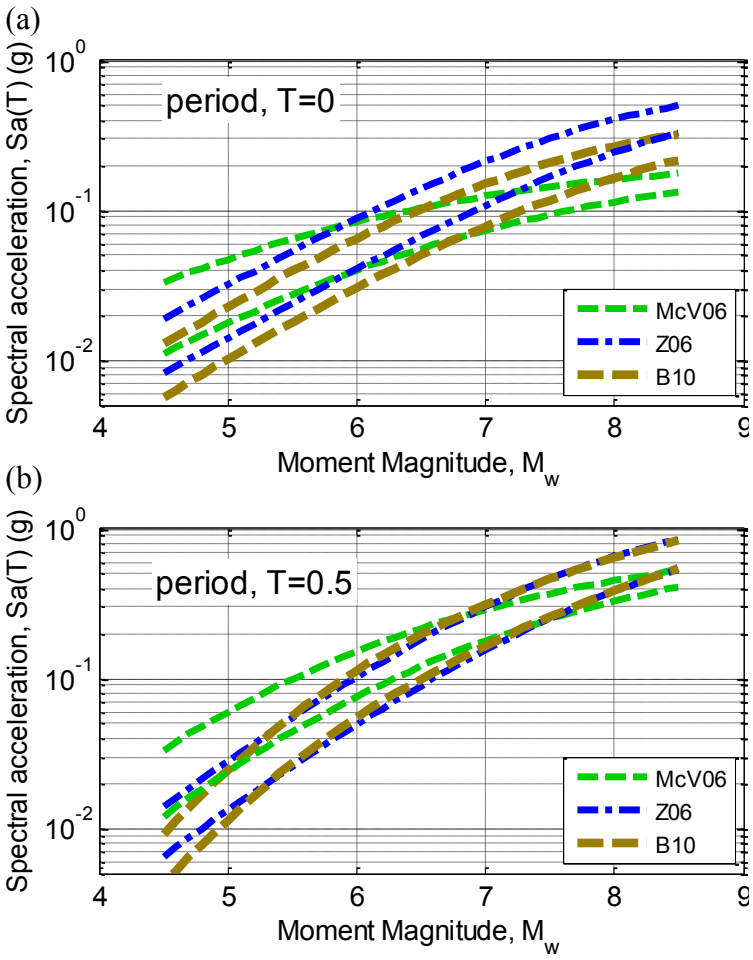

Figure 51: Magnitude scaling of the median B10 subduction interface model compared with the Z06 and McV06 models for path distances of 25 and 50 km: (a) Sa(0.0); and (b) Sa(0.5) (predictions for site class C, focal depth 40km).

9.2.3. Modification of the site response model

It was noted, with respect to subduction slab events, that the Z06 model uses five discrete site classes and uses a linear site response formulation. Because of the success of the CY08-based site response formulation used in the NZ-specific active shallow crustal and subduction slab B10 models, the same functional form was adopted for the B10 subduction interface model. The effects of site class on predicted response spectra for subduction interface events are shown for two scenarios in Figure 52. Figure 52a and Figure 52b clearly illustrate the effect of non-linear site response which leads to a small amplification (or even de-amplification) of short period spectral ordinates, and a large amplification of longer period spectral ordinates.

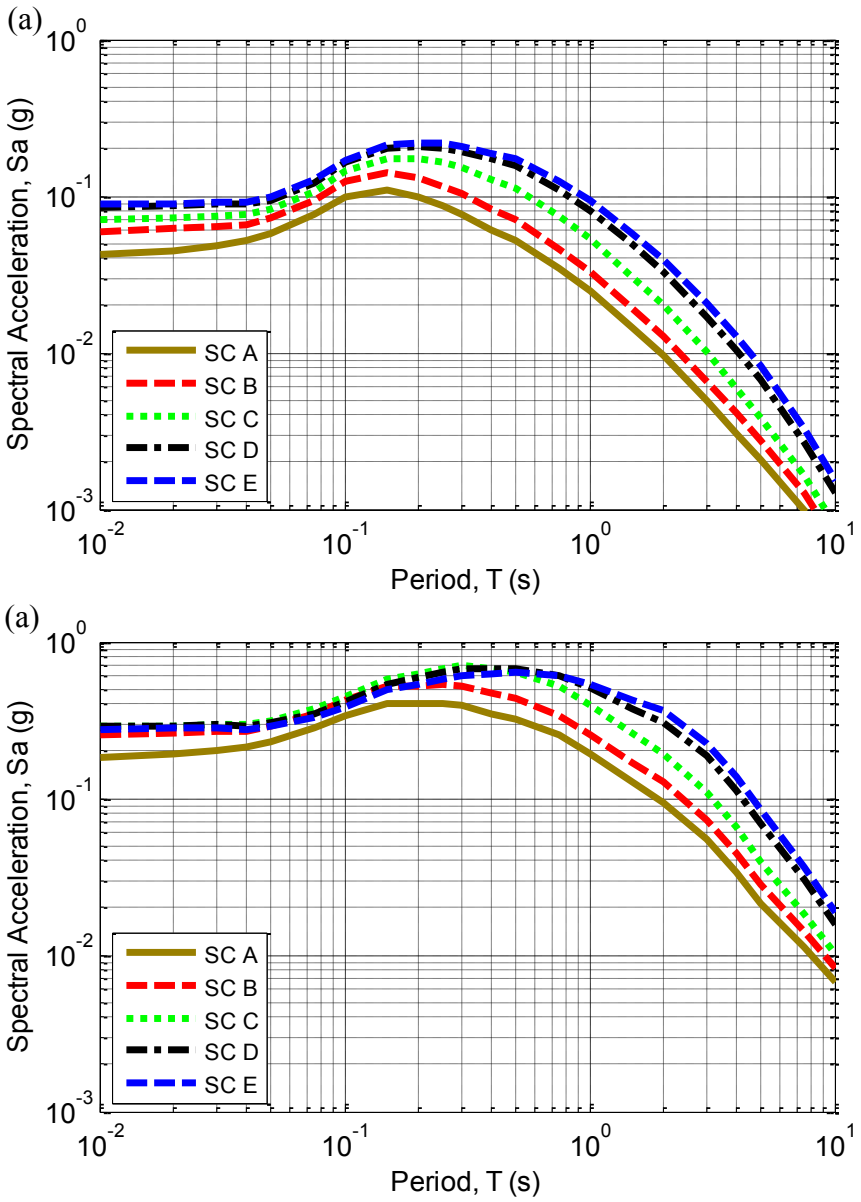

Figure 52: Effect of site class on the predicted response spectra for: (a) a M_w 6 event at distance of 25km; and (b) a M_w 8 event at distance of 25km (depth 15km in both cases).

9.2.4. Modification of the standard deviation model

Figure 49a and Figure 49b provided some evidence that the Z06 model may have a significantly higher standard deviation model than that exhibited by the NZ subduction interface data (Figure 33). As was noted with reference to subduction slab events, the Z06 model was developed using the same functional form for active shallow crustal, subduction interface, and subduction slab events (with the exception of a constant source term and additional geometric spreading for slab events (Zhao et al. 2006)). It was speculated that the use of the simple functional form of the Z06 model applied to these three different source types has lead to the large standard deviations in the Z06 model (as well as the omission of additional functional forms to represent, for example, the apparent reduction in geometric spreading in subduction slab events previously examined).

Because of the success of the CY08 variance model for use in the B10 active shallow crustal and subduction slab models it was also examined whether this same variance model was applicable for characterising the ground motion variability from subduction interface events. The CY08 variance model is functionally more complex than the Z06 model in that it is both magnitude and intensity dependent (Chiou and Youngs 2008). The observed standard deviation of the inter- and intra-event residuals from the NZ database using this variance model (presented in the next section) were found to not be statistically different than the standard normal distribution, and therefore the CY08 variance model was adopted for the B10 subduction interface model.

9.3. Functional form and parameters of the Bradley (2010) subduction interface model

The Bradley (2010) subduction interface model is based on the Z06 subduction interface model with the aforementioned modifications. The complete B10 subduction interface median model formulation is given by:

$$\begin{aligned} ln(y_{ref}) = {} & c_1 + c_7 max(min\{h, 125\} - 15, 0) \\ & + c_2(\boldsymbol{M} - 6) + \frac{c_2 - c_3}{c_n} ln\left(1 + e^{c_n(c_M - \boldsymbol{M})}\right) \\ & - ln[R_{RUP} + c_5 exp(c_6 \boldsymbol{M})] \\ & + c_\gamma \left(1 + c_{TVZ} \frac{R_{TVZ}}{R_{RUP}}\right) R_{RUP} \end{aligned} \tag{37}$$

and

$$\begin{aligned} ln(y) = {} & ln(y_{ref}) + \phi_1 log\left(\frac{min(V_{s30}, V_1)}{1130}\right) + b.ln\left(\frac{y_{ref} + \phi_4}{\phi_4}\right) \\ & + \phi_5 \left(1 - \frac{1}{cosh[\phi_6 max(0, Z_{1.0} - \phi_7)]}\right) + \frac{\phi_8}{cosh[0.15. max(0, Z_{1.0} - 15)]} \end{aligned} \tag{38}$$

where

$$V_1 = min\left(1130. max\left\{\left(\frac{T}{0.75}\right)^{-0.11}, 1\right\}, 1800\right) \tag{39}$$

$$b = \phi_2\left\{e^{\phi_3(min(V_{s30}, 1130) - 360)} - e^{\phi_3(1130 - 360)}\right\} \tag{40}$$

The predictor variables are:

$\boldsymbol{M}$	Moment magnitude
R_{RUP}	Closest distance to the fault rupture plane (km)
R_{TVZ}	Distance of wave propagation through the Taupo Volcanic Zone (TVZ) (km)
h	Focal depth of the fault rupture plane.
V_{s30}	Average shear wave velocity for the top 30m of the site (m/s)
$Z_{1.0}$	Depth to shear wave velocity of 1.0 km/s (m)

The period-independent parameter, c_2, for the B10 subduction interface median model are given in Table 13, while the period-dependent parameters of the reference model are given in Table 14. The site response model for subduction interface events is identical to that of the subduction slab and active shallow crustal models and

coefficients are given in Table 11. It is worthy of note that only the parameters c_1 (constant term), and c_3, c_M (small magnitude scaling) in the B10 interface model were constrained from the NZ database. Parameters c_5, c_6, c_7, c_γ (denoted as c, d, e, and b in Z06, respectively) and c_2, c_n, $\phi_1 - \phi_8$ were fixed at their values in the Z06 and CY08 models, respectively. c_{TVZ} (TVZ scaling) was taken to be the same as that for the B10 active shallow crustal and subduction slab models. The standard deviation model is also identical to that for the NZ-specific subduction slab and active shallow crustal models as given by Equations (32)-(35) and coefficients in Table 12.

Table 13: Period-independent coefficients for the reference model, $ln(y_{ref})$ (Equation (37))

c_2
1.06

Table 14: Period-dependent coefficients for the reference model, $ln(y_{ref})$ (Equation (37))[1]

Vibration Period (s)	c_1	c_3	c_n	c_M	c_5	c_6	c_7	c_γ	c_{TVZ}
pga	0.4066	1.2000	2.9960	5.8500	6.1600	0.4893	0.0512	-0.0056	2.000
0.01	0.5043	1.2030	2.9960	5.8171	6.1600	0.4893	0.0512	-0.0059	2.000
0.02	0.5420	1.2085	3.2920	5.8002	6.1580	0.4892	0.0512	-0.0061	2.000
0.03	0.5997	1.2155	3.5140	5.7866	6.1550	0.4890	0.0511	-0.0063	2.000
0.04	0.6474	1.2238	3.5630	5.7747	6.1508	0.4888	0.0508	-0.0065	2.000
0.05	0.7451	1.2332	3.5470	5.7640	6.1441	0.4884	0.0504	-0.0067	2.000
0.075	1.0574	1.2605	3.4480	5.7406	6.1200	0.4872	0.0495	-0.0073	2.000
0.1	1.3697	1.2924	3.3120	5.7202	6.0850	0.4854	0.0489	-0.0079	2.000
0.15	1.4621	1.3664	3.0440	5.6849	5.9871	0.4808	0.0479	-0.0072	2.000
0.2	1.3986	1.4502	2.8310	5.6544	5.8699	0.4755	0.0471	-0.0066	2.000
0.25	1.2773	1.5905	2.6580	5.6269	5.7547	0.4706	0.0464	-0.0059	2.000
0.3	1.1507	1.7348	2.5050	5.6016	5.6527	0.4665	0.0458	-0.0052	2.500
0.4	0.9124	1.9776	2.2610	5.5560	5.4997	0.4607	0.0445	-0.0042	3.200
0.5	0.7485	2.1668	2.0870	5.5151	5.4029	0.4571	0.0429	-0.0034	3.500
0.75	0.3256	2.6106	1.8120	5.4263	5.2900	0.4531	0.0387	-0.0025	4.500
1.0	0.0271	2.9800	1.6480	5.3500	5.2480	0.4517	0.0350	-0.0022	5.000
1.5	-0.5030	3.3838	1.5110	5.2199	5.2194	0.4507	0.0280	-0.0022	5.400
2.0	-0.8465	3.6246	1.4700	5.2973	5.2099	0.4504	0.0213	-0.002	5.800
3.0	-1.4638	3.6493	1.4560	5.4385	5.2040	0.4501	0.0106	-0.0015	6.000
4.0	-1.8531	3.6100	1.4650	5.5977	5.2020	0.4501	0.0041	-0.0019	6.150
5.0	-2.1662	3.5000	1.4780	5.7276	5.2010	0.4500	0.0010	-0.0024	6.300
7.5	-2.6510	3.4500	1.4980	5.9891	5.2000	0.4500	0.0000	-0.0027	6.425
10.0	-2.9410	3.4500	1.5020	6.1930	5.2000	0.4500	0.0000	-0.0029	6.550

[1]The units for *pga* and *psa* are g's.

9.4. Observed inter- and intra-event residuals of Bradley (2010) subduction interface model

This section presents the inter- and intra-event residuals obtained from applying the B10 subduction interface model to the NZ database. Similar to previous discussions only the inter- and intra-event residuals for vibration periods of 0.0 and 1.0 are presented here. Results for other vibration periods can be found in the appendix.

Figure 53 illustrates the observed inter- and intra-event residuals for Sa(0.0) from the NZ database using the B10 subduction interface model. It can be seen that based on the distributions of the inter- and intra-event residuals alone (i.e. Figure 53a and Figure 53b) that the B10 interface model is unbiased (both with respect to the median and standard deviation). Examination of the magnitude-dependence of the intra-event residuals also reveals no bias. It is also worthy of note that $M_w = 7.63$ event has inter-event residuals of approximately -1 at short periods (i.e. Sa(0.0) and Sa(0.2)) using the B10 subduction interface model, as compared to values of approximately -2 using the Z06 model. Figure 53d and Figure 53e also illustrate that there is no significant bias in the intra-event residuals obtained from the B10 interface model as a function of either magnitude or path distance.

Figure 53f illustrates that there is no significant bias observed for the inter-event residuals as a function of focal depth, h. This is to be expected, given that the same depth scaling as the Z06 model is adopted in the B10 slab model, which also did not exhibit bias (i.e. Figure 49f). Figure 53g illustrates the observed intra-event residuals as a function of site class. It can be seen that there is a slight under-prediction of site class B motions with a mean intra-event residual of approximately 0.4, but no bias for site class A, C, D, and E Sa(0.0) amplitudes.

Figure 54 illustrates the observed inter- and intra-event residuals for Sa(1.0) from the NZ database using the B10 subduction slab model. Similar to the results for Sa(0.0), it can be seen in Figure 54a and Figure 54b that the inter- and intra-event residuals cannot be rejected as different from the standard normal distribution. Figure 54c-Figure 54e also illustrate that the inter- and intra-event residuals do not exhibit any dependence with magnitude or distance.

Similar to the results for Sa(0.0), Figure 54f illustrates that the inter-event residuals obtained using the B10 interface model show no bias with respect to source depth (h). Figure 54g illustrates that there is a minor over-prediction for site class B Sa(1.0) amplitudes, similar to Sa(0.0), but no bias for site class A, C, D, and E amplitudes. The over-prediction of site class B events for Sa(0.0) and Sa(1.0) was not systematic across all vibration periods for subduction interface events. Furthermore, for active shallow crustal and subduction slab events there was no over-prediction bias for site class B (in fact in those active shallow crustal or subduction slab cases where there was a statistically significant bias at a single vibration period it was an under-prediction bias). Therefore it is not considered necessary to revise the site response model for subduction interface events.

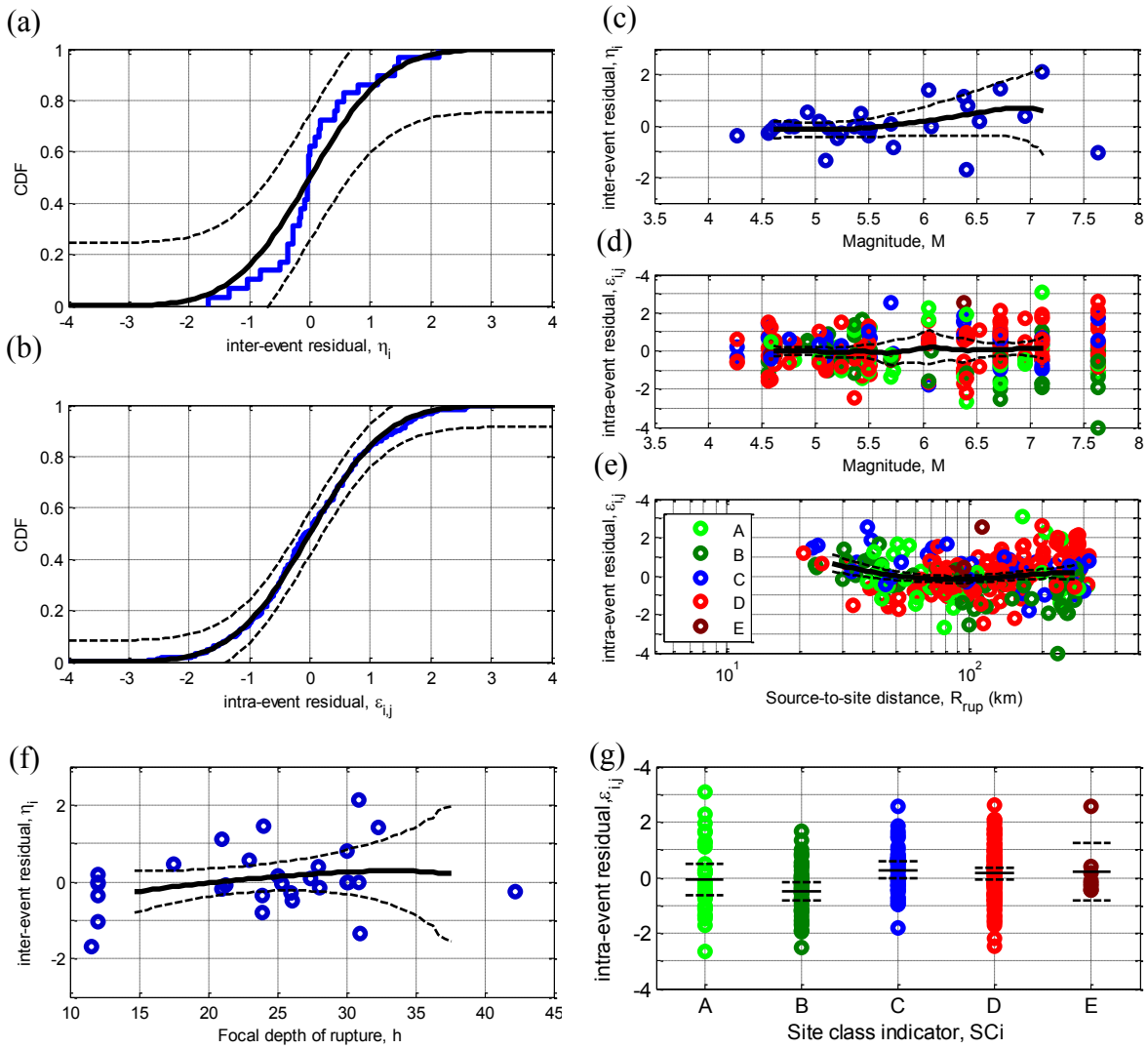

Figure 53: Residuals for Sa(0.0) using the B10 interface model: (a)&(b) distribution of inter- and intra-event residuals; (c)&(d) inter- and intra-event residuals as a function of magnitude; (e) intra-event residuals as a function of distance; (f) inter-event residuals as a function of depth; (g) intra-event residuals as a function of site class.

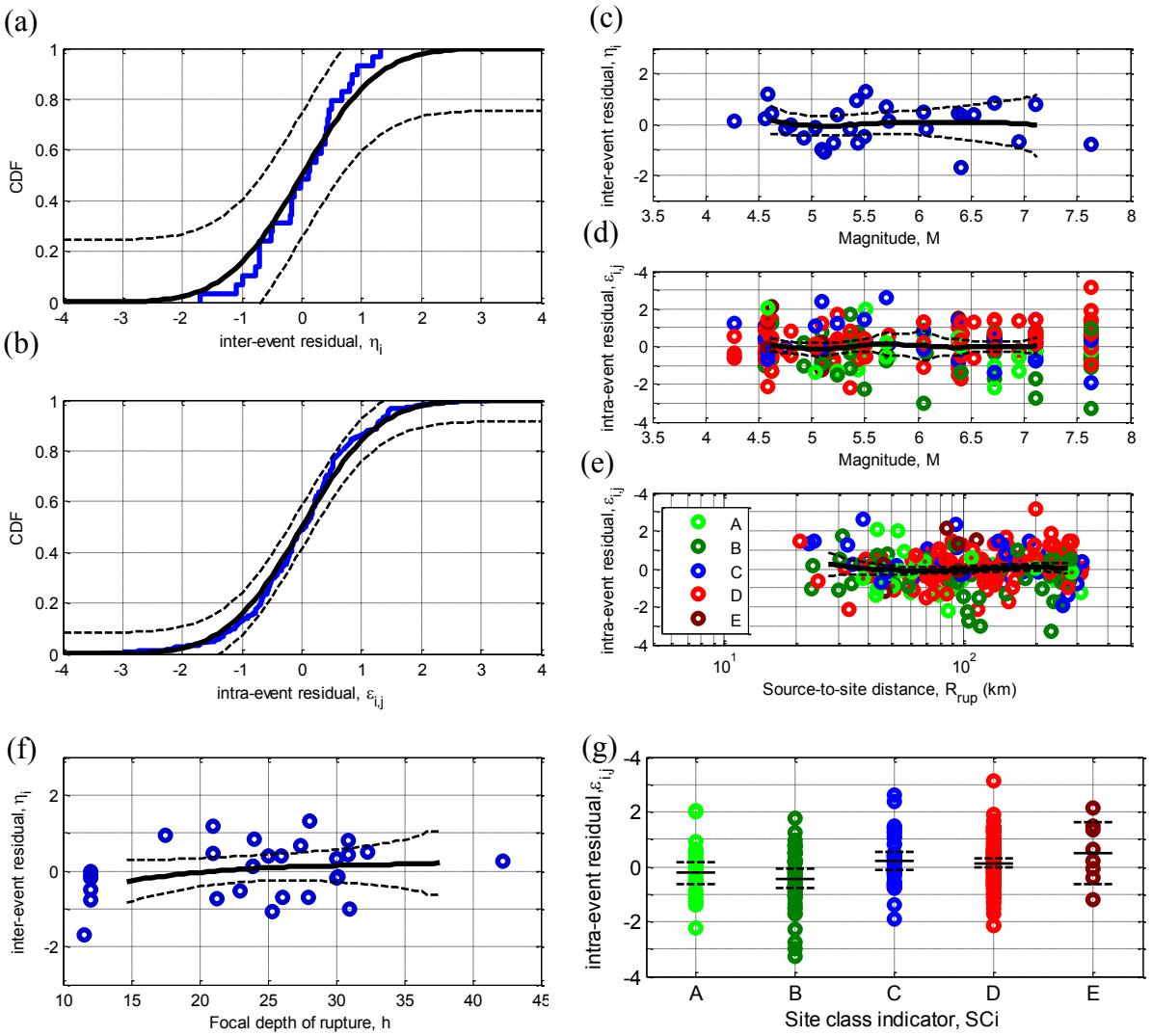

Figure 54: Residuals for Sa(1.0) using the B10 interface model: (a)&(b) distribution of inter- and intra-event residuals; (c)&(d) inter- and intra-event residuals as a function of magnitude; (e) intra-event residuals as a function of distance; (f) inter-event residuals as a function of depth; (g) intra-event residuals as a function of site class.

9.5. Standard deviation of the inter- and intra-event residuals

As was noted with respect to the B10 active shallow crustal and subduction slab models, the median of a GMPE represents only one aspect of the predicted distribution of spectral amplitudes that such GMPEs provide. The other component of equal importance is the standard deviation of the model. Therefore, in addition to examining the inter- and intra-event residuals for bias (i.e. that based on the mean), it is also important to examine the precision of the residuals (i.e. that based on the standard deviation).

The NZ database comprises a relatively small number of subduction interface events and recordings compared to active shallow crustal and subduction slab recordings (i.e. Table 2), and therefore it is difficult to make statistically meaningful inferences as to the precision of the B10 subduction interface model compared to that which was possible for the B10 active shallow crustal and subduction slab models. In examination of the standard deviation of the inter- and intra-event residuals emphasis was still given primarily to the identification of systematic trends which were apparent over multiple vibration periods considered. The two key features of the standard deviation model for consideration are: (i) the size of the inter- and intra-event standard deviations; and (ii) the magnitude dependence of the standard deviation of the inter- and intra-event residuals. Figure 53 and Figure 54 illustrated that the distribution (i.e. the median and standard deviation) of the normalised inter- and intra-event residuals for Sa(0.0) and Sa(1.0), respectively, were not statistically different from the standard normal distribution (other vibration periods can be found in the appendix). This suggests that the size of the inter- and intra-event standard deviations of the B10 subduction interface model (which adopts the CY08 standard deviation model) is approximately correct. Further insight can however be obtained from examining the standard deviation of the observed residuals as a function of predictor variables such as moment magnitude. Figure 55 illustrates that the standard deviations of both the inter- and intra-event residuals for Sa(1.0) using the B10 subduction interface model. It can be seen that for Sa(1.0) (and generally at all other vibration periods examined) that the inter-event standard deviation (i.e. Figure 55d) is not statistically different from the theoretical value of unity, and is not a function of magnitude. Conversely, Figure 55c illustrates that the standard deviation of the (normalised) inter-event residuals is less than unity for small magnitudes (i.e. $M_w < 5.5$). Such an observation appears to be systematic across all vibration periods considered.

Figure 56 compares the inter-event standard deviation of the B10 subduction interface model compared with the Z06 model. while the B10 model has a magnitude dependent standard deviation, it can be seen that the B10 standard deviation model is generally less than the Z06 model, and only becomes notably larger than the Z06 model for vibration periods greater than 1.0 seconds. Hence, while the scatter of the empirical small magnitude data possibly suggest that this inter-event standard deviation should be reduced (which would increase the scatter in the observed inter-event residuals), because of the very small number of subduction interface data it is considered unjustified to make such an adjustment. Furthermore, considering the fact that the intra-event standard deviation is notably larger than the inter-event standard deviation, even a significant reduction in the intra-event standard deviation will not have a significant effect on the total standard deviation. For example, if the inter-event standard deviation of PGA was reduced from 0.34 to 0.26 (i.e. a 25%

reduction), the total standard deviation would only reduce from 0.6893 to 0.65 (i.e. a 6% reduction).

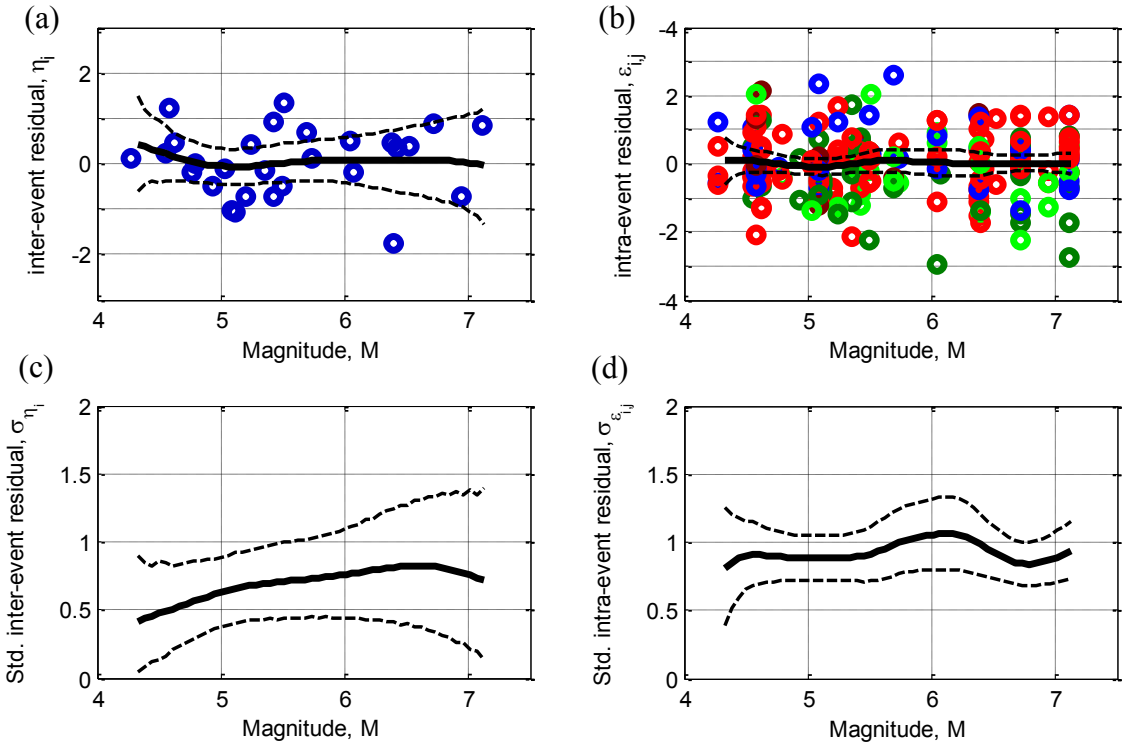

Figure 55: Inter- and intra-event residuals and their standard deviation as a function of magnitude for Sa(1.0) using the B10 interface model.

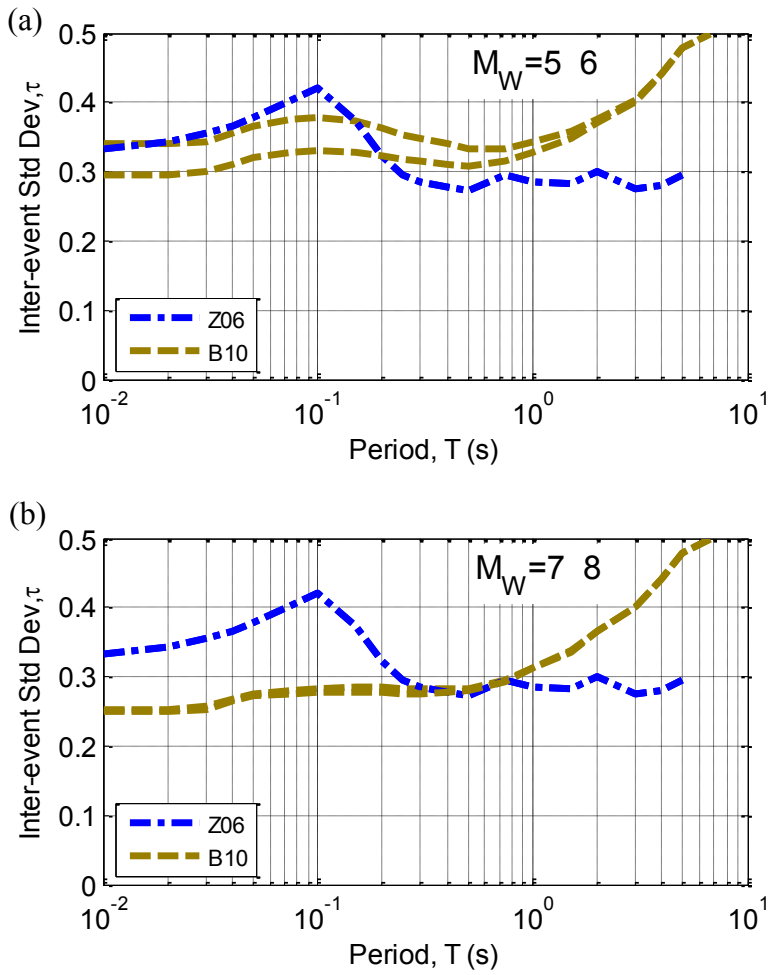

Figure 56: Magnitude and vibration period scaling of the B10 subduction interface standard deviation model in comparison to the Z06 model for: (a) $M_w = 5, 6$; and (b) $M_w = 7, 8$.

10.DISCUSSION

10.1. Comparison of the developed GMPEs with McV06

The McVerry *et al.* (2006) GMPE represents the presently employed model to conduct site-specific PSHA in NZ, upon which the current NZ loadings standard (NZS 1170.5 2004) is also based. Therefore it is informative to consider the efficacy of the developed NZ-specific models (B10) with the McV06 model. The following points represent, in the authors opinion, the key advantages of the presently developed models relative to McV06:

- The B10 models include large magnitude scaling at near-source distances based on global ground motions. The McV06 model used overseas ground motions for such M, R_{rup} scenarios, but the number of data considered were significantly less than that of the CY08 model (and consequently the B10 model).
- The B10 model contains NZ-specific scaling at smaller magnitudes, were the developed NZ database allows a good degree of constrain. It was observed that the McV06 model significantly over-predicted the amplitude of small magnitude events.
- The B10 model contains finite fault effects (both via R_{rup} and also consideration of hanging wall/ footwall effects), not considered in the McV06 model.
- The B10 model provides response spectral amplitudes at the surface of sites with standard site classes A-E used in NZS 1170.5 (2004), but these predictions are based on the use of specific V_{s30} and $Z_{1.0}$ values for each site class. Hence, for site-specific cases in which additional site investigation is performed it is possible to consider site effects in a continuous fashion (i.e. based on $V_{s,30}$ and $Z_{1.0}$ explicitly).
- The B10 model is applicable for 23 vibration periods from 0.0 to 10.0 seconds, compared to the 12 vibration periods from 0.0 to 3.0 seconds in the McV06 model. In particular, the maximum vibration period of 10.0 seconds makes the B10 model more applicable for emerging displacement-based design methods, for which the 3.0 second maximum period of the McV06 model is typically below the displacement response spectra corner period of large magnitude events.
- The B10 model predicts a smooth variation of pseudo-spectral amplitudes as a function of vibration period. This negates the need for post-PSHA smoothing of Uniform Hazard Spectra which are currently used in conjunction with the McV06 model for some studies.

11.CONCLUSIONS

This study has developed ground motion prediction equations (GMPEs) for geometric-mean pseudo-spectral acceleration amplitudes from New Zealand (NZ) earthquakes. The GMPEs were developed from a compiled database of 2437 three-component ground motion records using stringent quality criteria. Because the database is deficient in empirical records from large magnitude events recorded at close distances to the fault rupture plane then the NZ-specific GMPEs are developed based on modifying foreign GMPEs.

For active shallow crustal events, five different GMPEs were considered. It was found that the McVerry *et al.* (2006) model, which is the current model upon which seismic design guidelines and site-specific seismic hazard analyses in NZ are based, provided the poorest fit to the NZ database, and that the Chiou *et al.* (2010) (C10) modification of the Chiou and Youngs (2008) model was the most applicable. Discrepancies between the C10 model and the NZ database that were empirically identified were used to modify the C10 model for: (i) small magnitude scaling; (ii) scaling of short period ground motion from normal faulting events in volcanic crust; (iii) scaling of ground motions on very hard rock sites; (iv) anelastic attenuation in the NZ crust; and (v) consideration of the increased anelastic attenuation in the Taupo Volcanic Zone (TVZ).

For subduction slab events, three models were considered. It was found that all of the models had some significant biases with respect to applicability for NZ. The Zhao et al. (2006) (Z06) was selected because of the rigorous database upon which it was developed and modified by: (i) NZ-specific scaling at small magnitudes; (ii) path scaling at large distances; (iii) consideration of the increased TVZ attenuation; and (iv) revision of the standard deviation model. Based on these modifications the developed model showed no bias of the inter- and intra-event residuals as a function of various predictor variables. The standard deviation of the residuals using the revised standard deviation model also indicated that the model has an adequate precision.

Three GMPEs were considered for subduction interface events. The Zhao *et al.* (2006) (Z06) was the best performing model with only bias exhibited in the site response model, and possible over-prediction of large magnitude events. The Z06 interface model was modified to account for site response and magnitude scaling using the same functional forms as those of the developed active shallow crustal and subduction slab models. The developed model showed no bias of the inter- and intra-event residuals as a function of various predictor variables.

The developed GMPEs include specific features as evident in the NZ database; consistent scaling for parameters not well constrained by the NZ database; and pseudo-spectral amplitudes for vibration periods from 0.01 to 10 seconds. Hence, these models represent a significant advance in the state-of-the art for empirical ground motion prediction in NZ.

12.ACKNOWLEDGEMENTS

The author greatly appreciates the assistance of Dr. John Zhao who provided the initial ground motion database used in this study.

13.REFERENCES

Abrahamson, N. A., Atkinson, G. M., Boore, D. M., Bozorgnia, Y., Campbell, K. W., Chiou, B., Idriss, I. M., Silva, W. J., Youngs, R. R., 2008. Comparisons of the NGA Ground-Motion Relations, *Earthquake Spectra*, **24**, 45-66.

Abrahamson, N. A., Silva, W. J., 2008. Summary of the Abrahamson & Silva NGA ground motion relations, *Earthquake Spectra*, **24**, 67-97.

Ang, A. H. S., Tang, W. H., 2007. *Probability concepts in engineering: Emphasis on applications in civil and environmental engineering*. John Wiley & Sons.

Atkinson, G. M., 2008. Ground-Motion Prediction Equations for Eastern North America from a Referenced Empirical Approach: Implications for Epistemic Uncertainty, *Bulletin of the Seismological Society of America*, **98**, 1304-1318.

Atkinson, G. M., Boore, D. M., 2003. Empirical ground-motion relations for subduction-zone earthquakes and their application to cascadia and other regions, *Bulletin of the Seismological Society of America*, **93**, 1703–1729.

Atkinson, G. M., Morrison, M., 2009. Observations on Regional Variability in Ground-Motion Amplitudes for Small-to-Moderate Earthquakes in North America, *Bulletin of the Seismological Society of America*, **99**, 2393-2409.

Bommer, J. J., Abrahamson, N. A., 2006. Why do modern probabilistic seismic-hazard analyses often lead to increased hazard estimates?, *Bulletin of the Seismological Society of America*, **96**, 1967-1977.

Bommer, J. J., Stafford, P. J., Alarcon, J. E., Akkar, S., 2007. The Influence of Magnitude Range on Empirical Ground-Motion Prediction, *Bulletin of the Seismological Society of America*, **97**, 2152-2170.

Boore, D. M., Atkinson, G. M., 2008. Ground-motion prediction equations for the average horizontal component of PGA, PGV, and 5%-damped PSA at spectral periods between 0.01s and 10.0s, *Earthquake Spectra*, **24**, 99-138.

Campbell, K. W., 2003. Prediction of strong motion using the hybrid empirical method and its use in the development of ground motion (attenuation) relations in Eastern North America, *Bulletin of the Seismological Society of America*, **93**, 1012-1033.

Chiou, B., Darragh, R., Gregor, N., Silva, W. J., 2008. NGA project strong-motion database, *Earthquake Spectra*, **24**, 23-44.

Chiou, B., Youngs, R. R., 2006. *Chiou and Youngs PEER-NGA Empirical Ground Motion Model for the Average Horizontal Component of Peak Acceleration and Pseudo-Spectral Acceleration for Spectral Periods of 0.01 to 10 Seconds*, in *Interim Report for USGS Review*.

Chiou, B., Youngs, R. R., Abrahamson, N. A., Addo, K., 2010. Ground-motion attenuation model for small-to-moderate shallow crustal earthquakes in california and Its implications on regionalization of ground-motion prediction models, *Earthquake Spectra*, **(to appear)**.

Chiou, B. S. J., Youngs, R. R., 2008. An NGA Model for the average horizontal component of peak ground motion and response spectra, *Earthquake Spectra*, **24**, 173-215.

Cornell, C. A., 1968. Engineering seismic risk analysis, *Bulletin of the Seismological Society of America*, **58**, 1583–1606.

Cotton, F., Pousse, G., Bonilla, F., Scherbaum, F., 2008. On the Discrepancy of Recent European Ground-Motion Observations and Predictions from Empirical Models: Analysis of KiK-net Accelerometric Data and Point-Sources Stochastic

Simulations, *Bulletin of the Seismological Society of America*, **98**, 2244-2261.
Cousins, W. J., Zhao, J. X., Perrin, N., 1999. A model for the attenuation of peak ground acceleration in New Zealand earthquakes based on seismograph and accelerograph data, *Bulletin of the New Zealand Society for Earthquake Engineering*, **32**, 193-220.
Dhakal, Y. P., Takai, N., Sasatani, T., 2010. Empirical analysis of path effects on prediction equations of pseudo-velocity response spectra in northern Japan, *Earthquake Engineering & Structural Dynamics*, **39**, 443-461.
Douglas, J., 2004. An investigation of analysis of variance as a tool for exploring regional differences in strong ground motions, *Journal of Seismology*, **8**, 485-496.
Douglas, J., 2007. On the regional dependence of earthquake response spectra, *ISET Journal of Earthquake Technology*, **44**, 71–99.
Dowrick, D. J., Rhoades, D. A., 1998. Magnitudes of New Zealand earthquakes, *Bulletin of the New Zealand Society for Earthquake Engineering*, **31**, 260-280.
Eberhart-Phillips, D., Reyners, M., Bannister, S., Chadwick, M., Ellis, S., 2010. Setting up a versatile 3-D seismic velocity model for New Zealand, *Seismological Research Letters (submitted)*.
Ekström, G., 2010. *Global centroid moment tensor catalogue*, http://www.globalcmt.org/ (last accessed: 26 May 2010).
Engdahl, E. R., van der Hilst, R., Buland, R., 1998. Global teleseismic earthquake relocation with improved travel times and procedures for depth determination, *Bulletin of the Seismological Society of America*, **88**, 722-743.
Field, E. H., Dawson, T. E., Felzer, K. R., Frankel, A. D., Gupta, V., Jordan, T. H., Parsons, T., Petersen, M. D., Stein, R. S., Weldon II, R. J., Wills, C. J., 2008. *The uniform California earthquake rupture forecast, version 2 (UCERF 2)*. p. 715.
Field, E. H., Jordan, T. H., Cornell, C. A., 2003. OpenSHA: A developing community-modelling environment for seismic hazard analysis, *Seismological Research Letters*, **74**, 406-419.
Fry, B., Bannister, S., Beavan, J., Bland, L., Bradley, B. A., Cox, S., Cousins, J., Gale, N., Hancox, G., Holden, C., Jongens, R., Power, W., Prasetya, G., Reyners, M., Ristau, J., Robinson, R., Samsonov, S., Wilson, K., 2010. The Mw 7.6 Dusky Sound earthquake of 2009: Preliminary report, *Bulletin of the New Zealand Society for Earthquake Engineering*, **43**, 24-40.
Haines, A. J., 1981. A local magnitude scale for New Zealand earthquakes, *Bulletin of the Seismological Society of America*, **71**, 275-294.
Lindstrom, M. J., Bates, D. M., 1990. Nonlinear mixed effects models for repeated measures data, *Biometrics*, **46**, 673-687.
McVerry, G. H., Zhao, J. X., Abrahamson, N. A., Somerville, P. G., 2000. *Crustal and subduction zone attenuation relations for New Zealand earthquakes*, in *12th World Conference on Earthquake Engineering*: Auckland, New Zealand. p. 8.
McVerry, G. H., Zhao, J. X., Abrahamson, N. A., Somerville, P. G., 2006. New Zealand acceleration response spectrum attenuation relations for crustal and subduction zone earthquakes, *Bulletin of the New Zealand Society for Earthquake Engineering*, **39**, 1-58.
Morikawa, N., Sasatani, T., 2004. Source Models of Two Large Intraslab Earthquakes from Broadband Strong Ground Motions, *Bulletin of the Seismological Society of America*, **94**, 803-817.
Musson, R. M. W., 2010. Ground motion and probabilistic hazard, *Bulletin of Earthquake Engineering*, **7**, 575-589.
NZS 1170.5, 2004. *Structural design actions, Part 5: Earthquake actions - New*

Zealand. Standards New Zealand: Wellington, New Zealand.
Petersen, M. D., Frankel, A. D., Harmsen, S. C., Mueller, C. S., Haller, K. M., Wheeler, R. L., Wesson, R. L., Zeng, Y., Boyd, O. S., Perkins, D. M., Luco, N., Field, E. H., Wills, C. J., Rukstales, K. S., 2008. *Documentation for the 2008 Update of the United States National Seismic Hazard Maps*, in *Open-File Report 2008–1128*. United States Geological Survey (USGS). p. 127.
Power, M., Chiou, B., Abrahamson, N. A., Bozorgnia, Y., Shantz, T., Roblee, C., 2008. An overview of the NGA project*, Earthquake Spectra*, **24**, 3-21.
Ristau, J., 2008. Implementation of routine regional moment tensor analysis in New Zealand*, Seismological Research Letters*, **79**, 400-415.
Ruppert, D., Sheather, S. J., Wand, M. P., 1995. An effective bandwidth selector for local least squares regression*, Journal of the American Statistical Association*, **90**, 1257-1270.
Scasserra, G., Stewart, J. P., Bazzurro, P., Lanzo, G., Mollaioli, F., 2009. A Comparison of NGA Ground-Motion Prediction Equations to Italian Data*, Bulletin of the Seismological Society of America*, **99**, 2961-2978.
Scherbaum, F., Cotton, F., Smit, P., 2004. On the Use of Response Spectral-Reference Data for the Selection and Ranking of Ground-Motion Models for Seismic-Hazard Analysis in Regions of Moderate Seismicity: The Case of Rock Motion*, Bulletin of the Seismological Society of America*, **94**, 2164-2185.
Stafford, P. J., Strasser, F. O., Bommer, J. J., 2008. An evaluation of the applicability of the NGA models to ground-motion prediction in the Euro-Mediterranean region*, Bulletin of Earthquake Engineering*, **6**, 149-177.
Stirling, M. W., 2007. *Updating the national seismic hazard model for New Zealand*, in *8th Pacific Conference on Earthquake Engineering*: Singapore, Singapore. p. 8.
Stirling, M. W., McVerry, G. H., Berryman, K. R., 2002. A new seismic hazard model for New Zealand*, Bulletin of the Seismological Society of America*, **92**, 1878–1903.
Walling, M., Silva, W. J., Abrahamson, N. A., 2008. Nonlinear site amplification factors for constraining the NGA models*, Earthquake Spectra*, **24**, 243-255.
Wasserman, L., 2006. *All of non-parametric statistics*. Springer: New York.
Wells, D. L., Coppersmith, K. J., 1994. New empirical relationships among magnitude, rupture length, rupture width, rupture area, and surface displacement*, Bulletin of the Seismological Society of America*, **84**, 974-1002.
Youngs, R. R., Chiou, S. J., Silva, W. J., Humphrey, J. R., 1997. Strong ground motion attenuation relationships for subduction zone earthquakes*, Seismological Research Letters*, **68**, 94-127.
Zhao, J. X., 2010. Geometric Spreading Functions and Modeling of Volcanic Zones for Strong-Motion Attenuation Models Derived from Records in Japan*, Bulletin of the Seismological Society of America*, **100**, 712-732.
Zhao, J. X., Dowrick, D. J., McVerry, G. H., 1997. Attenuation of peak ground accelerations in New Zealand earthquakes*, Bulletin of the New Zealand Society for Earthquake Engineering*, **30**, 133-158.
Zhao, J. X., Gerstenberger, M., 2010. *Attenuation models for rapid post earthquake assessment in NZ*.
Zhao, J. X., Zhang, J., Asano, A., Ohno, Y., Oouchi, T., Takahashi, T., Ogawa, H., Irikura, K., Thio, H. K., Somerville, P. G., Fukushima, Y., Y., F., 2006. Attenuation relations of strong ground motion in Japan using site classification based on predominant period*, Bulletin of the Seismological Society of America*, **96**, 898-913.

APPENDIX A NZ STRONG MOTION DATABASE

This appendix contains the 213 events that comprise the developed NZ strong motion database. For each event the appendix provides: (i) and earthquake identification (EQ ID); the time of the event in year, month, day, hour, minute, and second (yyymmddhhmmssss); (iii) the latitude and longitude of the moment tensor solution of the event; (iv) the depth of the event (in km); (v) the moment magnitude; (vi) the focal mechanism; (vii) tectonic type; and (ix) number of recordings.

EQ ID	yyyymmddhhmmssss	Lat	Long	Depth	M_w	FM	Tectonic type	N_{record}
1	19760504135600	-44.729	167.659	25.0	6.53	R	I	2
2	19770118054100	-41.743	174.388	38.6	6.06	N	S	11
3	19820205175100	-40.684	175.871	33.7	5.33	N	S	2
4	19820902155800	-39.746	176.754	33.4	5.42	OB	S	2
5	19840308004000	-38.260	177.315	93.9	6.02	R	S	2
6	19880603232700	-45.042	167.583	74.2	6.66	OB	S	4
7	19890531055400	-45.297	167.088	30.0	6.42	OB	I	2
8	19890808075900	-40.129	174.398	117.5	5.55	R	S	2
9	19900210032700	-42.315	172.862	15.0	5.96	OB	C	2
10	19900219053400	-40.369	176.200	25.4	6.22	OB	S	10
11	19900513042300	-40.292	176.157	21.0	6.38	R	I	15
12	19900815155400	-40.390	176.364	32.5	5.13	N	S	4
13	19901004234800	-41.709	175.585	1.5	5.54	R	C	11
14	19901006024100	-41.634	175.495	17.5	5.42	R	I	9
15	19910128125800	-41.963	171.762	23.6	5.69	R	C	10
16	19910128180000	-41.969	171.767	18.8	5.83	R	C	8
17	19910215104800	-42.101	171.665	18.6	5.39	R	C	9
18	19910712044200	-39.412	175.973	61.9	5.27	OR	S	5
19	19910908135000	-40.291	175.111	84.4	5.57	R	S	18
20	19920302090500	-40.367	176.369	19.9	5.51	OB	S	5
21	19920330070200	-43.057	171.288	15.0	5.47	R	C	6
22	19920516175700	-38.350	178.201	23.9	5.73	R	I	5
23	19920527223000	-41.586	173.645	72.9	5.89	S	S	17
24	19920621174300	-37.817	177.026	36.1	6.21	N	C	7
25	19930411065900	-39.717	176.485	27.4	5.70	R	I	7
26	19930810005100	-45.214	167.007	28.0	6.95	R	I	6
27	19930810094600	-38.496	177.796	14.4	6.37	OB	C	14
28	19940618032500	-43.104	171.645	14.0	6.37	OR	C	10
29	19941215112000	-37.537	177.600	25.0	6.28	S	C	8
30	19950205225100	-37.801	178.948	21.0	7.11	N	C	28
31	19950322194300	-41.015	174.142	80.4	5.79	OR	S	43
32	19951124061800	-42.988	171.842	3.4	6.10	OR	C	9
33	19960829044700	-42.510	172.861	13.5	5.22	OB	C	2
34	19981020200300	-43.845	169.755	10.0	5.35	OB	C	2
35	19990103070000	-41.063	174.510	59.7	5.19	OB	S	17
36	19990818011647	-37.277	177.513	151.3	5.71	R	S	3
37	19991025203142	-38.697	175.975	159.0	5.98	OR	S	17
38	20000329143058	-41.043	175.462	27.7	5.21	OB	S	27
39	20000808103119	-39.265	176.306	57.0	5.26	OB	S	10
40	20001101103555	-45.129	167.128	30.0	6.08	R	I	2
41	20010924044956	-40.329	176.620	27.5	5.31	OB	S	11
42	20011015034938	-39.660	176.642	28.1	5.51	R	I	6
43	20011207192735	-44.170	168.666	16.4	5.76	R	C	12
44	20020224063735	-44.093	168.644	9.8	5.41	OB	C	5

45	20030125213031	-40.337	176.151	34.6	5.19	ON	S	41
46	20030212114351	-37.818	179.291	48.6	5.47	ON	S	2
47	20030803114614	-40.466	175.979	53.6	5.12	N	S	44
48	20030821121249	-45.102	166.809	30.9	7.11	R	I	25
49	20030821141227	-45.284	166.783	32.3	6.05	R	S	13
50	20030821195622	-45.216	166.811	32.1	5.27	R	S	3
51	20030822000221	-45.051	166.977	26.1	5.20	R	S	4
52	20030822152933	-45.154	166.899	38.3	4.98	R	S	3
53	20030823091354	-45.318	166.824	33.8	5.51	R	S	7
54	20030824144652	-45.179	166.903	23.0	4.93	R	I	2
55	20030826235627	-45.467	166.560	21.3	5.43	R	I	11
56	20030827012940	-45.444	166.662	25.3	5.12	R	I	3
57	20030827014254	-45.282	166.924	30.1	5.36	R	I	11
58	20030904084044	-45.161	166.811	27.7	5.47	R	S	14
59	20030929182232	-43.259	172.958	28.5	4.63	R	C	10
60	20030930193749	-45.648	166.983	6.1	5.55	N	C	8
61	20031102053214	-45.391	166.285	11.6	6.40	R	I	9
62	20031221172251	-39.260	174.866	144.7	4.26	OR	S	3
63	20040228144636	-45.238	166.842	25.6	4.24	R	S	2
64	20040401151329	-39.973	176.655	44.7	4.38	R	S	7
65	20040402120904	-41.102	175.075	30.2	4.33	N	S	19
66	20040417001841	-37.948	176.645	142.2	4.66	R	S	2
67	20040509203119	-38.248	178.292	15.0	4.29	N	C	2
68	20040511232203	-38.036	178.200	10.1	4.85	N	C	4
69	20040512012109	-38.028	178.222	10.9	4.56	N	C	4
70	20040512095257	-40.618	175.782	30.3	4.58	R	S	20
71	20040531024510	-37.389	177.647	119.8	4.62	R	S	6
72	20040623042829	-42.824	171.374	11.0	4.77	OR	C	15
73	20040718035806	-38.051	176.488	10.6	4.90	ON	C	6
74	20040718042223	-38.037	176.504	8.2	5.47	ON	C	16
75	20040718064015	-38.015	176.534	6.3	5.00	N	C	6
76	20040719060952	-41.729	172.480	18.0	4.41	R	C	8
77	20040819160339	-43.824	170.883	11.5	4.52	R	C	2
78	20040929034451	-41.436	172.371	5.6	4.02	S	C	4
79	20041002153129	-42.347	173.241	2.0	4.66	OB	C	3
80	20041004191750	-40.291	175.945	37.8	4.73	N	S	18
81	20041104083936	-40.595	175.044	42.2	4.56	R	I	10
82	20041122202632	-46.381	165.057	29.3	7.06	R	S	13
83	20041202033012	-44.063	168.819	10.3	4.06	OB	C	6
84	20050118083604	-41.429	175.733	8.5	5.21	R	C	43
85	20050118092600	-41.463	175.718	26.6	5.13	R	S	38
86	20050120185631	-41.097	175.065	31.4	5.30	N	S	66
87	20050131173153	-41.430	175.732	9.6	5.25	OB	C	42
88	20050213065531	-45.263	166.831	31.3	4.56	R	I	5
89	20050217213110	-39.894	174.631	31.8	4.74	OB	C	22
90	20050313150813	-40.102	173.598	150.8	5.37	OB	S	63

91	20050314080435	-45.020	166.574	26.0	5.24	R	S	6
92	20050402020750	-44.351	169.874	16.7	4.73	OB	C	5
93	20050411075137	-41.670	174.523	32.1	4.34	OR	S	28
94	20050416235843	-44.358	169.530	17.8	4.31	S	C	6
95	20050425081916	-45.859	166.818	94.2	4.53	ON	S	5
96	20050502153537	-43.934	169.017	18.6	5.43	OR	C	21
97	20050502154004	-43.937	169.008	15.9	5.00	S	C	12
98	20050511215846	-38.901	176.008	13.2	4.00	S	C	2
99	20050623082152	-41.977	173.892	6.9	4.50	S	C	2
100	20050623121558	-41.970	173.890	8.1	4.69	OR	C	2
101	20050710230924	-40.546	176.826	20.7	4.38	S	C	4
102	20050806115443	-41.943	171.675	12.8	4.20	R	C	10
103	20051012112018	-42.025	171.676	8.5	4.24	S	C	6
104	20051013181141	-42.698	172.522	12.2	4.49	S	C	9
105	20051019000533	-40.368	176.254	23.9	4.27	R	I	6
106	20051031213316	-41.685	174.186	5.4	4.27	OB	C	3
107	20051101053951	-41.687	174.179	9.6	4.59	S	C	8
108	20051103131650	-41.753	174.259	15.1	4.41	S	C	4
109	20051212135547	-40.438	176.022	29.4	4.58	OB	S	25
110	20051213080948	-41.099	174.866	32.1	4.29	OB	S	38
111	20060122165208	-39.899	176.514	25.2	4.21	R	I	3
112	20060313110216	-39.838	176.735	41.6	4.43	R	S	10
113	20060325152033	-40.415	176.850	12.0	4.66	S	C	4
114	20060325152422	-40.417	176.821	10.7	4.43	S	C	5
115	20060514173238	-40.914	174.445	61.0	4.54	S	S	47
116	20060604234838	-40.391	176.338	22.6	4.37	OB	C	6
117	20060705213223	-45.145	166.851	38.1	4.24	OB	S	2
118	20060708112718	-39.191	176.849	31.0	5.09	OB	S	15
119	20060723003738	-40.544	173.152	185.2	4.51	R	S	21
120	20060813042925	-41.777	172.651	91.4	5.30	ON	S	70
121	20060915114319	-40.943	174.463	51.4	4.61	N	S	46
122	20061002090226	-43.521	169.910	8.0	4.42	R	C	4
123	20061117143804	-41.043	174.334	76.0	4.75	OR	S	55
124	20061128185451	-38.175	176.844	86.2	4.93	OR	S	6
125	20061204185933	-38.254	177.510	46.6	4.51	OB	S	8
126	20070118033414	-39.547	175.813	53.7	4.82	N	S	5
127	20070204191426	-39.123	176.275	59.6	4.57	R	S	13
128	20070207004459	-40.999	174.456	54.5	4.18	N	S	35
129	20070306092728	-41.383	172.368	12.9	4.04	R	C	6
130	20070307070143	-40.355	175.351	16.8	4.29	R	C	6
131	20070425144036	-39.797	176.964	27.8	4.41	R	S	7
132	20070513132510	-41.216	173.549	89.7	4.58	OR	S	39
133	20070516131829	-40.369	174.635	93.2	4.28	R	S	28
134	20070712054227	-38.728	176.200	96.8	4.61	OB	S	3
135	20070808033834	-44.027	169.619	12.0	4.08	S	C	2
136	20070825014332	-40.453	174.865	51.4	4.60	N	S	28

137	20070929131238	-37.776	176.824	2.0	4.75	ON	C	6
138	20071001021207	-38.938	175.927	5.0	4.19	S	C	2
139	20071003191510	-42.161	172.882	69.7	5.39	OB	S	45
140	20071006125222	-42.202	172.904	67.8	4.32	N	S	8
141	20071015122933	-44.721	167.302	24.0	6.72	R	I	38
142	20071015212822	-44.729	167.299	5.0	6.01	R	C	31
143	20071016002632	-44.735	167.398	5.0	4.45	R	C	3
144	20071016143434	-44.768	167.282	5.0	4.66	R	C	3
145	20071016163847	-44.698	167.241	7.4	4.95	OB	C	8
146	20071024011230	-42.166	172.040	8.6	4.54	R	C	15
147	20071106221738	-42.100	172.893	57.0	4.86	OB	S	29
148	20071129155332	-45.064	167.257	117.1	5.24	R	S	15
149	20071220075516	-38.878	178.495	44.2	6.58	N	S	53
150	20071221223511	-38.816	178.371	34.4	4.59	N	S	3
151	20071227080703	-38.953	175.673	117.5	4.71	OB	S	16
152	20071228180337	-38.780	176.298	79.8	4.88	OB	S	19
153	20080120184147	-44.946	166.975	12.0	5.50	R	I	9
154	20080215053227	-44.430	167.327	5.0	4.18	ON	C	3
155	20080413024242	-45.145	166.810	12.0	4.80	R	I	4
156	20080501190033	-43.225	171.025	2.0	4.48	R	C	3
157	20080612210624	-37.556	177.089	5.0	5.24	ON	C	3
158	20080712000856	-45.817	166.760	125.7	5.12	OB	S	11
159	20080825112519	-39.652	176.754	29.3	5.49	N	S	34
160	20080901012150	-39.112	175.849	85.5	5.17	S	S	11
161	20080905023537	-42.343	172.717	9.2	4.50	S	C	6
162	20080914092512	-40.231	174.499	84.0	4.62	N	S	26
163	20080924224041	-42.207	173.944	14.4	4.98	R	C	9
164	20080926072302	-42.249	173.827	17.8	5.03	R	C	20
165	20081024174747	-39.634	176.749	28.3	4.22	N	S	10
166	20081205055145	-43.841	169.224	16.8	4.34	OB	C	6
167	20081217203357	-36.801	177.876	149.3	5.20	OB	S	3
168	20081226194959	-40.507	174.819	52.9	4.68	OB	S	30
169	20090130082657	-42.749	172.431	8.5	4.54	OB	C	2
170	20090321202818	-37.733	176.731	164.5	5.13	R	S	14
171	20090324005310	-45.176	167.033	34.8	4.10	OB	S	2
172	20090327164642	-44.250	170.006	15.9	4.57	S	C	13
173	20090408111258	-38.707	178.477	17.6	5.07	N	C	4
174	20090514234737	-41.357	174.083	42.5	3.92	OB	S	2
175	20090715092229	-45.765	166.570	12.0	7.63	R	I	32
176	20090715234120	-45.521	167.033	65.0	5.04	OB	S	6
177	20090716021309	-45.400	166.750	12.0	4.81	R	C	3
178	20090716063001	-45.702	166.551	5.0	5.00	OB	C	3
180	20090717063924	-45.381	166.484	5.0	5.16	S	C	6
181	20090718153346	-45.548	166.631	12.0	5.03	R	I	4
182	20090724132840	-45.286	166.651	12.0	4.02	R	I	2
183	20090730020648	-45.686	166.477	12.0	4.76	R	I	2

184	20090805083138	-45.479	166.287	5.0	6.10	R	I	10
185	20090825045724	-46.156	166.153	12.0	5.17	OB	C	3
186	20090826075239	-40.439	176.558	36.7	4.29	N	S	6
187	20090827141049	-41.442	174.709	33.9	4.70	ON	S	29
188	19730105135400	-38.986	175.372	155.0	6.57	R	S	11
189	19950210014400	-37.916	179.514	12.0	6.49	N	C	17
190	19960531233100	-40.634	175.334	40.8	4.81	UN	S	10
191	19970620153630	-41.166	174.442	39.8	5.07	UN	S	12
192	20000427091445	-40.230	174.024	136.7	5.13	UN	S	18
193	20000516070326	-40.022	174.760	107.8	4.91	UN	S	15
194	20001030163218	-40.758	174.956	53.6	4.89	UN	S	21
195	20010404212529	-41.679	174.168	30.9	4.62	UN	I	13
196	20020326052250	-40.306	176.343	37.7	4.67	UN	S	10
197	20020504125953	-41.397	172.346	10.2	5.31	UN	C	28
198	20021207055937	-40.728	174.957	43.9	4.71	UN	S	45
199	20021224074206	-42.003	173.983	6.4	4.87	UN	C	13
200	20011008192734	-40.953	174.453	5.9	4.67	UN	C	11
201	20011022020328	-41.611	174.400	13.2	4.63	UN	C	9
202	20011102050633	-41.191	174.549	37.5	4.63	UN	S	26
203	20011109045638	-41.527	173.286	87.9	4.85	UN	S	16
204	20020629122728	-39.309	178.080	41.0	5.24	UN	S	11
205	20021006070525	-41.024	175.453	28.3	4.27	UN	S	18
206	20030115235356	-40.881	174.109	65.6	4.43	UN	S	30
207	20030218220208	-40.307	176.589	21.0	4.59	UN	I	11
208	20030629175848	-41.749	174.227	8.1	4.62	UN	C	19
209	20030821124541	-45.153	167.299	53.5	5.55	UN	S	11
210	20030801143544	-40.611	175.331	38.2	4.33	UN	S	25
211	20040730121311	-41.142	174.583	62.6	4.10	UN	S	16
212	20050118003821	-40.957	174.431	52.2	4.27	UN	S	29
213	20061116224208	-41.063	174.180	56.8	4.23	UN	S	20

APPENDIX B DEVELOPMENT OF CHIOU ET AL. - BASED (C10) MODEL

Chiou et al. (2010) modified the Chiou and Youngs (2008) (CY08) model based on the observation that the CY08 model over-predicted ground motions from small magnitude events in California. The modification of Chiou et al. (2010) involved changing the numerical values of four of the parameters in the CY08 model: c_1, c_3, c_M, and $c_{\gamma 2}$. Chiou et al. (2010) however only computed these modified coefficients for PGV, PGA, Sa(0.2) and Sa(1.0). As part of the present study, foreign GMPEs were examined against the NZ database for spectral periods of 0.0. 0.2, 0.5, 1.0, and 5.0 seconds. Hence, because Chiou et al. (2010) do not provide these parameter values for periods of 0.2, 0.5, and 5.0 seconds was desired to use interpolation to determine the approximate values to use. The developed model based on this interpolation is referred to as the Chiou et al. – based model (C10).

Figure B-1 illustrates the variation of c_1 with period in the CY08 model and the values computed from Chiou et al. (2010). It can be seen that the values are essentially identical, and hence the values of c_1 used by CY08 were adopted for the C10 model.

Figure B-2 illustrates the variation of the parameter c_3 with period in the CY08 model and the values computed from Chiou et al. (2010). In addition a parametric fit, which passes through the Chiou et al. (2010) determined values, and also tends to the CY08 parameter values at long periods is also shown. While there is a significant amount of speculation as to how c_3 varies with period for $1 < T < 3$ seconds, the parametric fit is only needed to compute c_3 at $T = 0.2$, 0.5, and 5 seconds then it is deemed adequate.

Figure B-2 illustrates the variation of the parameter c_M with period in the CY08 model and the values computed from Chiou et al. (2010). In addition a parametric fit, which passes through the Chiou et al. (2010) determined values, and also tends to the CY08 parameter values at long periods is also shown. As for the case of c_3, as the parametric fit is only needed to compute c_M at $T = 0.2$, 0.5, and 5 seconds it is deemed adequate.

Figure B-4 illustrates the variation of the parameter $c_{\gamma 2}$ with period in the CY08 model and the values computed from Chiou et al. (2010). In addition a parametric fit, which passes through the Chiou et al. (2010) determined values, and also tends to the CY08 parameter values at long periods is also shown. As for the case of c_3, as the parametric fit is only needed to compute c_M at $T = 0.2$, 0.5, and 5 seconds it is deemed adequate.

Chiou et al. (2010) also computed the inter- and intra-event standard deviations for their small magnitude model, however, it is possible that the data used (from the ShakeMap database) contains poor metadata, and this is expected to cause an increase in the size of the standard deviations. As a result, the C10-based model adopts the CY08 standard deviation model. If the NZ database exhibits a significantly larger standard deviation for small magnitude events then this will be evident upon examining the standard deviation of the inter- and intra-event residuals.

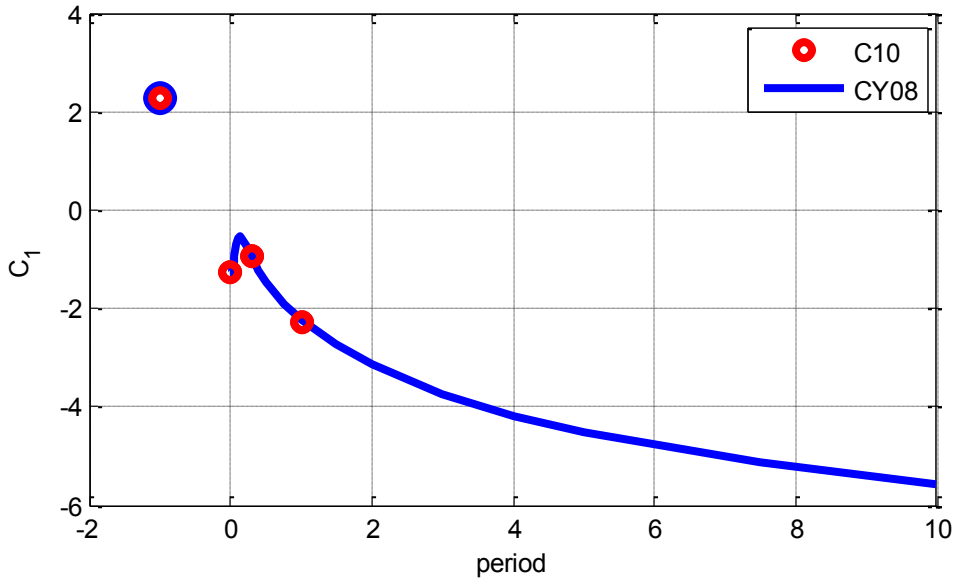

Figure B-1: Variation of parameter c_1.

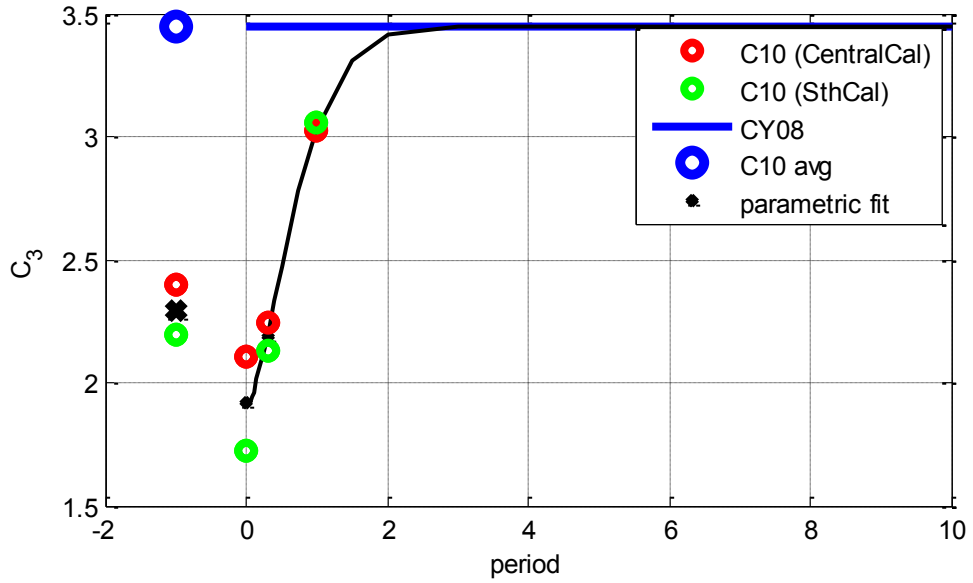

Figure B-2: Variation of parameter c_3.

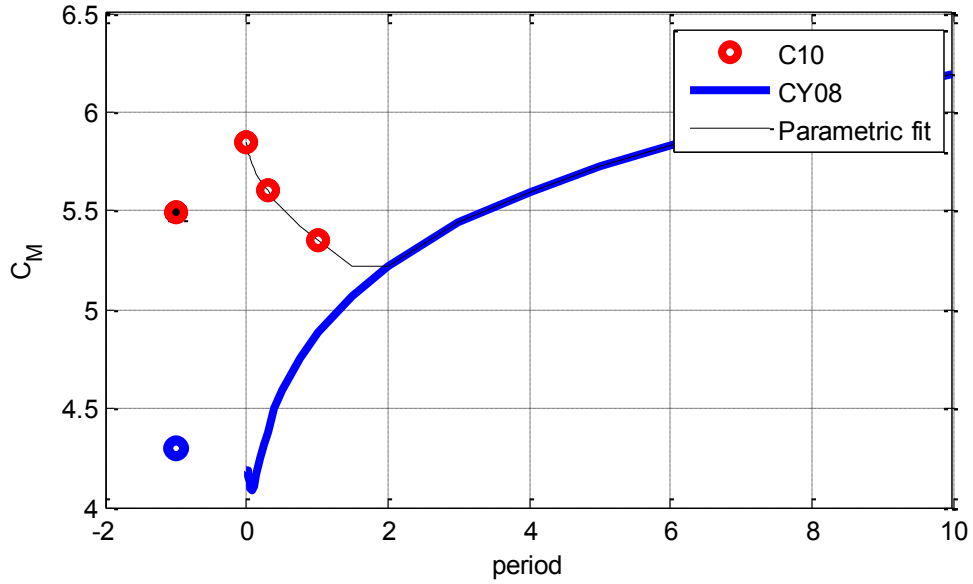

Figure B-3: Variation of parameter c_M.

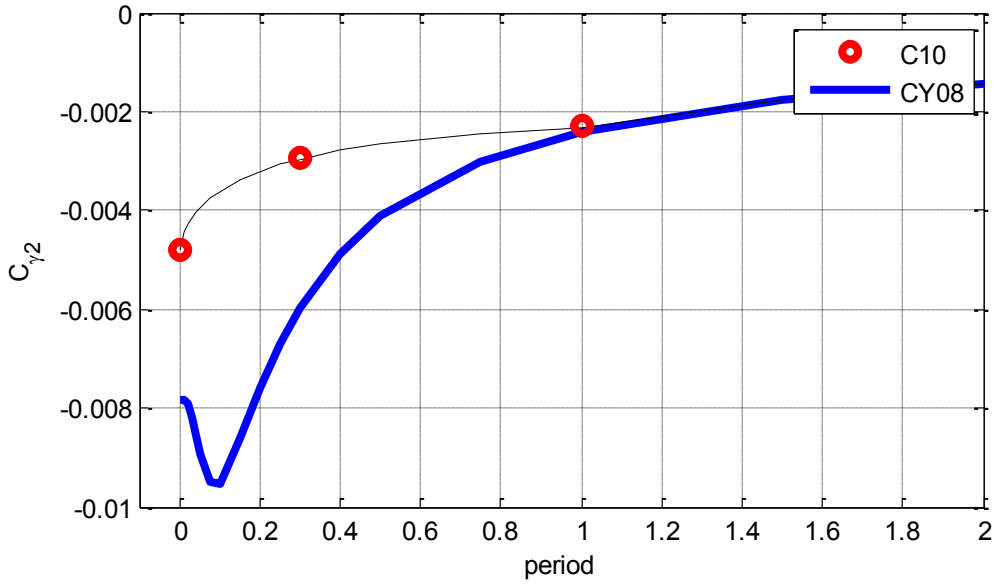

Figure B-4: Variation of parameter $c_{\gamma 2}$.

B.1. References

Chiou, B., Youngs, R. R., Abrahamson, N. A., Addo, K., 2010. Ground-motion attenuation model for small-to-moderate shallow crustal earthquakes in california and Its implications on regionalization of ground-motion prediction models, Earthquake Spectra, (to appear).

Chiou, B. S. J., Youngs, R. R., 2008. An NGA Model for the average horizontal component of peak ground motion and response spectra, Earthquake Spectra, 24, 173-215.

APPENDIX C PREDICTOR VARIABLE SCALING FOR ALTERNATIVE GROUND MOTION PREDICTION EQUATIONS CONSIDERED

C.1. Parameter scaling of the median of crustal prediction equations

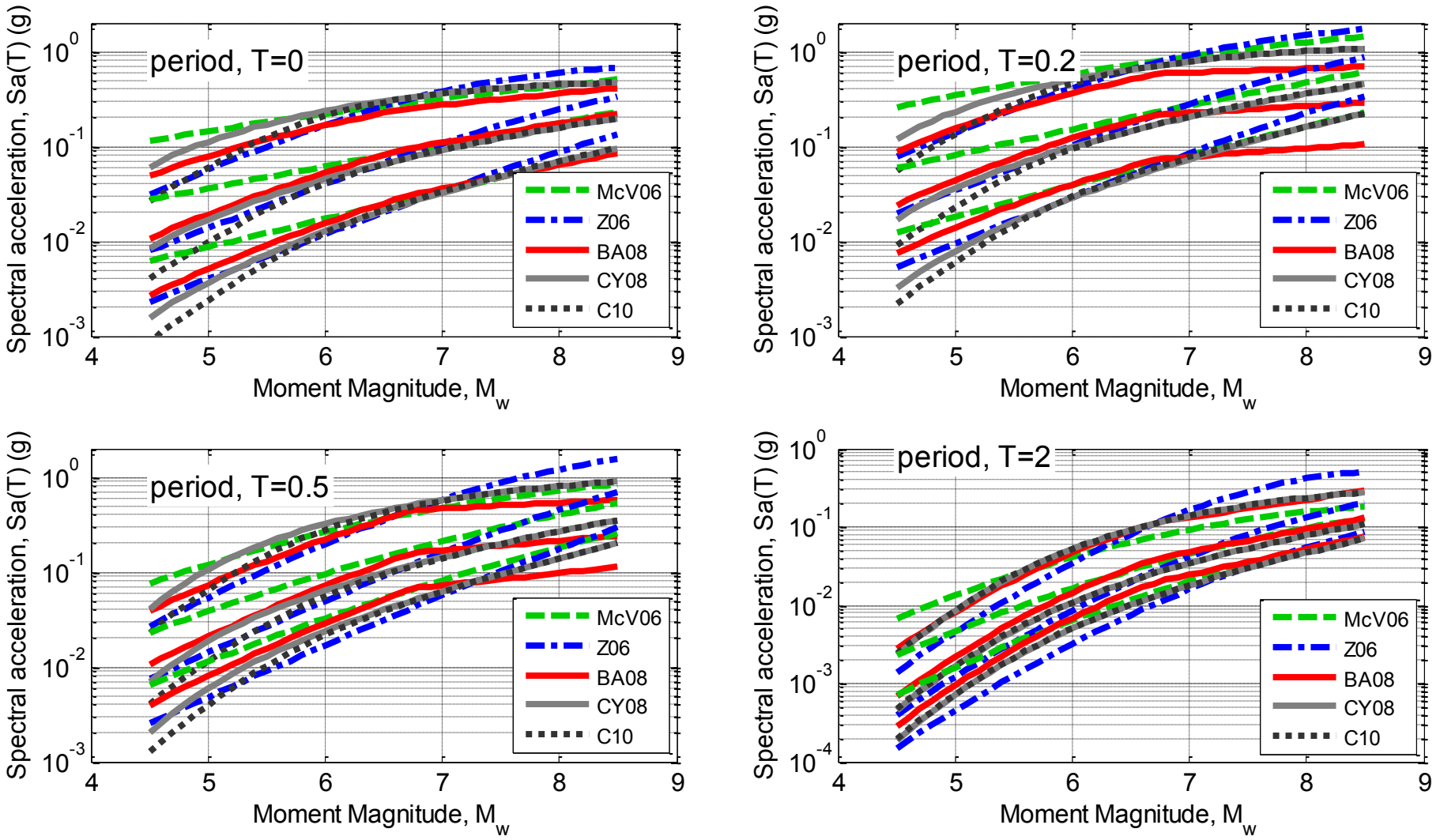

Figure C-1: Magnitude scaling of the median of crustal ground motion prediction equations for distances of 10, 50, and 120 km: (a) Sa(0.0); (b) Sa(0.2); (c) Sa(0.5); and (d) Sa(1.0). (predictions for site class C and strike-slip focal mechanism).

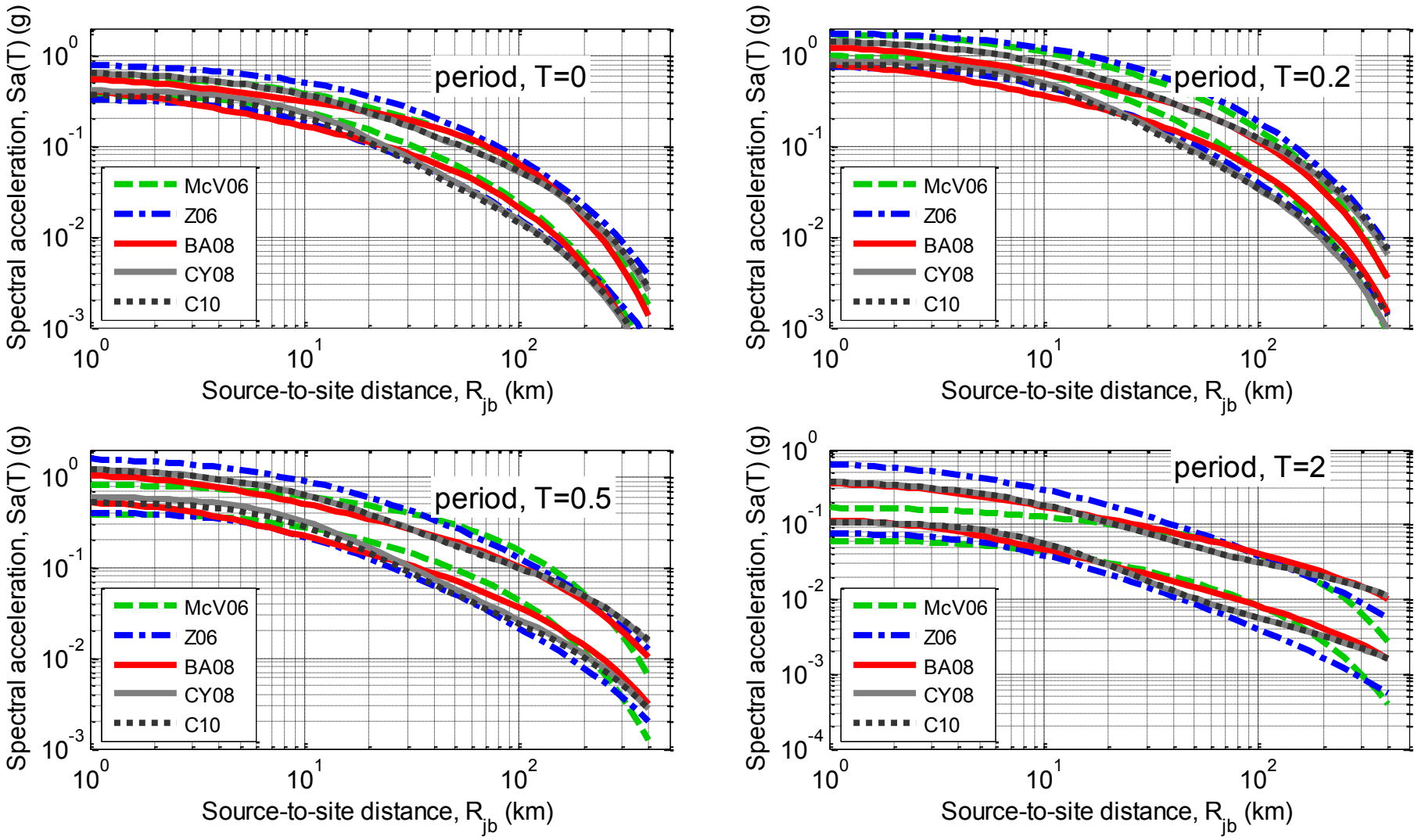

Figure C-2: Path distance scaling of the median of crustal ground motion prediction equations for magnitudes of 6 and 7.5: (a) Sa(0.0); (b) Sa(0.2); (c) Sa(0.5); and (d) Sa(1.0). (predictions for site class C and strike-slip focal mechanism).

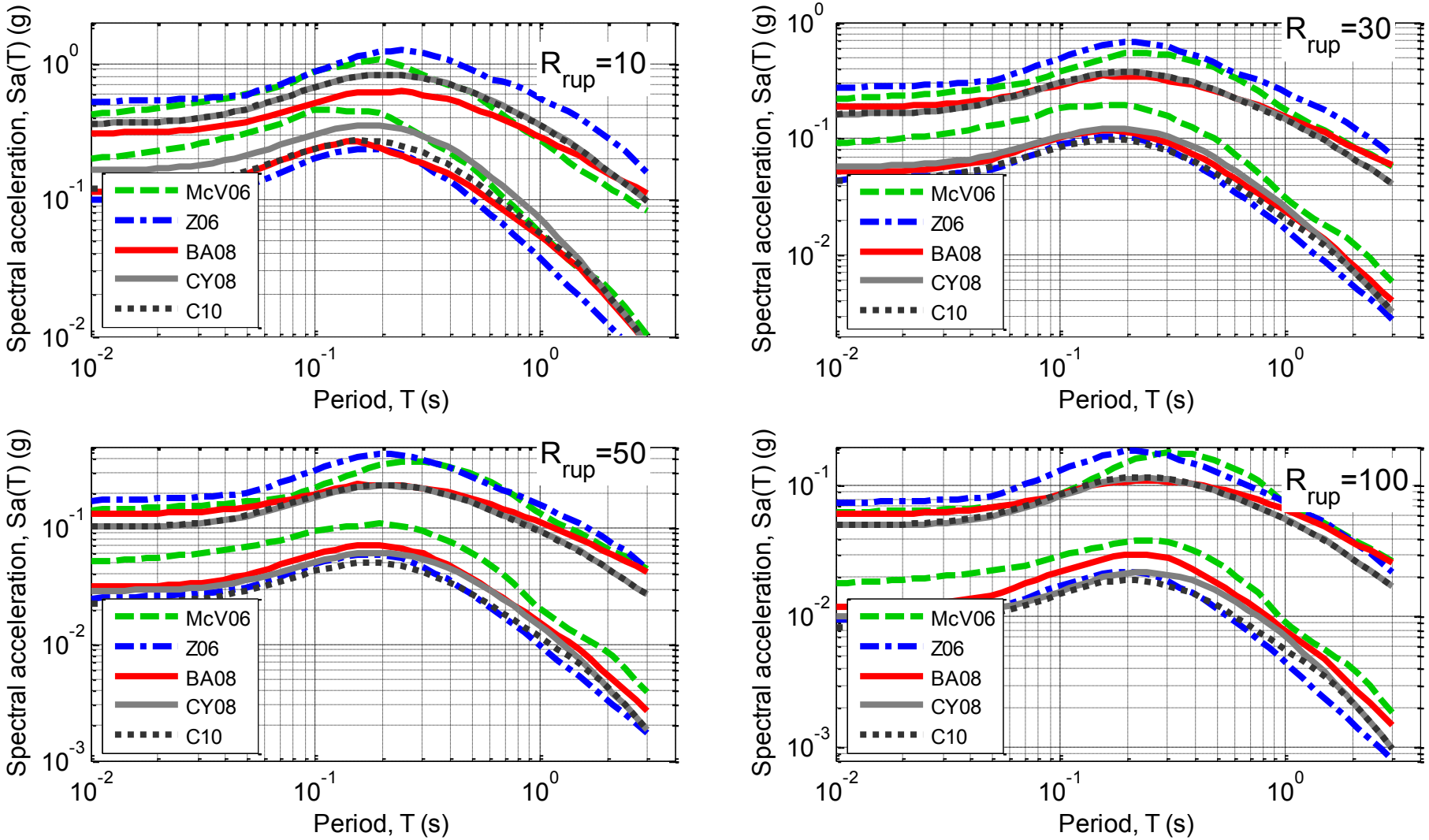

Figure C-3: Vibration period scaling of the median of crustal ground motion prediction equations for magnitudes of 5.5 and 7.5: (a) R_{rup} = 10km; (b) R_{rup} = 30km; (c) R_{rup} = 50km; and (d) R_{rup} = 100km. (predictions for site class C and strike-slip focal mechanism).

C.2. Parameter scaling of the standard deviation of crustal prediction equations

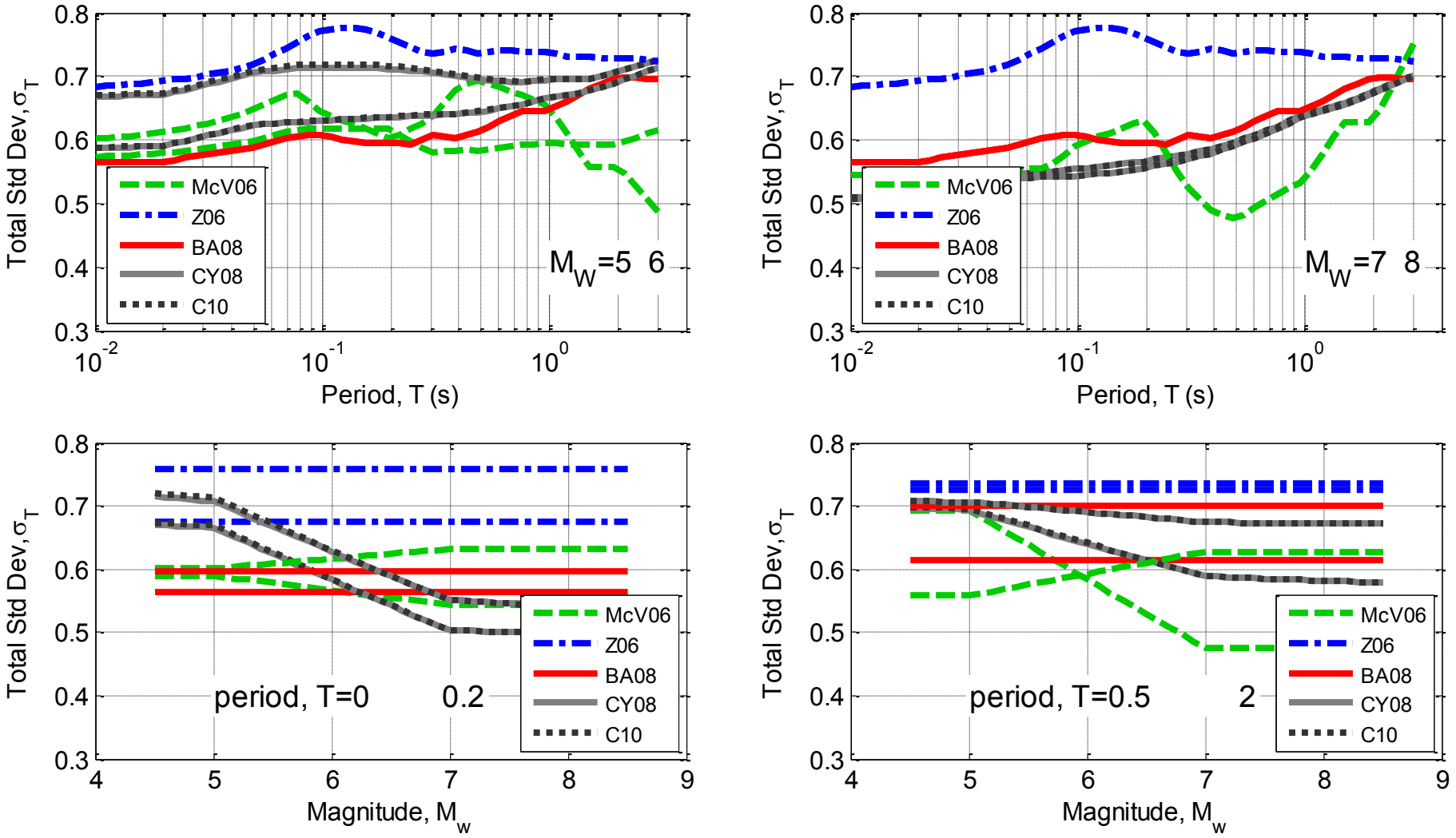

Figure C-4: Total standard deviation scaling of crustal ground motion prediction equations with period and magnitude.

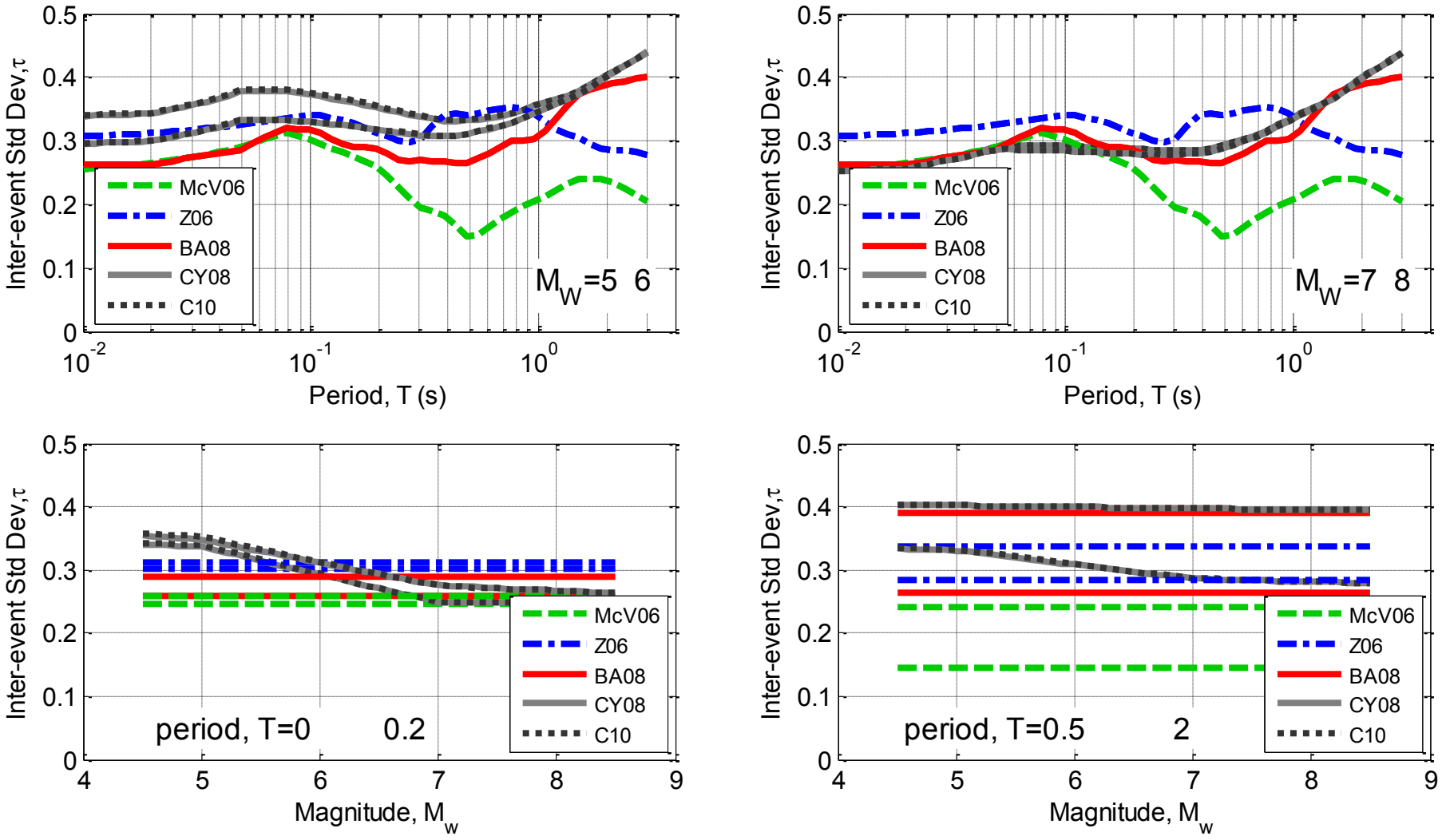

Figure C-5: Inter-event standard deviation scaling of crustal ground motion prediction equations with period and magnitude.

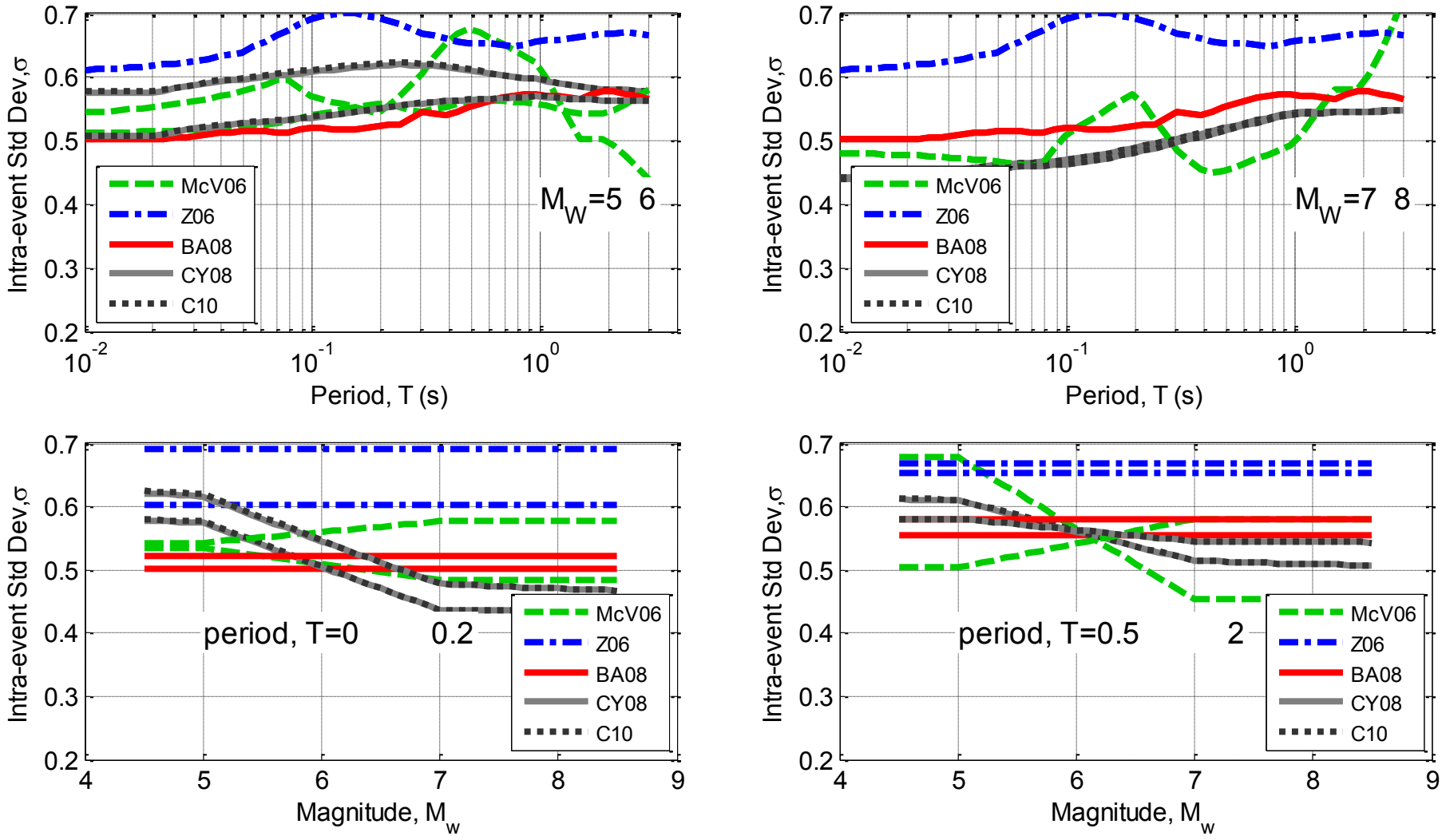

Figure C-6: Intra-event standard deviation scaling of crustal ground motion prediction equations with period and magnitude.

C.3. Parameter scaling of the median of slab prediction equations

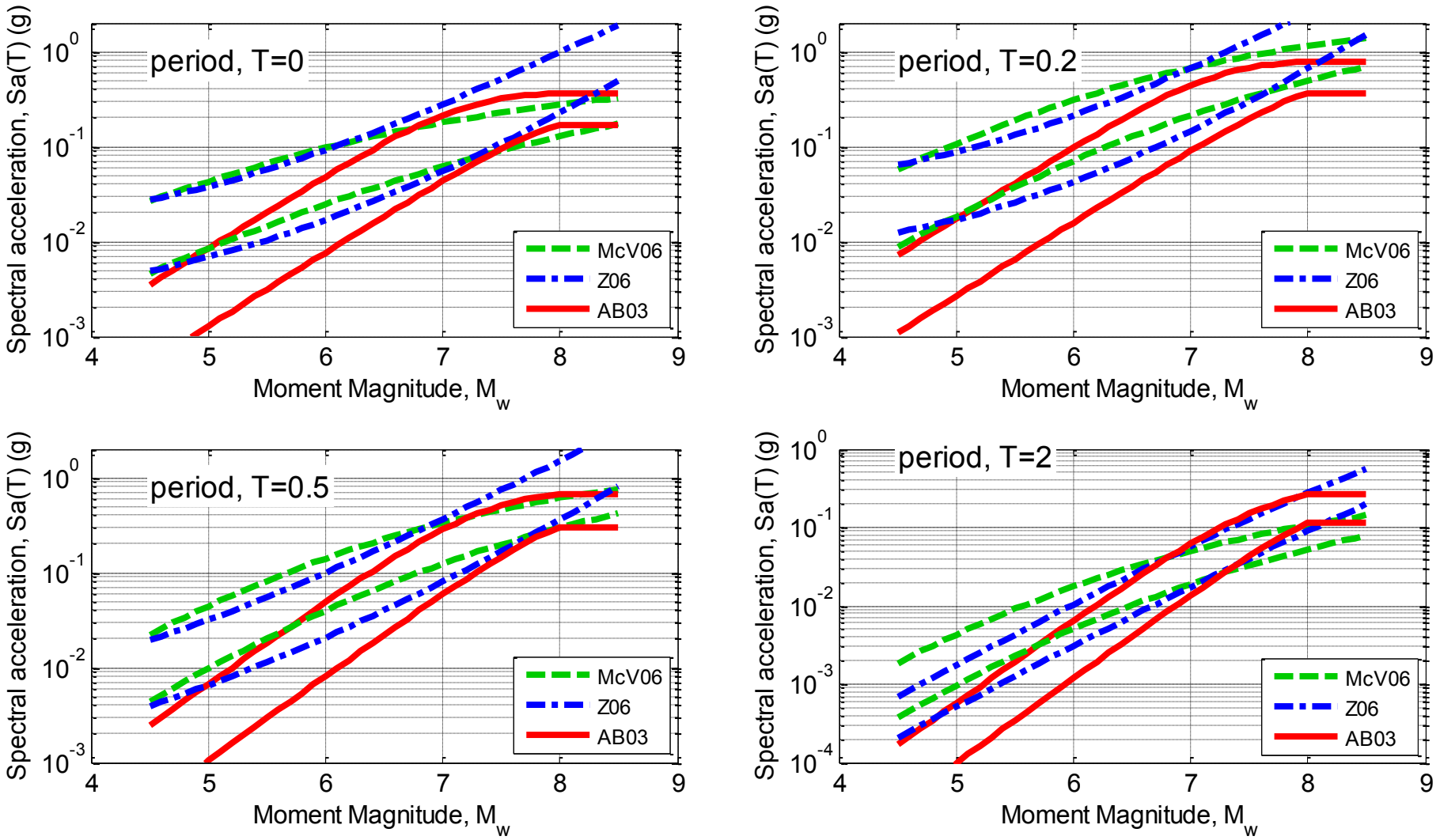

Figure C-7: Magnitude scaling of the median of slab ground motion prediction equations for distances of 50, and 120 km: (a) Sa(0.0); (b) Sa(0.2); (c) Sa(0.5); and (d) Sa(1.0). (predictions for site class C, depth 40km).

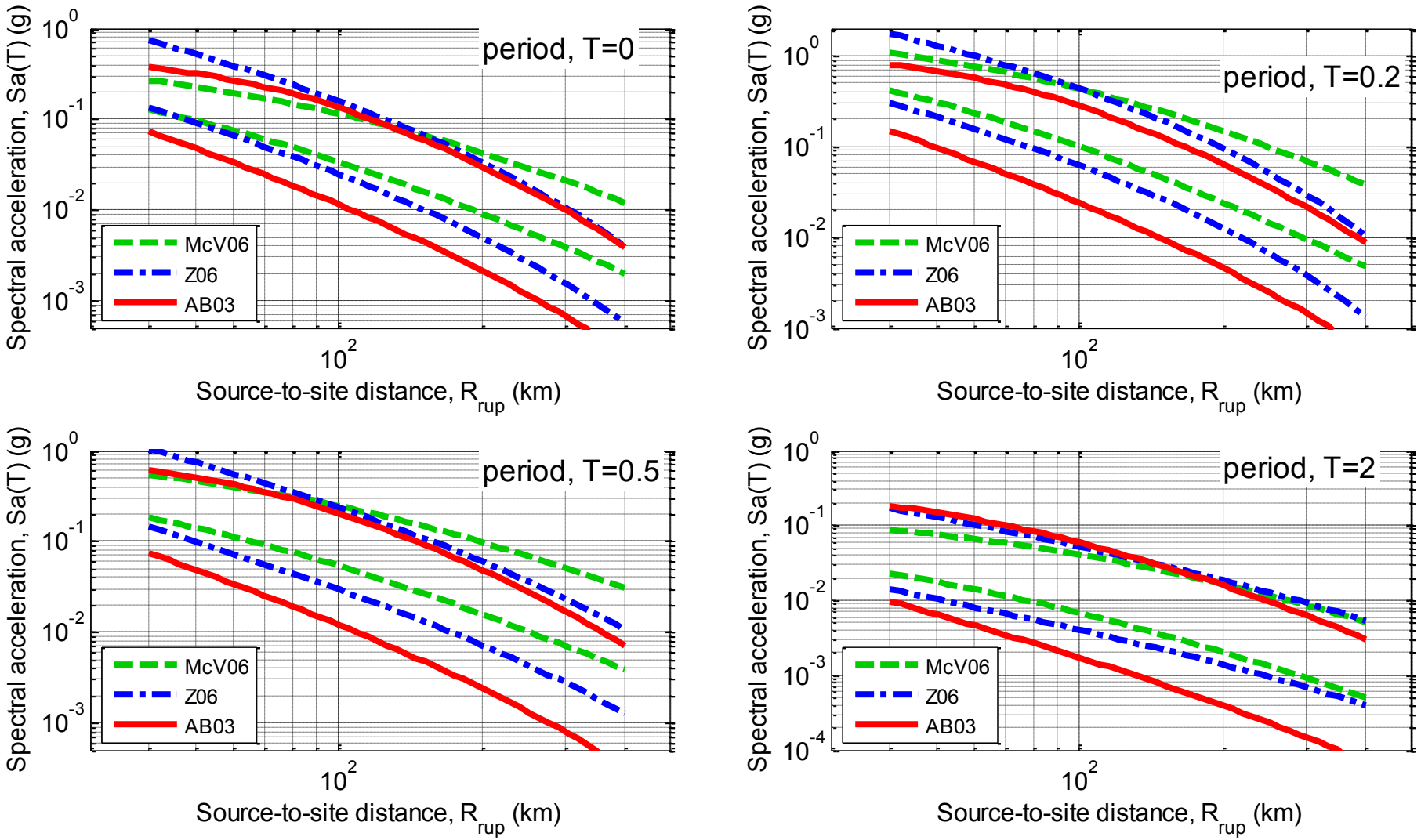

Figure C-8: Path distance scaling of the median of slab ground motion prediction equations for magnitudes of 6 and 7.5: (a) Sa(0.0); (b) Sa(0.2); (c) Sa(0.5); and (d) Sa(1.0). (predictions for site class C, depth 40km).

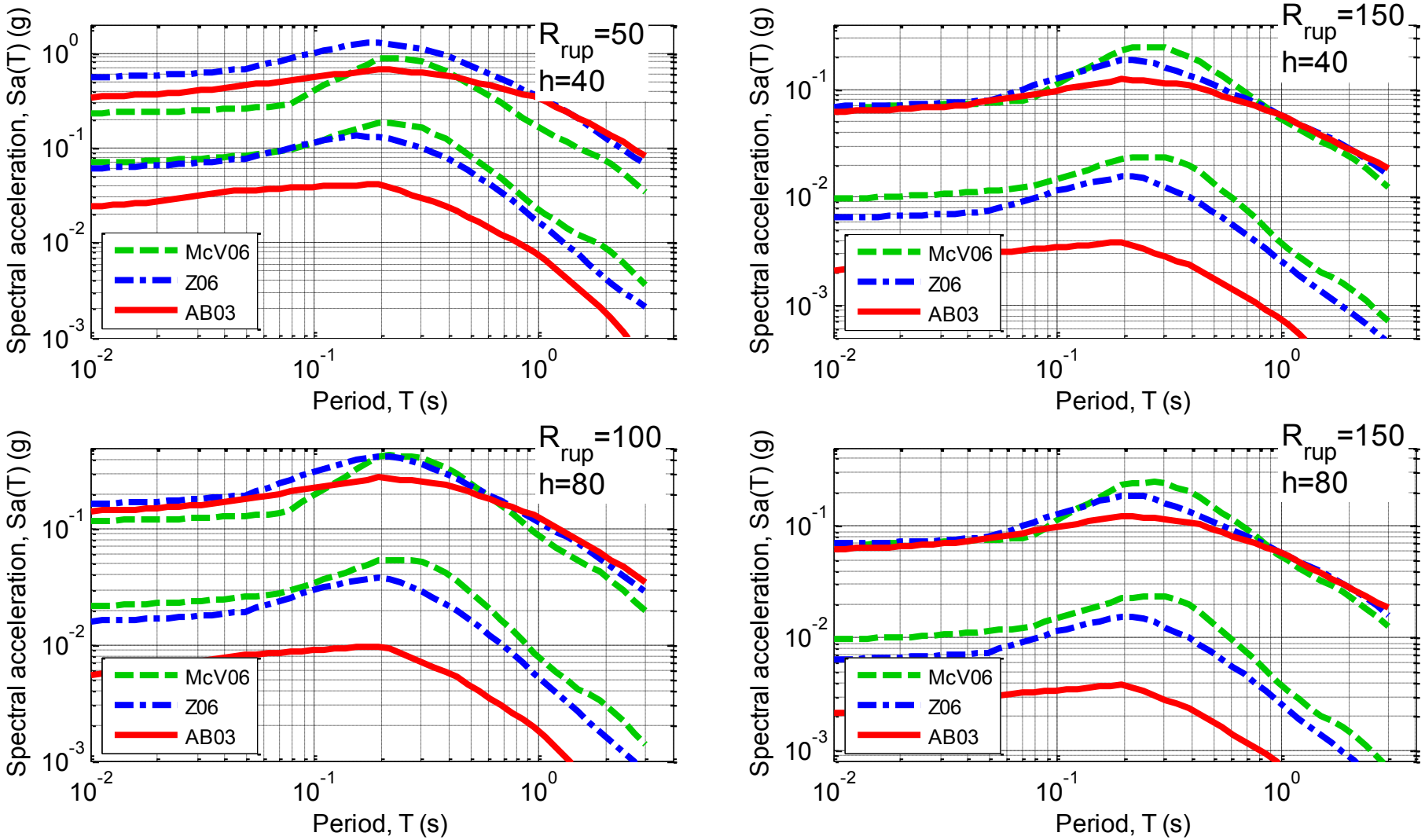

Figure C-9: Vibration period scaling of the median of slab ground motion prediction equations for magnitudes of 5.5 and 7.5: (a) R_{rup} = 50km, h=40km; (b) R_{rup} = 150km, h=40km; (c) R_{rup} = 100km, h=80km; and (d) R_{rup} = 150km, h=80km. (predictions for site class C).

C.4. Parameter scaling of the standard deviation of slab prediction equations

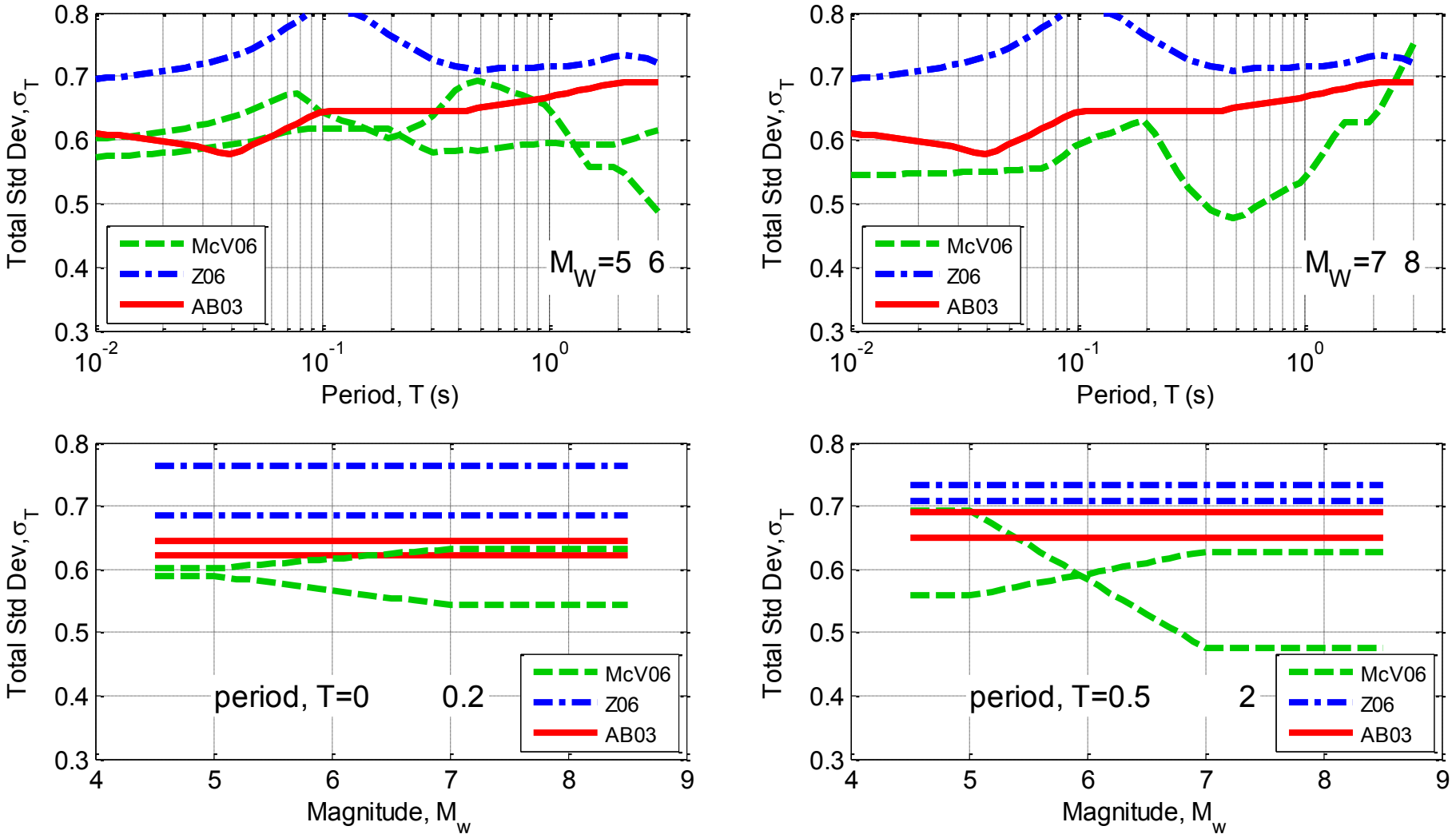

Figure C-10: Total standard deviation scaling of slab ground motion prediction equations with period and magnitude.

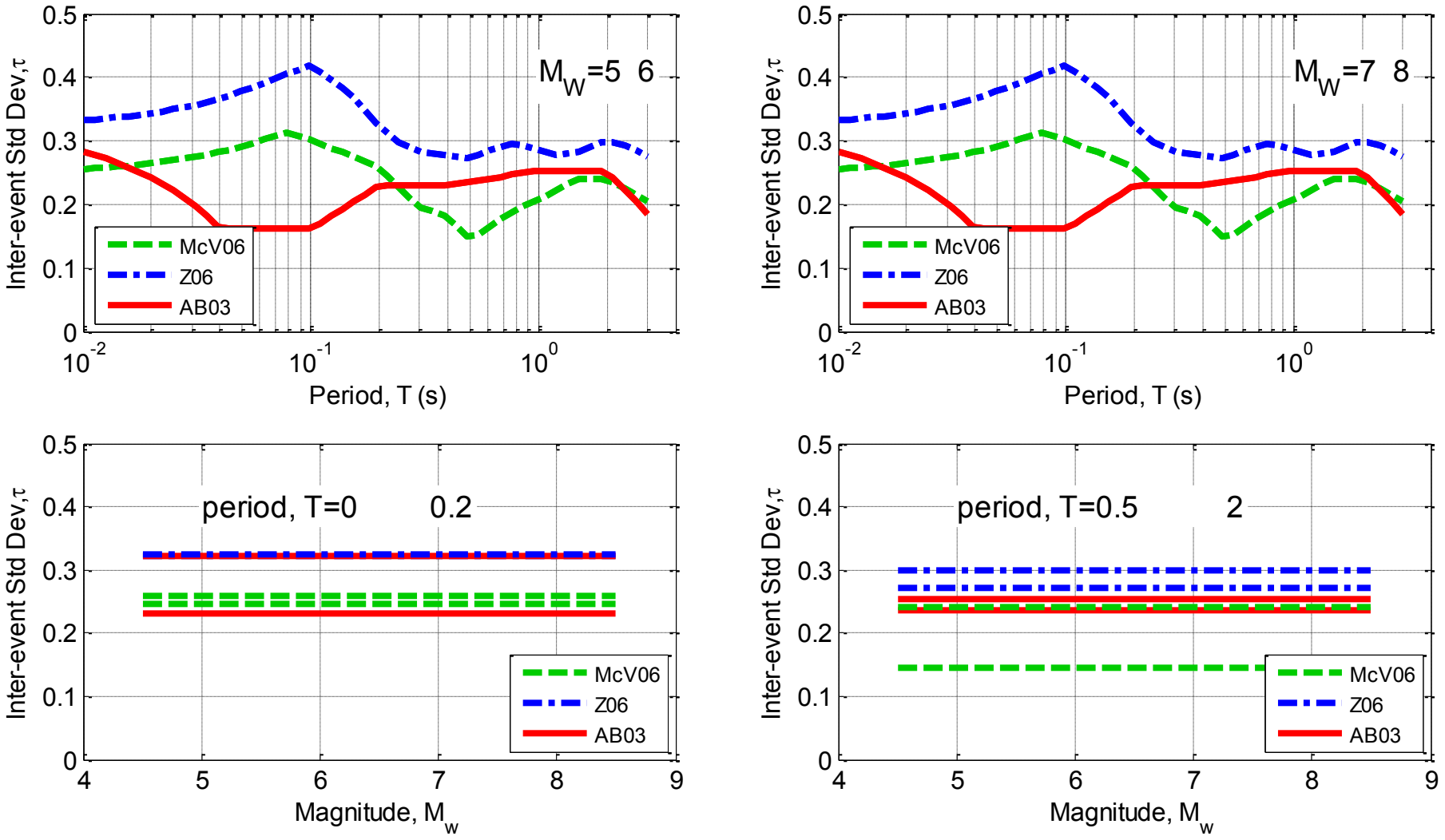

Figure C-11: Inter-event standard deviation scaling of slab ground motion prediction equations with period and magnitude.

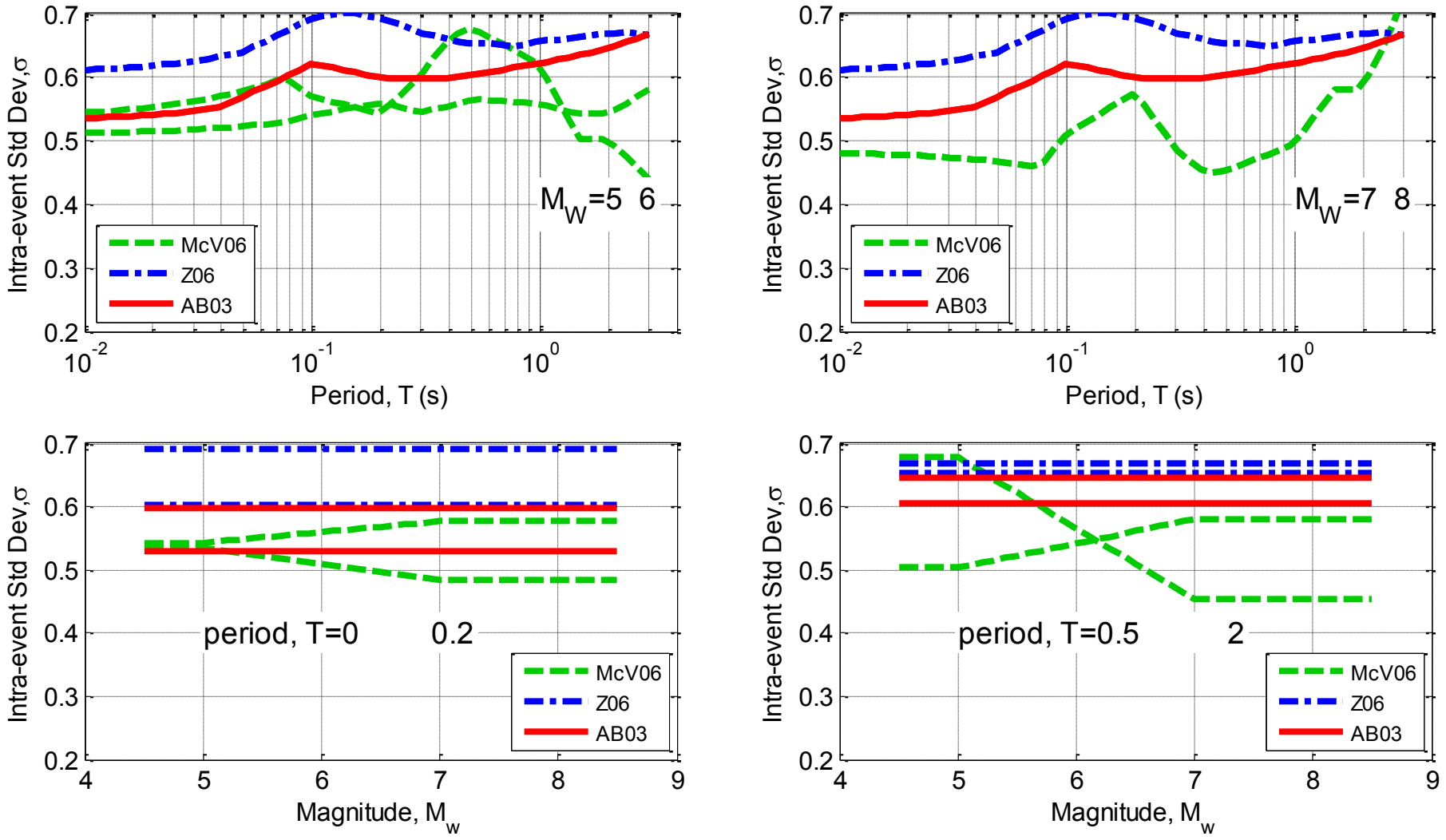

Figure C-12: Intra-event standard deviation scaling of slab ground motion prediction equations with period and magnitude.

C.5. Parameter scaling of the median of interface prediction equations

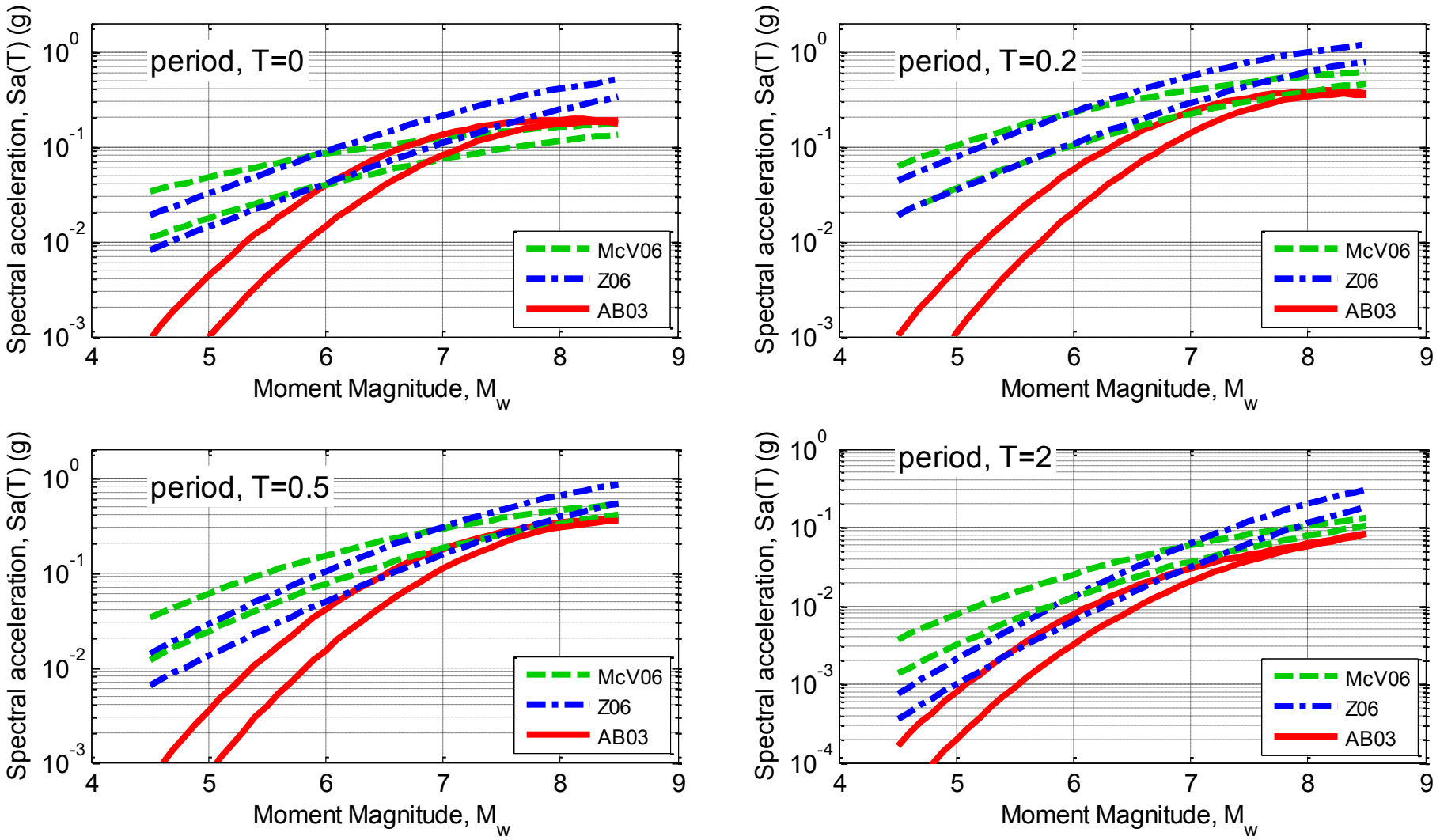

Figure C-13: Magnitude scaling of the median of interface ground motion prediction equations for distances of 15, and 25 km: (a) Sa(0.0); (b) Sa(0.2); (c) Sa(0.5); and (d) Sa(1.0). (predictions for site class C, depth 15km).

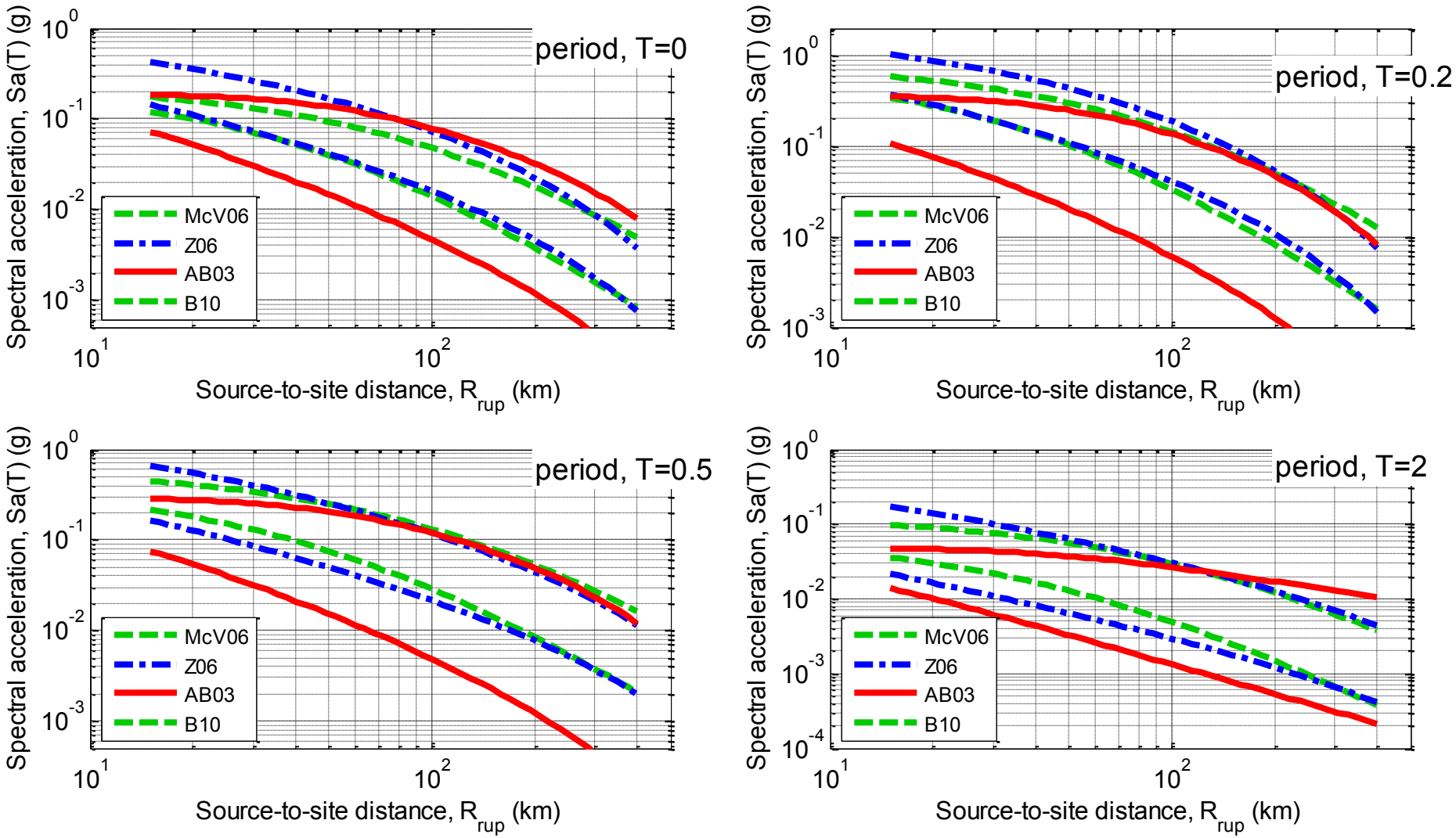

Figure C-14: Path distance scaling of the median of interface ground motion prediction equations for magnitudes of 6 and 7.5: (a) Sa(0.0); (b) Sa(0.2); (c) Sa(0.5); and (d) Sa(1.0). (predictions for site class C, depth 15km).

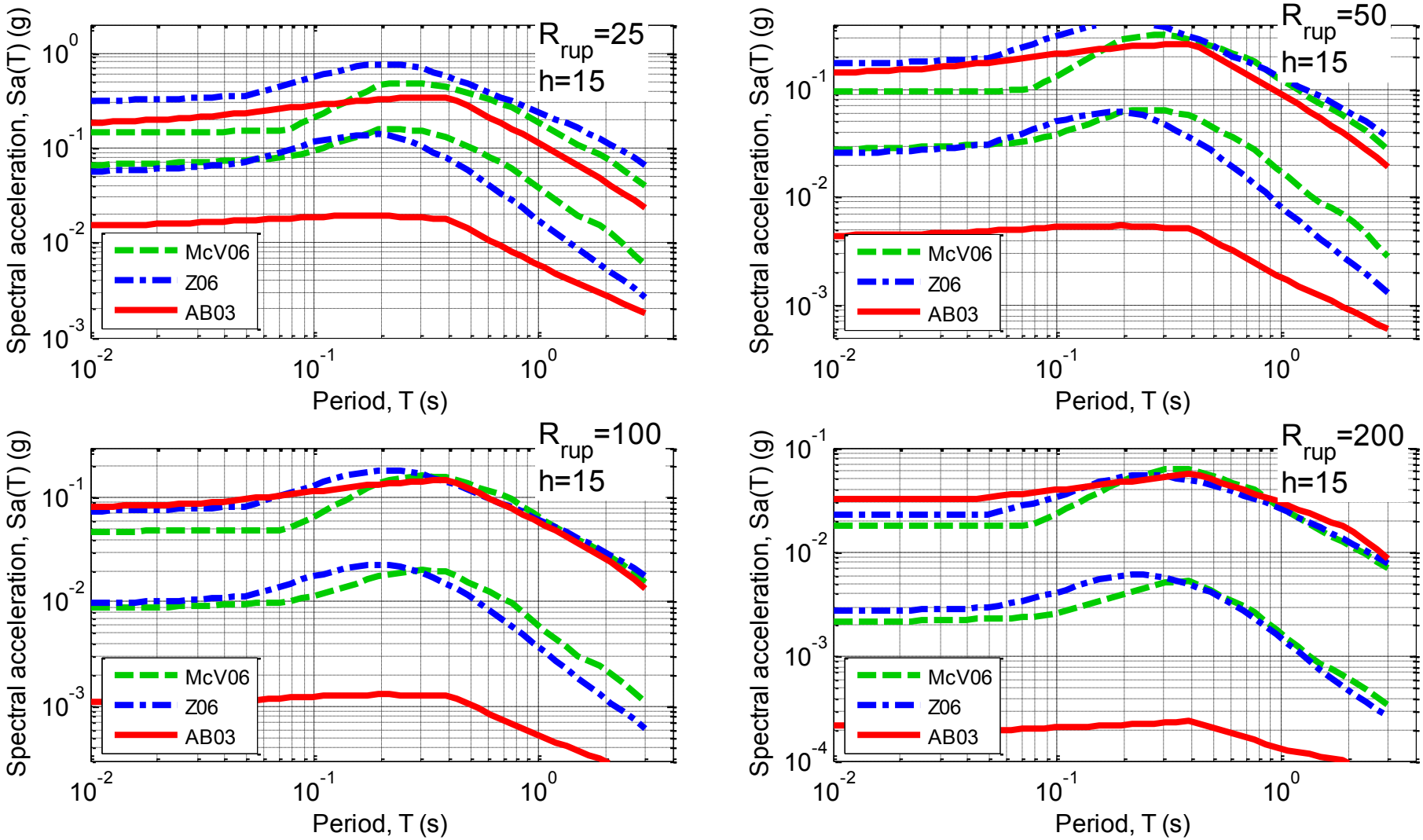

Figure C-15: Vibration period scaling of the median of interface ground motion prediction equations for magnitudes of 5.5 and 7.5: (a) R_{rup} = 25km; (b) R_{rup} = 50km; (c) R_{rup} = 100km; and (d) R_{rup} = 200km. (predictions for site class C and depth 15km).

C.6. Parameter scaling of the standard deviation of interface prediction equations

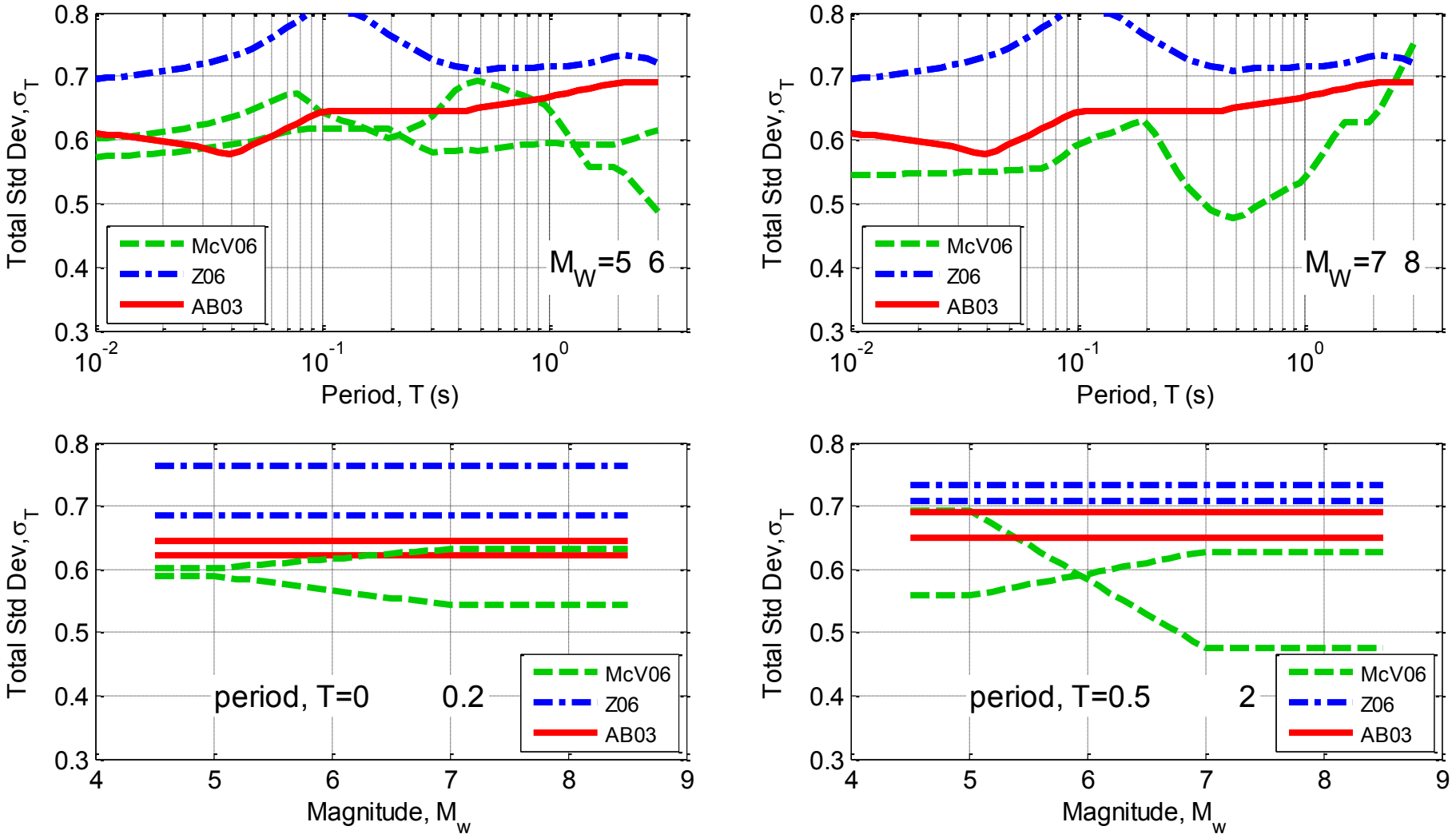

Figure C-16: Total standard deviation scaling of interface ground motion prediction equations with period and magnitude.

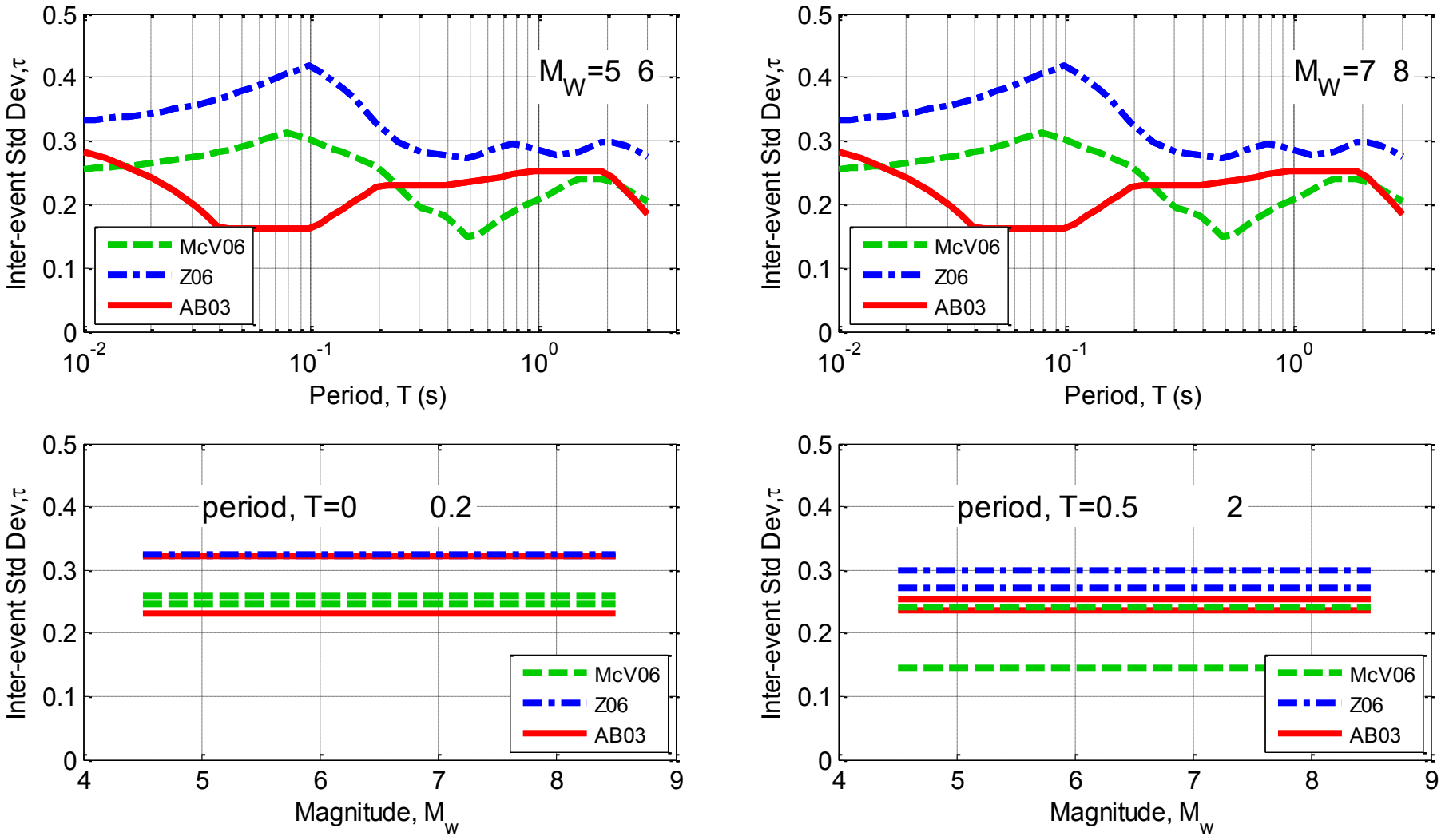

Figure C-17: Inter-event standard deviation scaling of interface ground motion prediction equations with period and magnitude.

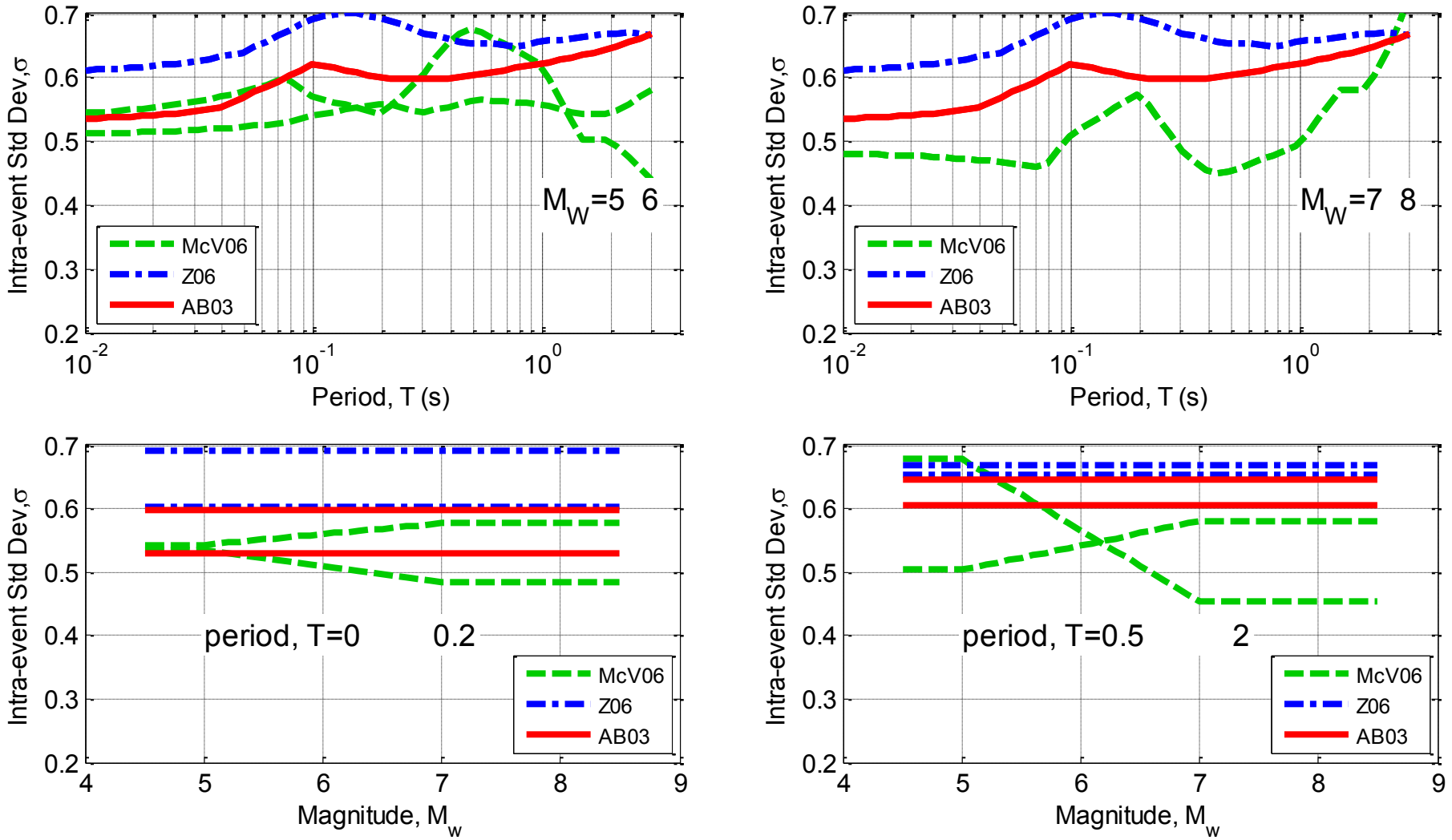

Figure C-18: Intra-event standard deviation scaling of interface ground motion prediction equations with period and magnitude.

APPENDIX D OBSERVED RESIDUALS OF VARIOUS GROUND MOTION PREDICTION EQUATIONS

D.1. McVerry et al. (2006) Crustal model

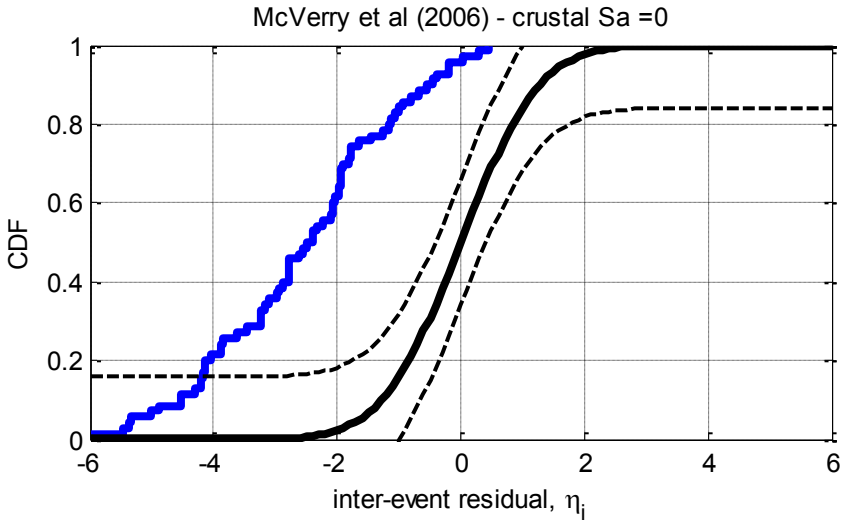

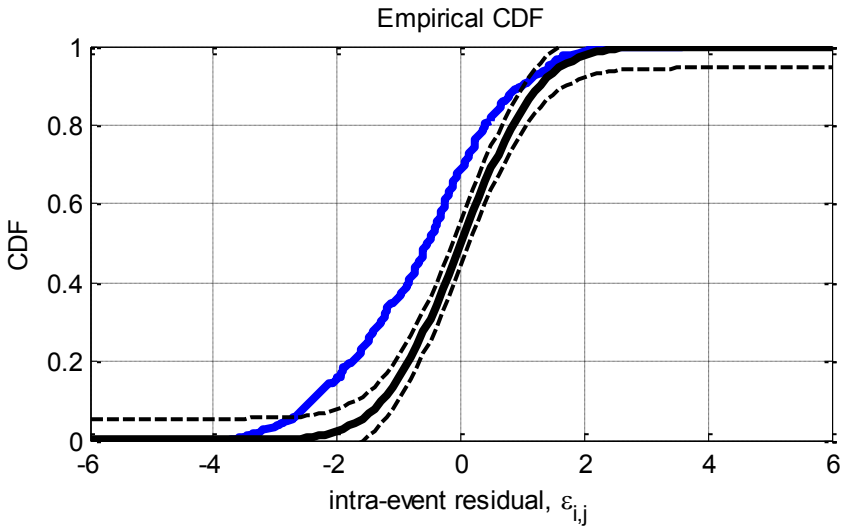

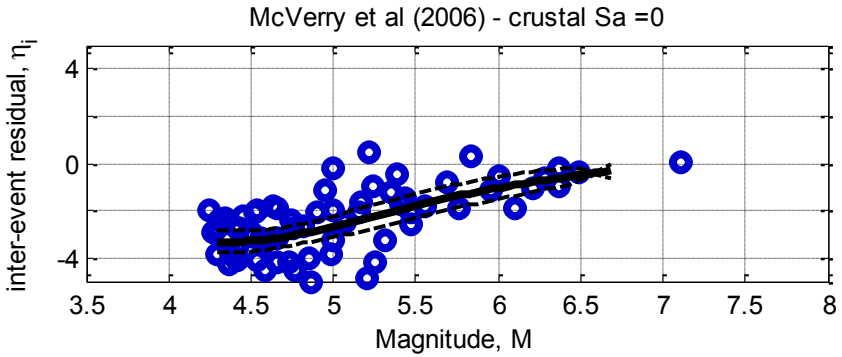

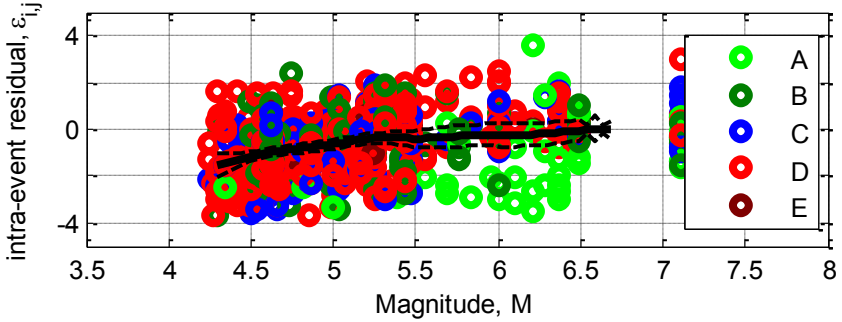

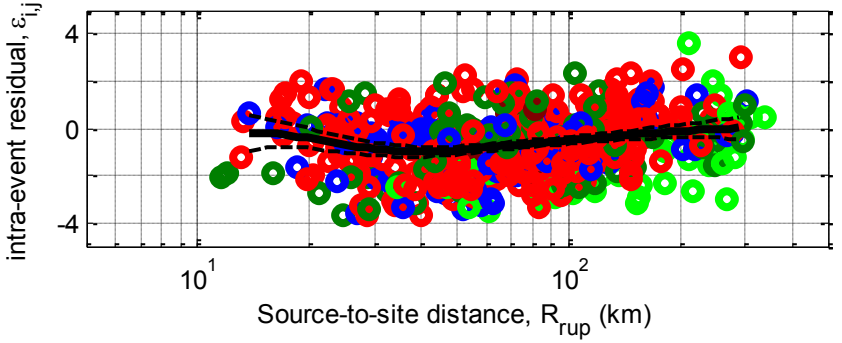

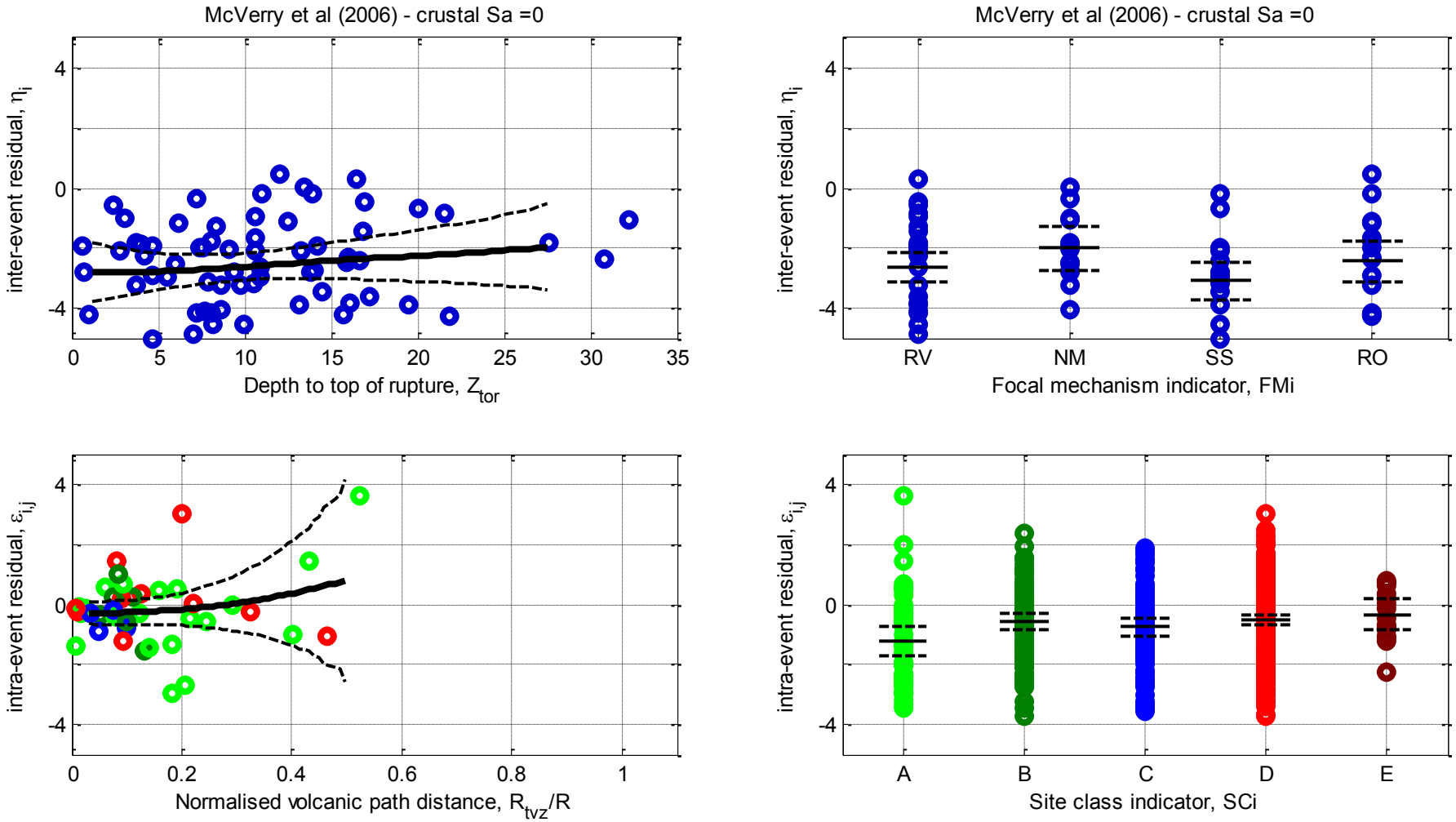

Figure D-1: Residuals for Sa(0.0) using the McVerry et al. (2006) crustal model

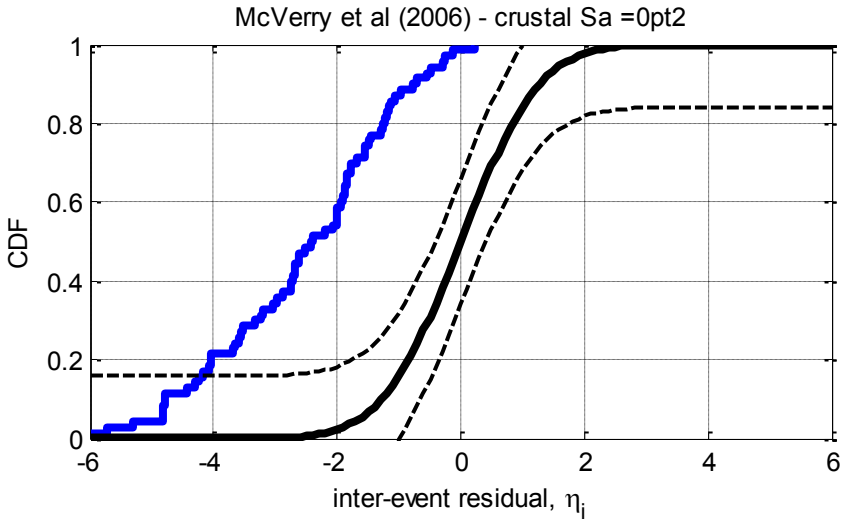
McVerry et al (2006) - crustal Sa =0pt2
CDF
inter-event residual, η_i

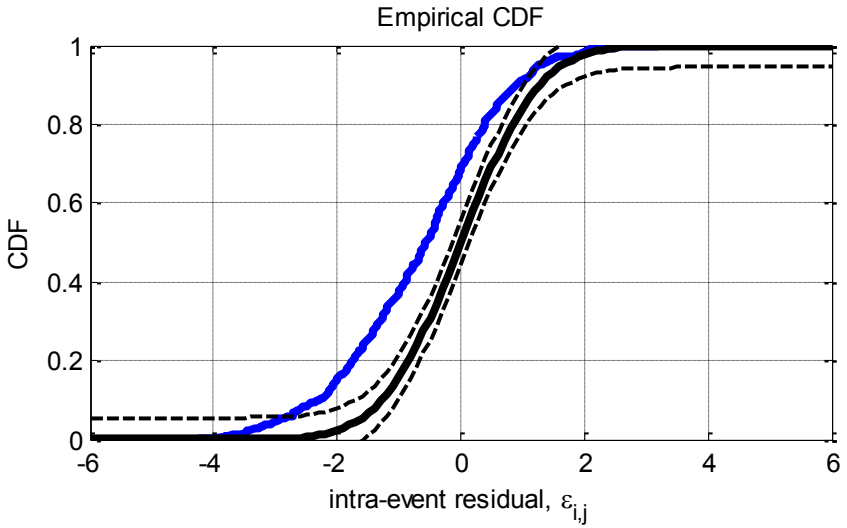
Empirical CDF
CDF
intra-event residual, $\varepsilon_{i,j}$

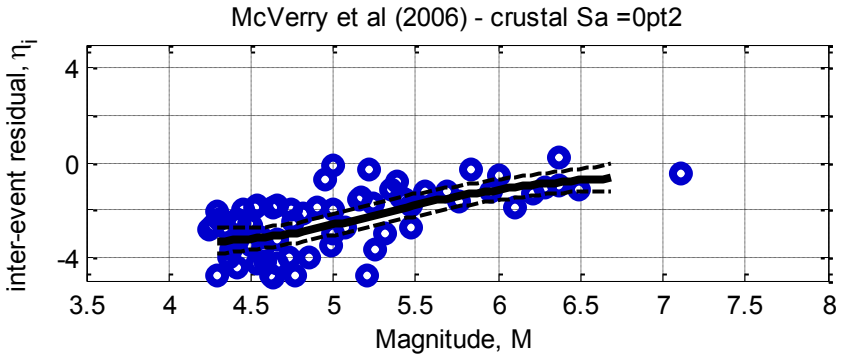
McVerry et al (2006) - crustal Sa =0pt2
inter-event residual, η_i
Magnitude, M

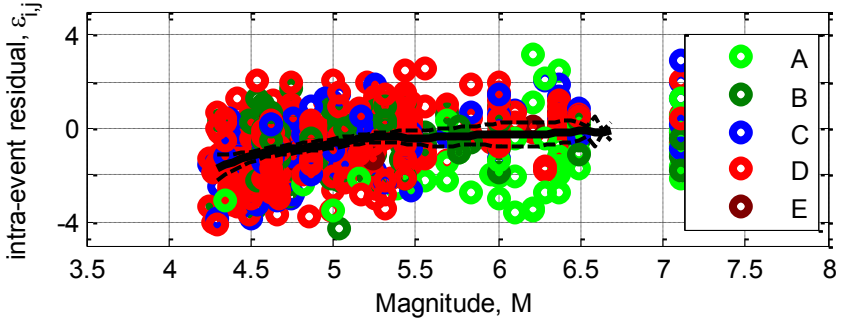
intra-event residual, $\varepsilon_{i,j}$
Magnitude, M
A
B
C
D
E

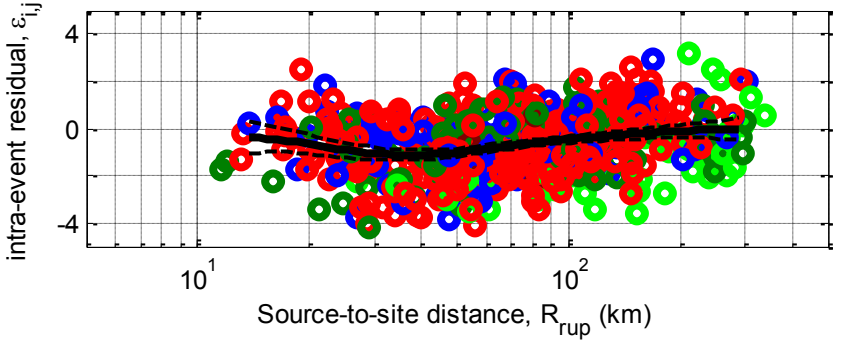
intra-event residual, $\varepsilon_{i,j}$
Source-to-site distance, R_{rup} (km)

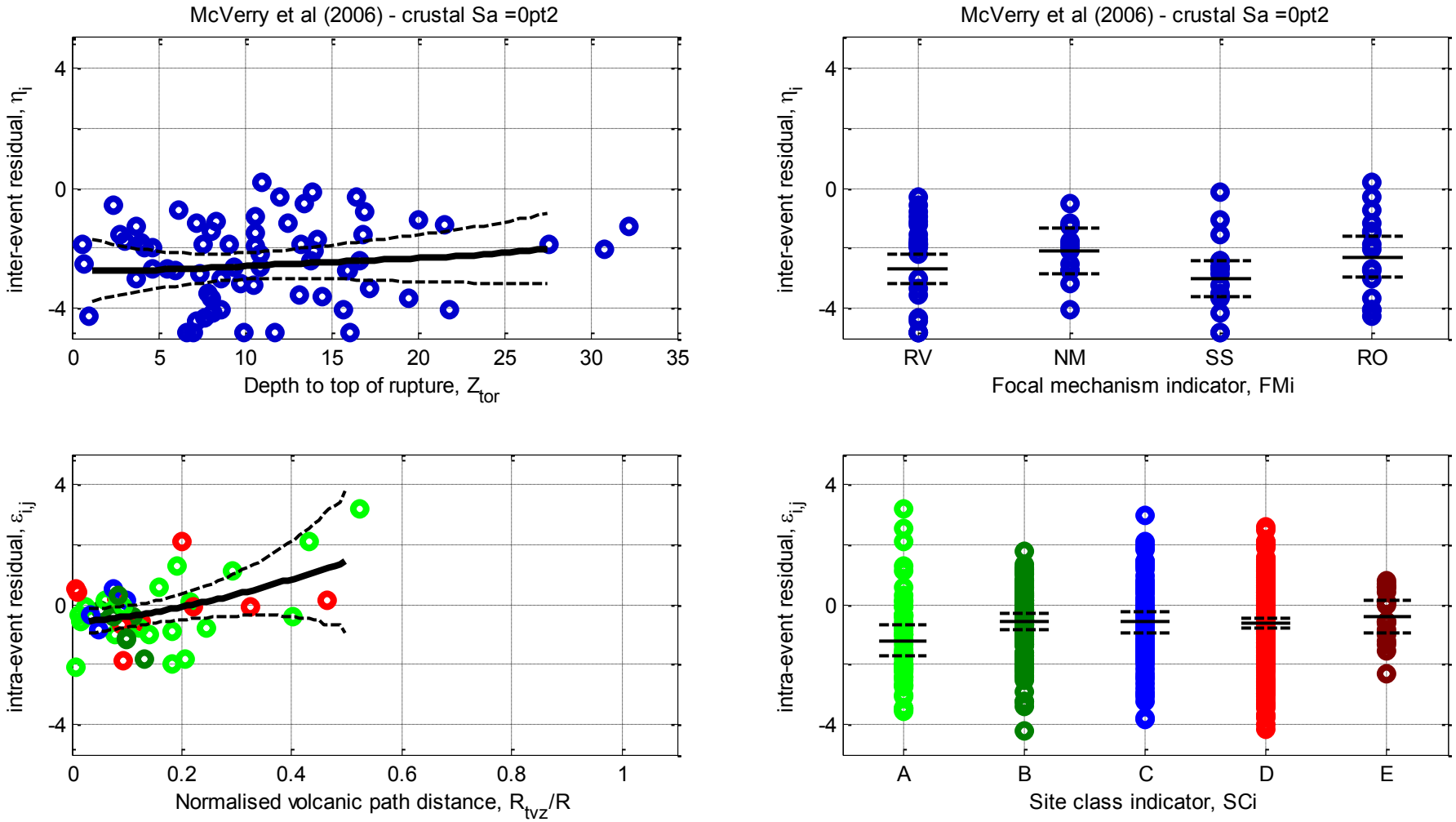

Figure D-2: Residuals for Sa(0.2) using the McVerry et al. (2006) crustal model

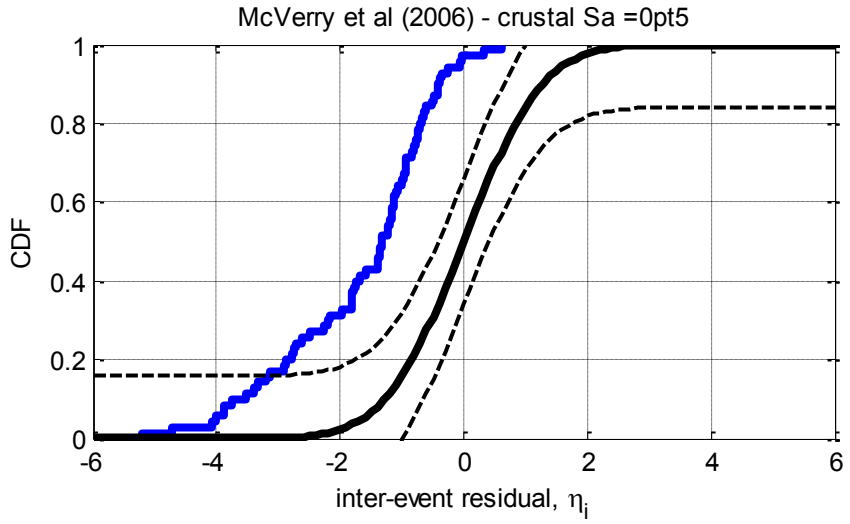
McVerry et al (2006) - crustal Sa =0pt5
CDF
inter-event residual, η_i

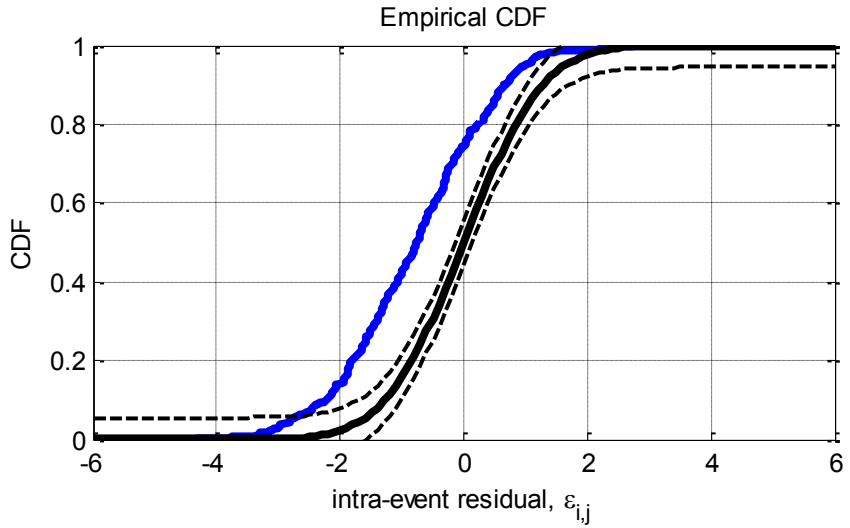
Empirical CDF
CDF
intra-event residual, $\varepsilon_{i,j}$

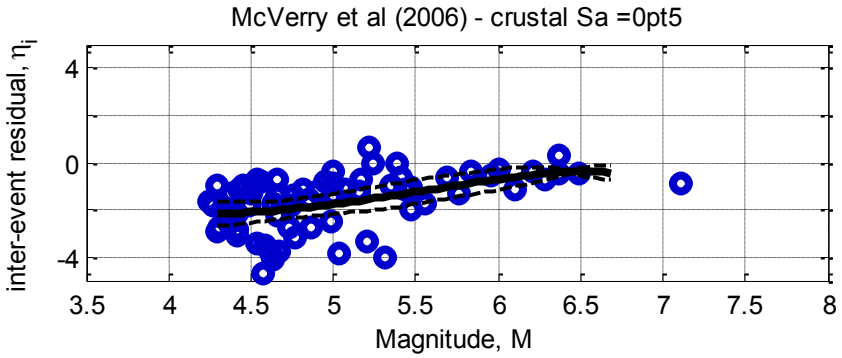
McVerry et al (2006) - crustal Sa =0pt5
inter-event residual, η_i
Magnitude, M

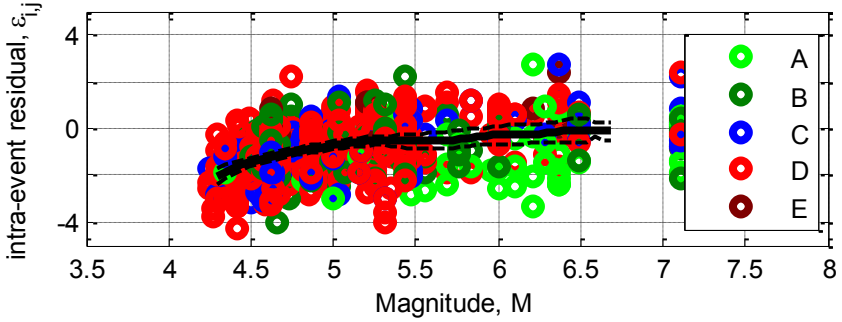
intra-event residual, $\varepsilon_{i,j}$
Magnitude, M
A
B
C
D
E

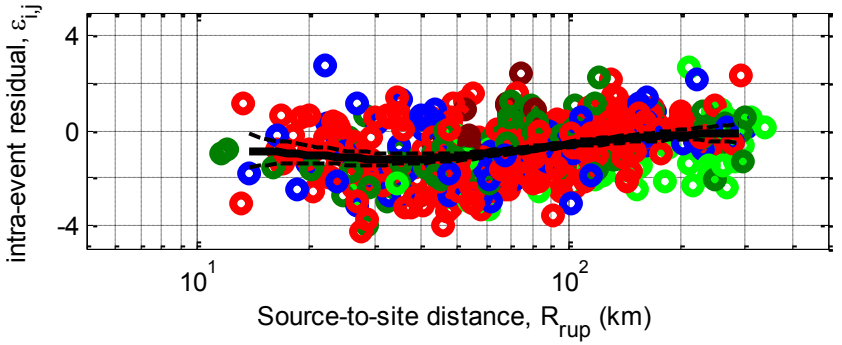
intra-event residual, $\varepsilon_{i,j}$
Source-to-site distance, R_{rup} (km)

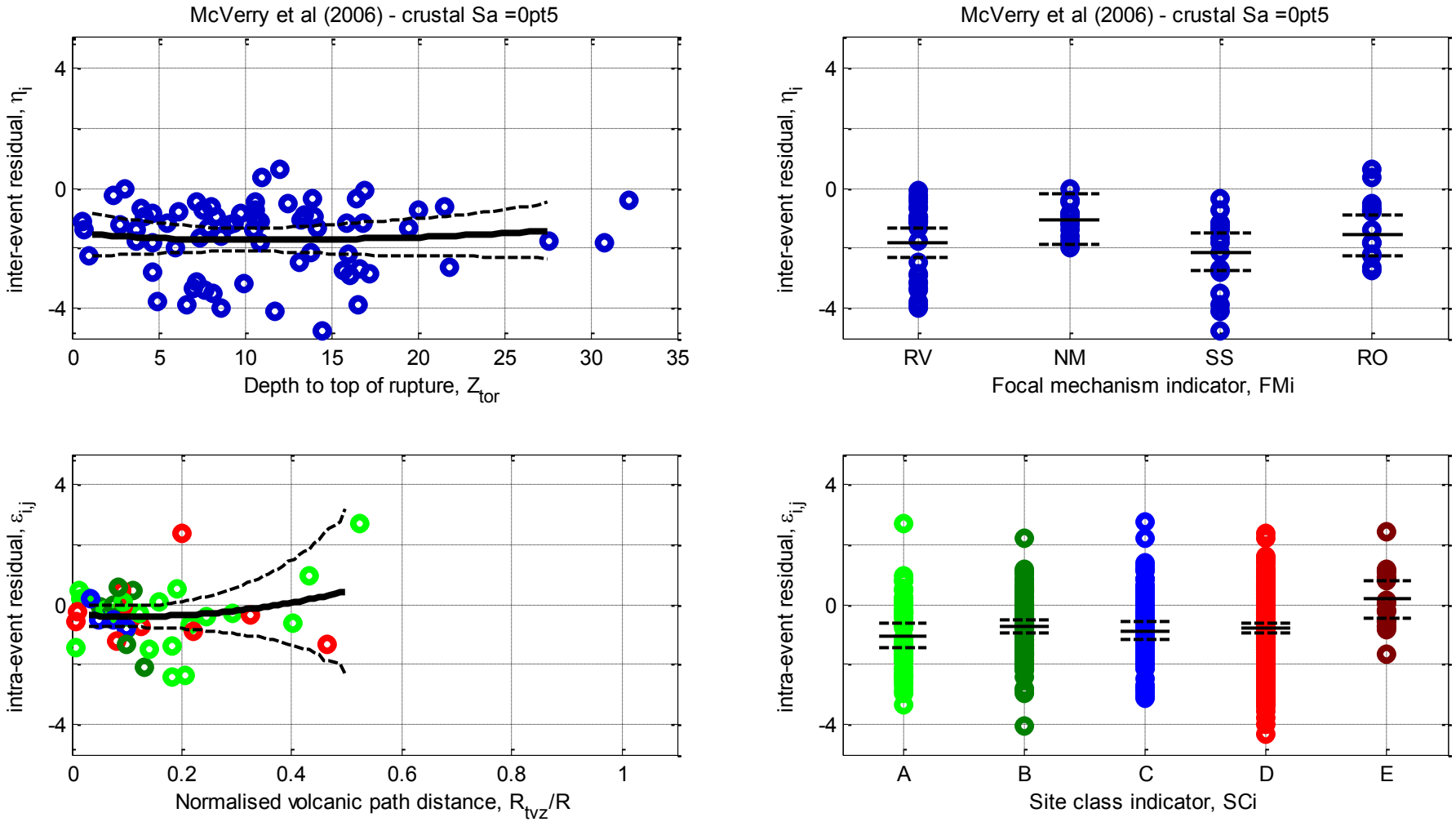

Figure D-3: Residuals for Sa(0.5) using the McVerry et al. (2006) crustal model

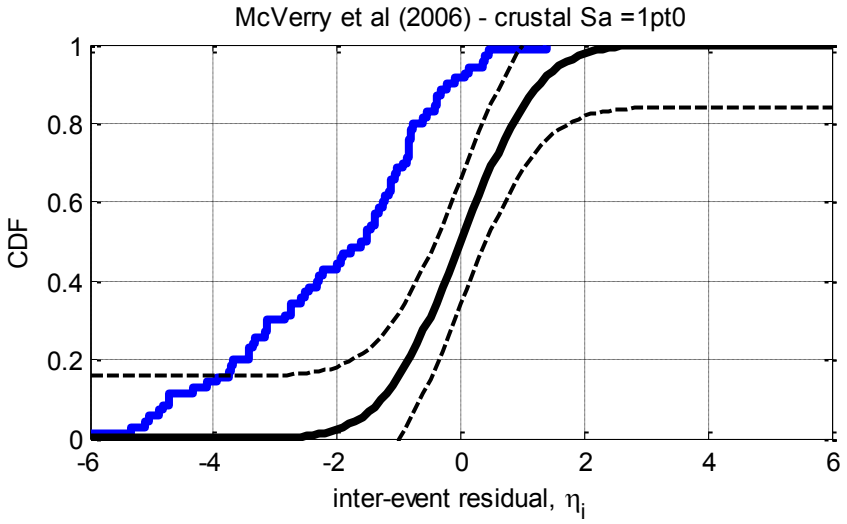
McVerry et al (2006) - crustal Sa =1pt0
CDF
inter-event residual, η_i

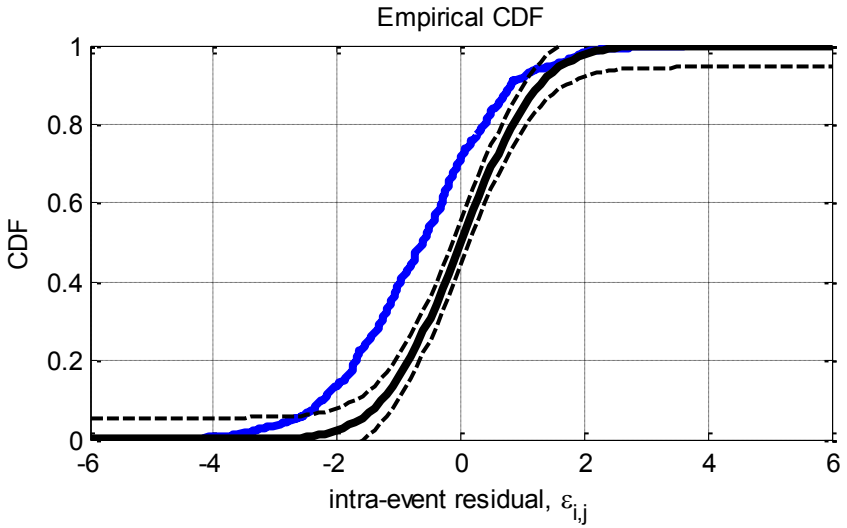
Empirical CDF
CDF
intra-event residual, $\varepsilon_{i,j}$

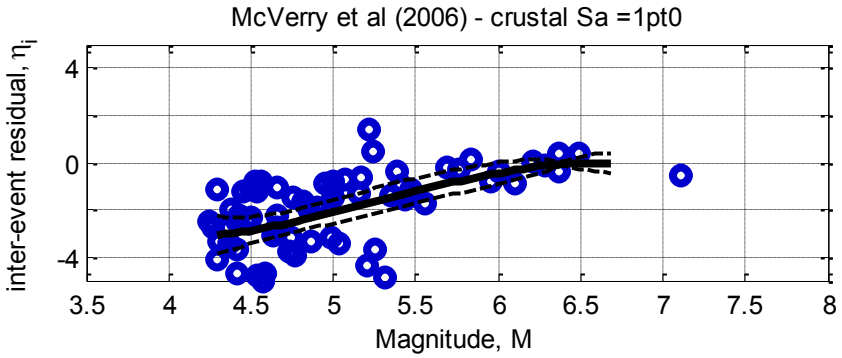
McVerry et al (2006) - crustal Sa =1pt0
inter-event residual, η_i
Magnitude, M

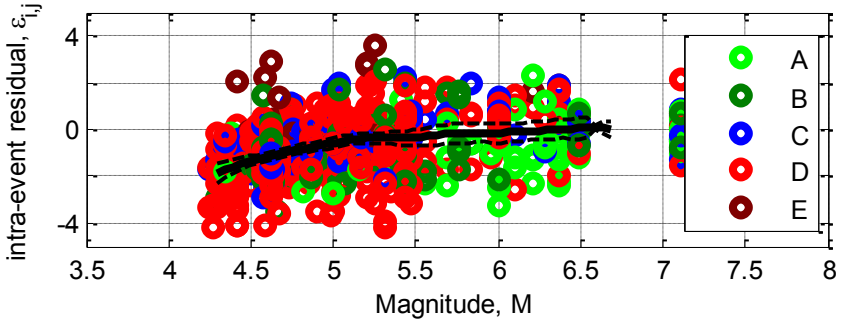
intra-event residual, $\varepsilon_{i,j}$
A
B
C
D
E
Magnitude, M

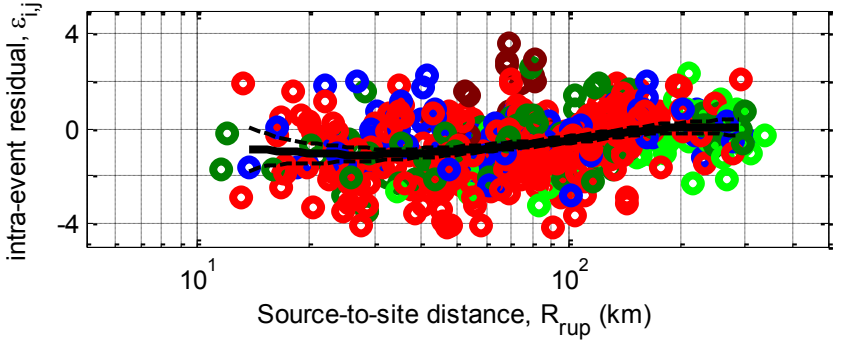
intra-event residual, $\varepsilon_{i,j}$
Source-to-site distance, R_{rup} (km)

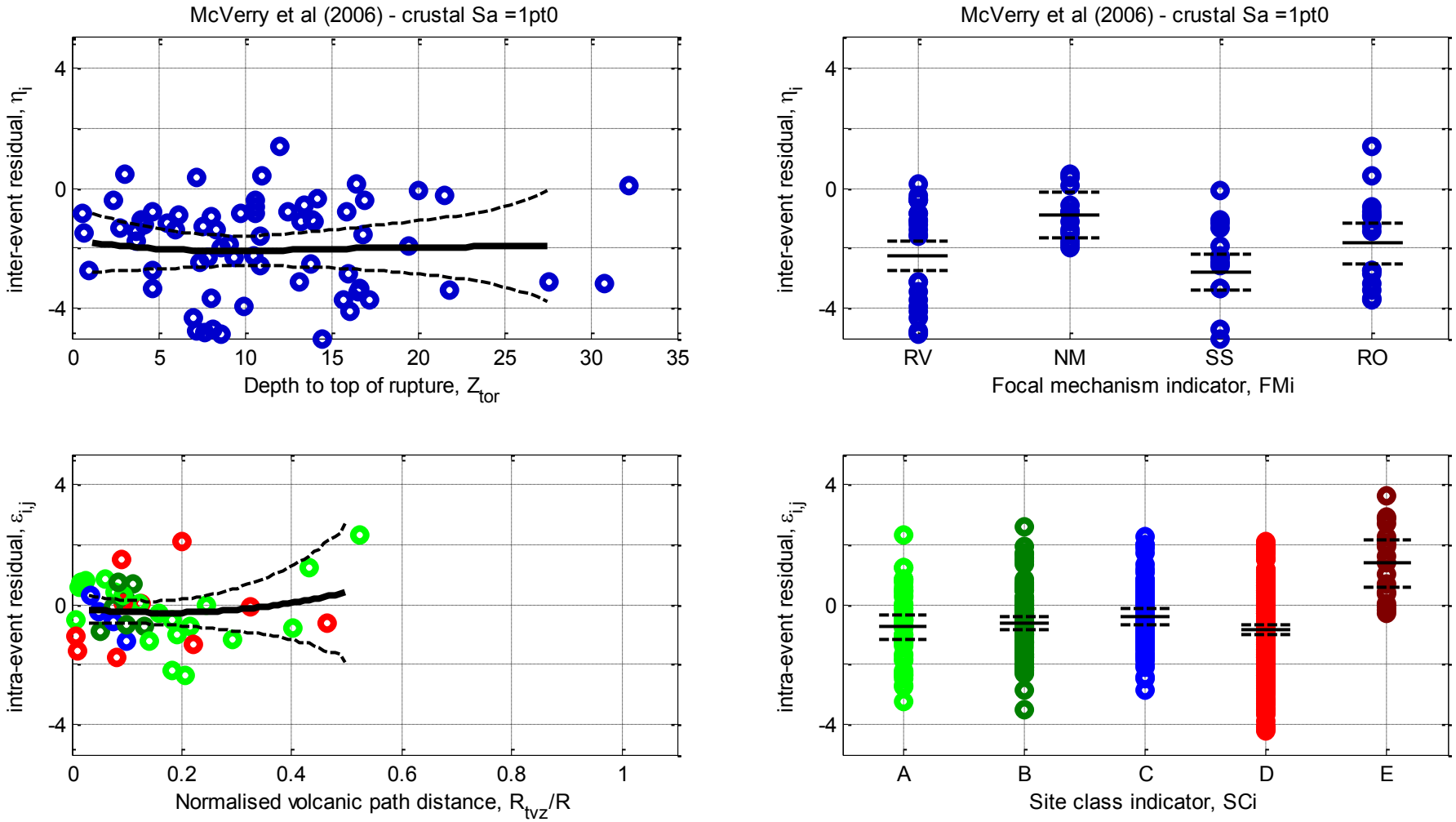

Figure D-4: Residuals for Sa(1.0) using the McVerry et al. (2006) crustal model

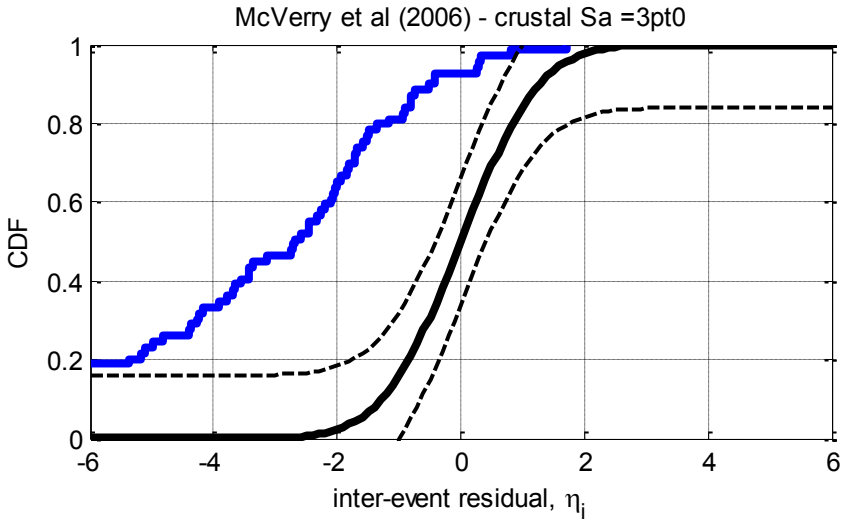
McVerry et al (2006) - crustal Sa =3pt0
CDF
inter-event residual, η_i

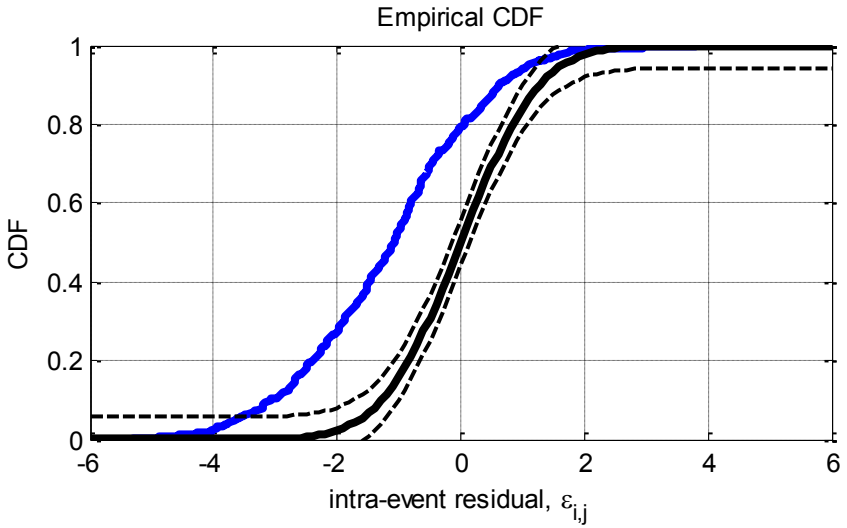
Empirical CDF
CDF
intra-event residual, $\varepsilon_{i,j}$

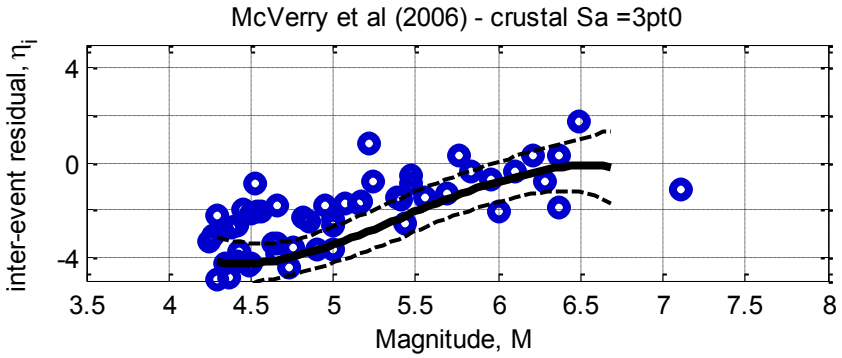
McVerry et al (2006) - crustal Sa =3pt0
inter-event residual, η_i
Magnitude, M

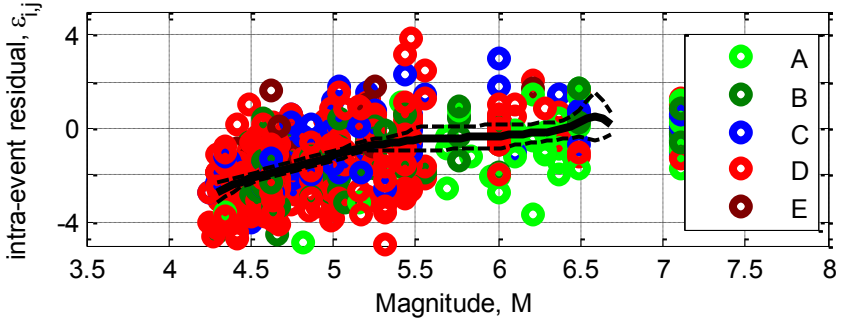
intra-event residual, $\varepsilon_{i,j}$
Magnitude, M
A
B
C
D
E

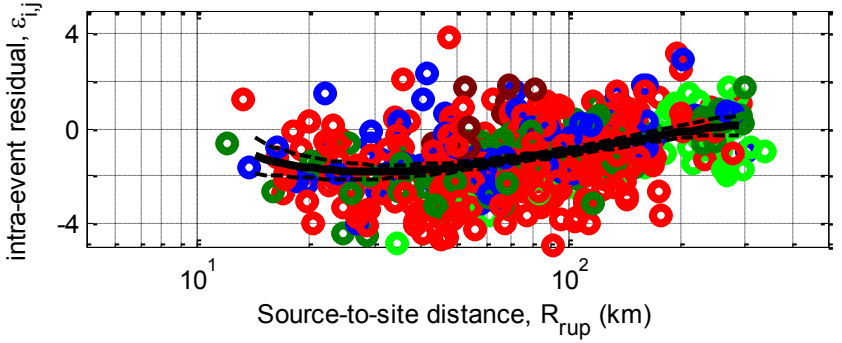
intra-event residual, $\varepsilon_{i,j}$
Source-to-site distance, R_{rup} (km)

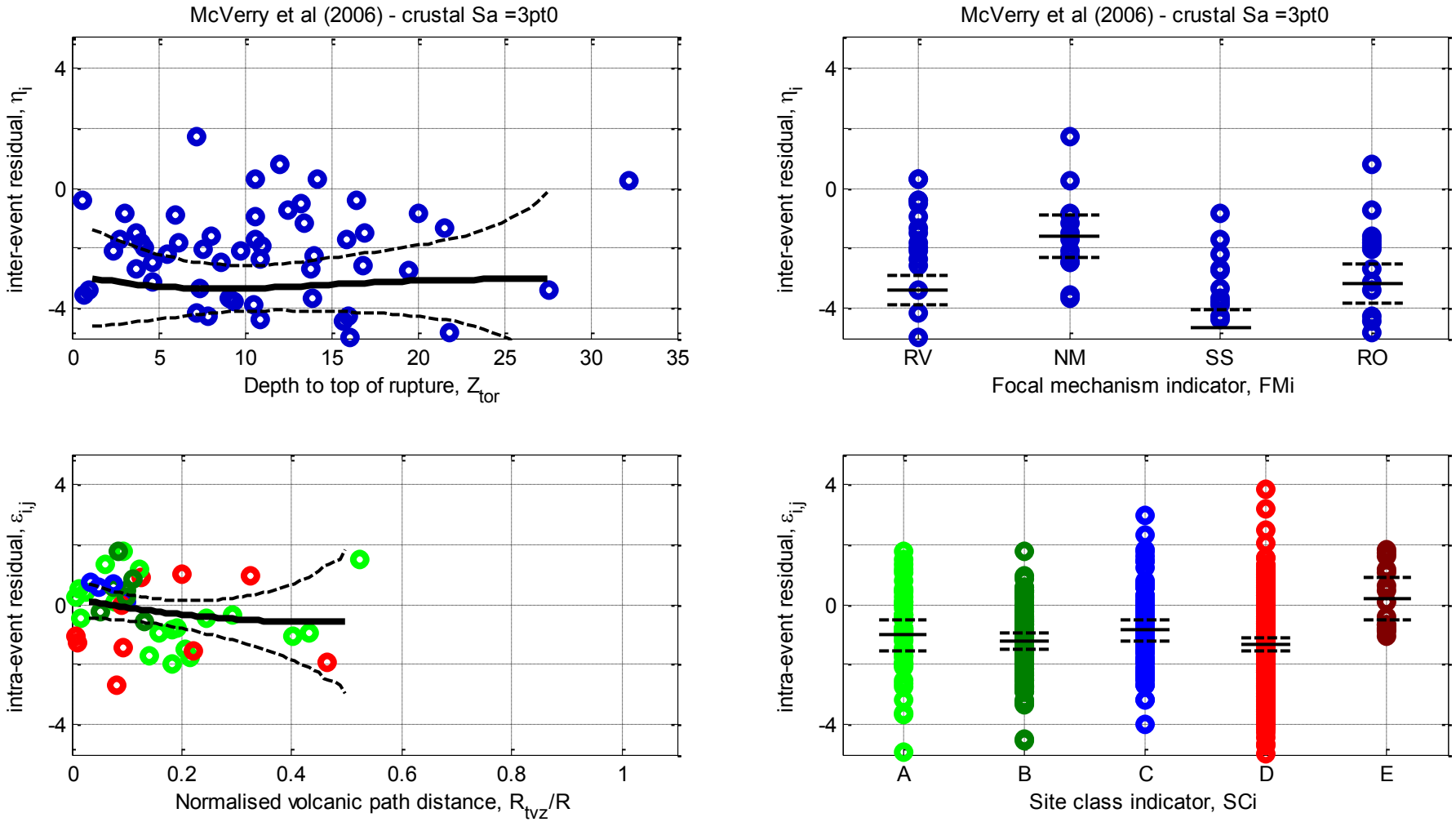

Figure D-5: Residuals for Sa(3.0) using the McVerry et al. (2006) crustal model

D.2. Zhao et al. (2006) Crustal model

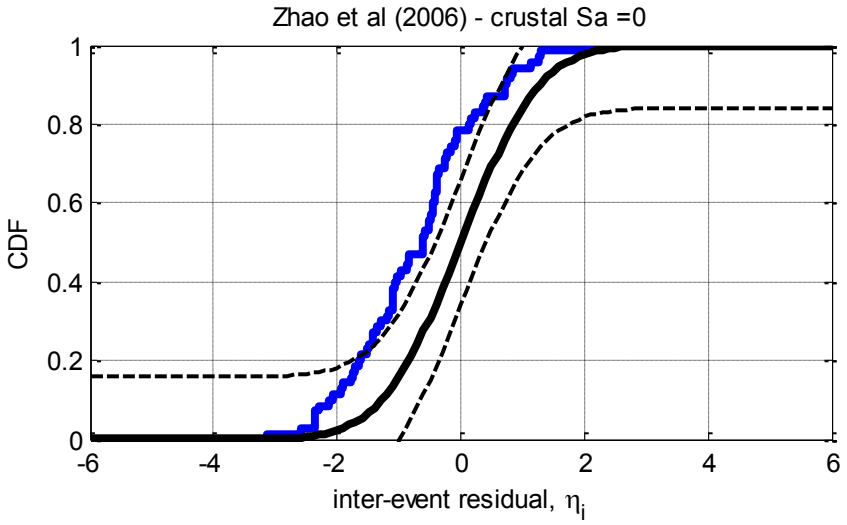

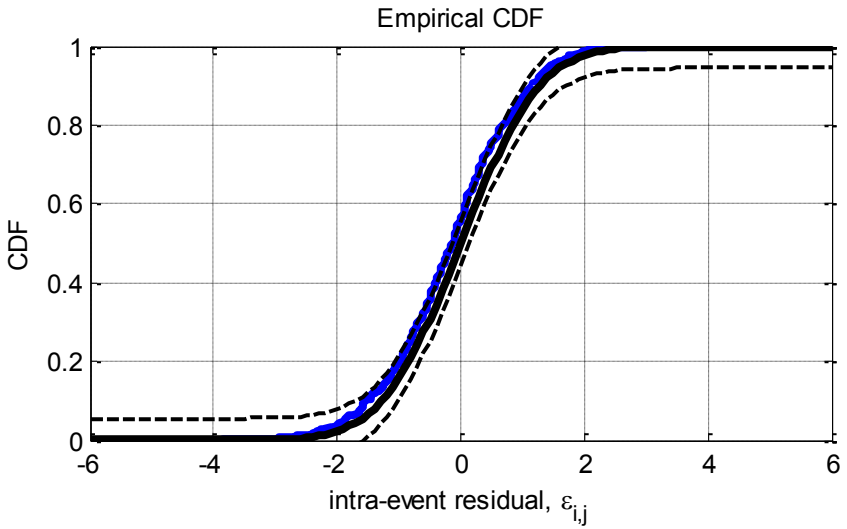

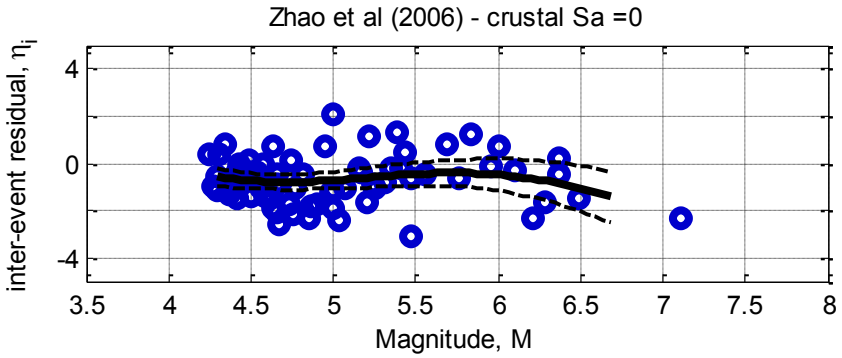

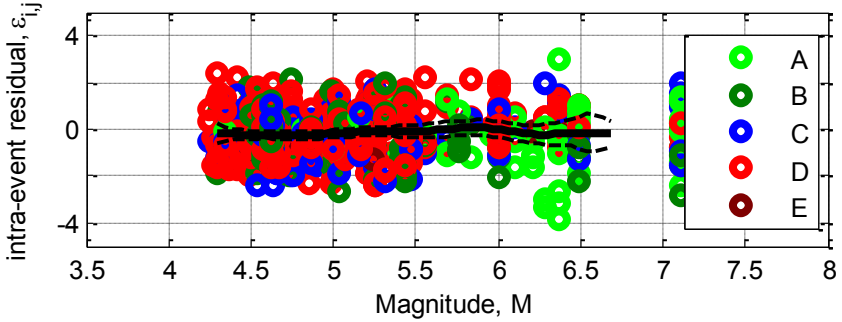

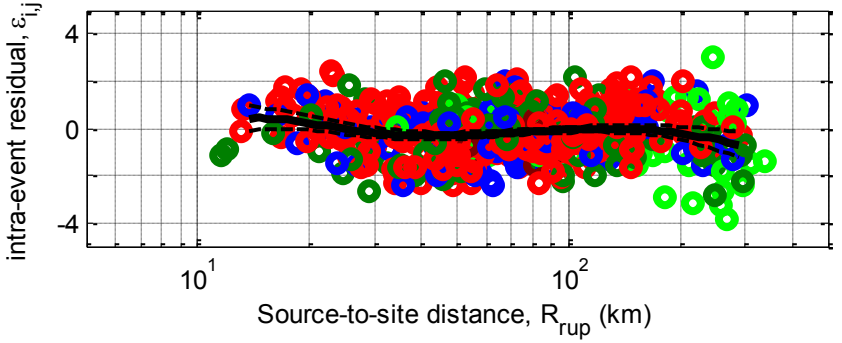

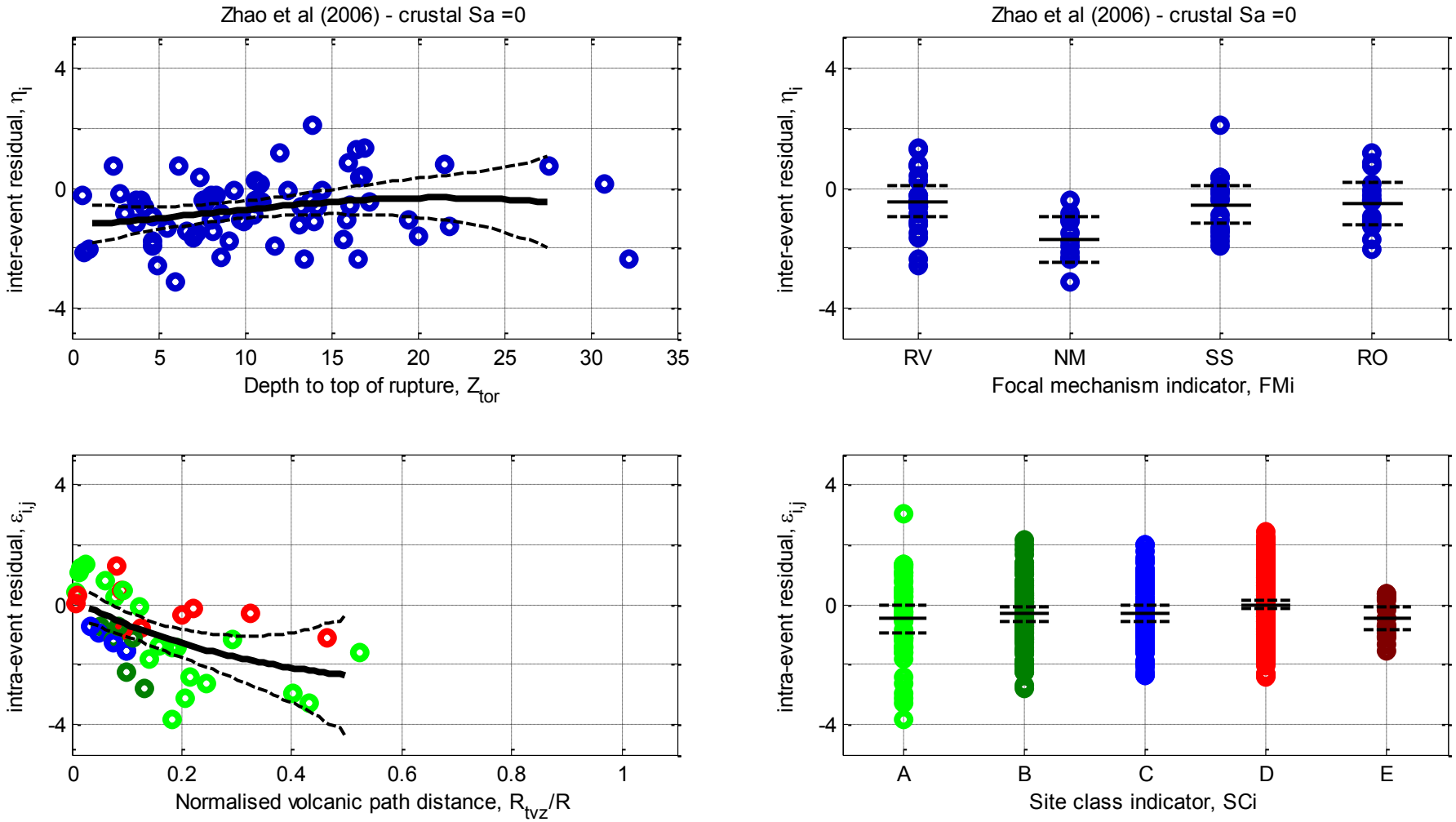

Figure D-6: Residuals for Sa(0.0) using the Zhao et al. (2006) crustal model

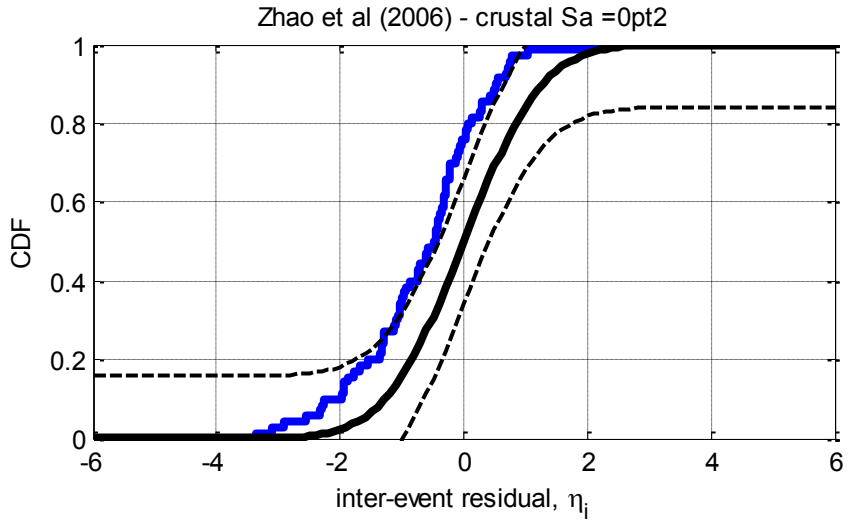
Zhao et al (2006) - crustal Sa =0pt2
CDF
inter-event residual, η_i

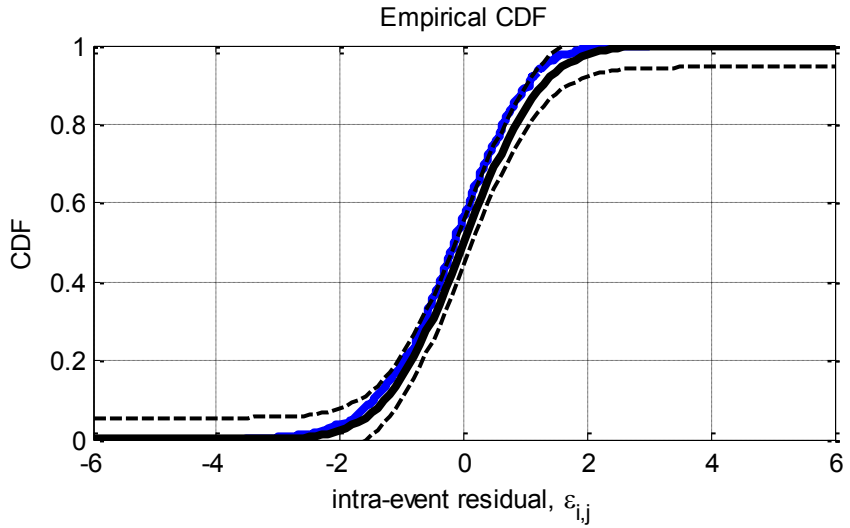
Empirical CDF
CDF
intra-event residual, $\varepsilon_{i,j}$

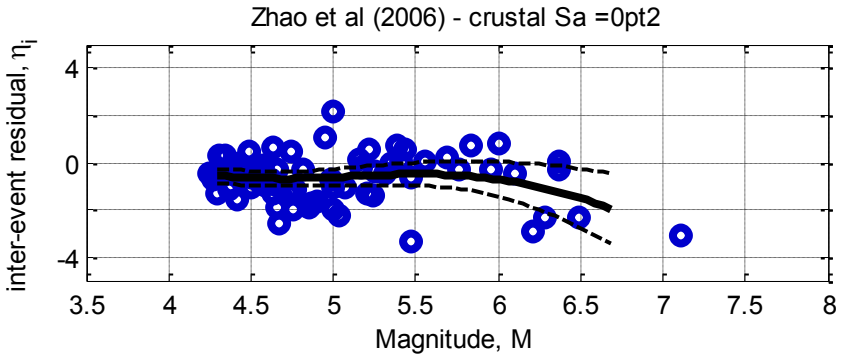
Zhao et al (2006) - crustal Sa =0pt2
inter-event residual, η_i
Magnitude, M

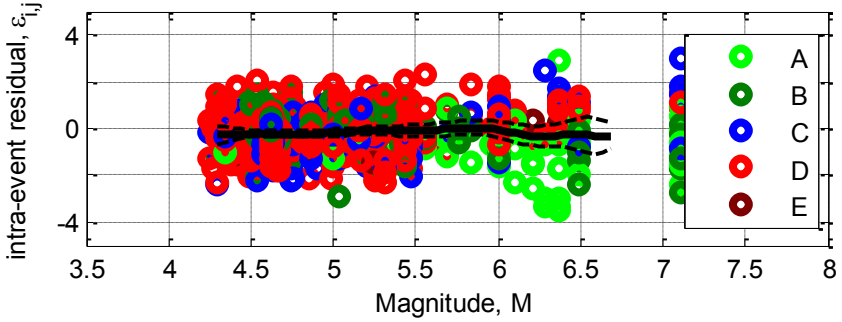
intra-event residual, $\varepsilon_{i,j}$
Magnitude, M
A
B
C
D
E

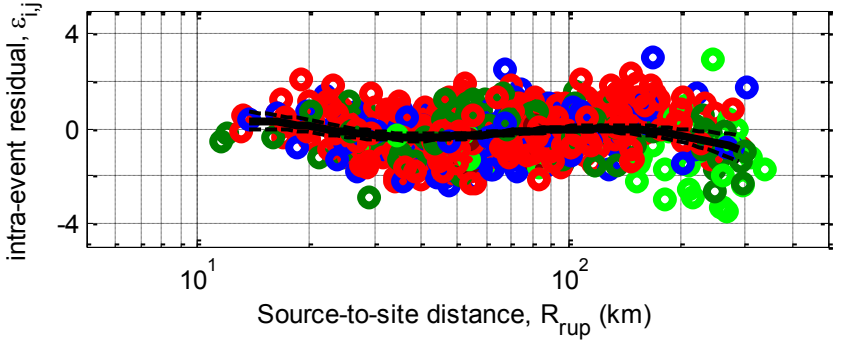
intra-event residual, $\varepsilon_{i,j}$
Source-to-site distance, R_{rup} (km)

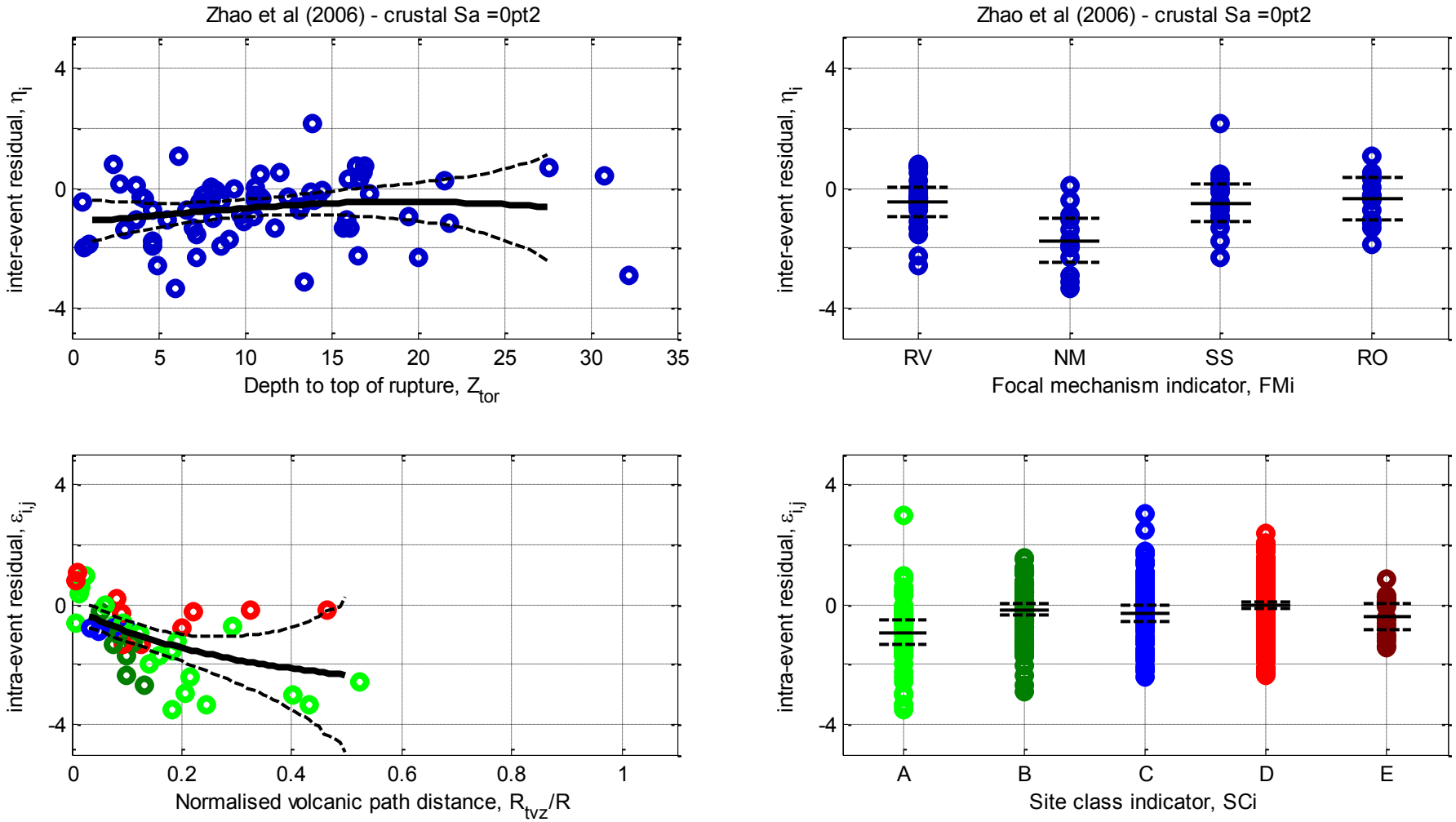

Figure D-7: Residuals for Sa(0.2) using the Zhao et al. (2006) crustal model

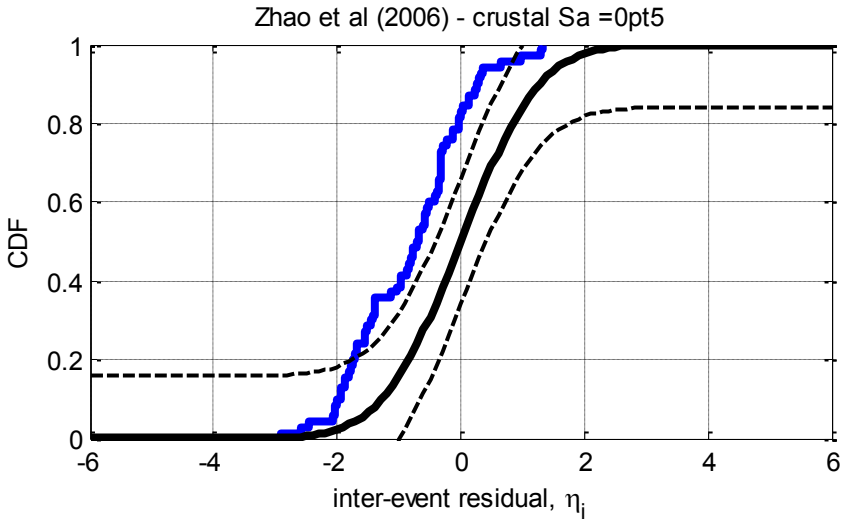
Zhao et al (2006) - crustal Sa =0pt5
CDF
inter-event residual, η_i

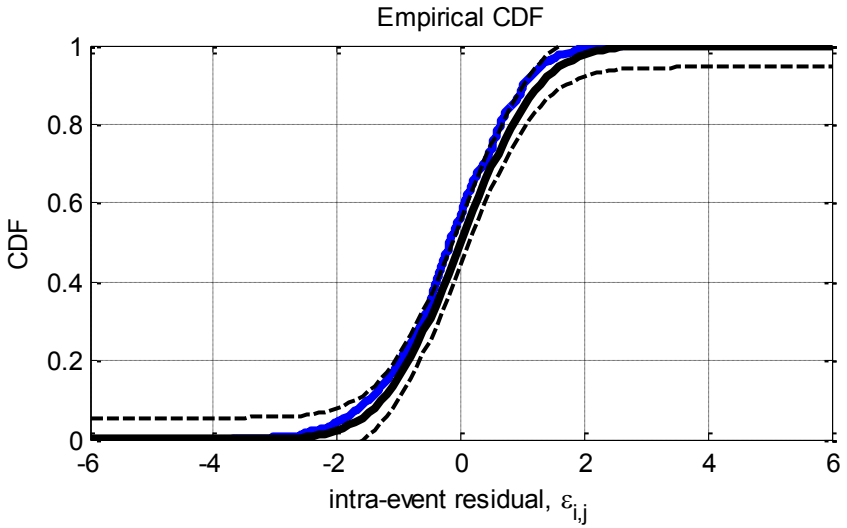
Empirical CDF
CDF
intra-event residual, $\varepsilon_{i,j}$

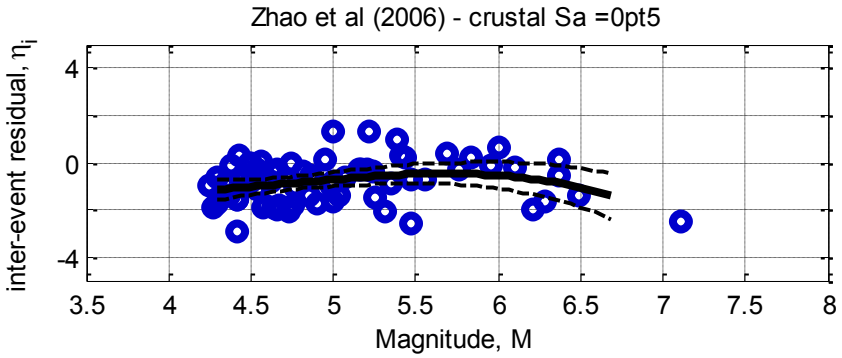
Zhao et al (2006) - crustal Sa =0pt5
inter-event residual, η_i
Magnitude, M

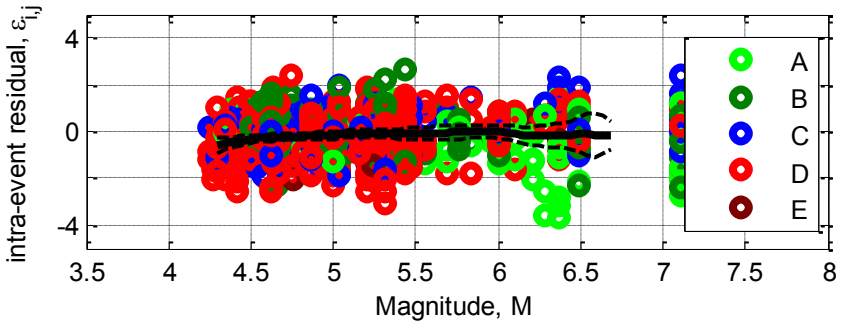
intra-event residual, $\varepsilon_{i,j}$
Magnitude, M
A
B
C
D
E

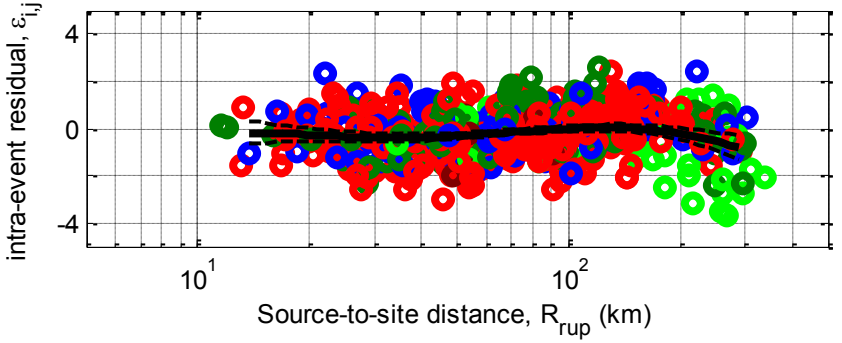
intra-event residual, $\varepsilon_{i,j}$
Source-to-site distance, R_{rup} (km)

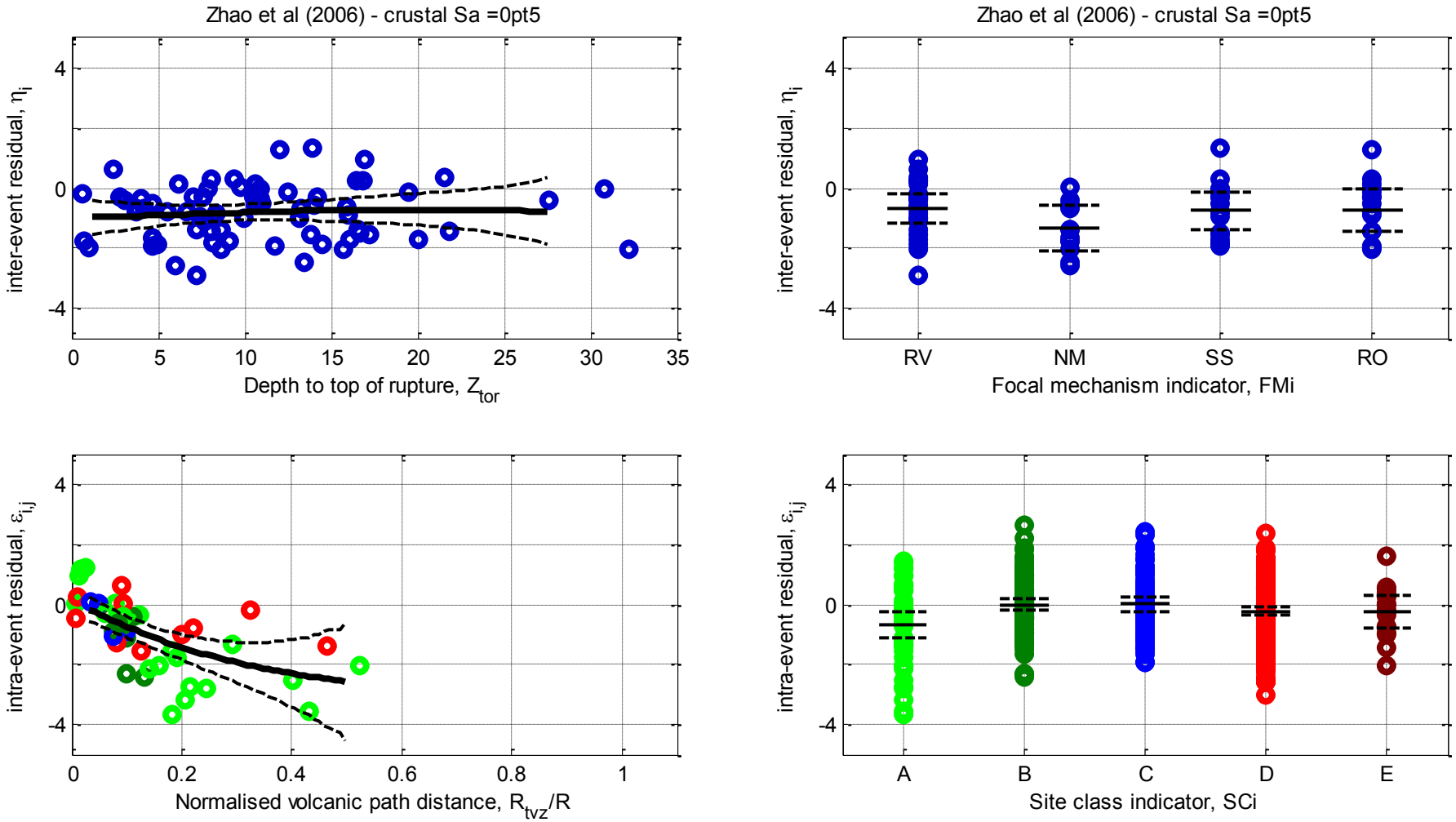

Figure D-8: Residuals for Sa(0.5) using the Zhao et al. (2006) crustal model

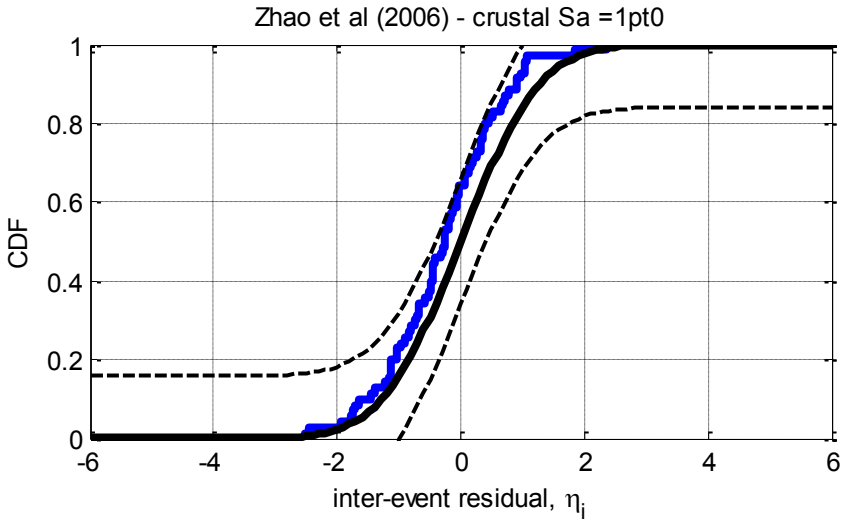
Zhao et al (2006) - crustal Sa =1pt0
CDF
inter-event residual, η_i

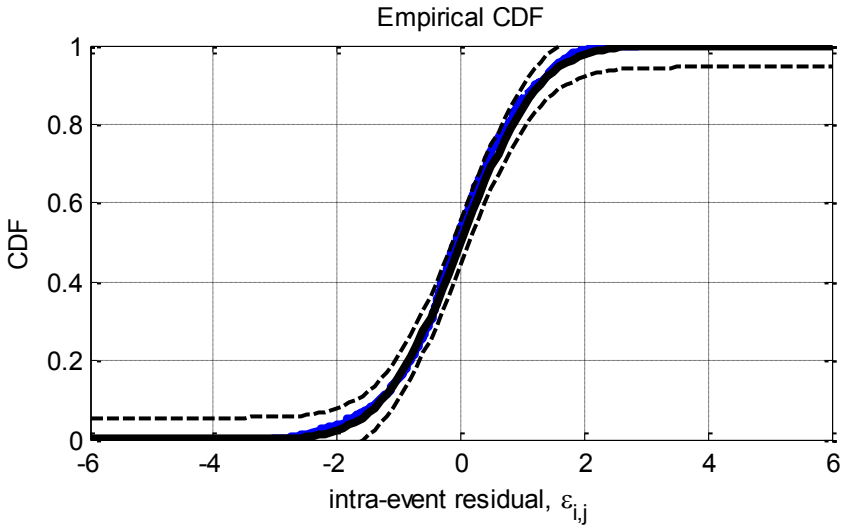
Empirical CDF
CDF
intra-event residual, $\varepsilon_{i,j}$

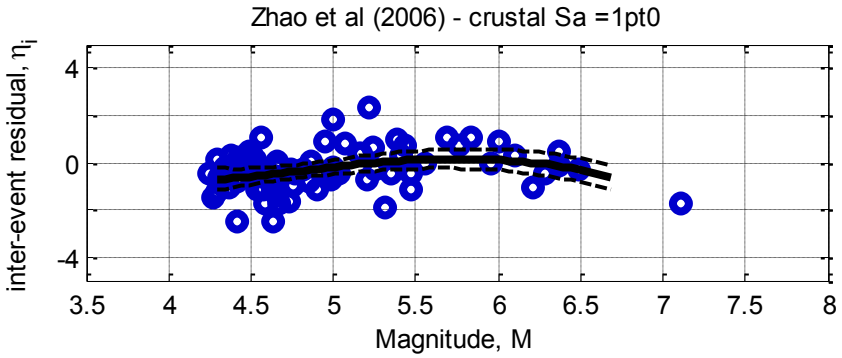
Zhao et al (2006) - crustal Sa =1pt0
inter-event residual, η_i
Magnitude, M

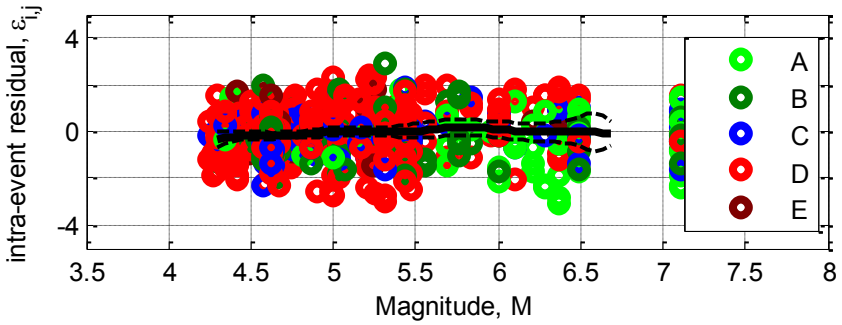
intra-event residual, $\varepsilon_{i,j}$
Magnitude, M
A
B
C
D
E

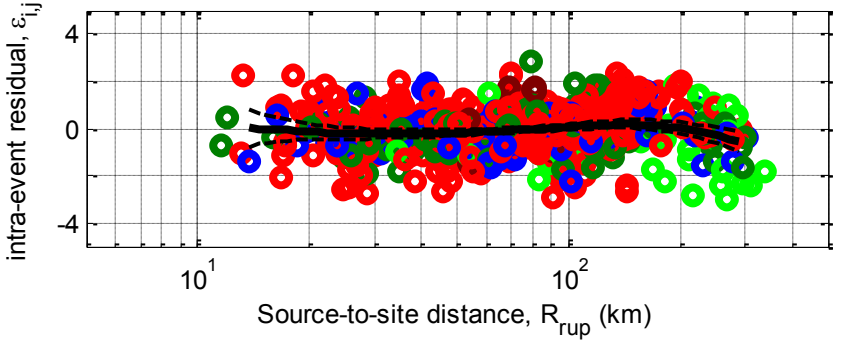
intra-event residual, $\varepsilon_{i,j}$
Source-to-site distance, R_{rup} (km)

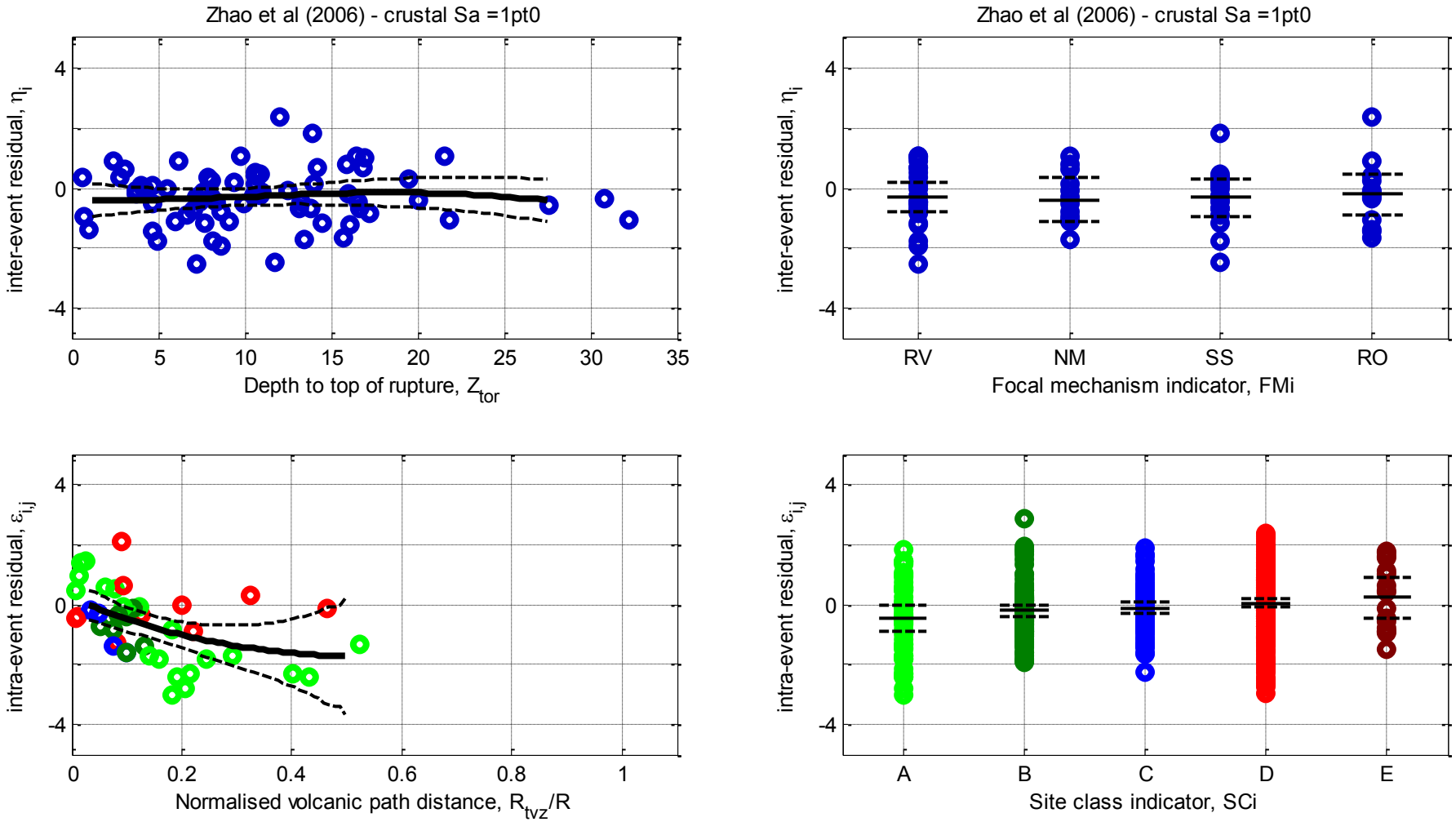

Figure D-9: Residuals for Sa(1.0) using the Zhao et al. (2006) crustal model

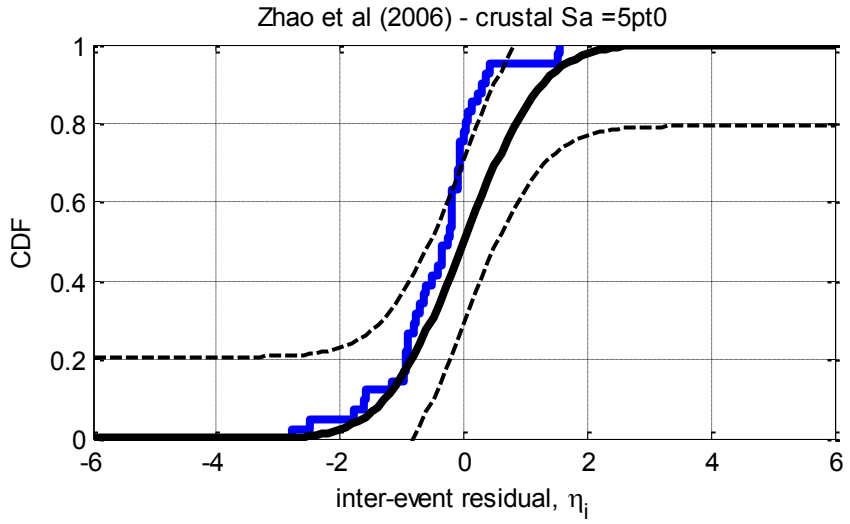
Zhao et al (2006) - crustal Sa =5pt0
CDF
inter-event residual, η_i

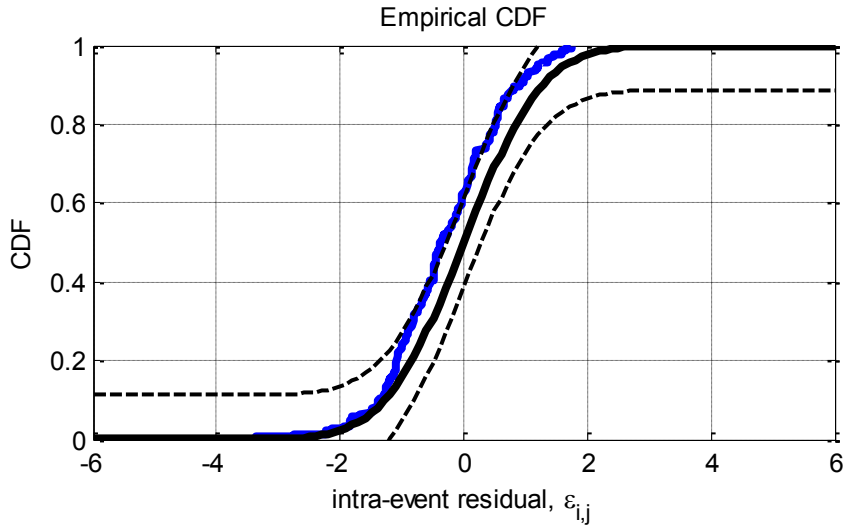
Empirical CDF
CDF
intra-event residual, $\varepsilon_{i,j}$

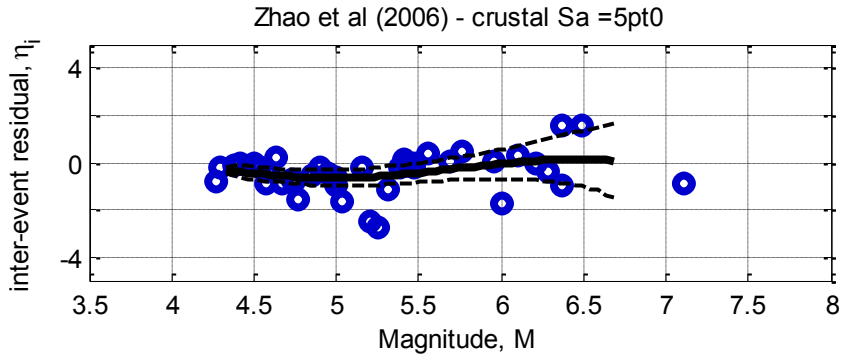
Zhao et al (2006) - crustal Sa =5pt0
inter-event residual, η_i
Magnitude, M

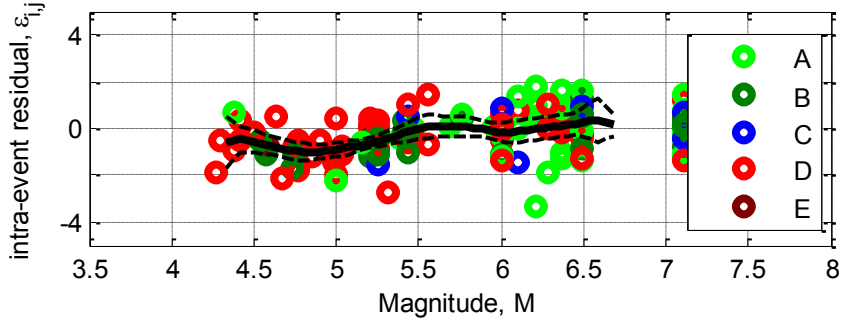
intra-event residual, $\varepsilon_{i,j}$
Magnitude, M
A
B
C
D
E

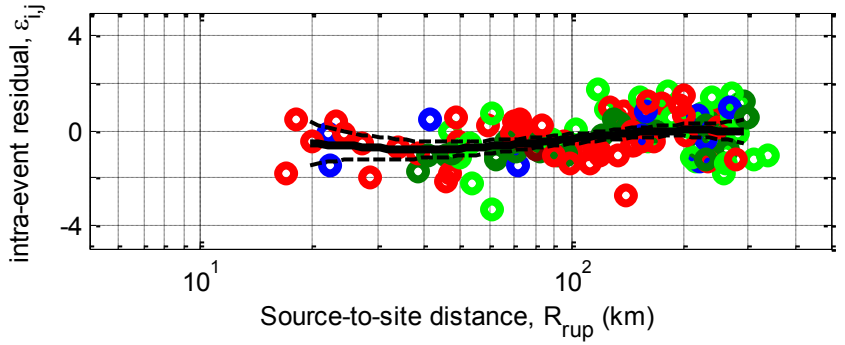
intra-event residual, $\varepsilon_{i,j}$
Source-to-site distance, R_{rup} (km)

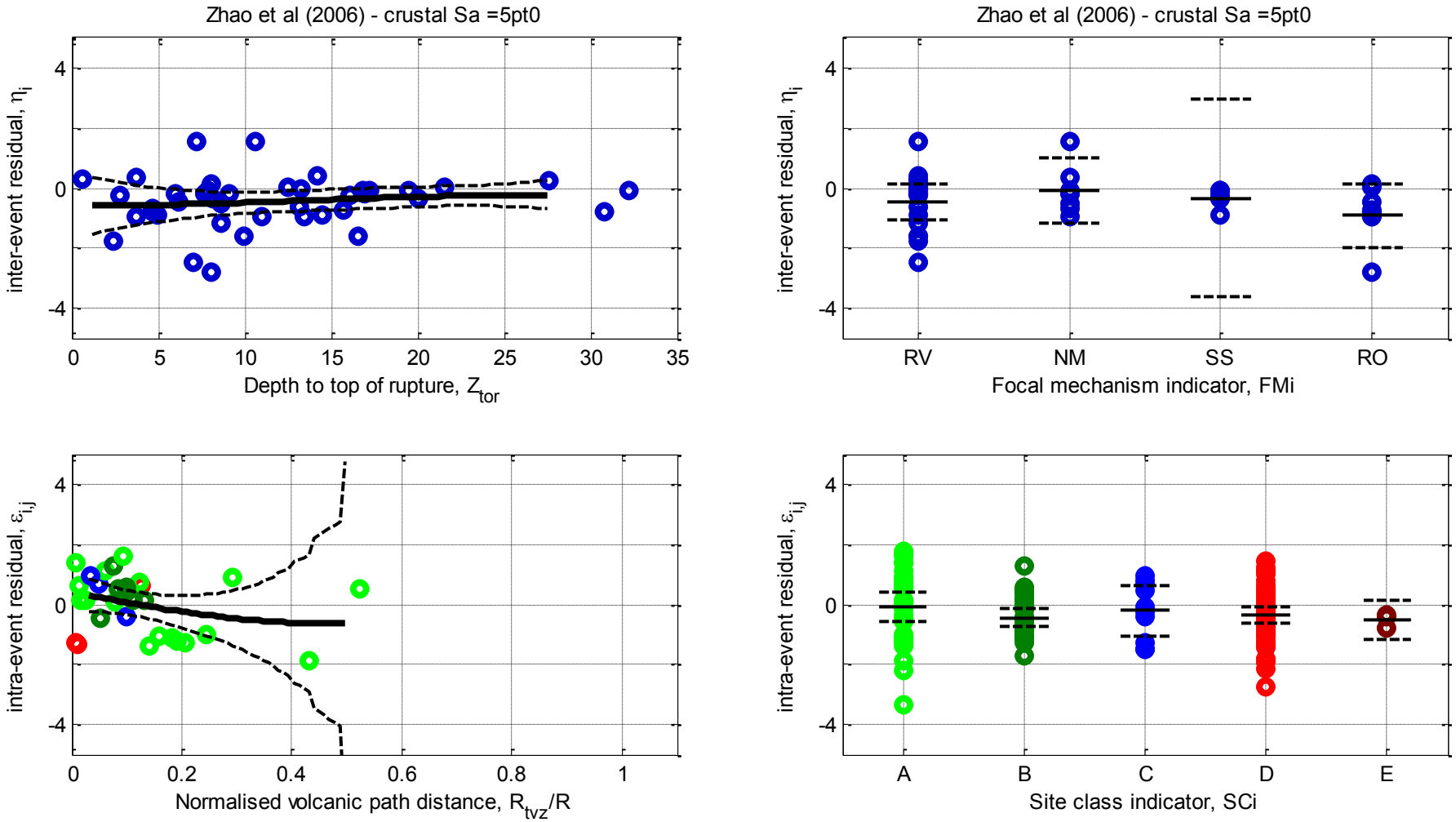

Figure D-10: Residuals for Sa(5.0) using the Zhao et al. (2006) crustal model

D.3. Boore and Atkinson (2008) Crustal model

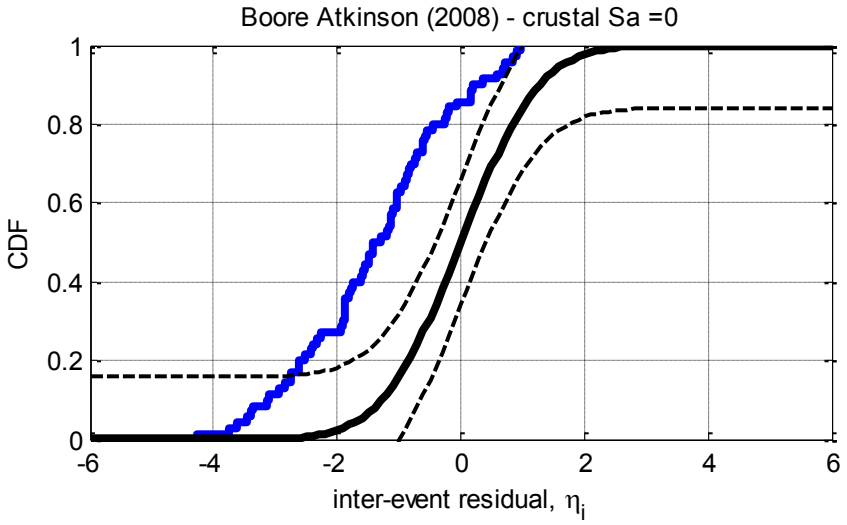

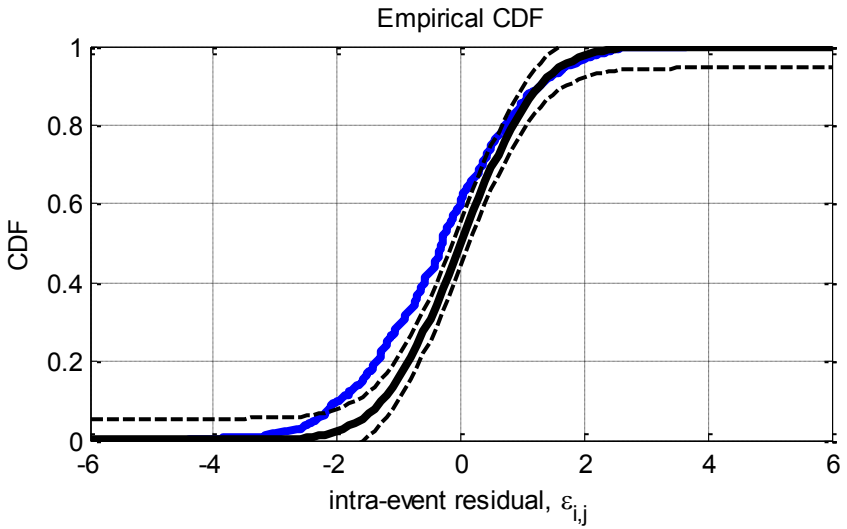

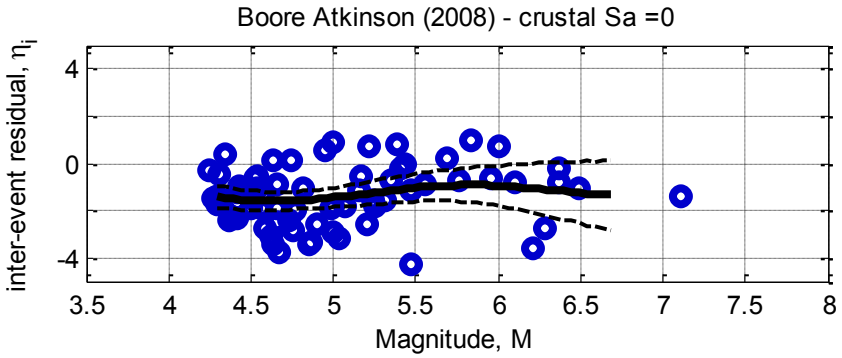

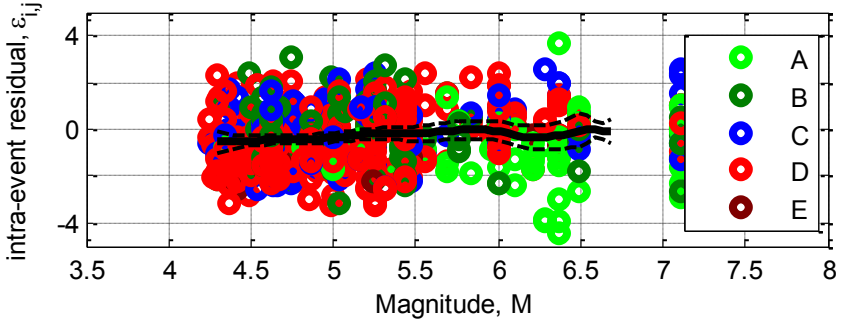

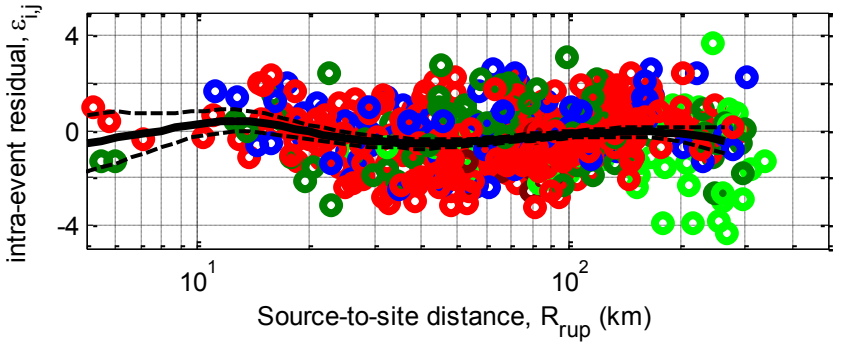

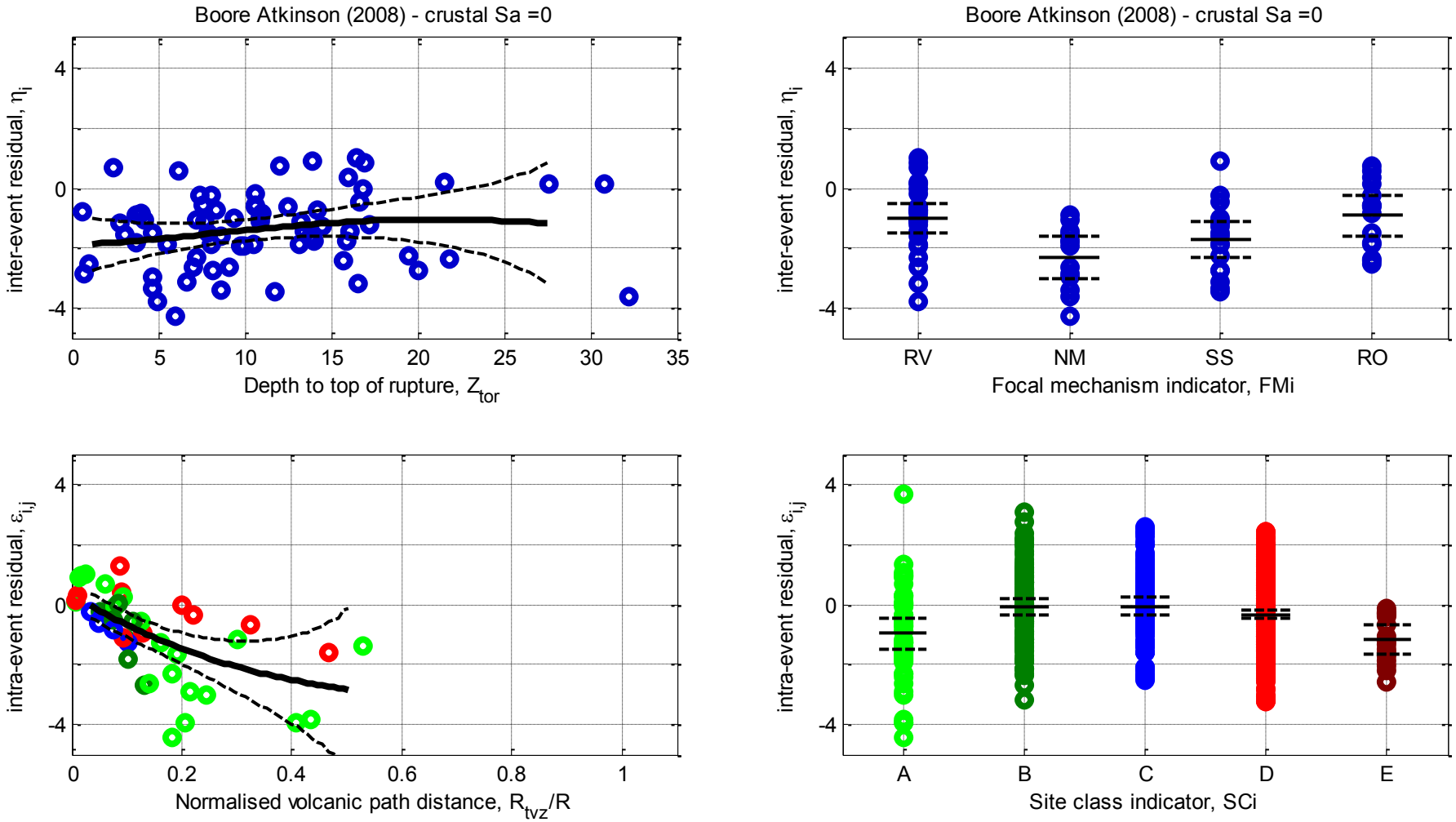

Figure D-11: Residuals for Sa(0.0) using the Boore and Atkinson (2008) crustal model

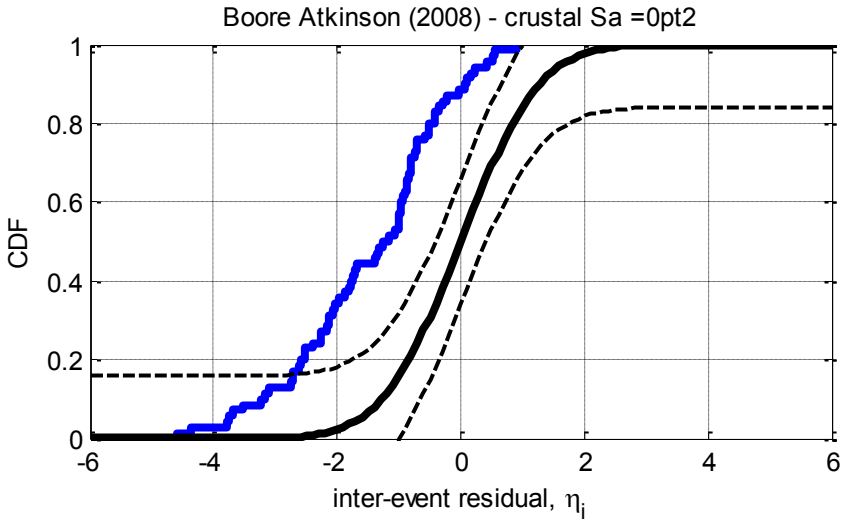
Boore Atkinson (2008) - crustal Sa =0pt2
CDF
inter-event residual, η_i

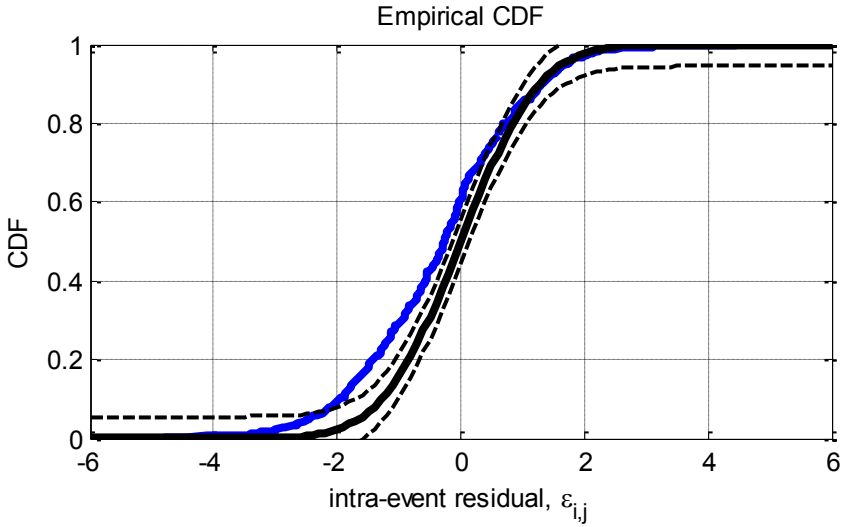
Empirical CDF
CDF
intra-event residual, $\varepsilon_{i,j}$

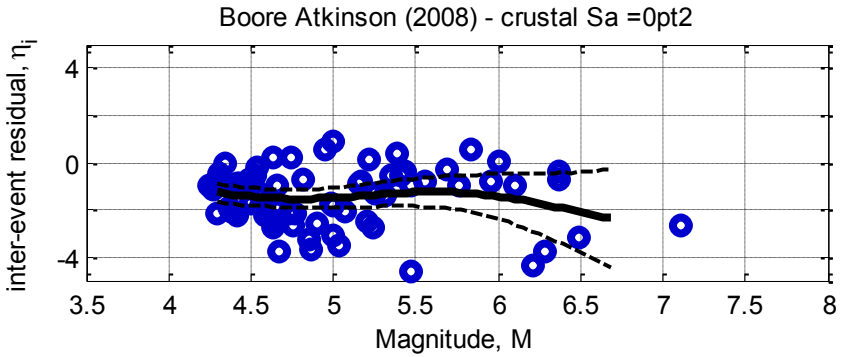
Boore Atkinson (2008) - crustal Sa =0pt2
inter-event residual, η_i
Magnitude, M

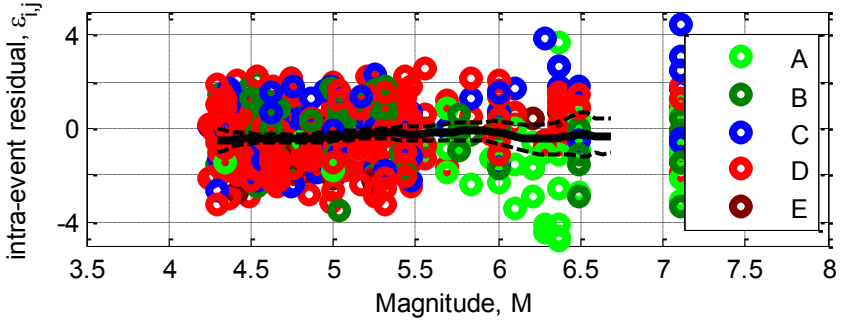
intra-event residual, $\varepsilon_{i,j}$
Magnitude, M
A
B
C
D
E

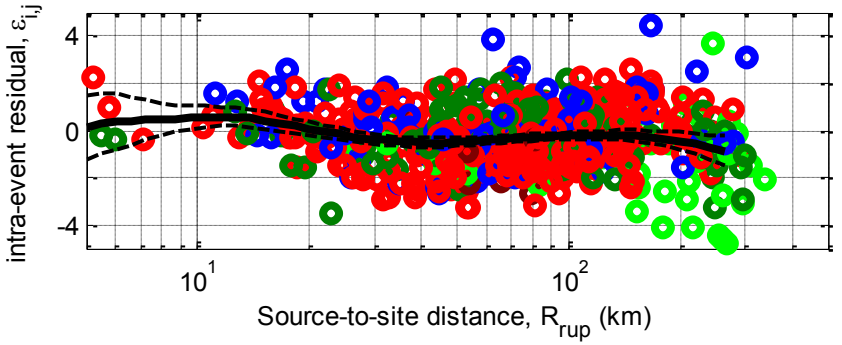
intra-event residual, $\varepsilon_{i,j}$
Source-to-site distance, R_{rup} (km)

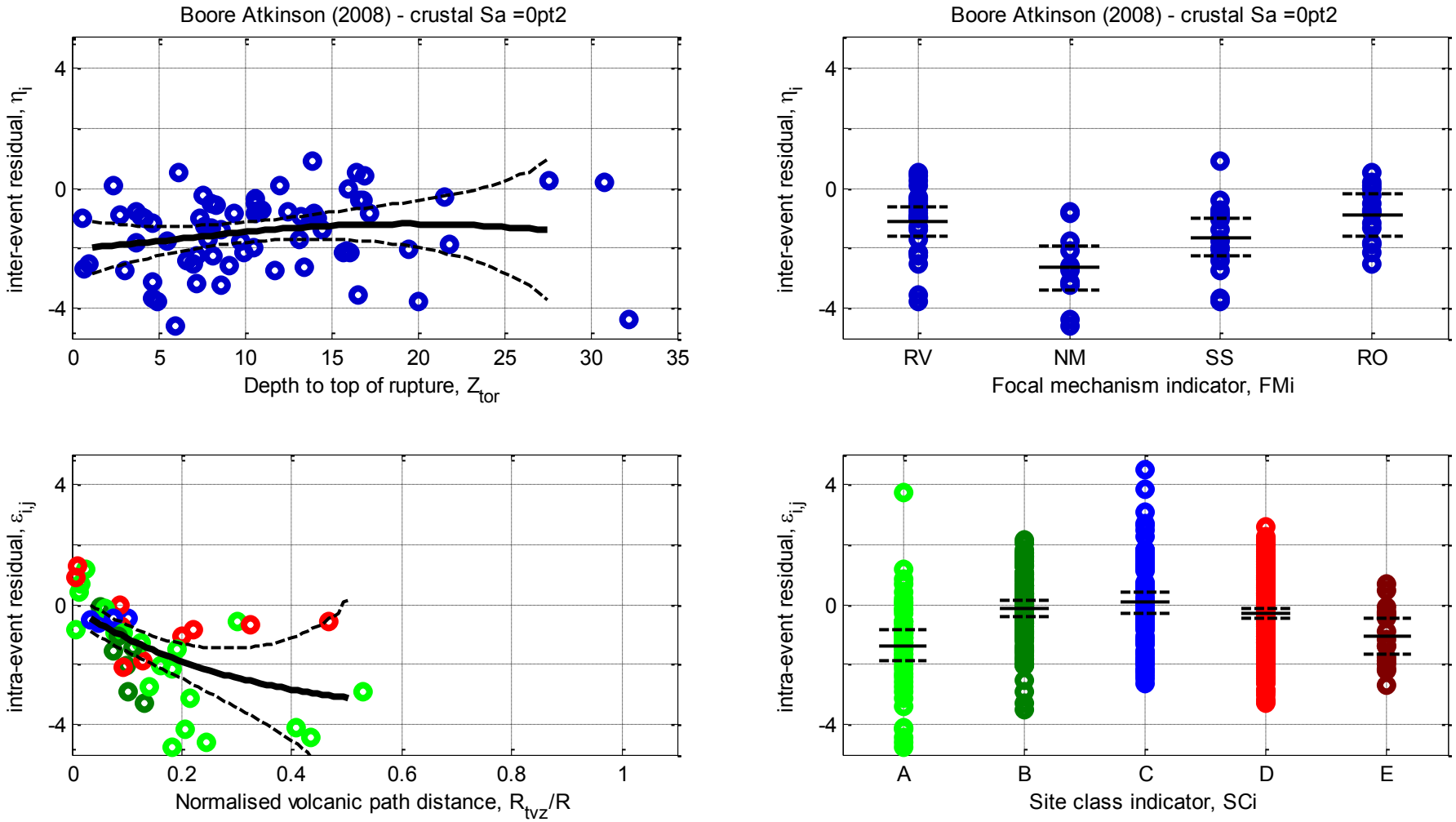

Figure D-12: Residuals for Sa(0.2) using the Boore and Atkinson (2008) crustal model

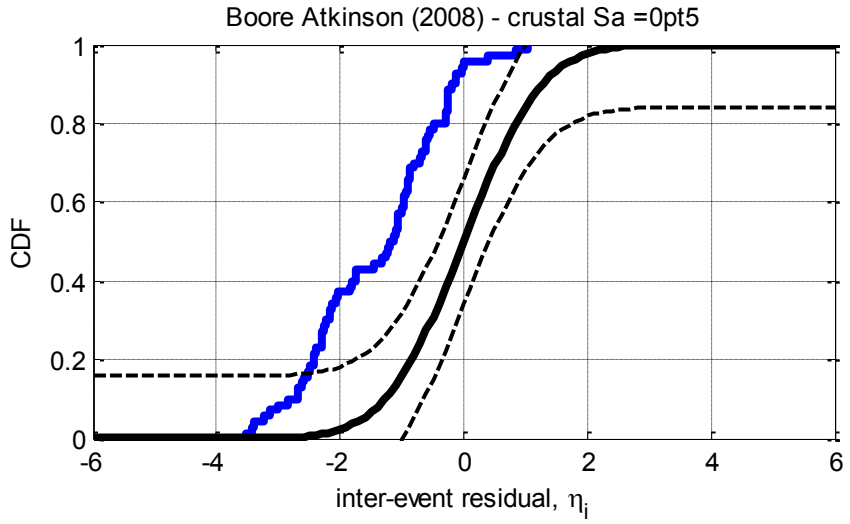
Boore Atkinson (2008) - crustal Sa =0pt5
CDF
inter-event residual, η_i

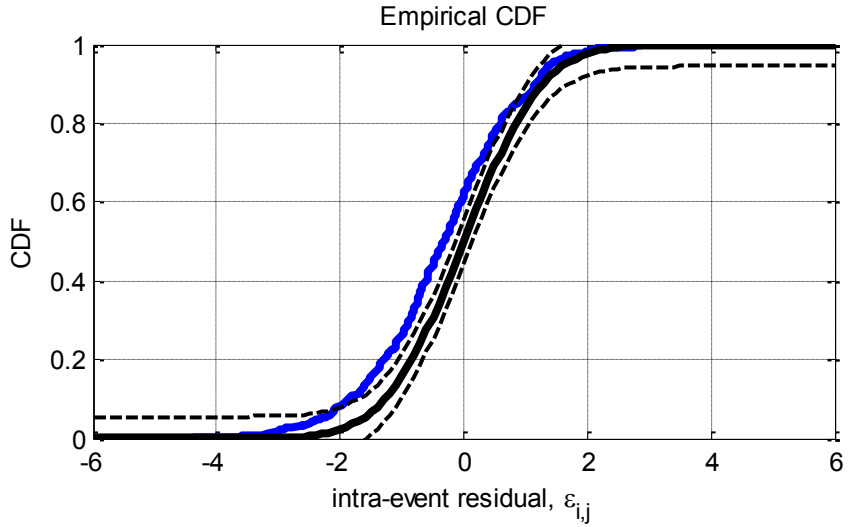
Empirical CDF
CDF
intra-event residual, $\varepsilon_{i,j}$

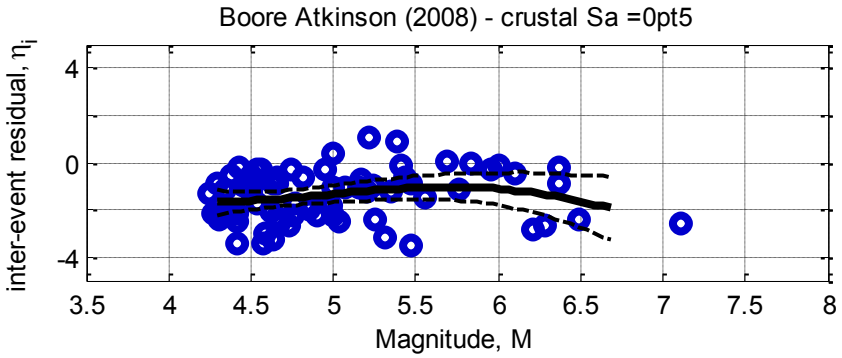
Boore Atkinson (2008) - crustal Sa =0pt5
inter-event residual, η_i
Magnitude, M

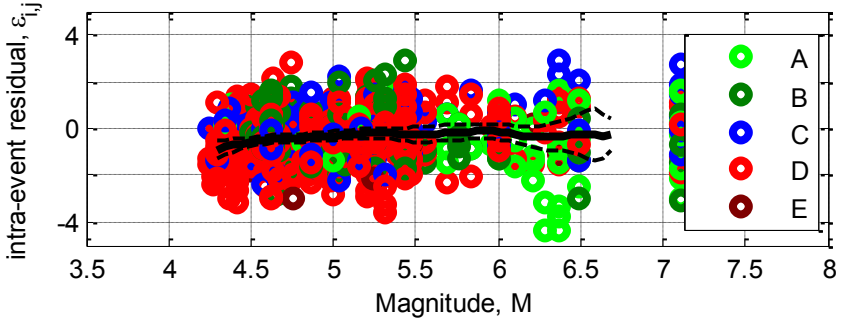
intra-event residual, $\varepsilon_{i,j}$
A
B
C
D
E
Magnitude, M

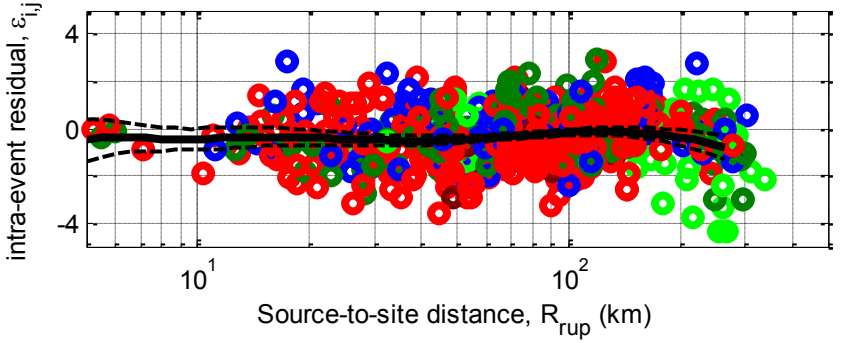
intra-event residual, $\varepsilon_{i,j}$
Source-to-site distance, R_{rup} (km)

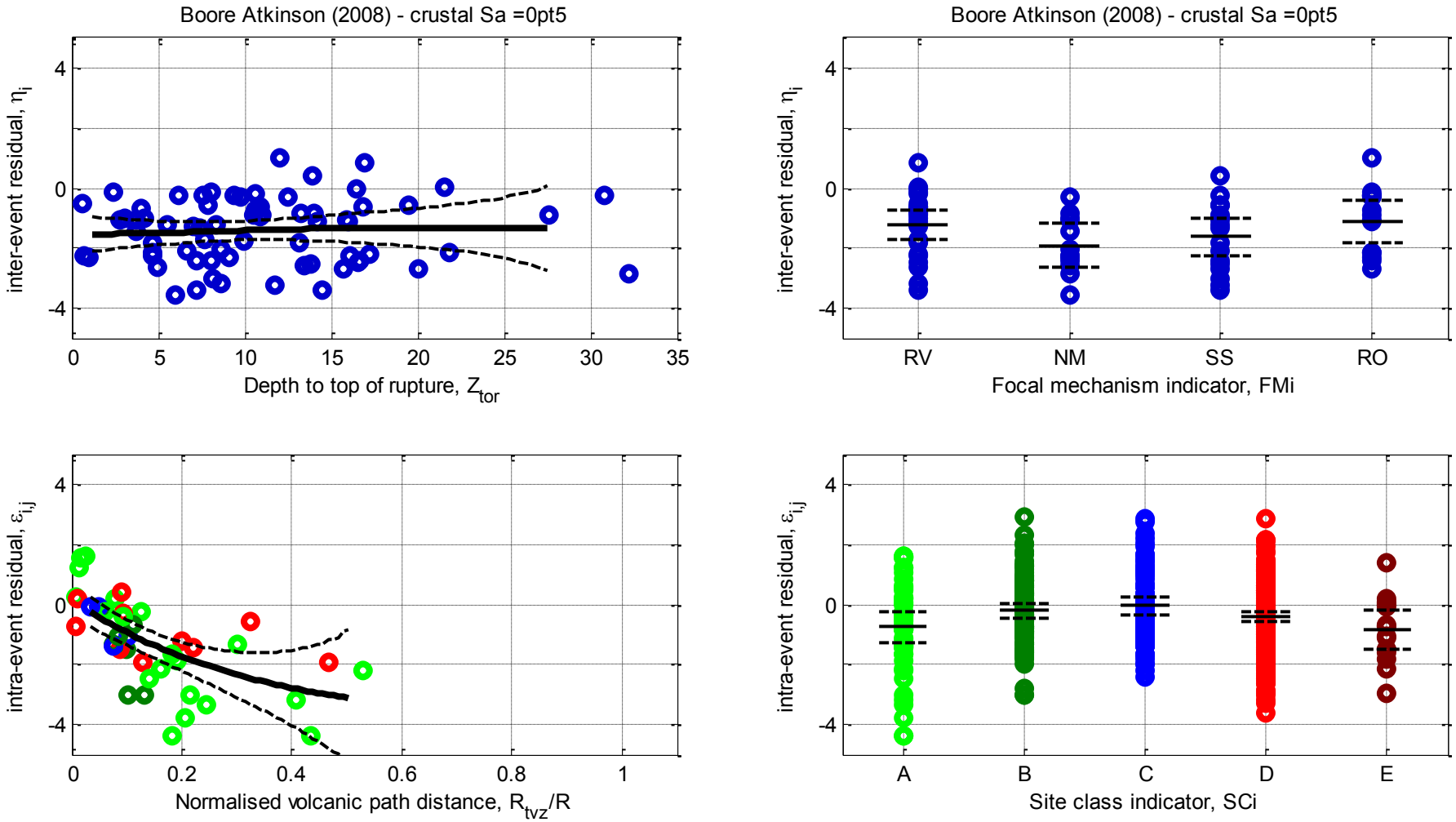

Figure D-13: Residuals for Sa(0.5) using the Boore and Atkinson (2008) crustal model

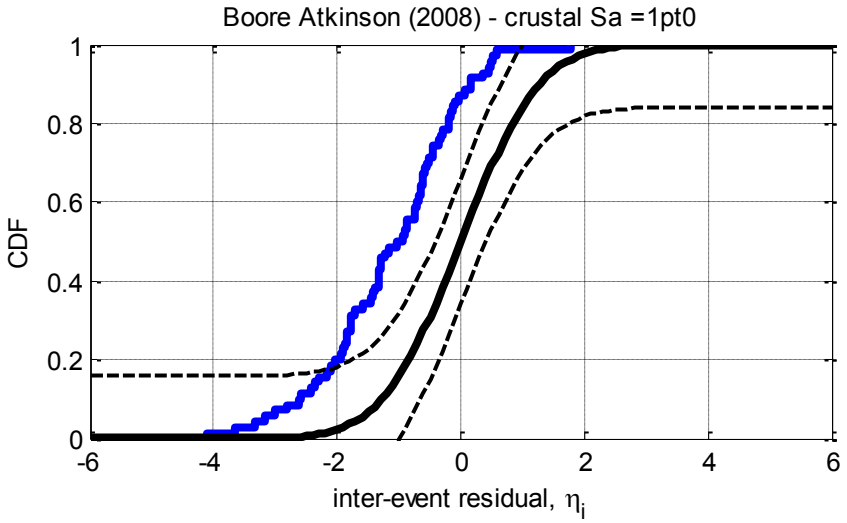
Boore Atkinson (2008) - crustal Sa =1pt0
CDF
inter-event residual, η_i

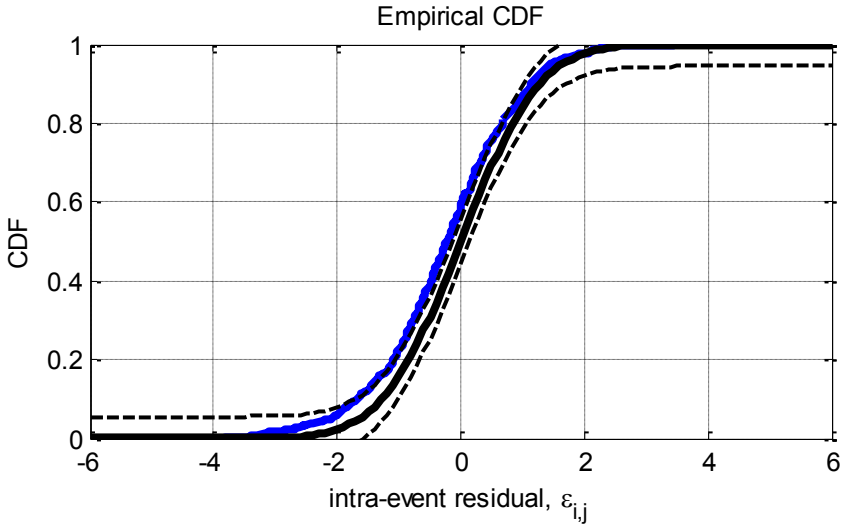
Empirical CDF
CDF
intra-event residual, $\varepsilon_{i,j}$

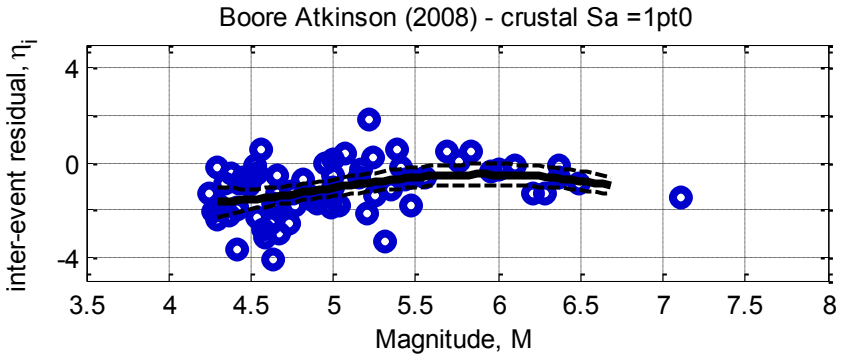
Boore Atkinson (2008) - crustal Sa =1pt0
inter-event residual, η_i
Magnitude, M

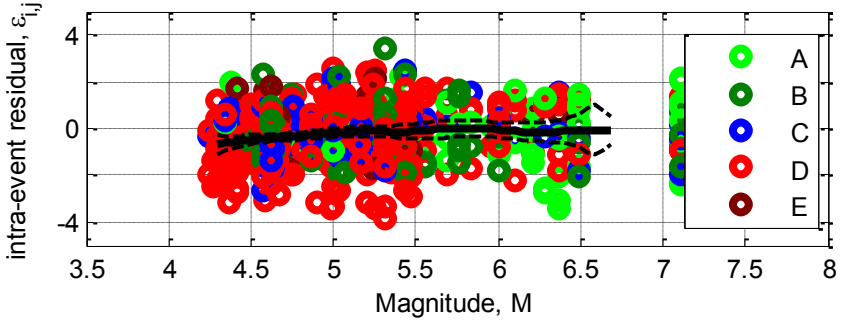
intra-event residual, $\varepsilon_{i,j}$
Magnitude, M
A
B
C
D
E

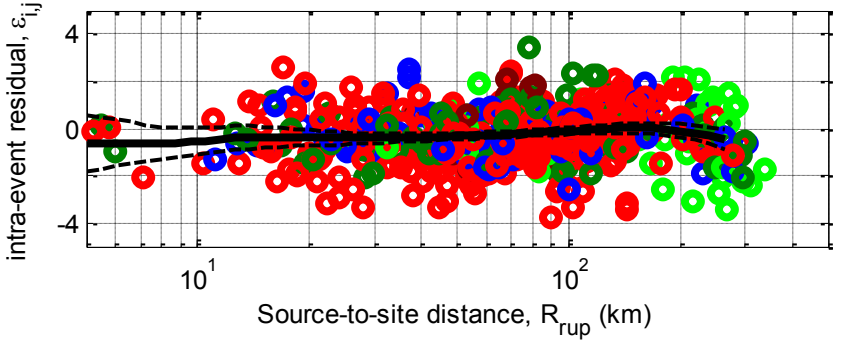
intra-event residual, $\varepsilon_{i,j}$
Source-to-site distance, R_{rup} (km)

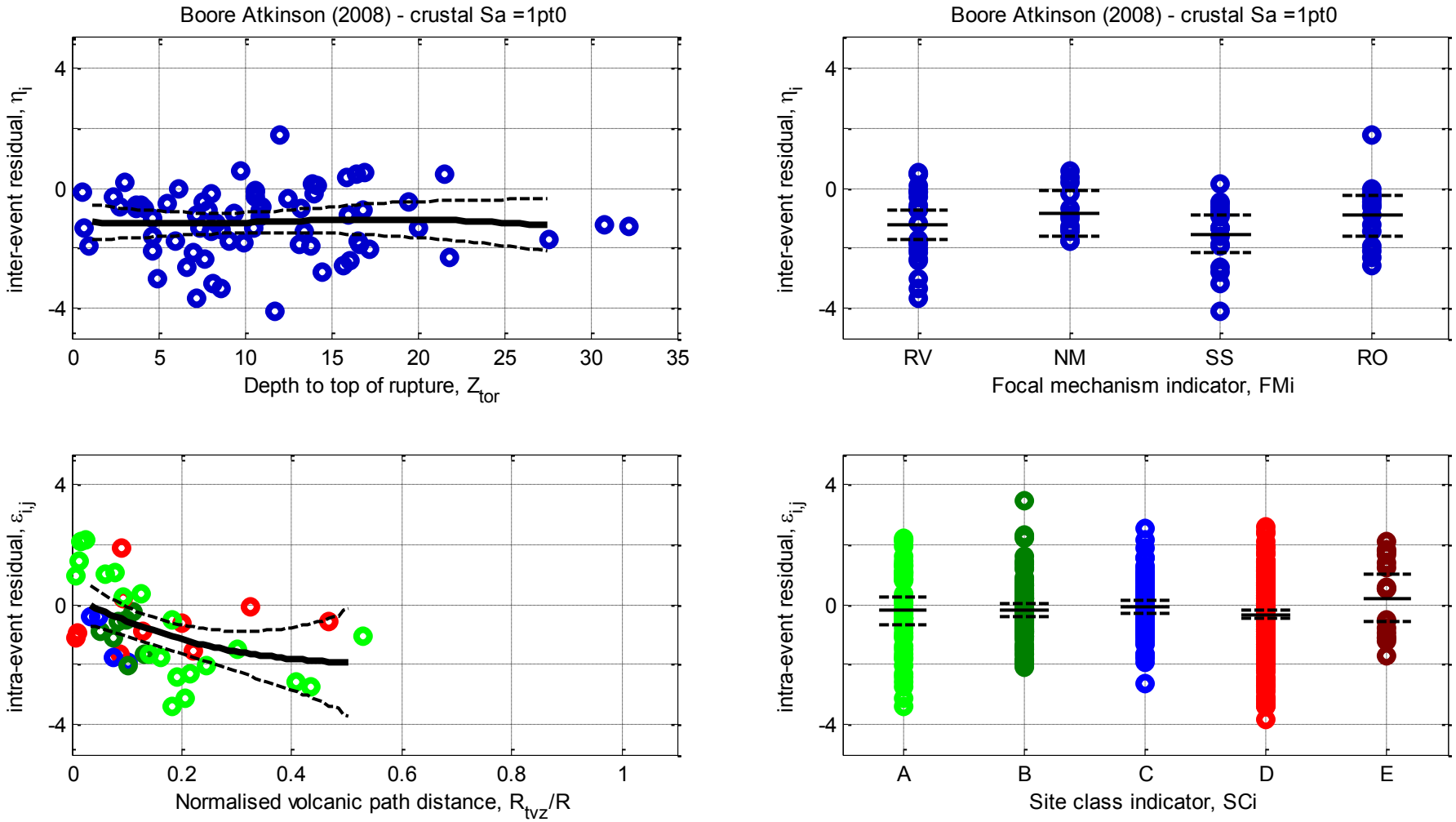

Figure D-14: Residuals for Sa(1.0) using the Boore and Atkinson (2008) crustal model

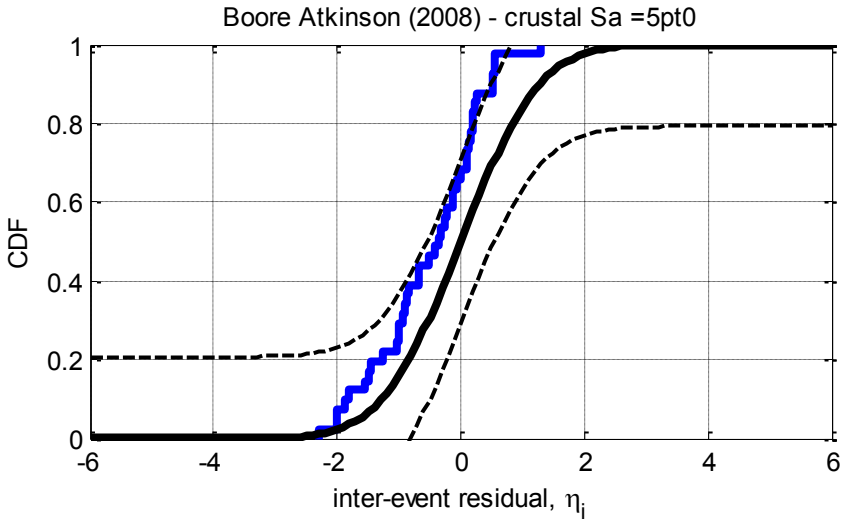
Boore Atkinson (2008) - crustal Sa =5pt0
CDF
inter-event residual, η_i

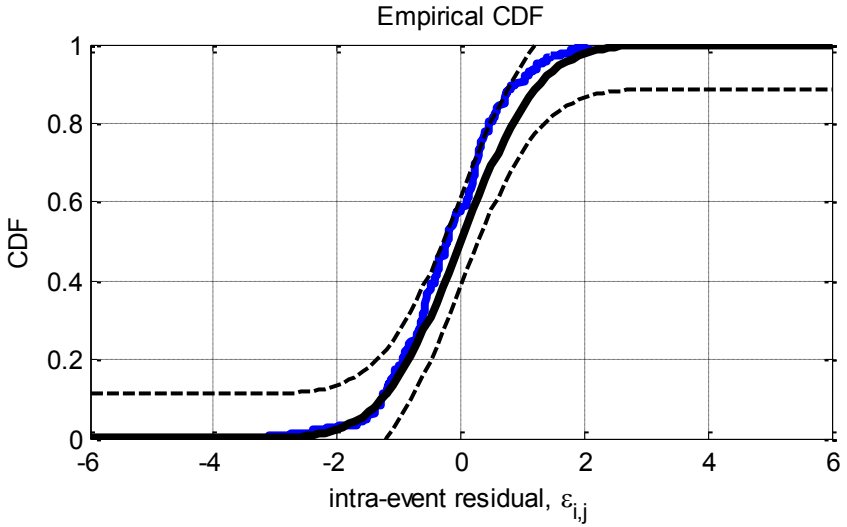
Empirical CDF
CDF
intra-event residual, $\varepsilon_{i,j}$

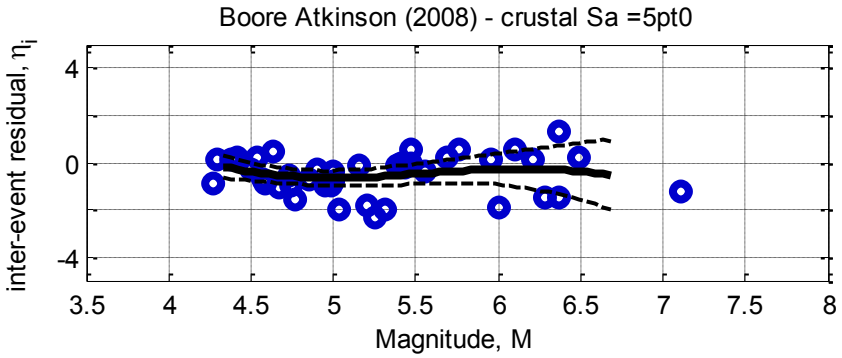
Boore Atkinson (2008) - crustal Sa =5pt0
inter-event residual, η_i
Magnitude, M

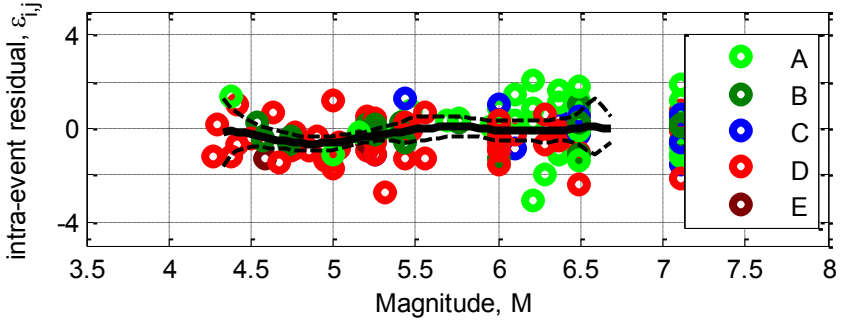
intra-event residual, $\varepsilon_{i,j}$
Magnitude, M
A
B
C
D
E

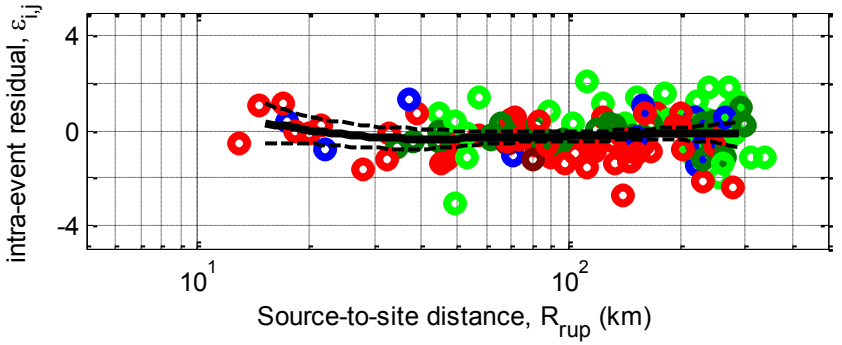
intra-event residual, $\varepsilon_{i,j}$
Source-to-site distance, R_{rup} (km)

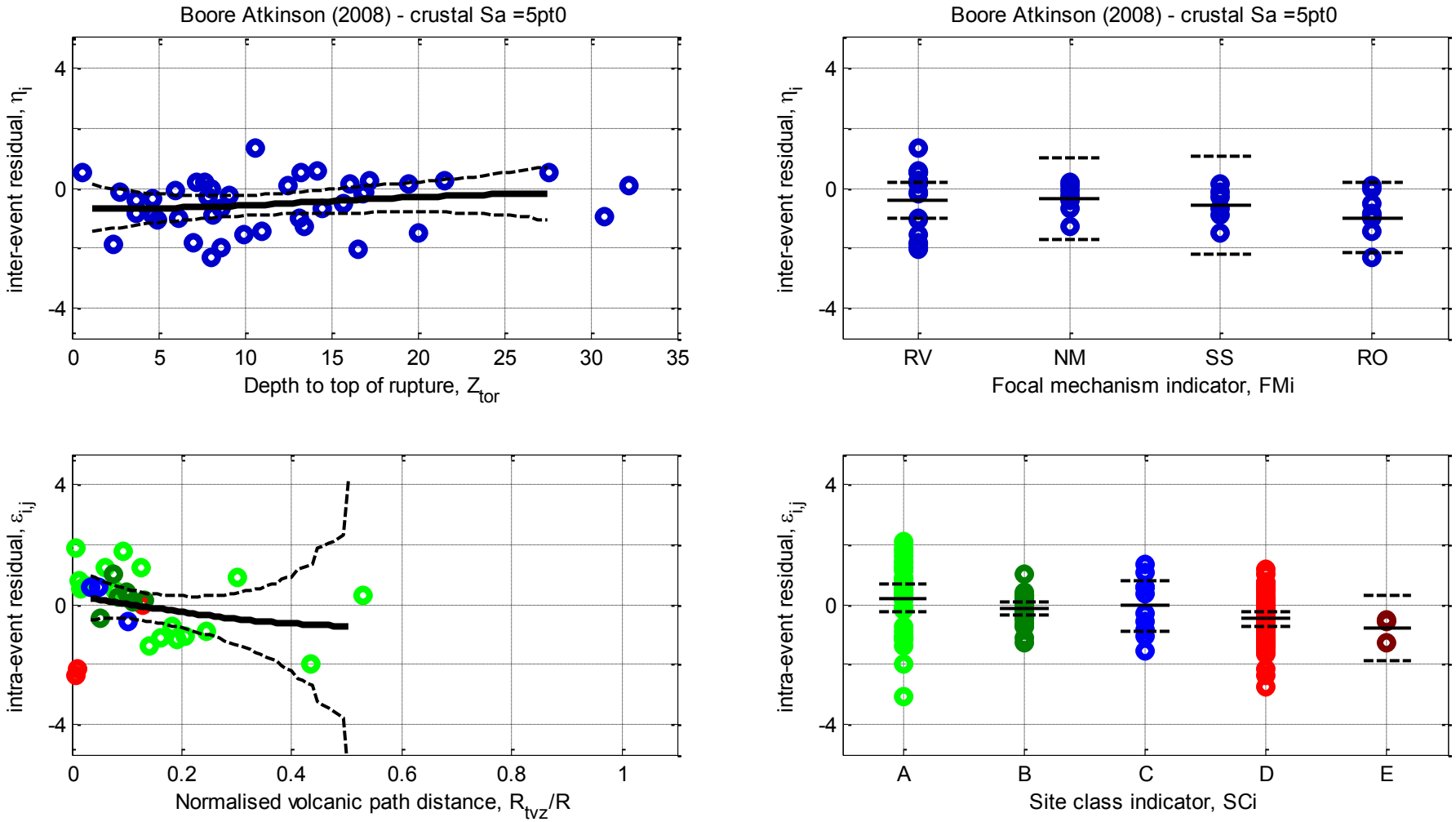

Figure D-15: Residuals for Sa(5.0) using the Boore and Atkinson (2008) crustal model

D.4. Chiou and Youngs (2008) Crustal model

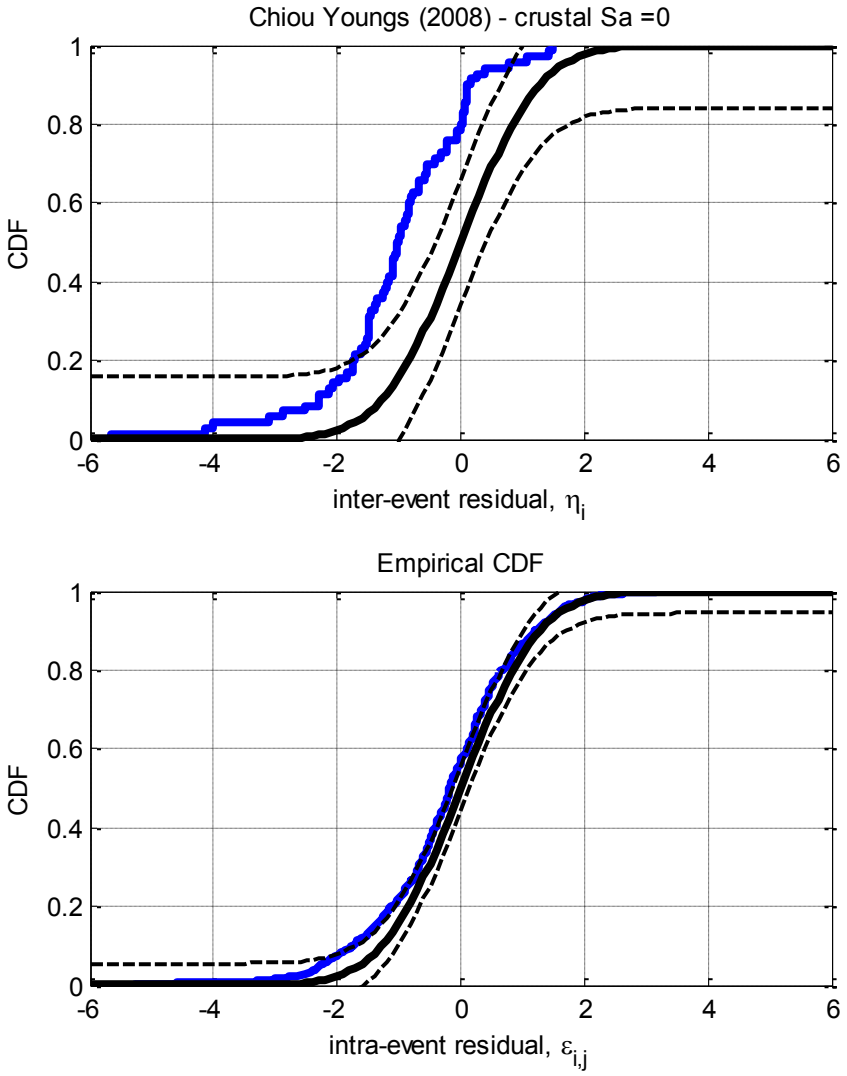

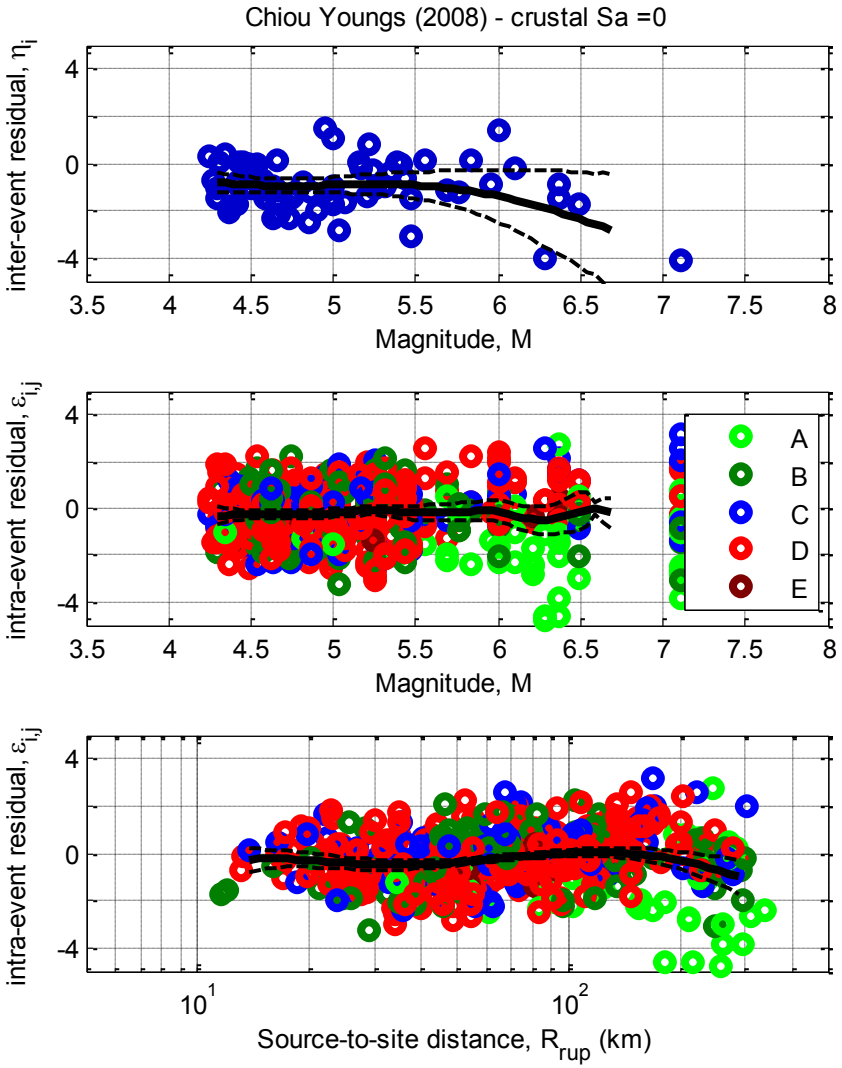

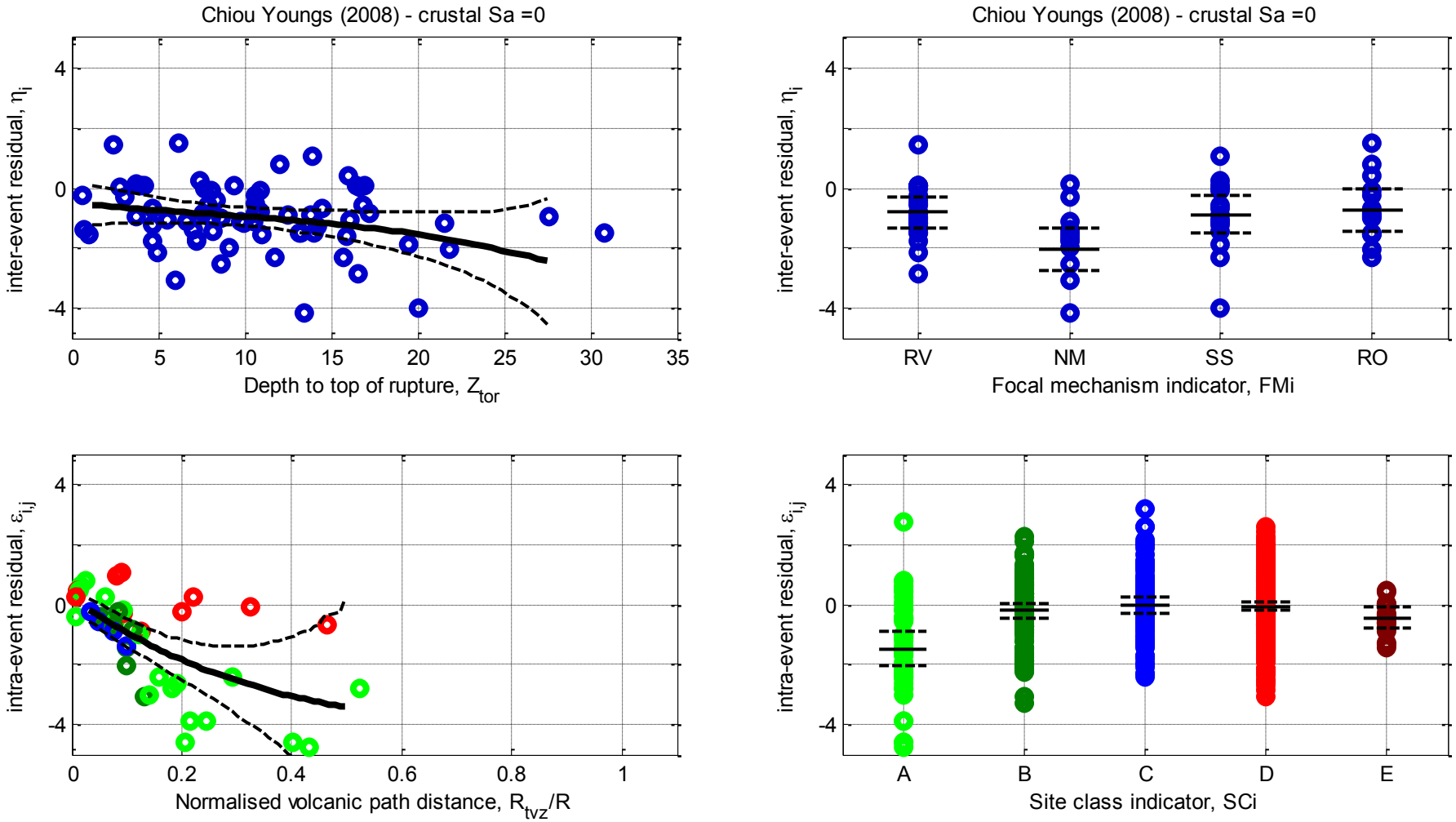

Figure D-16: Residuals for Sa(0.0) using the Chiou and Youngs (2008) crustal model

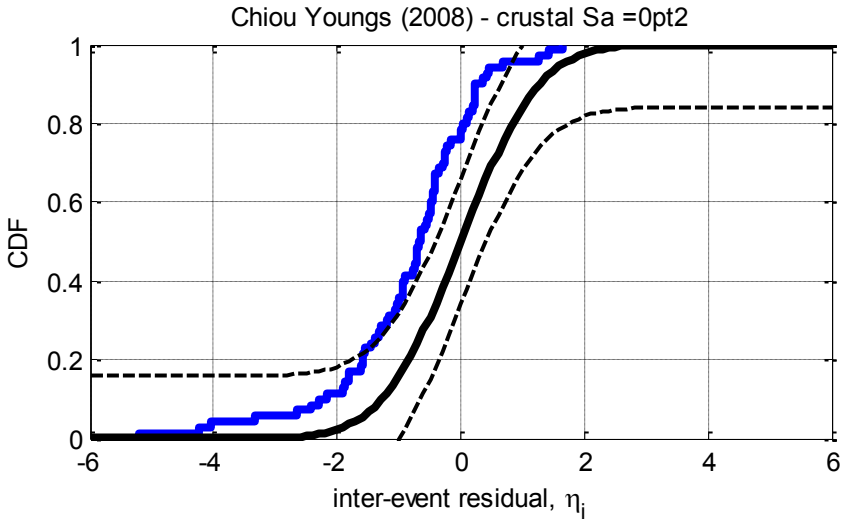
Chiou Youngs (2008) - crustal Sa =0pt2
CDF
inter-event residual, η_i

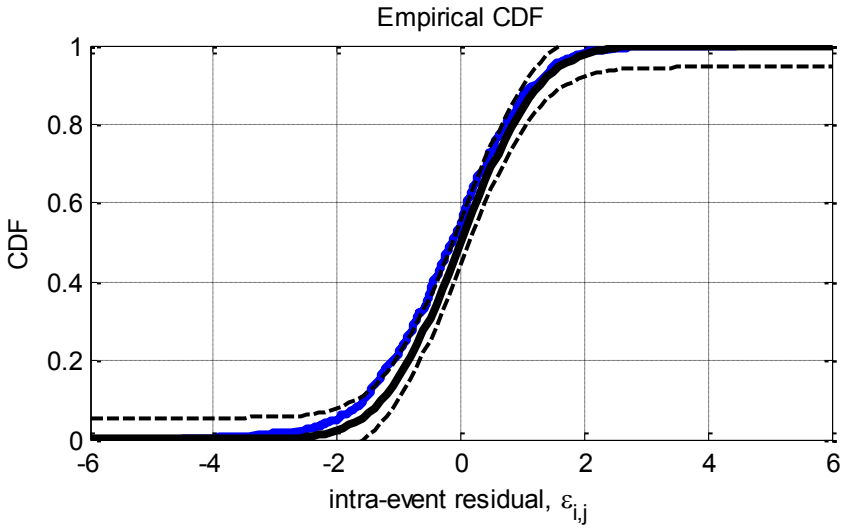
Empirical CDF
CDF
intra-event residual, $\varepsilon_{i,j}$

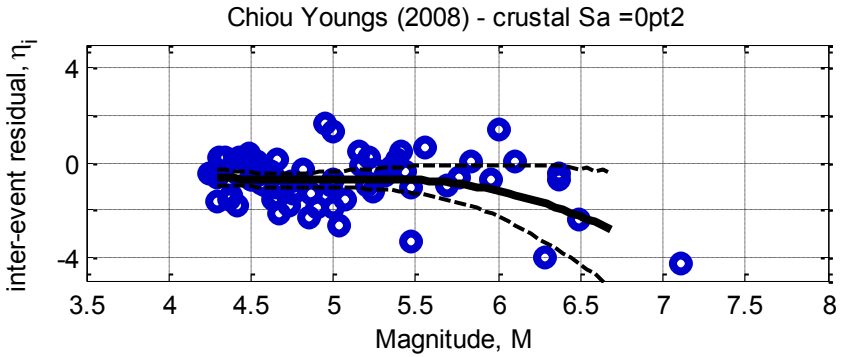
Chiou Youngs (2008) - crustal Sa =0pt2
inter-event residual, η_i
Magnitude, M

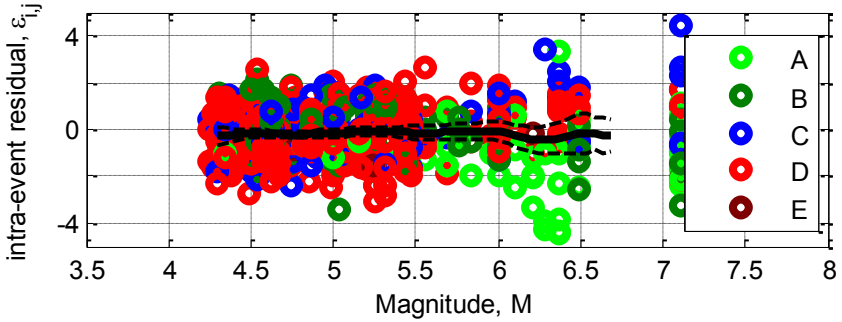
intra-event residual, $\varepsilon_{i,j}$
Magnitude, M
A
B
C
D
E

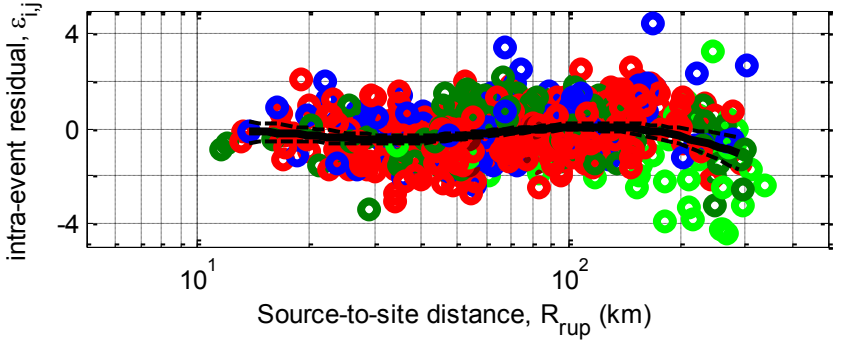
intra-event residual, $\varepsilon_{i,j}$
Source-to-site distance, R_{rup} (km)

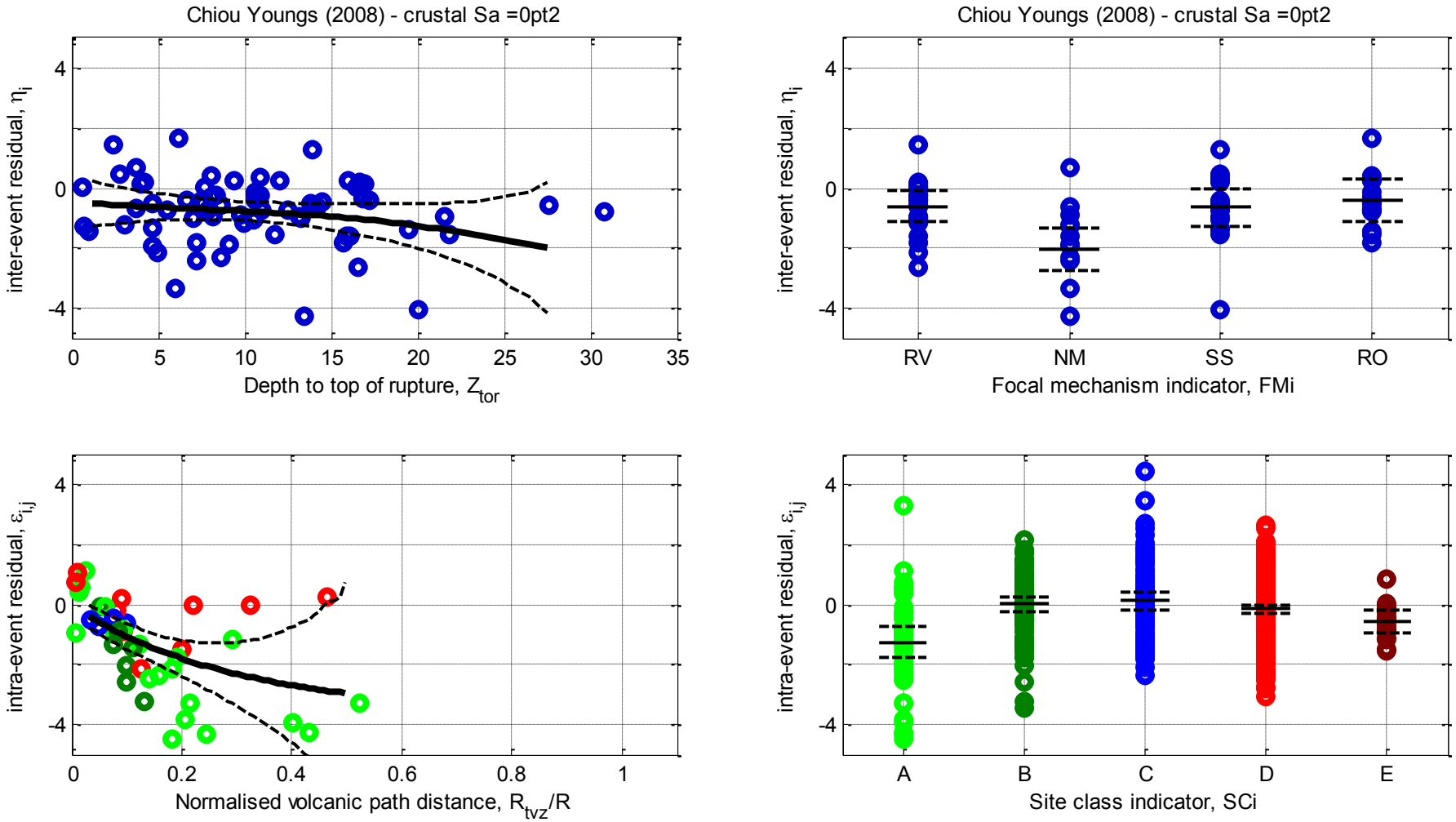

Figure D-17: Residuals for Sa(0.2) using the Chiou and Youngs (2008) crustal model

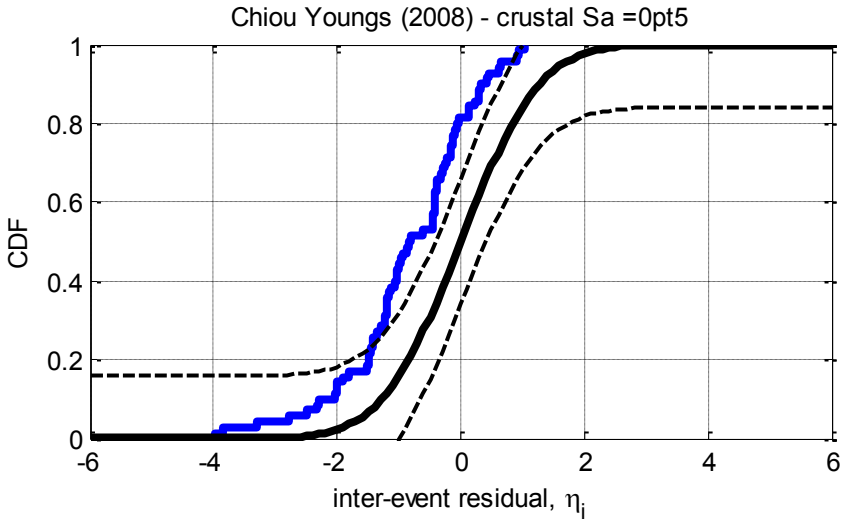
Chiou Youngs (2008) - crustal Sa =0pt5
CDF
inter-event residual, η_i

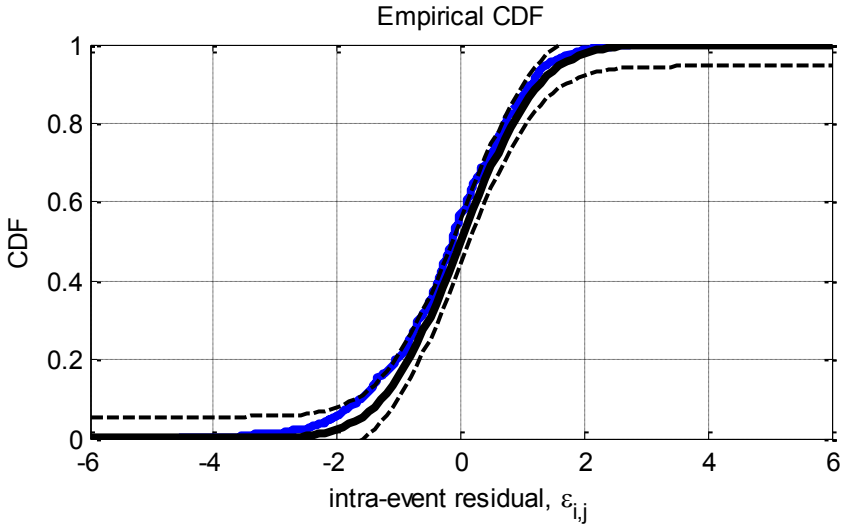
Empirical CDF
CDF
intra-event residual, $\varepsilon_{i,j}$

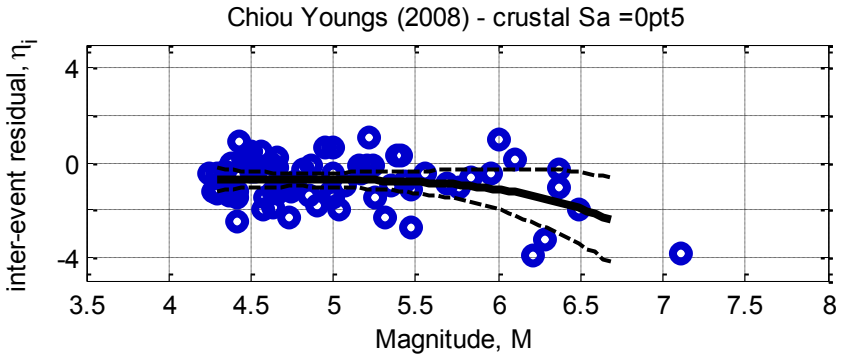
Chiou Youngs (2008) - crustal Sa =0pt5
inter-event residual, η_i
Magnitude, M

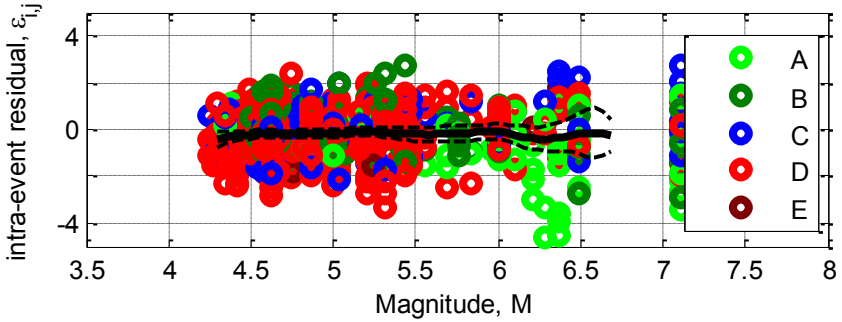
intra-event residual, $\varepsilon_{i,j}$
Magnitude, M
A
B
C
D
E

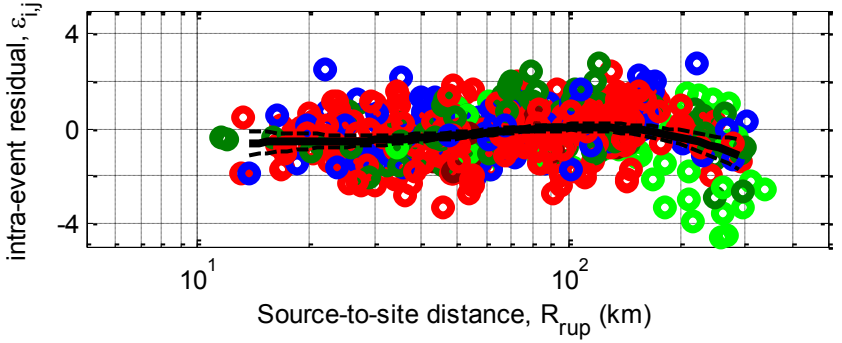
intra-event residual, $\varepsilon_{i,j}$
Source-to-site distance, R_{rup} (km)

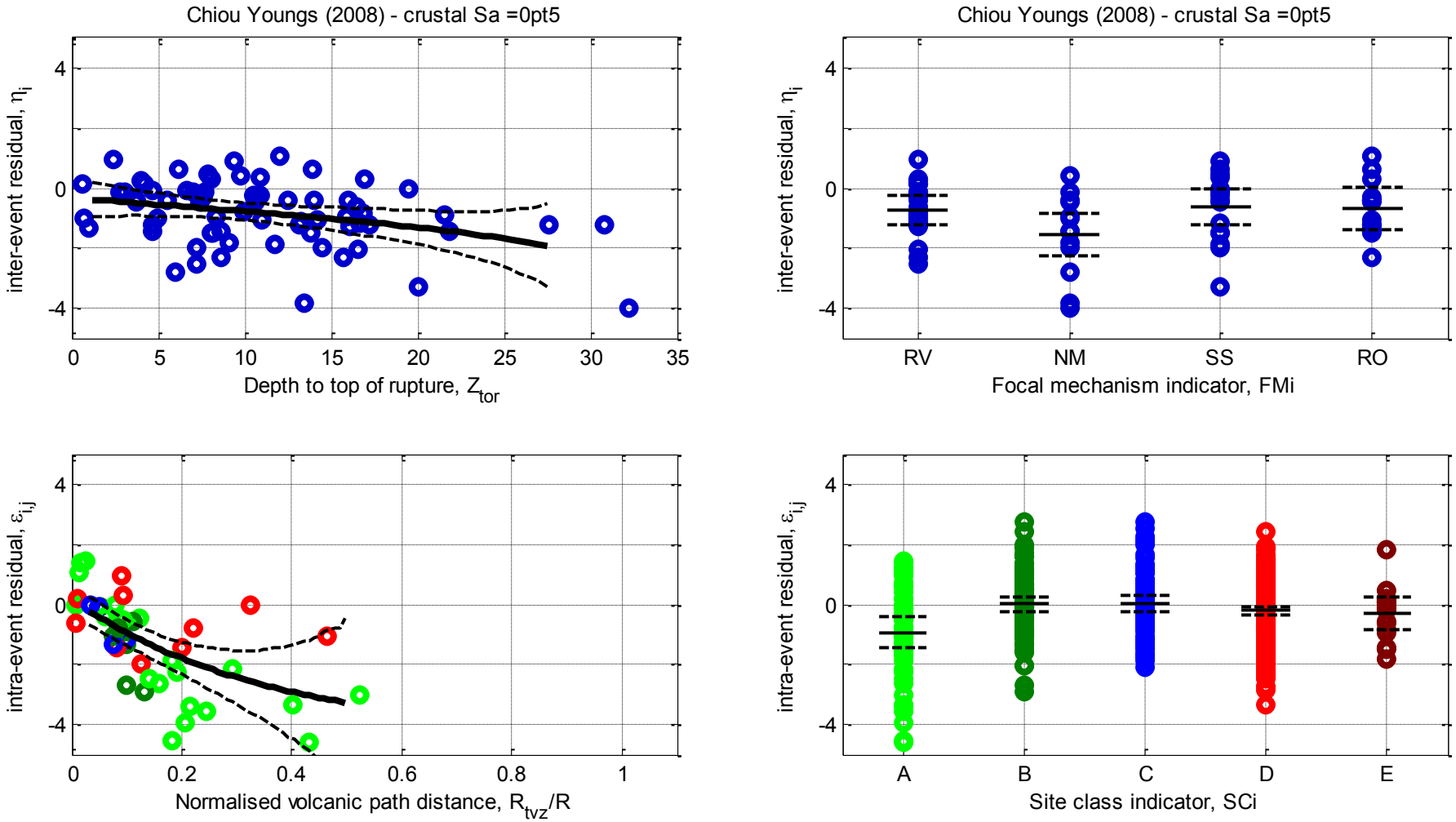

Figure D-18: Residuals for Sa(0.5) using the Chiou and Youngs (2008) crustal model

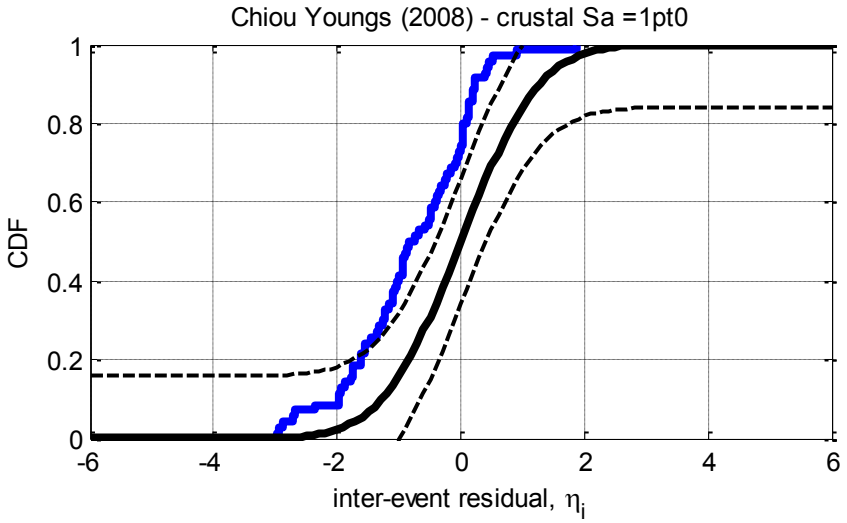
Chiou Youngs (2008) - crustal Sa =1pt0
CDF
inter-event residual, η_i

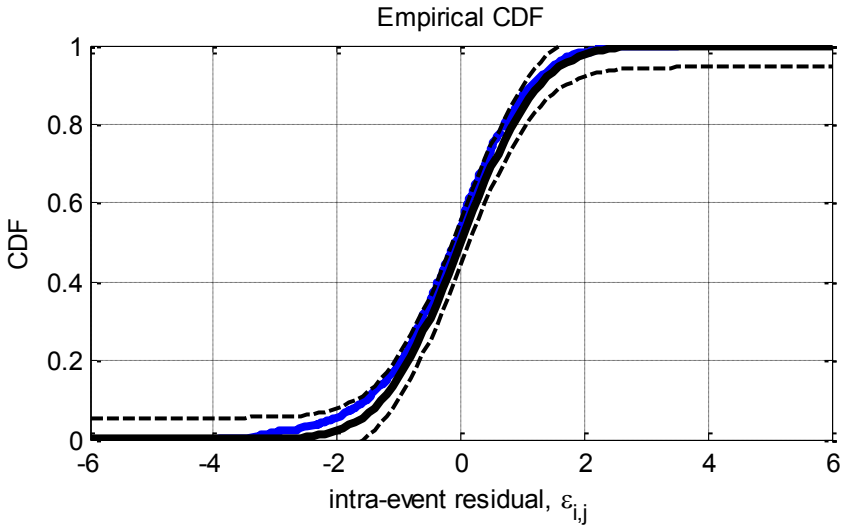
Empirical CDF
CDF
intra-event residual, $\varepsilon_{i,j}$

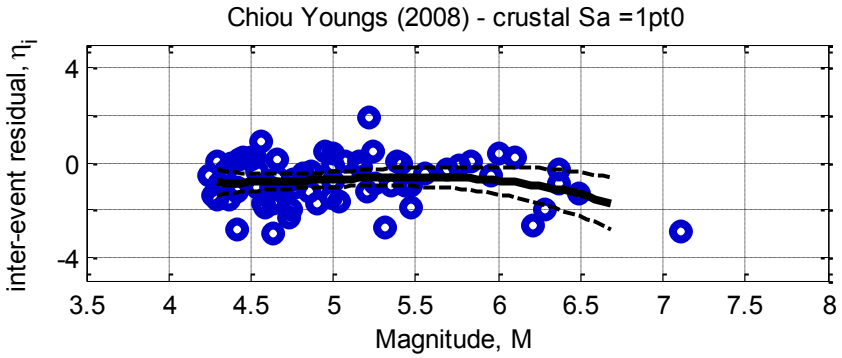
Chiou Youngs (2008) - crustal Sa =1pt0
inter-event residual, η_i
Magnitude, M

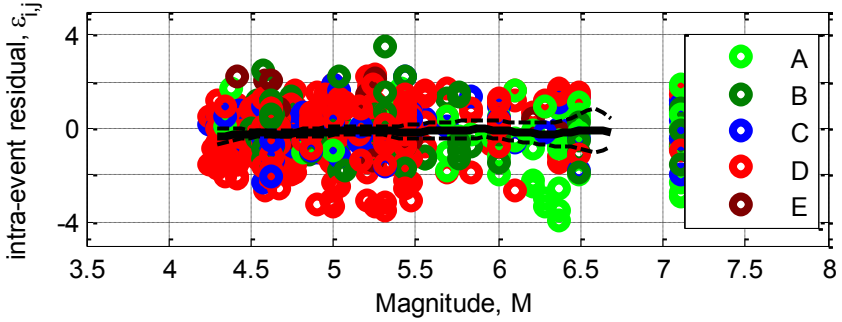
intra-event residual, $\varepsilon_{i,j}$
Magnitude, M
A
B
C
D
E

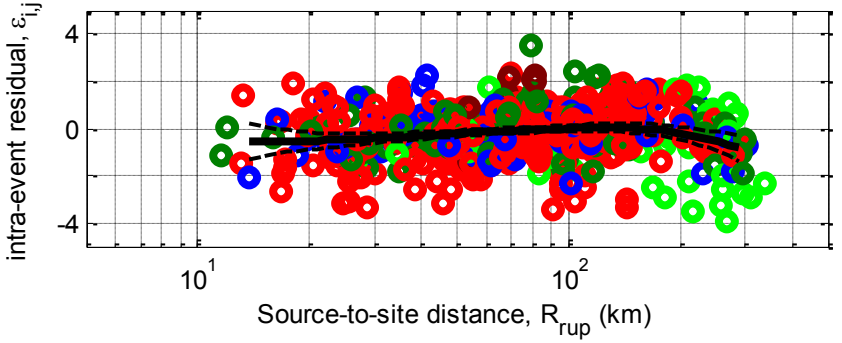
intra-event residual, $\varepsilon_{i,j}$
Source-to-site distance, R_{rup} (km)

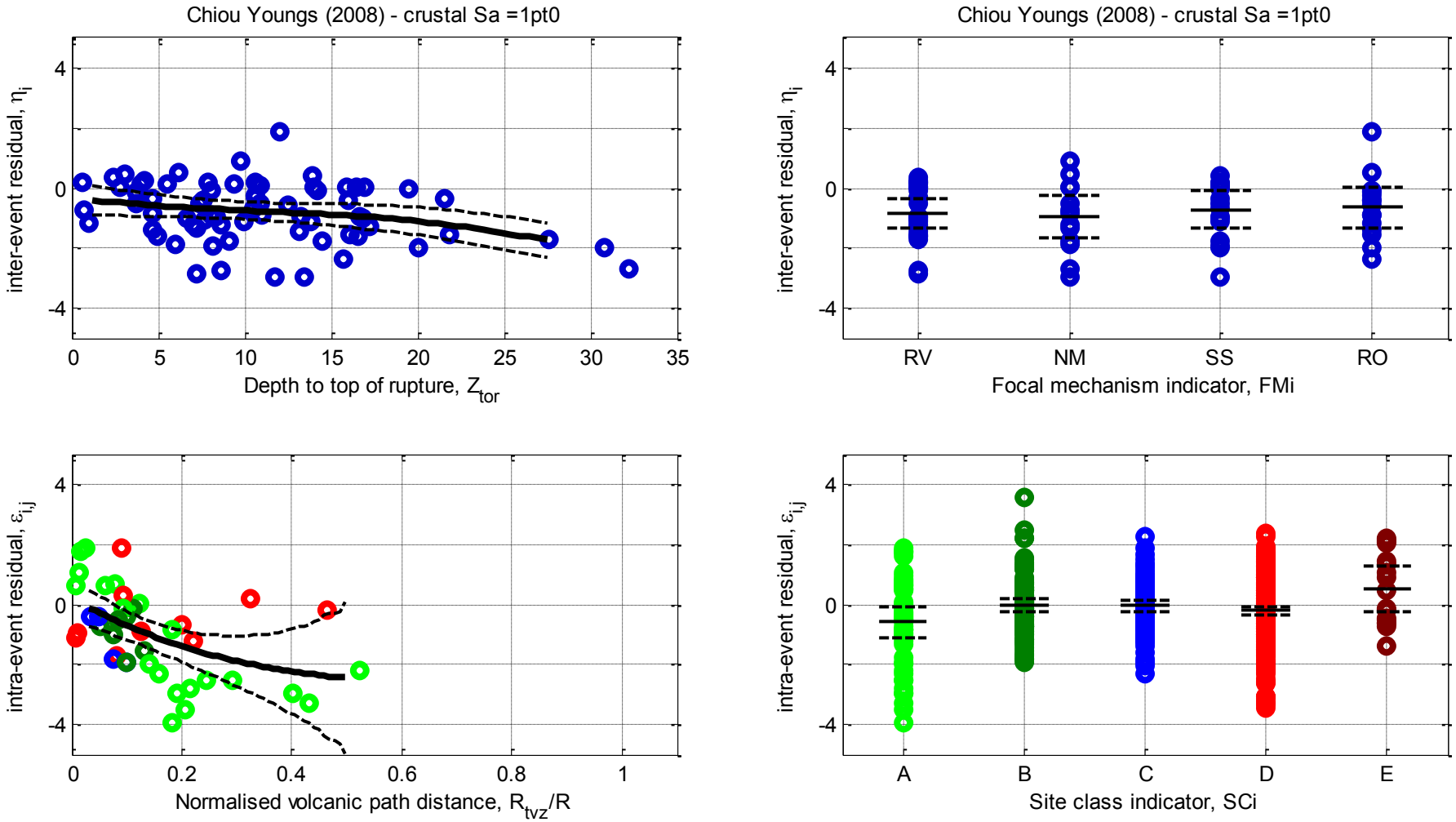

Figure D-19: Residuals for Sa(1.0) using the Chiou and Youngs (2008) crustal model

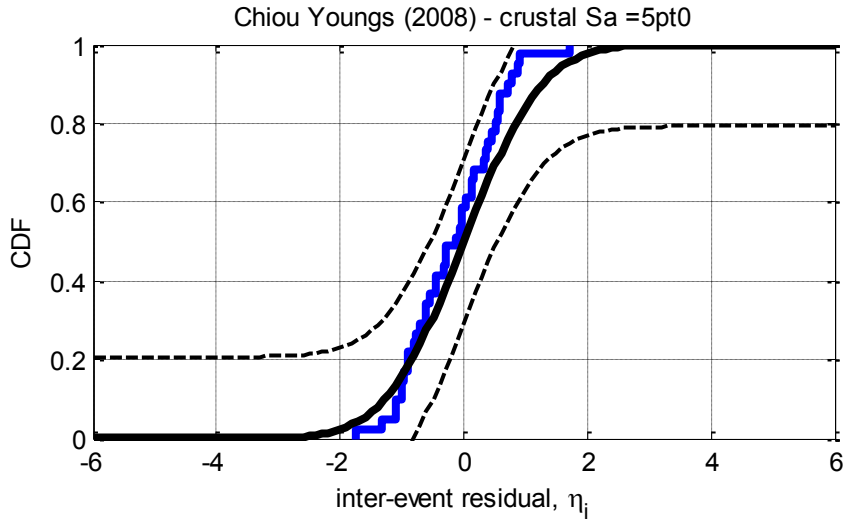
Chiou Youngs (2008) - crustal Sa =5pt0
CDF
inter-event residual, η_i

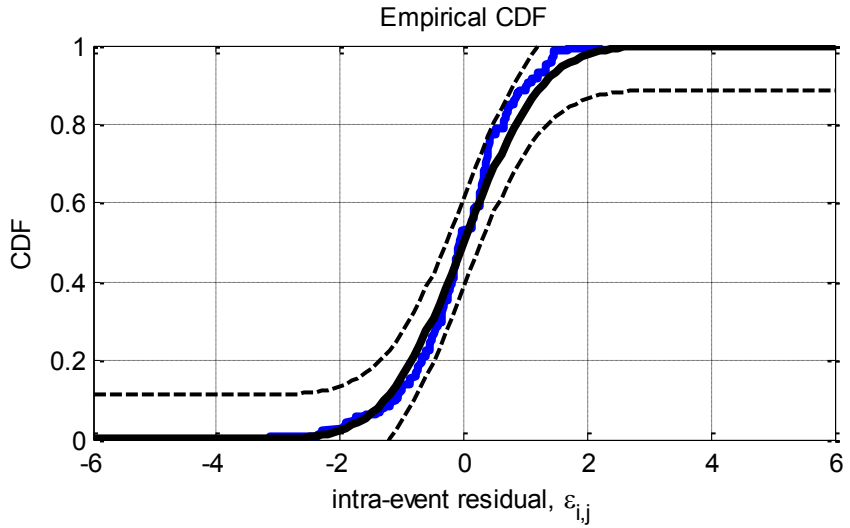
Empirical CDF
CDF
intra-event residual, $\varepsilon_{i,j}$

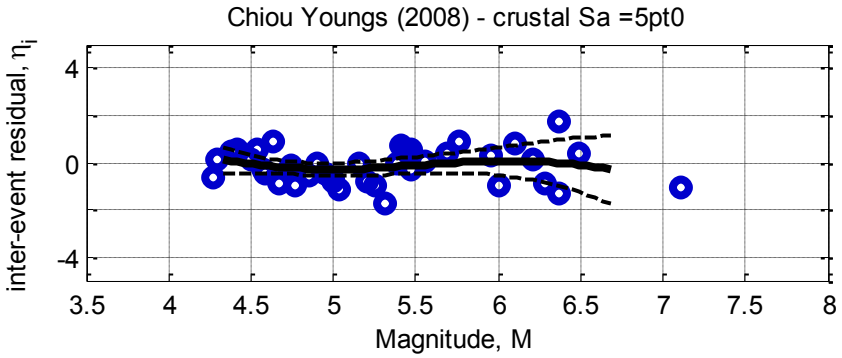
Chiou Youngs (2008) - crustal Sa =5pt0
inter-event residual, η_i
Magnitude, M

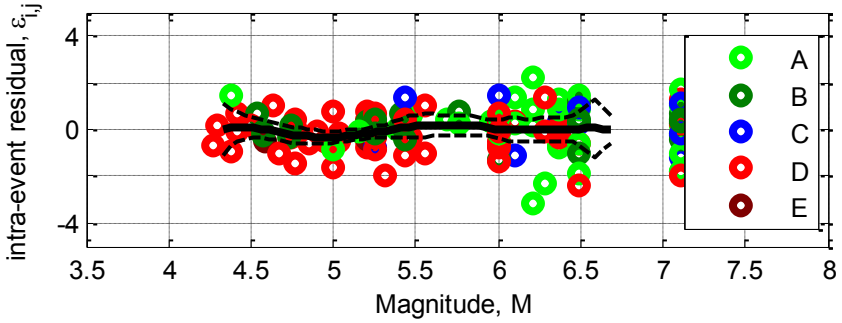
intra-event residual, $\varepsilon_{i,j}$
Magnitude, M
A
B
C
D
E

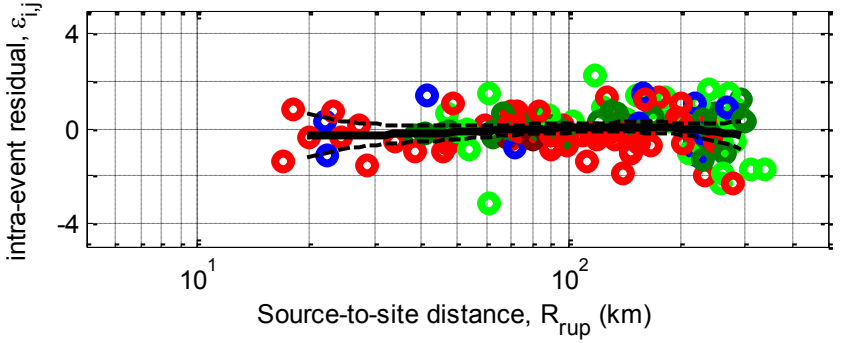
intra-event residual, $\varepsilon_{i,j}$
Source-to-site distance, R_{rup} (km)

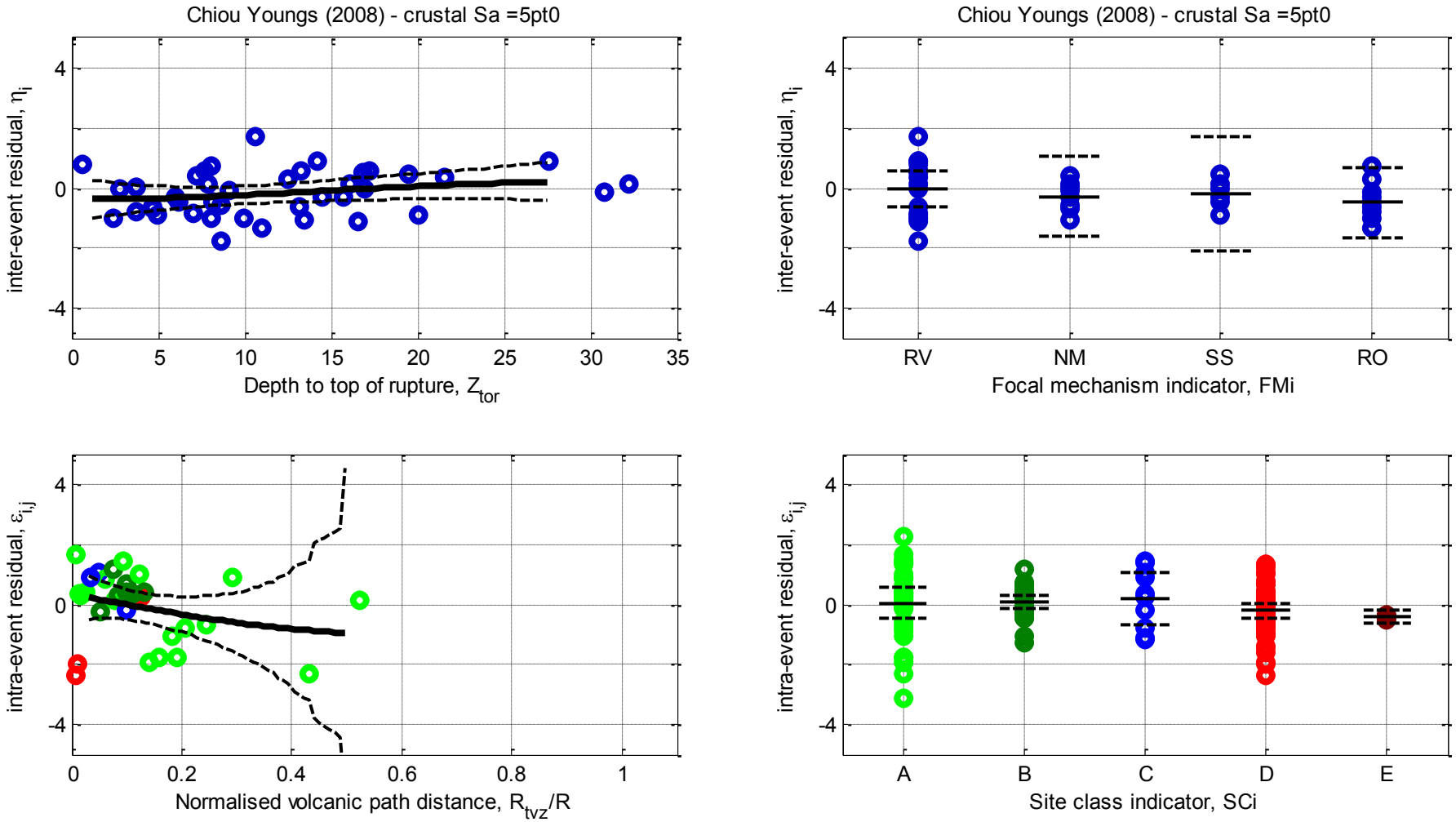

Figure D-20: Residuals for Sa(5.0) using the Chiou and Youngs (2008) crustal model

D.5. Chiou et al. (2010) Crustal model

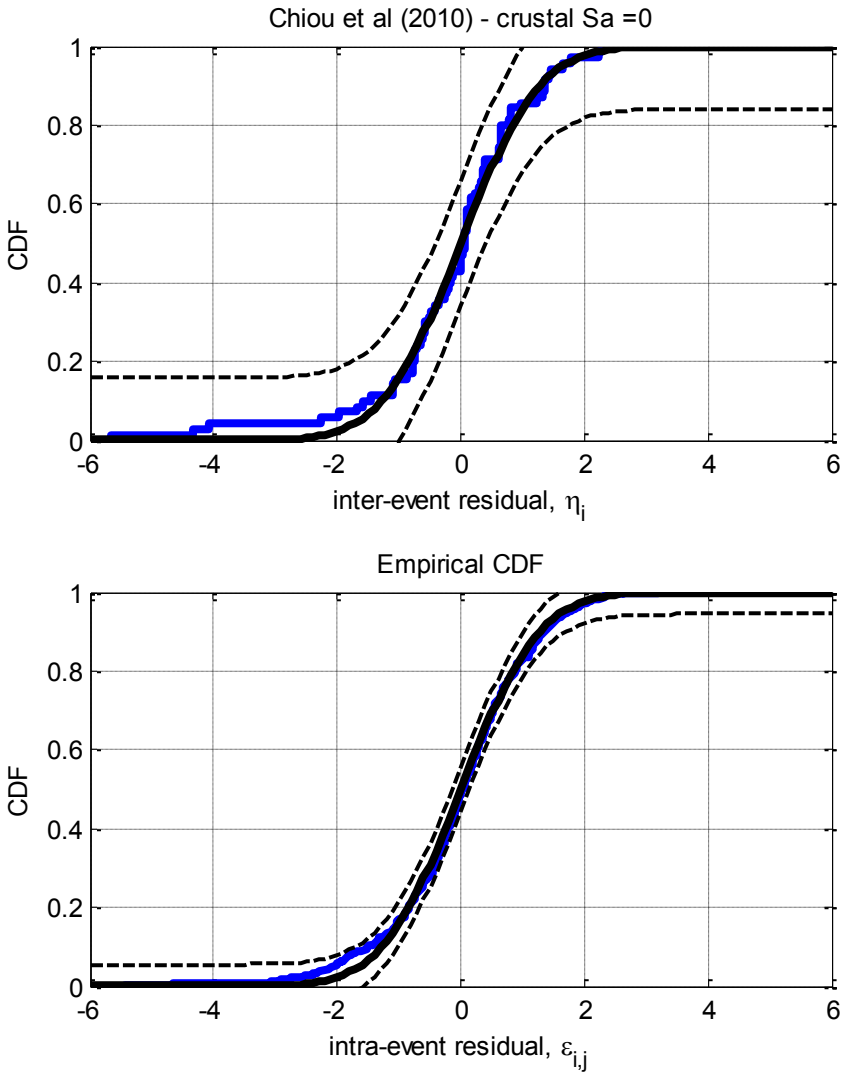

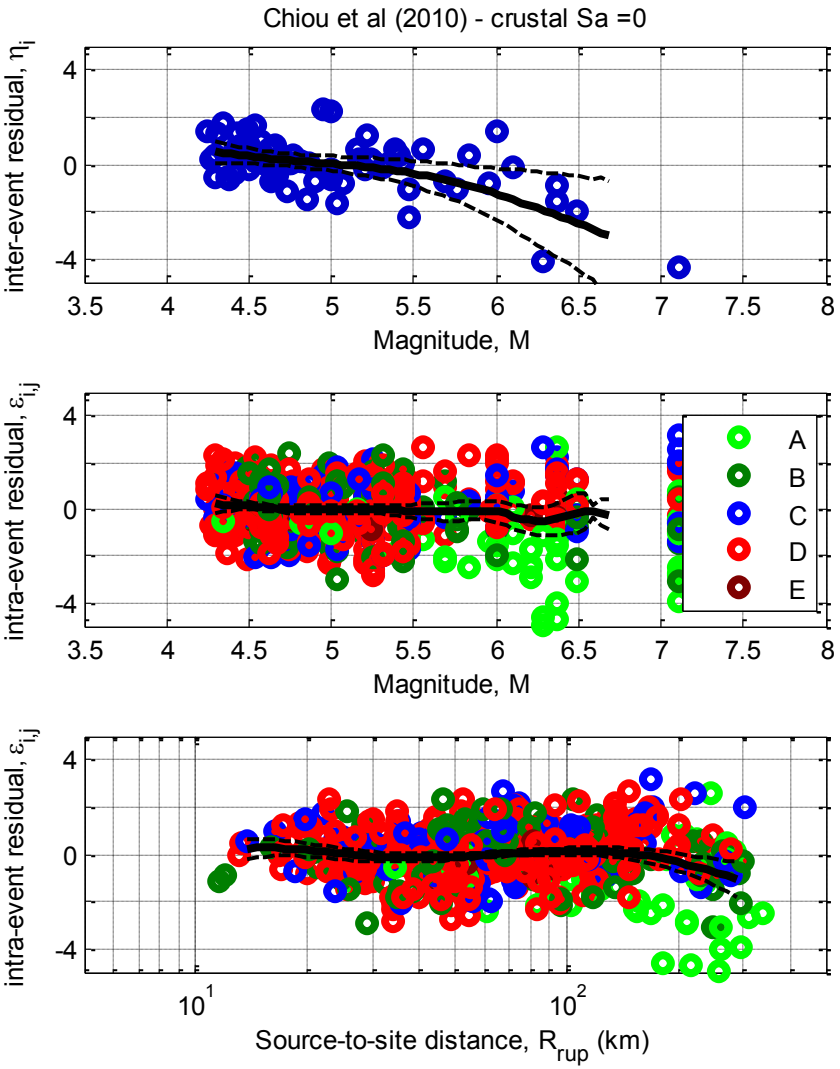

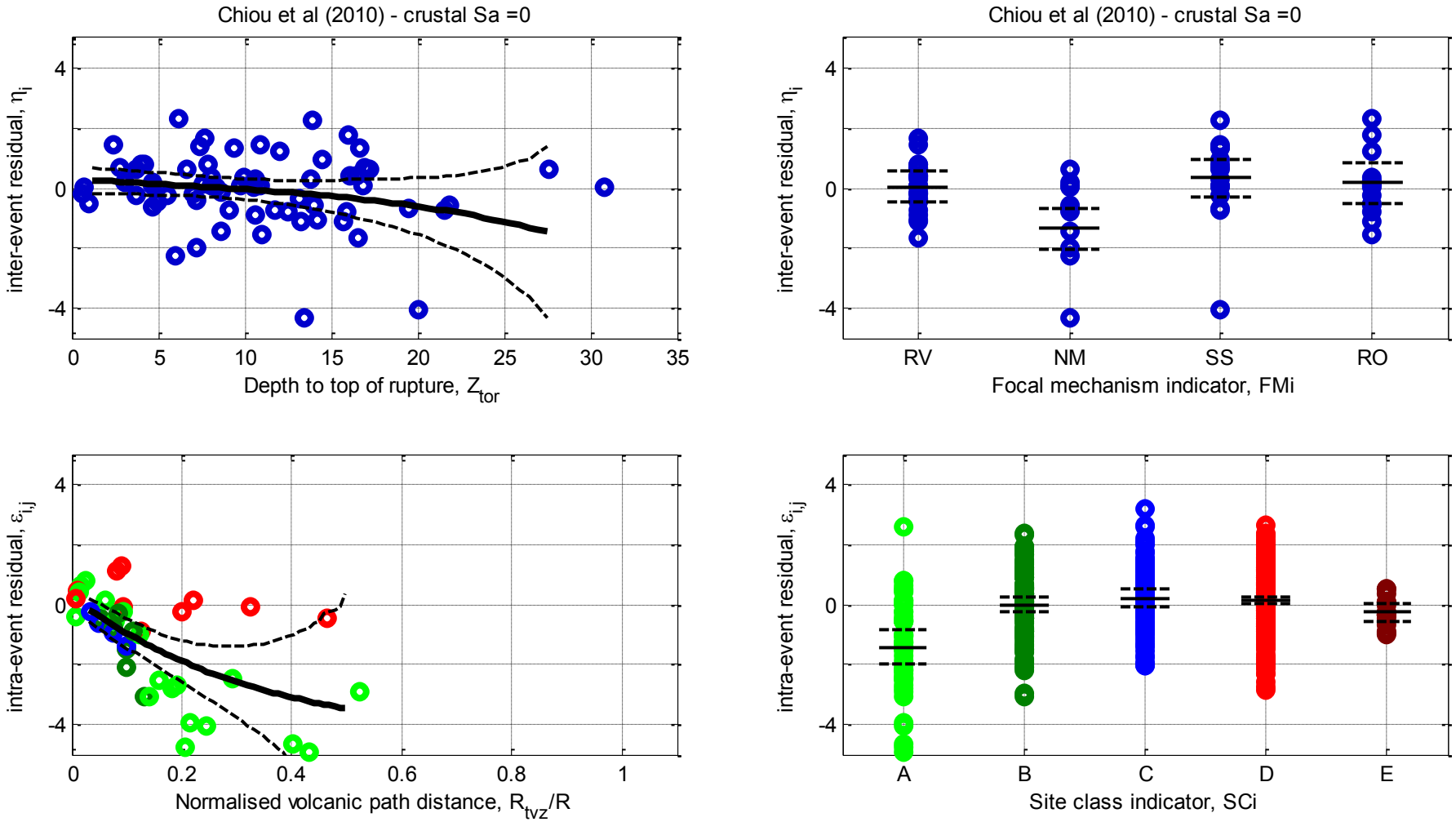

Figure D-21: Residuals for Sa(0.0) using the Chiou et al. (2010) crustal model

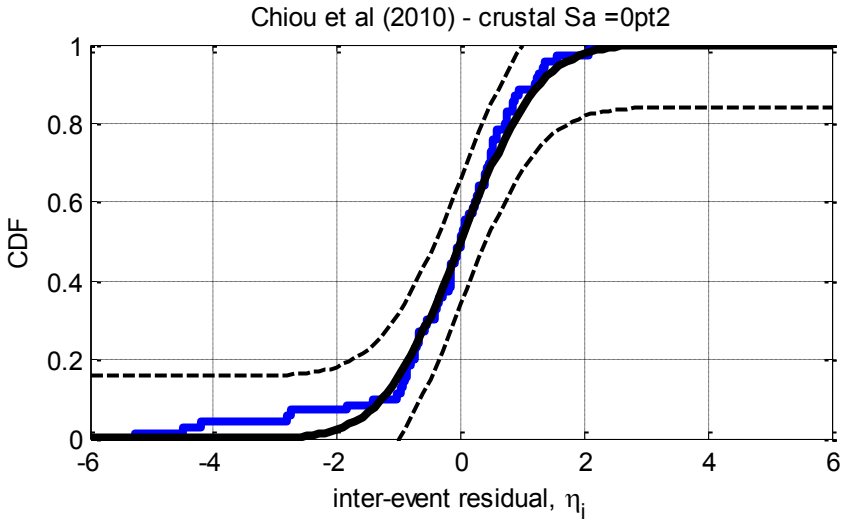
Chiou et al (2010) - crustal Sa =0pt2
CDF
inter-event residual, η_i

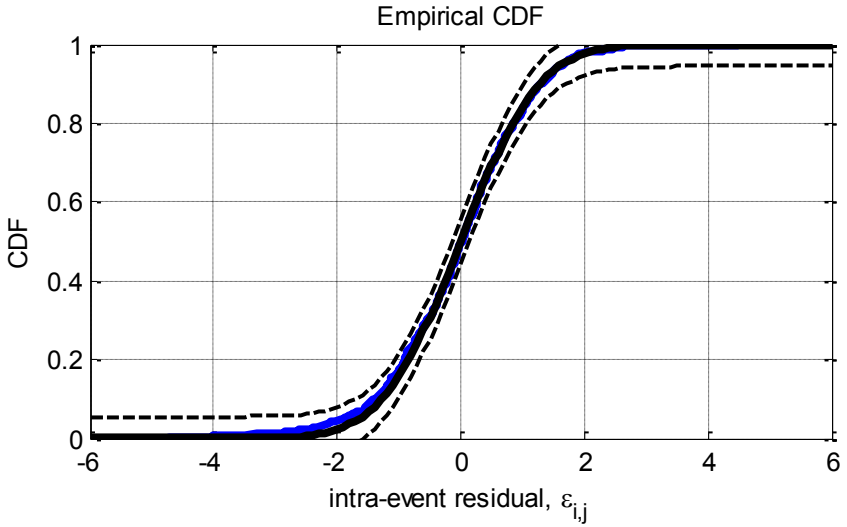
Empirical CDF
CDF
intra-event residual, $\varepsilon_{i,j}$

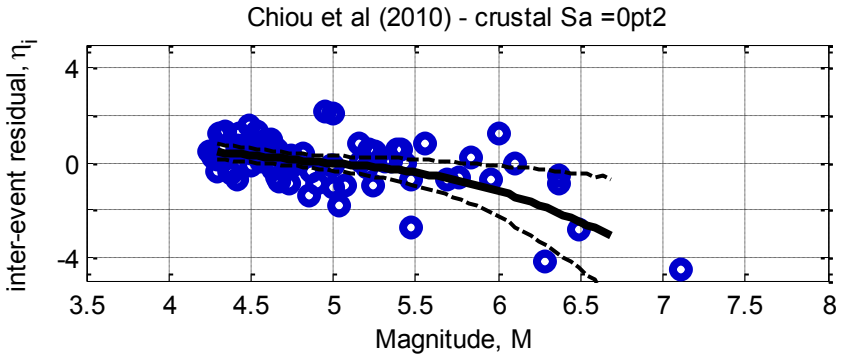
Chiou et al (2010) - crustal Sa =0pt2
inter-event residual, η_i
Magnitude, M

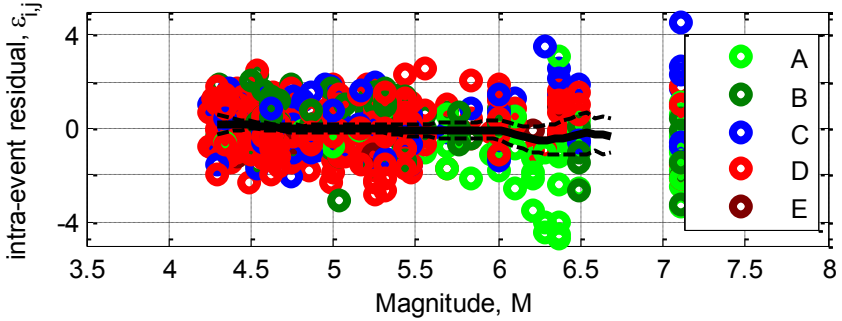
intra-event residual, $\varepsilon_{i,j}$
Magnitude, M
A
B
C
D
E

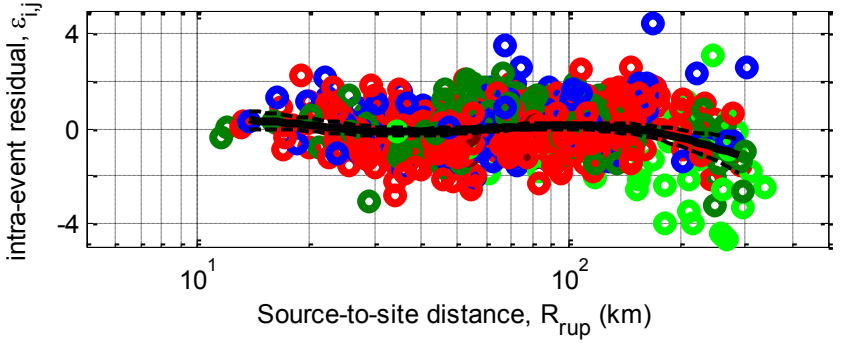
intra-event residual, $\varepsilon_{i,j}$
Source-to-site distance, R_{rup} (km)

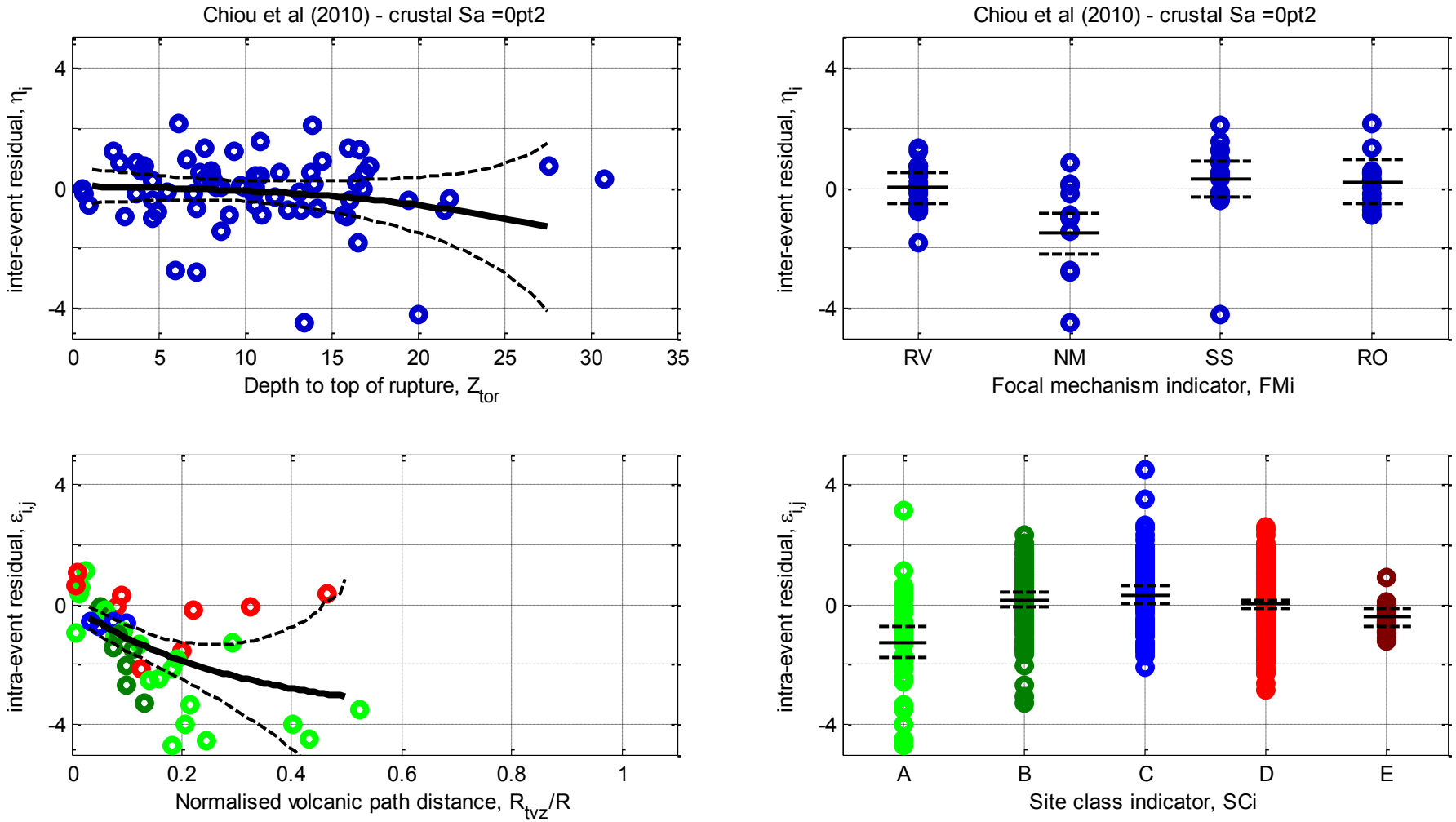

Figure D-22: Residuals for Sa(0.2) using the Chiou et al. (2010) crustal model

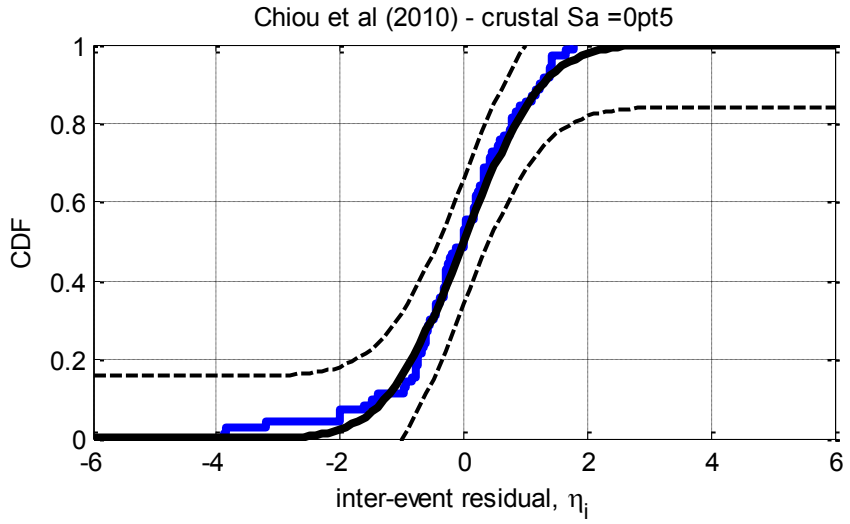
Chiou et al (2010) - crustal Sa =0pt5
CDF
inter-event residual, η_i

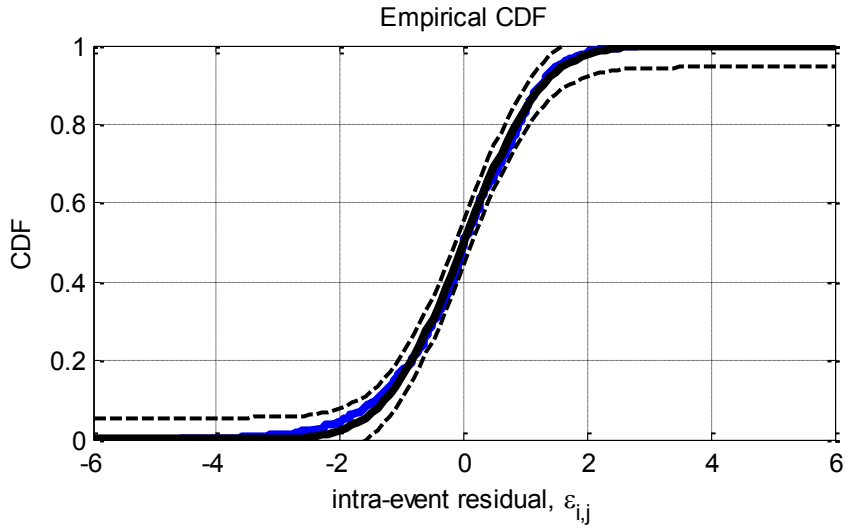
Empirical CDF
CDF
intra-event residual, $\varepsilon_{i,j}$

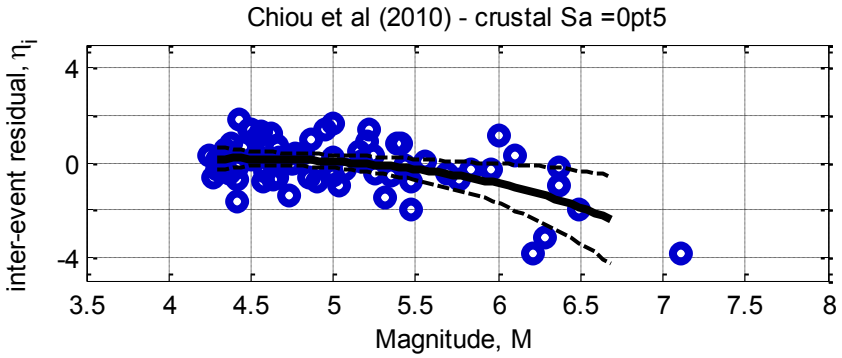
Chiou et al (2010) - crustal Sa =0pt5
inter-event residual, η_i
Magnitude, M

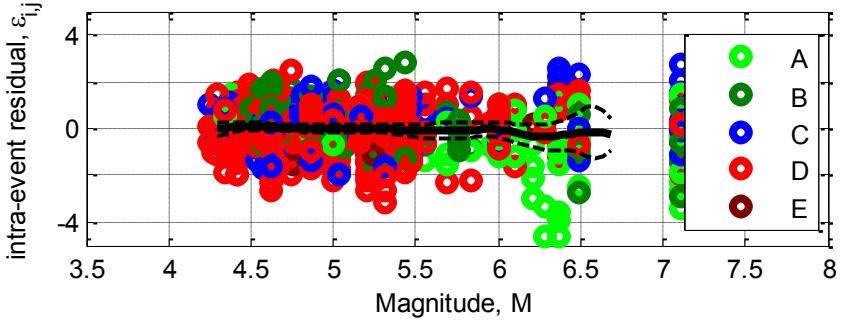
intra-event residual, $\varepsilon_{i,j}$
Magnitude, M
A
B
C
D
E

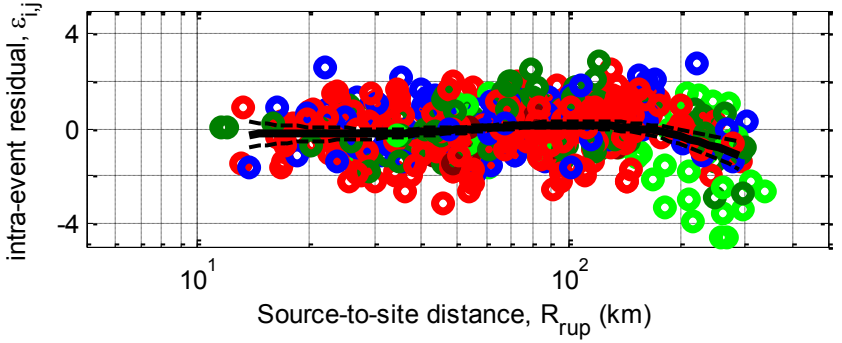
intra-event residual, $\varepsilon_{i,j}$
Source-to-site distance, R_{rup} (km)

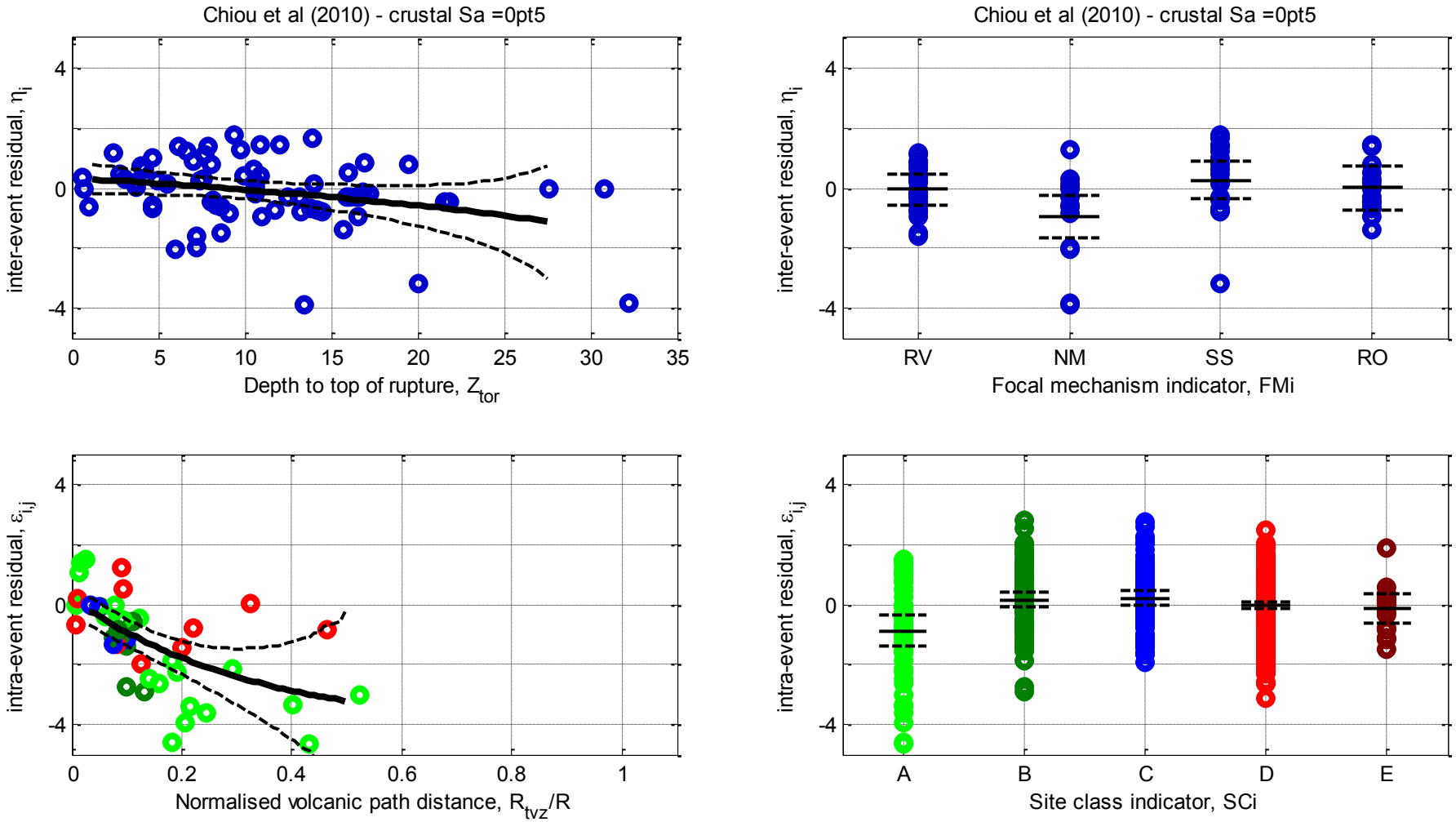

Figure D-23: Residuals for Sa(0.5) using the Chiou et al. (2010) crustal model

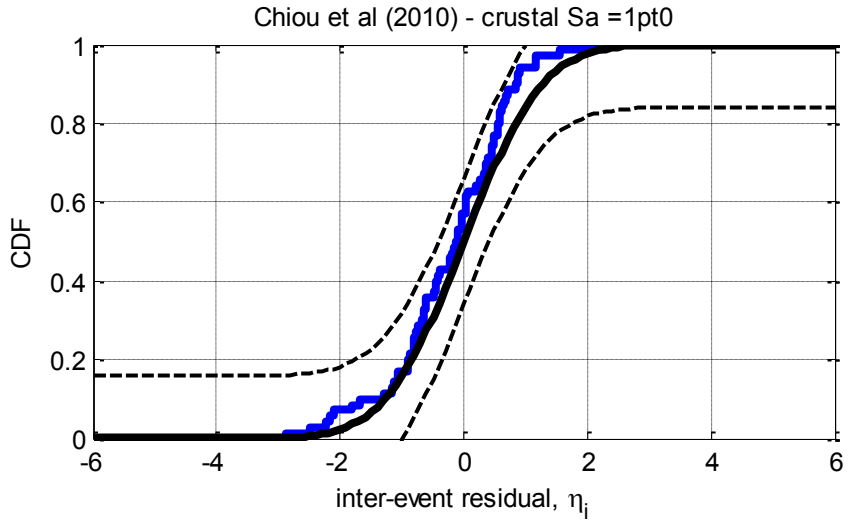
Chiou et al (2010) - crustal Sa =1pt0
CDF
inter-event residual, η_i

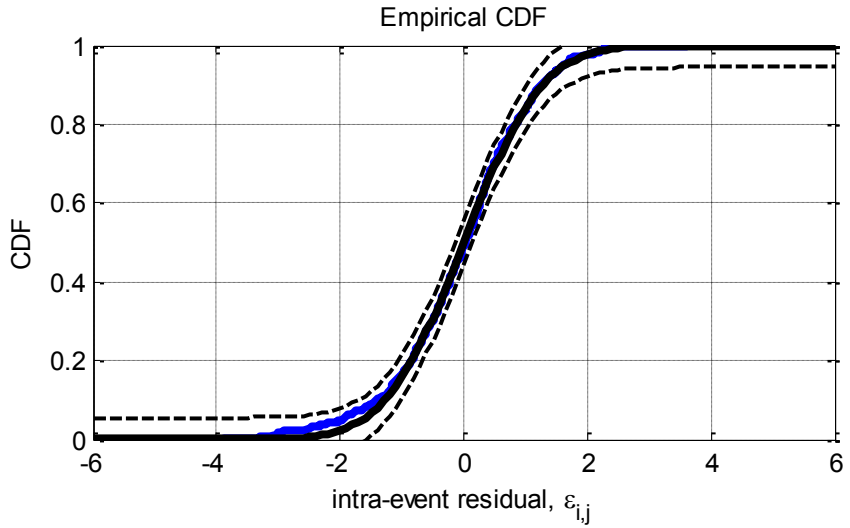
Empirical CDF
CDF
intra-event residual, $\varepsilon_{i,j}$

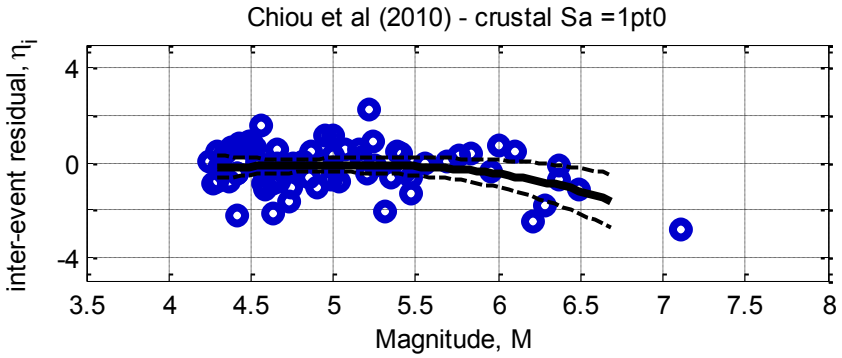
Chiou et al (2010) - crustal Sa =1pt0
inter-event residual, η_i
Magnitude, M

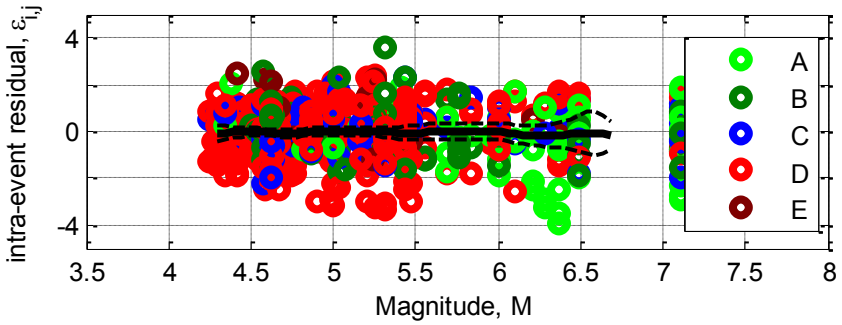
intra-event residual, $\varepsilon_{i,j}$
Magnitude, M
A
B
C
D
E

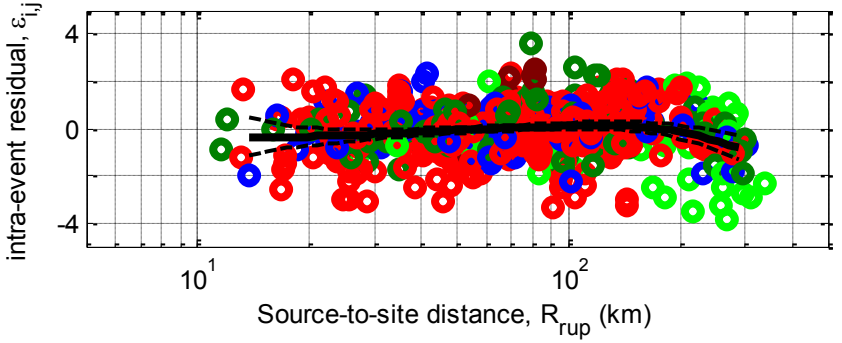
intra-event residual, $\varepsilon_{i,j}$
Source-to-site distance, R_{rup} (km)

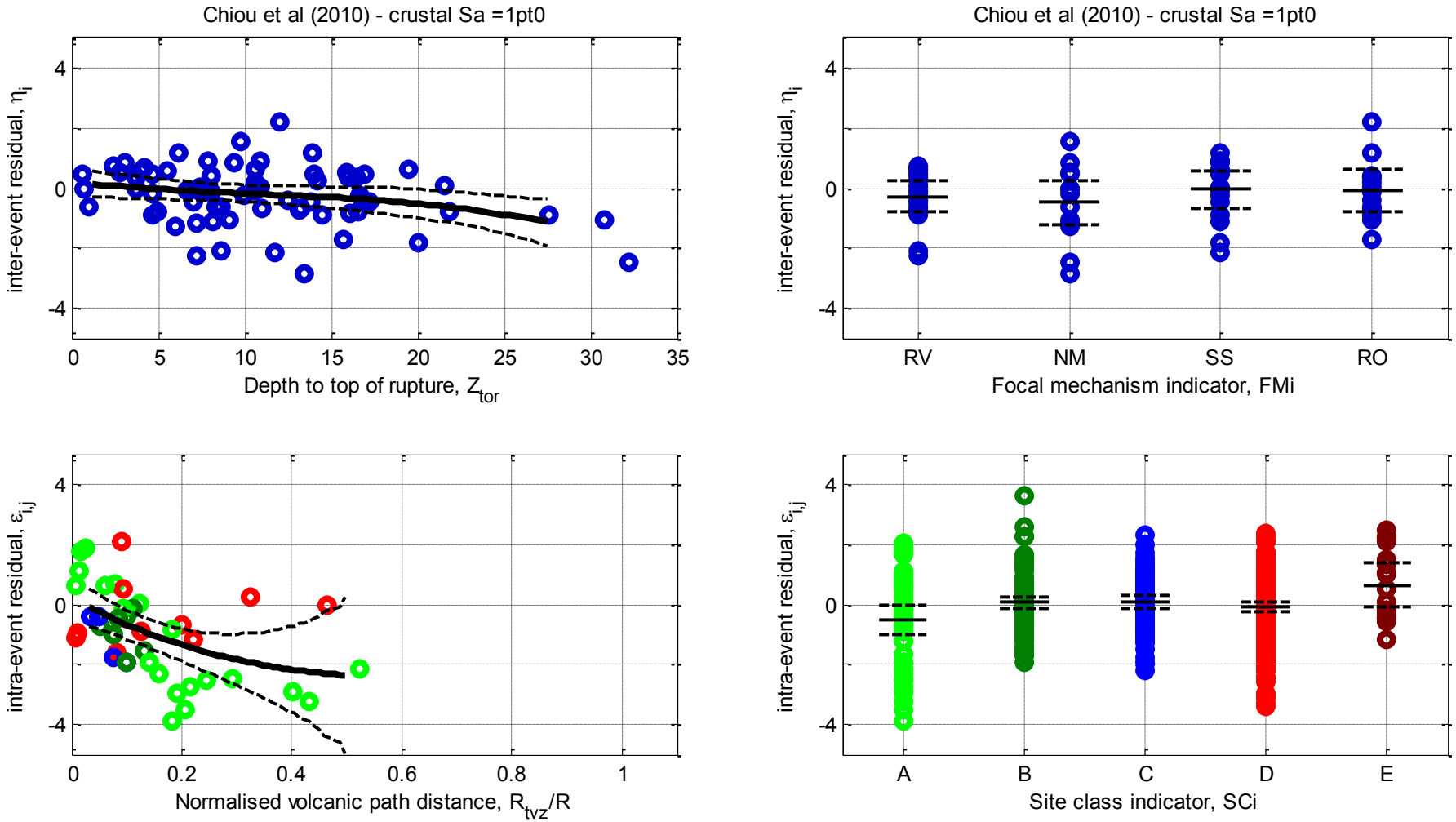

Figure D-24: Residuals for Sa(1.0) using the Chiou et al. (2010) crustal model

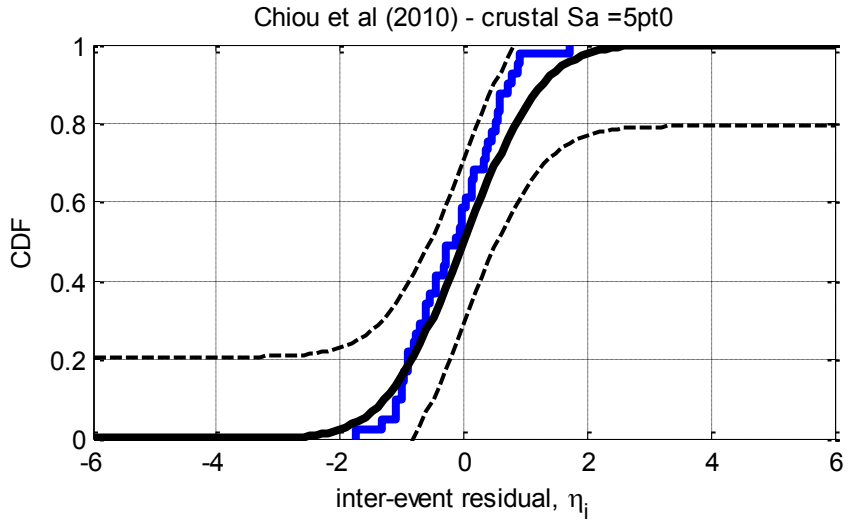
Chiou et al (2010) - crustal Sa =5pt0
CDF
inter-event residual, η_i

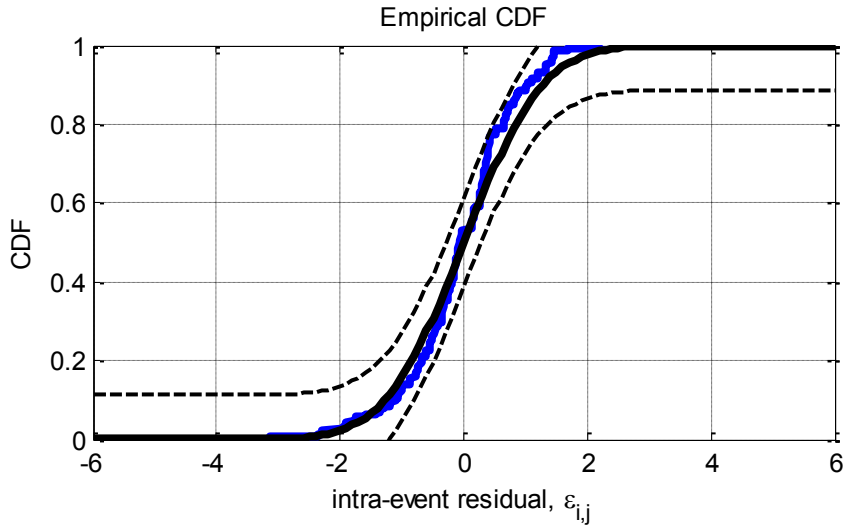
Empirical CDF
CDF
intra-event residual, $\varepsilon_{i,j}$

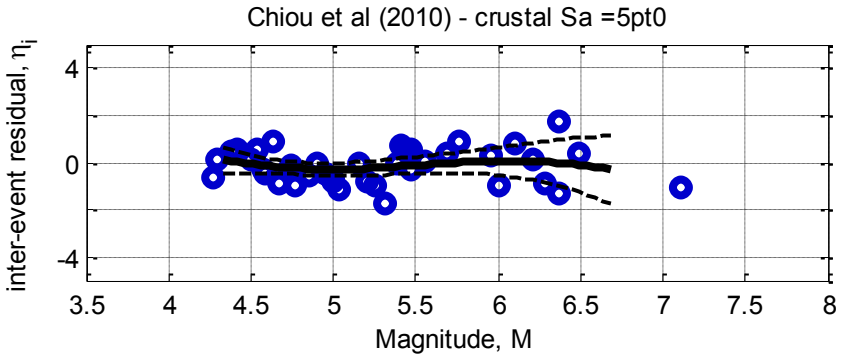
Chiou et al (2010) - crustal Sa =5pt0
inter-event residual, η_i
Magnitude, M

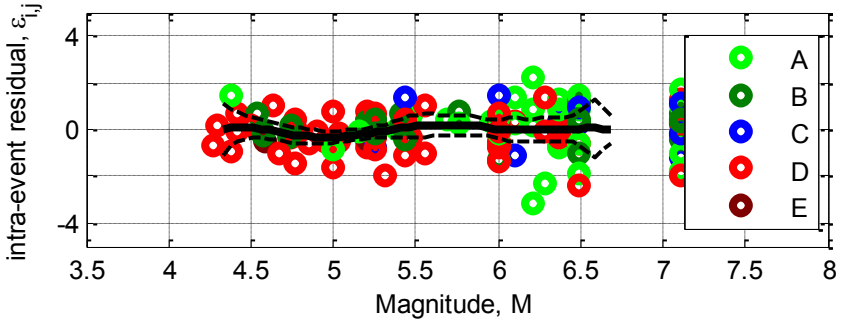
intra-event residual, $\varepsilon_{i,j}$
Magnitude, M
A
B
C
D
E

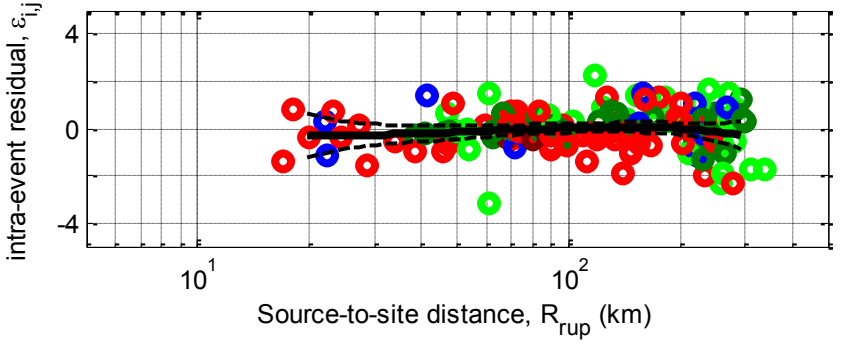
intra-event residual, $\varepsilon_{i,j}$
Source-to-site distance, R_{rup} (km)

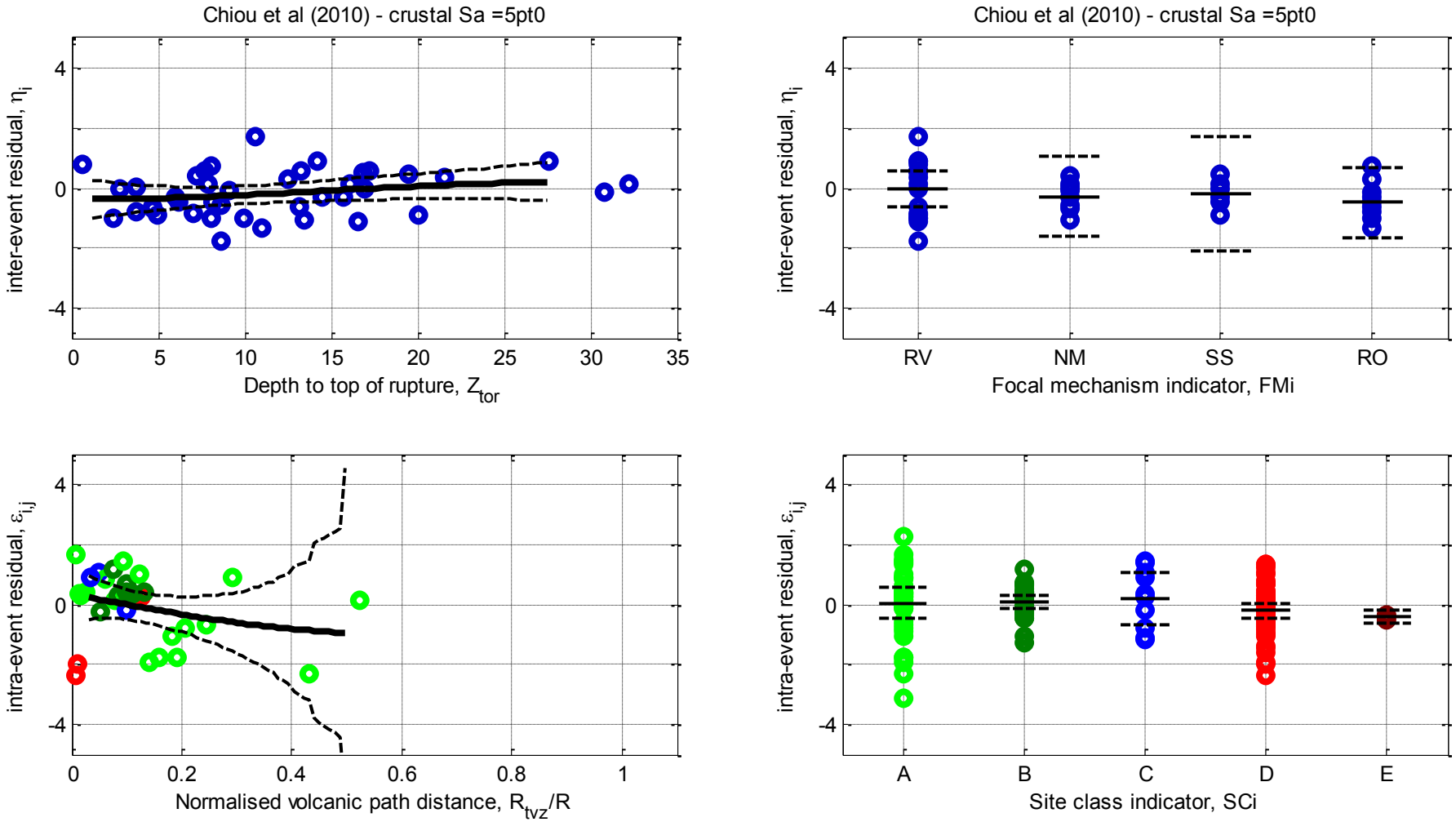

Figure D-25: Residuals for Sa(5.0) using the Chiou et al. (2010) crustal model

D.6. Bradley (2010) Crustal model

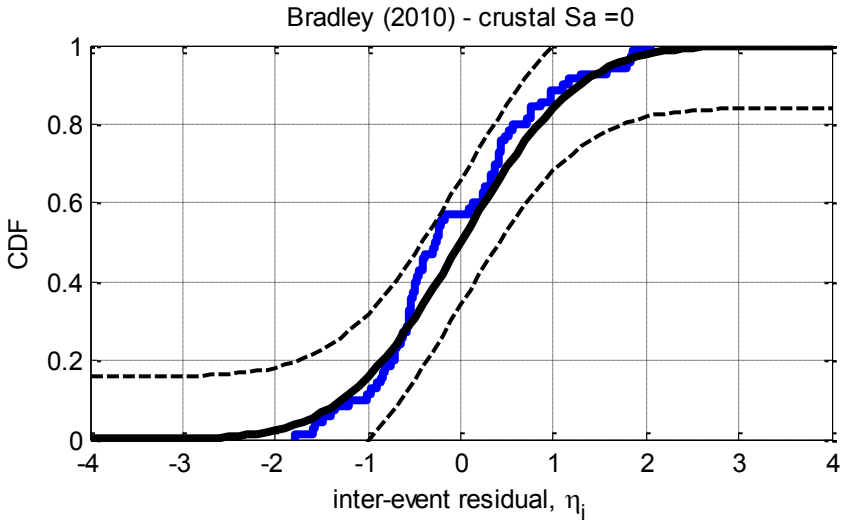

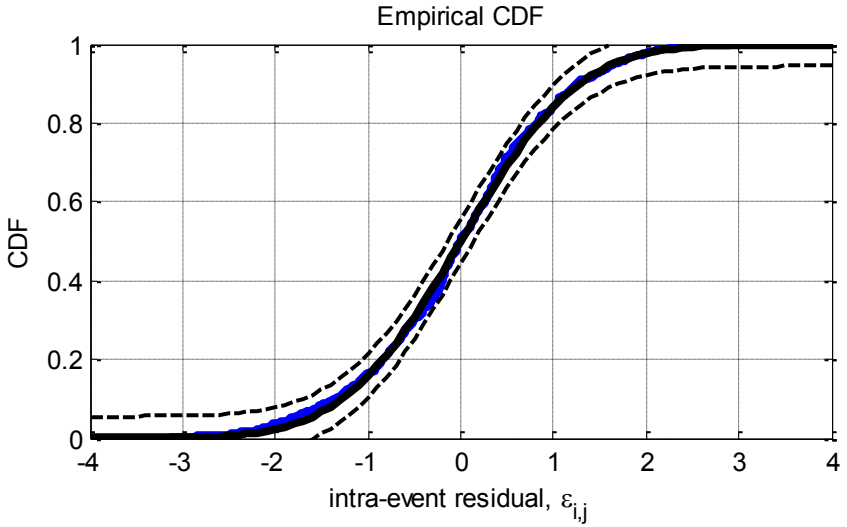

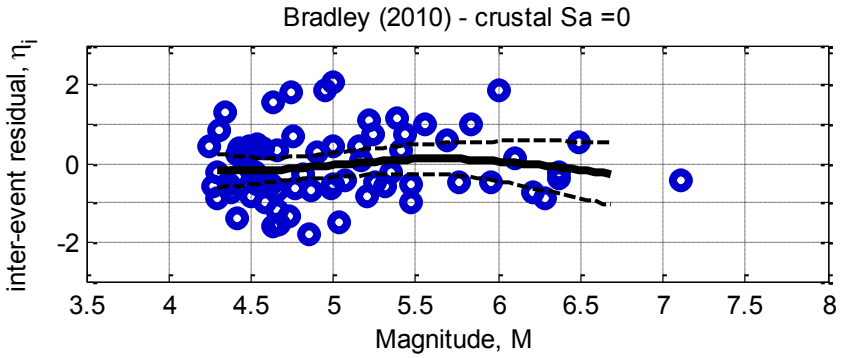

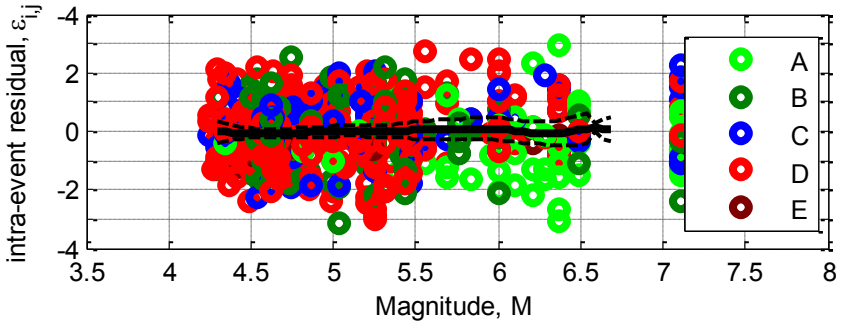

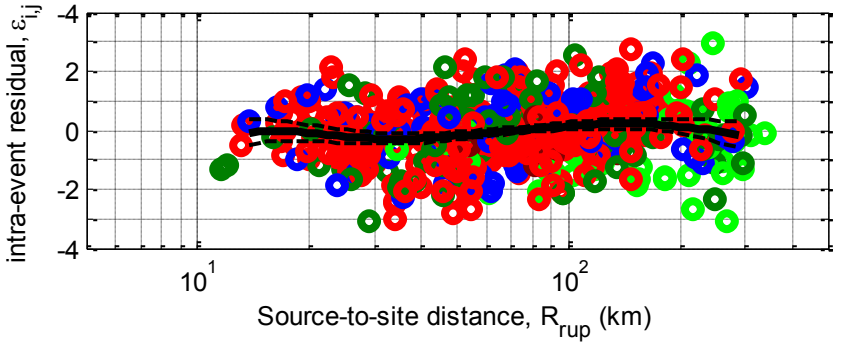

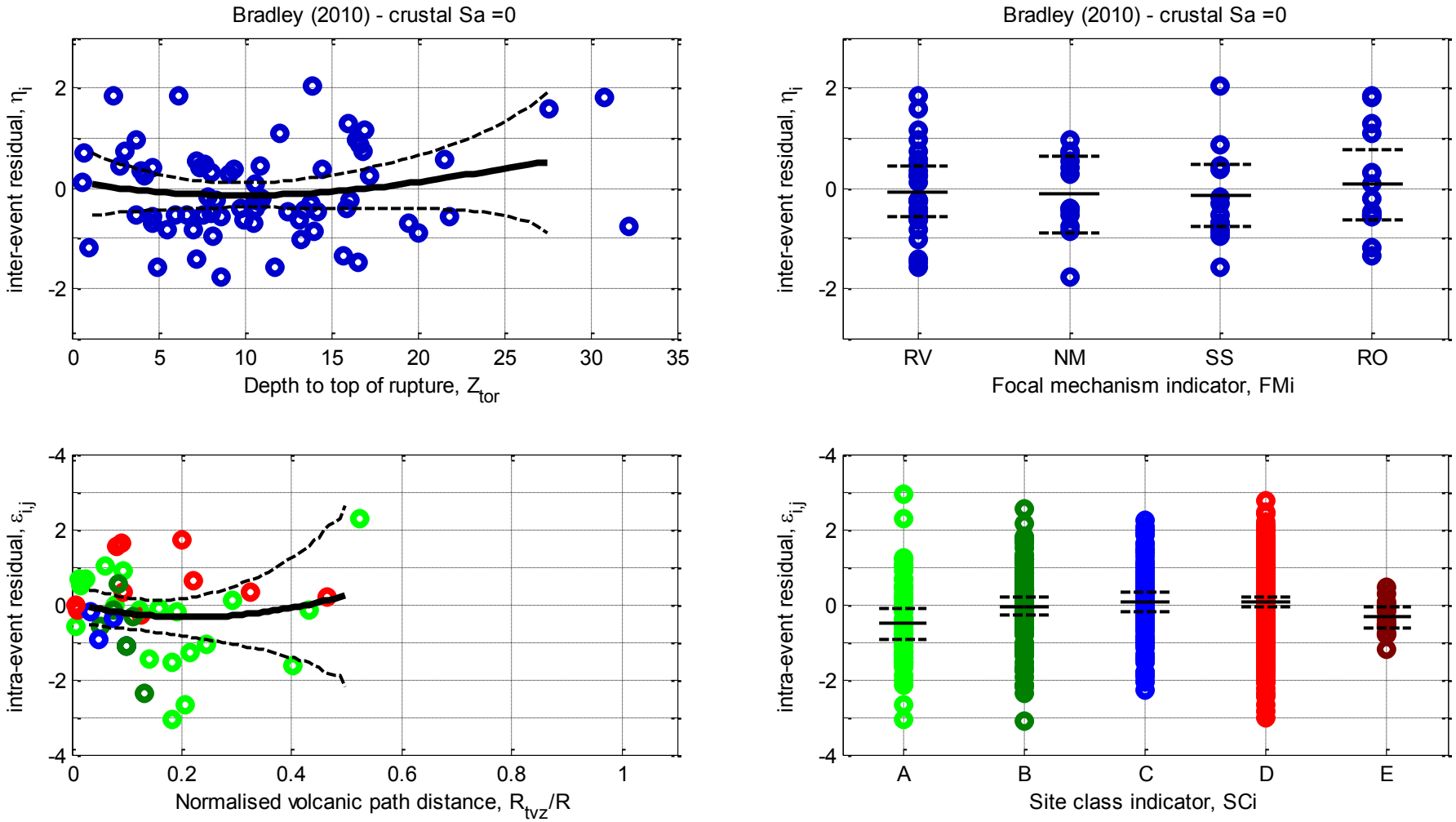

Figure D-26: Residuals for Sa(0.0) using the Bradley (2010) crustal model

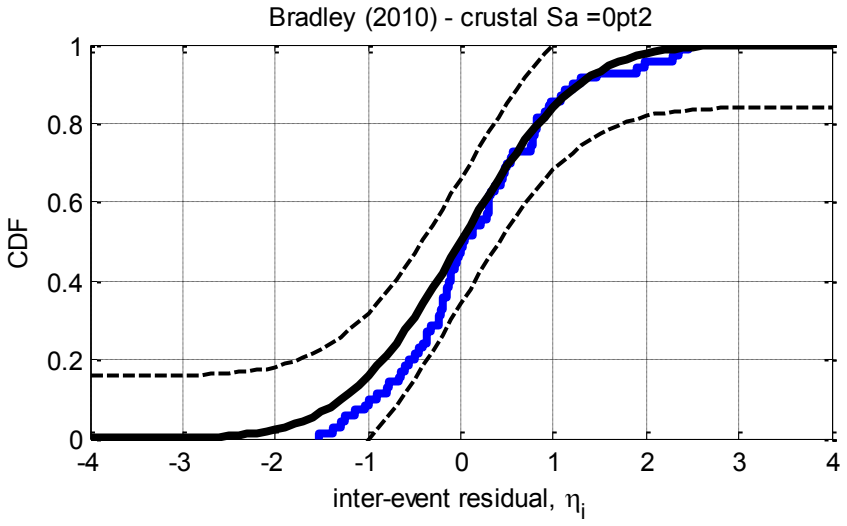
Bradley (2010) - crustal Sa =0pt2
CDF
inter-event residual, η_i

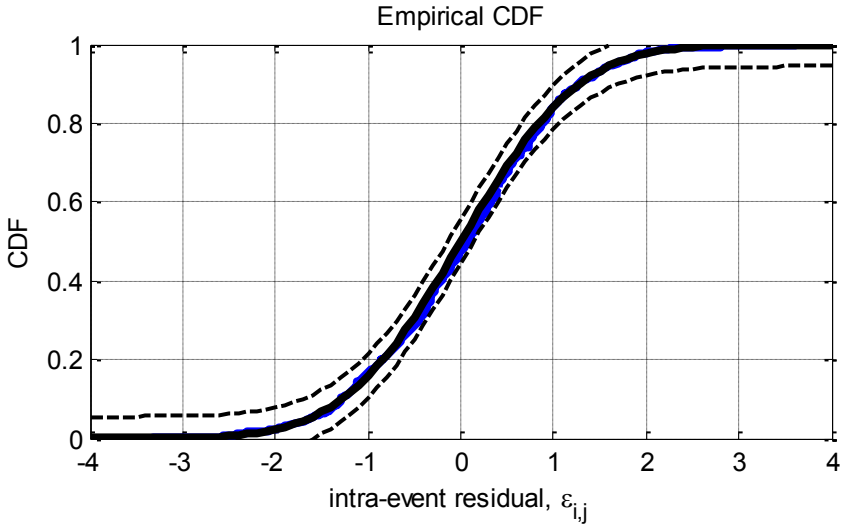
Empirical CDF
CDF
intra-event residual, $\varepsilon_{i,j}$

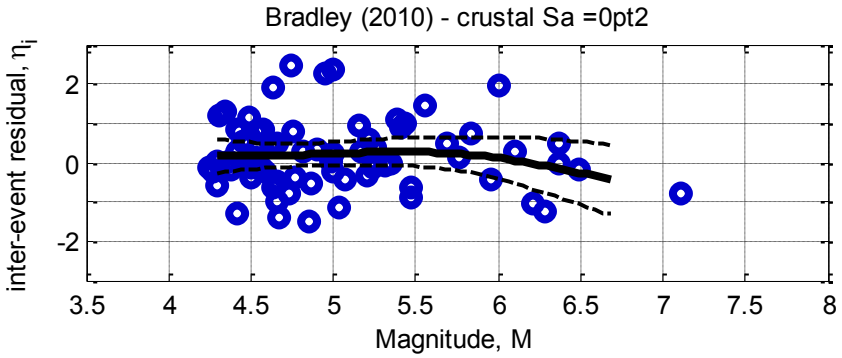
Bradley (2010) - crustal Sa =0pt2
inter-event residual, η_i
Magnitude, M

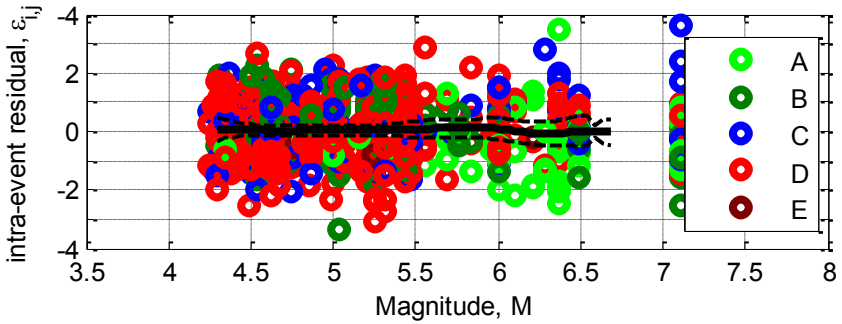
intra-event residual, $\varepsilon_{i,j}$
Magnitude, M
A
B
C
D
E

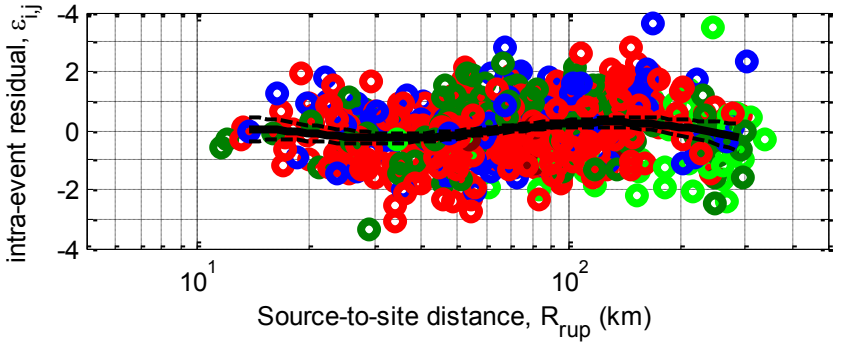
intra-event residual, $\varepsilon_{i,j}$
Source-to-site distance, R_{rup} (km)

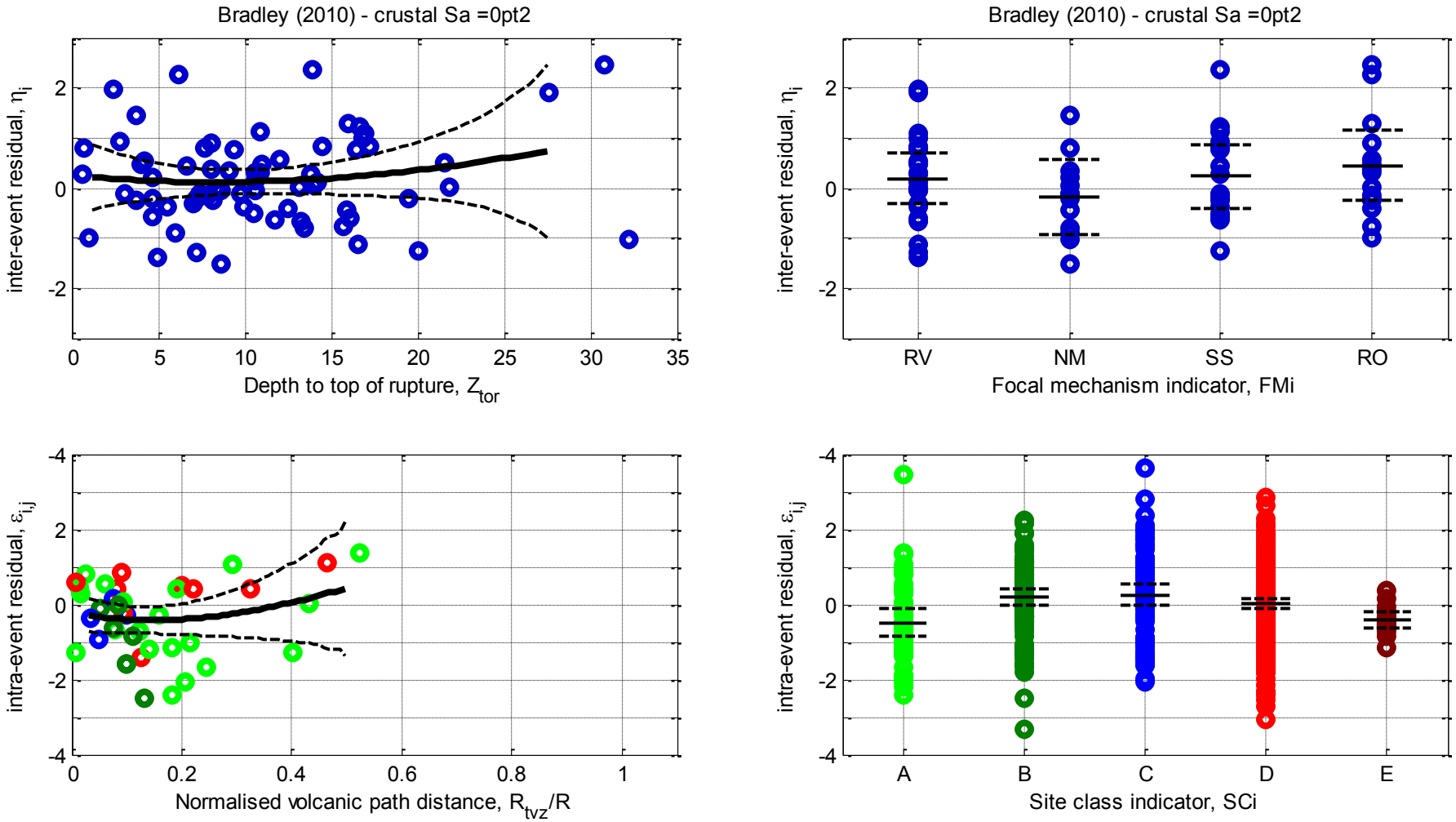

Figure D-27: Residuals for Sa(0.2) using the Bradley (2010) crustal model

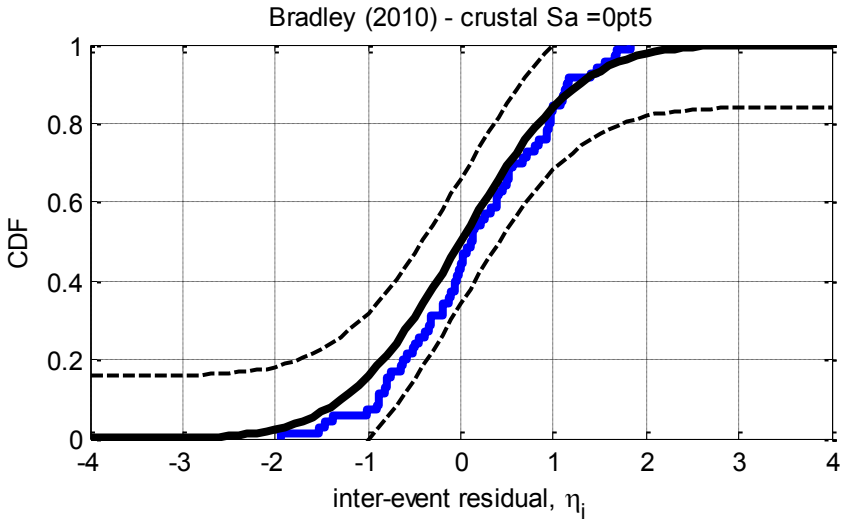
Bradley (2010) - crustal Sa =0pt5
CDF
inter-event residual, η_i

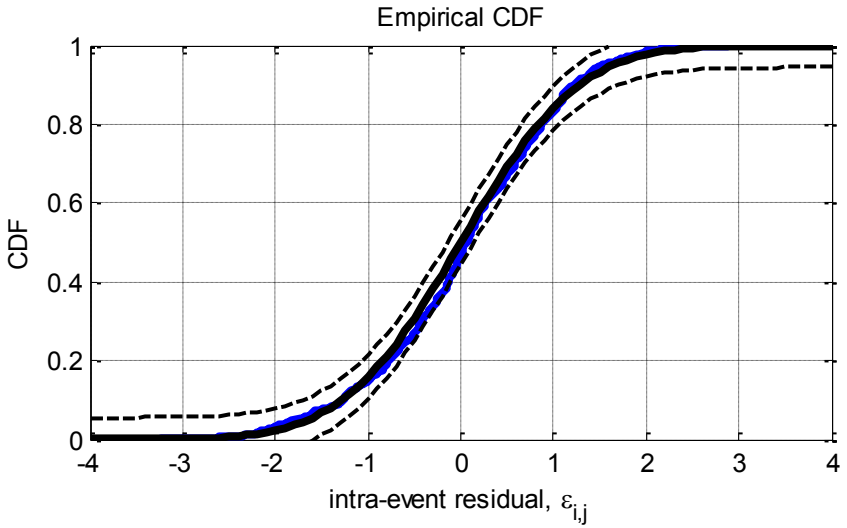
Empirical CDF
CDF
intra-event residual, $\varepsilon_{i,j}$

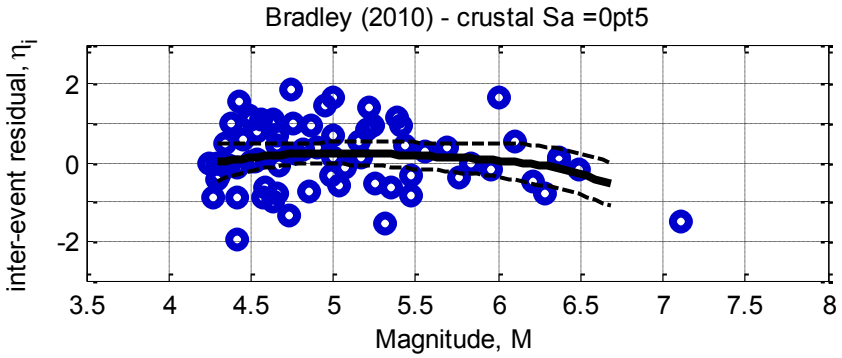
Bradley (2010) - crustal Sa =0pt5
inter-event residual, η_i
Magnitude, M

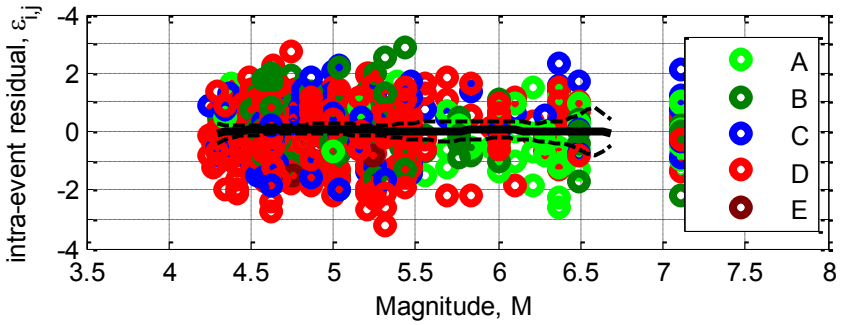
intra-event residual, $\varepsilon_{i,j}$
Magnitude, M
A
B
C
D
E

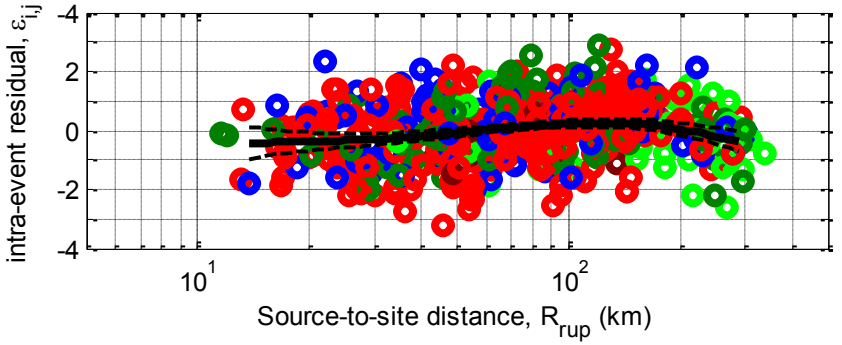
intra-event residual, $\varepsilon_{i,j}$
Source-to-site distance, R_{rup} (km)

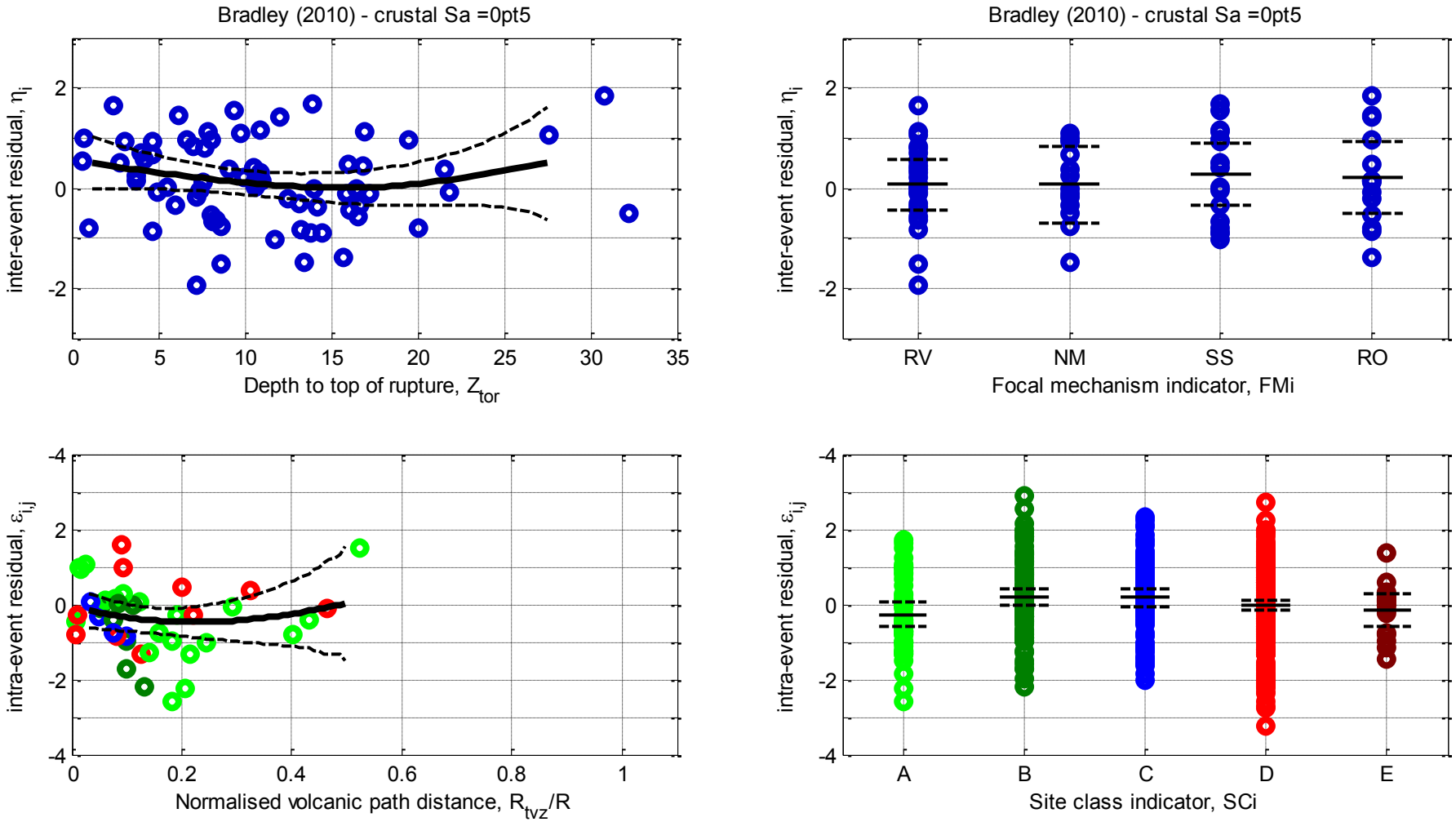

Figure D-28: Residuals for Sa(0.5) using the Bradley (2010) crustal model

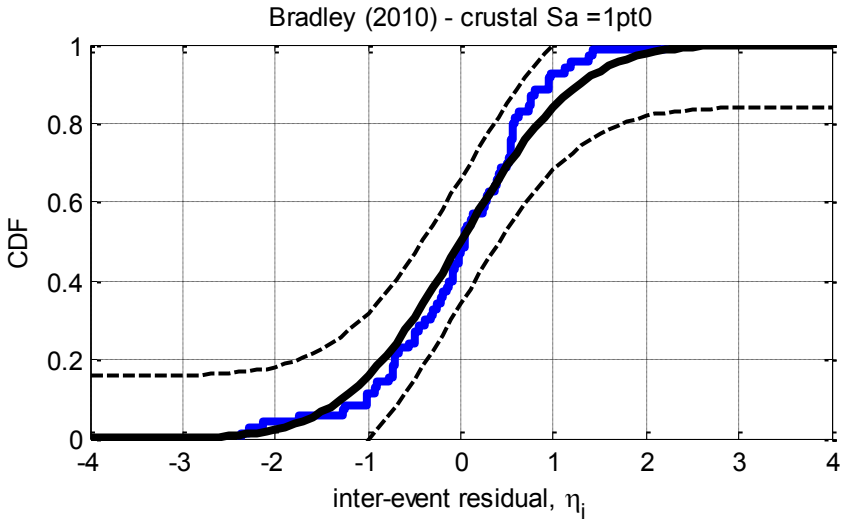
Bradley (2010) - crustal Sa =1pt0
CDF
inter-event residual, η_i

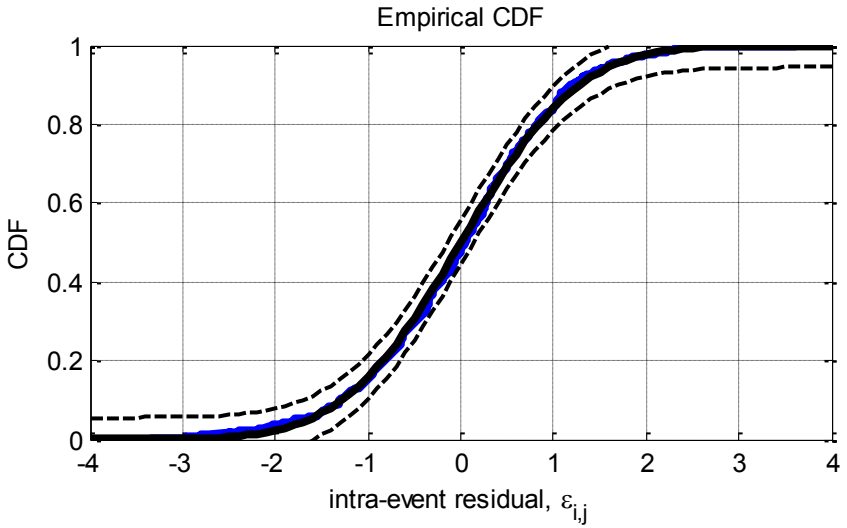
Empirical CDF
CDF
intra-event residual, $\varepsilon_{i,j}$

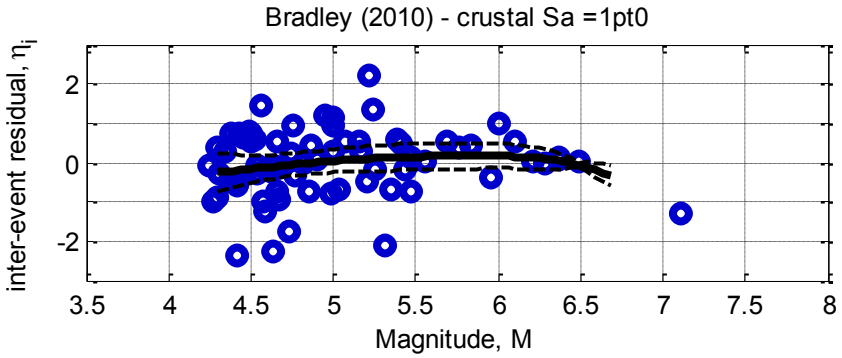
Bradley (2010) - crustal Sa =1pt0
inter-event residual, η_i
Magnitude, M

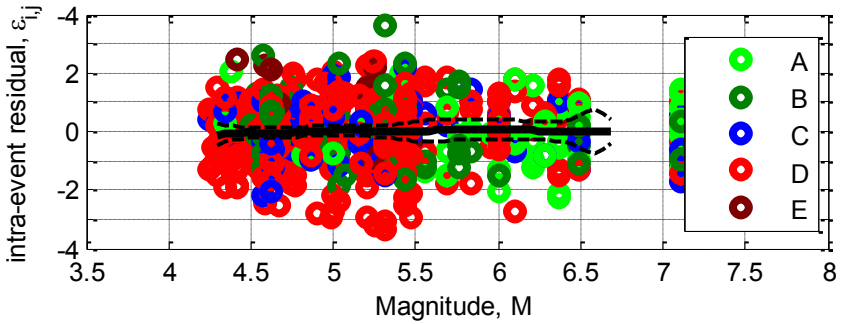
intra-event residual, $\varepsilon_{i,j}$
Magnitude, M
A
B
C
D
E

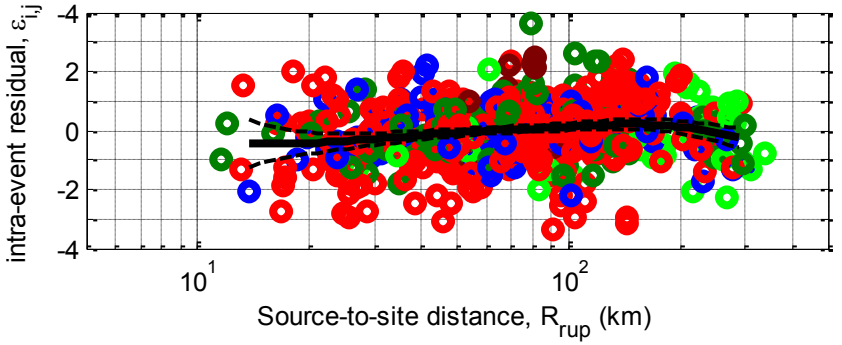
intra-event residual, $\varepsilon_{i,j}$
Source-to-site distance, R_{rup} (km)

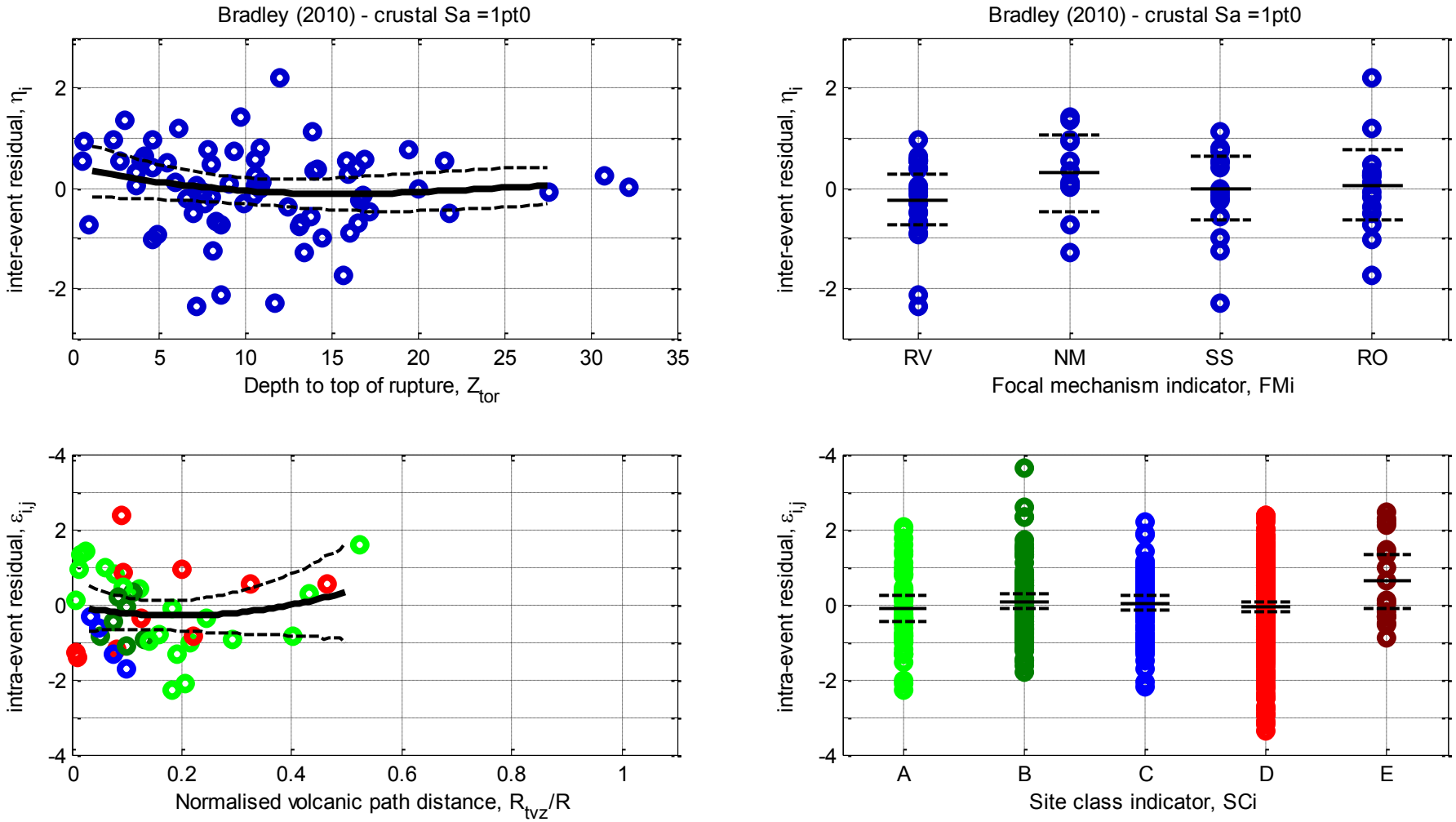

Figure D-29: Residuals for Sa(1.0) using the Bradley (2010) crustal model

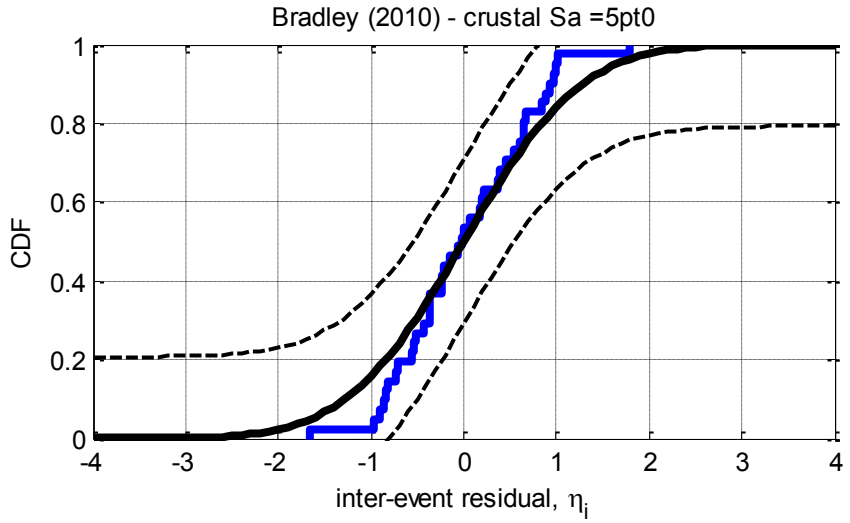
Bradley (2010) - crustal Sa =5pt0
CDF
inter-event residual, η_i

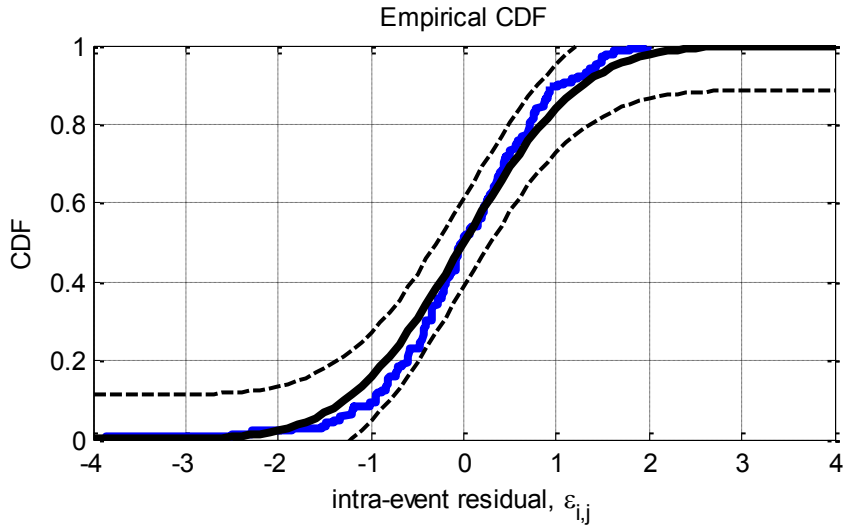
Empirical CDF
CDF
intra-event residual, $\varepsilon_{i,j}$

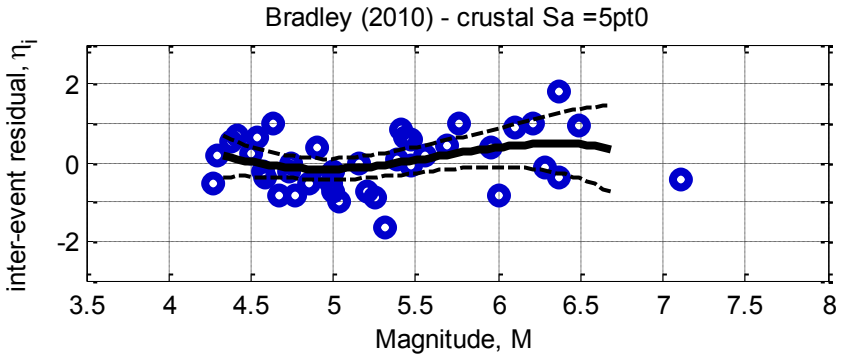
Bradley (2010) - crustal Sa =5pt0
inter-event residual, η_i
Magnitude, M

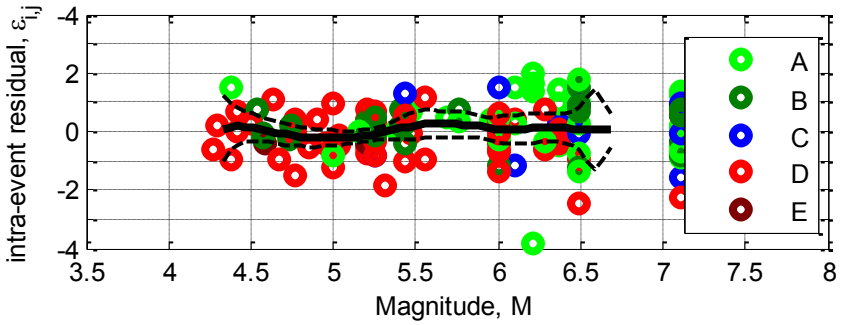
intra-event residual, $\varepsilon_{i,j}$
A
B
C
D
E
Magnitude, M

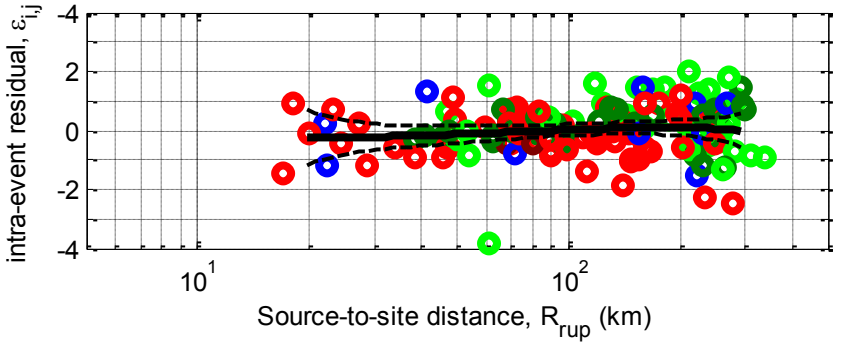
intra-event residual, $\varepsilon_{i,j}$
Source-to-site distance, R_{rup} (km)

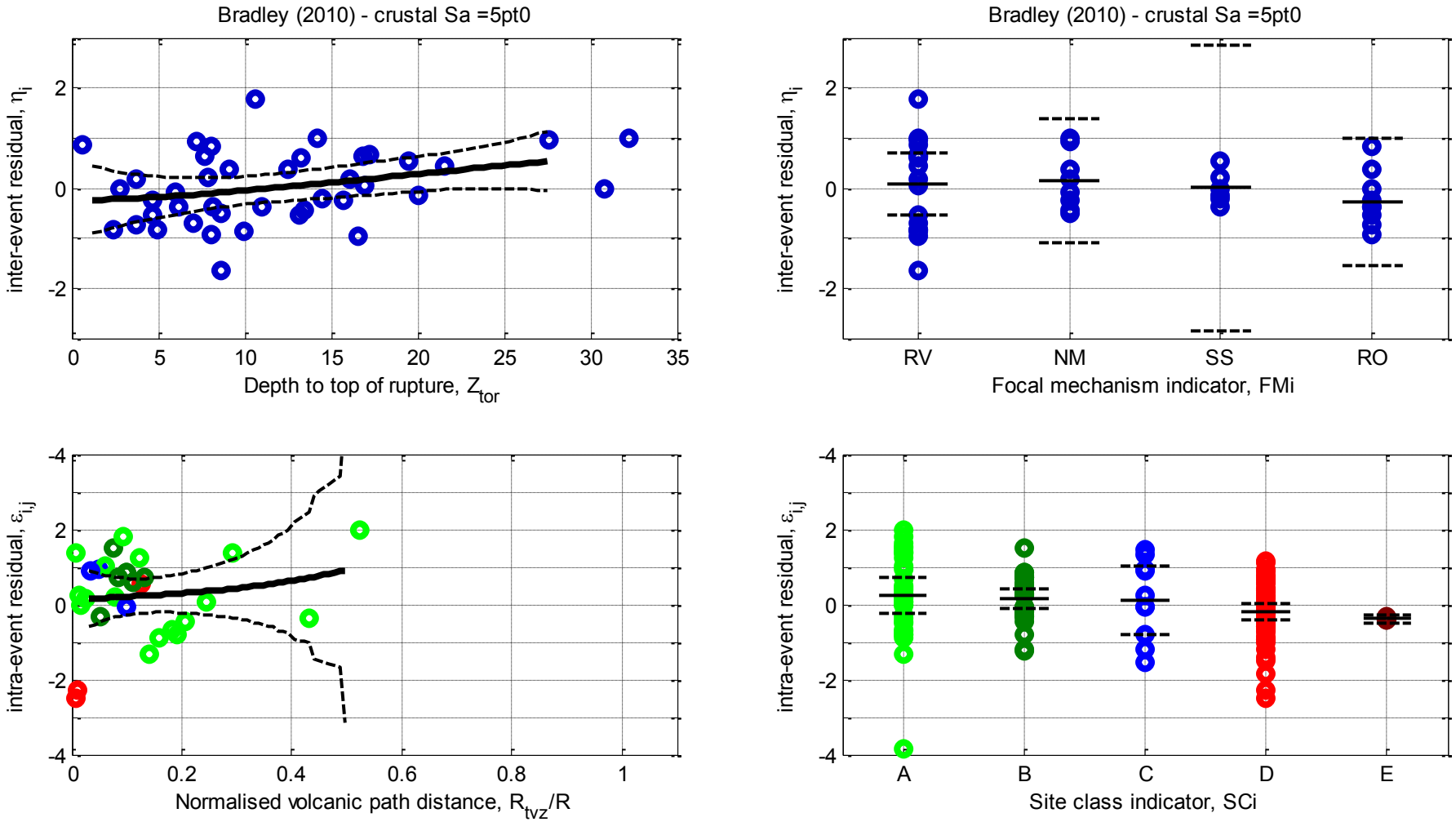

Figure D-30: Residuals for Sa(5.0) using the Bradley (2010) crustal model

D.7. McVerry et al. (2006) Slab model

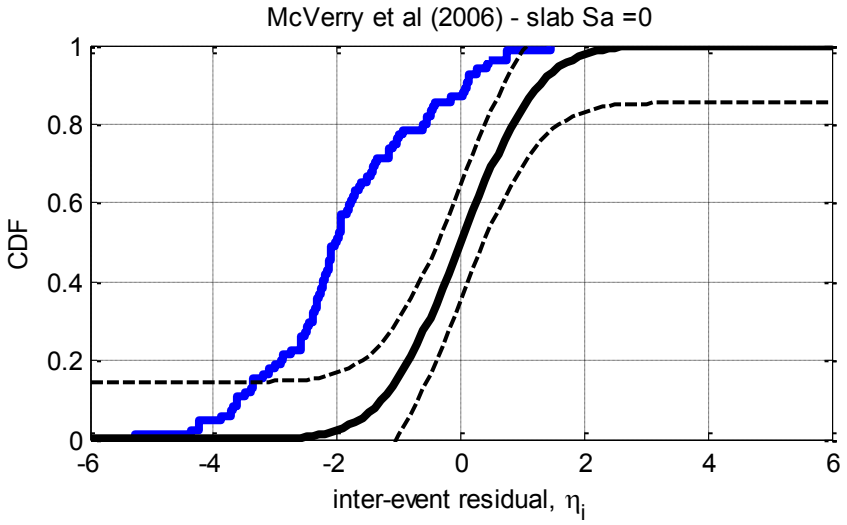

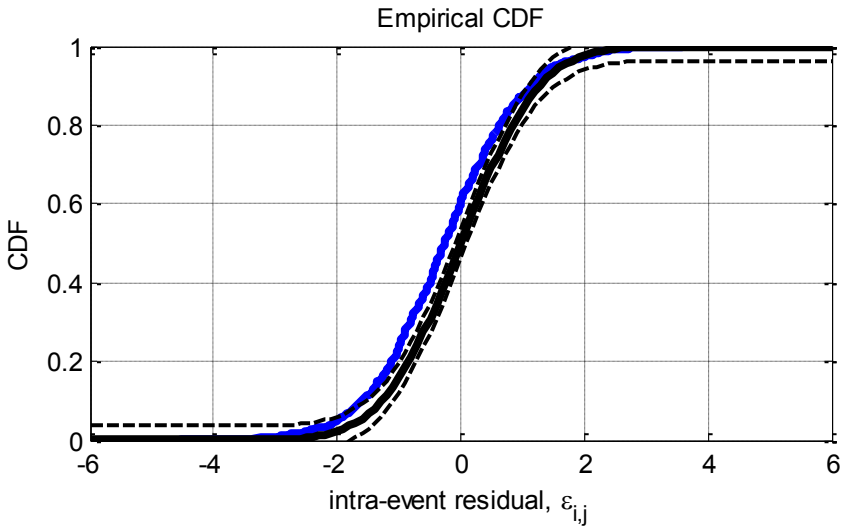

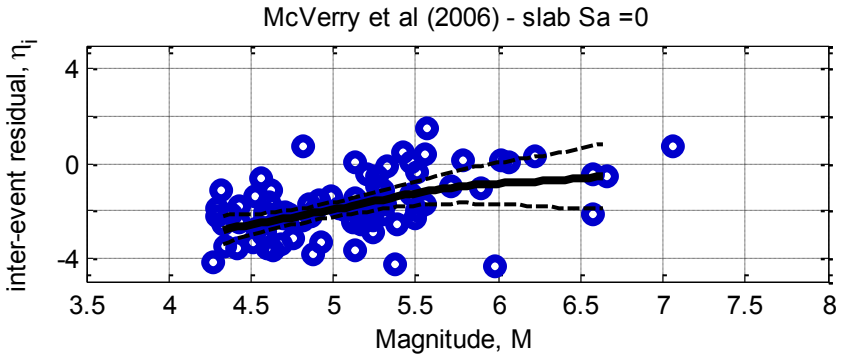

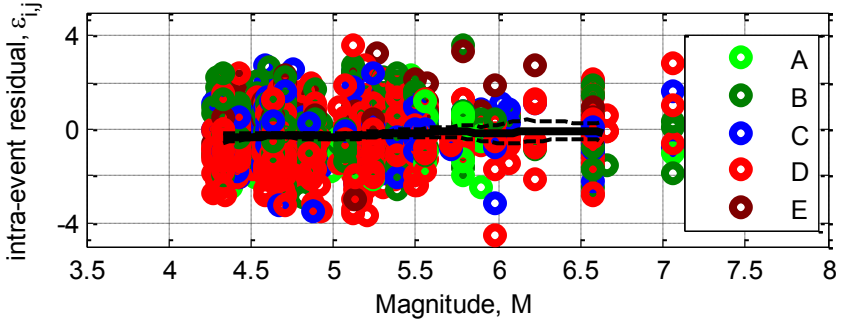

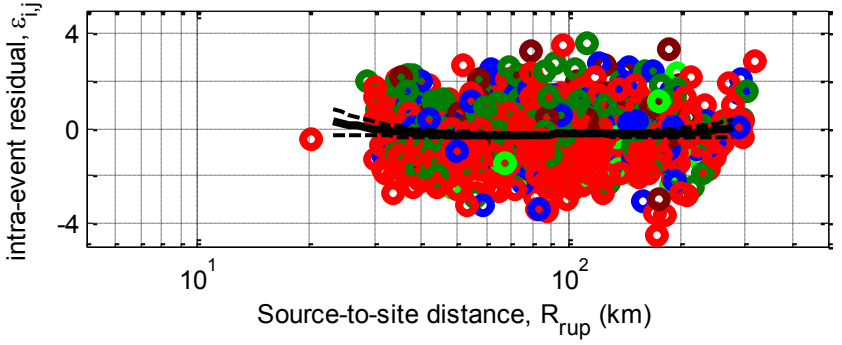

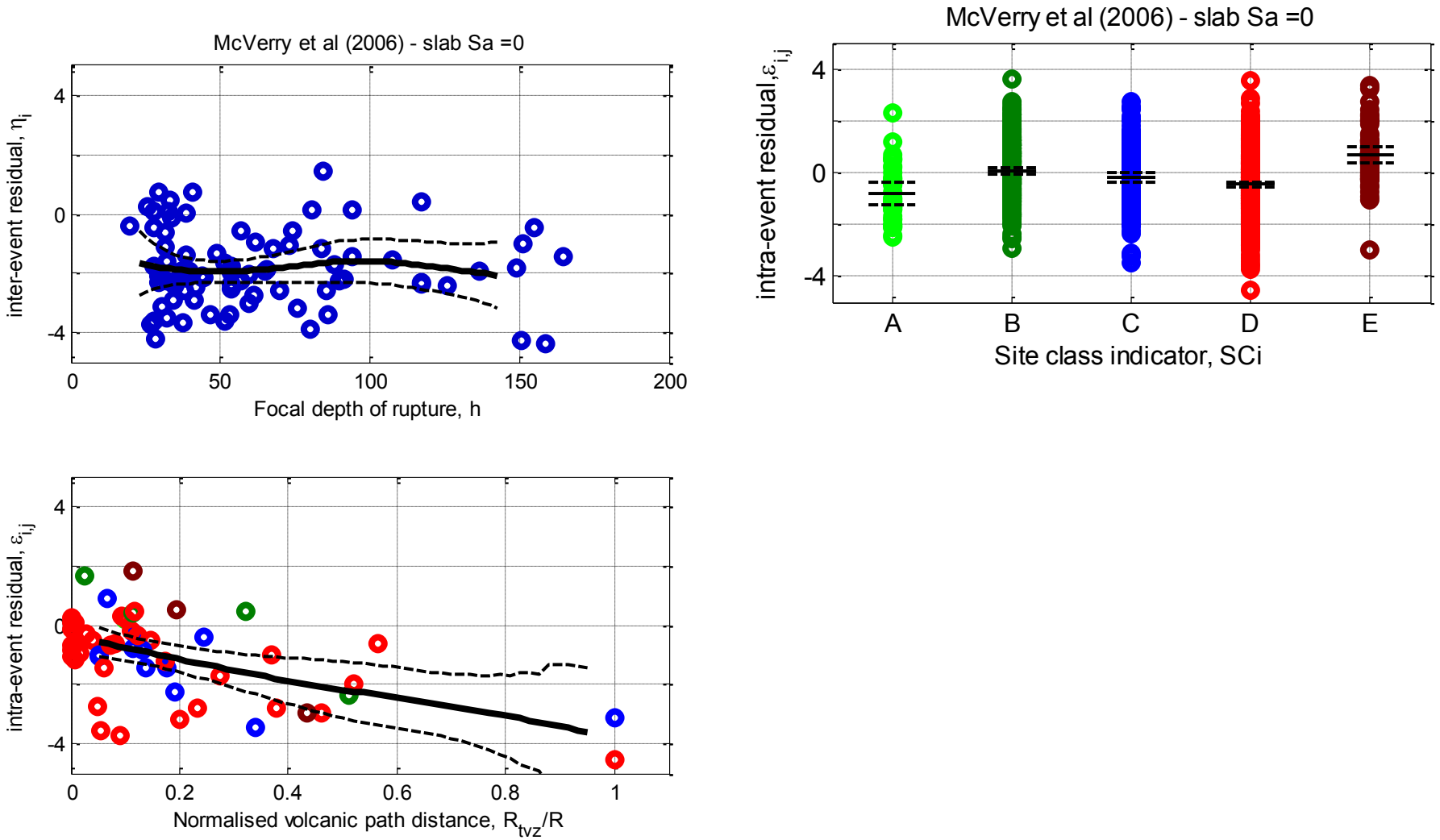

Figure D-31: Residuals for Sa(0.0) using the McVerry et al. (2006) slab model

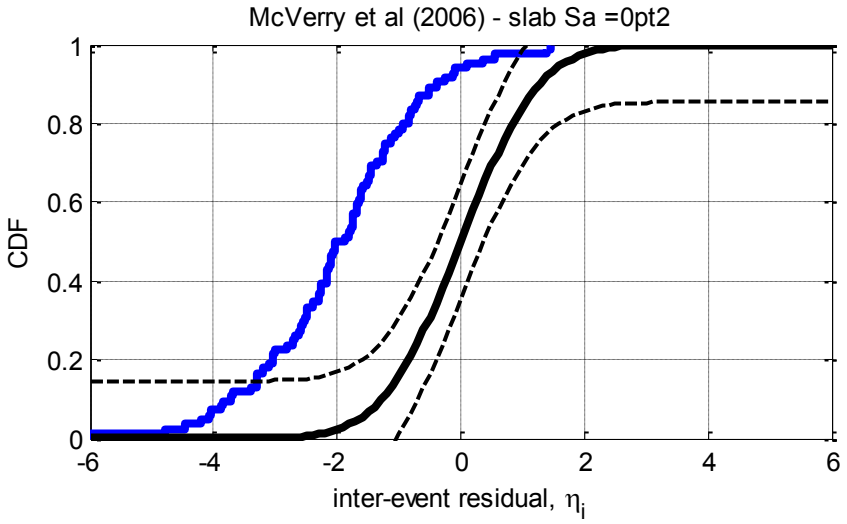
McVerry et al (2006) - slab Sa =0pt2
CDF
inter-event residual, η_i

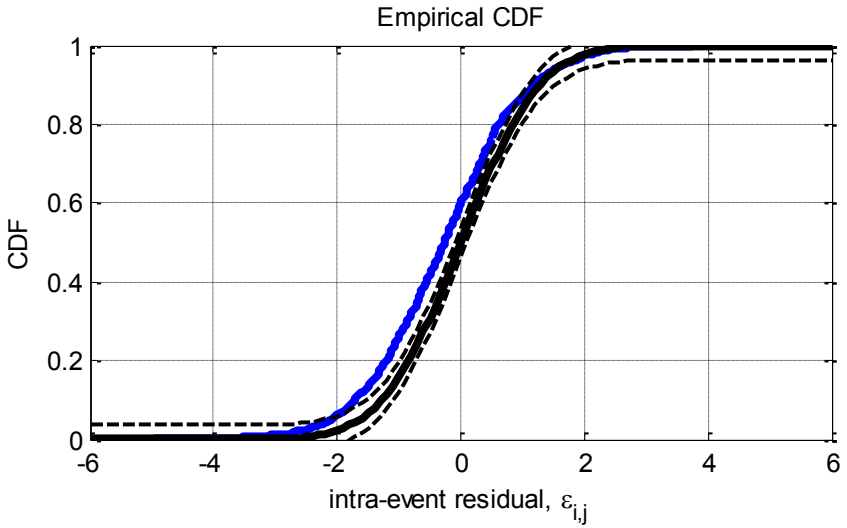
Empirical CDF
CDF
intra-event residual, $\varepsilon_{i,j}$

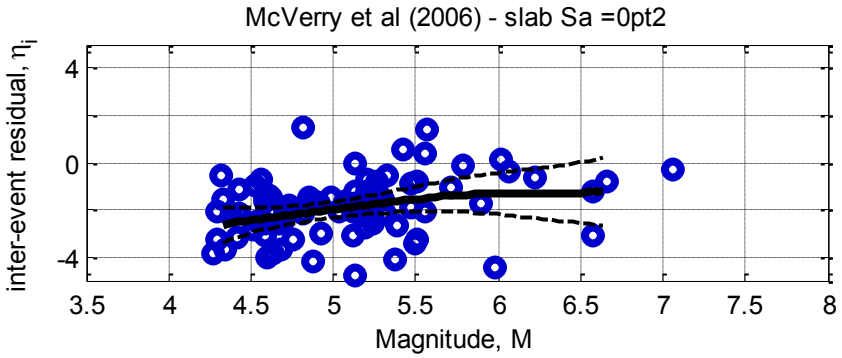
McVerry et al (2006) - slab Sa =0pt2
inter-event residual, η_i
Magnitude, M

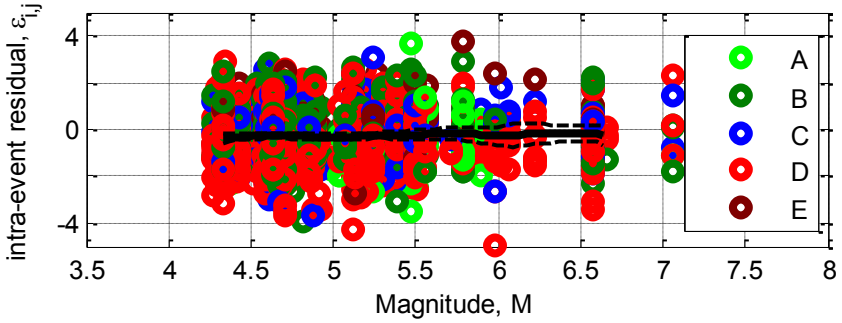
intra-event residual, $\varepsilon_{i,j}$
A
B
C
D
E
Magnitude, M

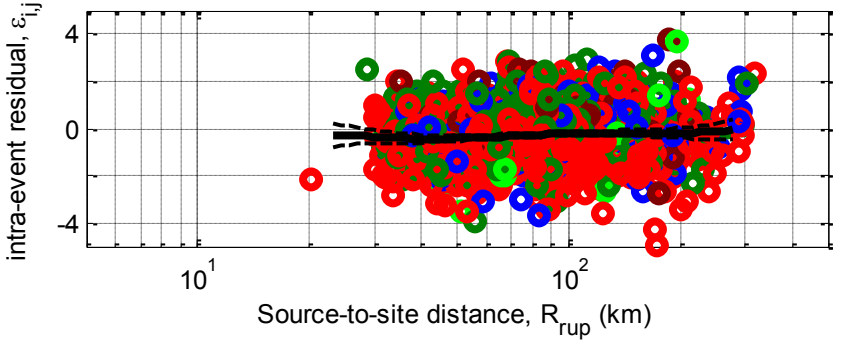
intra-event residual, $\varepsilon_{i,j}$
Source-to-site distance, R_{rup} (km)

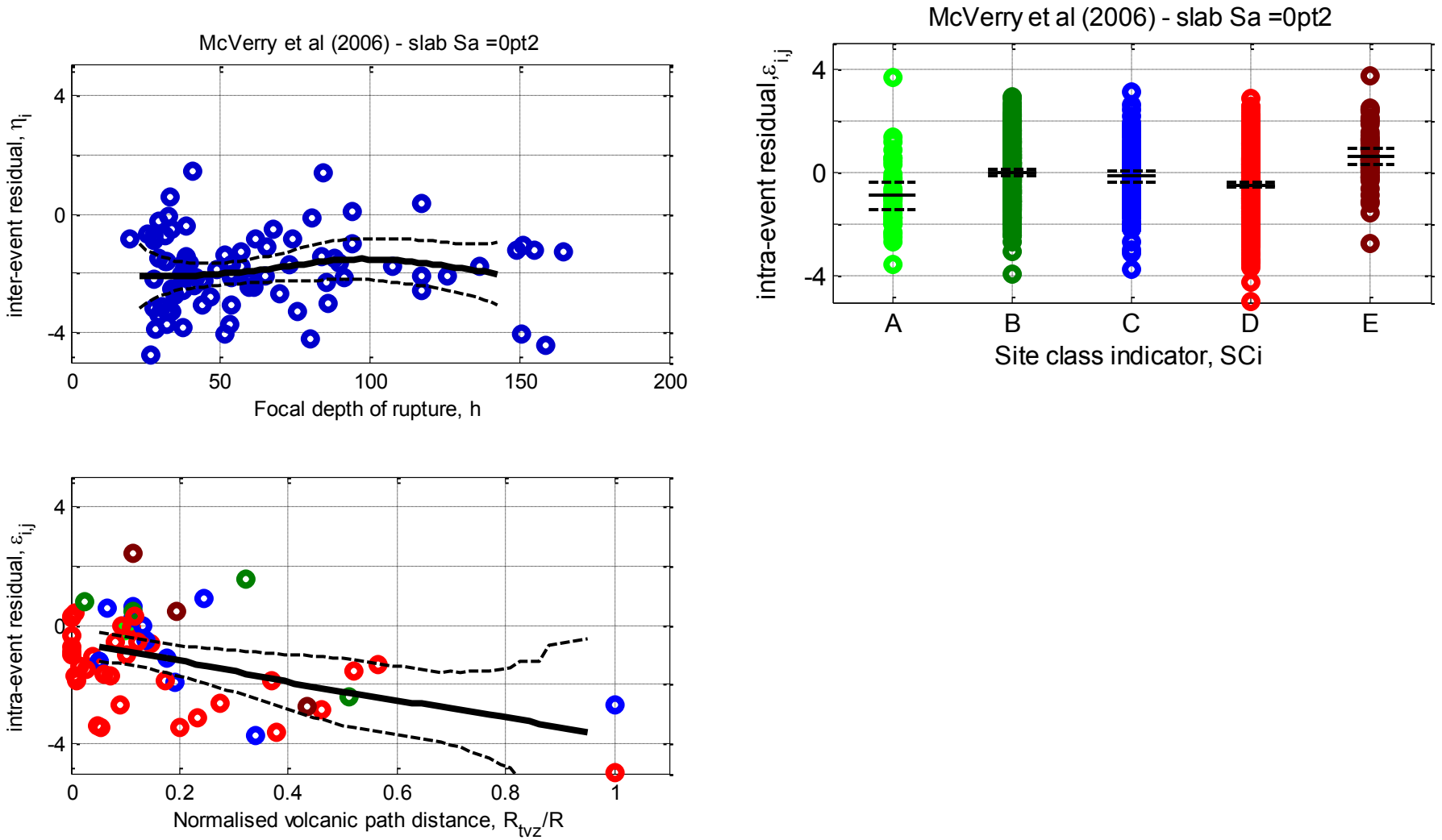

Figure D-32: Residuals for Sa(0.2) using the McVerry et al. (2006) slab model

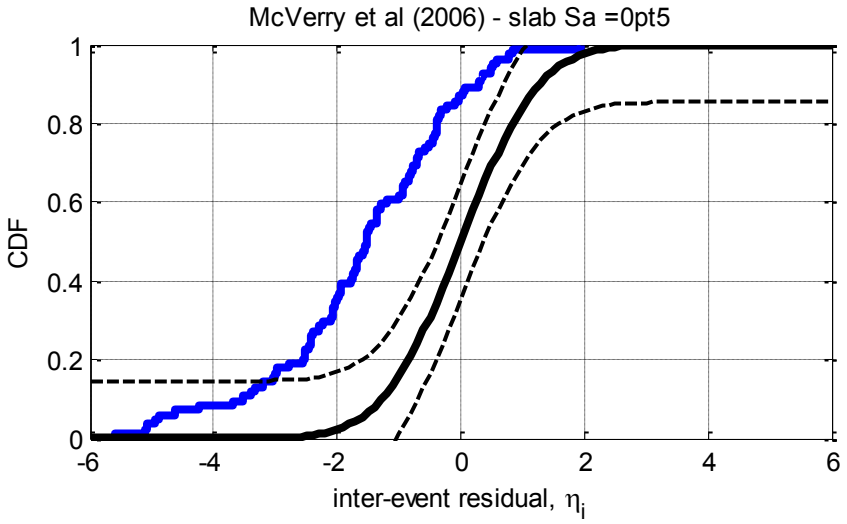
McVerry et al (2006) - slab Sa =0pt5
CDF
inter-event residual, η_i

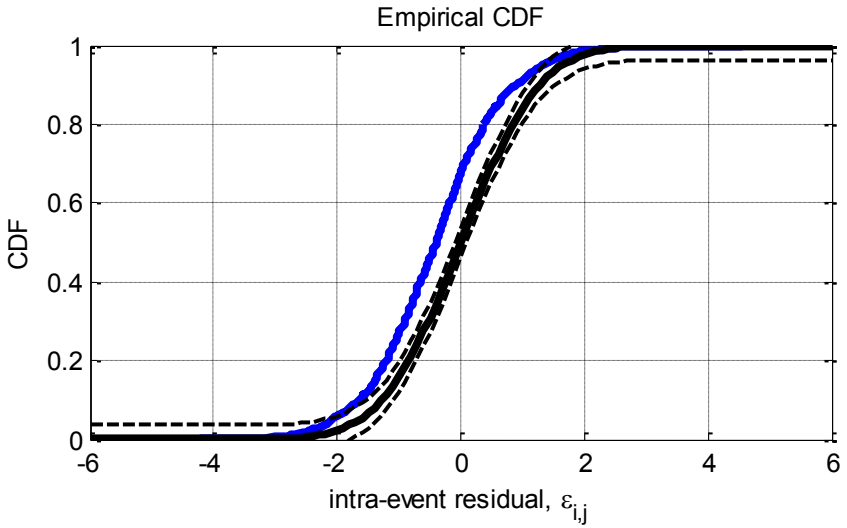
Empirical CDF
CDF
intra-event residual, $\varepsilon_{i,j}$

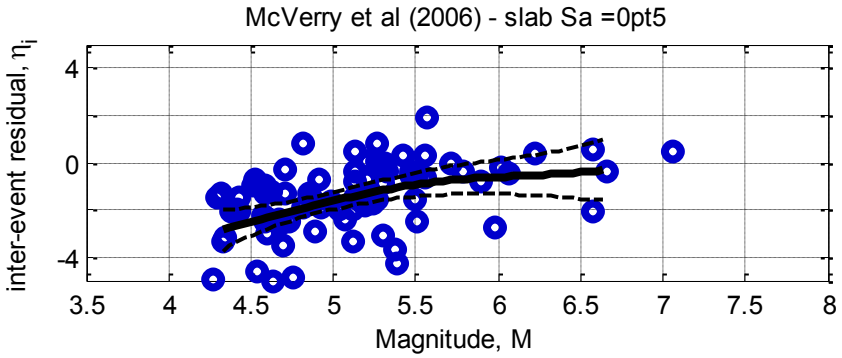
McVerry et al (2006) - slab Sa =0pt5
inter-event residual, η_i
Magnitude, M

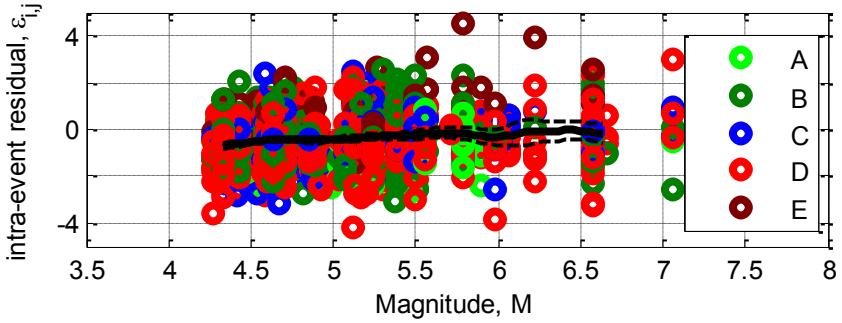
intra-event residual, $\varepsilon_{i,j}$
Magnitude, M
A
B
C
D
E

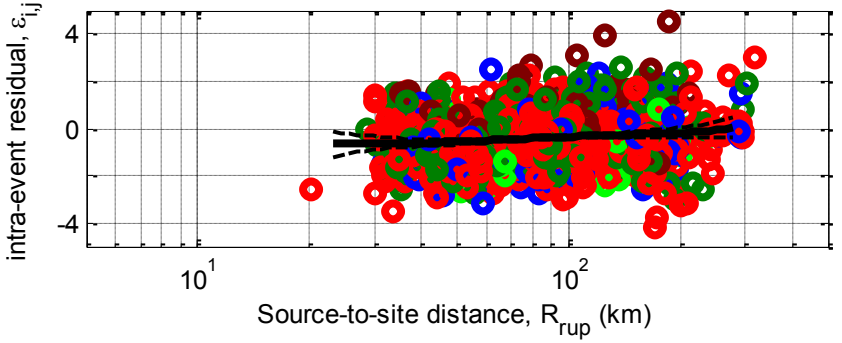
intra-event residual, $\varepsilon_{i,j}$
Source-to-site distance, R_{rup} (km)

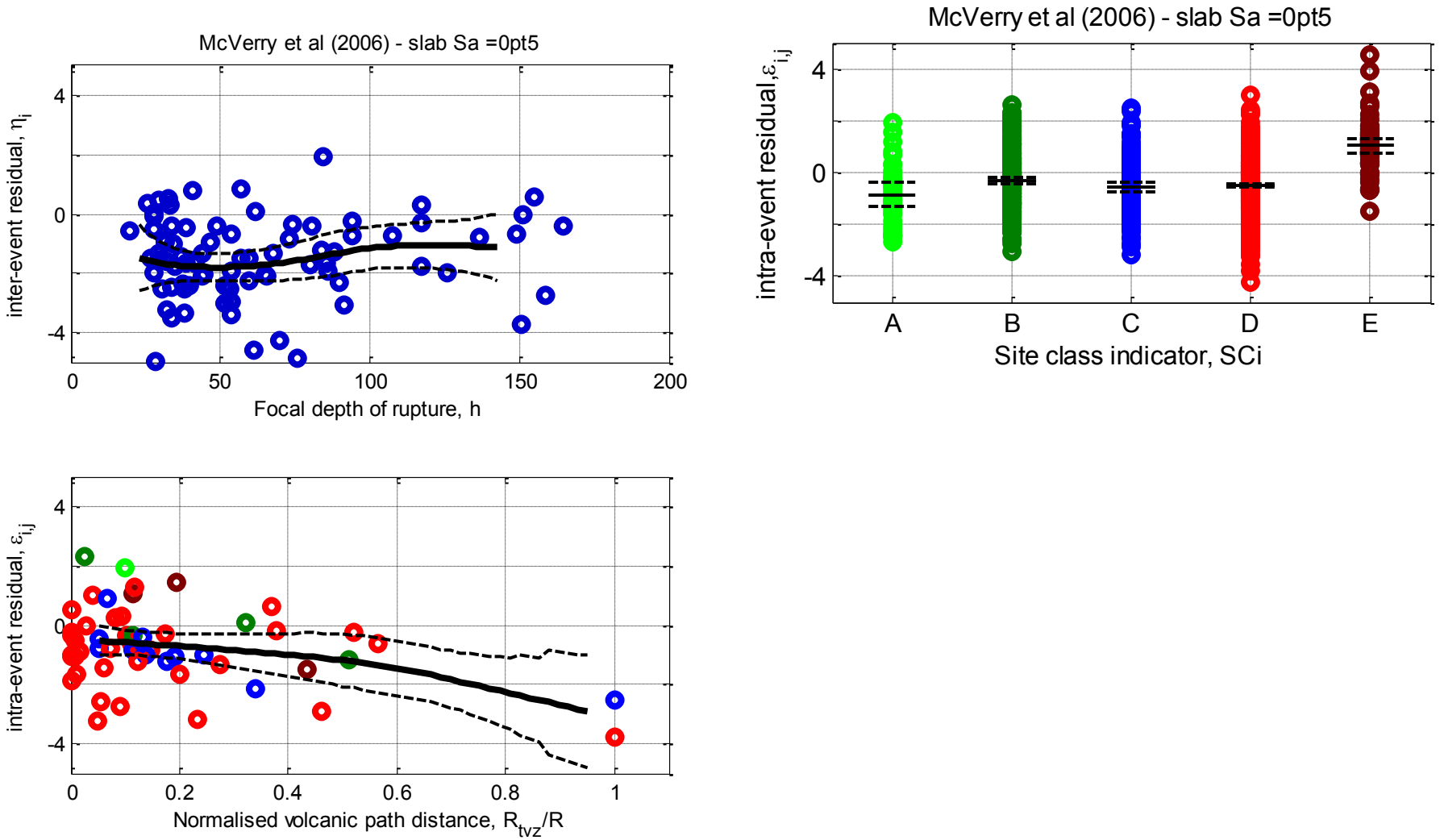

Figure D-33: Residuals for Sa(0.5) using the McVerry et al. (2006) slab model

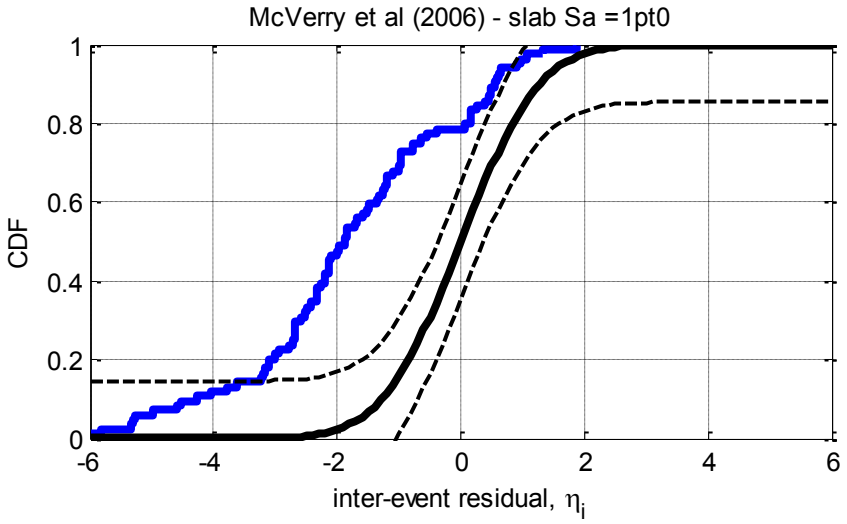
McVerry et al (2006) - slab Sa =1pt0
CDF
inter-event residual, η_i

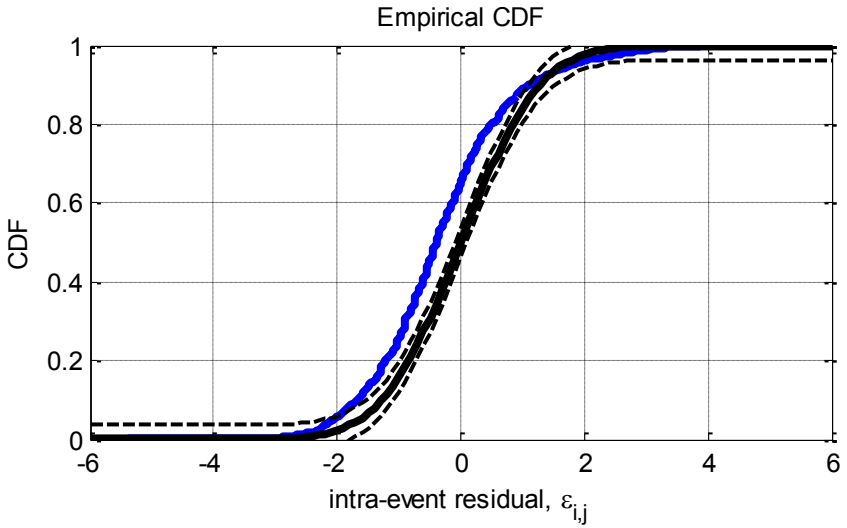
Empirical CDF
CDF
intra-event residual, $\varepsilon_{i,j}$

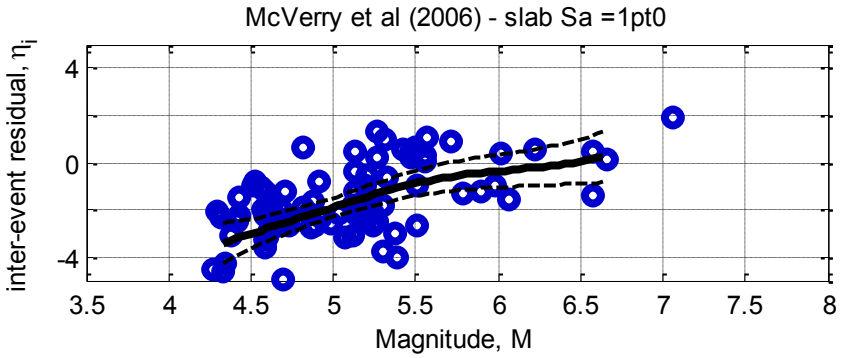
McVerry et al (2006) - slab Sa =1pt0
inter-event residual, η_i
Magnitude, M

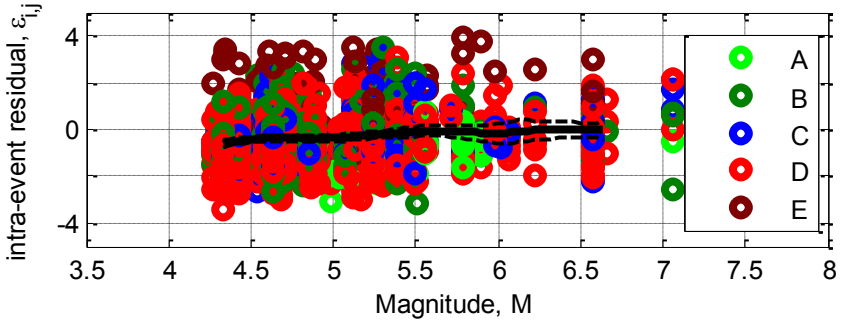
intra-event residual, $\varepsilon_{i,j}$
Magnitude, M
A
B
C
D
E

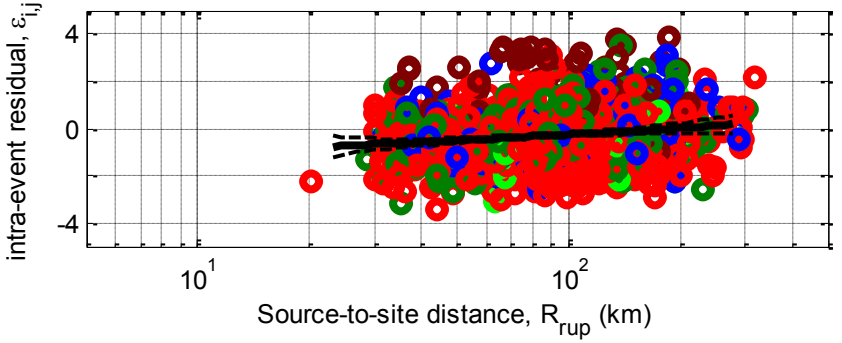
intra-event residual, $\varepsilon_{i,j}$
Source-to-site distance, R_{rup} (km)

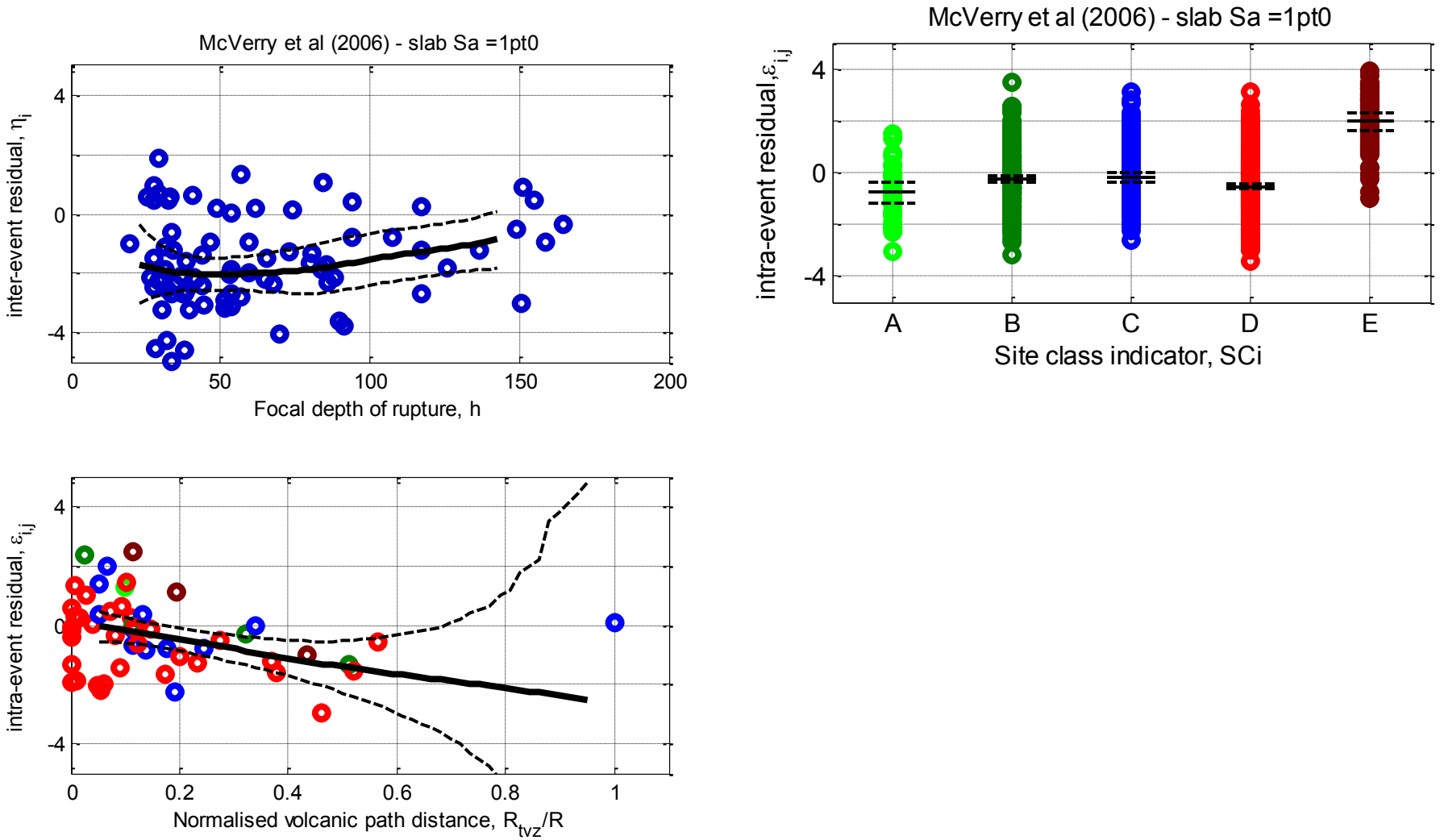

Figure D-34: Residuals for Sa(1.0) using the McVerry et al. (2006) slab model

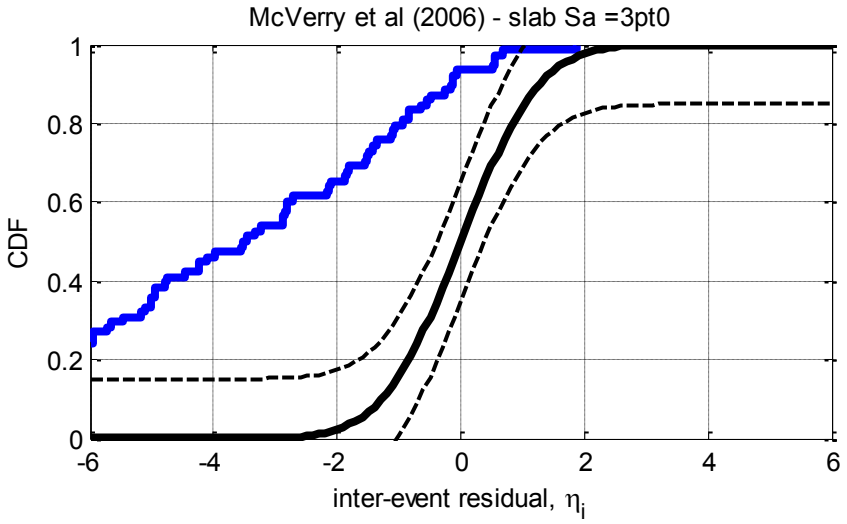
McVerry et al (2006) - slab Sa =3pt0
CDF
inter-event residual, η_i

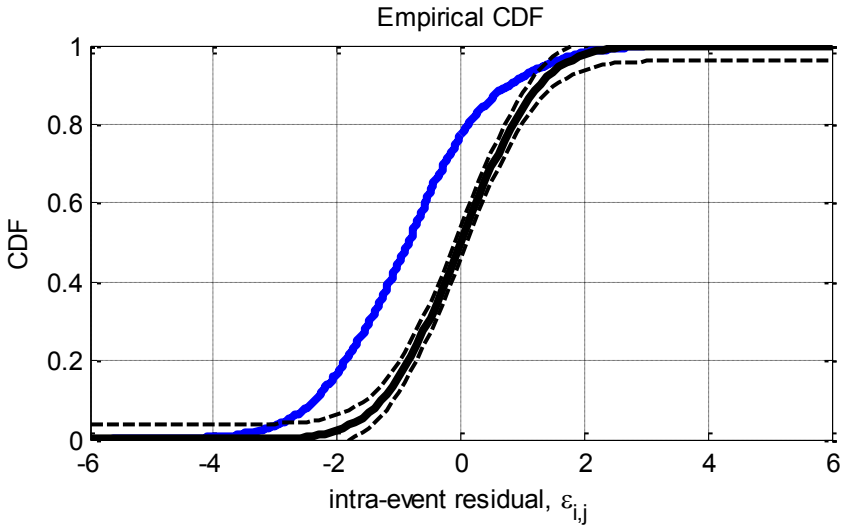
Empirical CDF
CDF
intra-event residual, $\varepsilon_{i,j}$

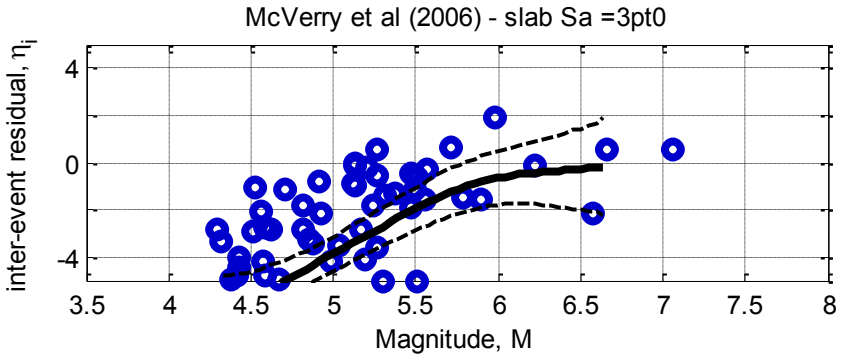
McVerry et al (2006) - slab Sa =3pt0
inter-event residual, η_i
Magnitude, M

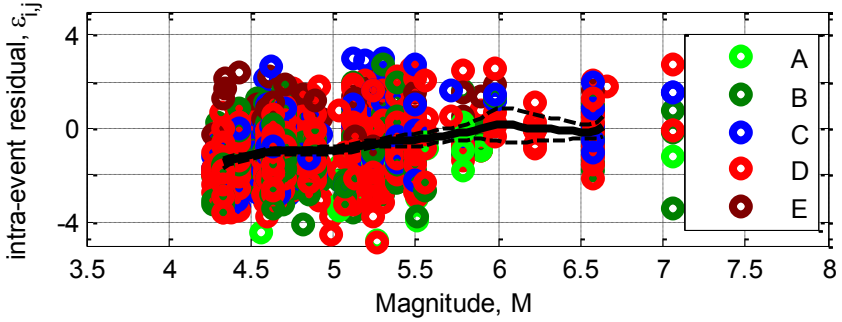
intra-event residual, $\varepsilon_{i,j}$
A
B
C
D
E
Magnitude, M

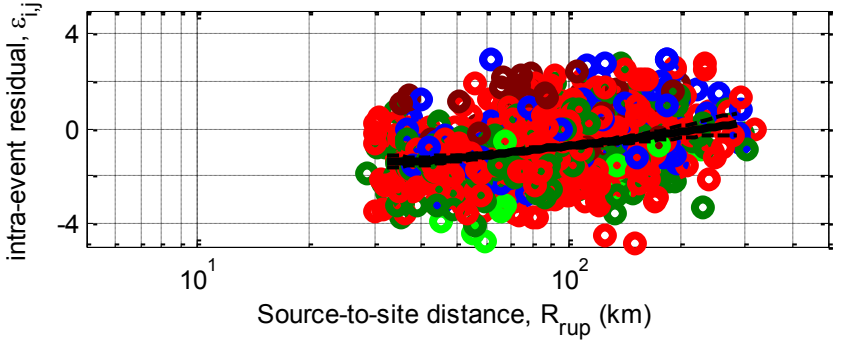
intra-event residual, $\varepsilon_{i,j}$
Source-to-site distance, R_{rup} (km)

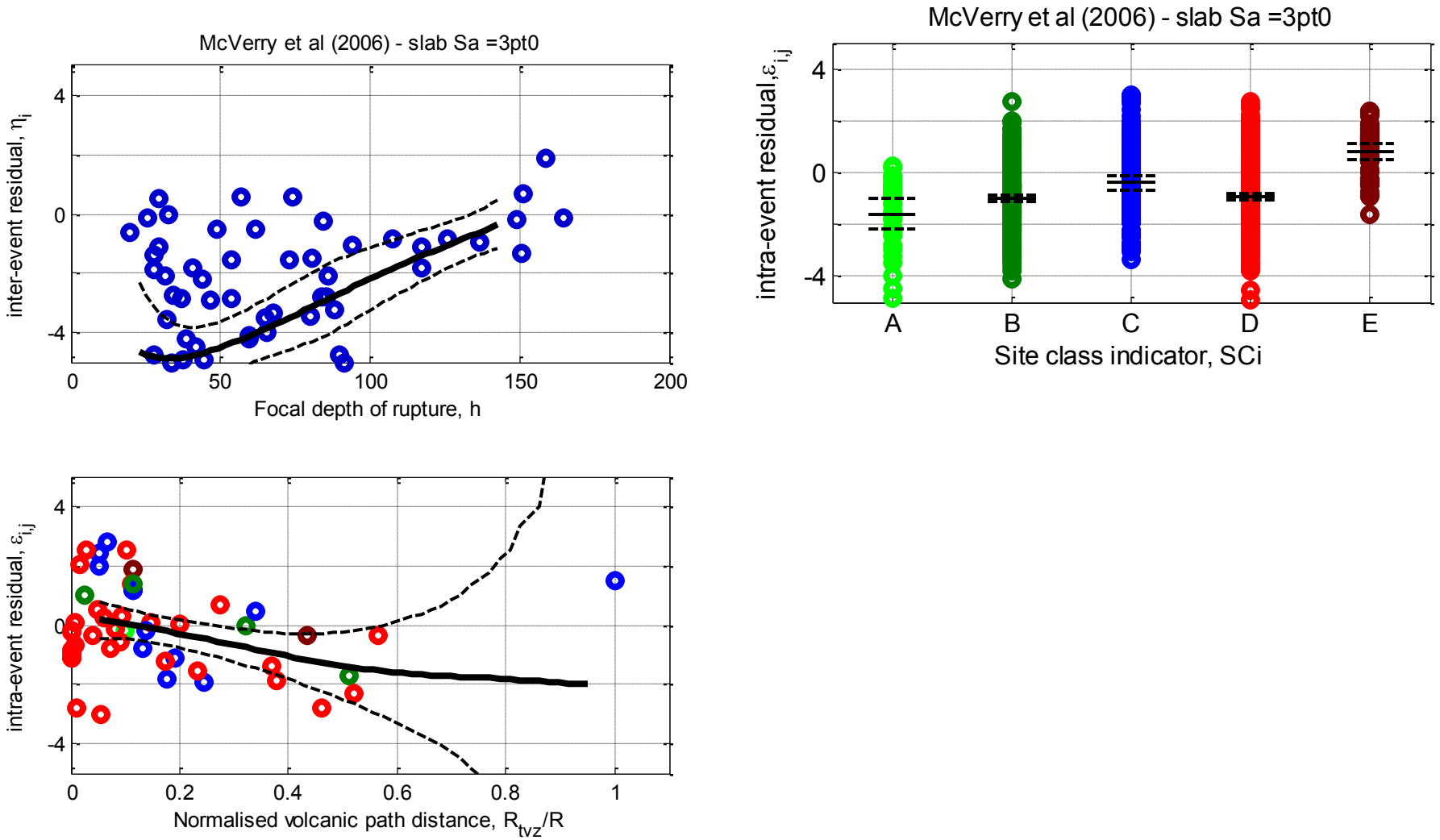

Figure D-35: Residuals for Sa(3.0) using the McVerry et al. (2006) slab model

D.8. Zhao et al. (2006) Slab model

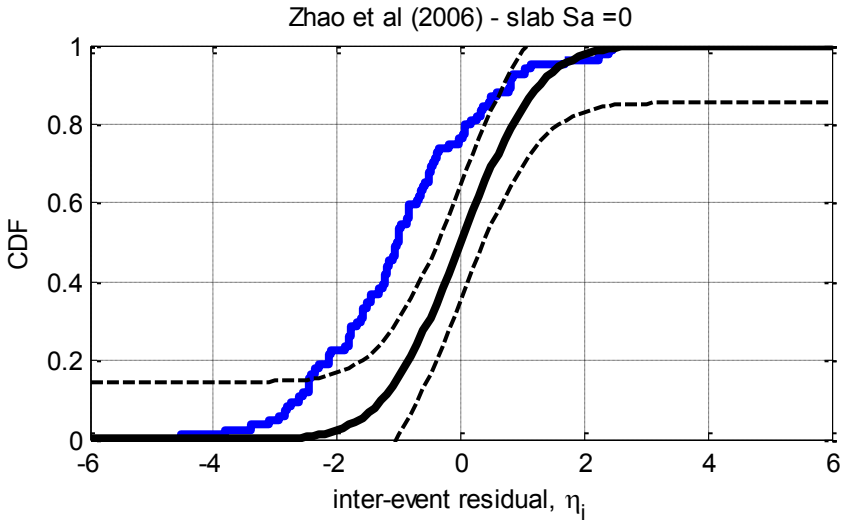

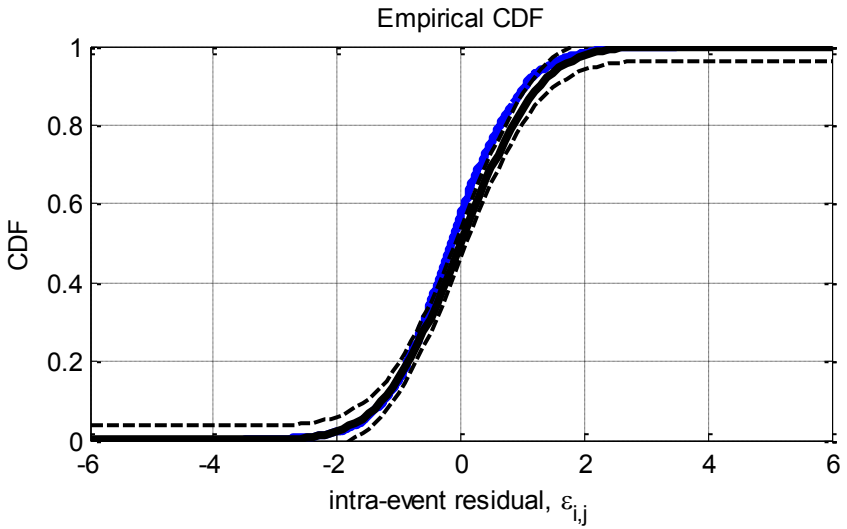

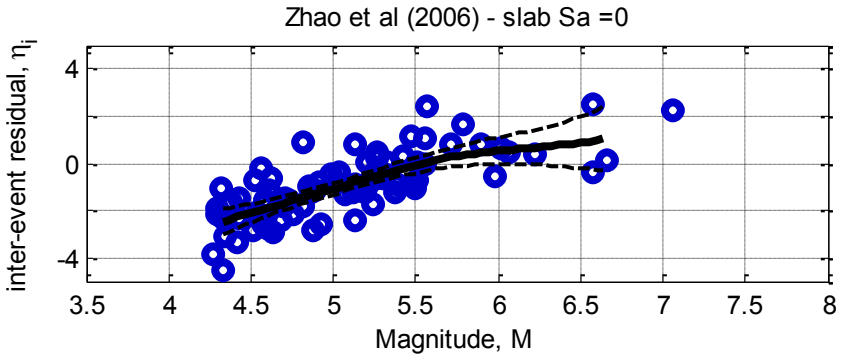

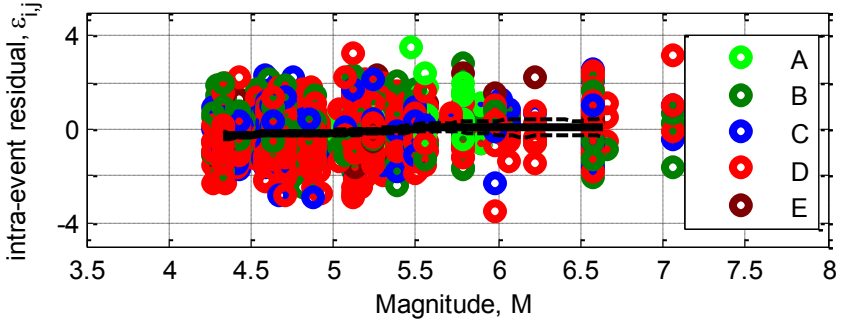

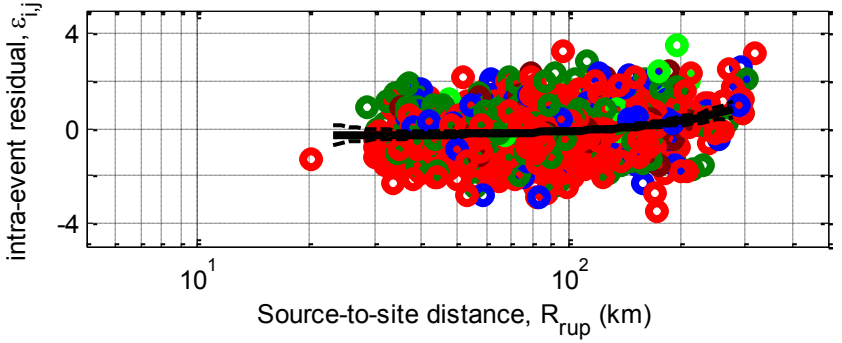

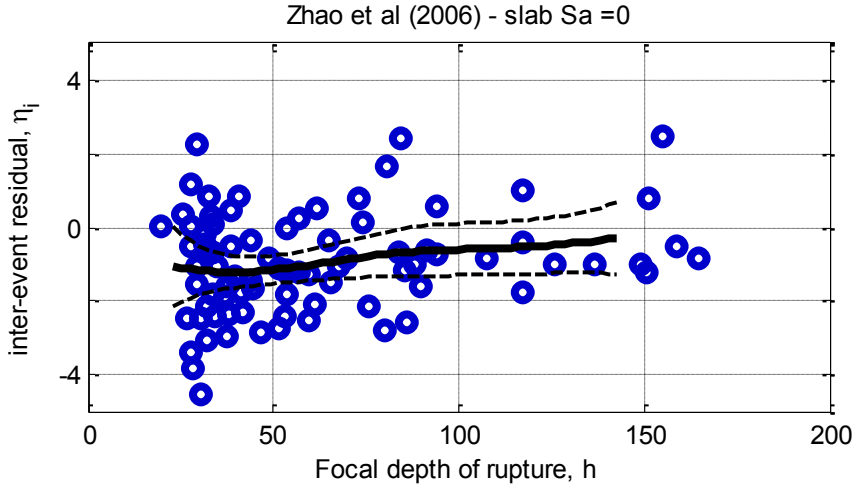

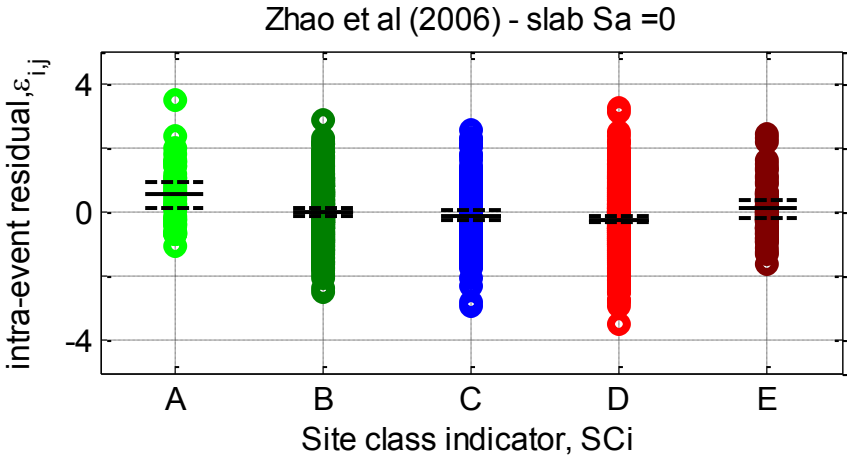

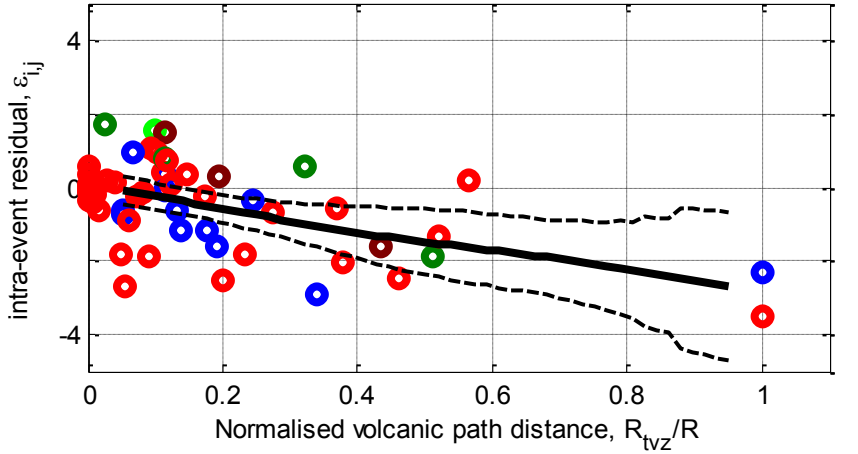

Figure D-36: Residuals for Sa(0.0) using the Zhao et al. (2006) slab model

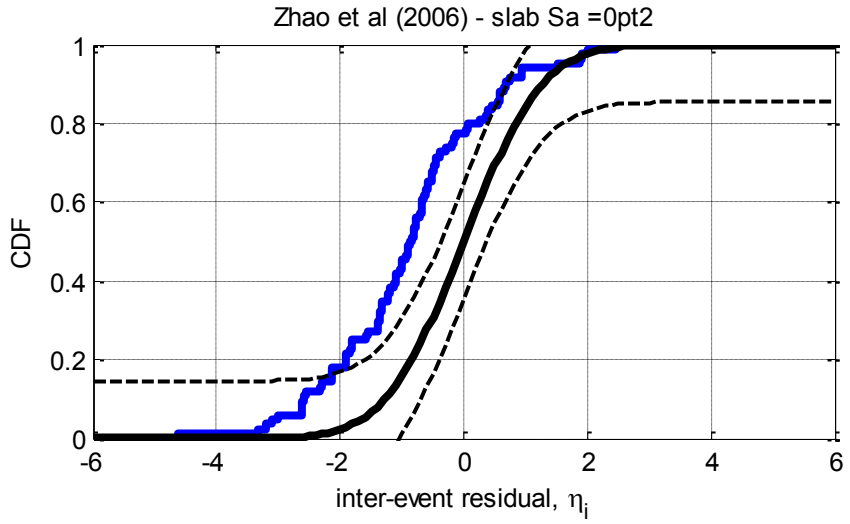
Zhao et al (2006) - slab Sa =0pt2
CDF
inter-event residual, η_i

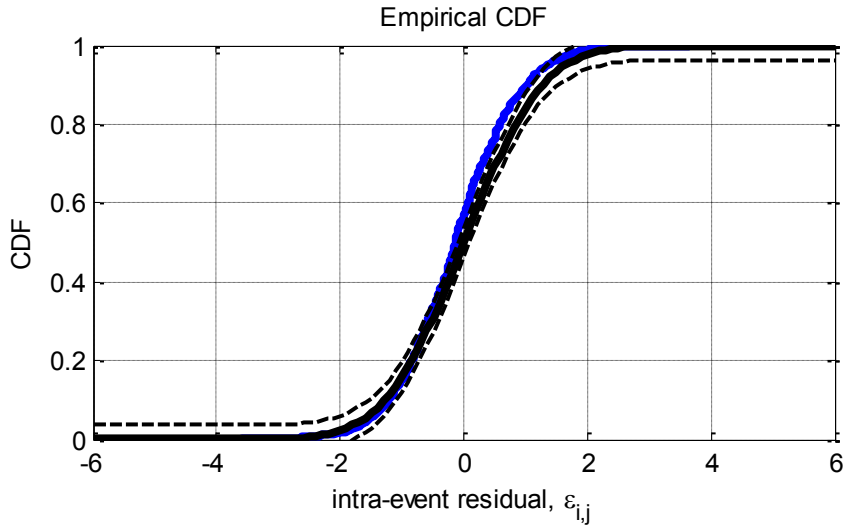
Empirical CDF
CDF
intra-event residual, $\varepsilon_{i,j}$

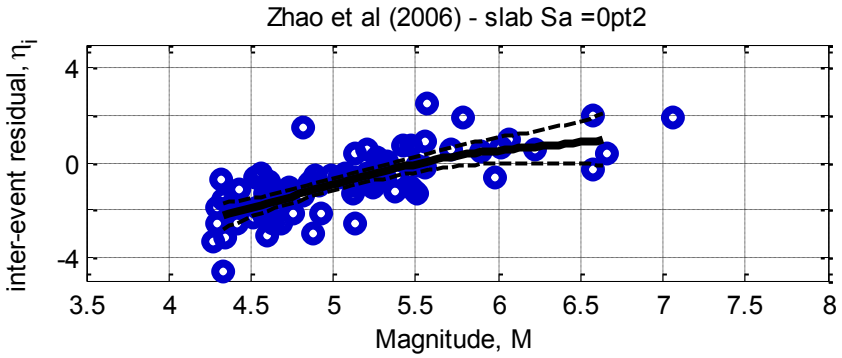
Zhao et al (2006) - slab Sa =0pt2
inter-event residual, η_i
Magnitude, M

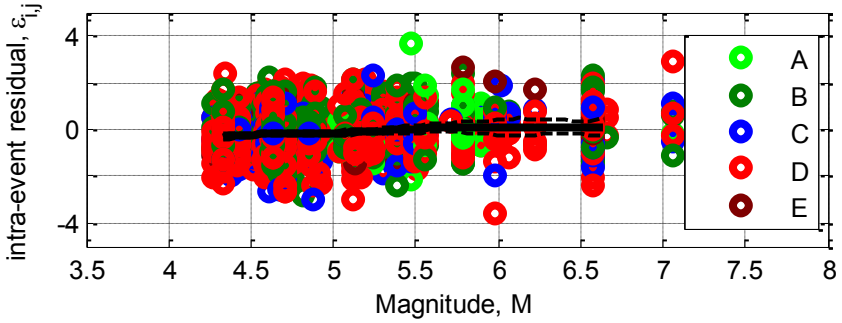
intra-event residual, $\varepsilon_{i,j}$
Magnitude, M
A
B
C
D
E

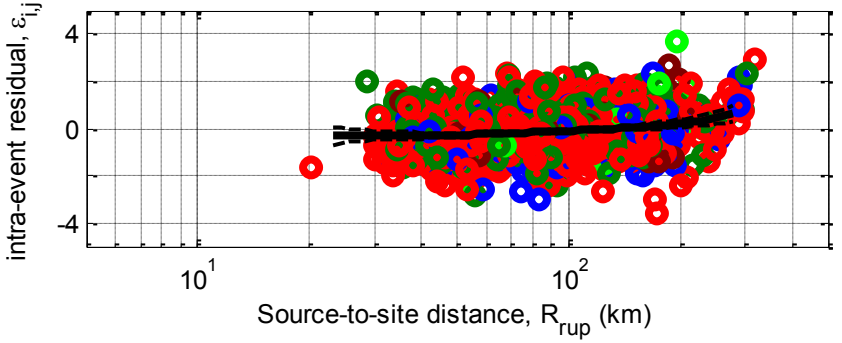
intra-event residual, $\varepsilon_{i,j}$
Source-to-site distance, R_{rup} (km)

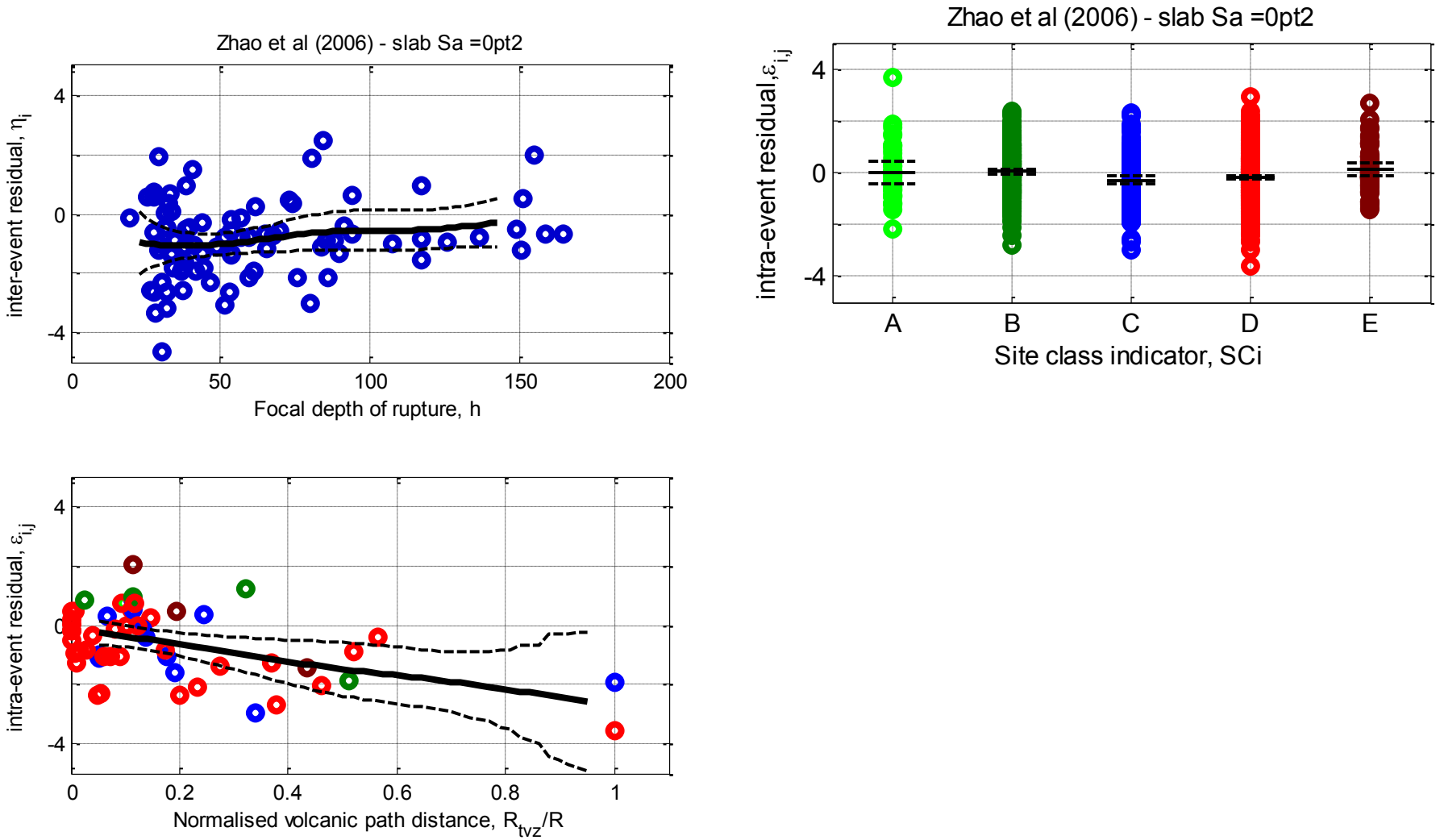

Figure D-37: Residuals for Sa(0.2) using the Zhao et al. (2006) slab model

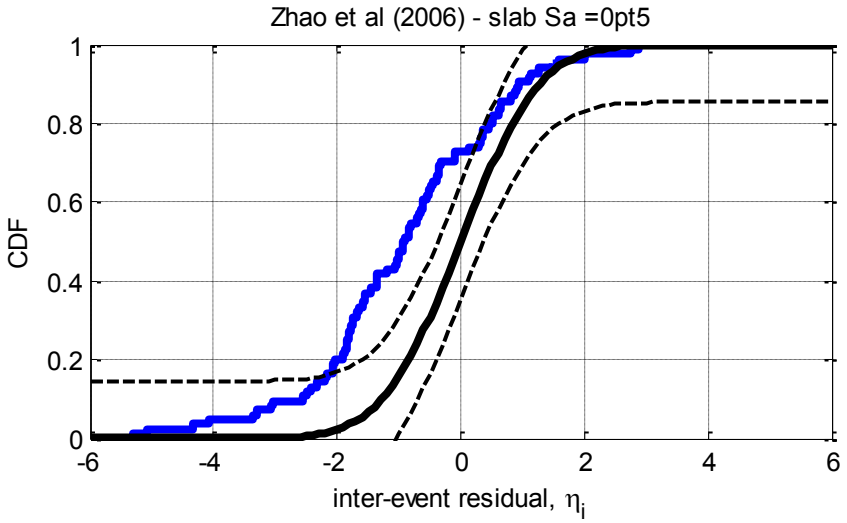
Zhao et al (2006) - slab Sa =0pt5
CDF
inter-event residual, η_i

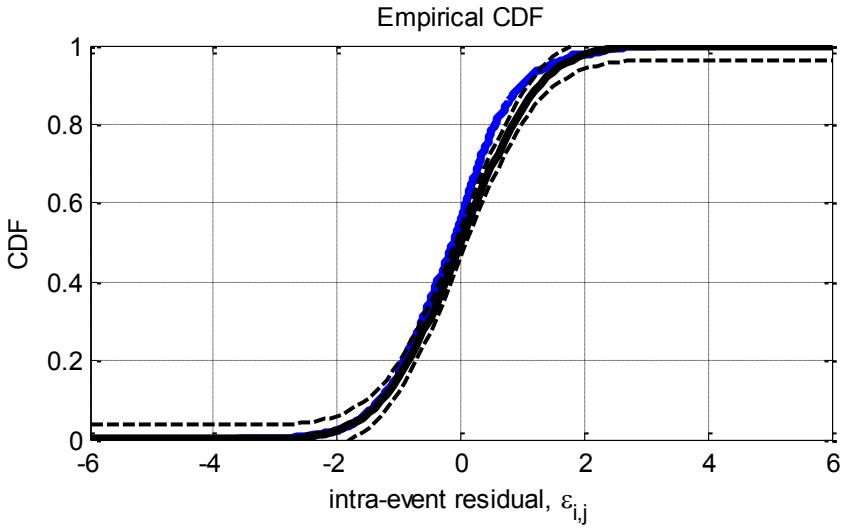
Empirical CDF
CDF
intra-event residual, $\varepsilon_{i,j}$

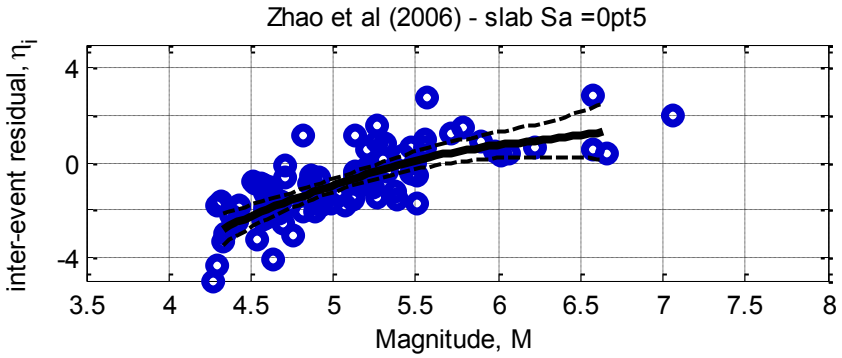
Zhao et al (2006) - slab Sa =0pt5
inter-event residual, η_i
Magnitude, M

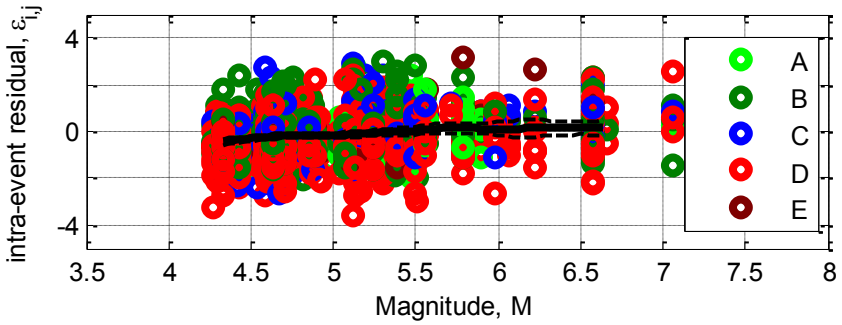
intra-event residual, $\varepsilon_{i,j}$
Magnitude, M
A
B
C
D
E

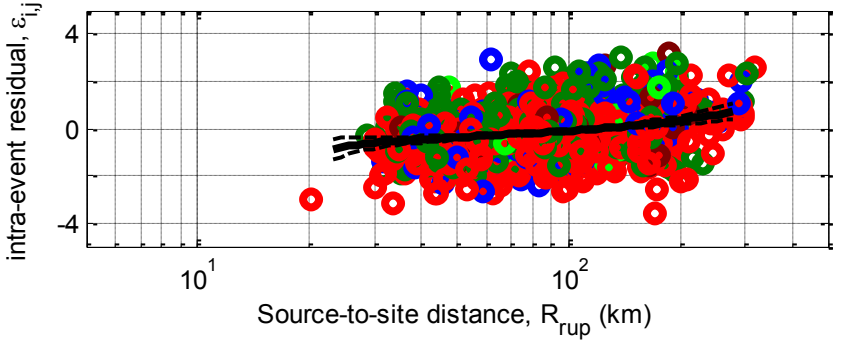
intra-event residual, $\varepsilon_{i,j}$
Source-to-site distance, R_{rup} (km)

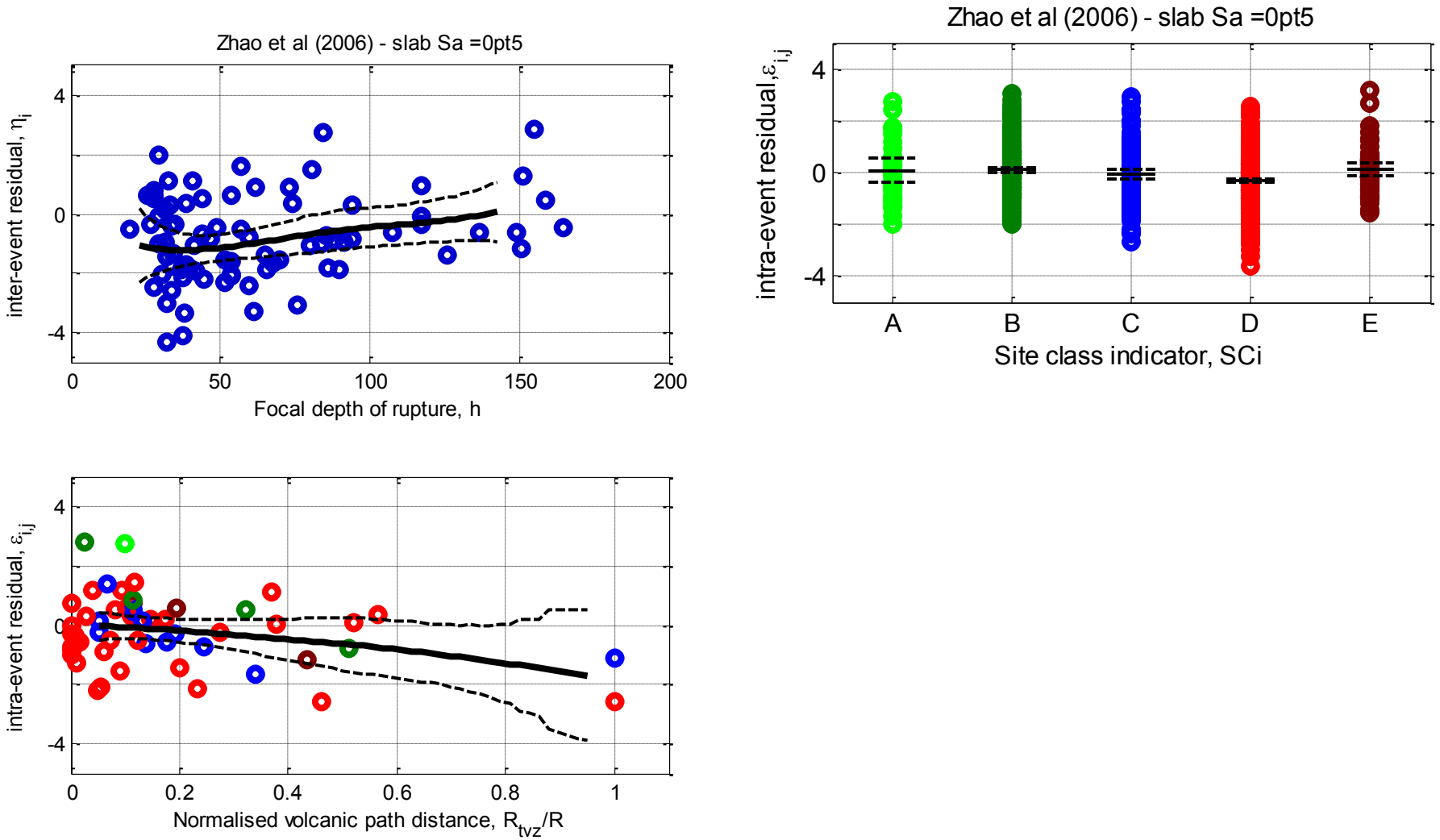

Figure D-38: Residuals for Sa(0.5) using the Zhao et al. (2006) slab model

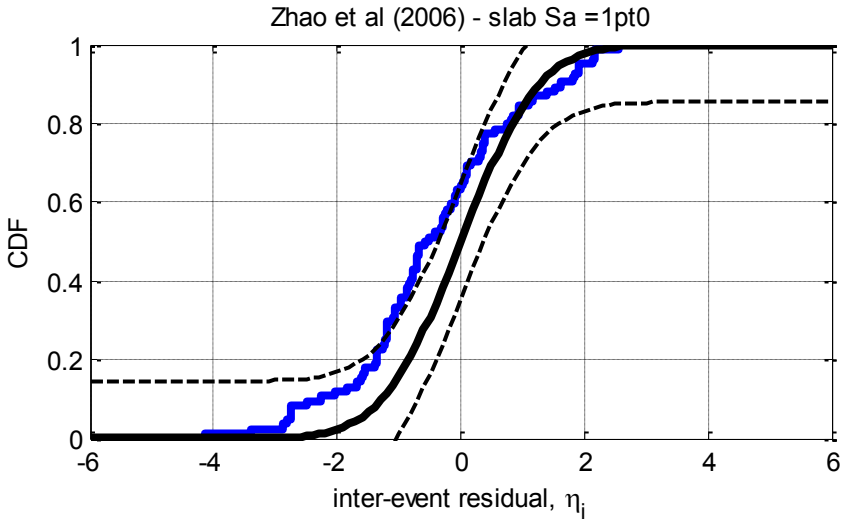
Zhao et al (2006) - slab Sa =1pt0
CDF
inter-event residual, η_i

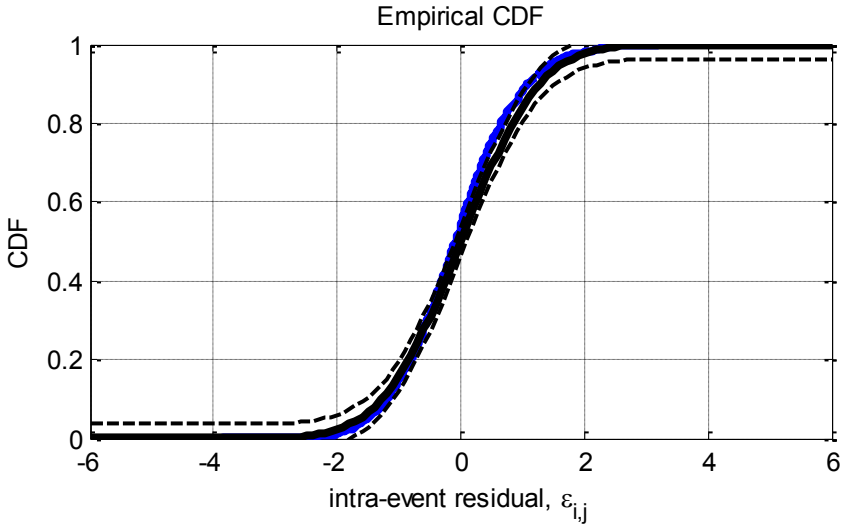
Empirical CDF
CDF
intra-event residual, $\varepsilon_{i,j}$

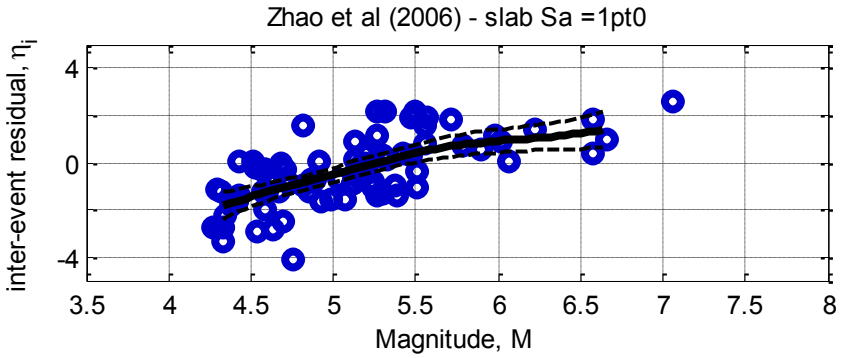
Zhao et al (2006) - slab Sa =1pt0
inter-event residual, η_i
Magnitude, M

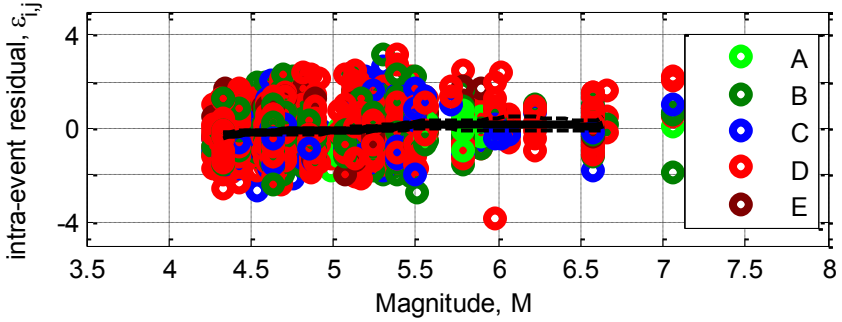
intra-event residual, $\varepsilon_{i,j}$
Magnitude, M
A
B
C
D
E

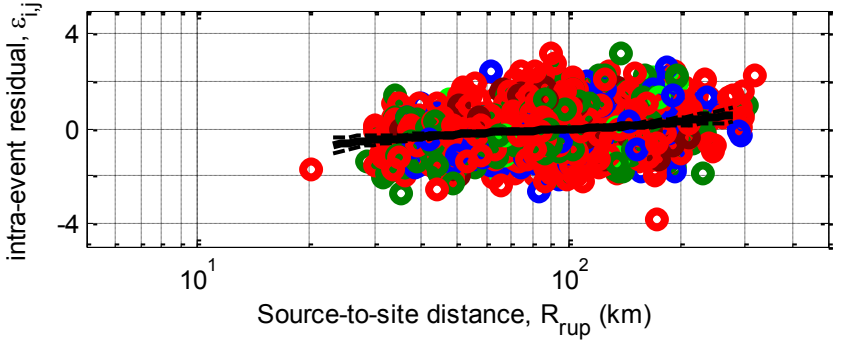
intra-event residual, $\varepsilon_{i,j}$
Source-to-site distance, R_{rup} (km)

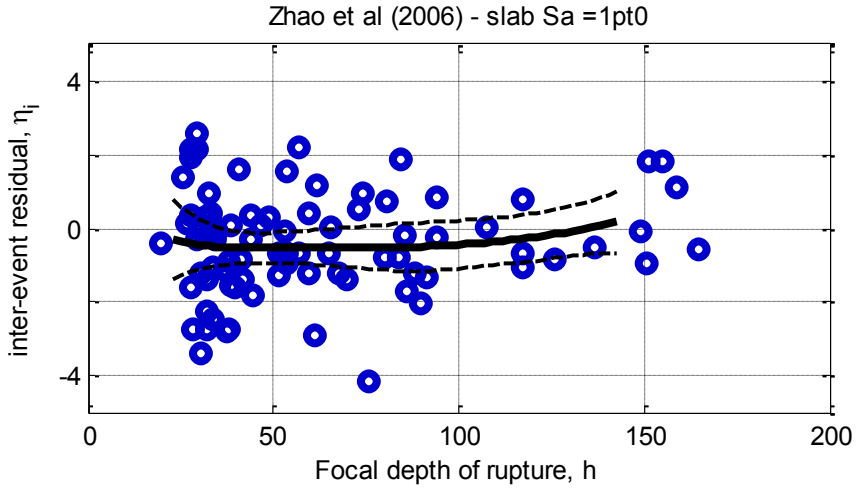

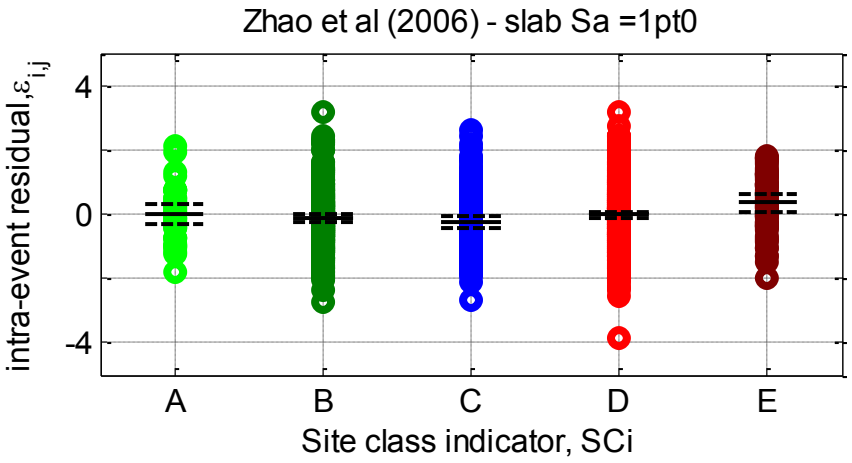

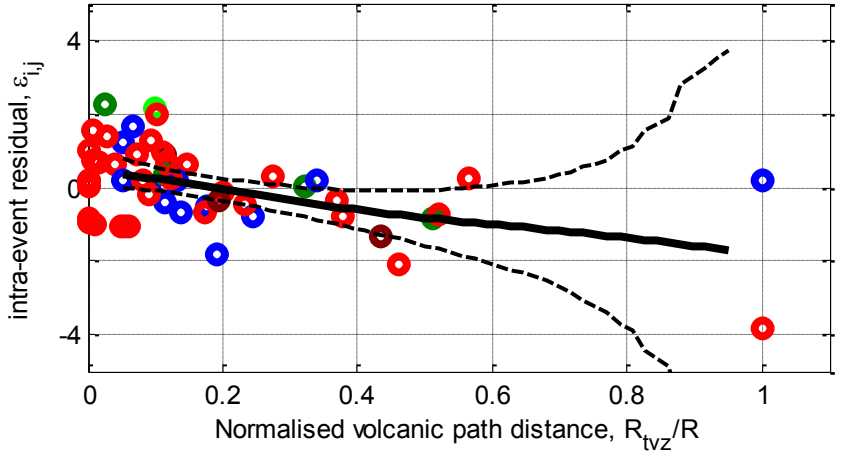

Figure D-39: Residuals for Sa(1.0) using the Zhao et al. (2006) slab model

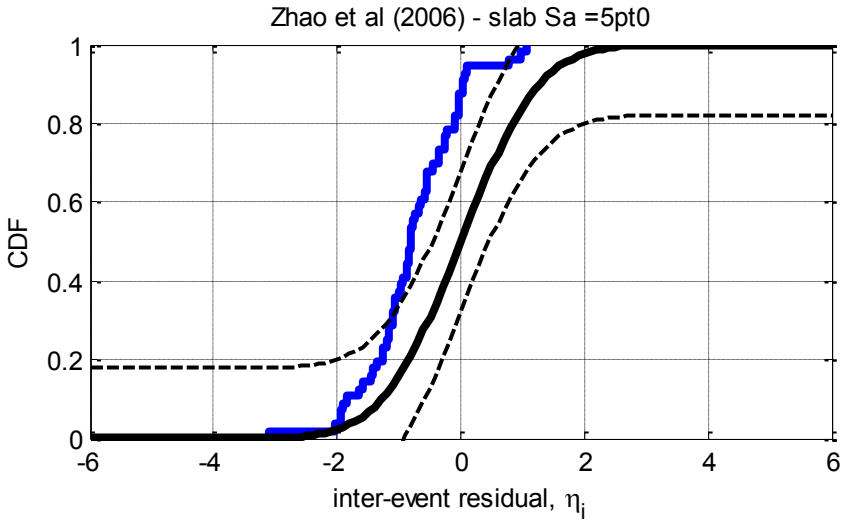
Zhao et al (2006) - slab Sa =5pt0
CDF
inter-event residual, η_i

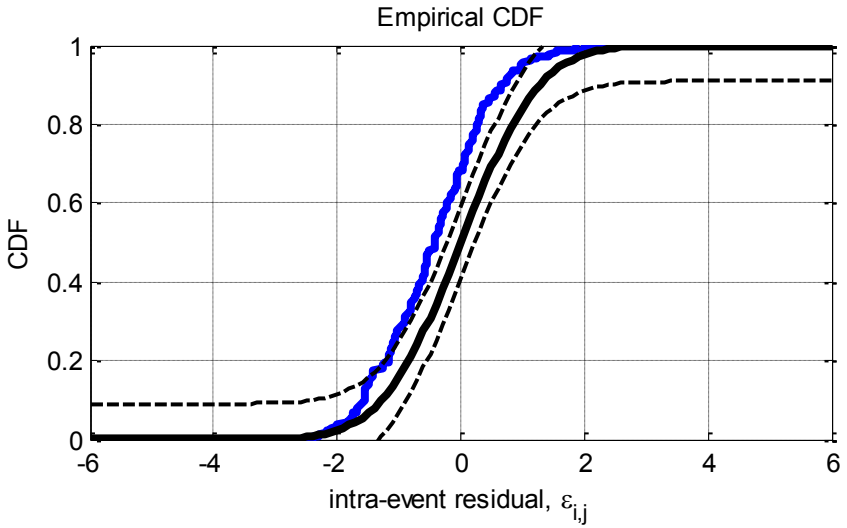
Empirical CDF
CDF
intra-event residual, $\varepsilon_{i,j}$

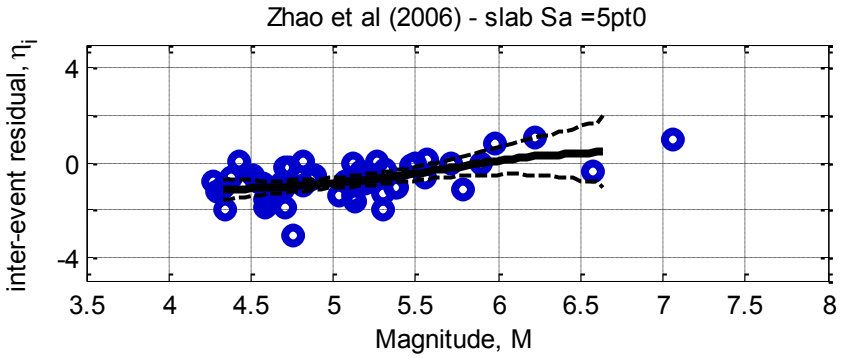
Zhao et al (2006) - slab Sa =5pt0
inter-event residual, η_i
Magnitude, M

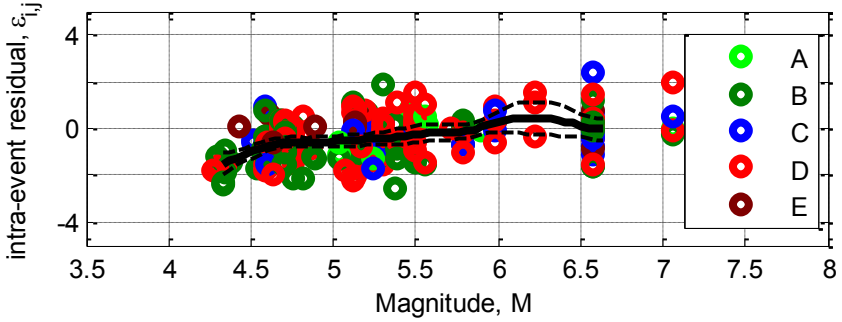
intra-event residual, $\varepsilon_{i,j}$
Magnitude, M
A
B
C
D
E

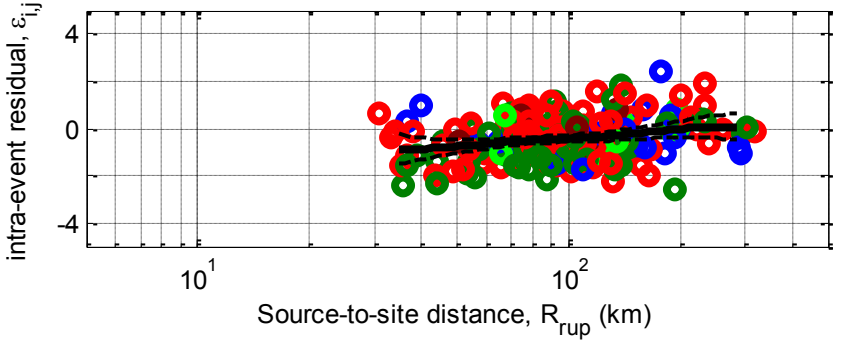
intra-event residual, $\varepsilon_{i,j}$
Source-to-site distance, R_{rup} (km)

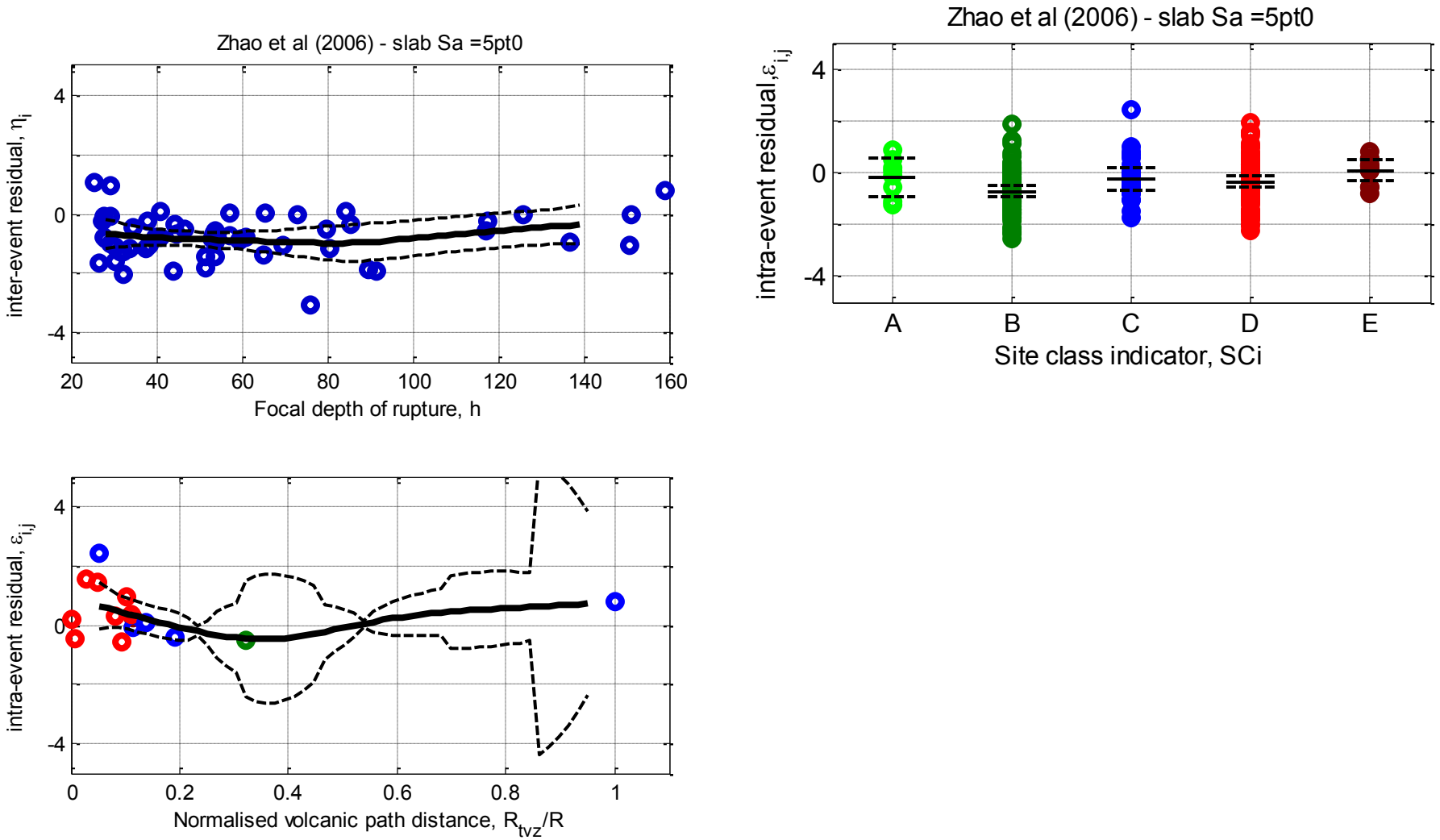

Figure D-40: Residuals for Sa(5.0) using the Zhao et al. (2006) slab model

D.9. Atkinson and Boore (2003) Slab model

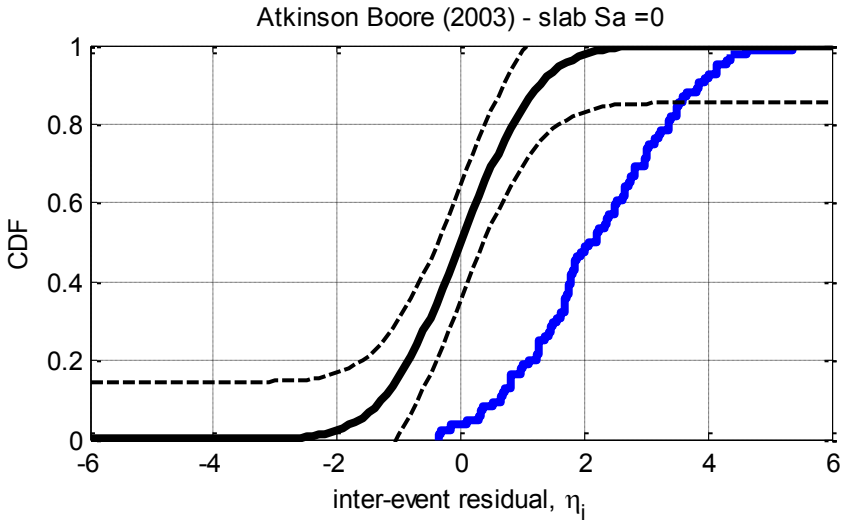

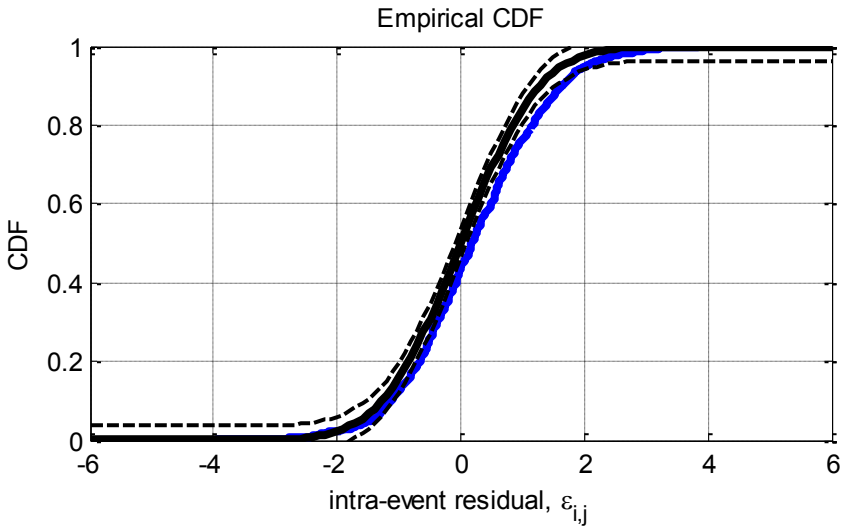

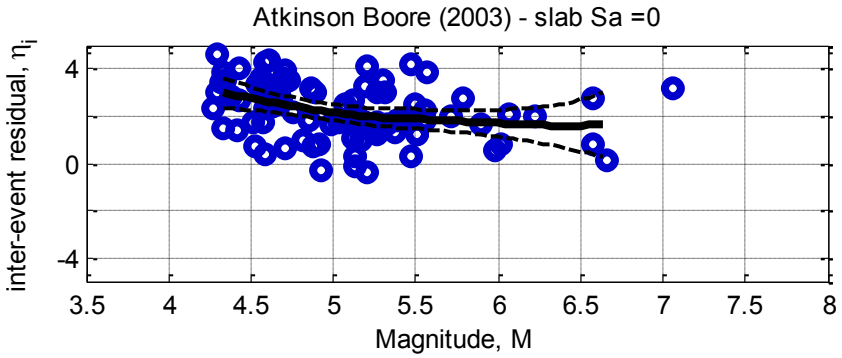

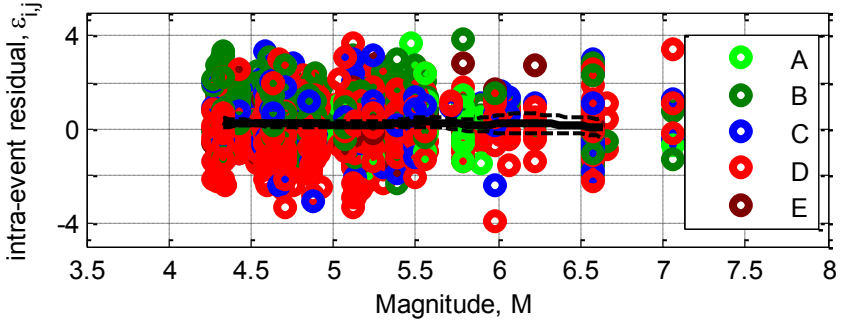

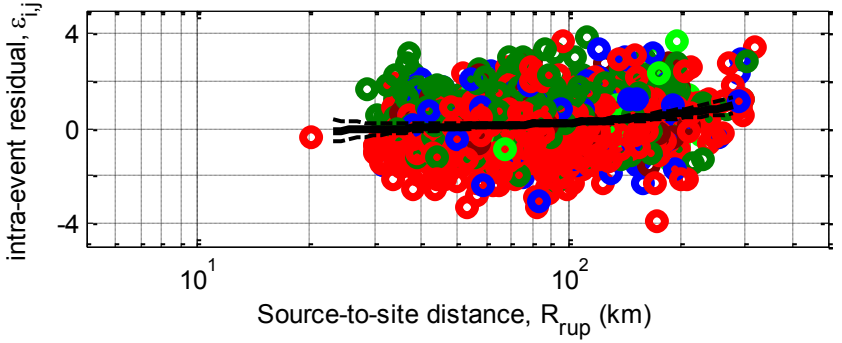

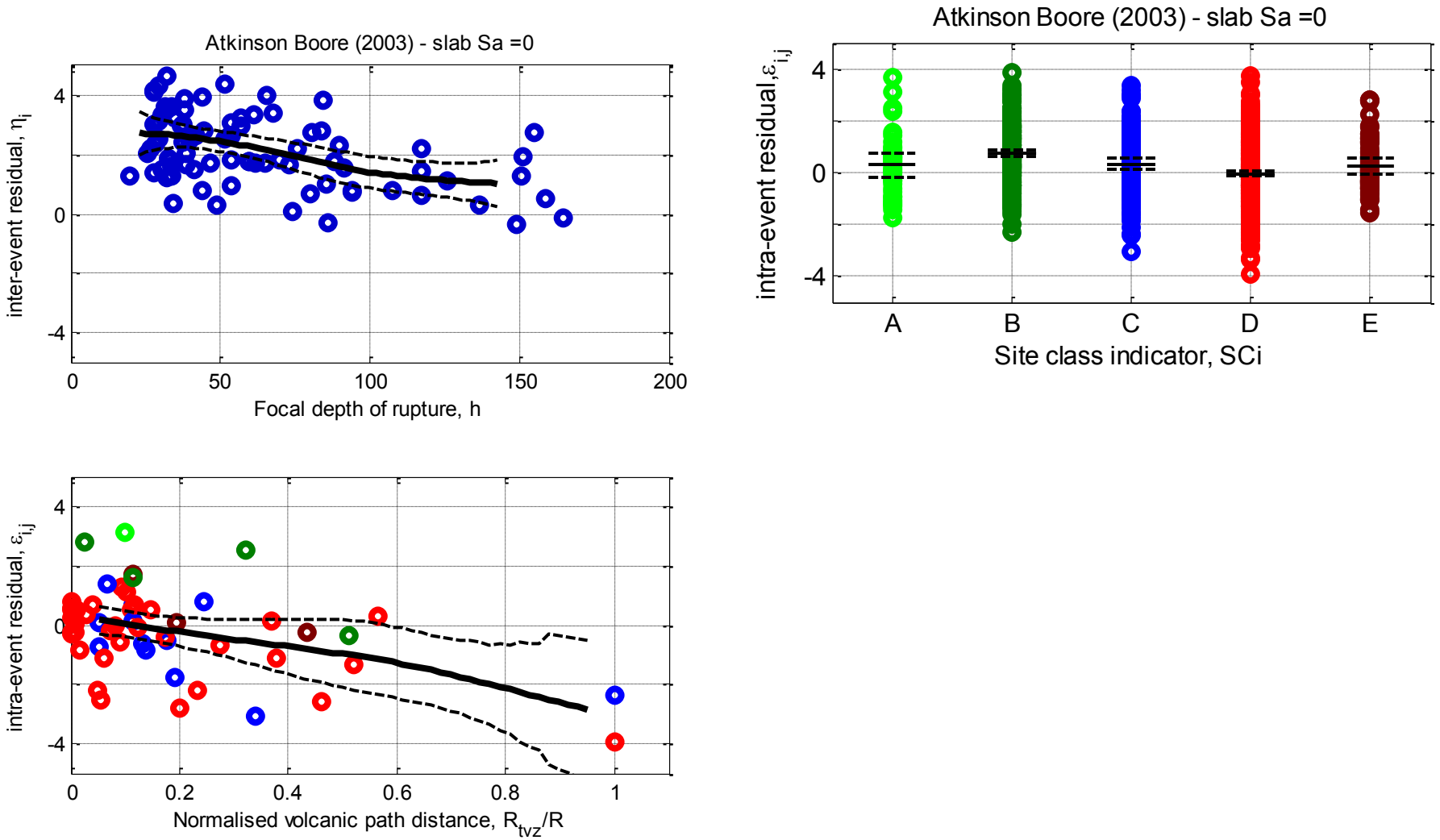

Figure D-41: Residuals for Sa(0.0) using the Atkinson and Boore (2003) slab model

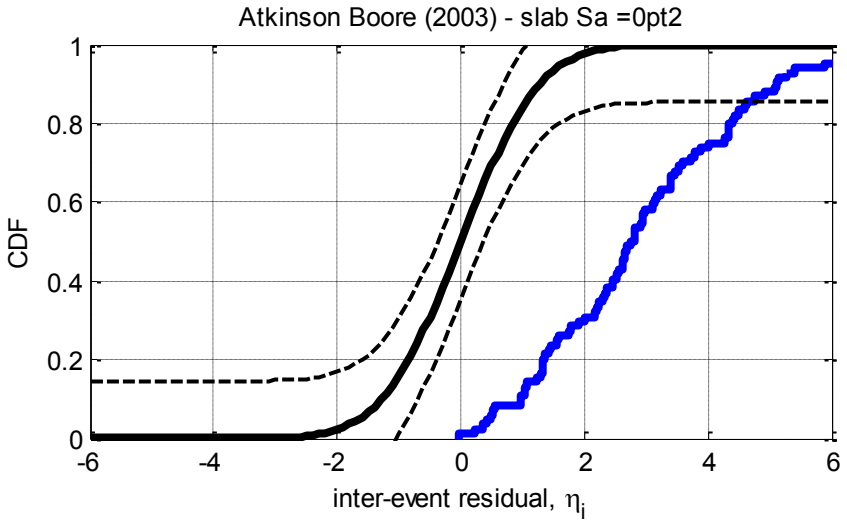
Atkinson Boore (2003) - slab Sa =0pt2
CDF
inter-event residual, η_i

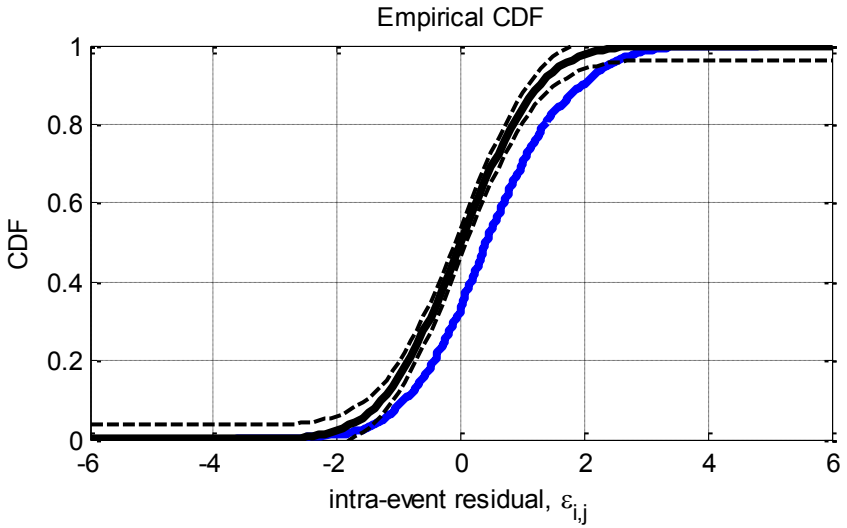
Empirical CDF
CDF
intra-event residual, $\varepsilon_{i,j}$

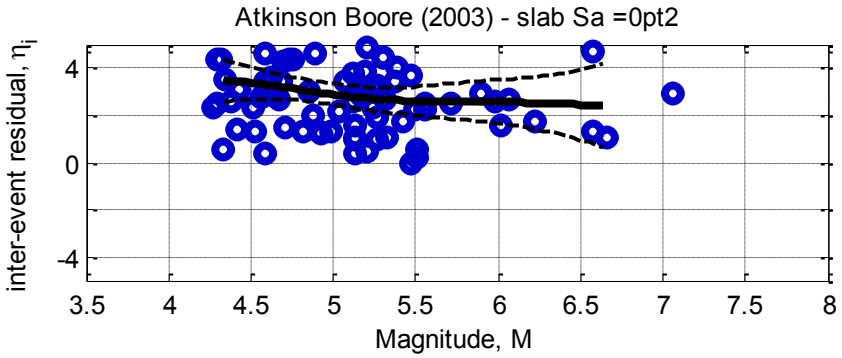
Atkinson Boore (2003) - slab Sa =0pt2
inter-event residual, η_i
Magnitude, M

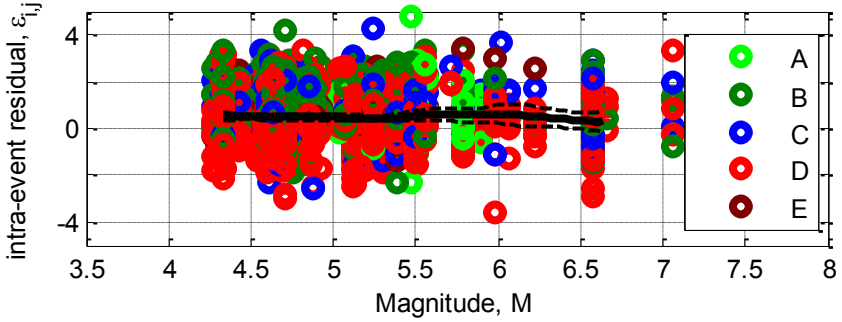
intra-event residual, $\varepsilon_{i,j}$
A
B
C
D
E
Magnitude, M

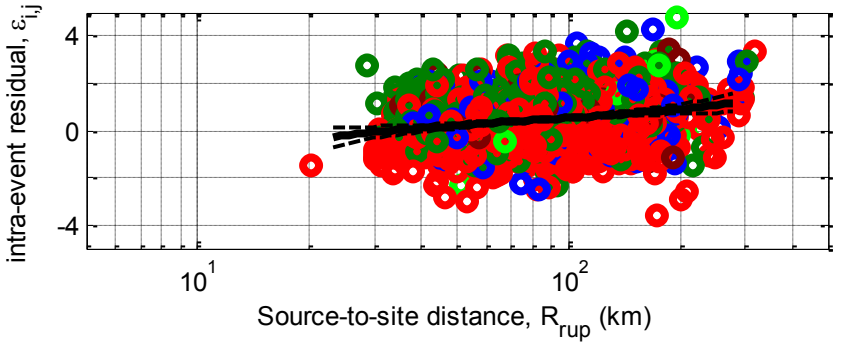
intra-event residual, $\varepsilon_{i,j}$
Source-to-site distance, R_{rup} (km)

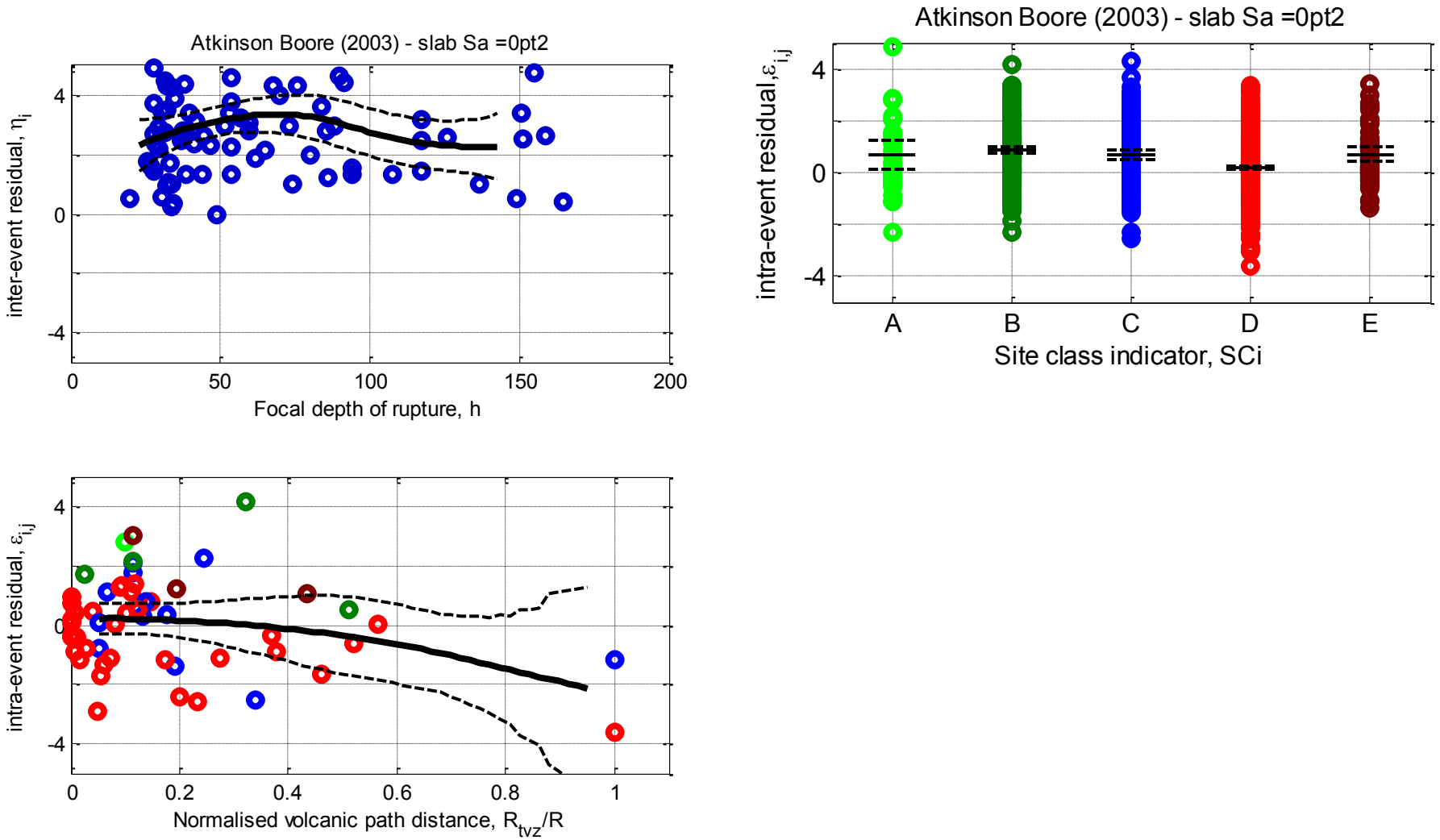

Figure D-42: Residuals for Sa(0.2) using the Atkinson and Boore (2003) slab model

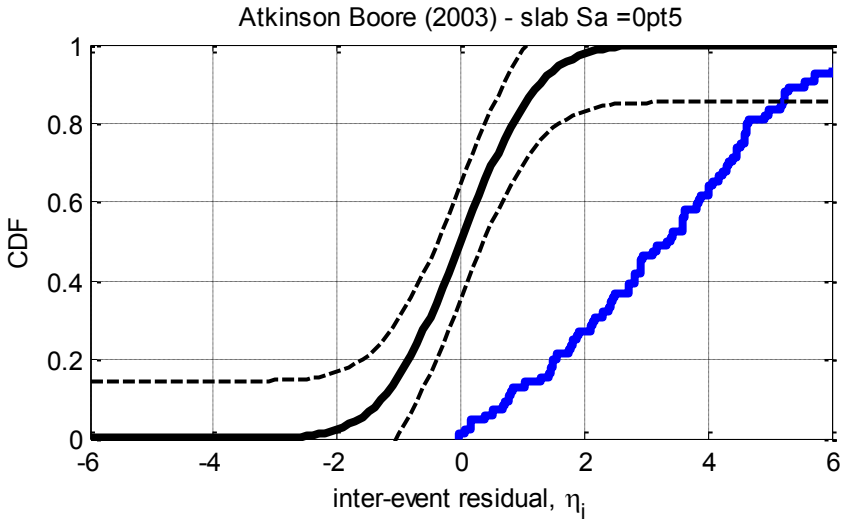
Atkinson Boore (2003) - slab Sa =0pt5
CDF
inter-event residual, η_i

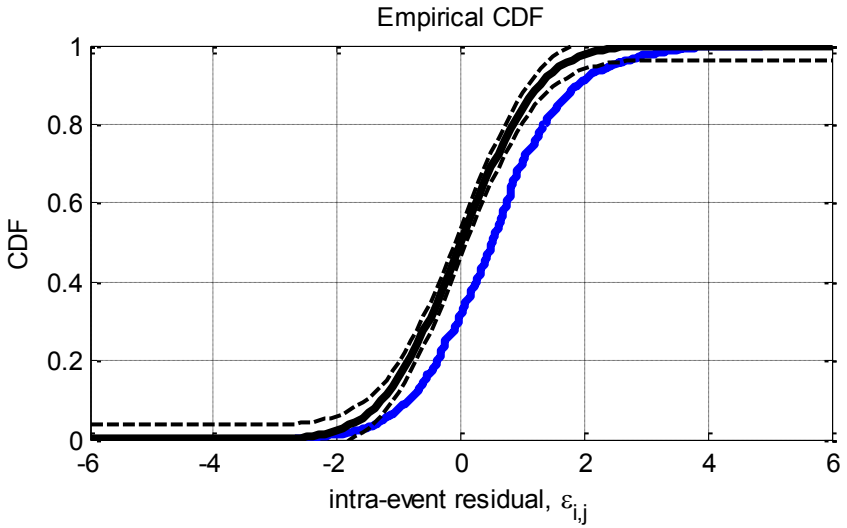
Empirical CDF
CDF
intra-event residual, $\varepsilon_{i,j}$

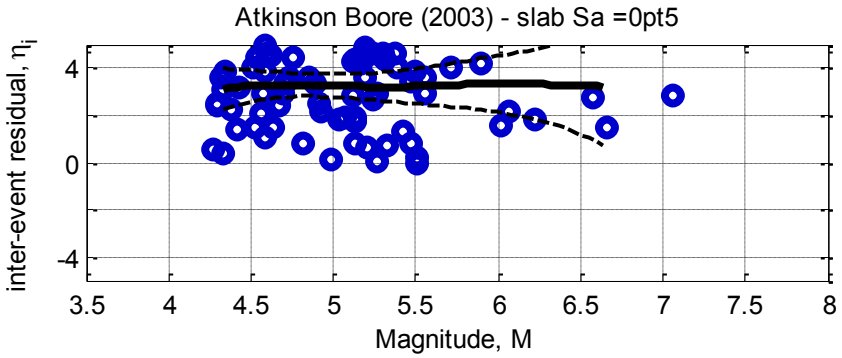
Atkinson Boore (2003) - slab Sa =0pt5
inter-event residual, η_i
Magnitude, M

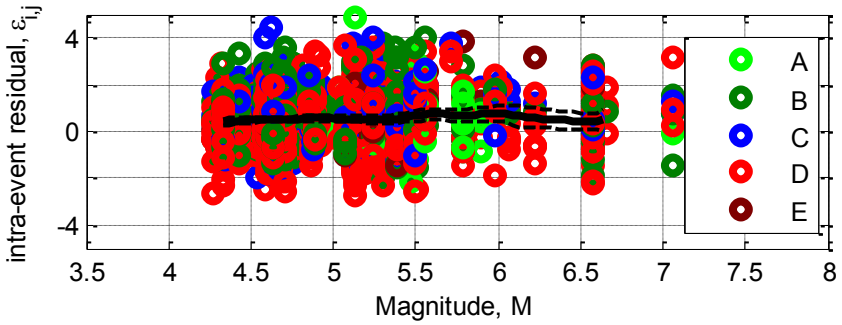
intra-event residual, $\varepsilon_{i,j}$
Magnitude, M
A
B
C
D
E

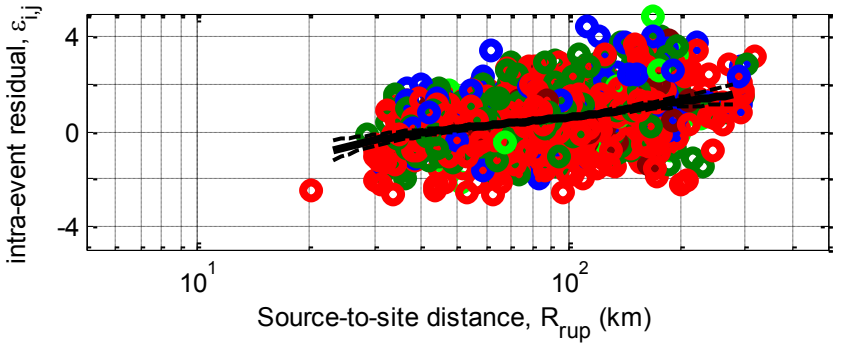
intra-event residual, $\varepsilon_{i,j}$
Source-to-site distance, R_{rup} (km)

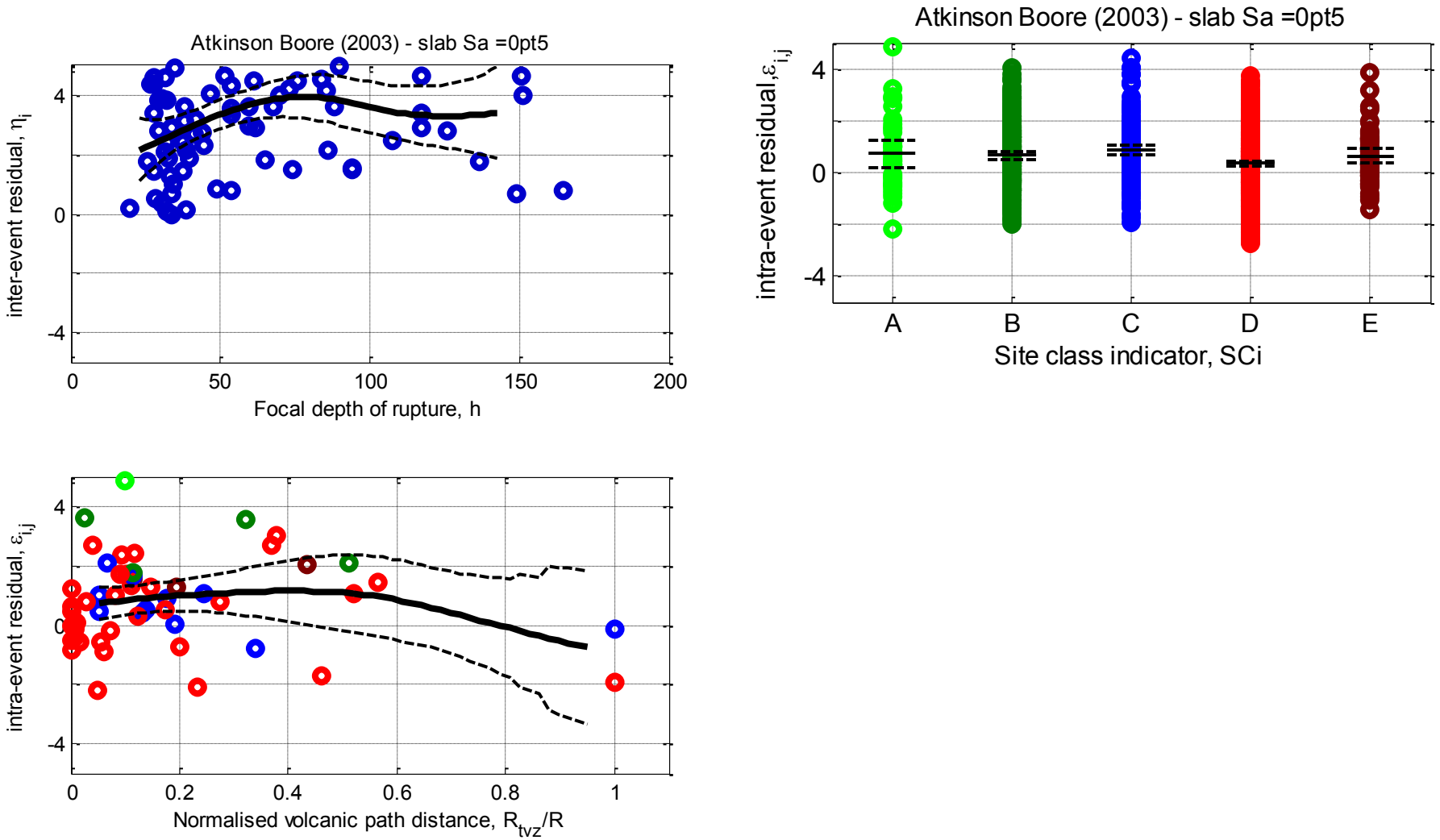

Figure D-43: Residuals for Sa(0.5) using the Atkinson and Boore (2003) slab model

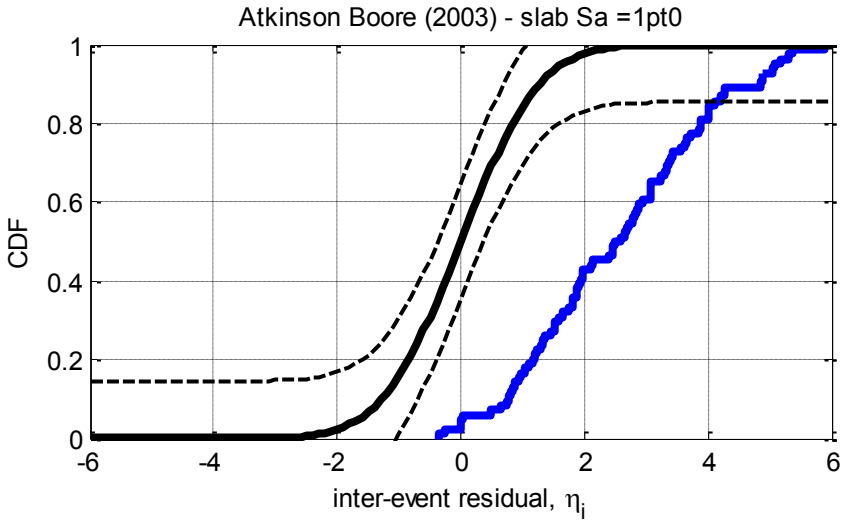
Atkinson Boore (2003) - slab Sa =1pt0
CDF
inter-event residual, η_i

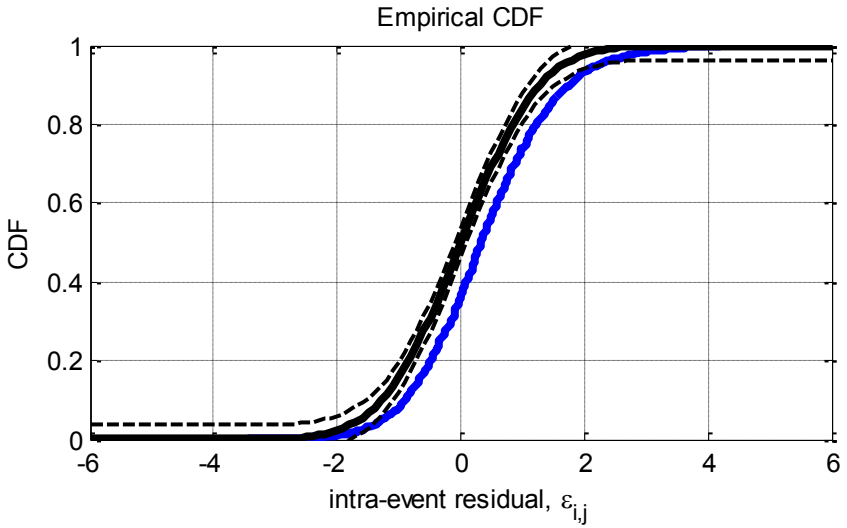
Empirical CDF
CDF
intra-event residual, $\varepsilon_{i,j}$

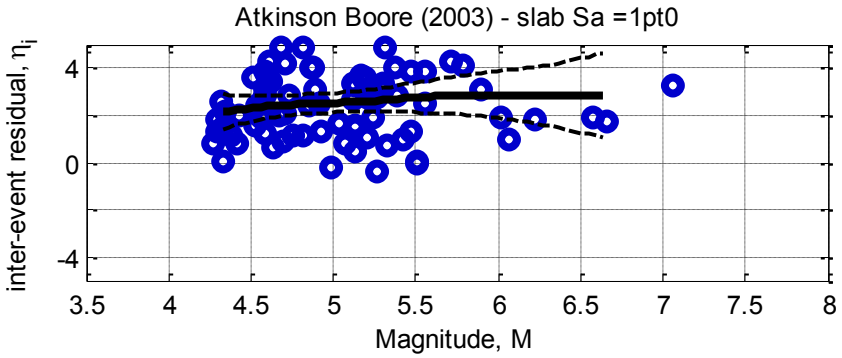
Atkinson Boore (2003) - slab Sa =1pt0
inter-event residual, η_i
Magnitude, M

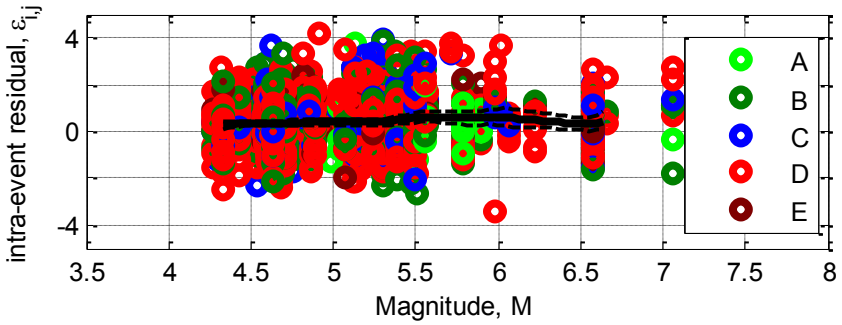
intra-event residual, $\varepsilon_{i,j}$
A
B
C
D
E
Magnitude, M

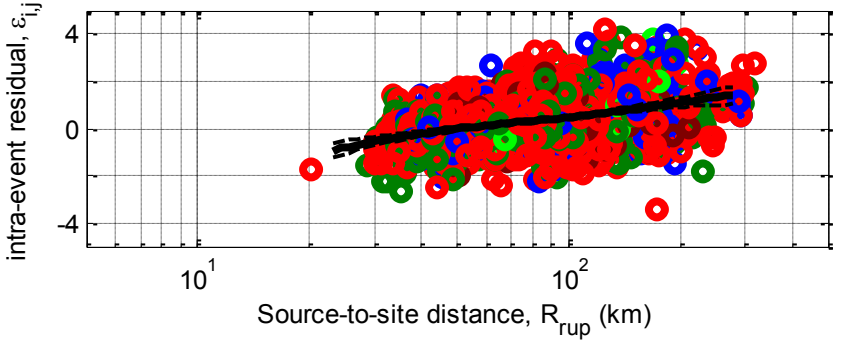
intra-event residual, $\varepsilon_{i,j}$
Source-to-site distance, R_{rup} (km)

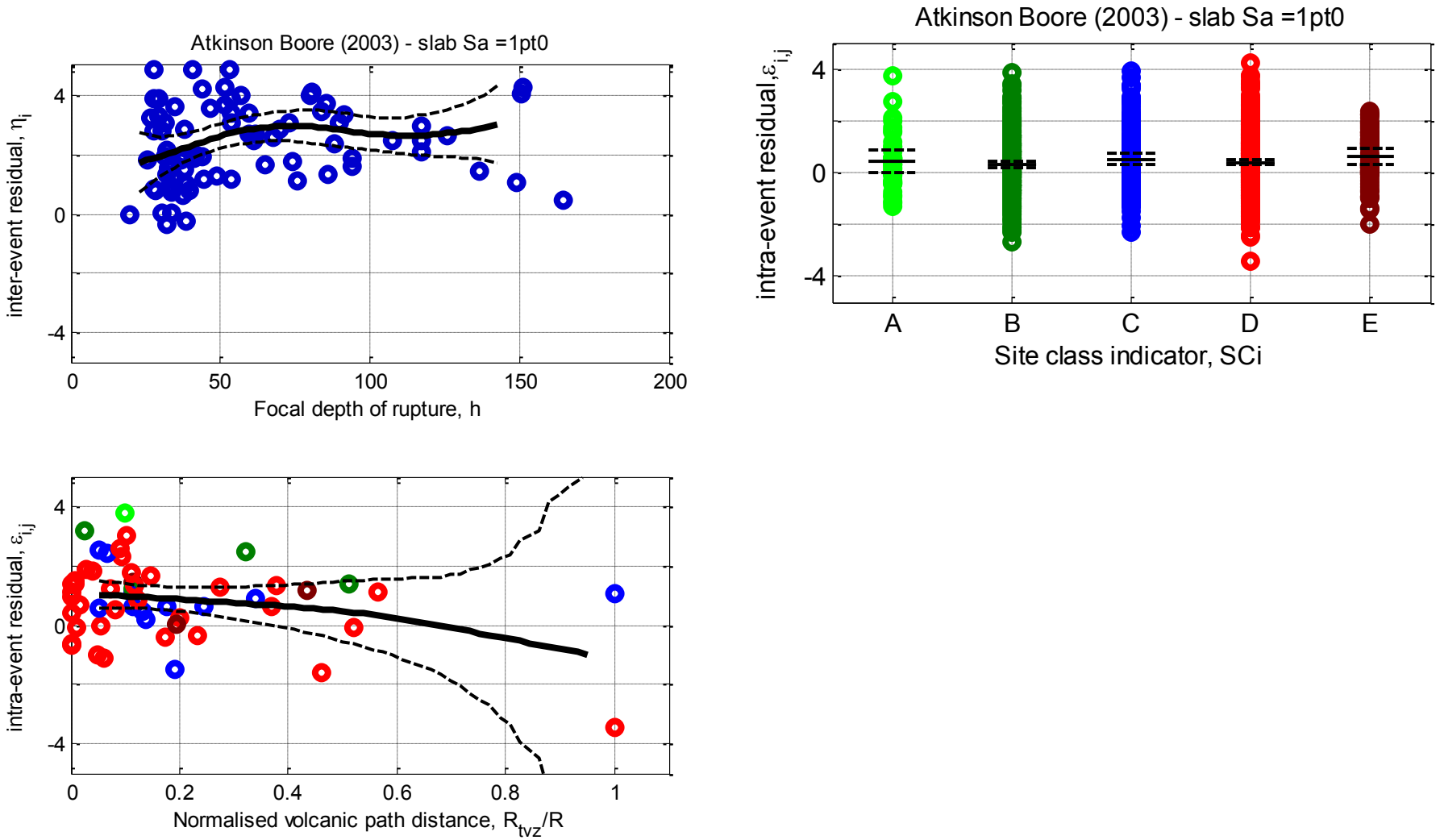

Figure D-44: Residuals for Sa(1.0) using the Atkinson and Boore (2003) slab model

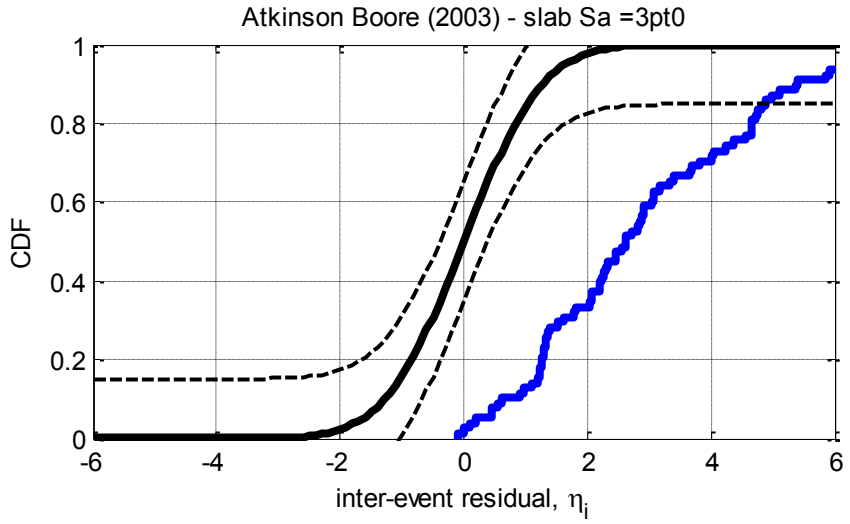
Atkinson Boore (2003) - slab Sa =3pt0
CDF
inter-event residual, η_i

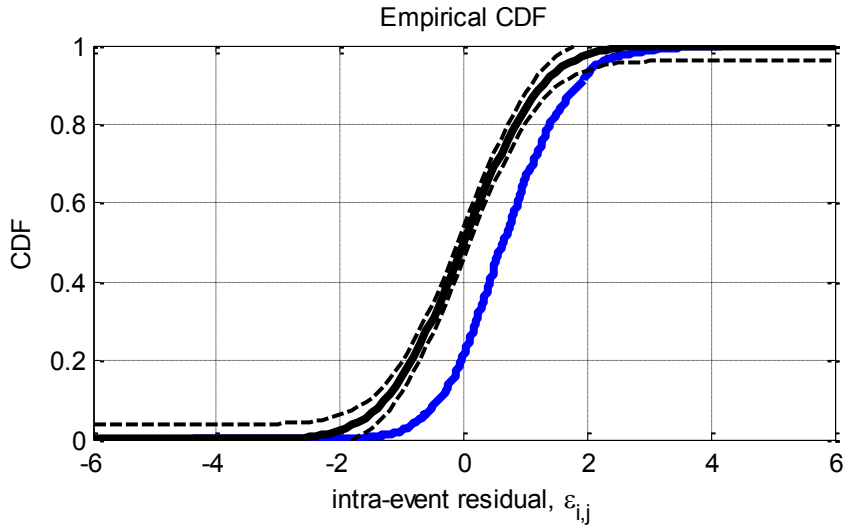
Empirical CDF
CDF
intra-event residual, $\varepsilon_{i,j}$

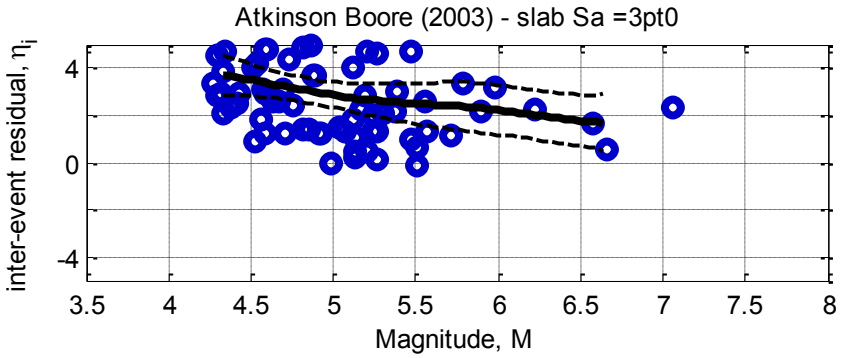
Atkinson Boore (2003) - slab Sa =3pt0
inter-event residual, η_i
Magnitude, M

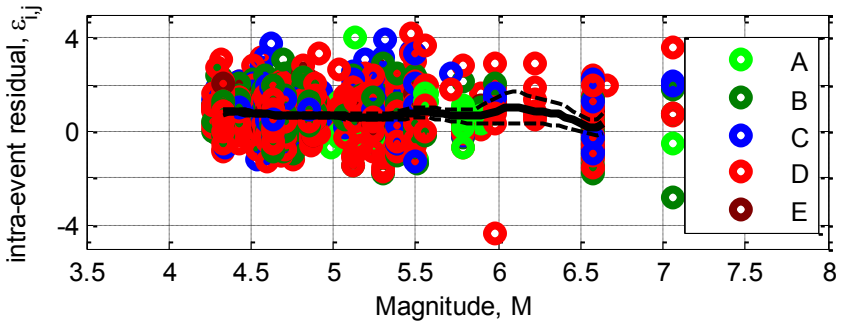
intra-event residual, $\varepsilon_{i,j}$
A
B
C
D
E
Magnitude, M

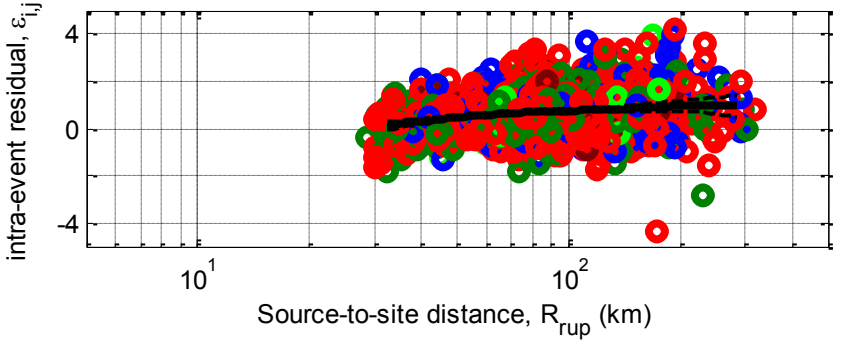
intra-event residual, $\varepsilon_{i,j}$
Source-to-site distance, R_{rup} (km)

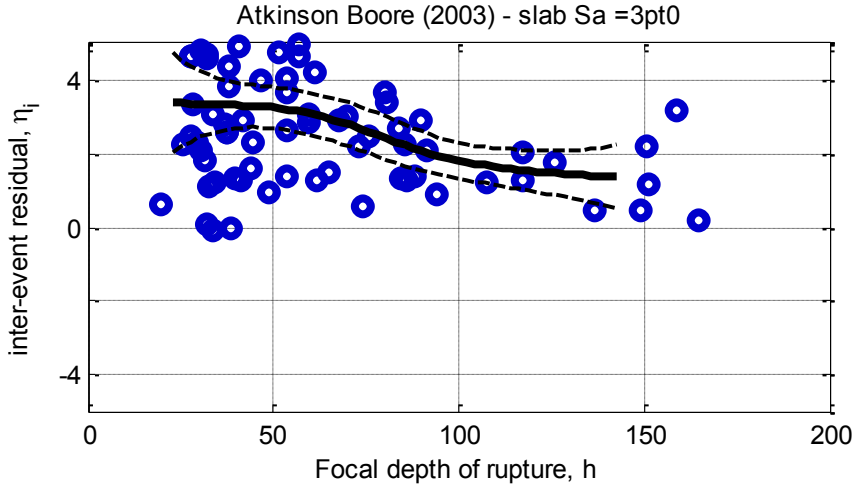

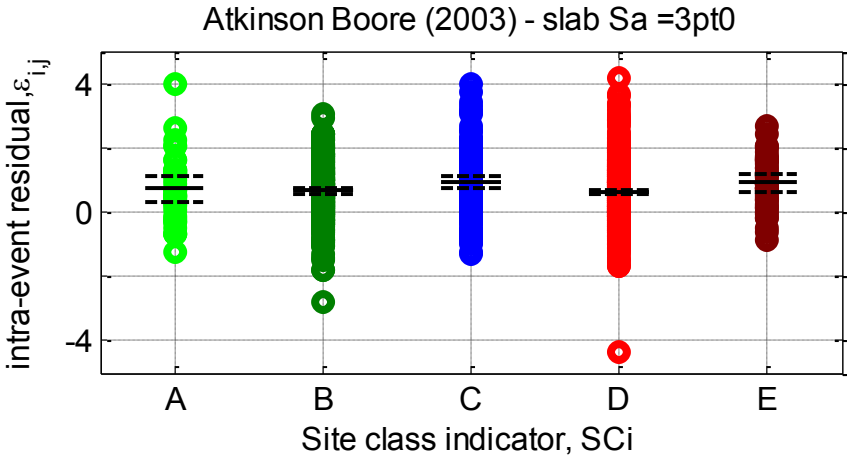

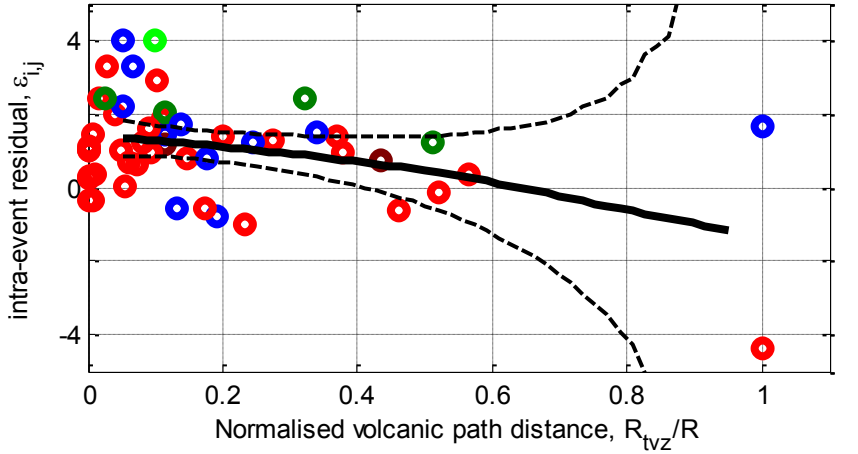

Figure D-45: Residuals for Sa(3.0) using the Atkinson and Boore (2003) slab model

D.10. Bradley (2010) Slab model

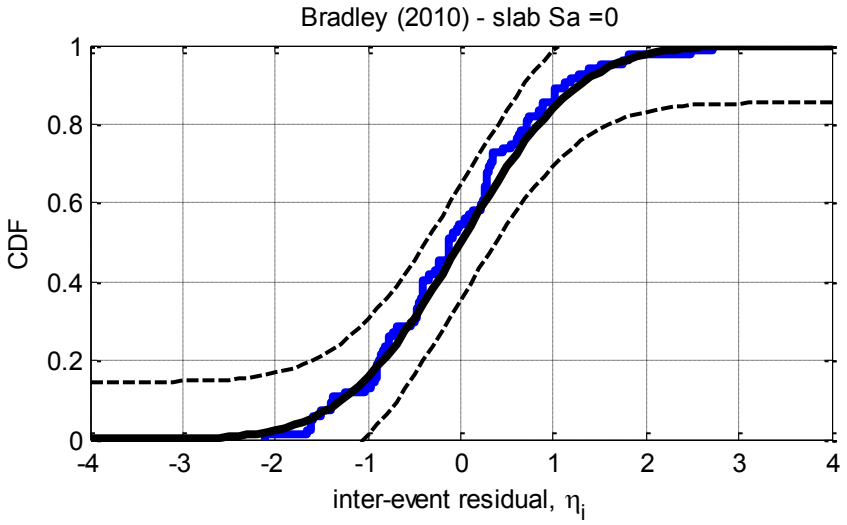

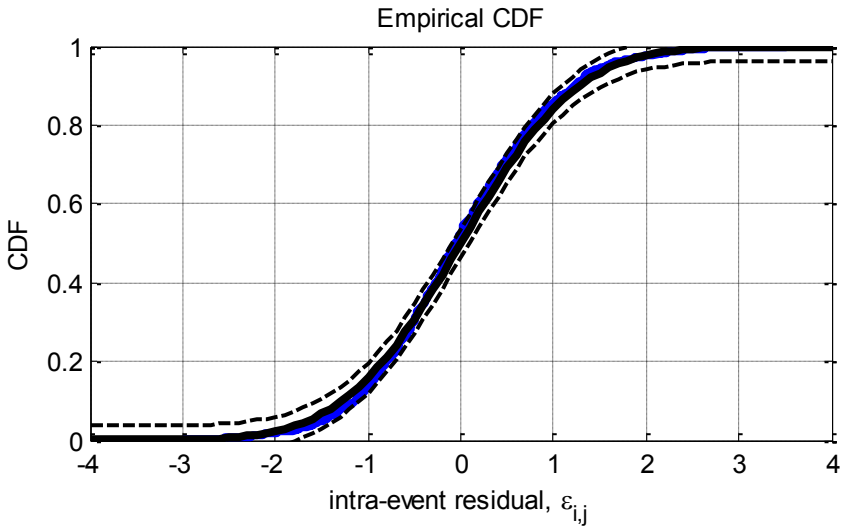

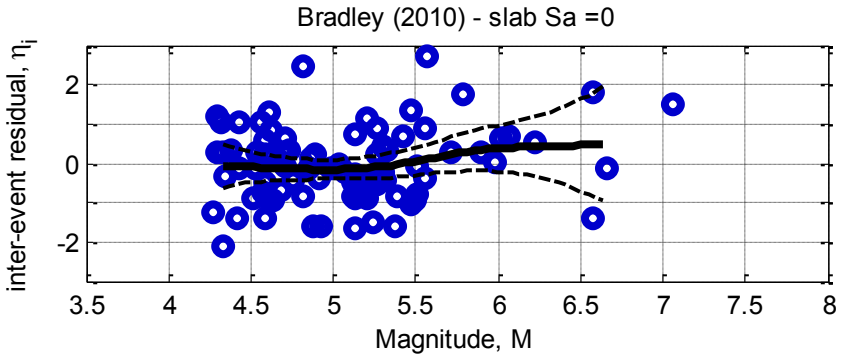

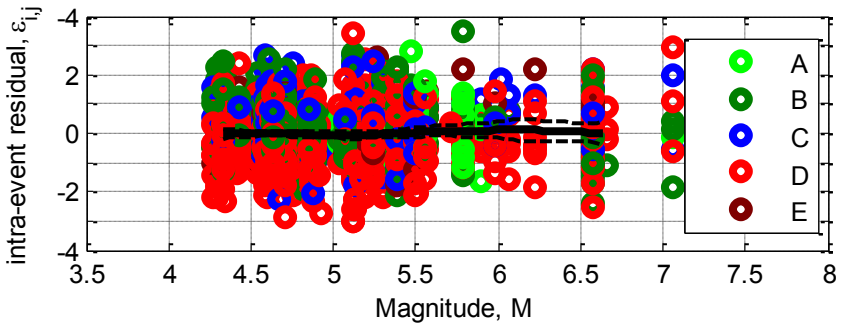

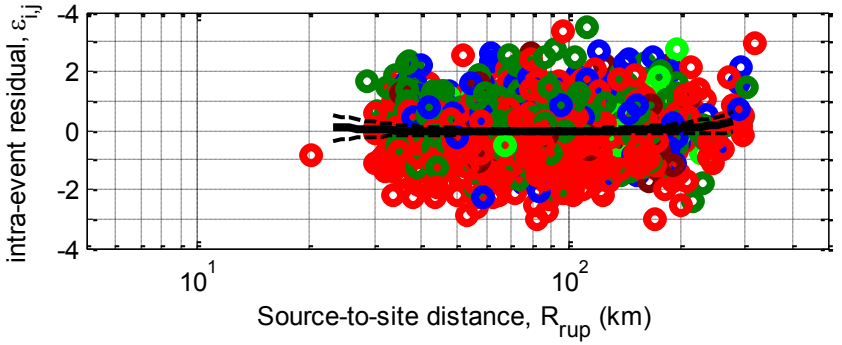

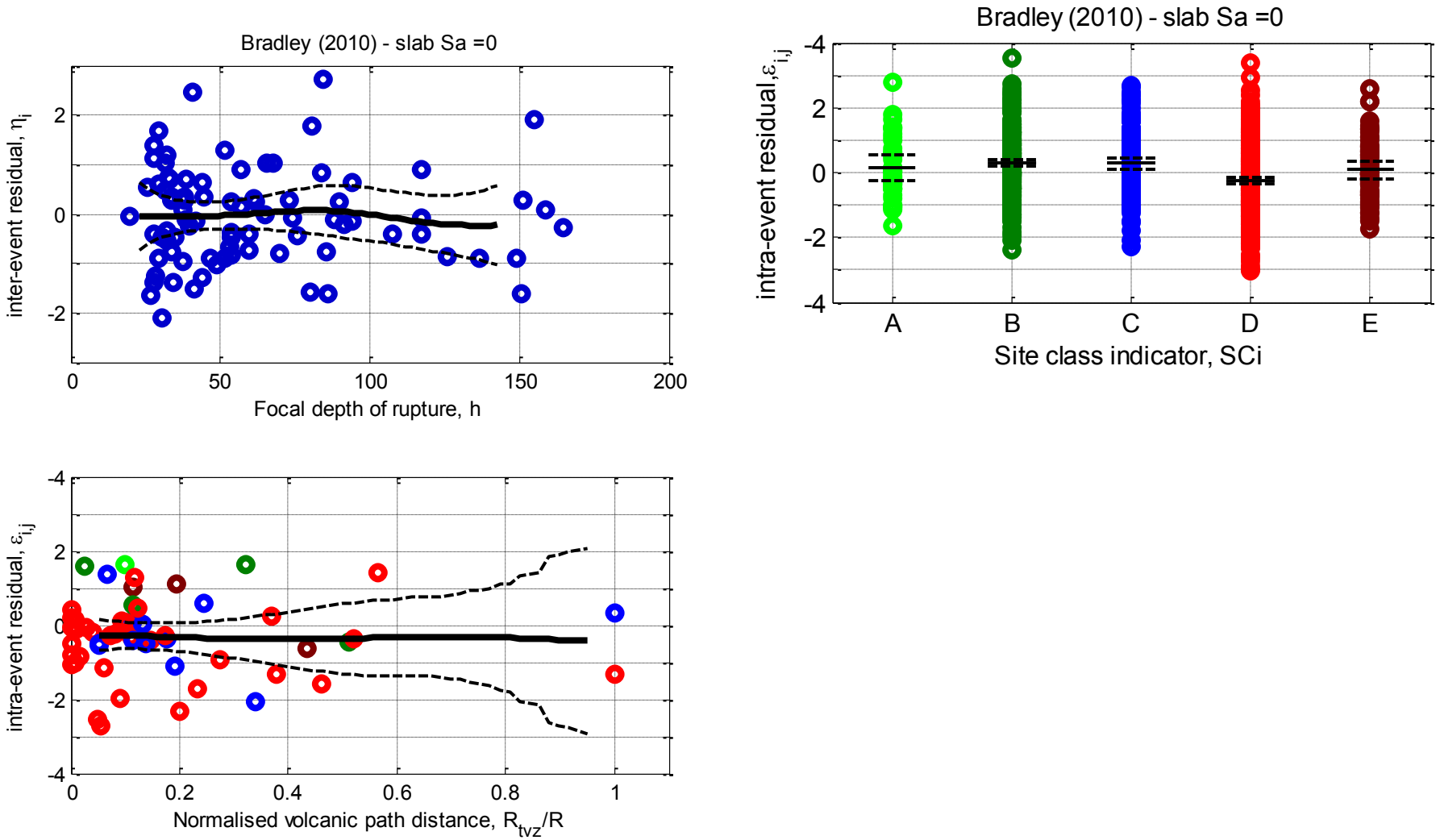

Figure D-46: Residuals for Sa(0.0) using the Bradley (2010) slab model

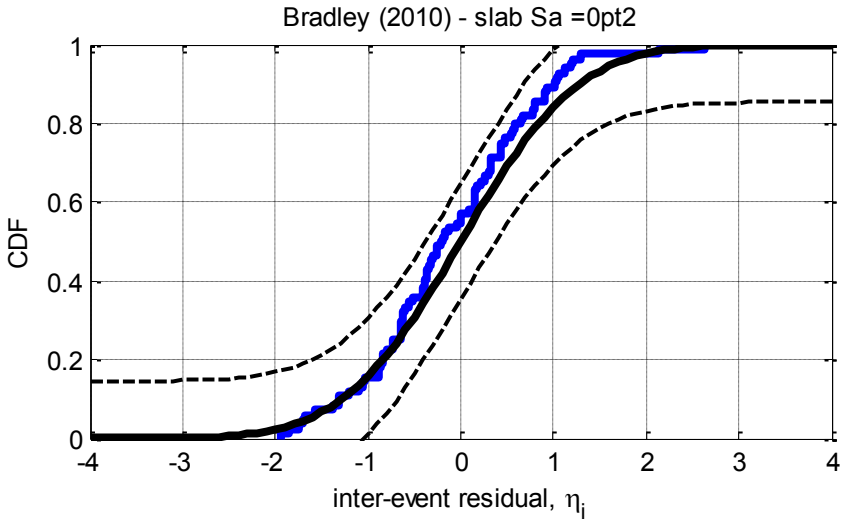
Bradley (2010) - slab Sa =0pt2
CDF
inter-event residual, η_i

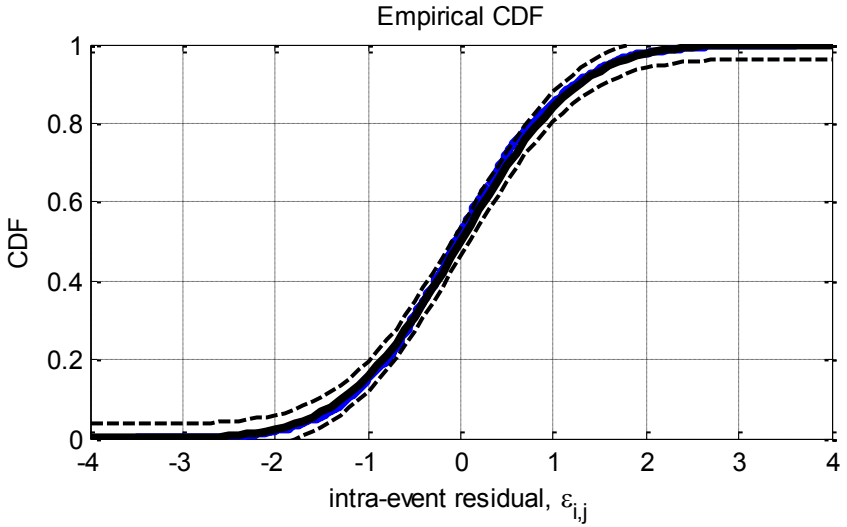
Empirical CDF
CDF
intra-event residual, $\varepsilon_{i,j}$

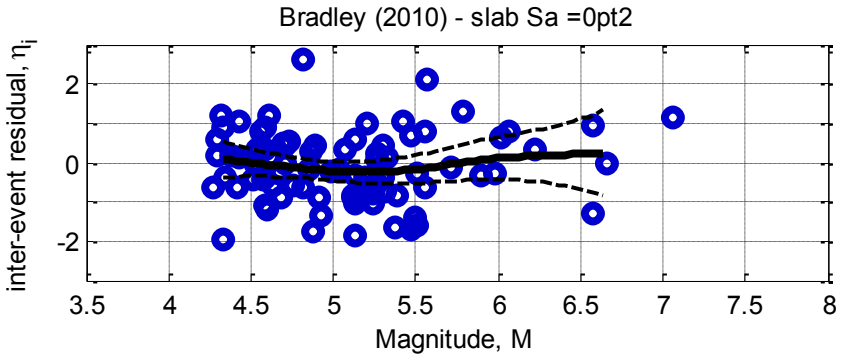
Bradley (2010) - slab Sa =0pt2
inter-event residual, η_i
Magnitude, M

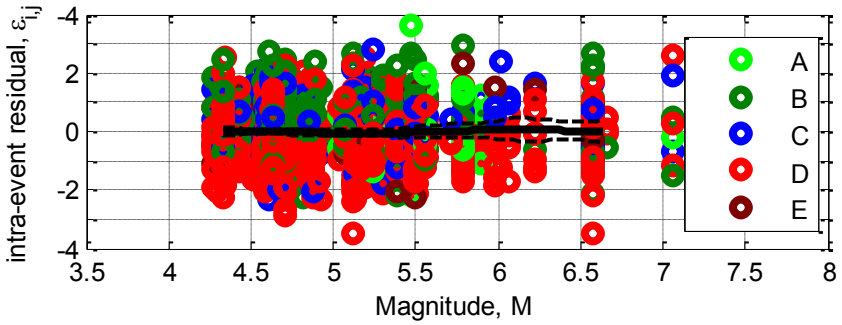
intra-event residual, $\varepsilon_{i,j}$
A
B
C
D
E
Magnitude, M

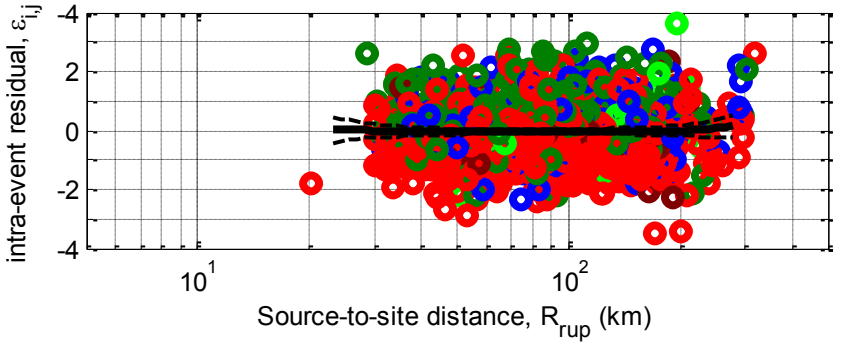
intra-event residual, $\varepsilon_{i,j}$
Source-to-site distance, R_{rup} (km)

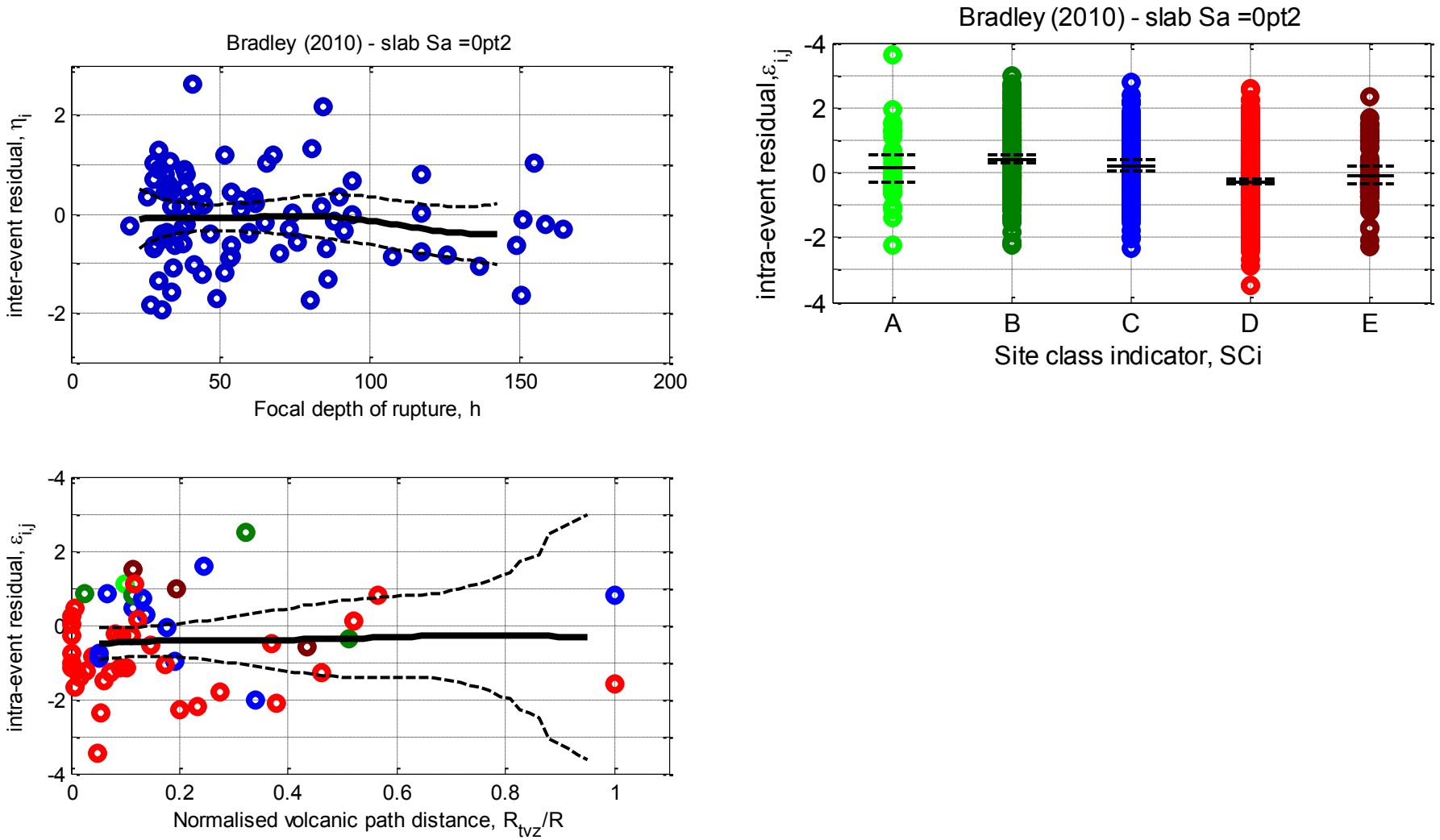

Figure D-47: Residuals for Sa(0.2) using the Bradley (2010) slab model

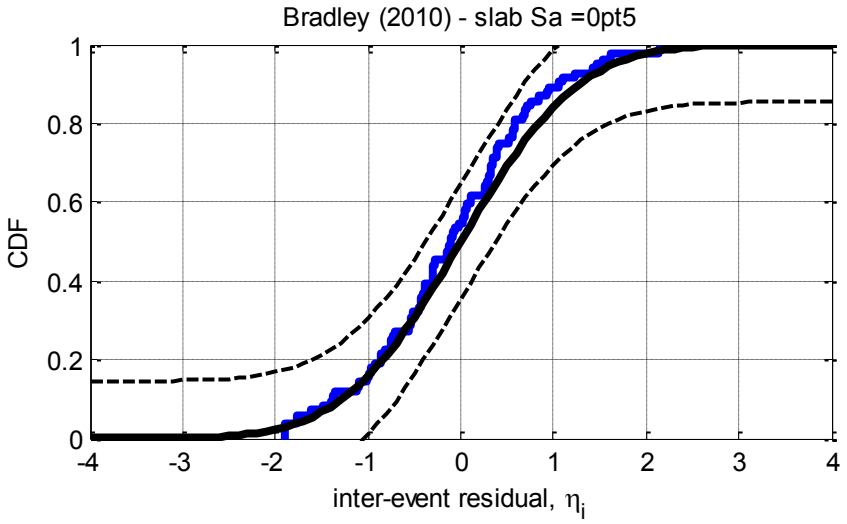
Bradley (2010) - slab Sa =0pt5
CDF
inter-event residual, η_i

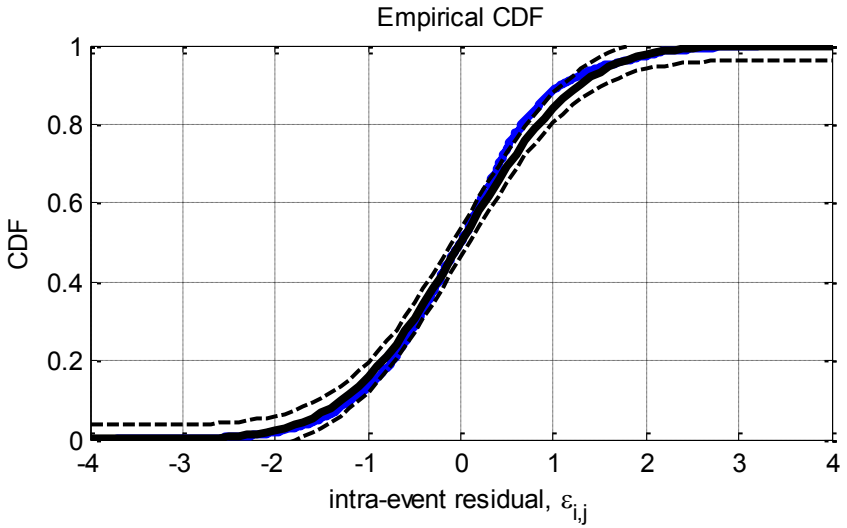
Empirical CDF
CDF
intra-event residual, $\varepsilon_{i,j}$

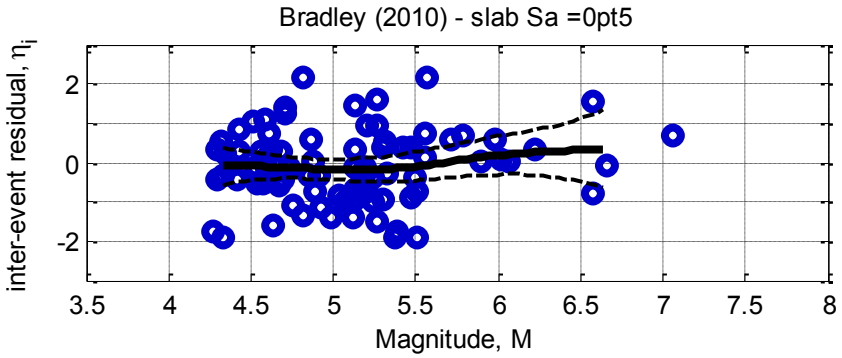
Bradley (2010) - slab Sa =0pt5
inter-event residual, η_i
Magnitude, M

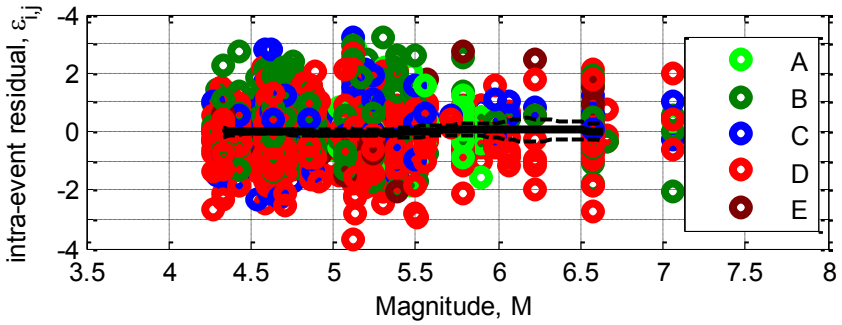
intra-event residual, $\varepsilon_{i,j}$
A
B
C
D
E
Magnitude, M

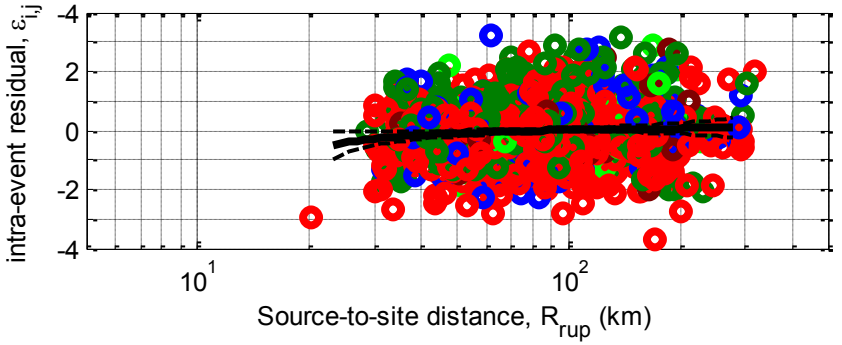
intra-event residual, $\varepsilon_{i,j}$
Source-to-site distance, R_{rup} (km)

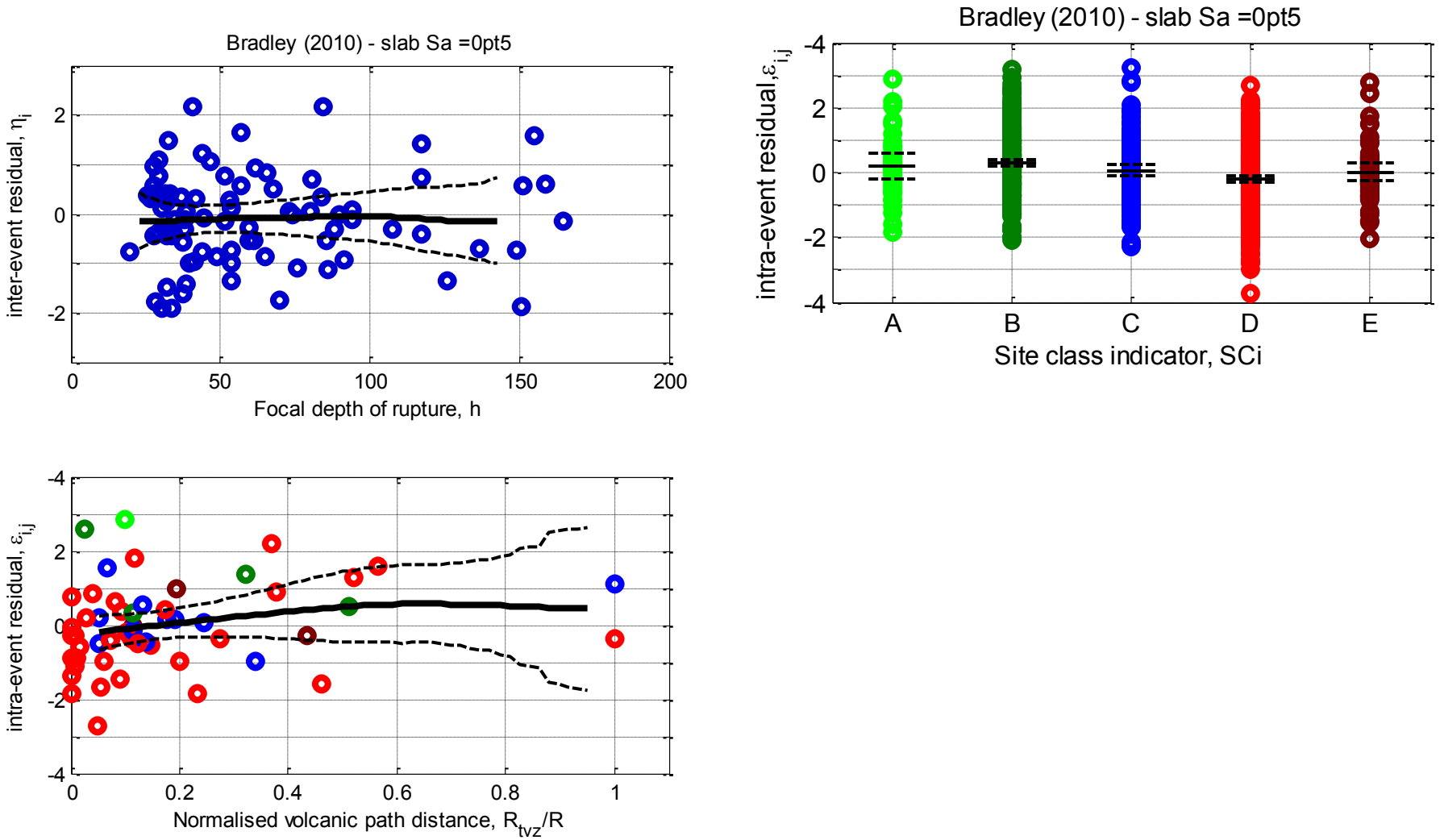

Figure D-48: Residuals for Sa(0.5) using the Bradley (2010) slab model

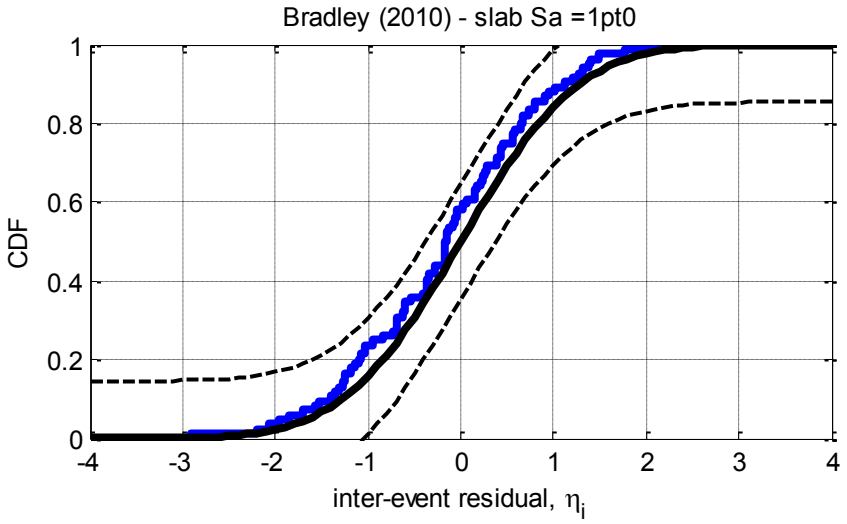
Bradley (2010) - slab Sa =1pt0
CDF
inter-event residual, η_i

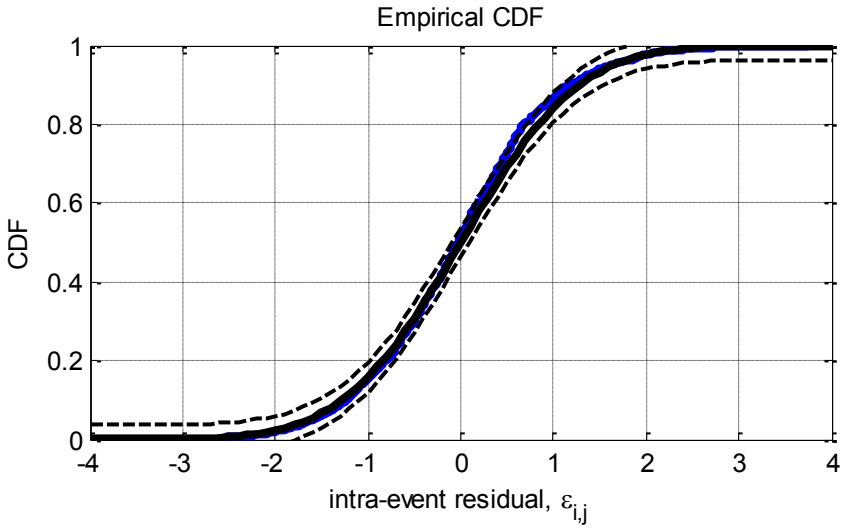
Empirical CDF
CDF
intra-event residual, $\varepsilon_{i,j}$

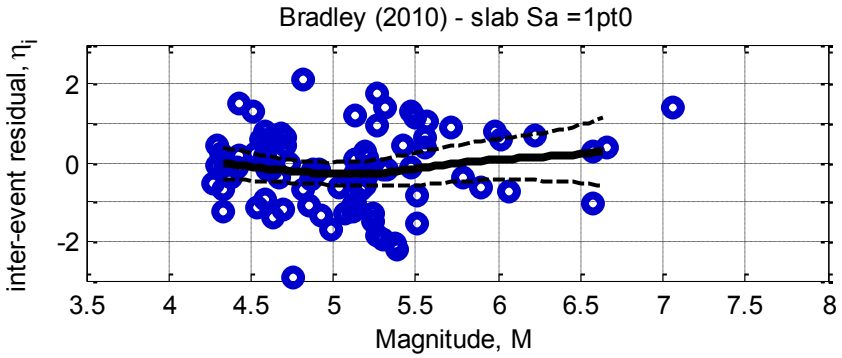
Bradley (2010) - slab Sa =1pt0
inter-event residual, η_i
Magnitude, M

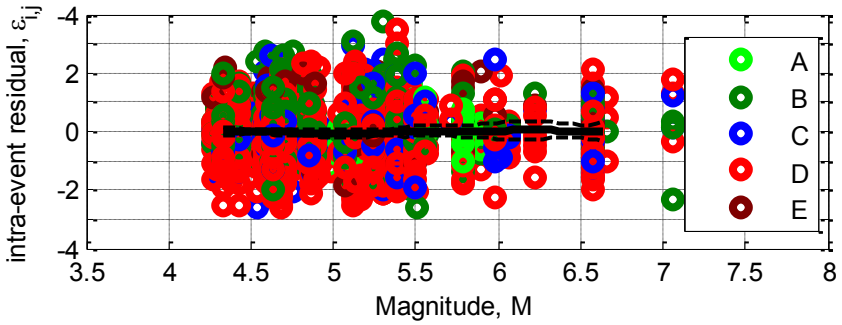
intra-event residual, $\varepsilon_{i,j}$
A
B
C
D
E
Magnitude, M

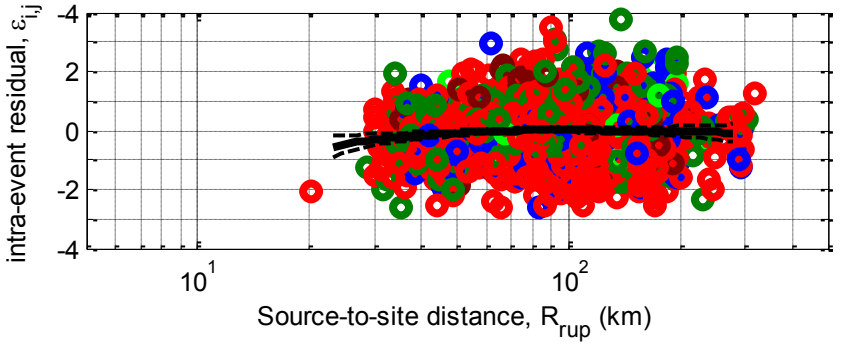
intra-event residual, $\varepsilon_{i,j}$
Source-to-site distance, R_{rup} (km)

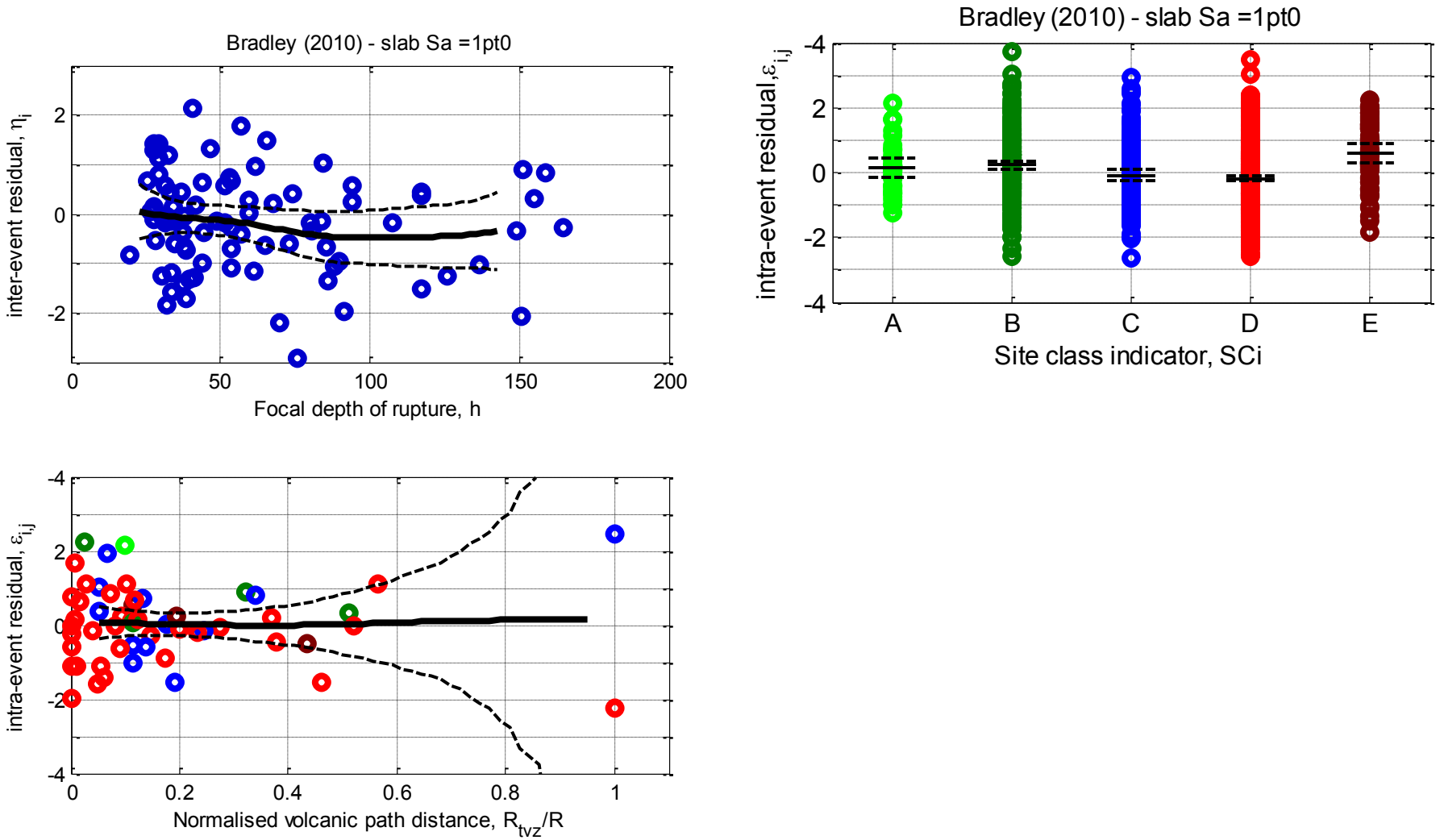

Figure D-49: Residuals for Sa(1.0) using the Bradley (2010) slab model

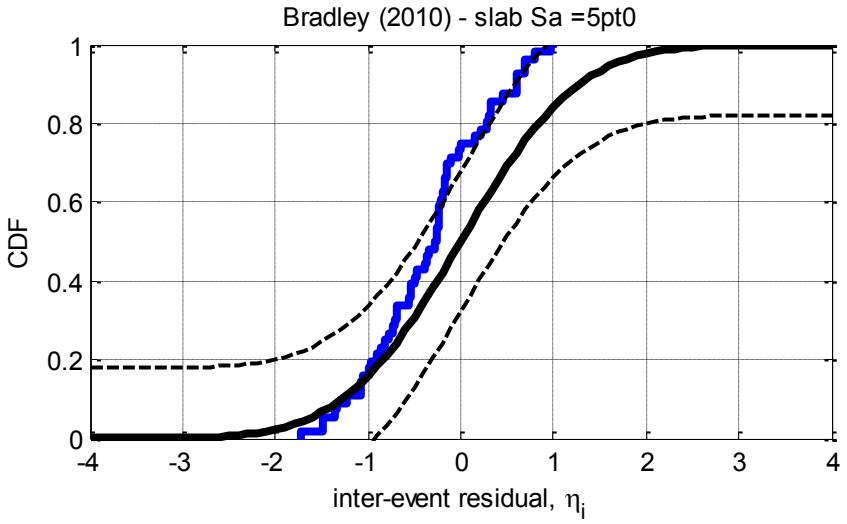
Bradley (2010) - slab Sa =5pt0
CDF
inter-event residual, η_i

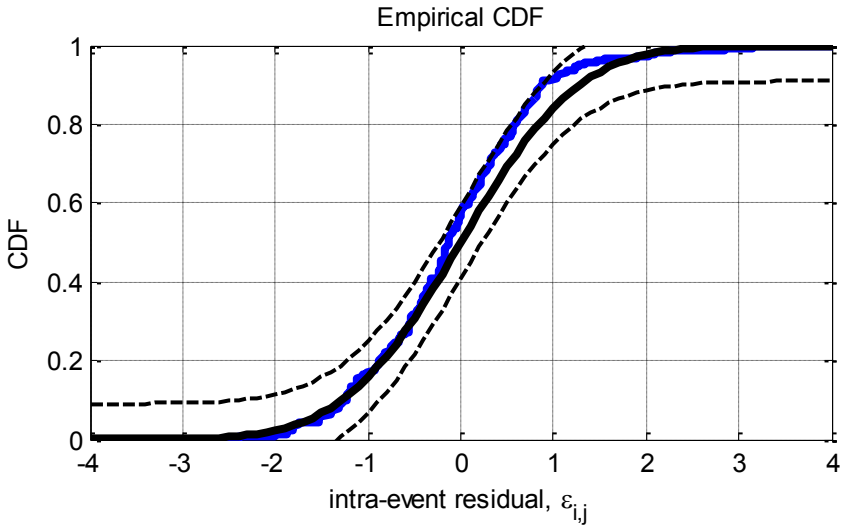
Empirical CDF
CDF
intra-event residual, $\varepsilon_{i,j}$

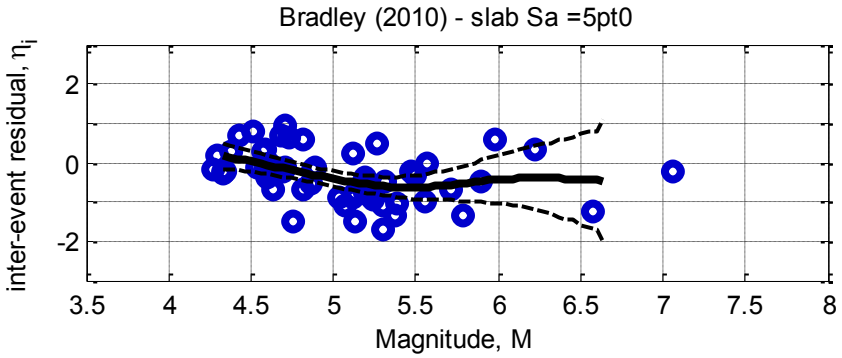
Bradley (2010) - slab Sa =5pt0
inter-event residual, η_i
Magnitude, M

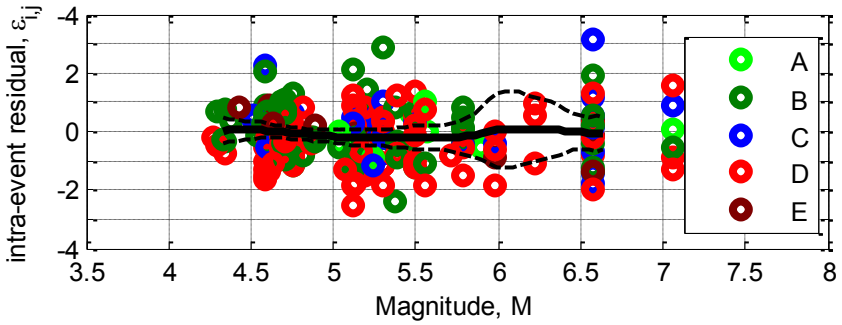
intra-event residual, $\varepsilon_{i,j}$
A
B
C
D
E
Magnitude, M

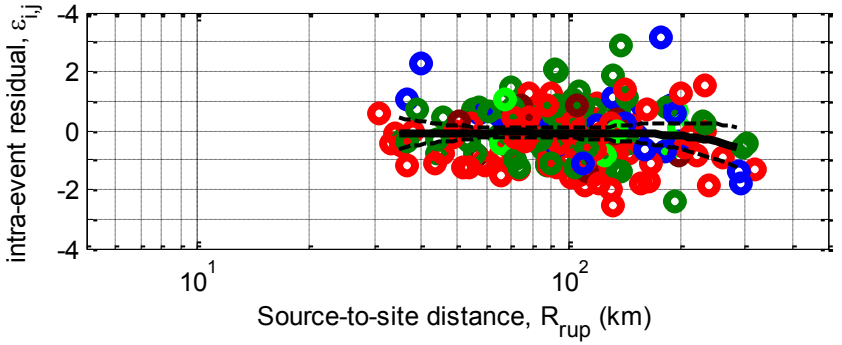
intra-event residual, $\varepsilon_{i,j}$
Source-to-site distance, R_{rup} (km)

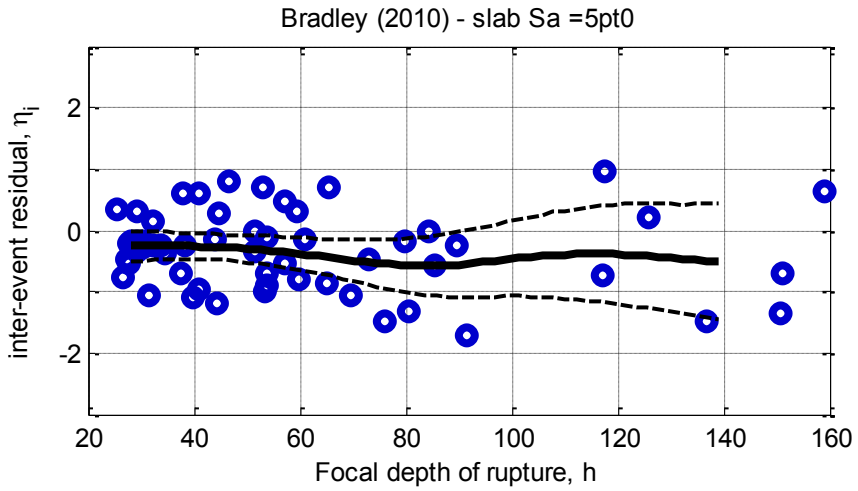

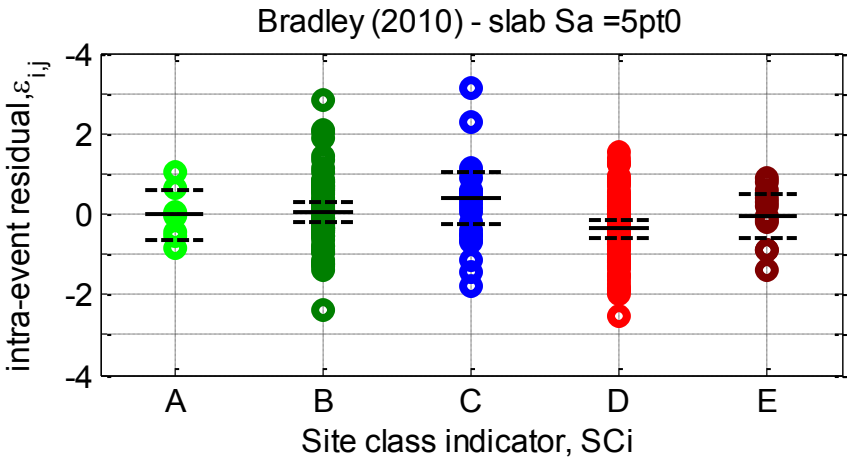

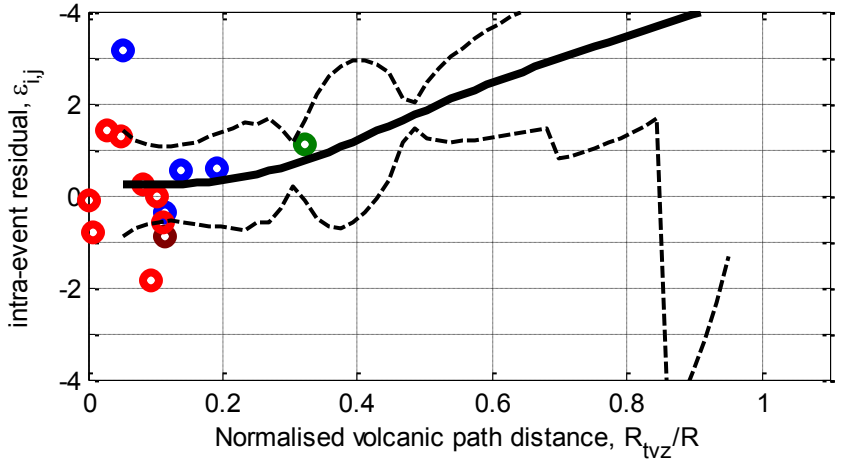

Figure D-50: Residuals for Sa(5.0) using the Bradley (2010) slab model

D.11. McVerry et al. (2006) Interface model

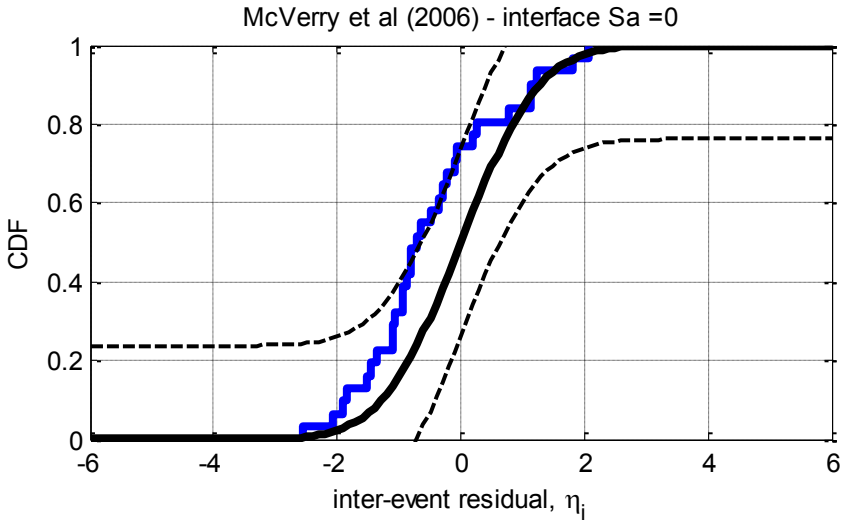

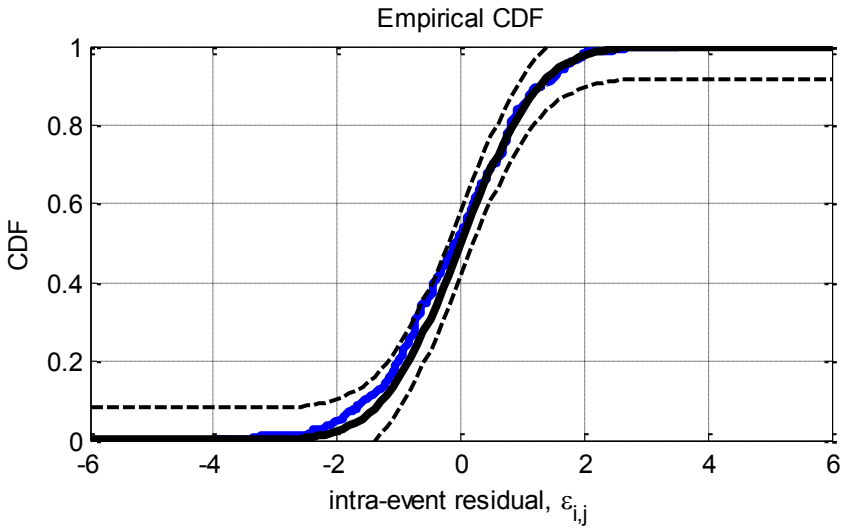

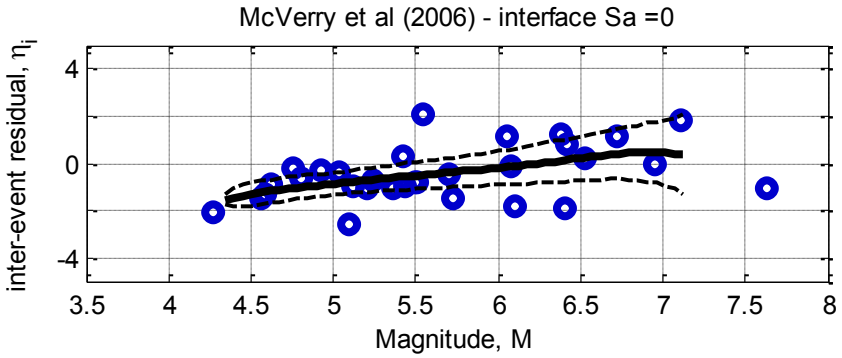

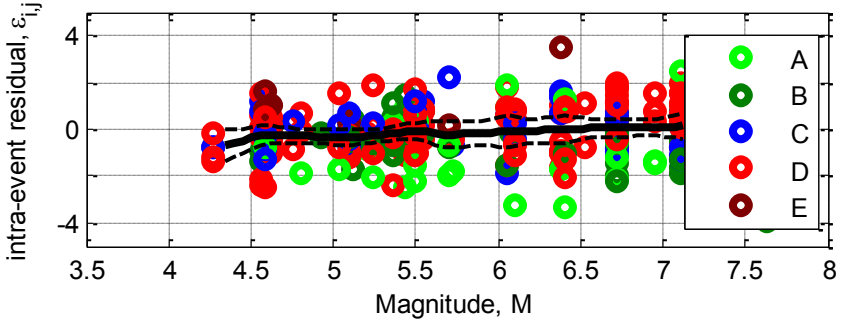

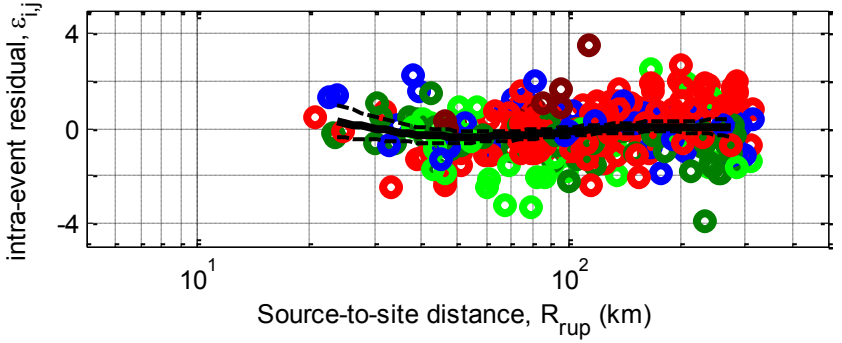

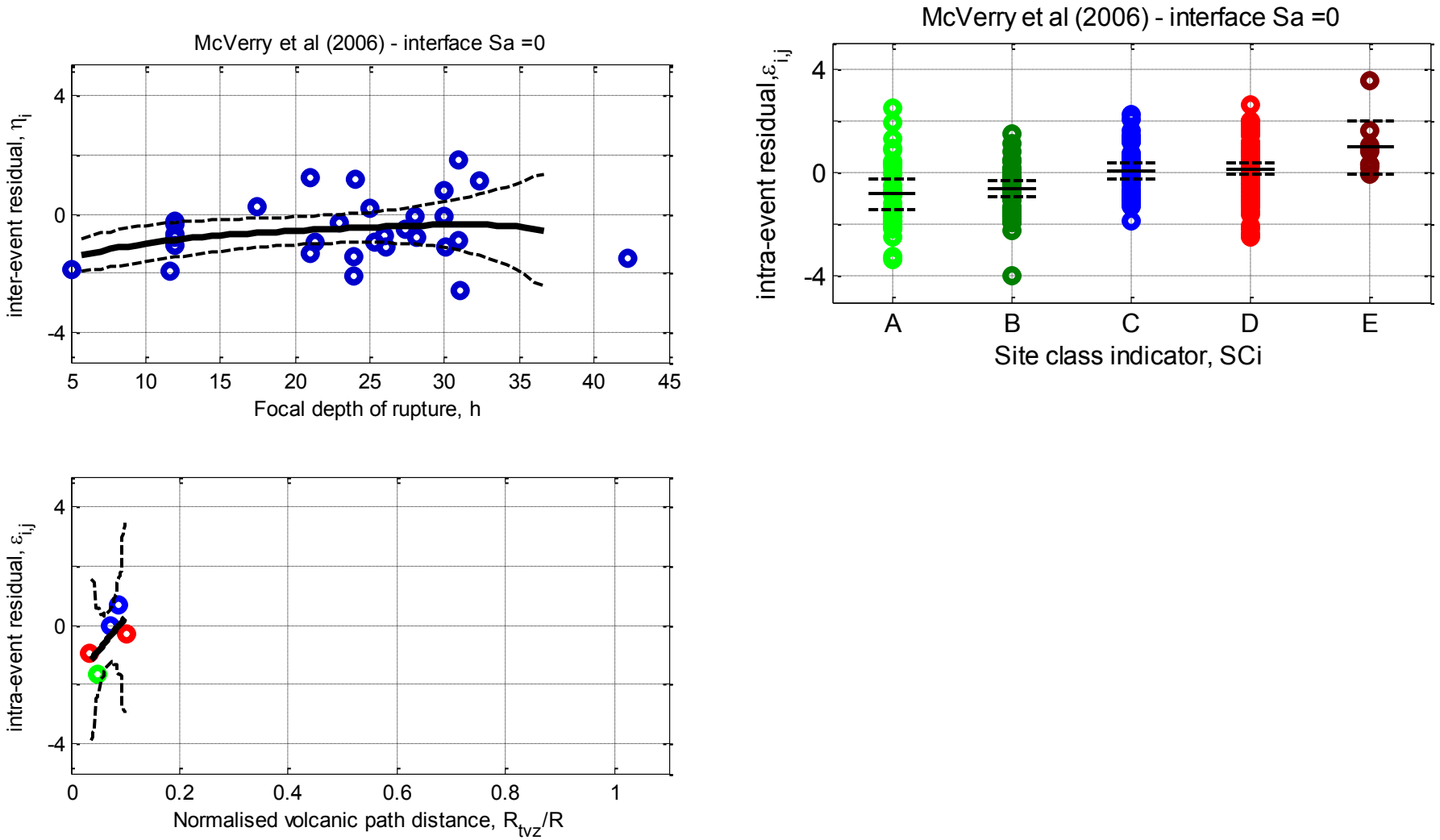

Figure D-51: Residuals for Sa(0.0) using the McVerry et al. (2006) interface model

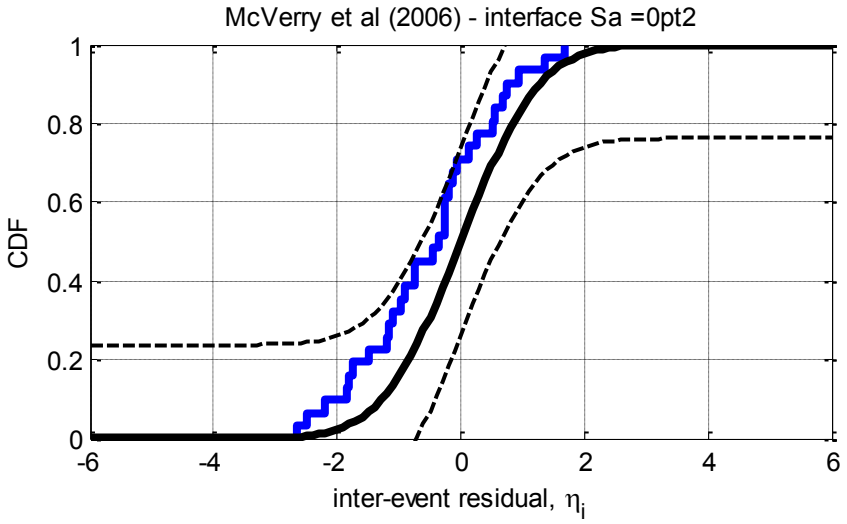
McVerry et al (2006) - interface Sa =0pt2
CDF
inter-event residual, η_i

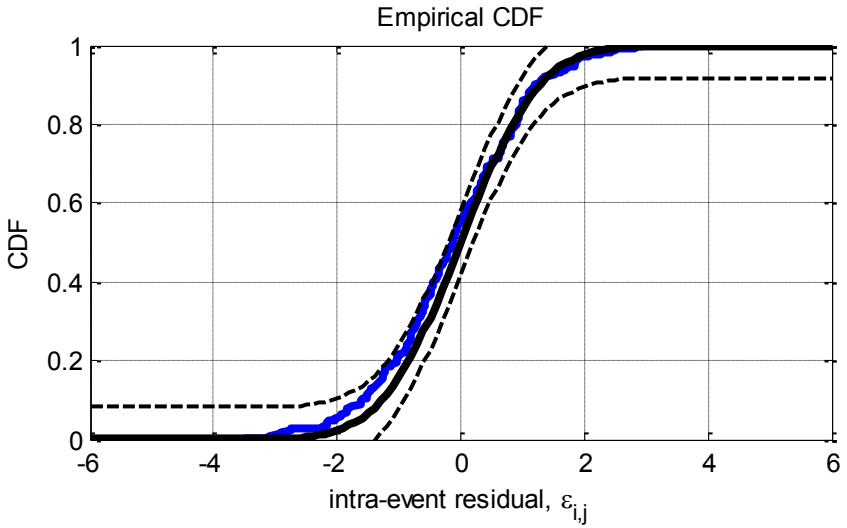
Empirical CDF
CDF
intra-event residual, $\varepsilon_{i,j}$

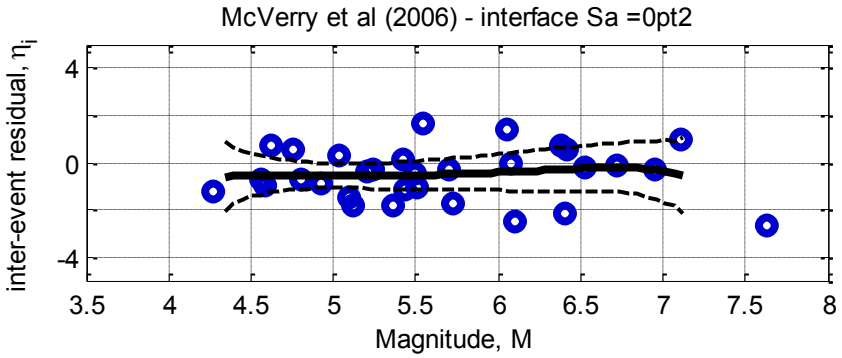
McVerry et al (2006) - interface Sa =0pt2
inter-event residual, η_i
Magnitude, M

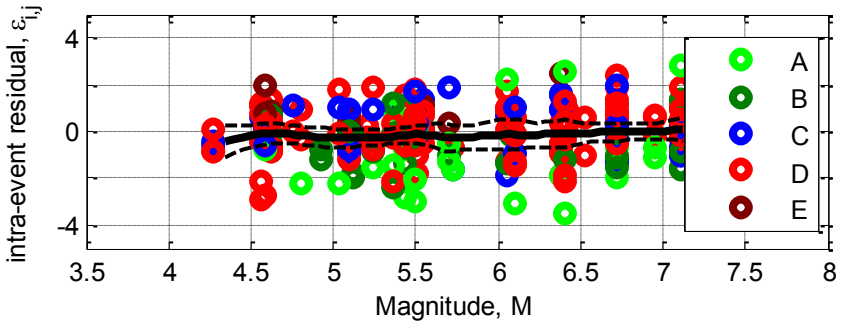
intra-event residual, $\varepsilon_{i,j}$
Magnitude, M
A
B
C
D
E

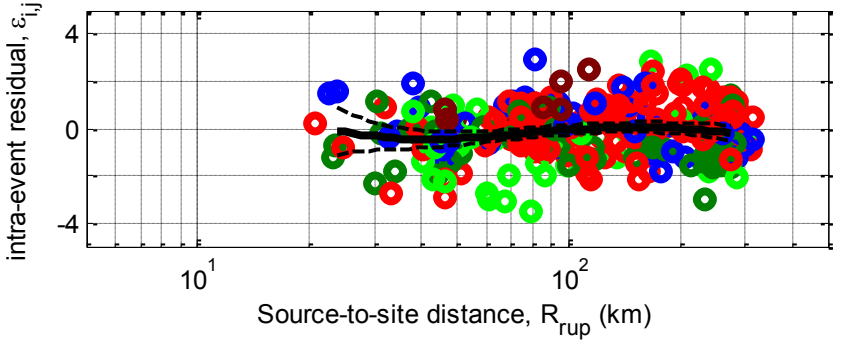
intra-event residual, $\varepsilon_{i,j}$
Source-to-site distance, R_{rup} (km)

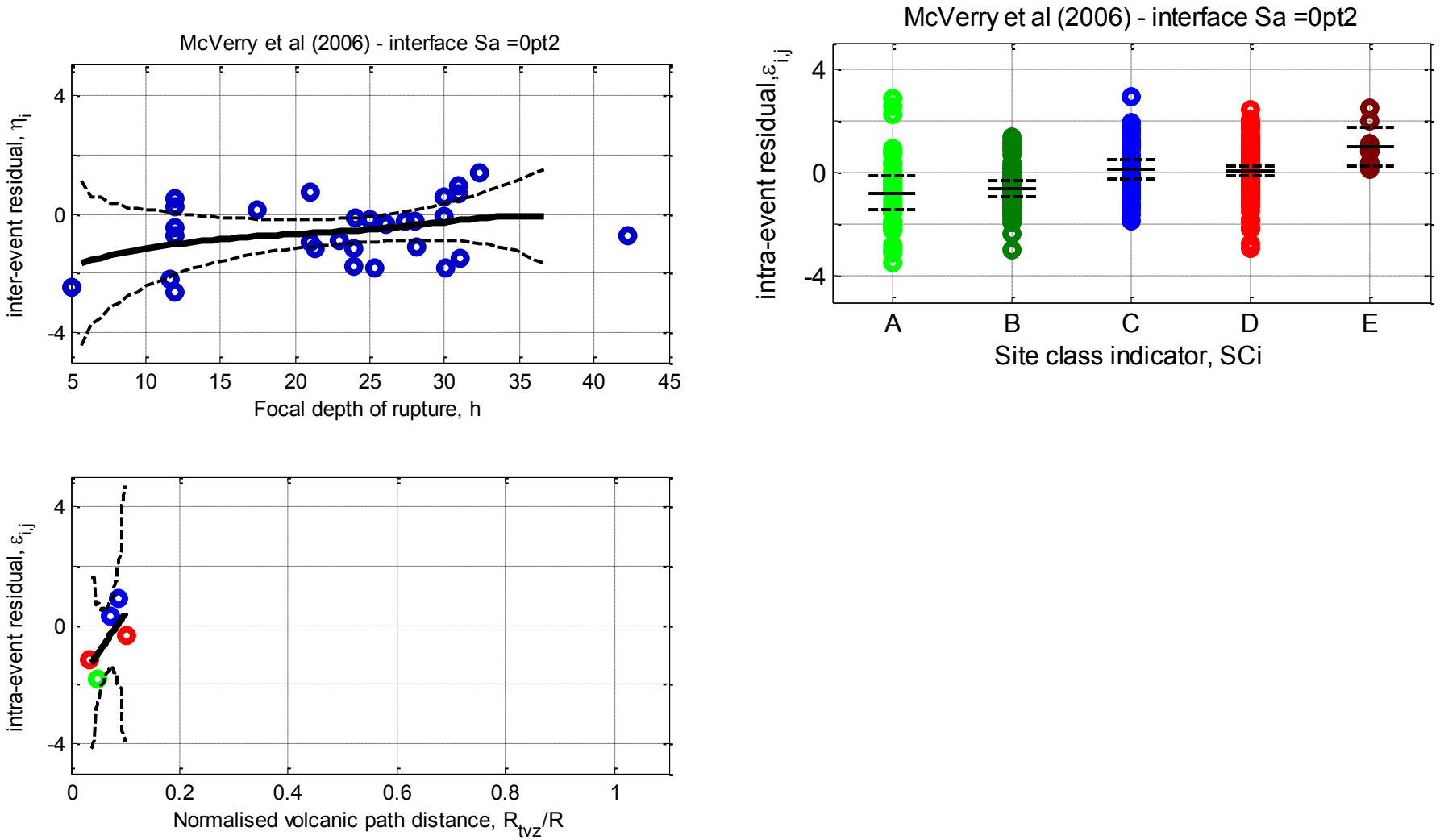

Figure D-52: Residuals for Sa(0.2) using the McVerry et al. (2006) interface model

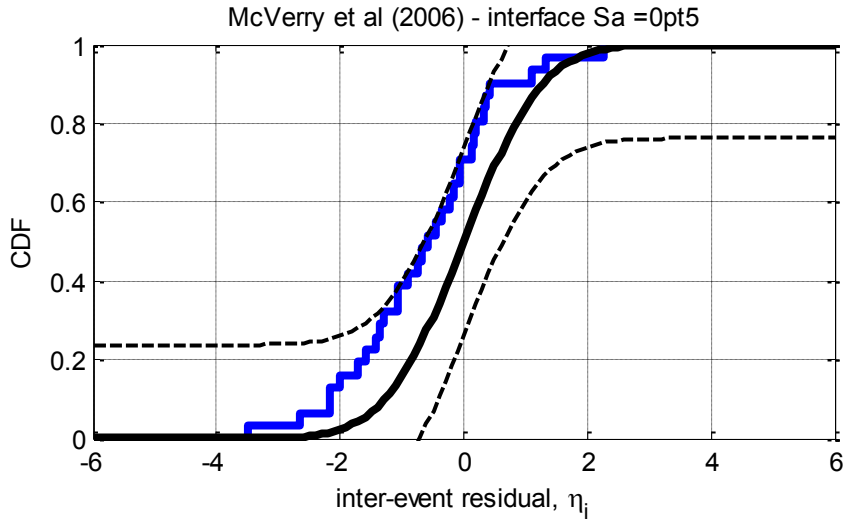
McVerry et al (2006) - interface Sa =0pt5
CDF
inter-event residual, η_i

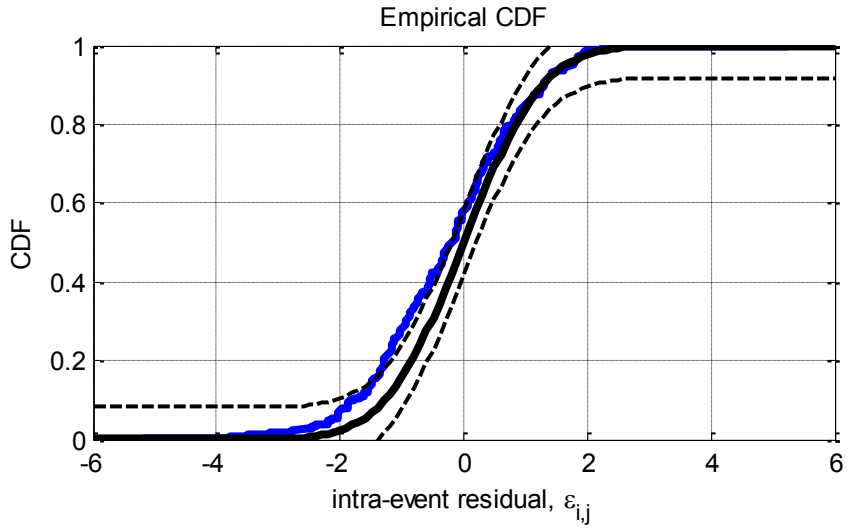
Empirical CDF
CDF
intra-event residual, $\varepsilon_{i,j}$

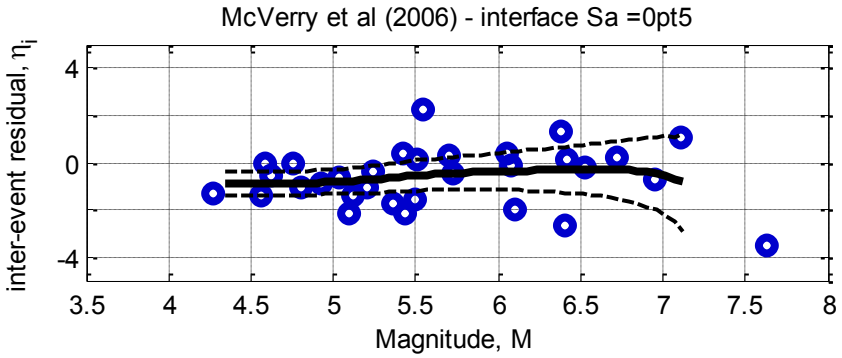
McVerry et al (2006) - interface Sa =0pt5
inter-event residual, η_i
Magnitude, M

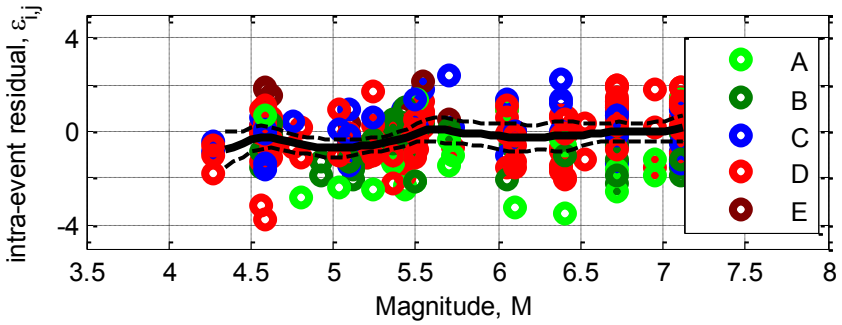
intra-event residual, $\varepsilon_{i,j}$
Magnitude, M
A
B
C
D
E

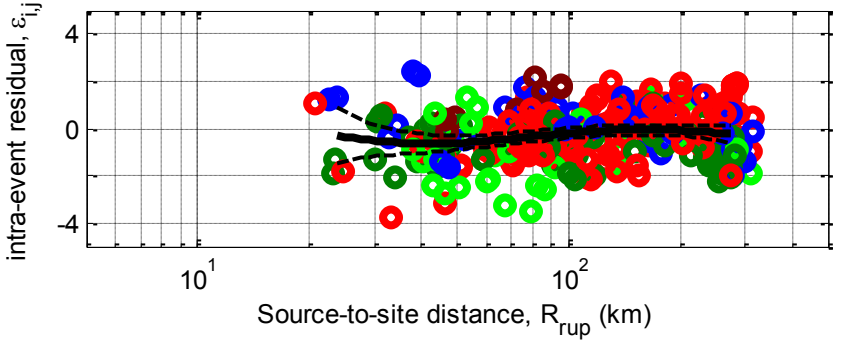
intra-event residual, $\varepsilon_{i,j}$
Source-to-site distance, R_{rup} (km)

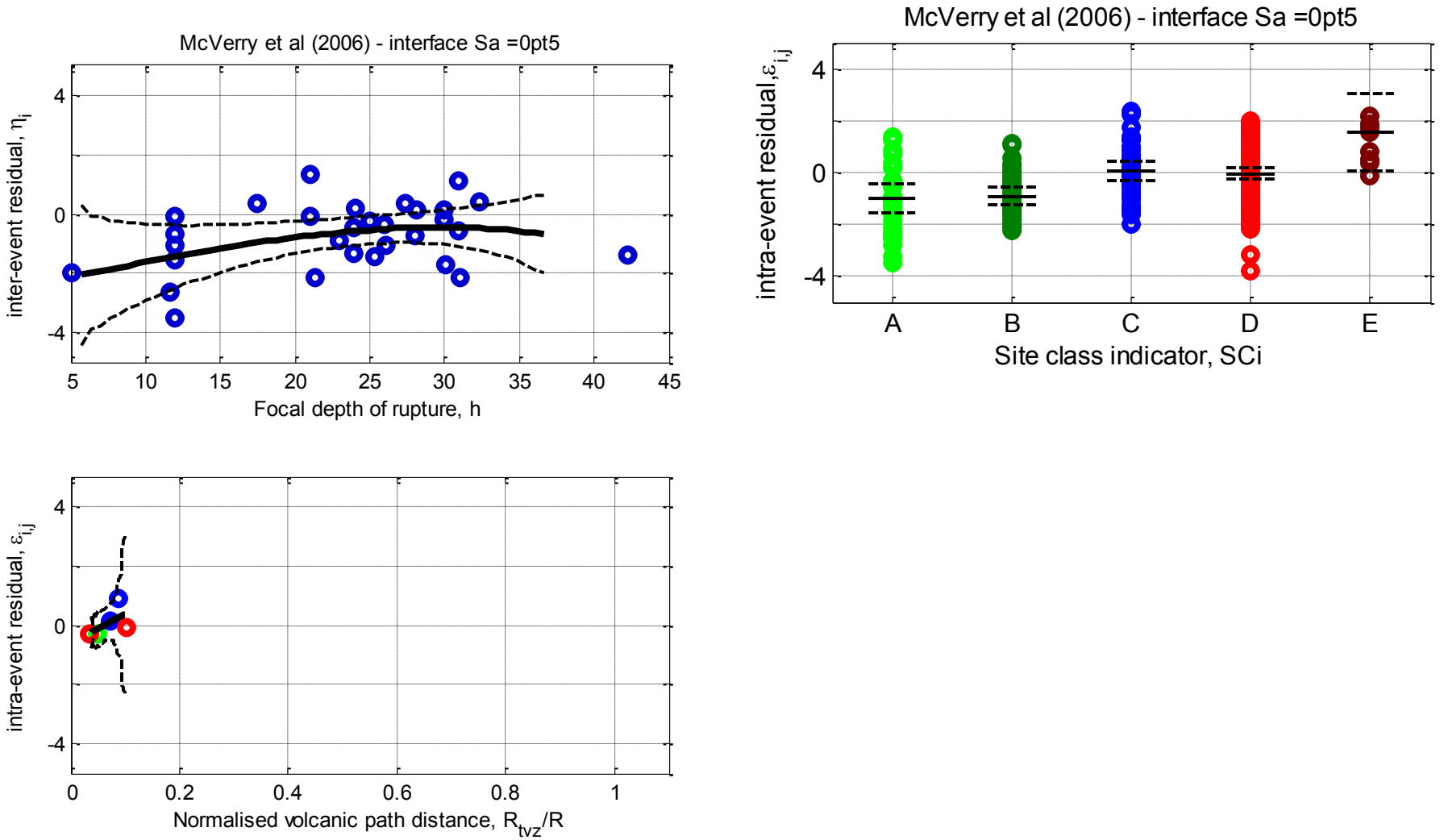

Figure D-53: Residuals for Sa(0.5) using the McVerry et al. (2006) interface model

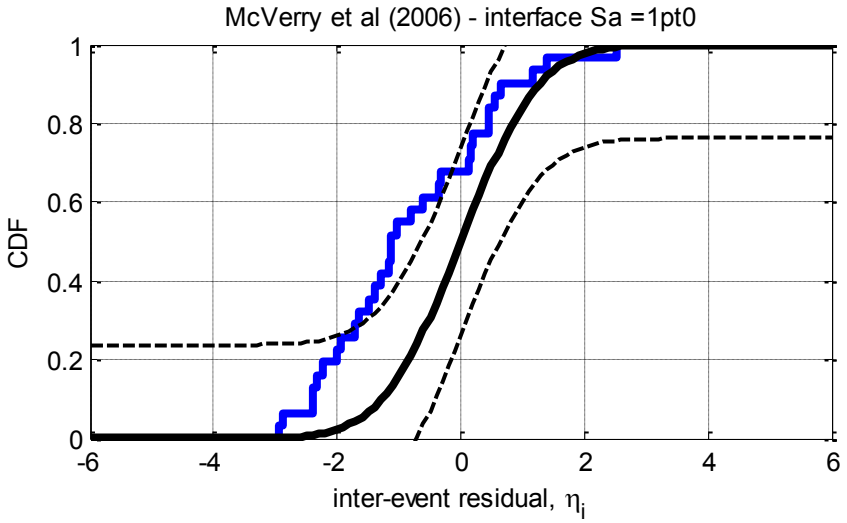
McVerry et al (2006) - interface Sa =1pt0
CDF
inter-event residual, η_i

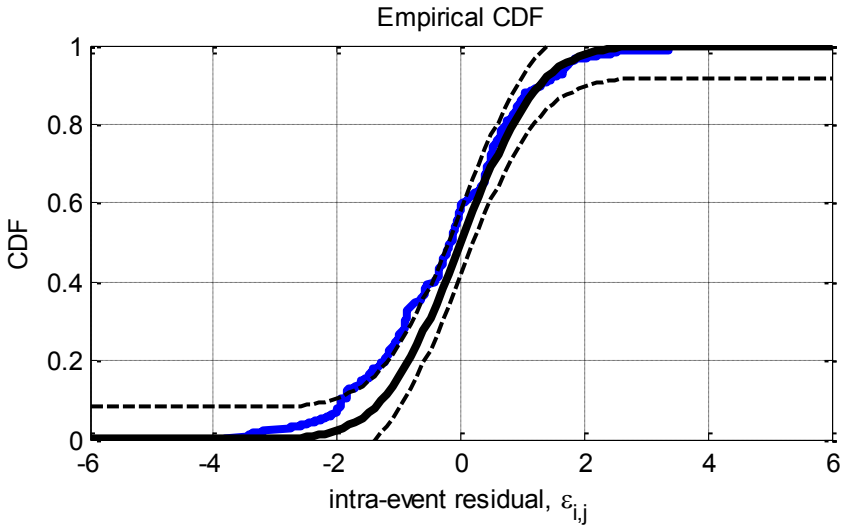
Empirical CDF
CDF
intra-event residual, $\varepsilon_{i,j}$

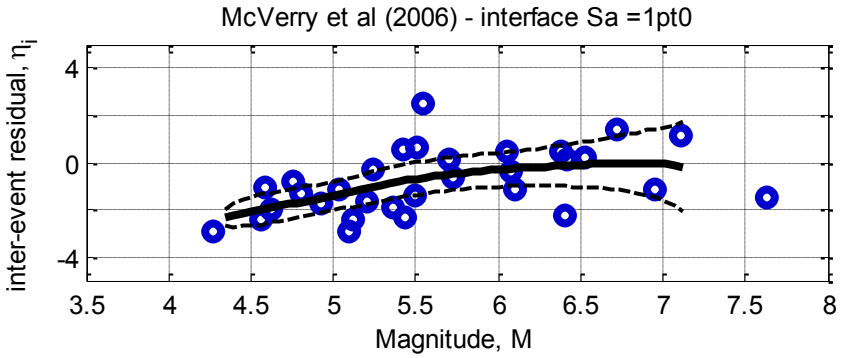
McVerry et al (2006) - interface Sa =1pt0
inter-event residual, η_i
Magnitude, M

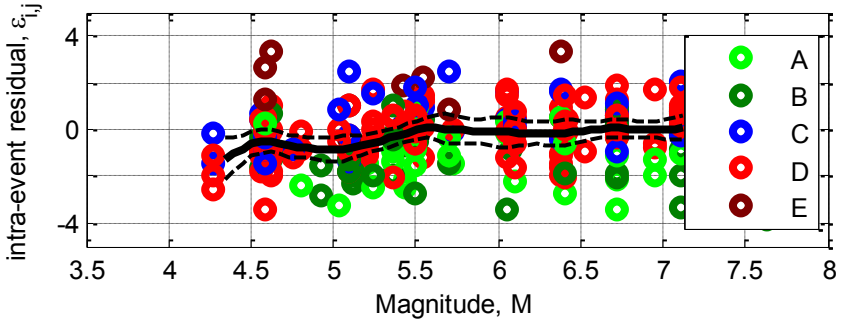
intra-event residual, $\varepsilon_{i,j}$
Magnitude, M
A
B
C
D
E

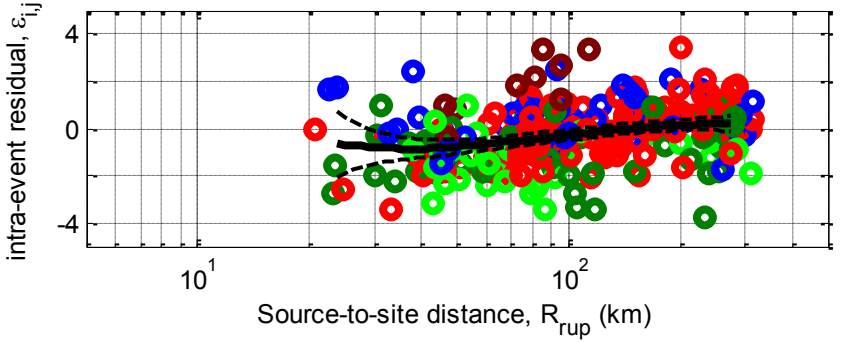
intra-event residual, $\varepsilon_{i,j}$
Source-to-site distance, R_{rup} (km)

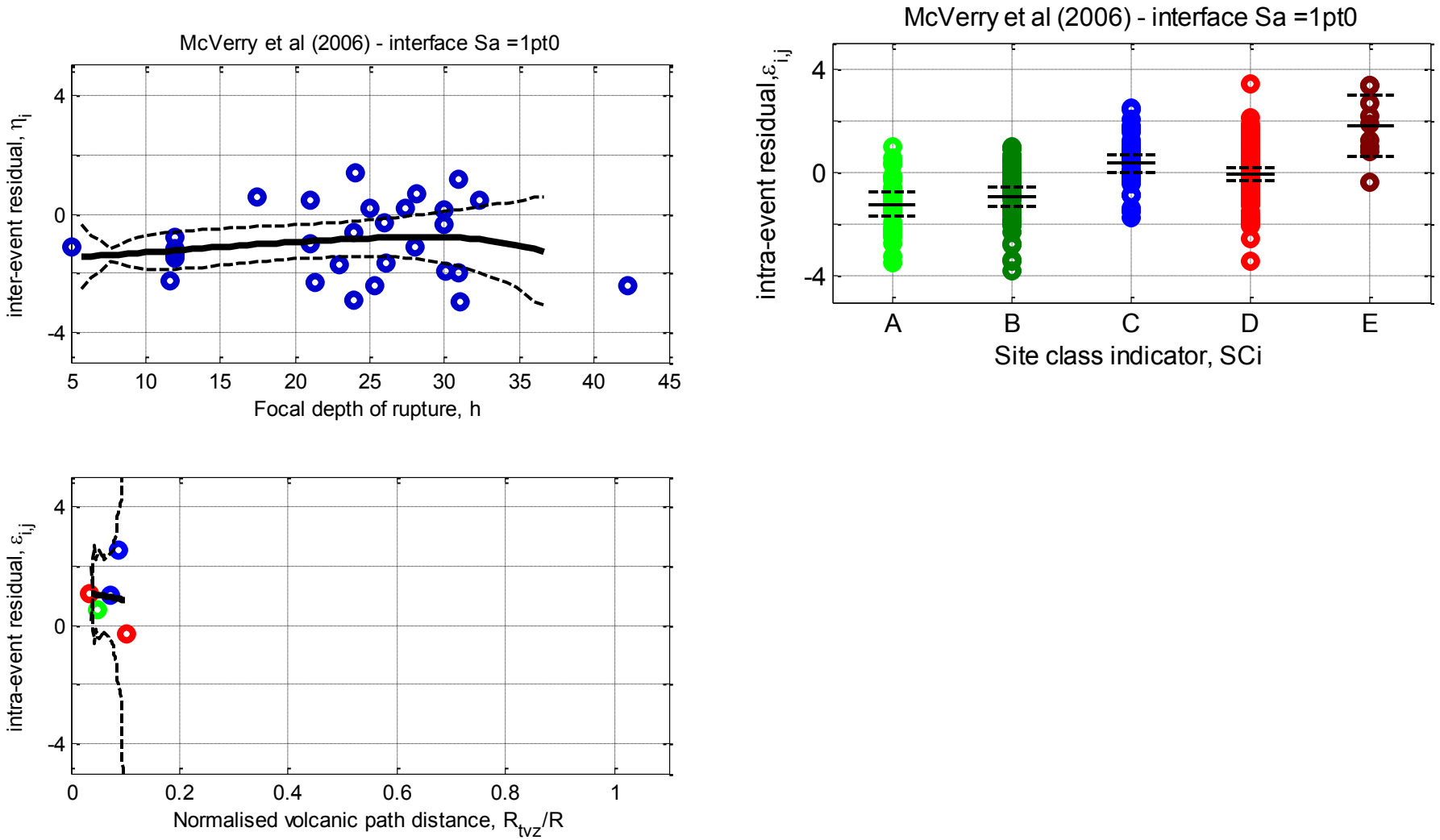

Figure D-54: Residuals for Sa(1.0) using the McVerry et al. (2006) interface model

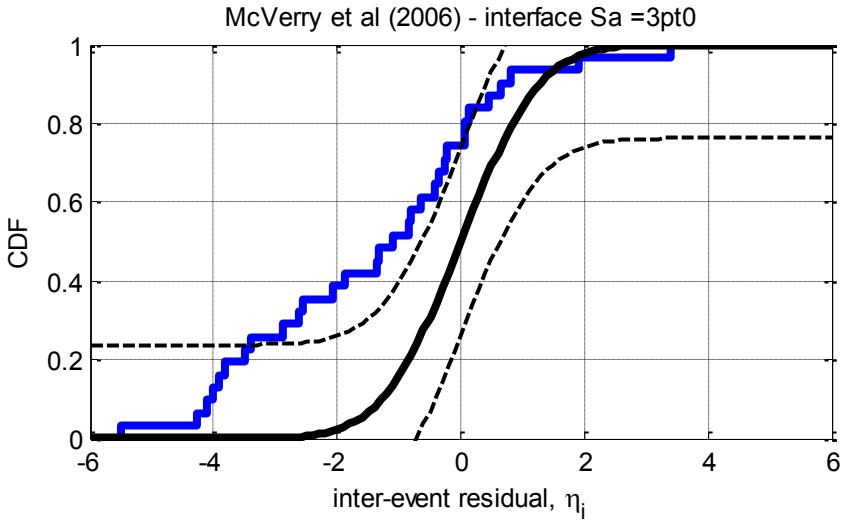
McVerry et al (2006) - interface Sa =3pt0
CDF
inter-event residual, η_i

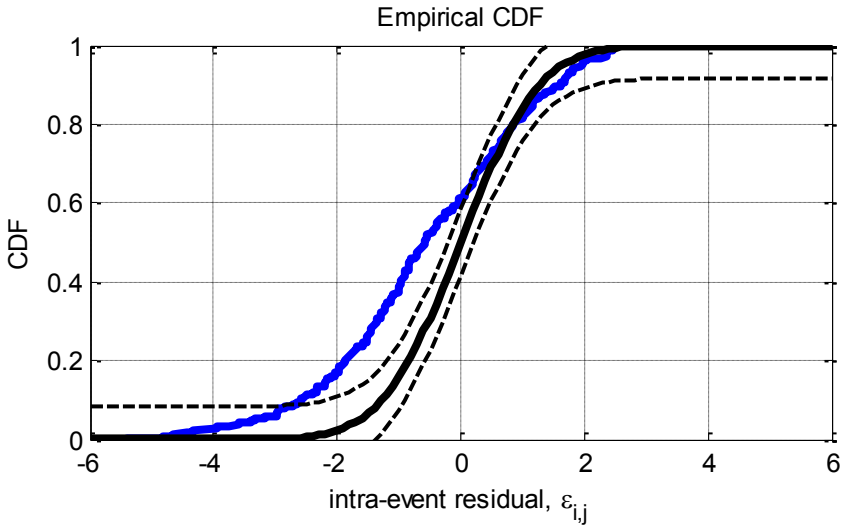
Empirical CDF
CDF
intra-event residual, $\varepsilon_{i,j}$

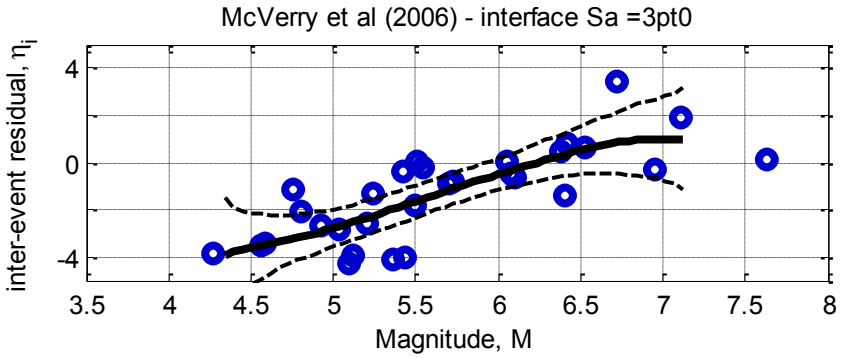
McVerry et al (2006) - interface Sa =3pt0
inter-event residual, η_i
Magnitude, M

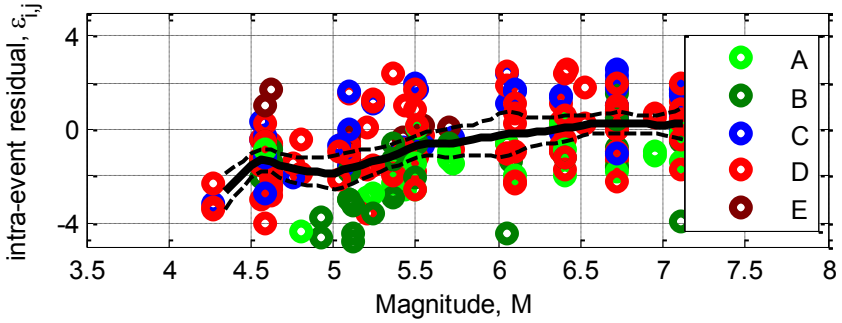
intra-event residual, $\varepsilon_{i,j}$
Magnitude, M
A
B
C
D
E

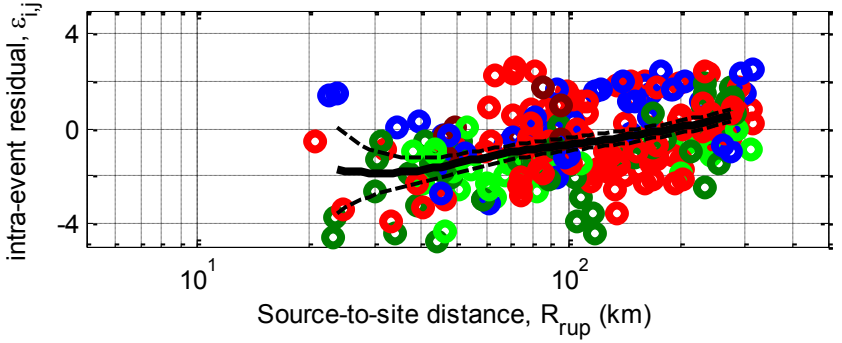
intra-event residual, $\varepsilon_{i,j}$
Source-to-site distance, R_{rup} (km)

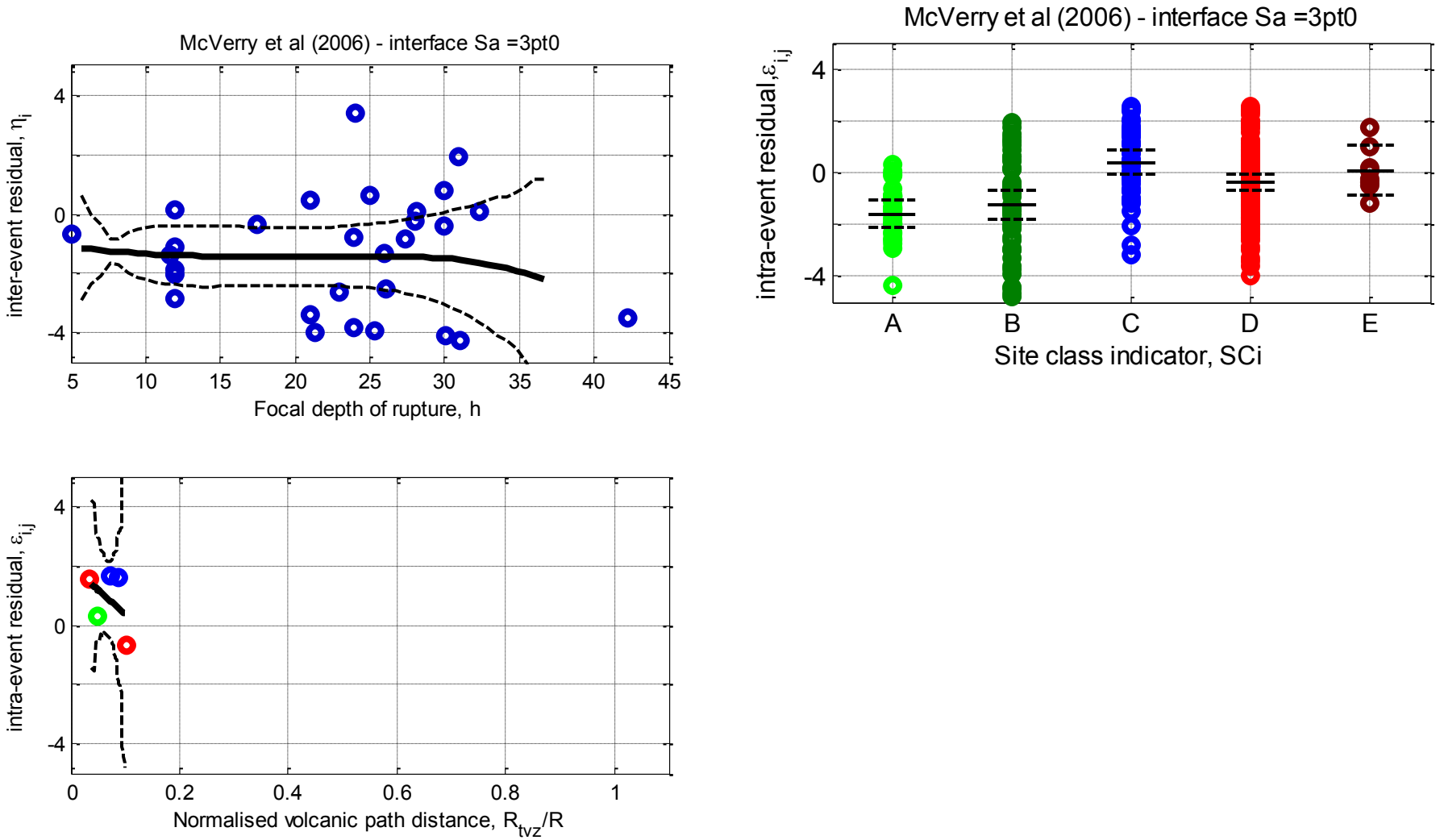

Figure D-55: Residuals for Sa(3.0) using the McVerry et al. (2006) interface model

D.12. Zhao et al. (2006) Interface model

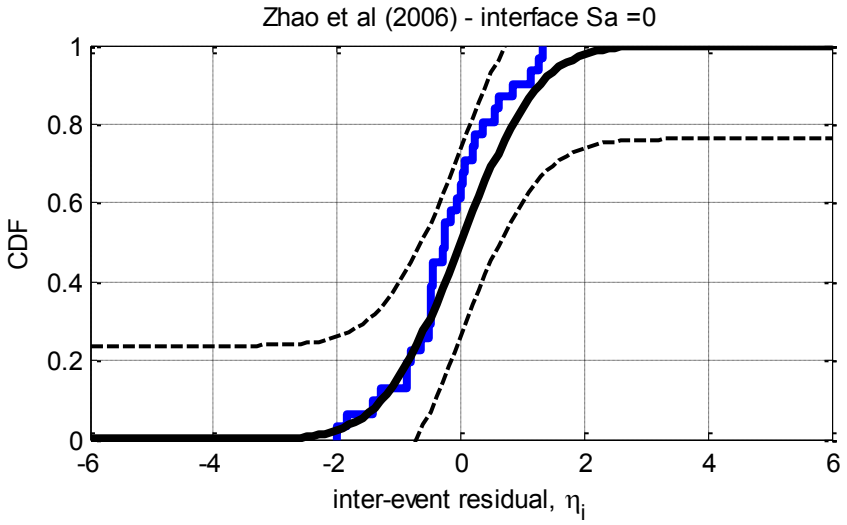

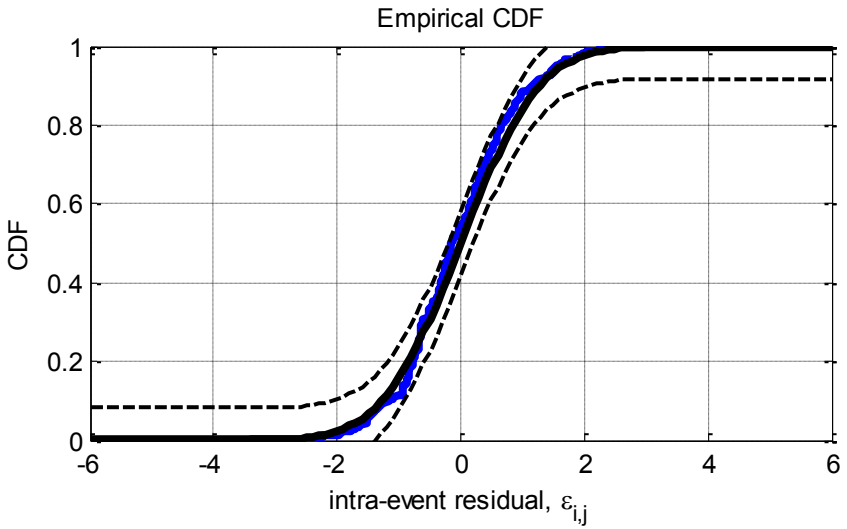

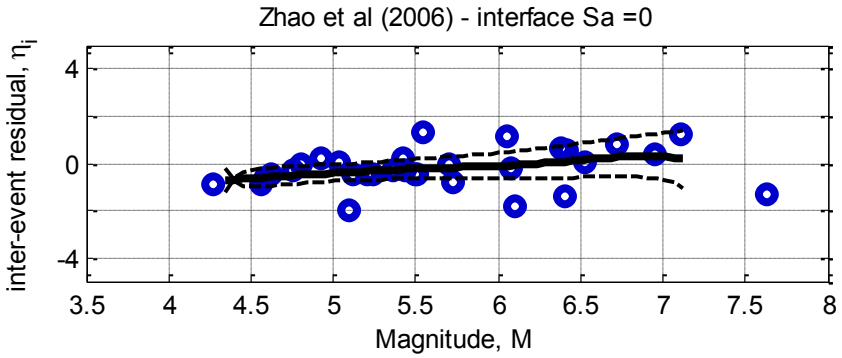

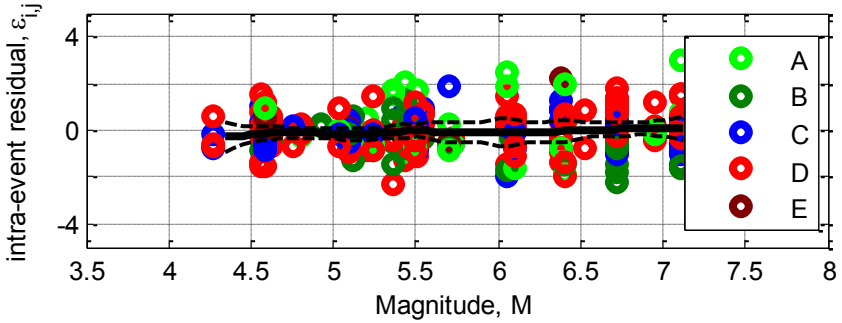

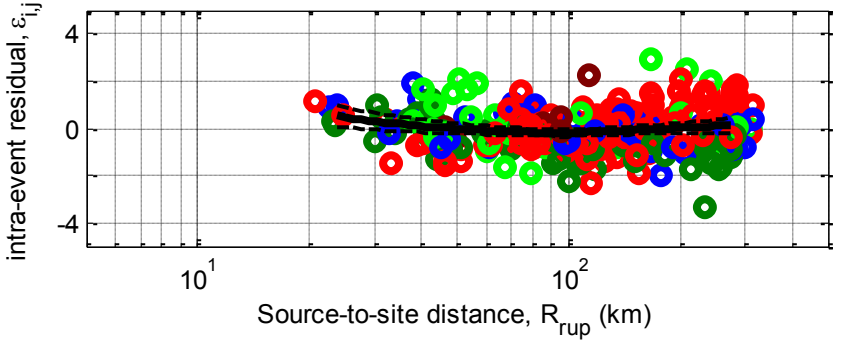

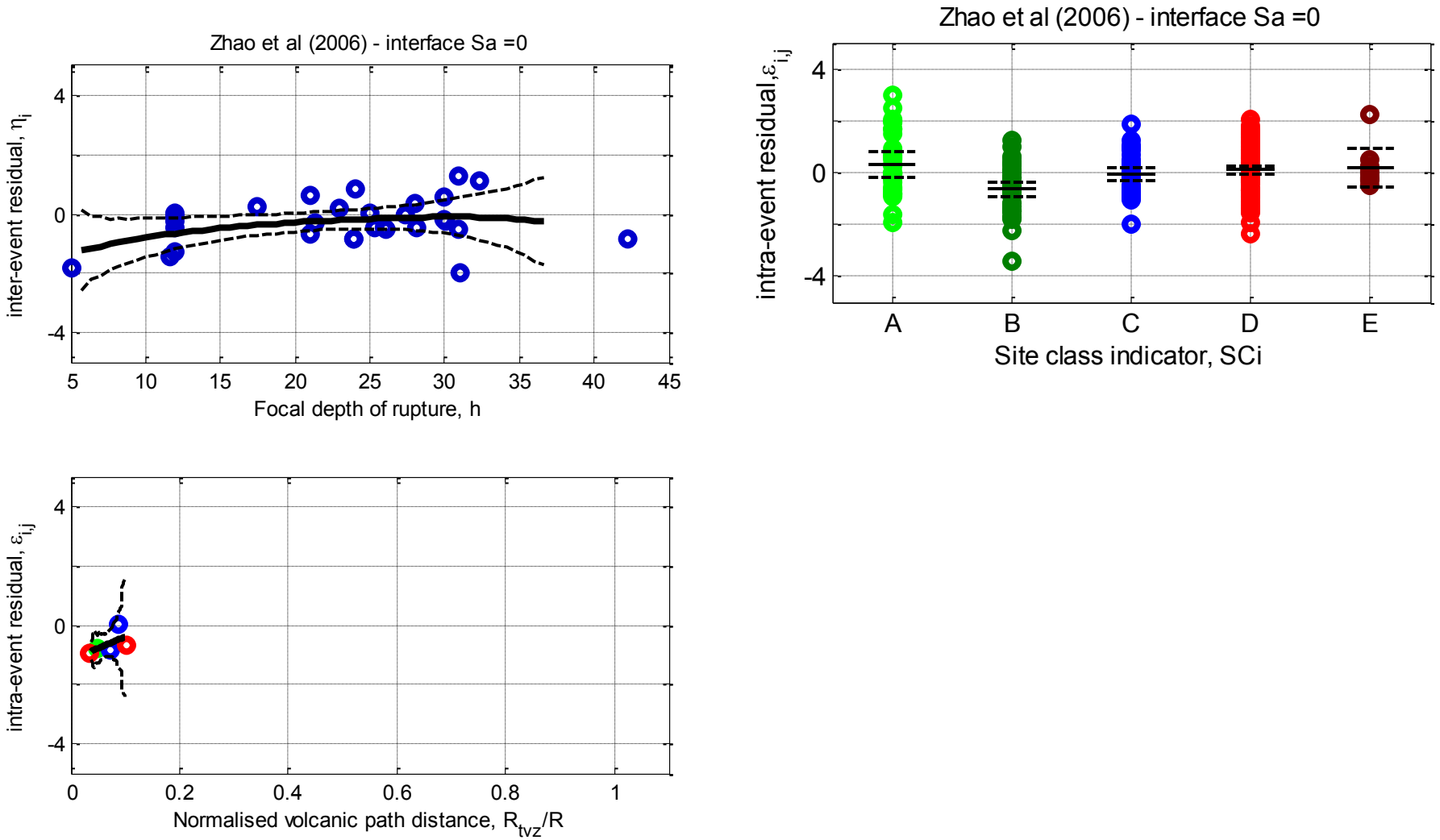

Figure D-56: Residuals for Sa(0.0) using the Zhao et al. (2006) interface model

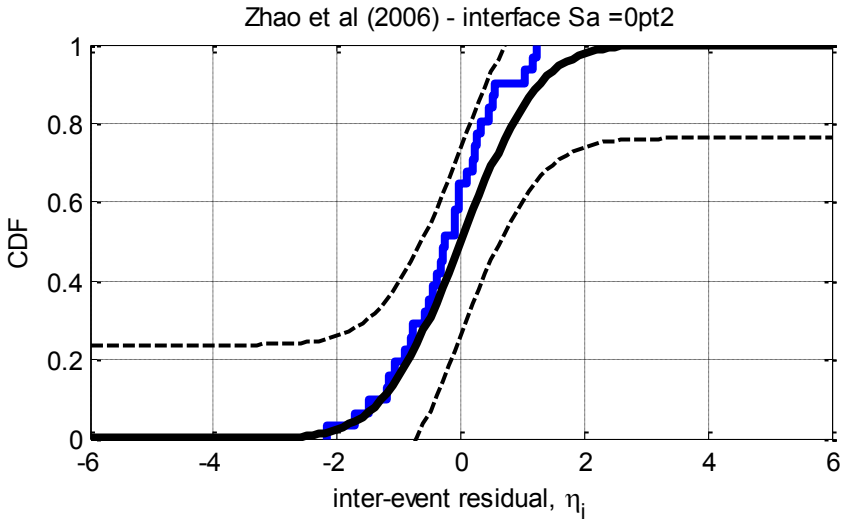
Zhao et al (2006) - interface Sa =0pt2
CDF
inter-event residual, η_i

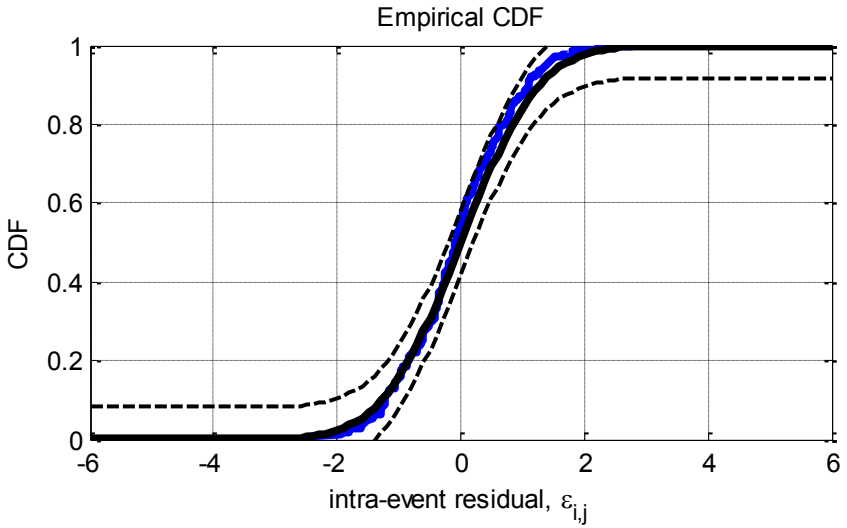
Empirical CDF
CDF
intra-event residual, $\varepsilon_{i,j}$

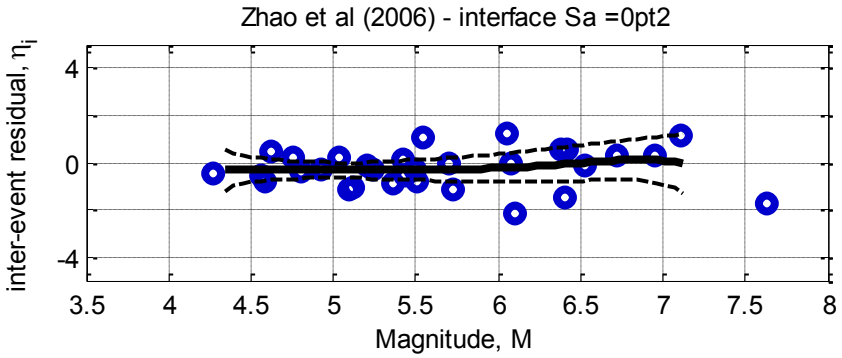
Zhao et al (2006) - interface Sa =0pt2
inter-event residual, η_i
Magnitude, M

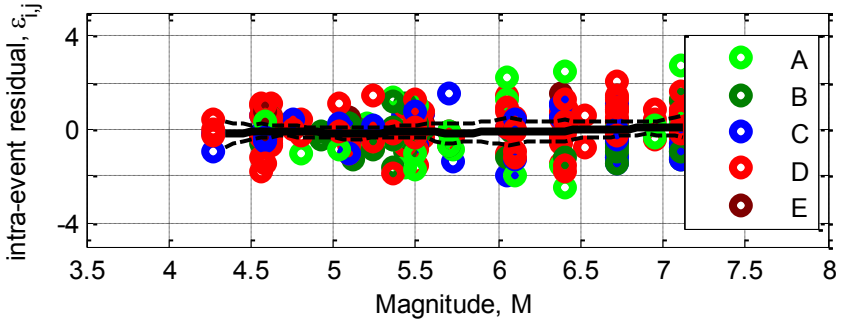
intra-event residual, $\varepsilon_{i,j}$
Magnitude, M
A
B
C
D
E

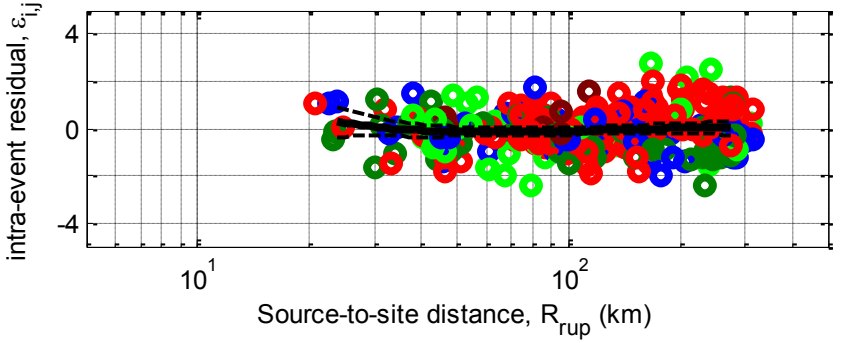
intra-event residual, $\varepsilon_{i,j}$
Source-to-site distance, R_{rup} (km)

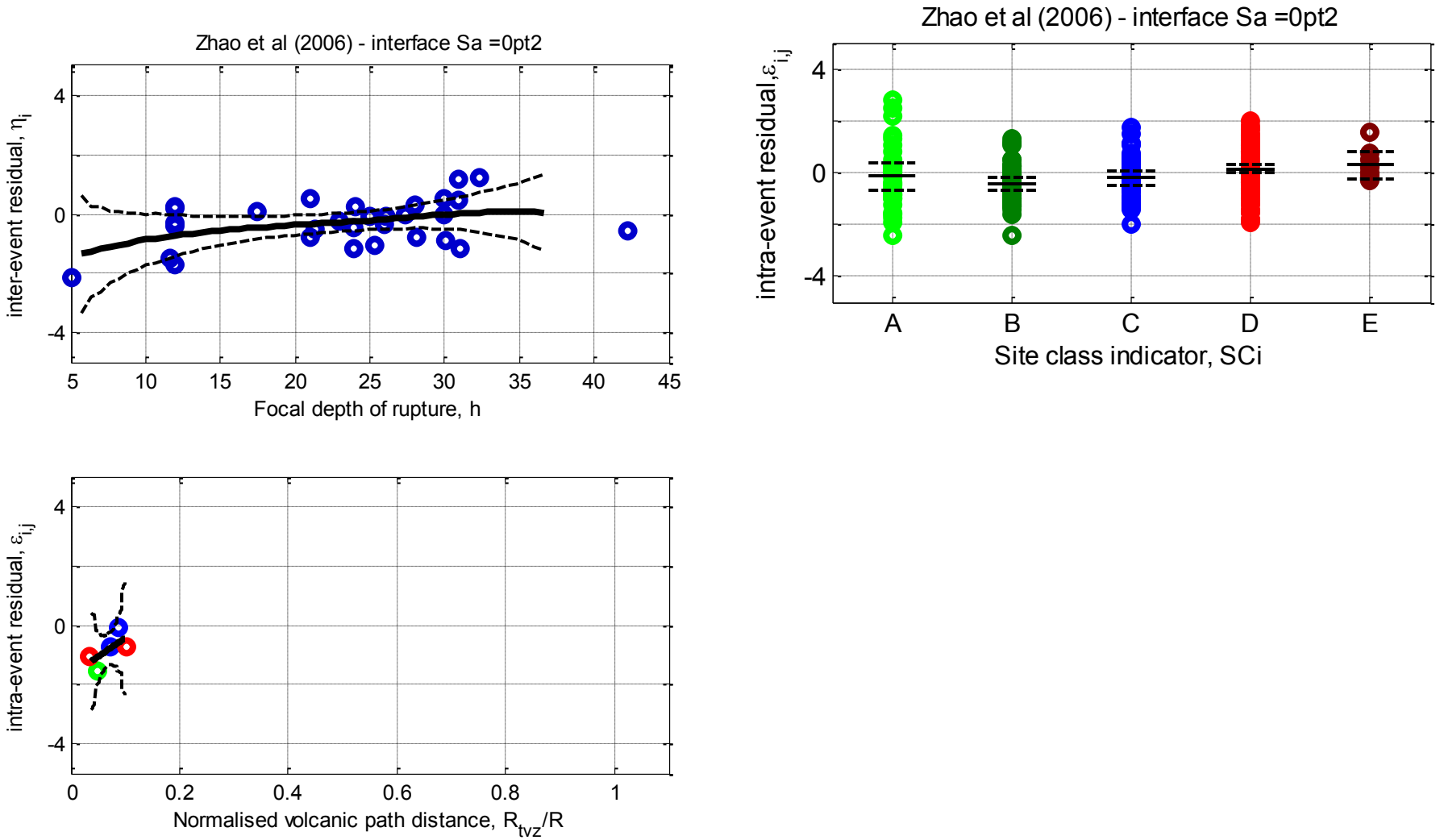

Figure D-57: Residuals for Sa(0.2) using the Zhao et al. (2006) interface model

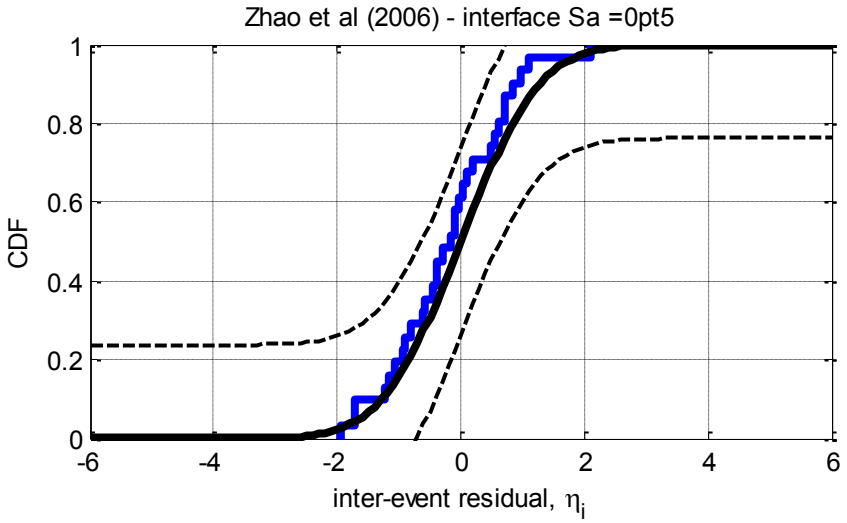
Zhao et al (2006) - interface Sa =0pt5
CDF
inter-event residual, η_i

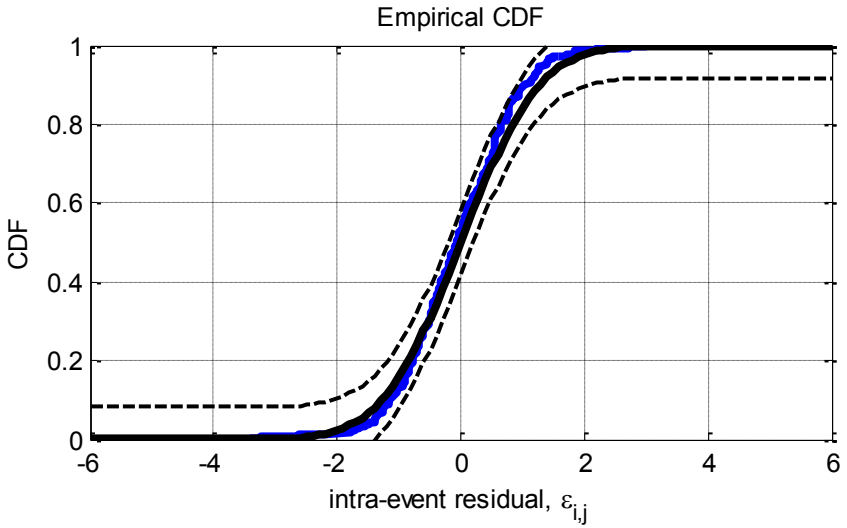
Empirical CDF
CDF
intra-event residual, $\varepsilon_{i,j}$

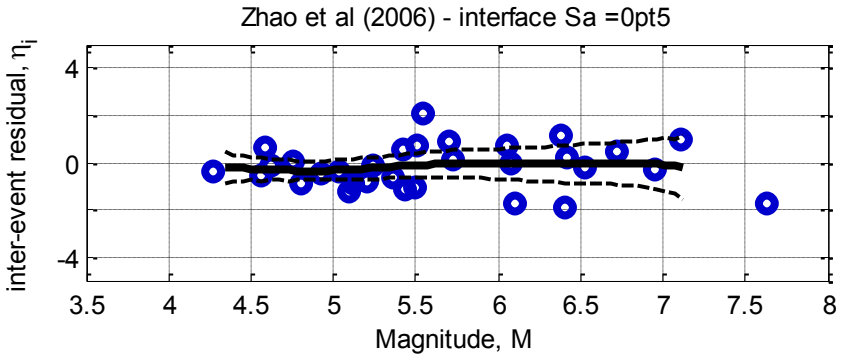
Zhao et al (2006) - interface Sa =0pt5
inter-event residual, η_i
Magnitude, M

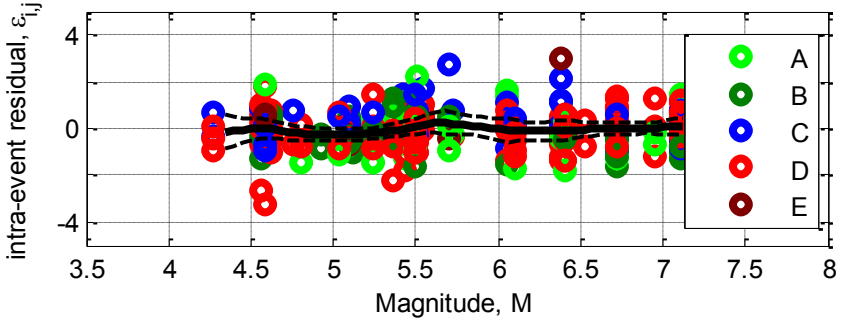
intra-event residual, $\varepsilon_{i,j}$
Magnitude, M
A
B
C
D
E

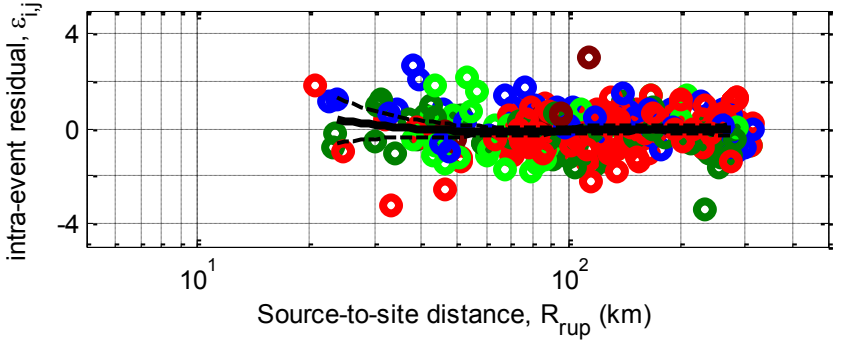
intra-event residual, $\varepsilon_{i,j}$
Source-to-site distance, R_{rup} (km)

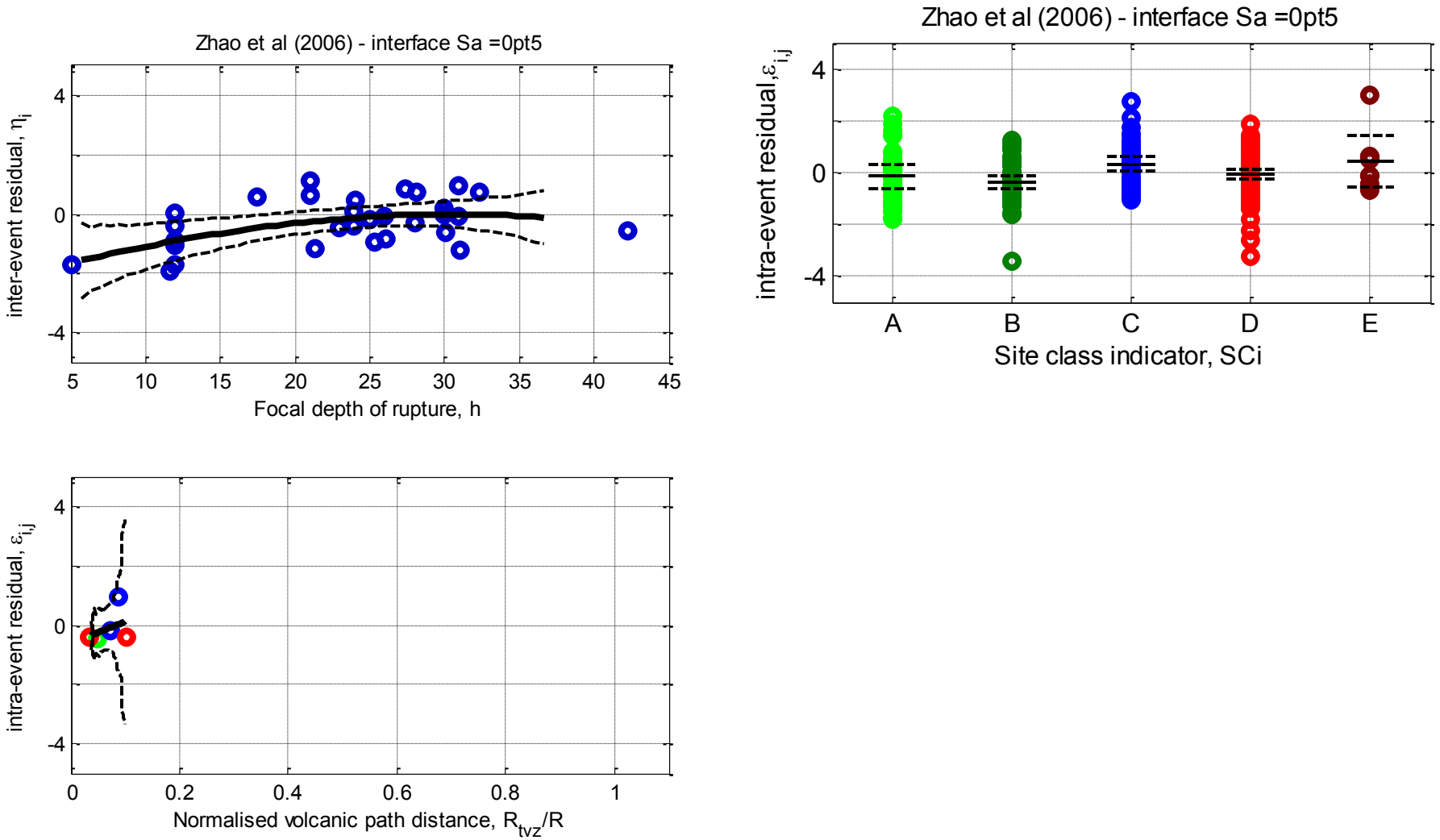

Figure D-58: Residuals for Sa(0.5) using the Zhao et al. (2006) interface model

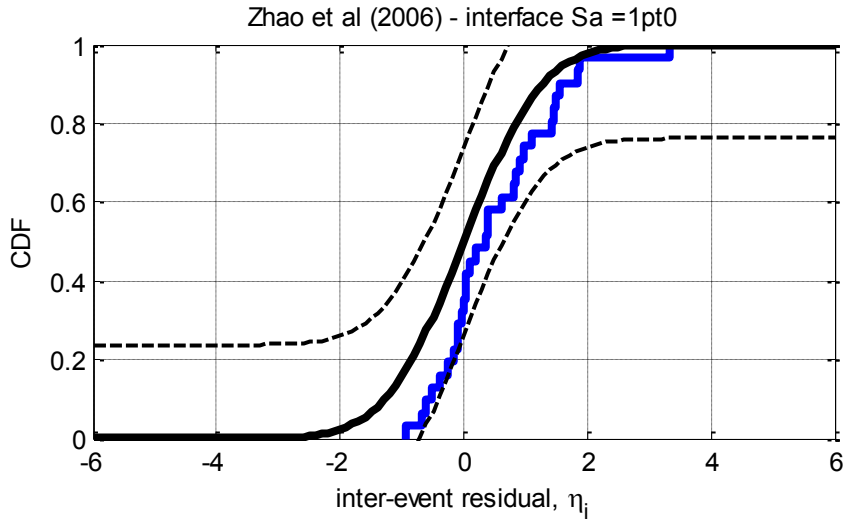
Zhao et al (2006) - interface Sa =1pt0
CDF
inter-event residual, η_i

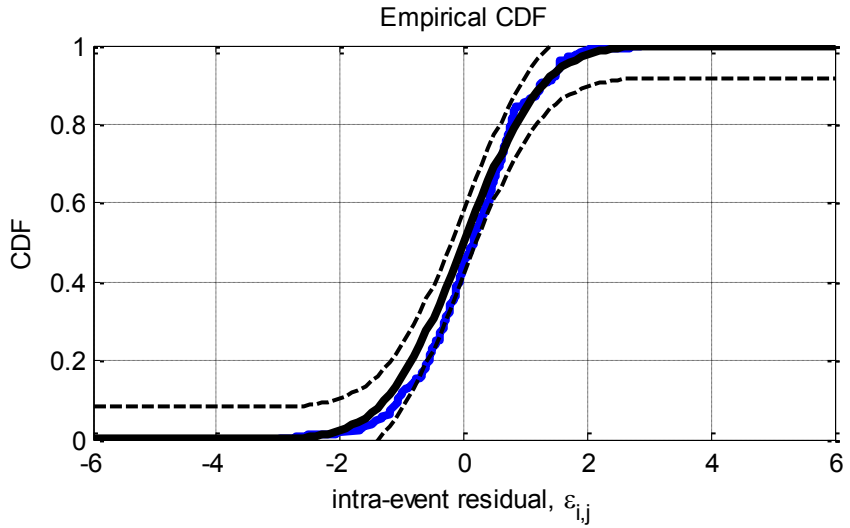
Empirical CDF
CDF
intra-event residual, $\varepsilon_{i,j}$

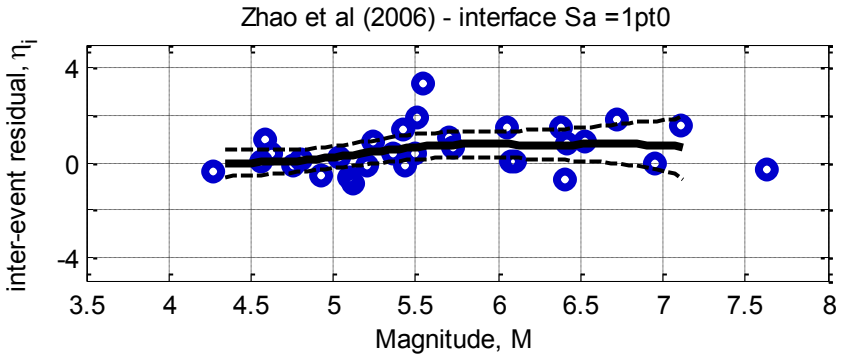
Zhao et al (2006) - interface Sa =1pt0
inter-event residual, η_i
Magnitude, M

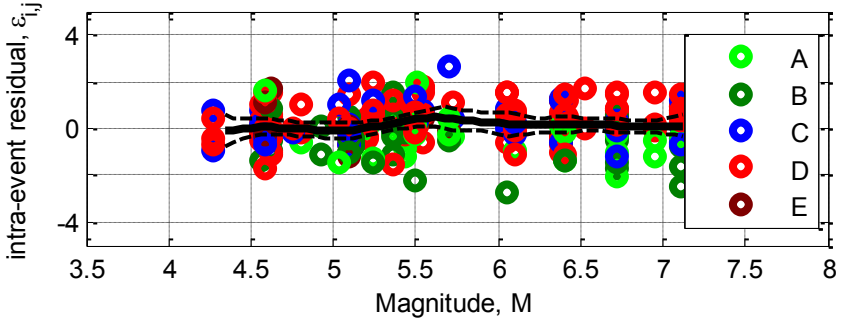
intra-event residual, $\varepsilon_{i,j}$
A
B
C
D
E
Magnitude, M

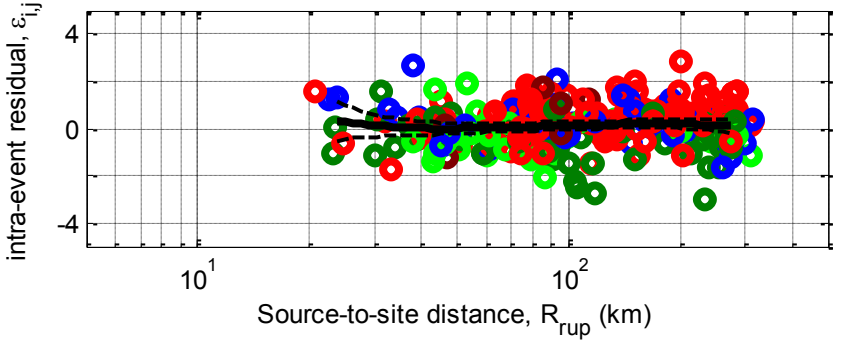
intra-event residual, $\varepsilon_{i,j}$
Source-to-site distance, R_{rup} (km)

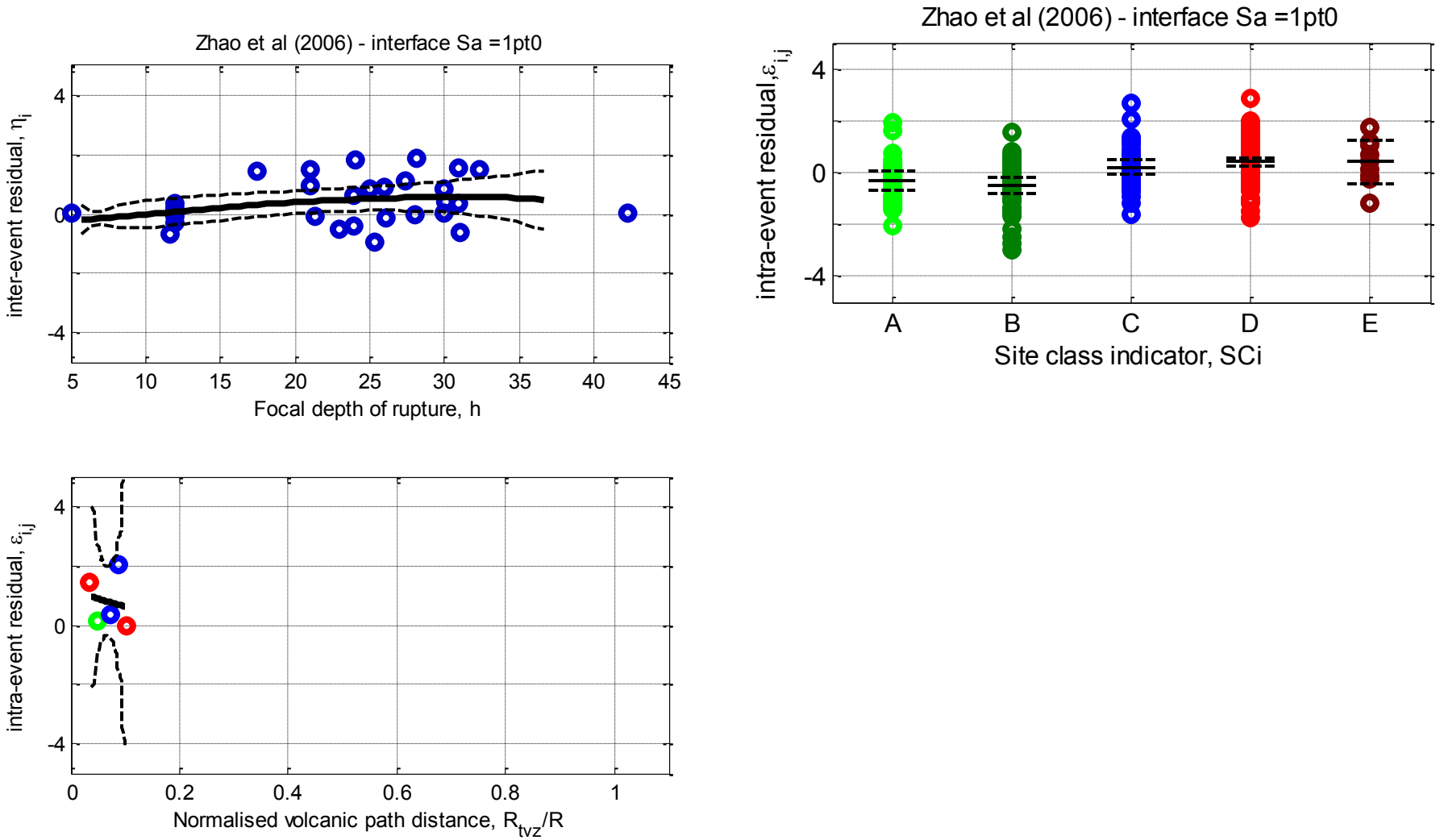

Figure D-59: Residuals for Sa(1.0) using the Zhao et al. (2006) interface model

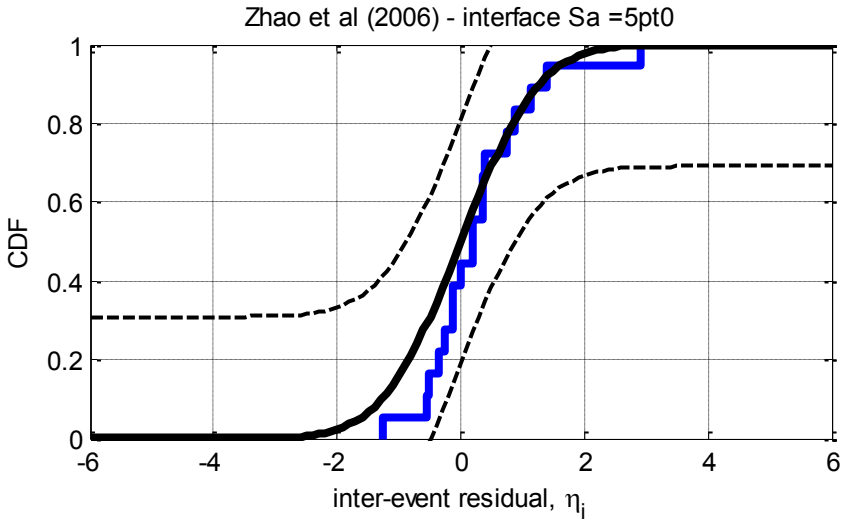
Zhao et al (2006) - interface Sa =5pt0
CDF
inter-event residual, η_i

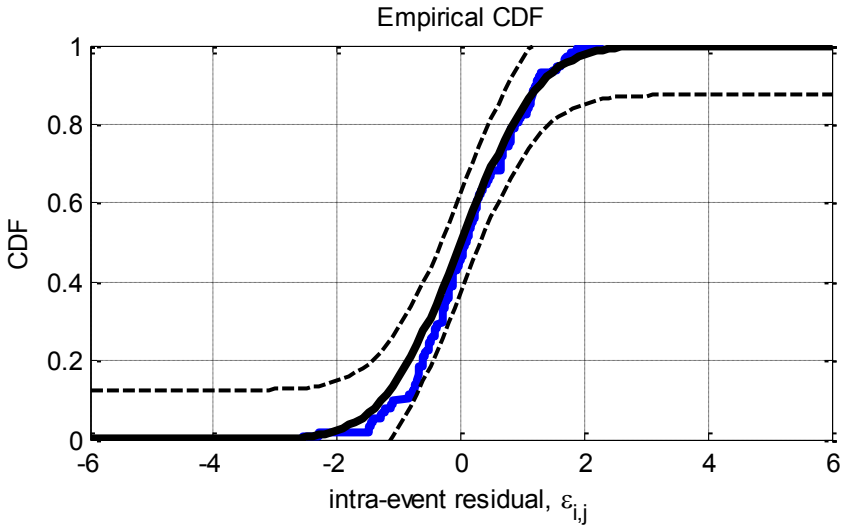
Empirical CDF
CDF
intra-event residual, $\varepsilon_{i,j}$

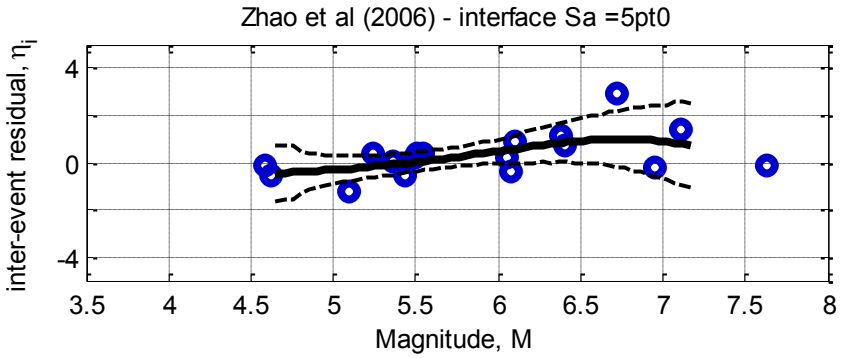
Zhao et al (2006) - interface Sa =5pt0
inter-event residual, η_i
Magnitude, M

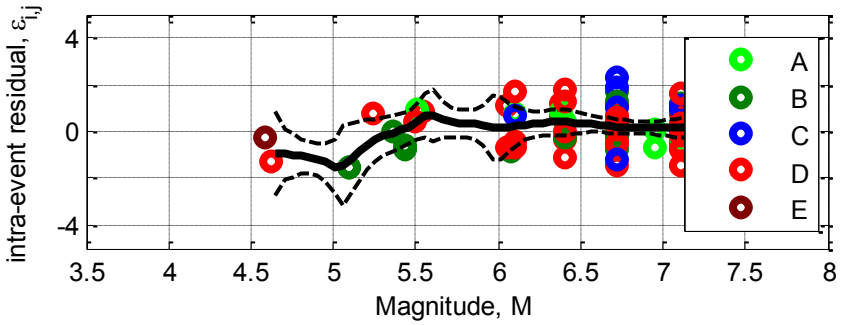
intra-event residual, $\varepsilon_{i,j}$
Magnitude, M
A
B
C
D
E

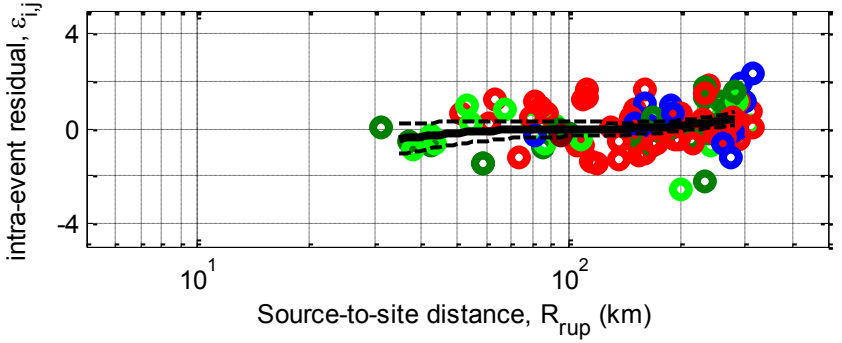
intra-event residual, $\varepsilon_{i,j}$
Source-to-site distance, R_{rup} (km)

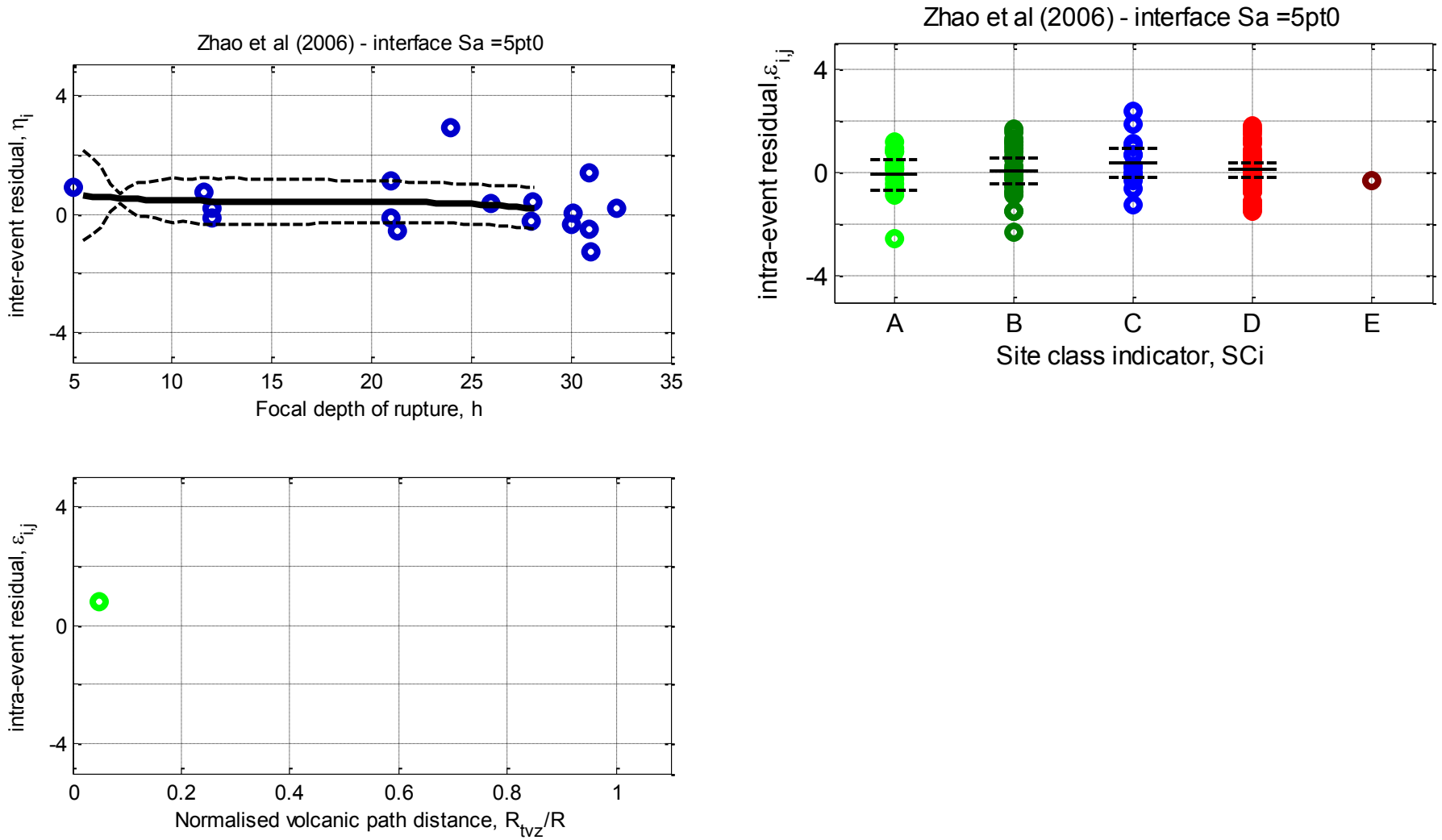

Figure D-60: Residuals for Sa(5.0) using the Zhao et al. (2006) interface model

D.13. Atkinson and Boore (2003) Interface model

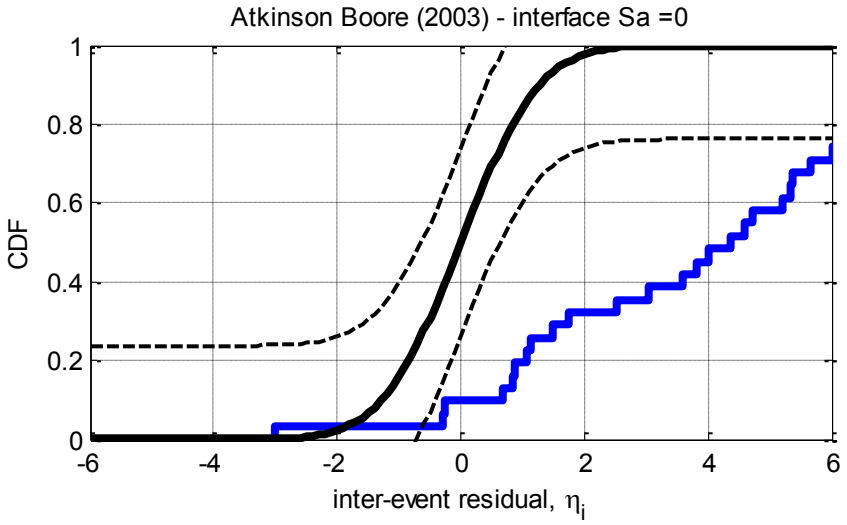

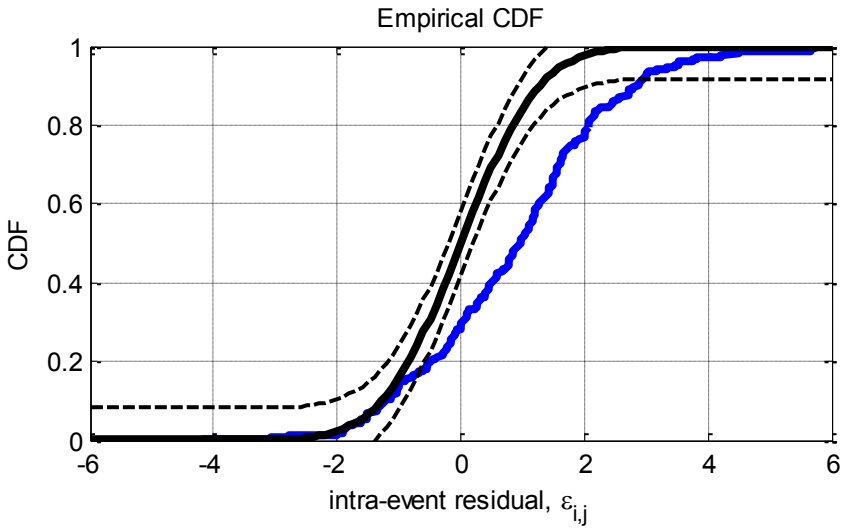

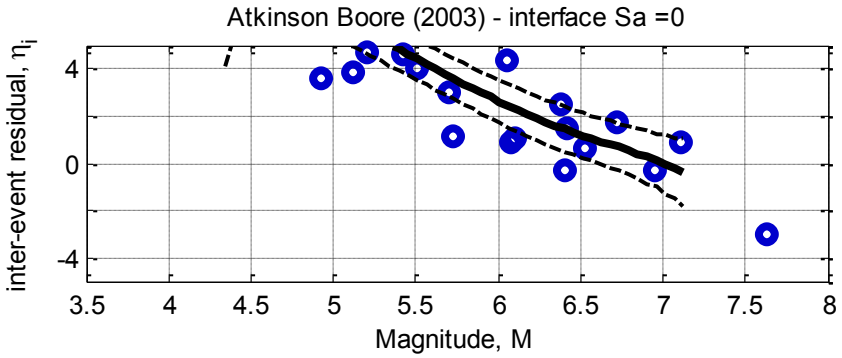

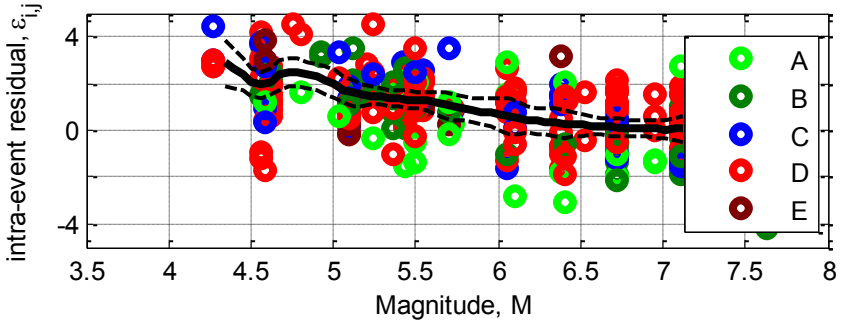

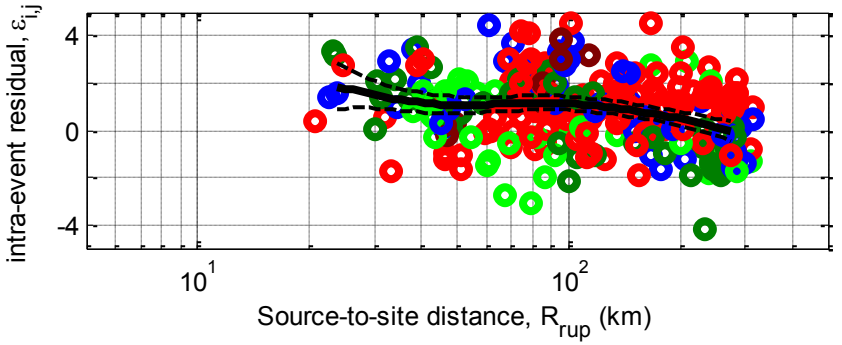

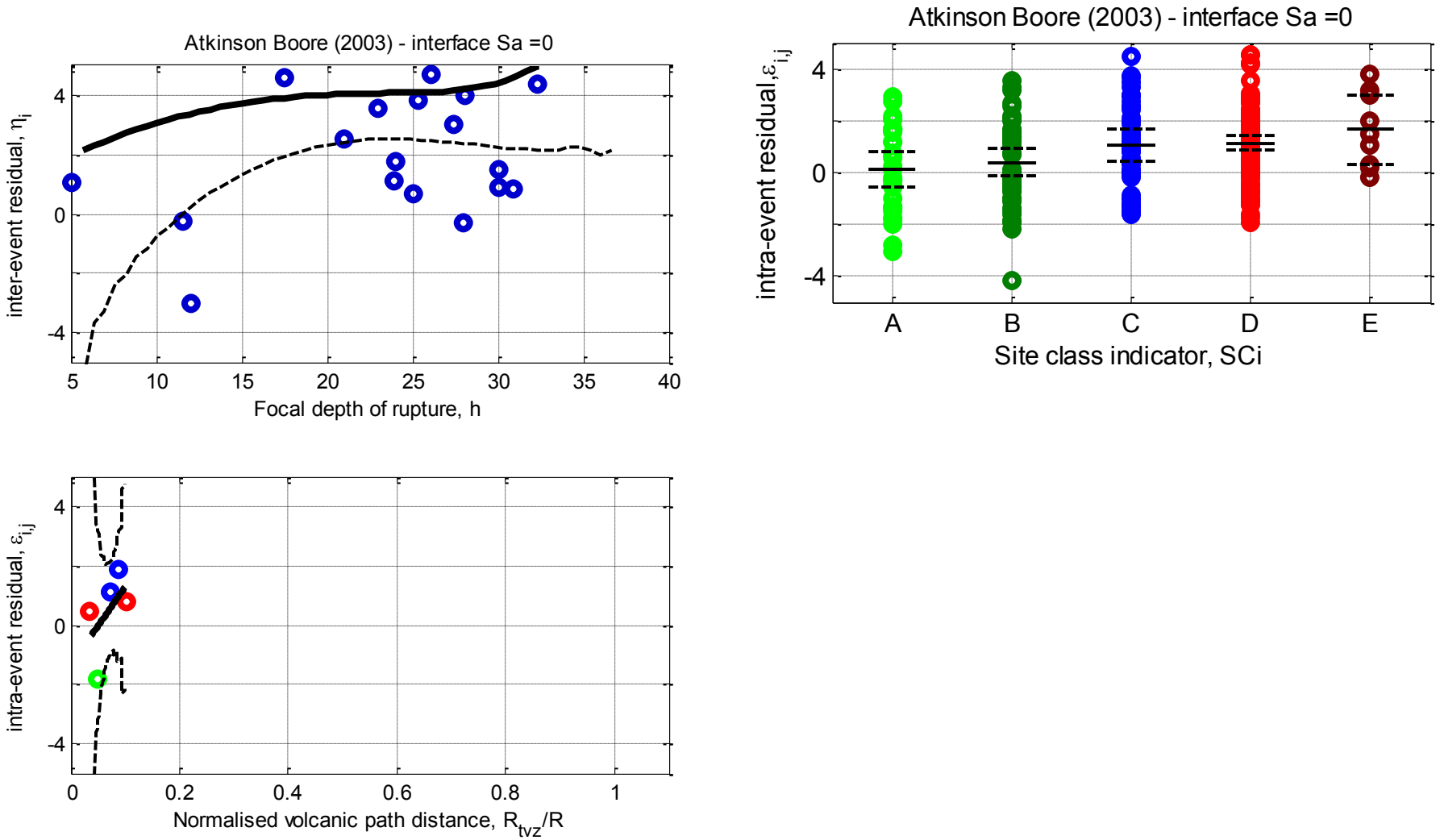

Figure D-61: Residuals for Sa(0.0) using the Atkinson and Boore (2003) interface model

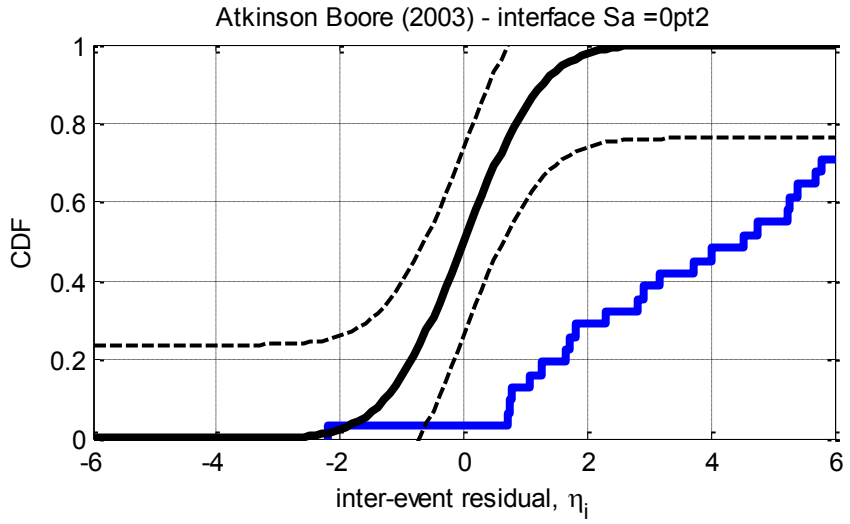
Atkinson Boore (2003) - interface Sa =0pt2
CDF
inter-event residual, η_i

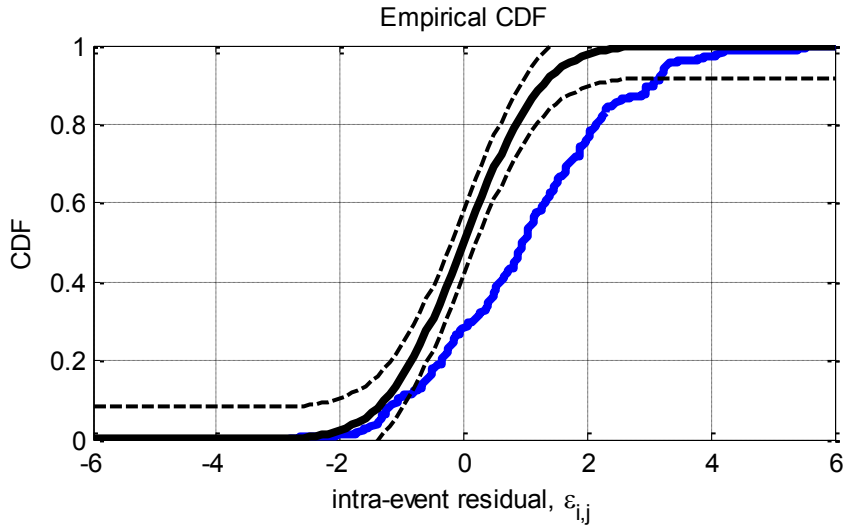
Empirical CDF
CDF
intra-event residual, $\varepsilon_{i,j}$

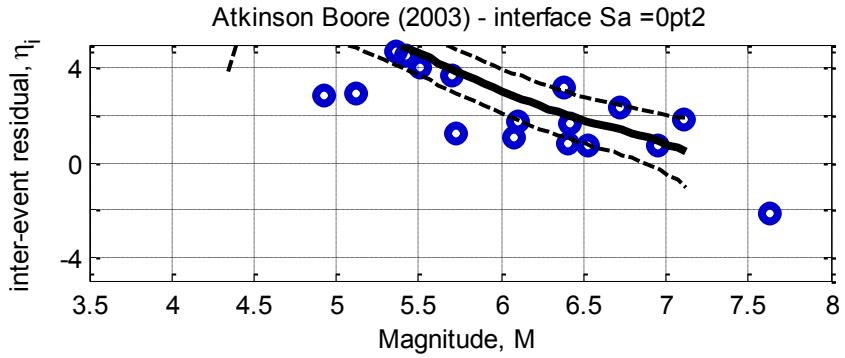
Atkinson Boore (2003) - interface Sa =0pt2
inter-event residual, η_i
Magnitude, M

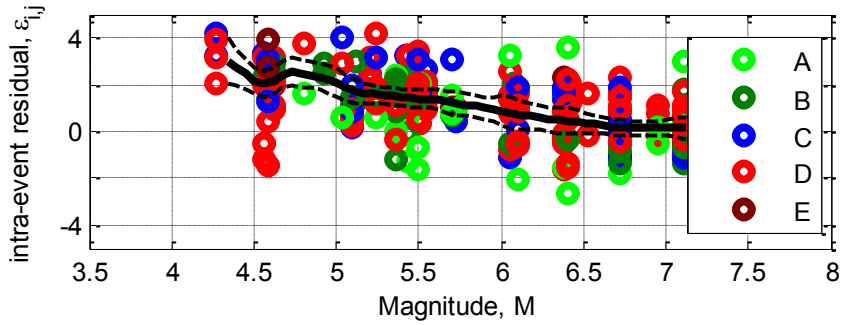
intra-event residual, $\varepsilon_{i,j}$
A
B
C
D
E
Magnitude, M

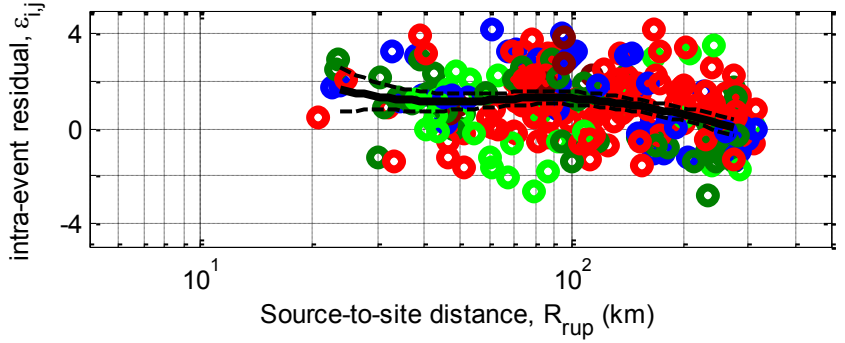
intra-event residual, $\varepsilon_{i,j}$
Source-to-site distance, R_{rup} (km)

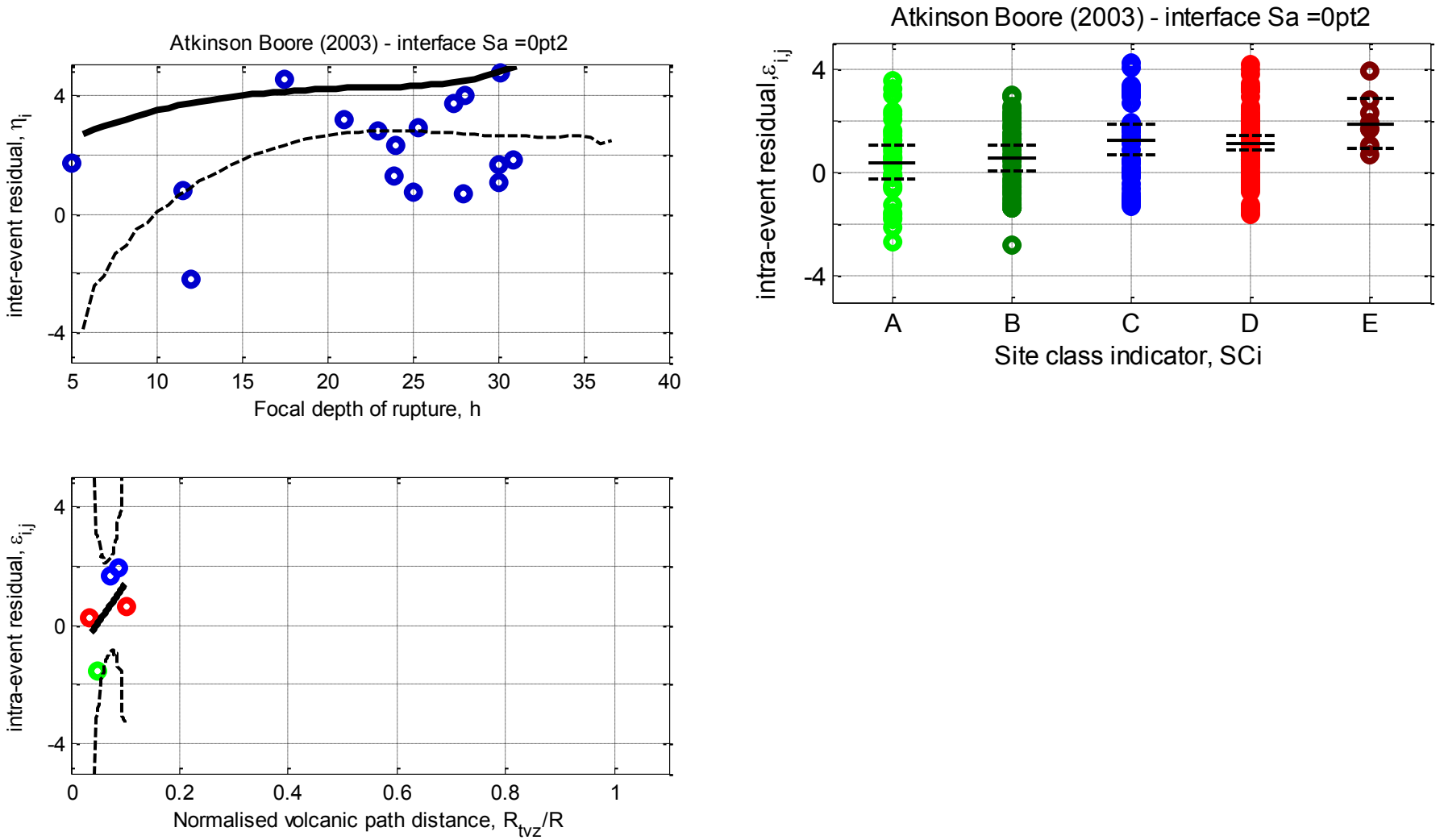

Figure D-62: Residuals for Sa(0.2) using the Atkinson and Boore (2003) interface model

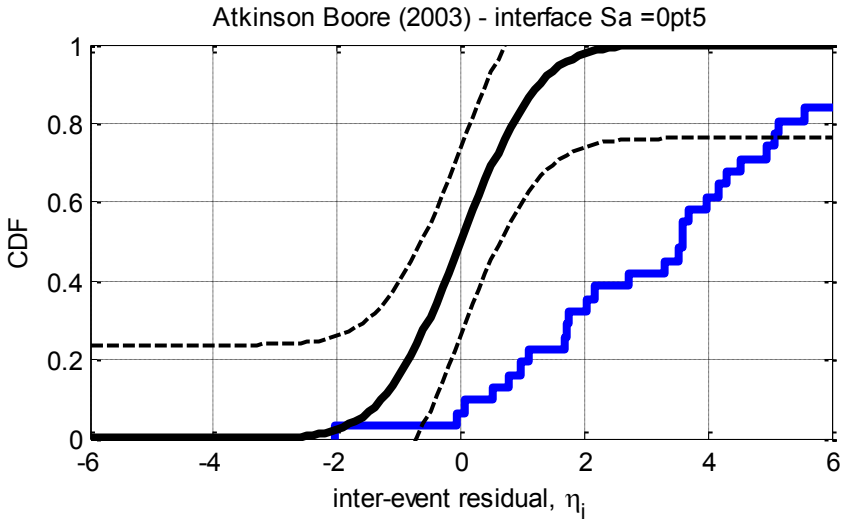
Atkinson Boore (2003) - interface Sa =0pt5
CDF
inter-event residual, η_i

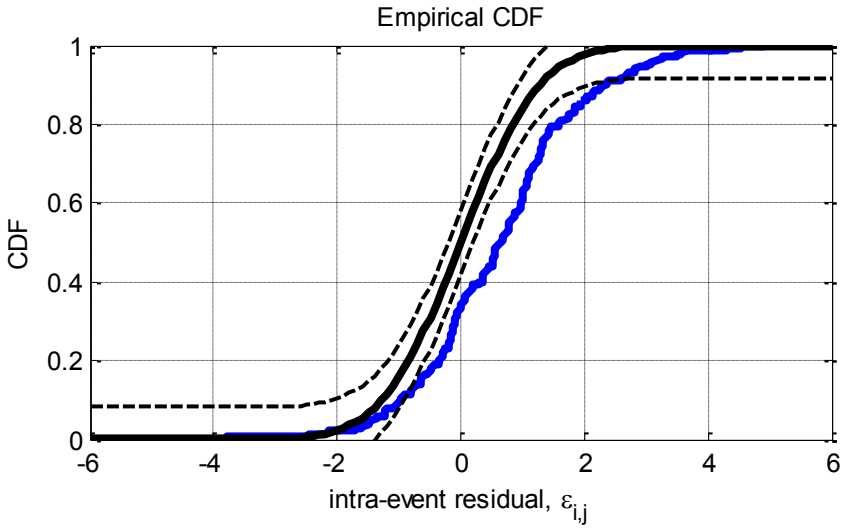
Empirical CDF
CDF
intra-event residual, $\varepsilon_{i,j}$

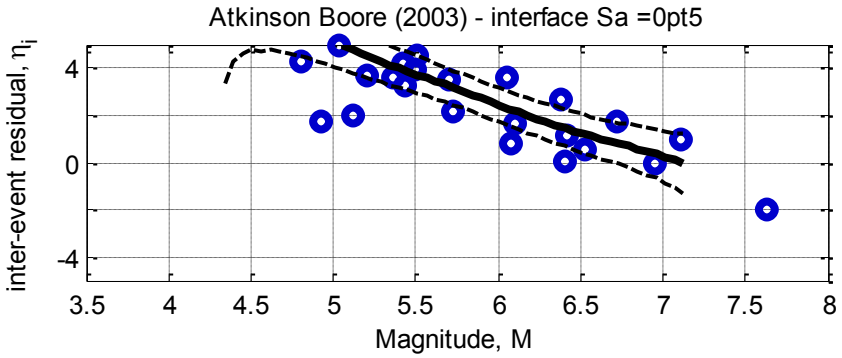
Atkinson Boore (2003) - interface Sa =0pt5
inter-event residual, η_i
Magnitude, M

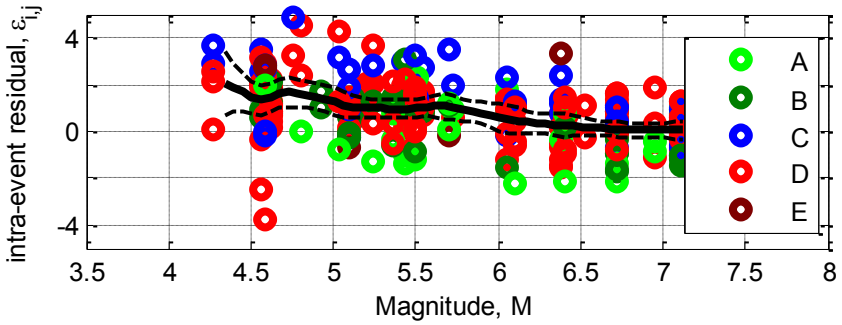
intra-event residual, $\varepsilon_{i,j}$
Magnitude, M
A
B
C
D
E

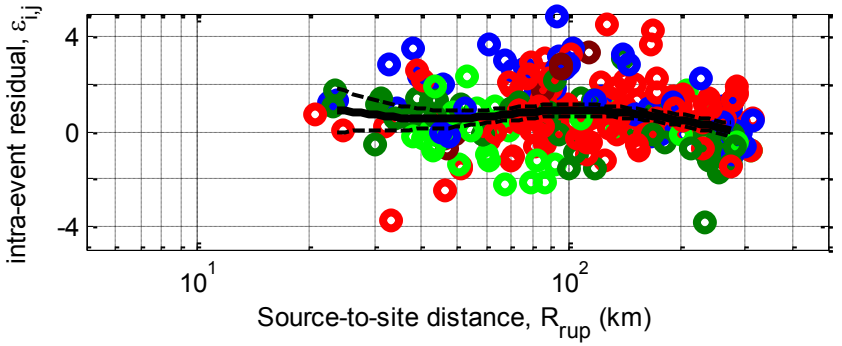
intra-event residual, $\varepsilon_{i,j}$
Source-to-site distance, R_{rup} (km)

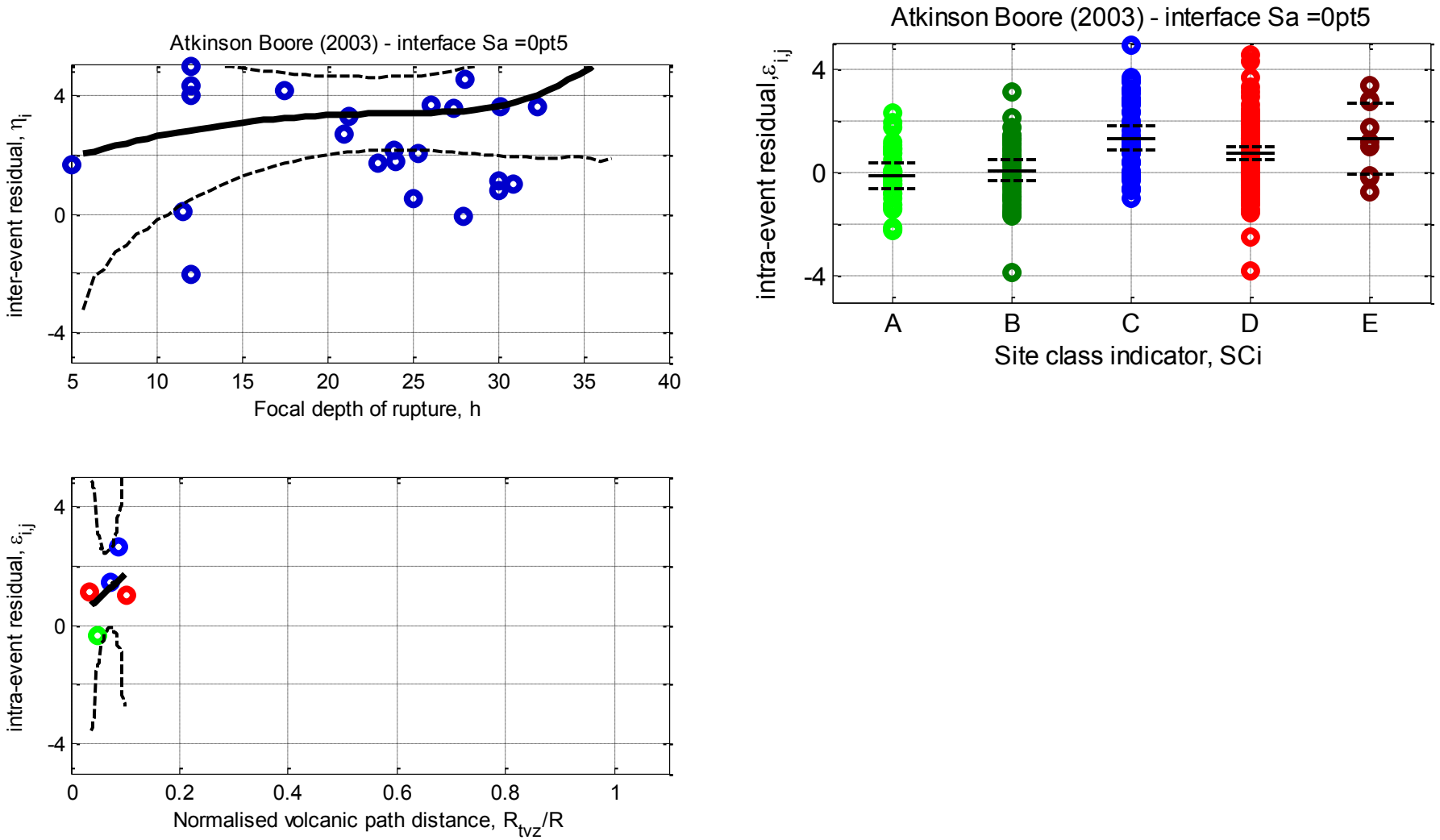

Figure D-63: Residuals for Sa(0.5) using the Atkinson and Boore (2003) interface model

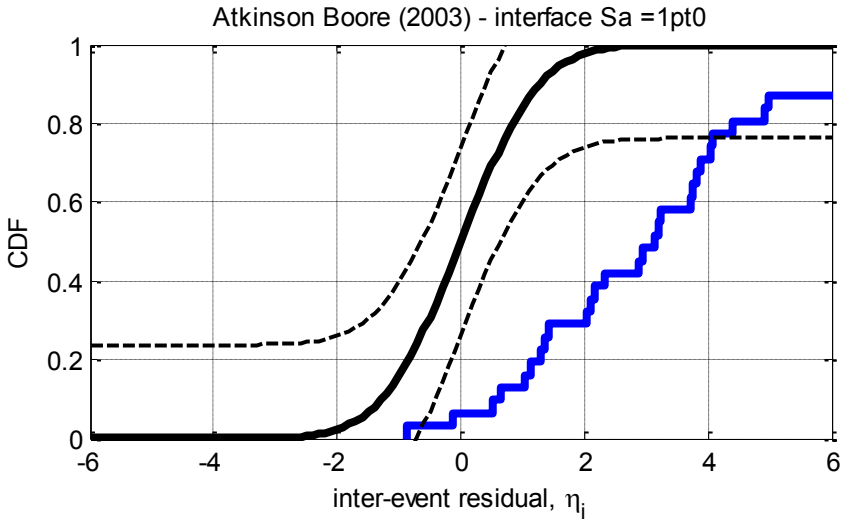
Atkinson Boore (2003) - interface Sa =1pt0
CDF
inter-event residual, η_i

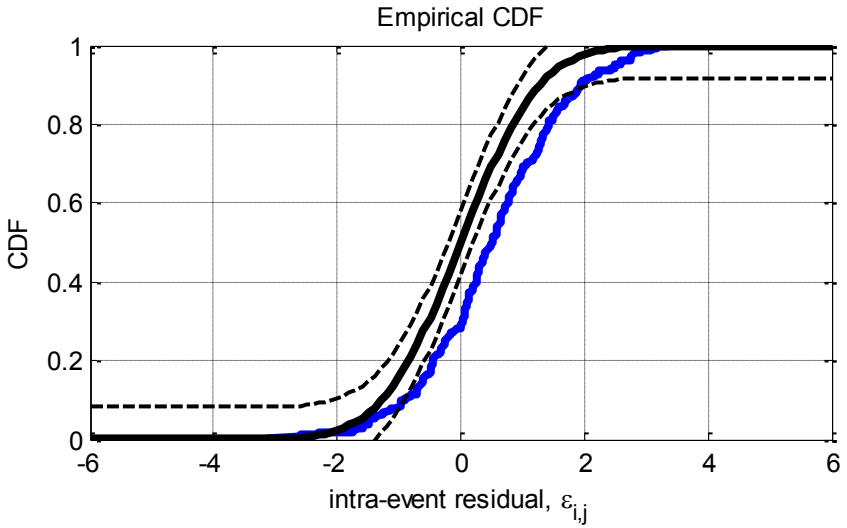
Empirical CDF
CDF
intra-event residual, $\varepsilon_{i,j}$

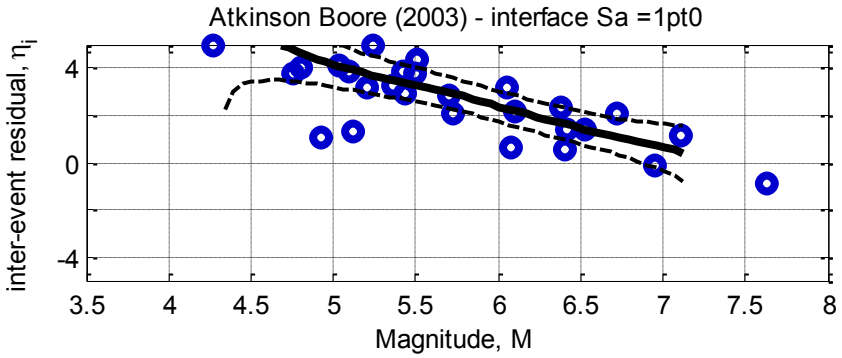
Atkinson Boore (2003) - interface Sa =1pt0
inter-event residual, η_i
Magnitude, M

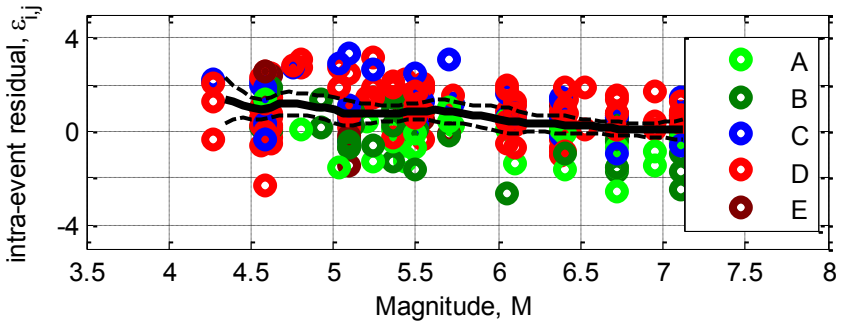
intra-event residual, $\varepsilon_{i,j}$
A
B
C
D
E
Magnitude, M

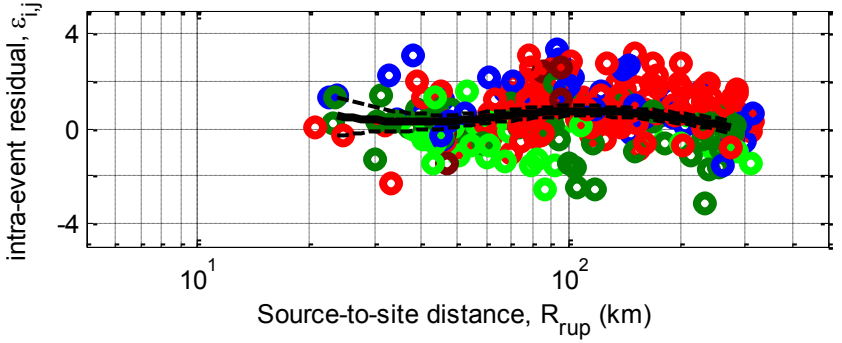
intra-event residual, $\varepsilon_{i,j}$
Source-to-site distance, R_{rup} (km)

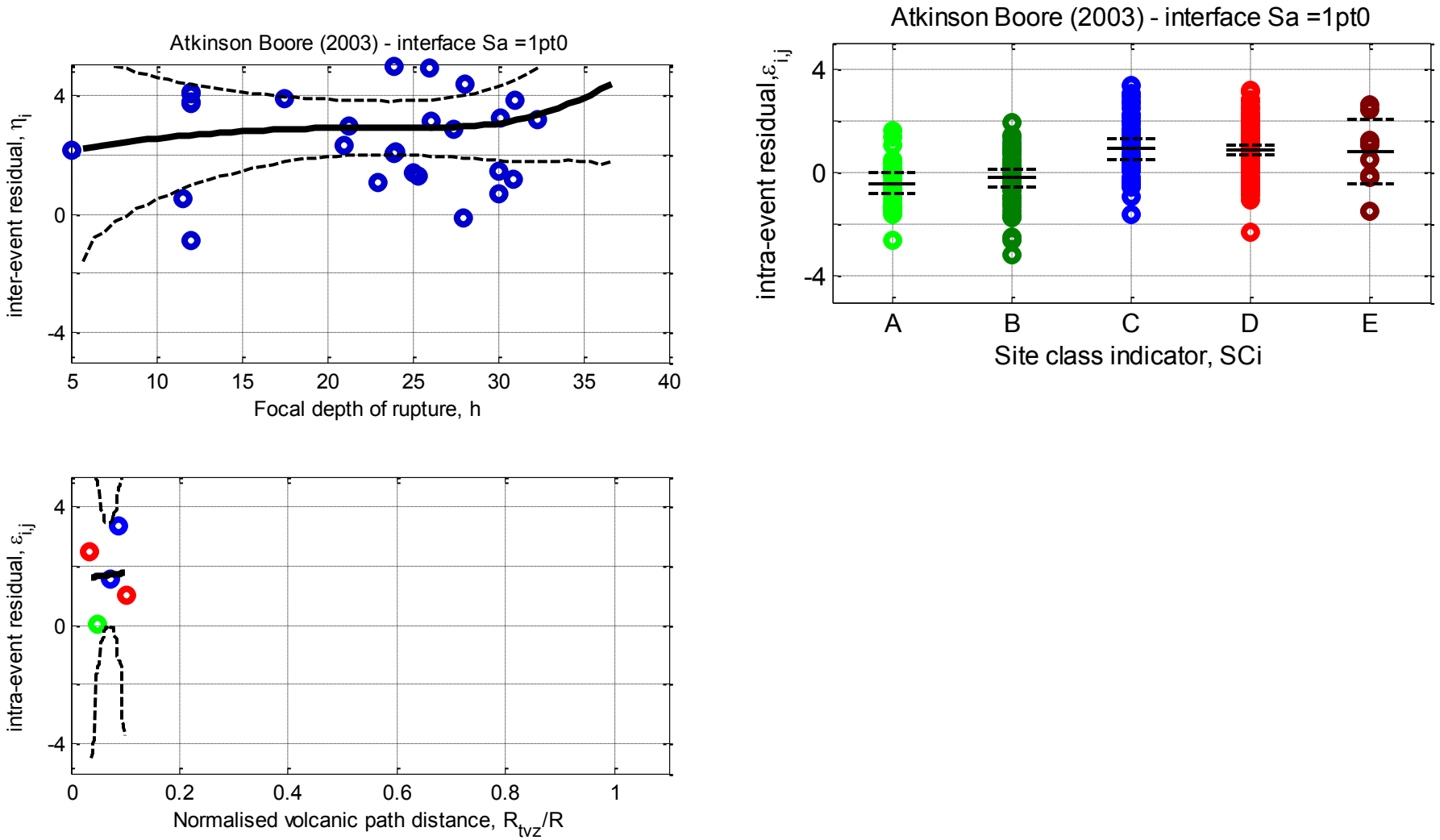

Figure D-64: Residuals for Sa(1.0) using the Atkinson and Boore (2003) interface model

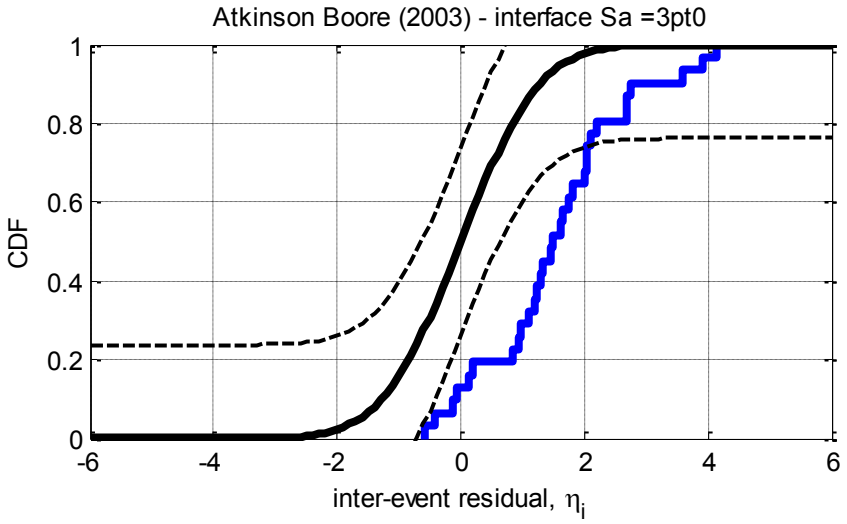
Atkinson Boore (2003) - interface Sa =3pt0
CDF
inter-event residual, η_i

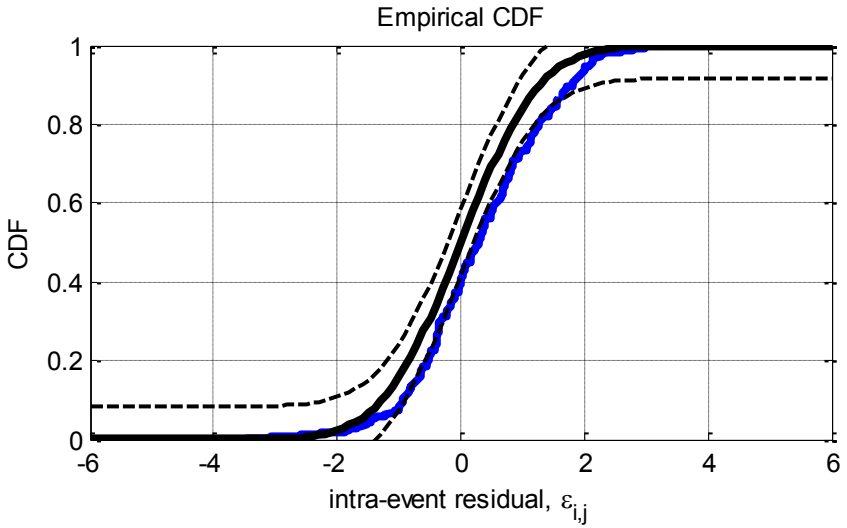
Empirical CDF
CDF
intra-event residual, $\varepsilon_{i,j}$

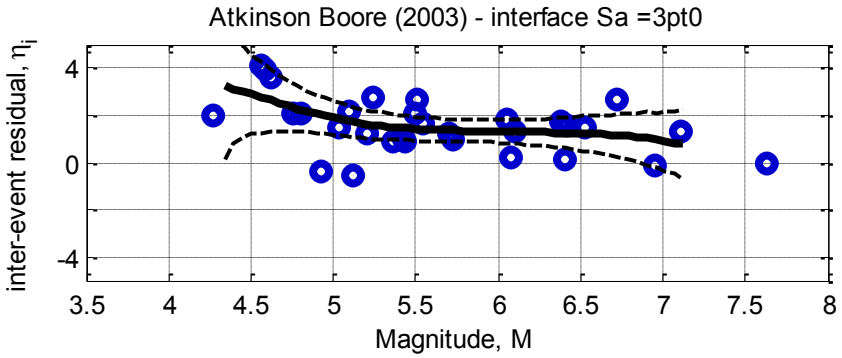
Atkinson Boore (2003) - interface Sa =3pt0
inter-event residual, η_i
Magnitude, M

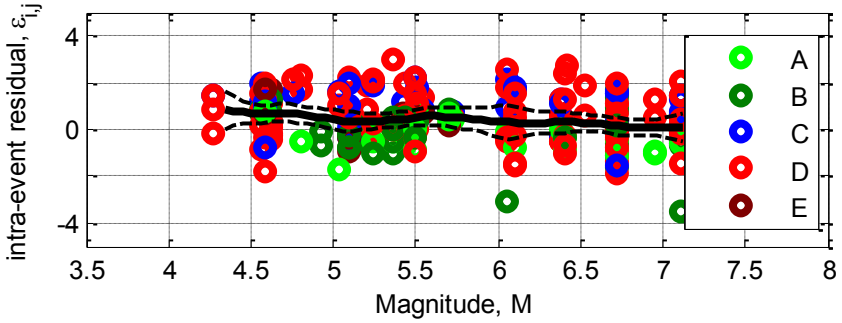
intra-event residual, $\varepsilon_{i,j}$
Magnitude, M
A
B
C
D
E

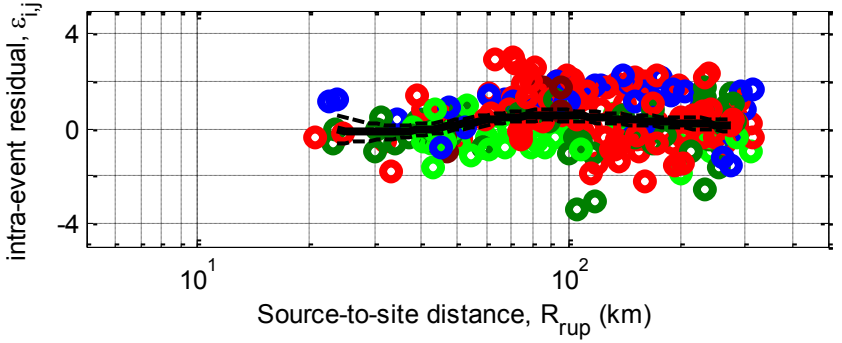
intra-event residual, $\varepsilon_{i,j}$
Source-to-site distance, R_{rup} (km)

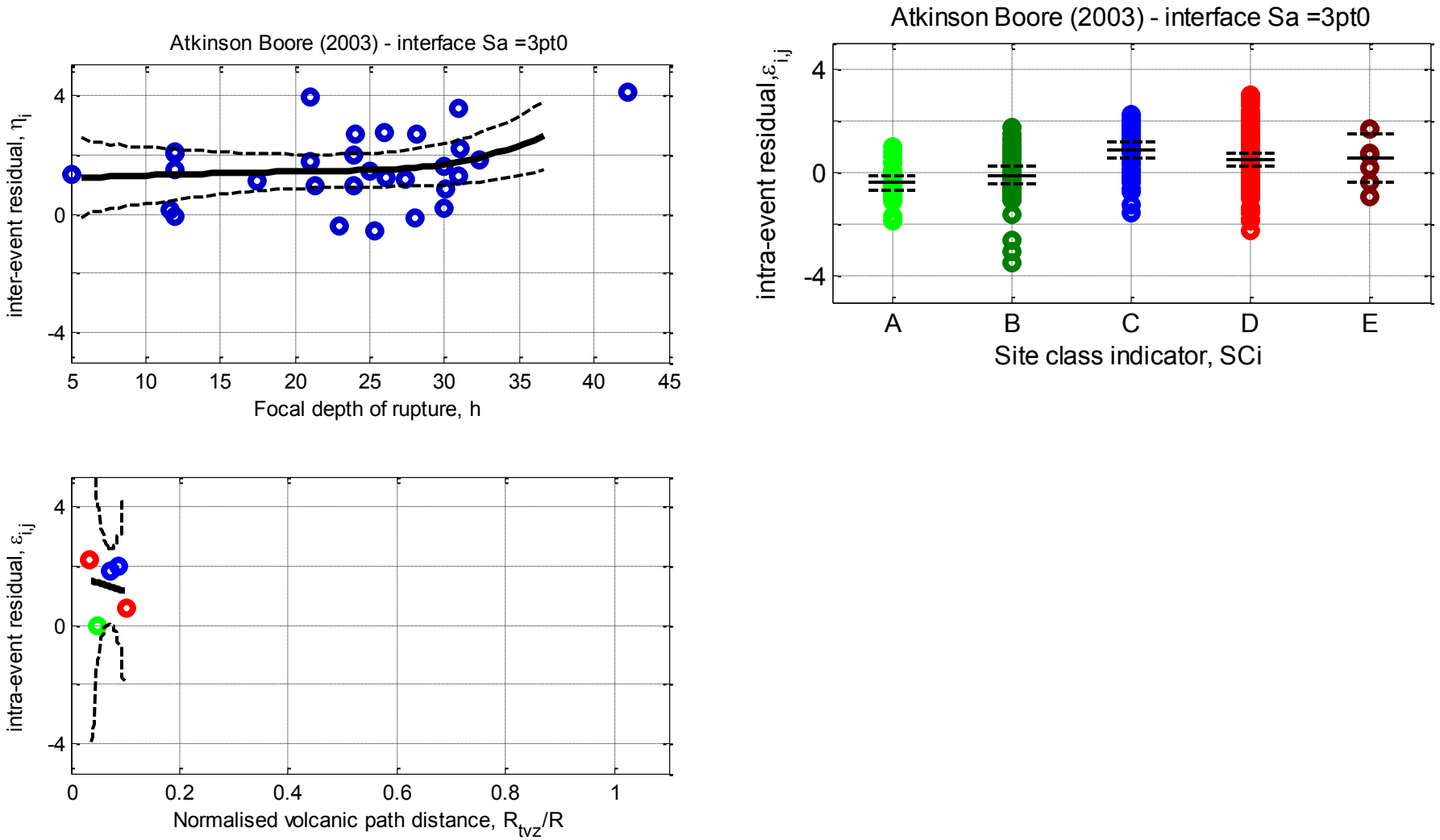

Figure D-65: Residuals for Sa(3.0) using the Atkinson and Boore (2003) interface model

D.14. Bradley (2010) Interface model

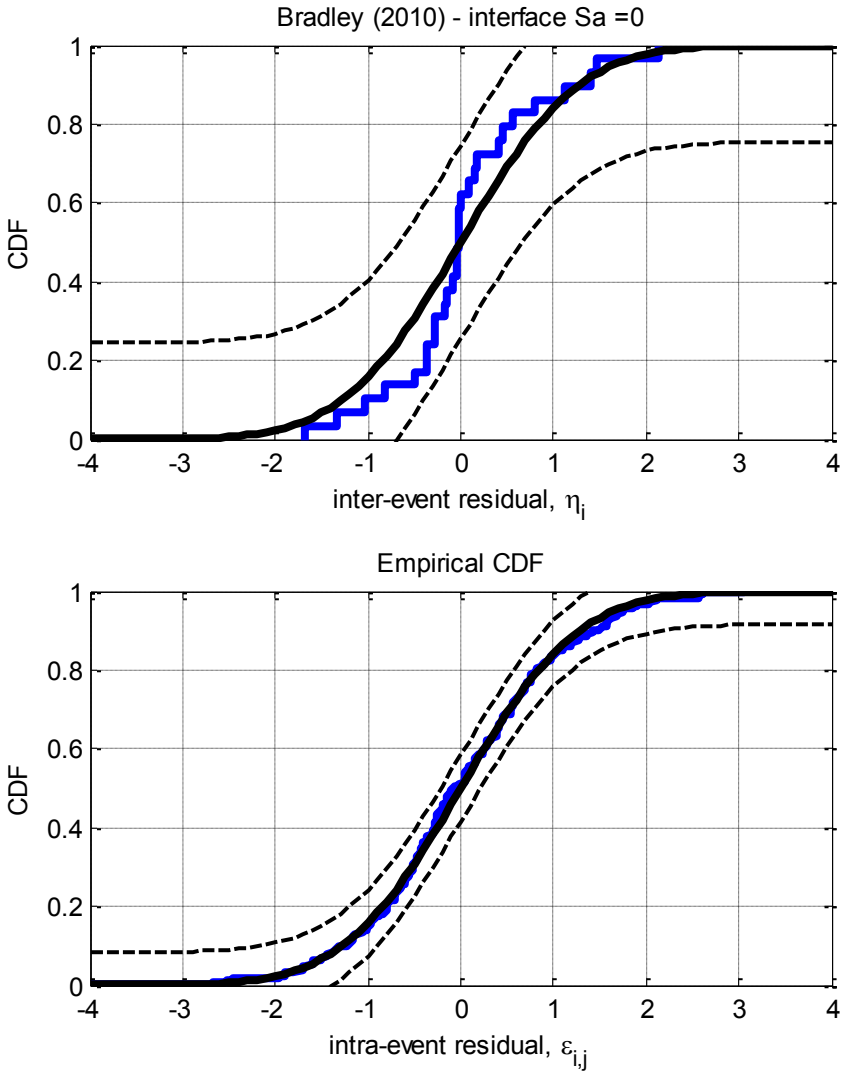

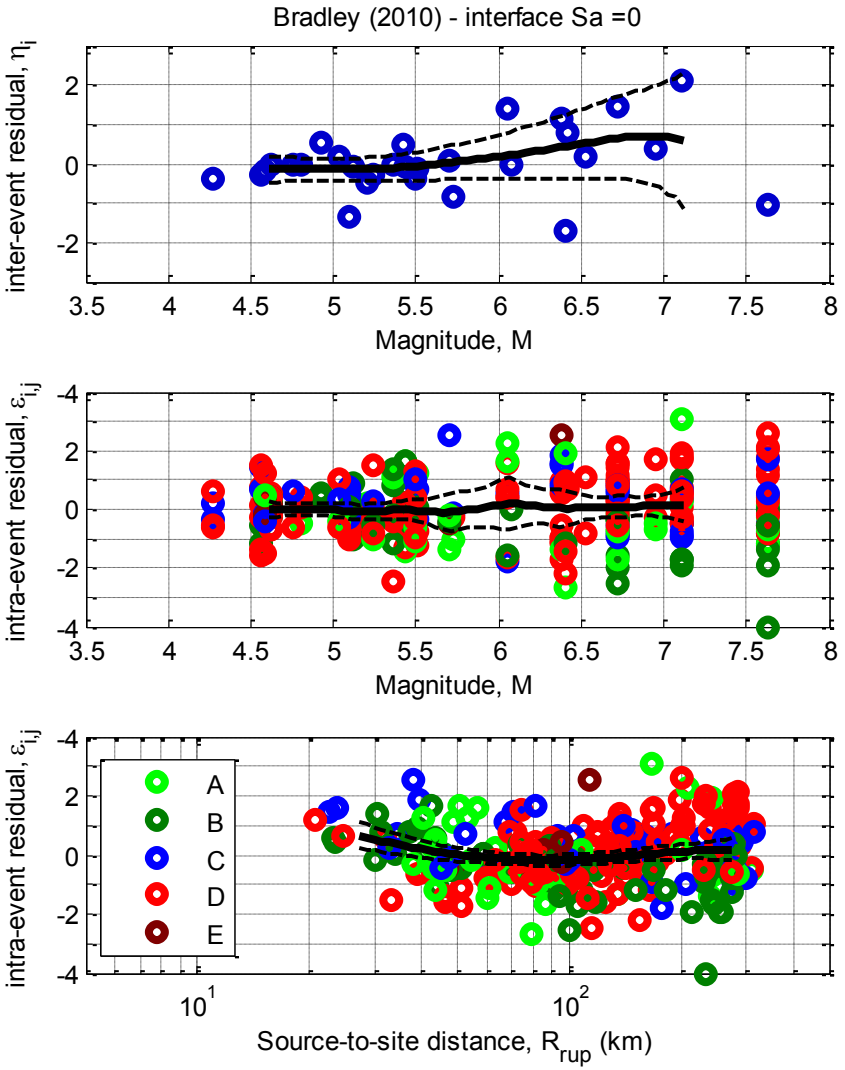

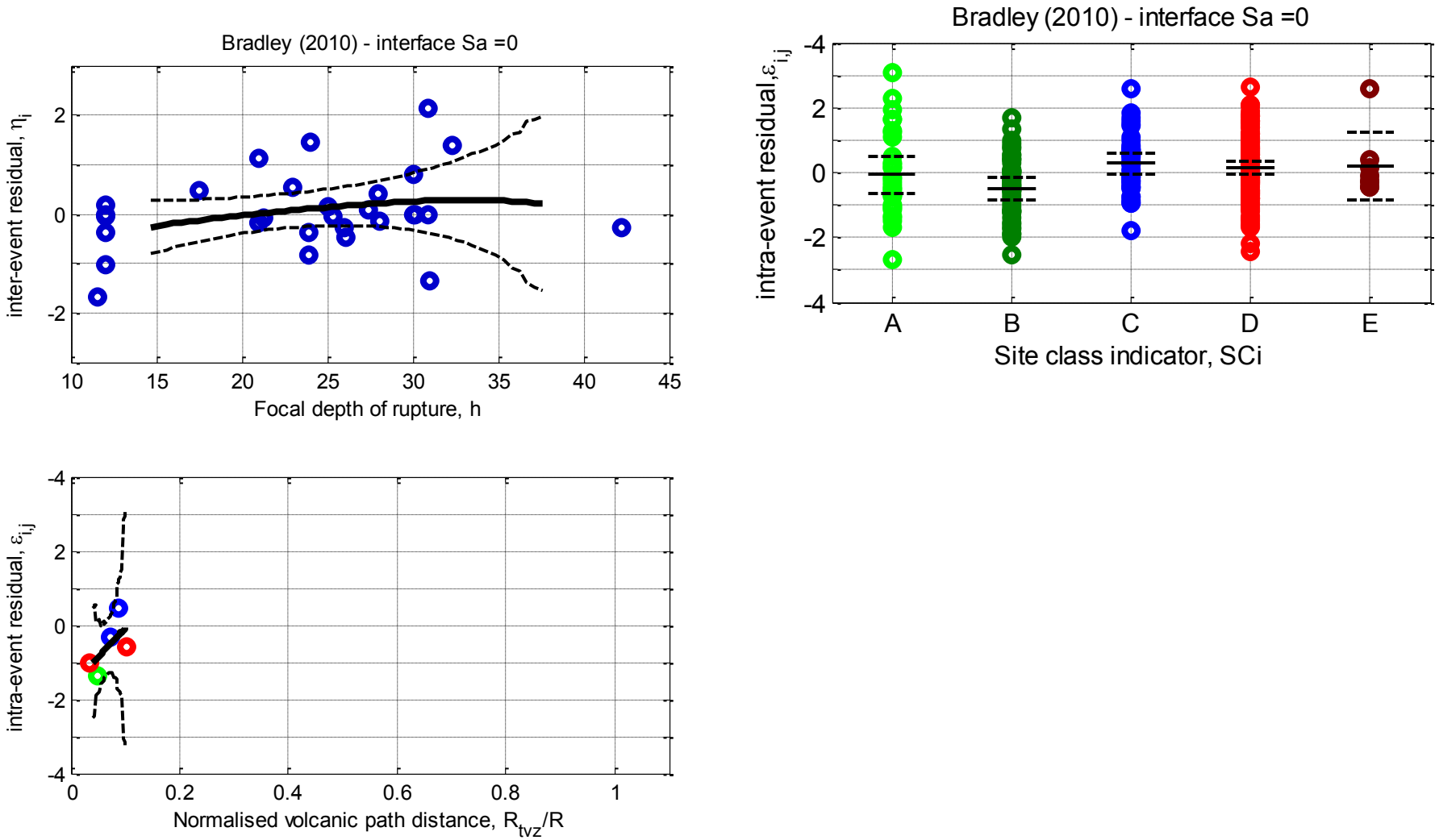

Figure D-66: Residuals for Sa(0.0) using the Bradley (2010) interface model

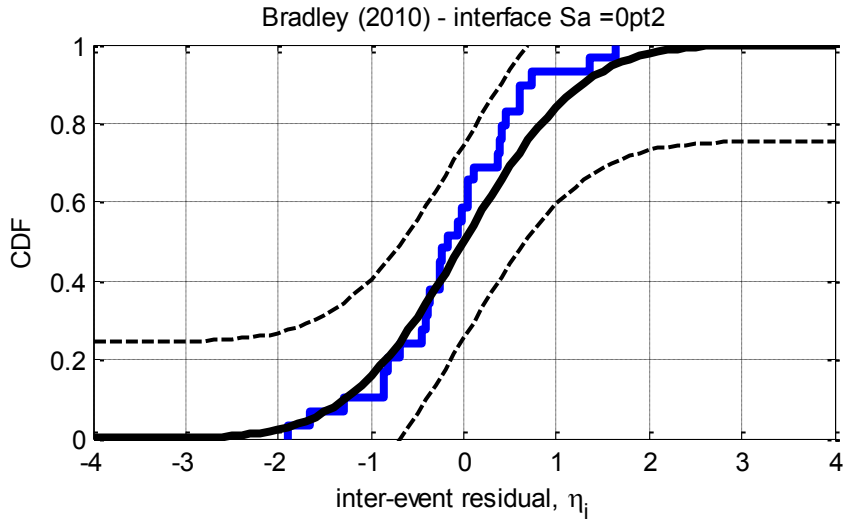
Bradley (2010) - interface Sa =0pt2
CDF
inter-event residual, η_i

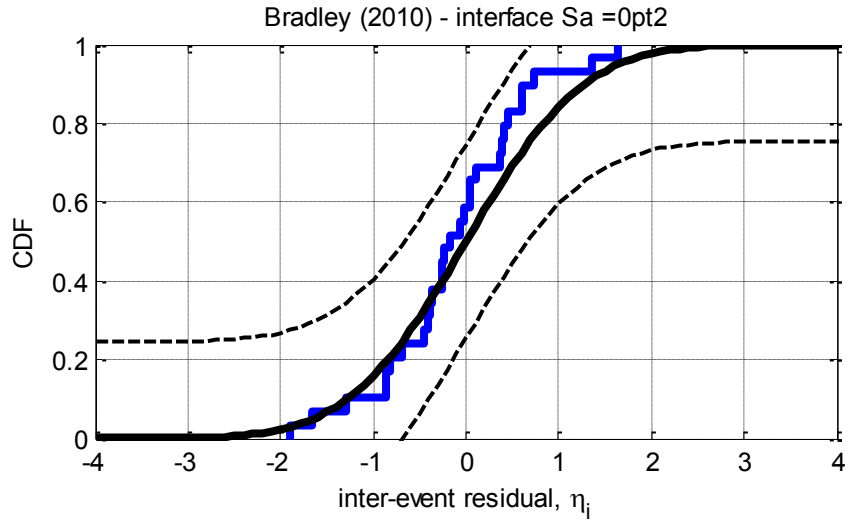
Bradley (2010) - interface Sa =0pt2
CDF
inter-event residual, η_i

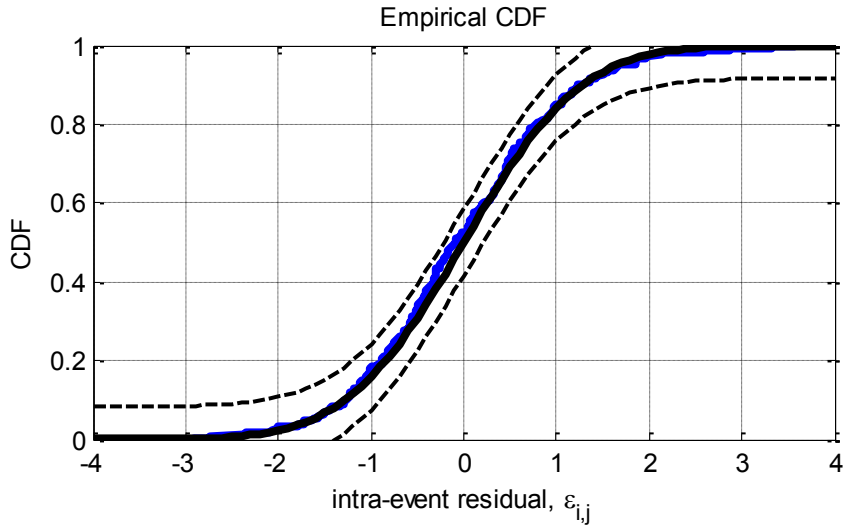
Empirical CDF
CDF
intra-event residual, $\varepsilon_{i,j}$

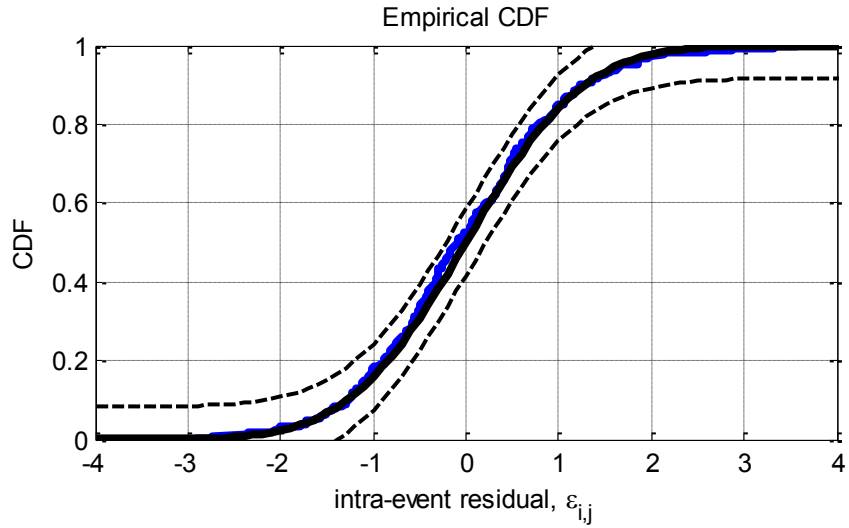
Empirical CDF
CDF
intra-event residual, $\varepsilon_{i,j}$

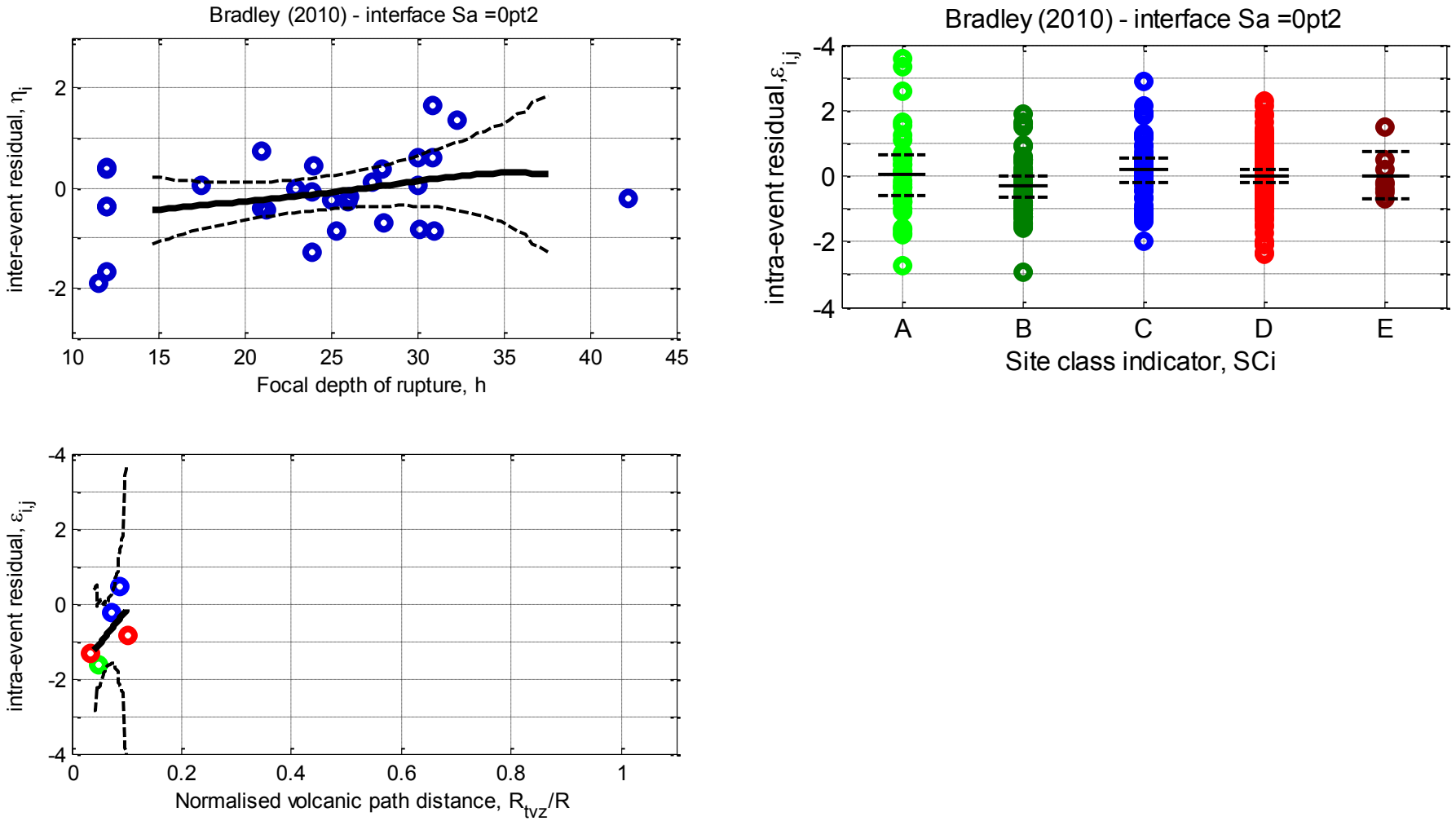

Figure D-67: Residuals for Sa(0.2) using the Bradley (2010) interface model

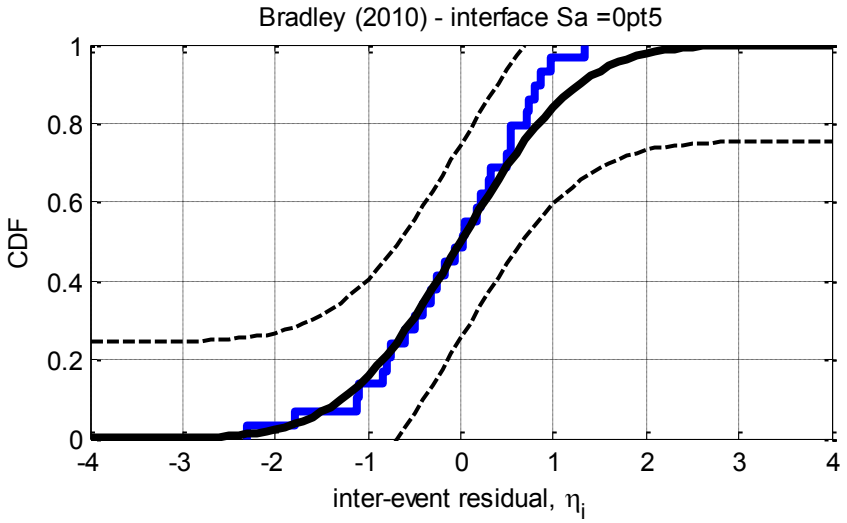
Bradley (2010) - interface Sa =0pt5
CDF
inter-event residual, η_i

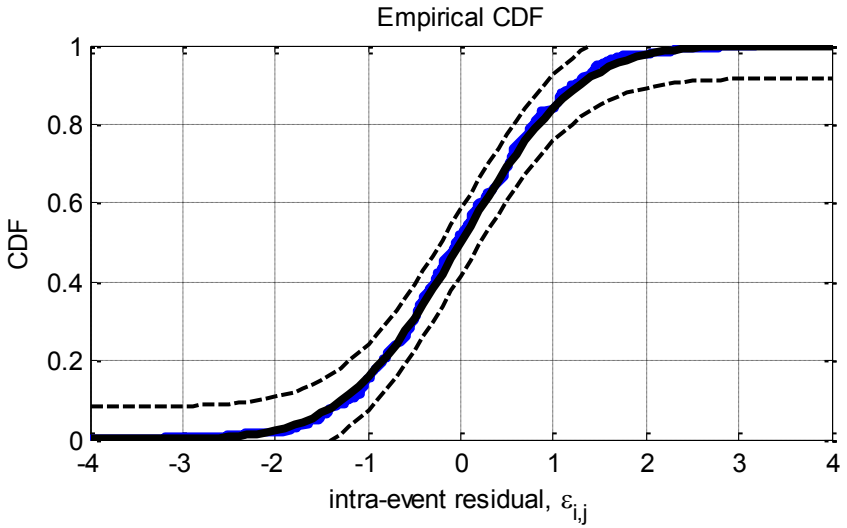
Empirical CDF
CDF
intra-event residual, $\varepsilon_{i,j}$

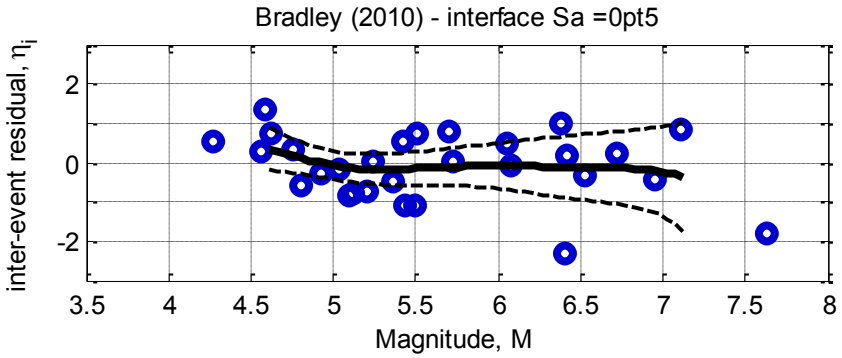
Bradley (2010) - interface Sa =0pt5
inter-event residual, η_i
Magnitude, M

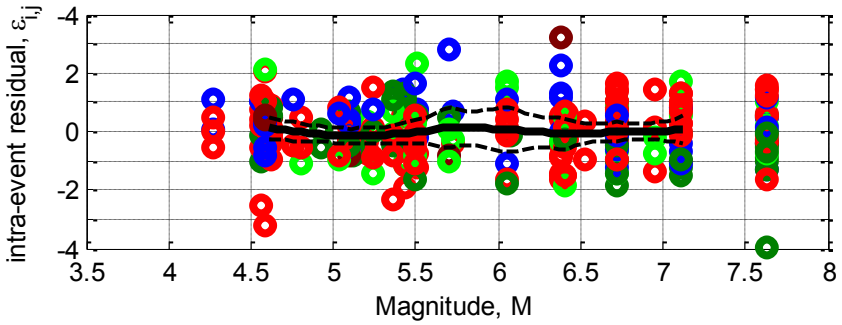
intra-event residual, $\varepsilon_{i,j}$
Magnitude, M

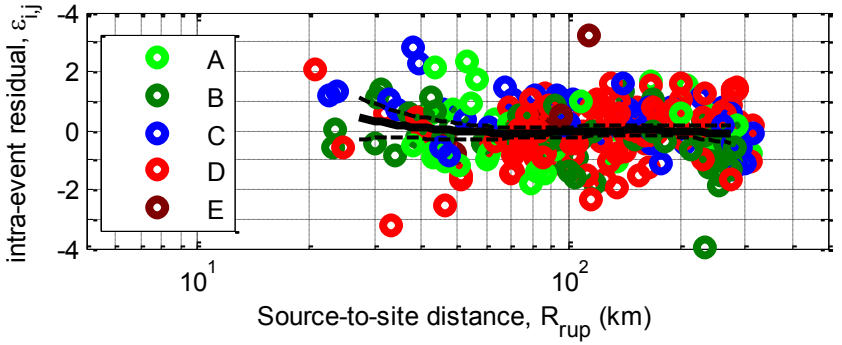
intra-event residual, $\varepsilon_{i,j}$
A
B
C
D
E
Source-to-site distance, R_{rup} (km)

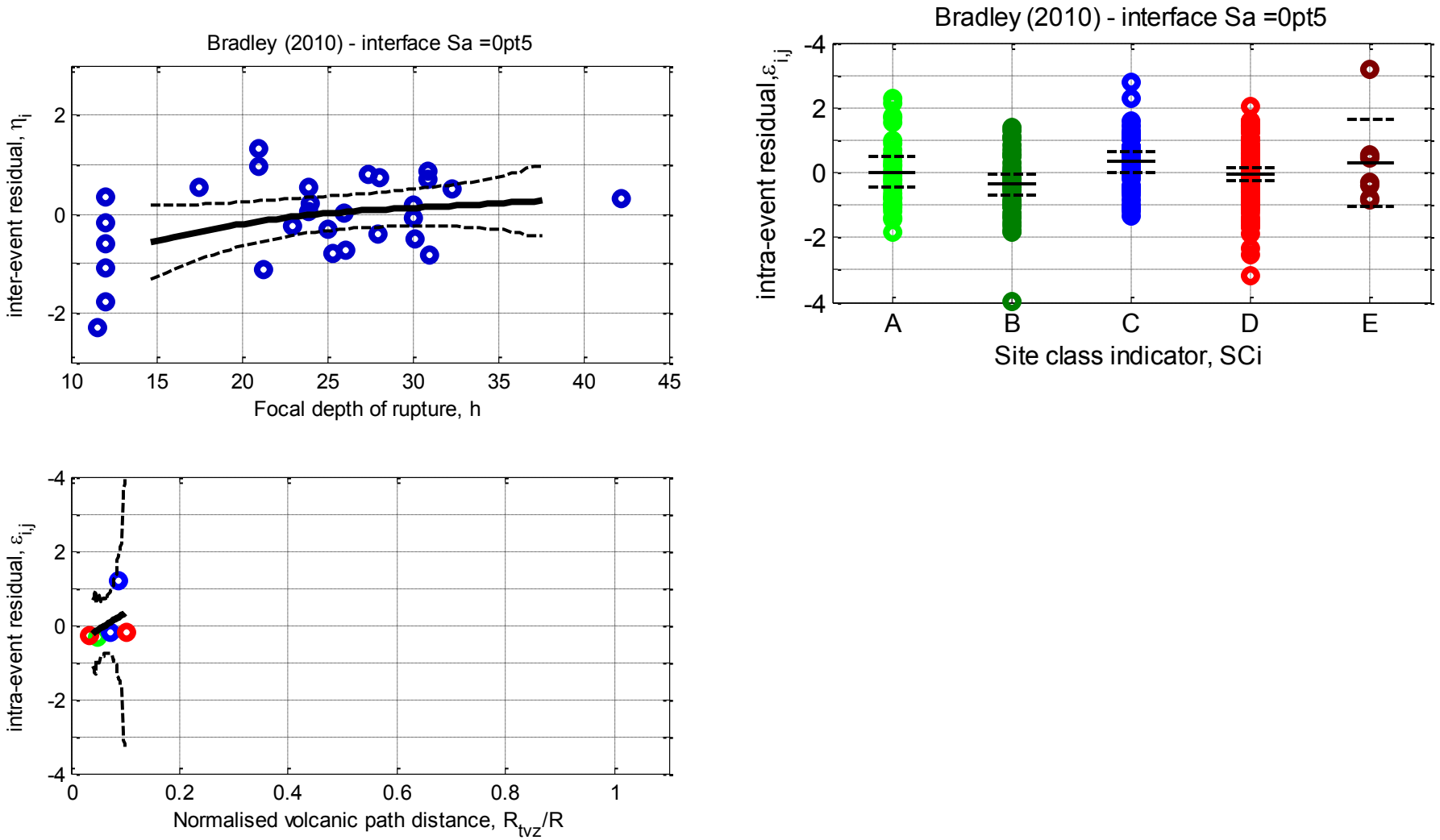

Figure D-68: Residuals for Sa(0.5) using the Bradley (2010) interface model

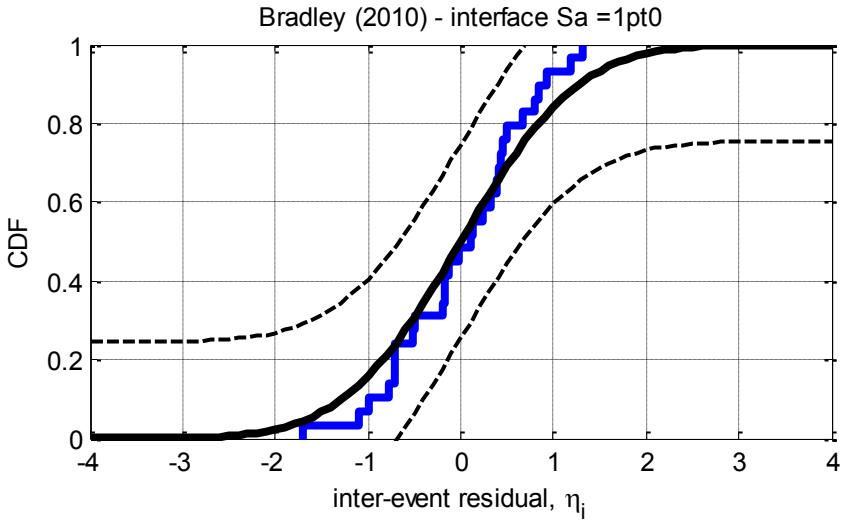
Bradley (2010) - interface Sa =1pt0
CDF
inter-event residual, η_i

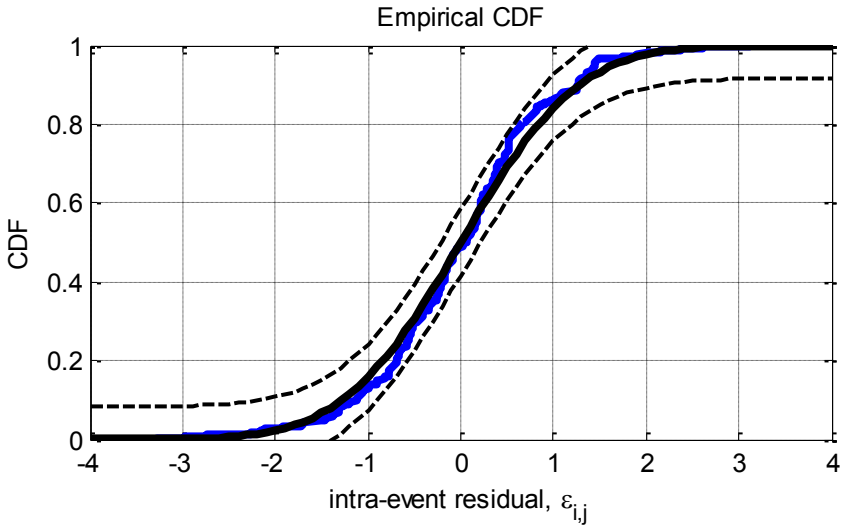
Empirical CDF
CDF
intra-event residual, $\varepsilon_{i,j}$

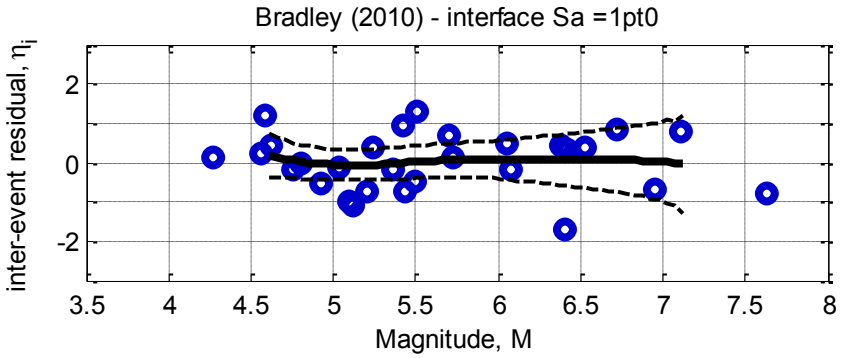
Bradley (2010) - interface Sa =1pt0
inter-event residual, η_i
Magnitude, M

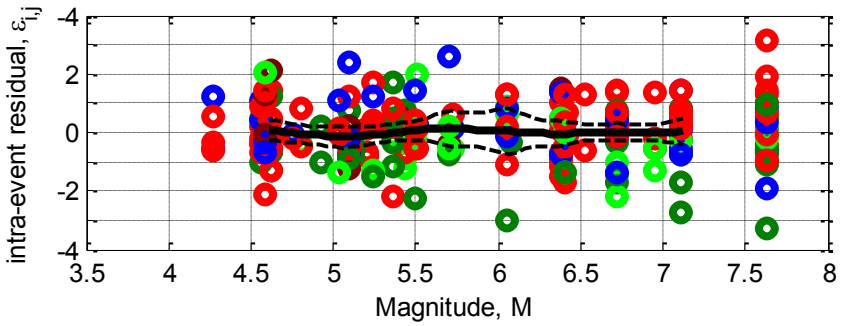
intra-event residual, $\varepsilon_{i,j}$
Magnitude, M

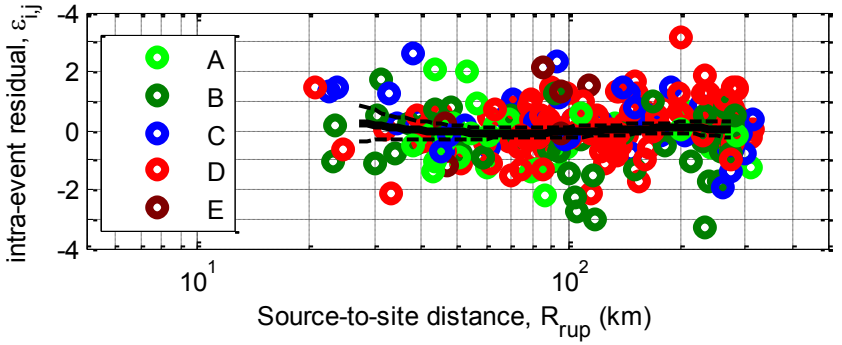
intra-event residual, $\varepsilon_{i,j}$
A
B
C
D
E
Source-to-site distance, R_{rup} (km)

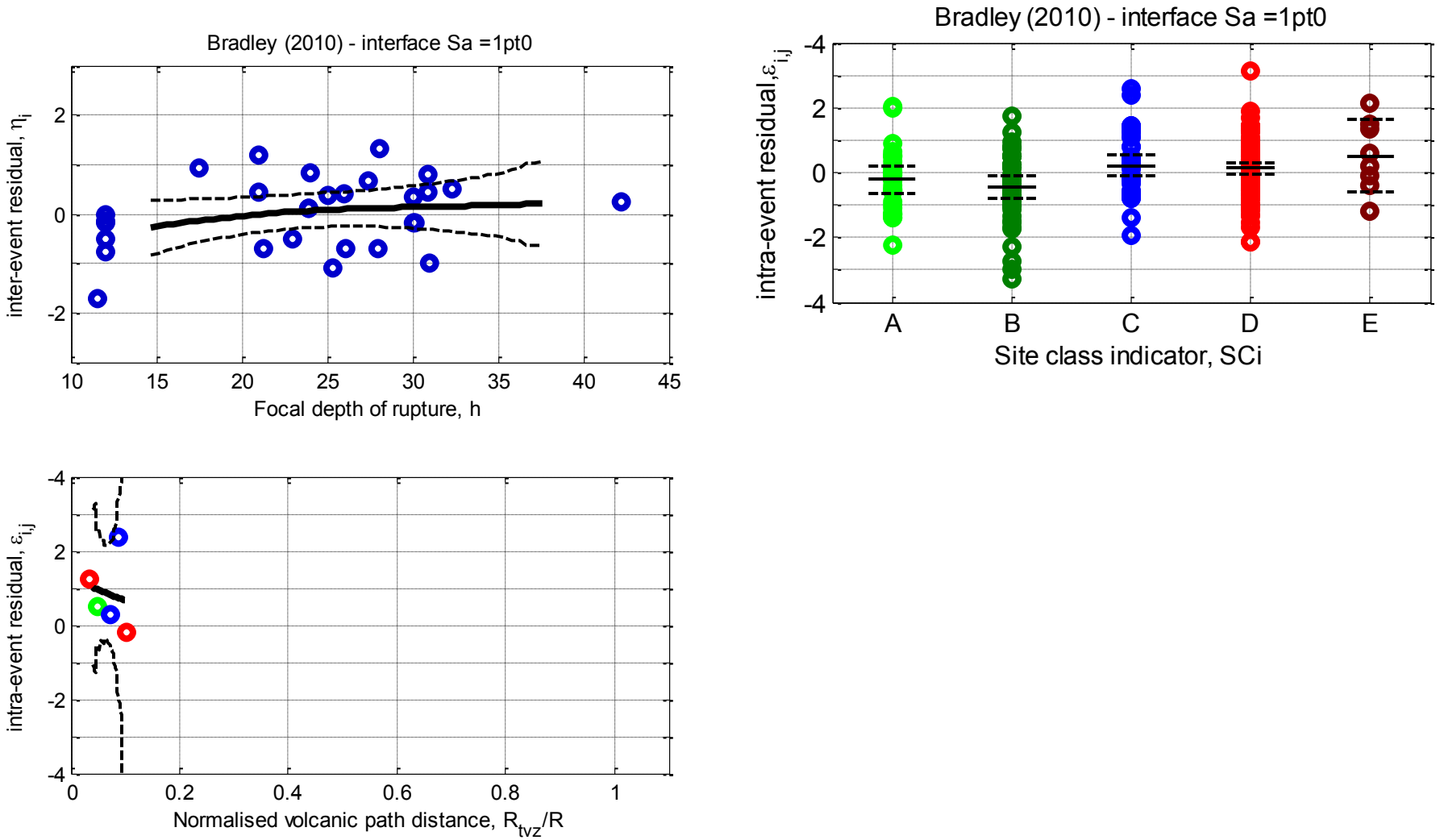

Figure D-69: Residuals for Sa(1.0) using the Bradley (2010) interface model

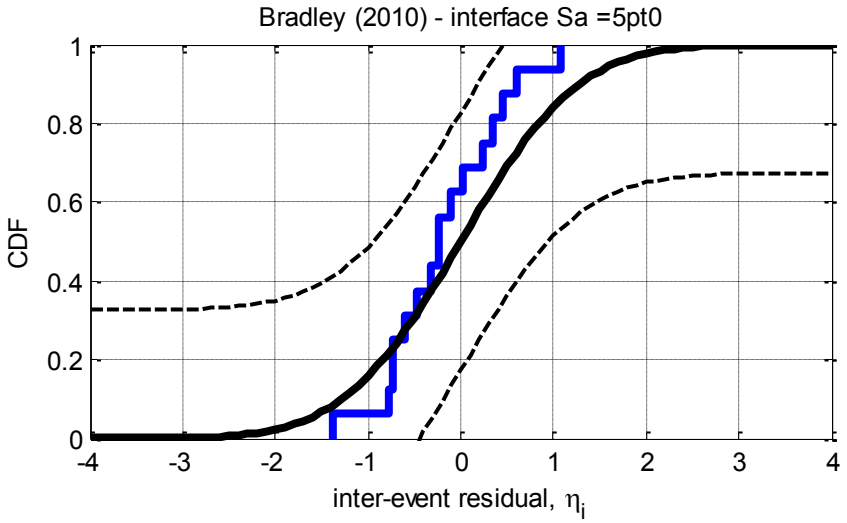
Bradley (2010) - interface Sa =5pt0
CDF
inter-event residual, η_i

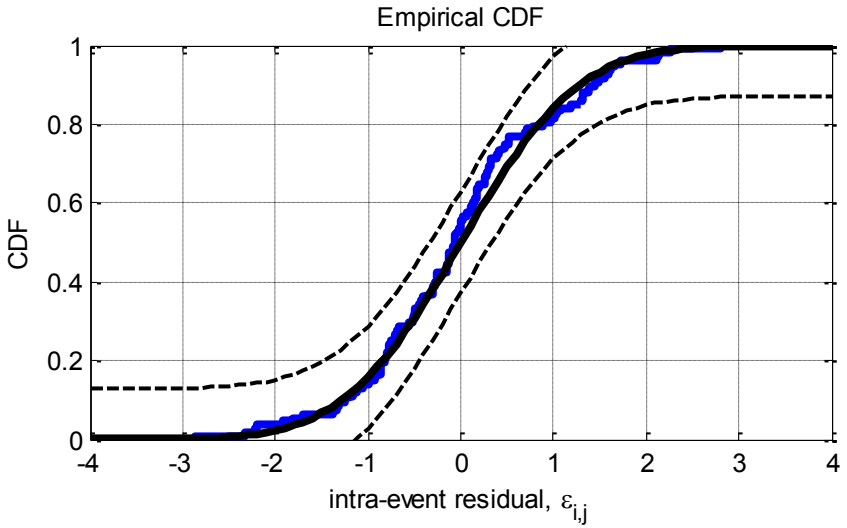
Empirical CDF
CDF
intra-event residual, $\varepsilon_{i,j}$

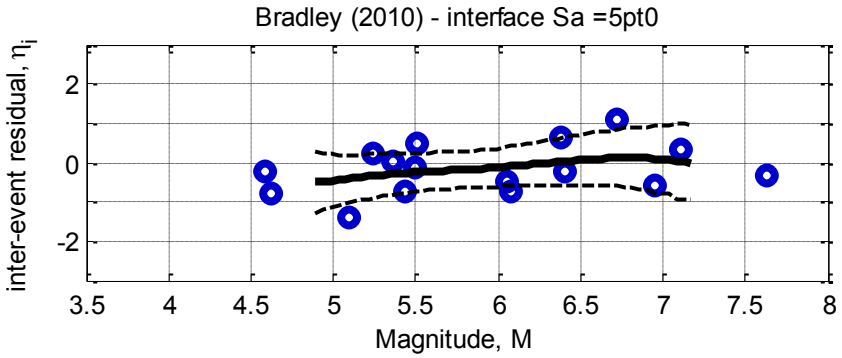
Bradley (2010) - interface Sa =5pt0
inter-event residual, η_i
Magnitude, M

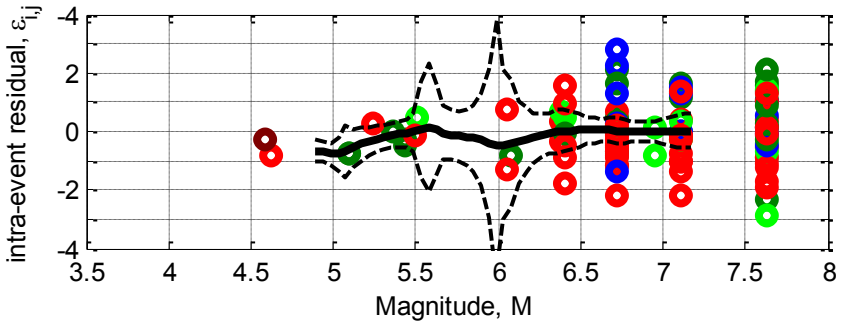
intra-event residual, $\varepsilon_{i,j}$
Magnitude, M

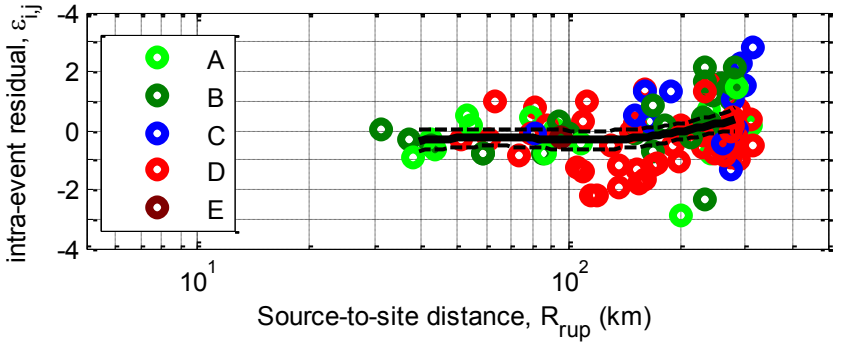
intra-event residual, $\varepsilon_{i,j}$
A
B
C
D
E
Source-to-site distance, R_{rup} (km)

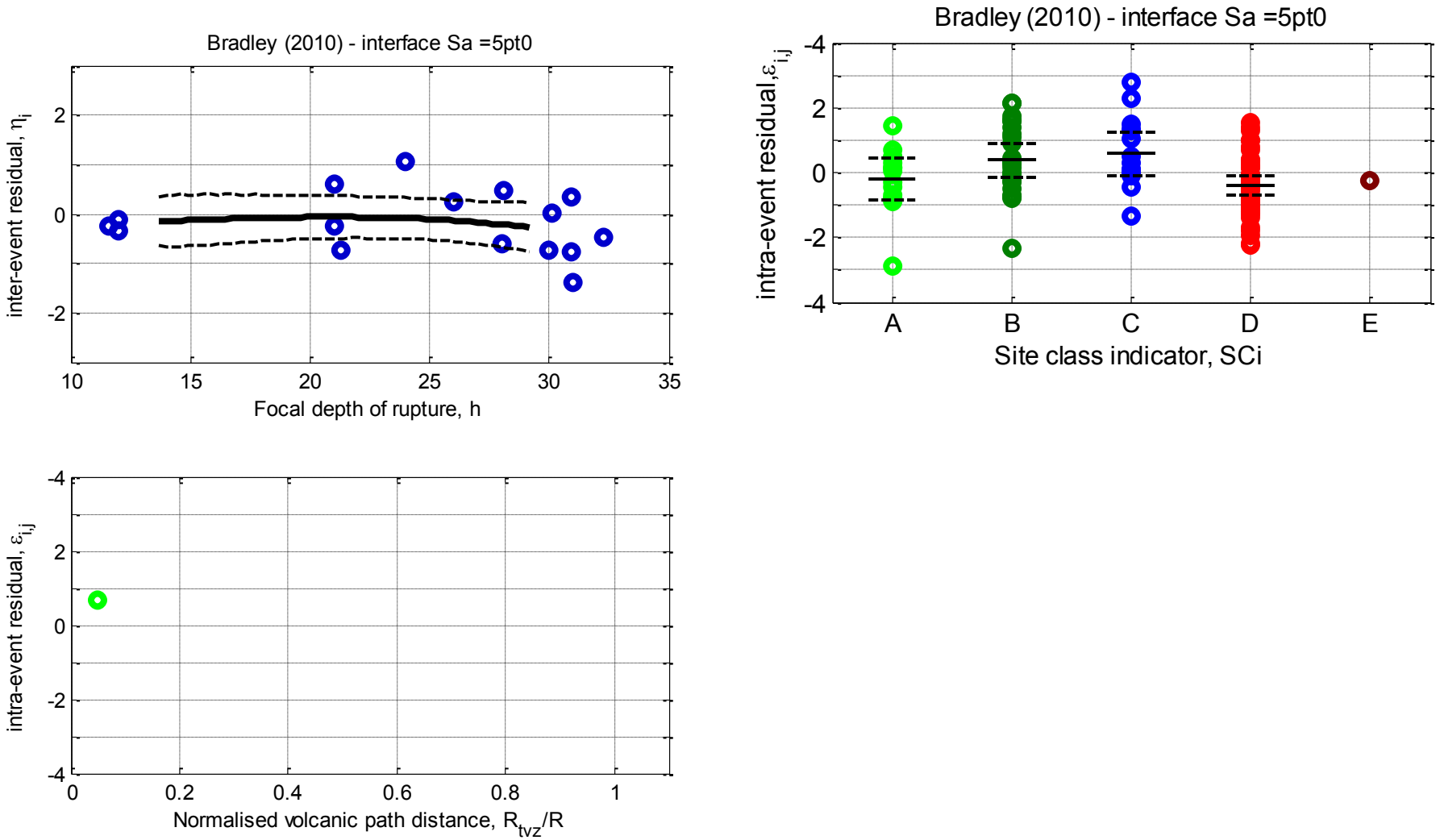

Figure D-70: Residuals for Sa(5.0) using the Bradley (2010) interface model

APPENDIX E OBSERVED RESIDUAL STANDARD DEVIATIONS OF THE DEVELOPED GROUND MOTION PREDICTION EQUATIONS

E.1. Bradley (2010) Crustal model

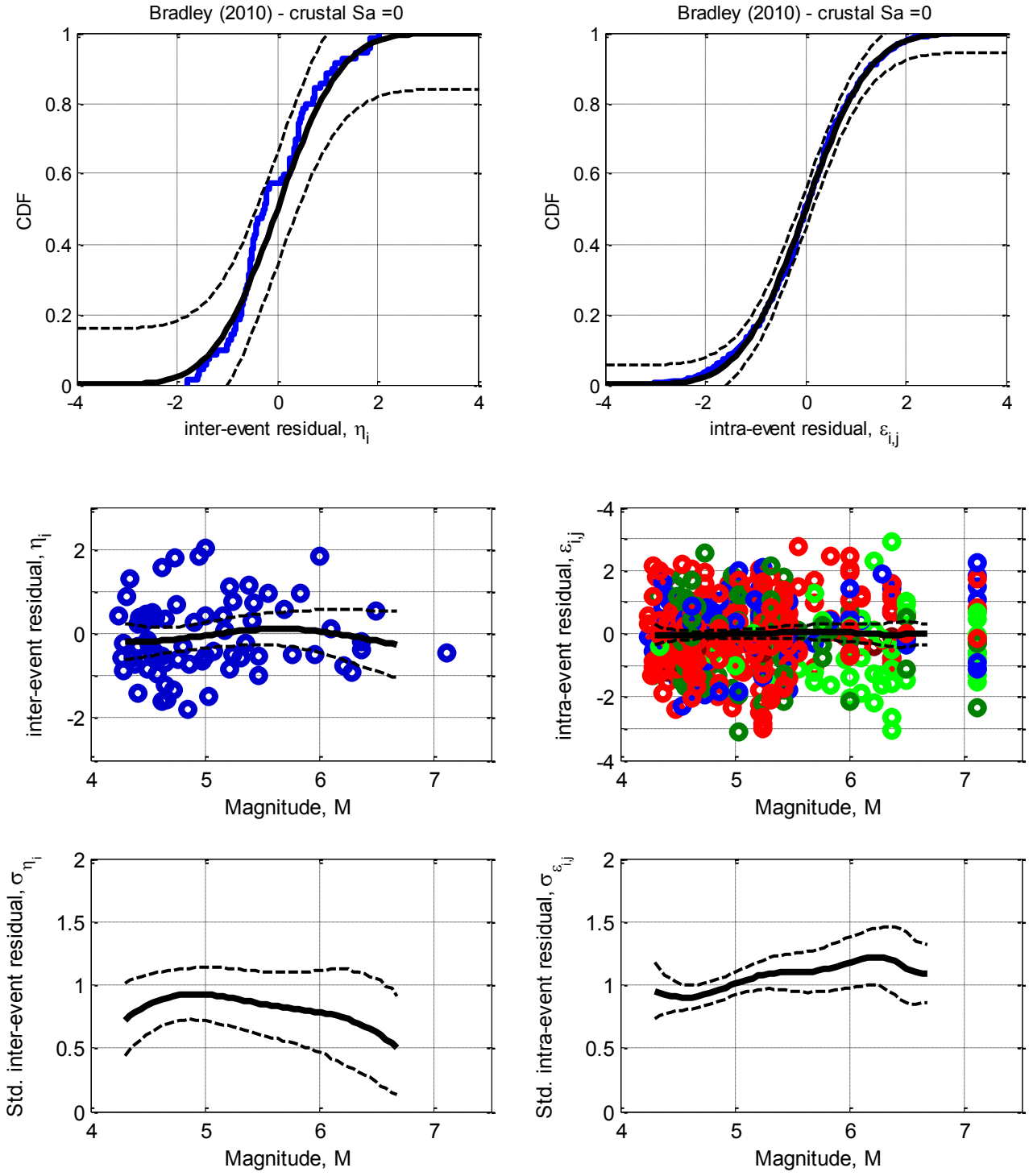

Figure E-1: Residuals for Sa(0.0) using the Bradley (2010) crustal model

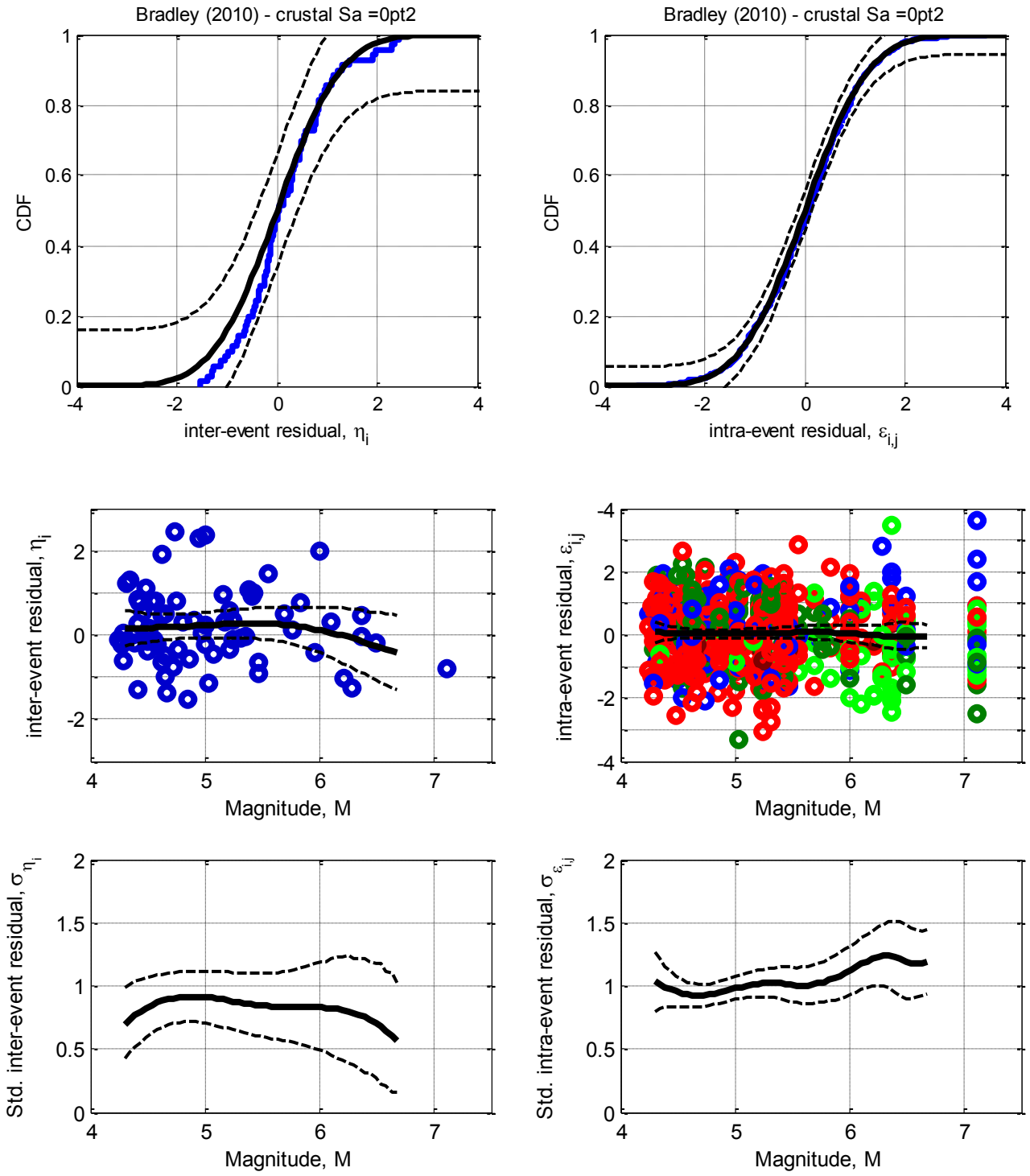

Figure E-2: Residuals for Sa(0.2) using the Bradley (2010) crustal model

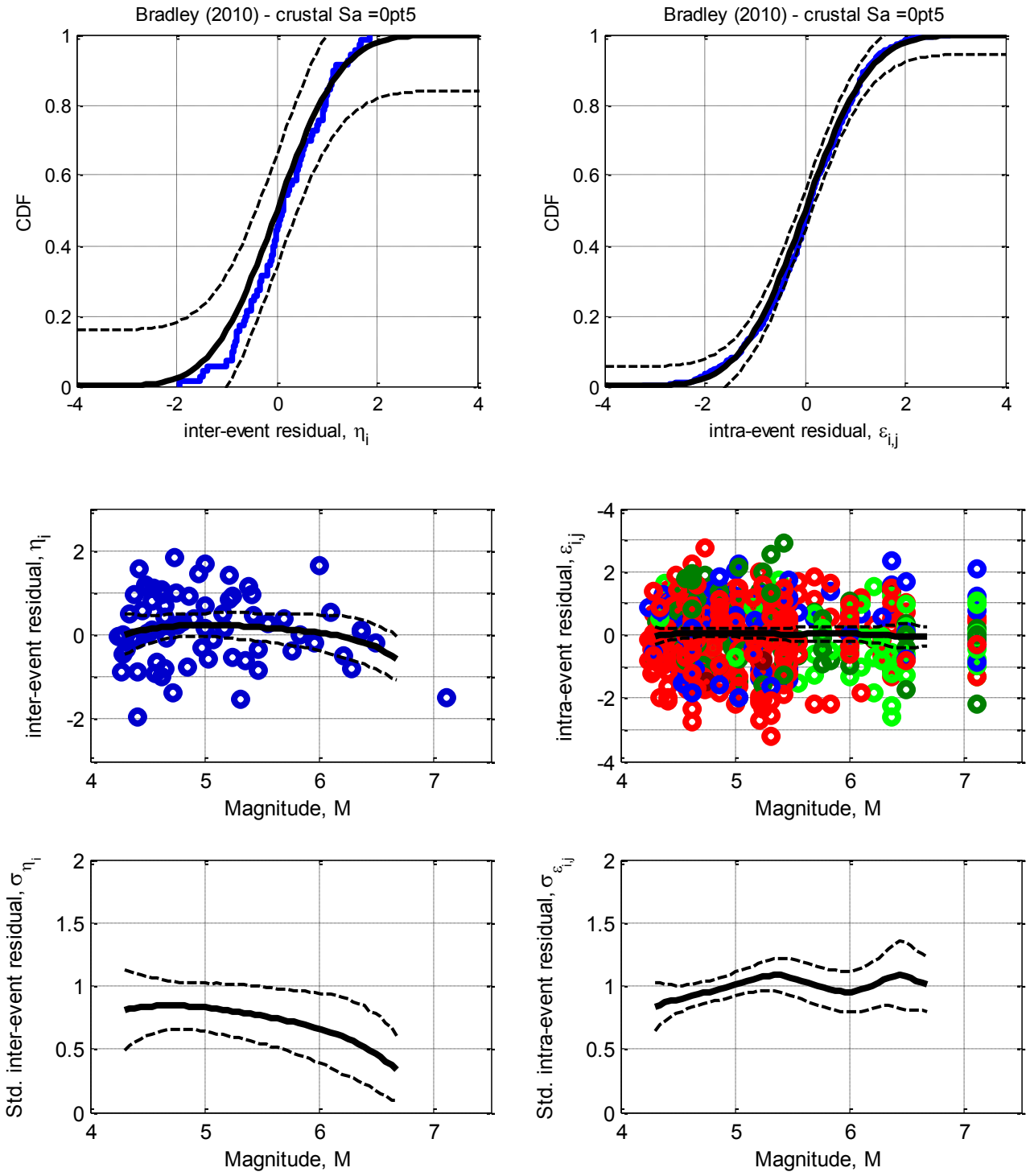

Figure E-3: Residuals for Sa(0.5) using the Bradley (2010) crustal model

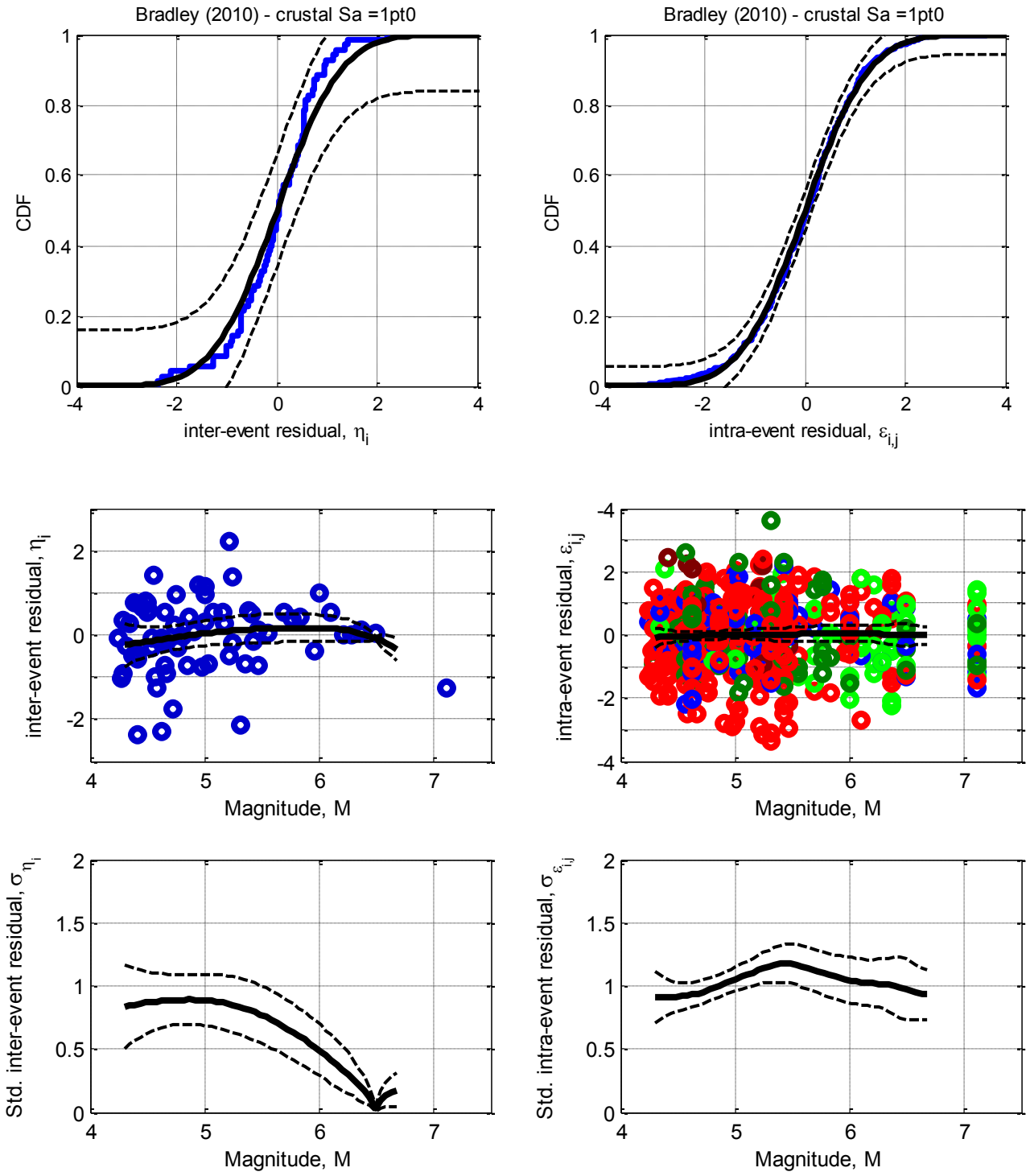

Figure E-4: Residuals for Sa(1.0) using the Bradley (2010) crustal model

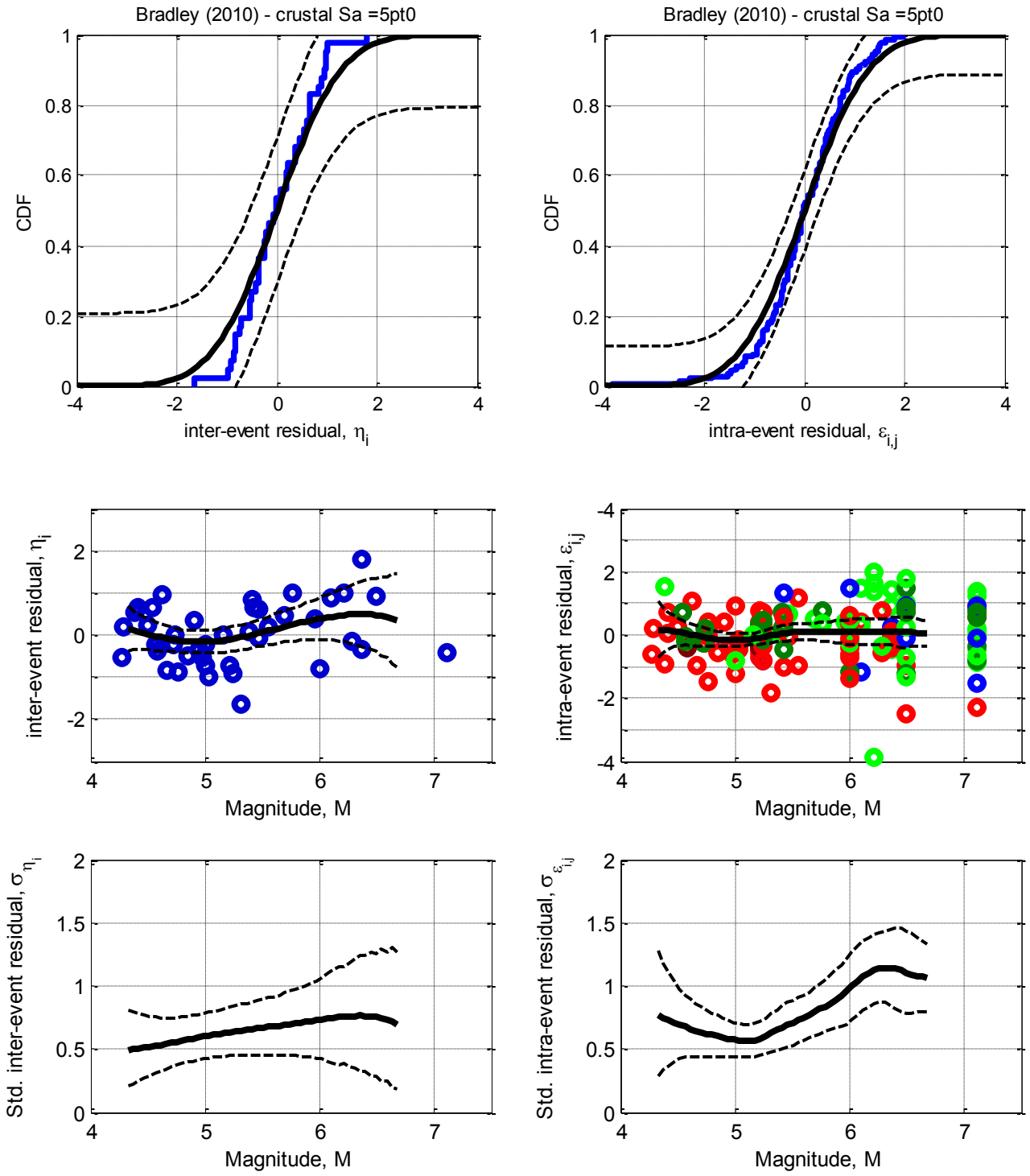

Figure E-5: Residuals for Sa(5.0) using the Bradley (2010) crustal model

E.2. Bradley (2010) Slab model

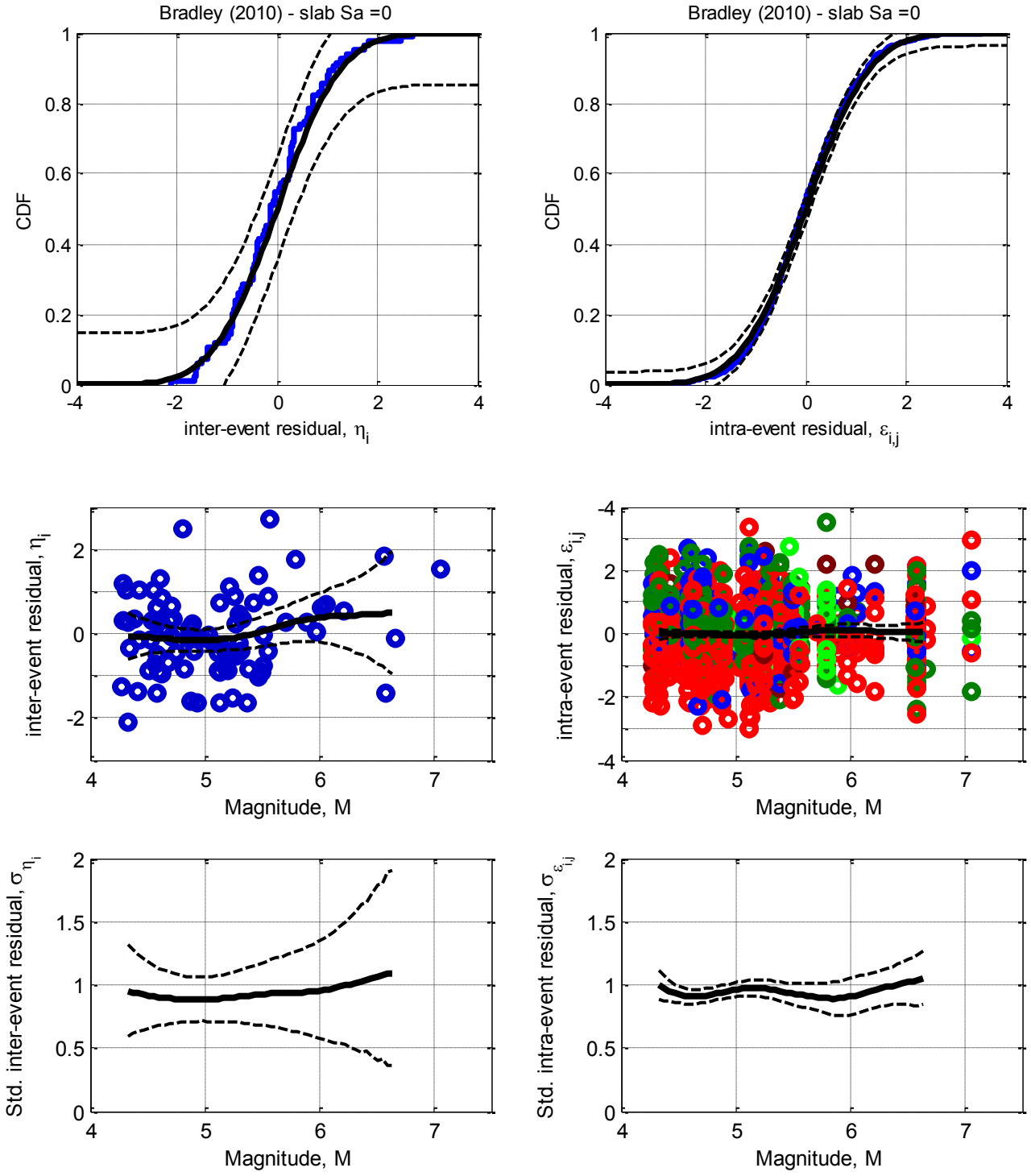

Figure E-6: Residuals for Sa(0.0) using the Bradley (2010) slab model

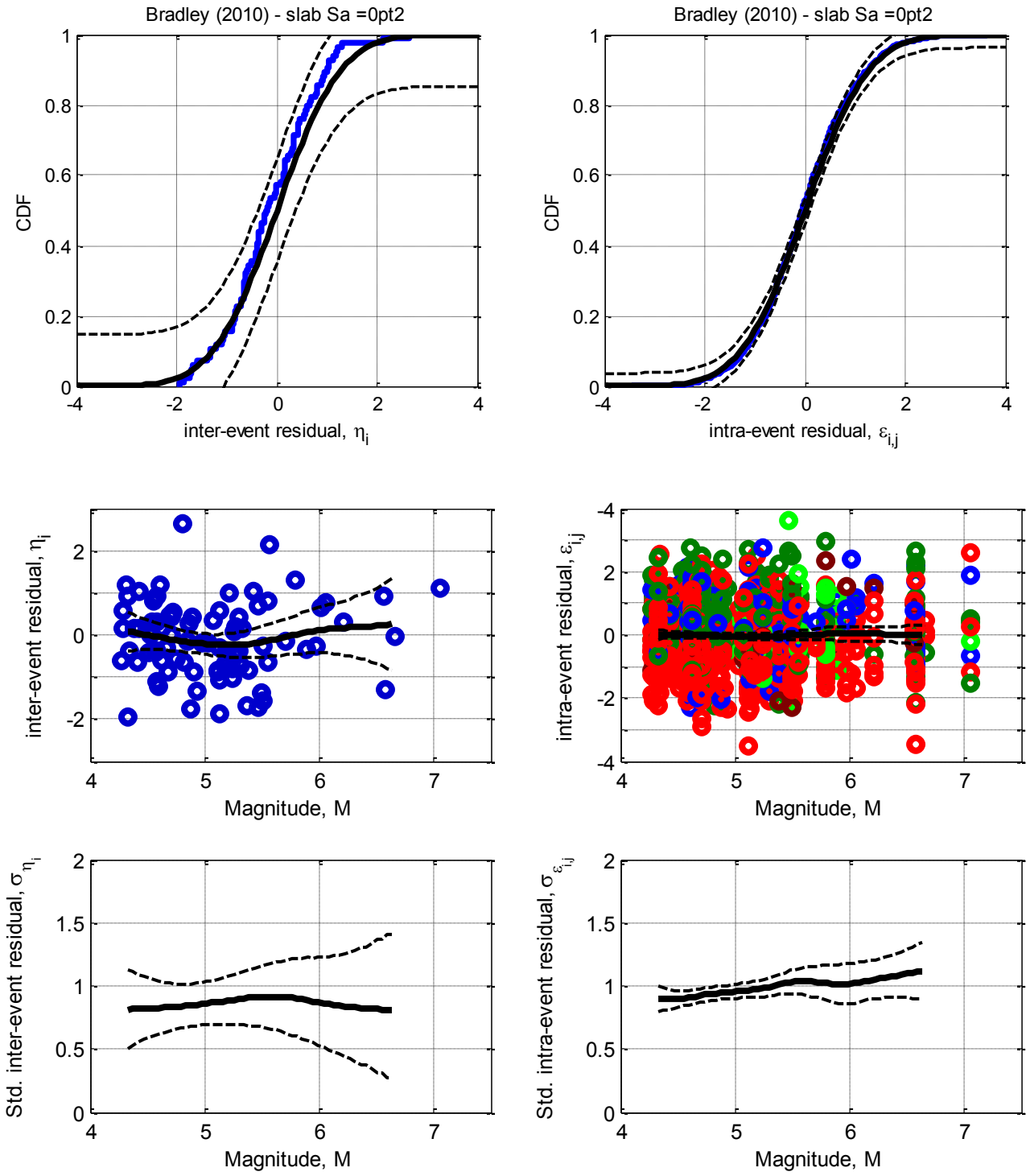

Figure E-7: Residuals for Sa(0.2) using the Bradley (2010) slab model

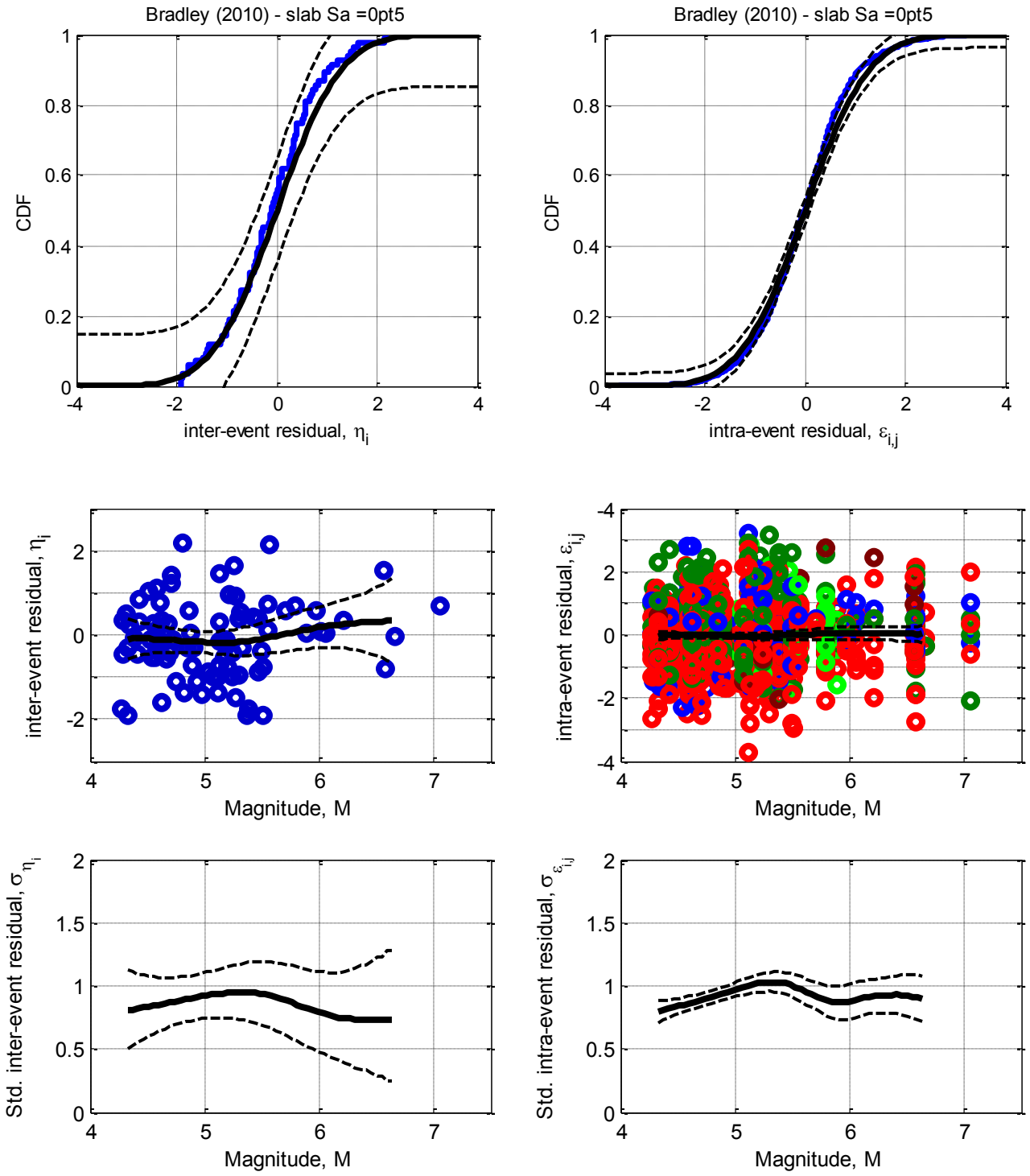

Figure E-8: Residuals for Sa(0.5) using the Bradley (2010) slab model

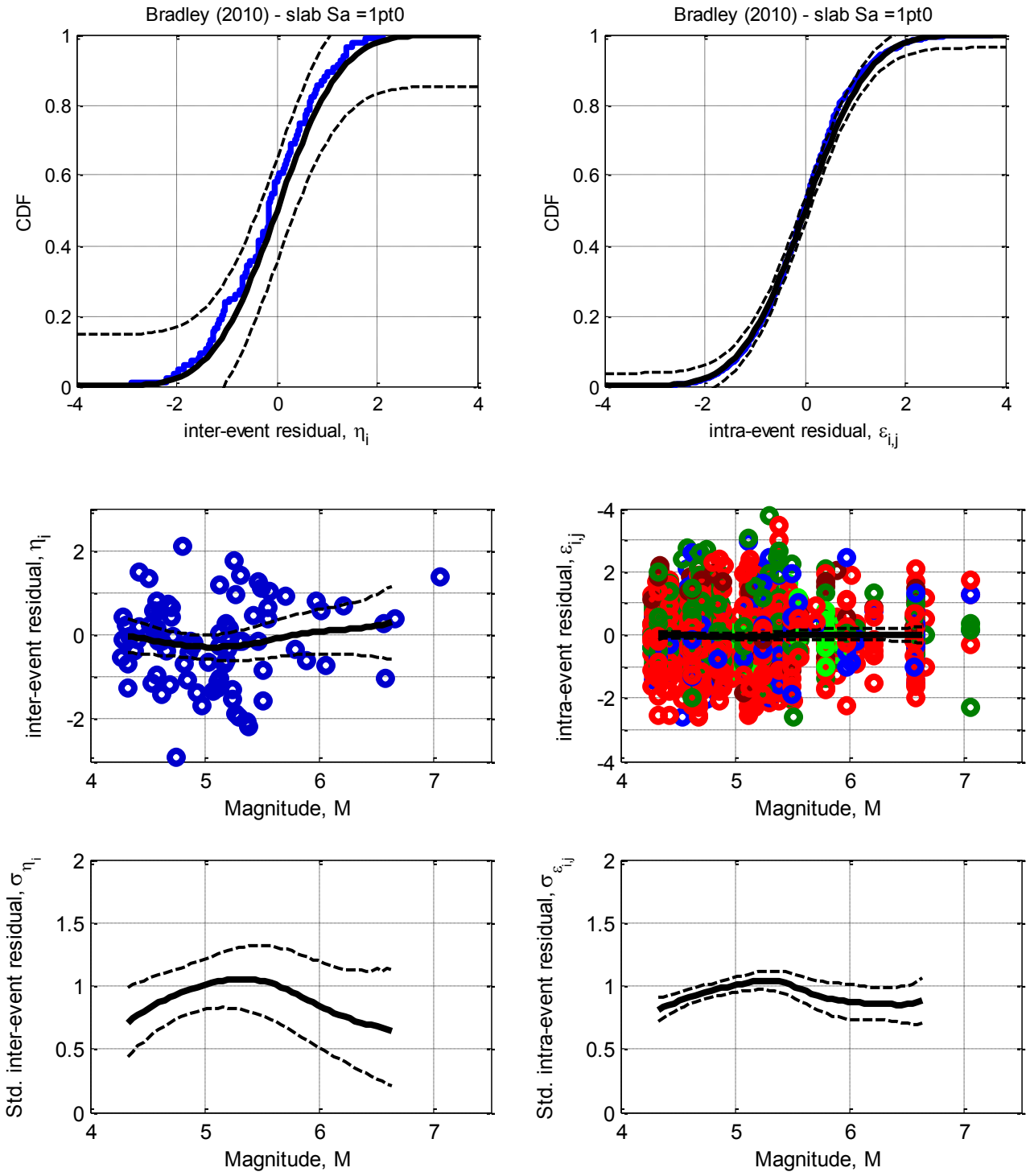

Figure E-9: Residuals for Sa(1.0) using the Bradley (2010) slab model

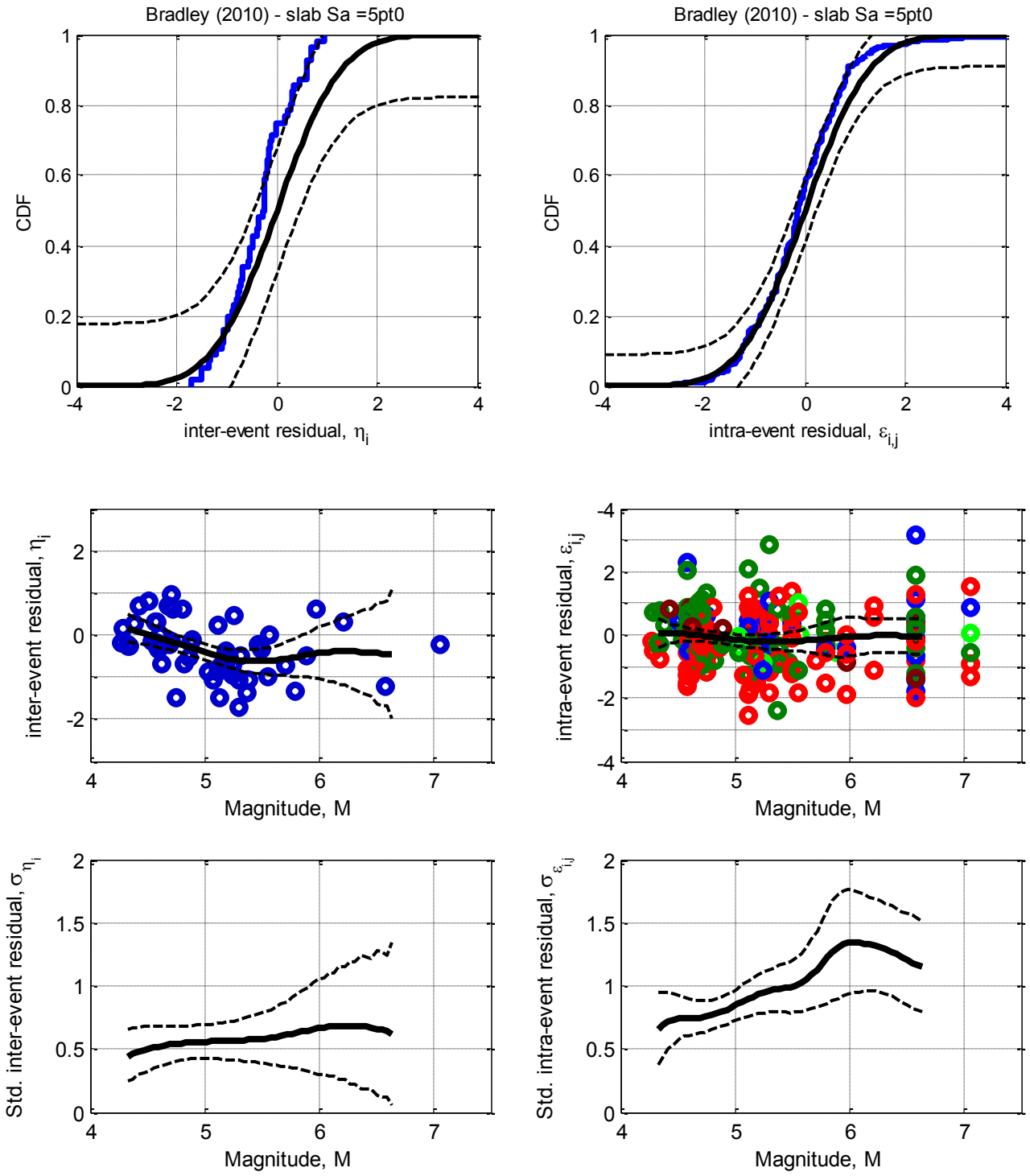

Figure E-10: Residuals for Sa(5.0) using the Bradley (2010) slab model

E.1. Bradley (2010) Interface model

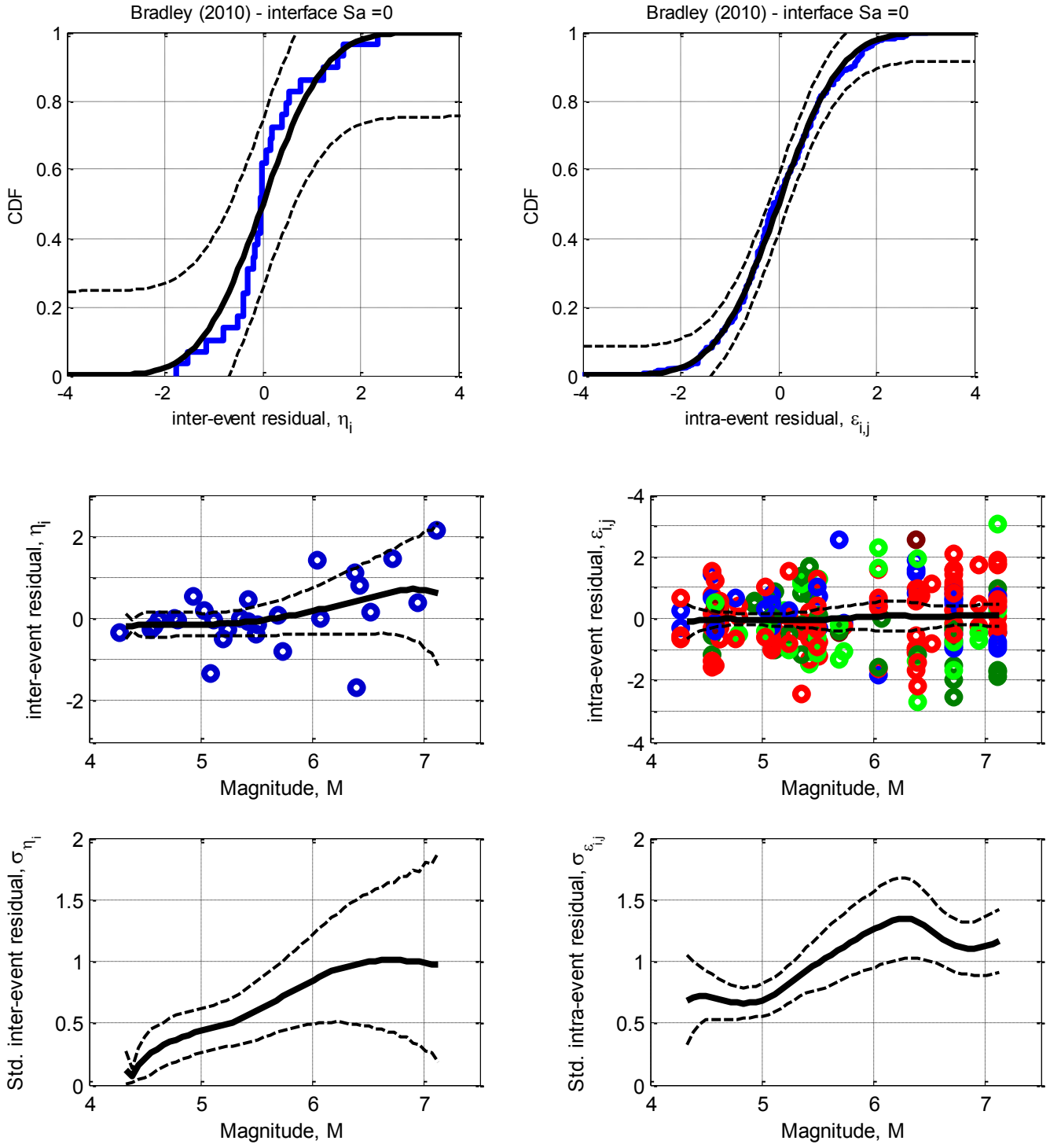

Figure E-11: Residuals for Sa(0.0) using the Bradley (2010) interface model

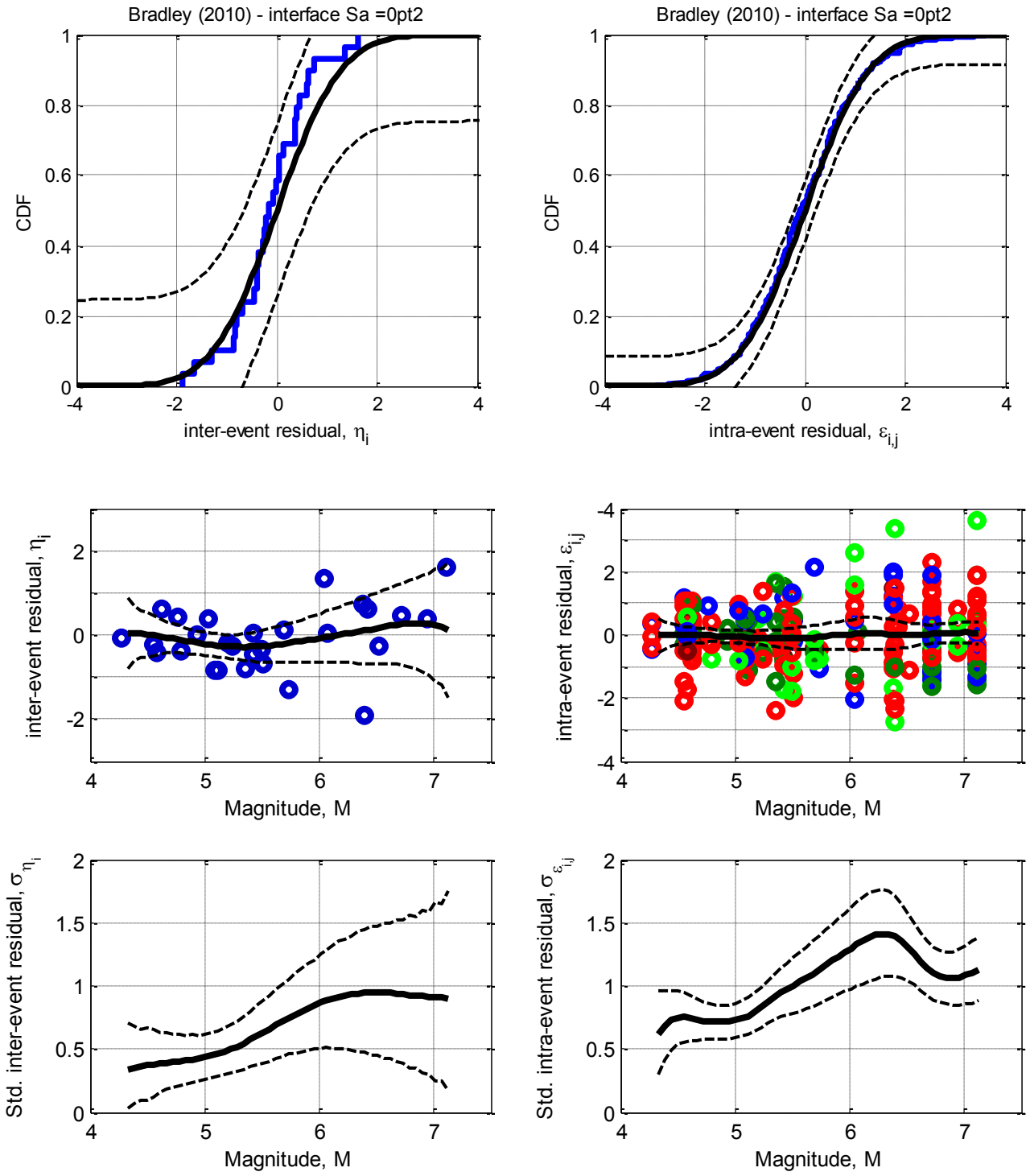

Figure E-12: Residuals for Sa(0.2) using the Bradley (2010) interface model

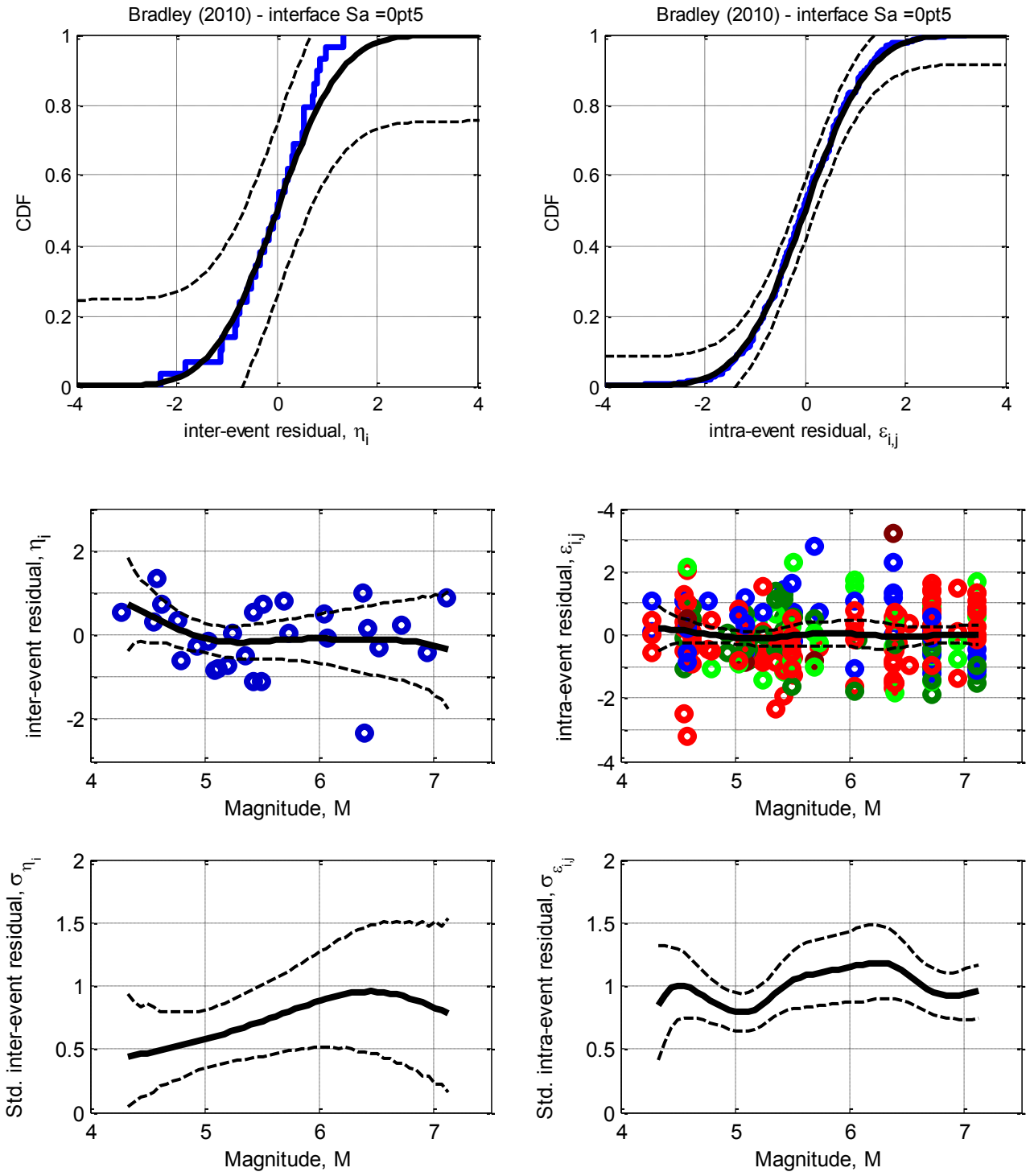

Figure E-13: Residuals for Sa(0.5) using the Bradley (2010) interface model

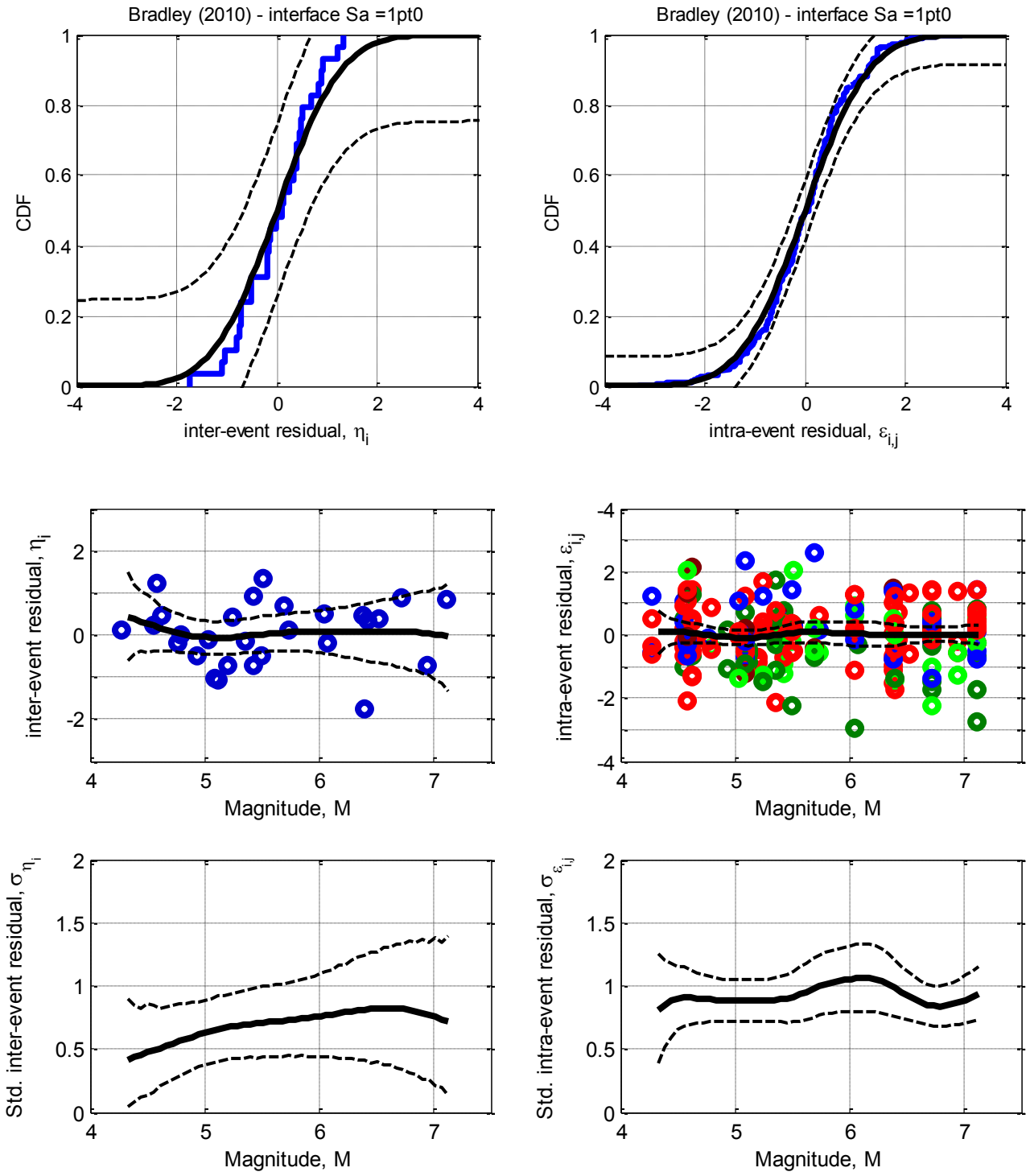

Figure E-14: Residuals for Sa(1.0) using the Bradley (2010) interface model

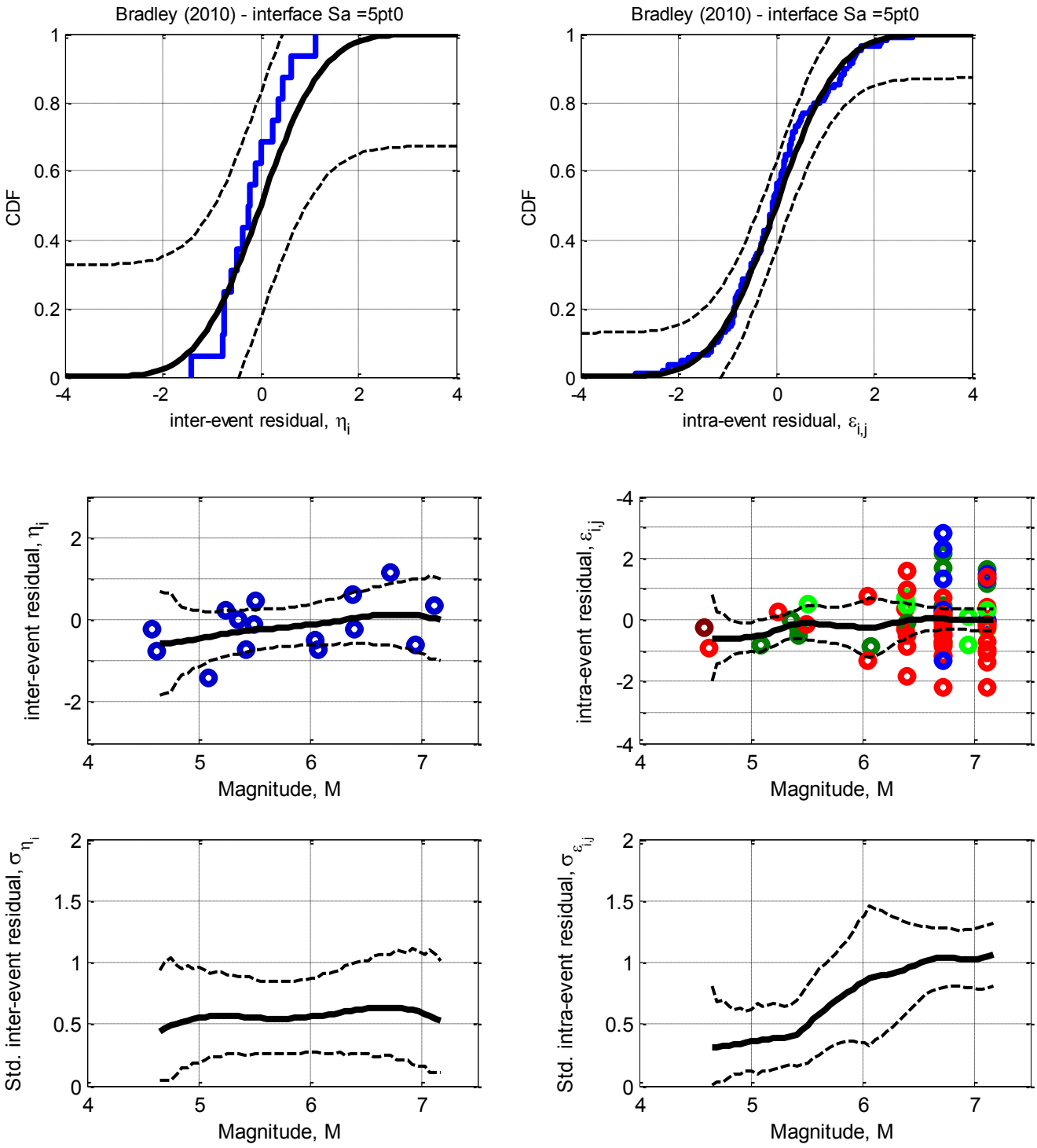

Figure E-15: Residuals for Sa(5.0) using the Bradley (2010) interface model

APPENDIX F PREDICTOR VARIABLE SCALING FOR DEVELOPED NZ-SPECIFIC GROUND MOTION PREDICTION EQUATIONS

F.1. Parameter scaling of the median of crustal prediction equations

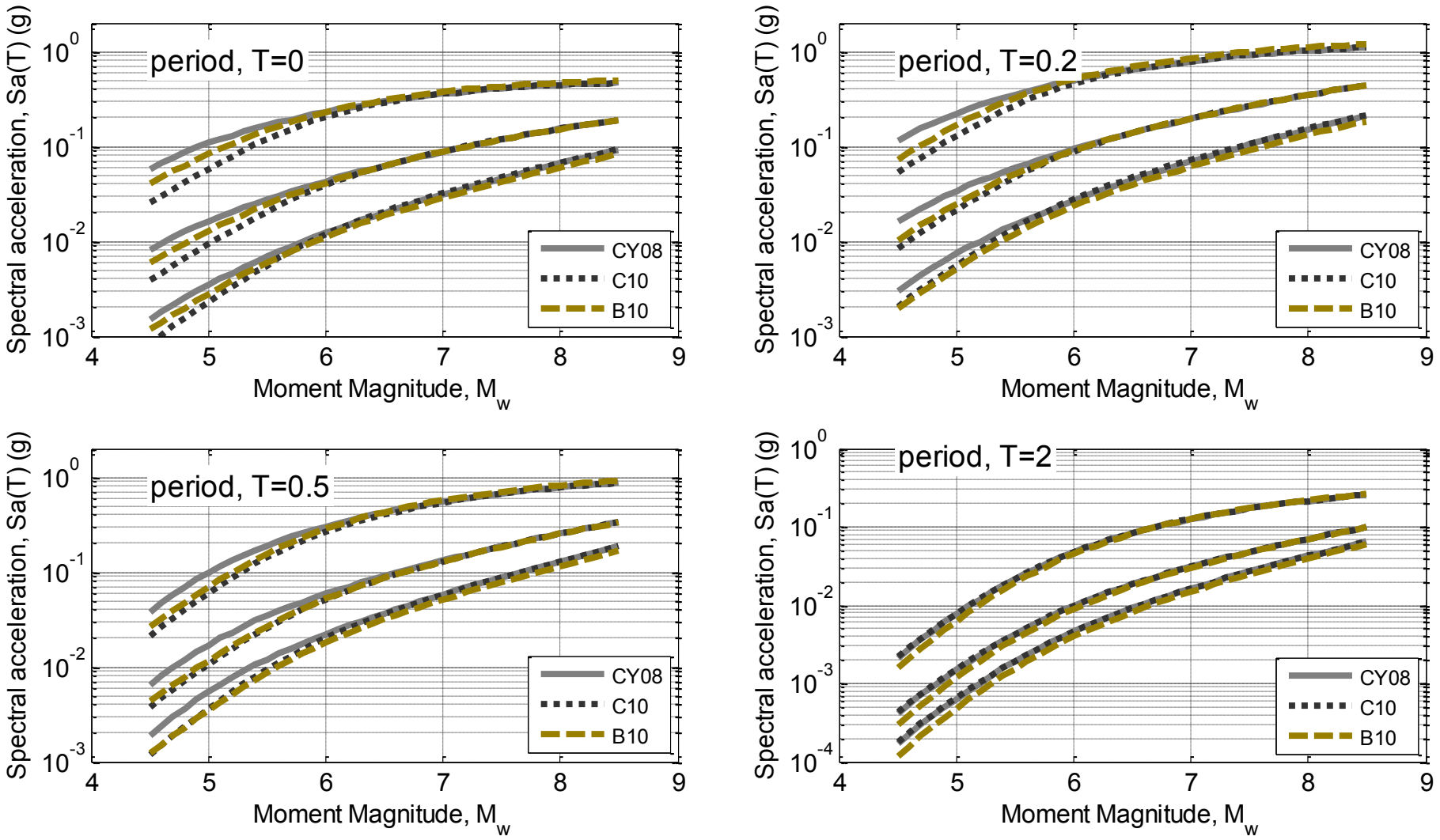

Figure F-1: Magnitude scaling of the median of crustal ground motion prediction equations for distances of 10, 50, and 120 km: (a) Sa(0.0); (b) Sa(0.2); (c) Sa(0.5); and (d) Sa(1.0). (predictions for site class C and strike-slip focal mechanism).

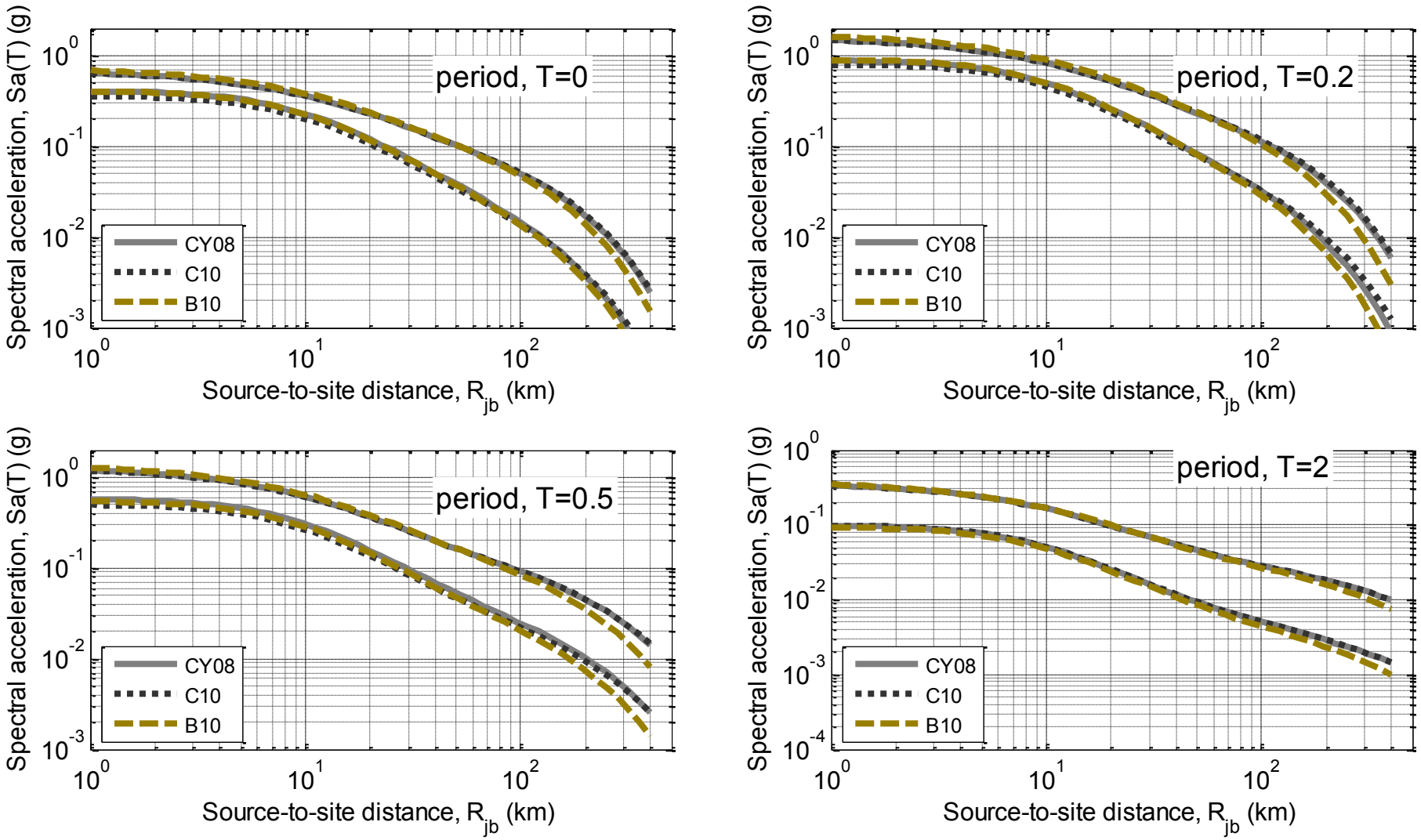

Figure F-2: Path distance scaling of the median of crustal ground motion prediction equations for magnitudes of 6 and 7.5: (a) Sa(0.0); (b) Sa(0.2); (c) Sa(0.5); and (d) Sa(1.0). (predictions for site class C and strike-slip focal mechanism).

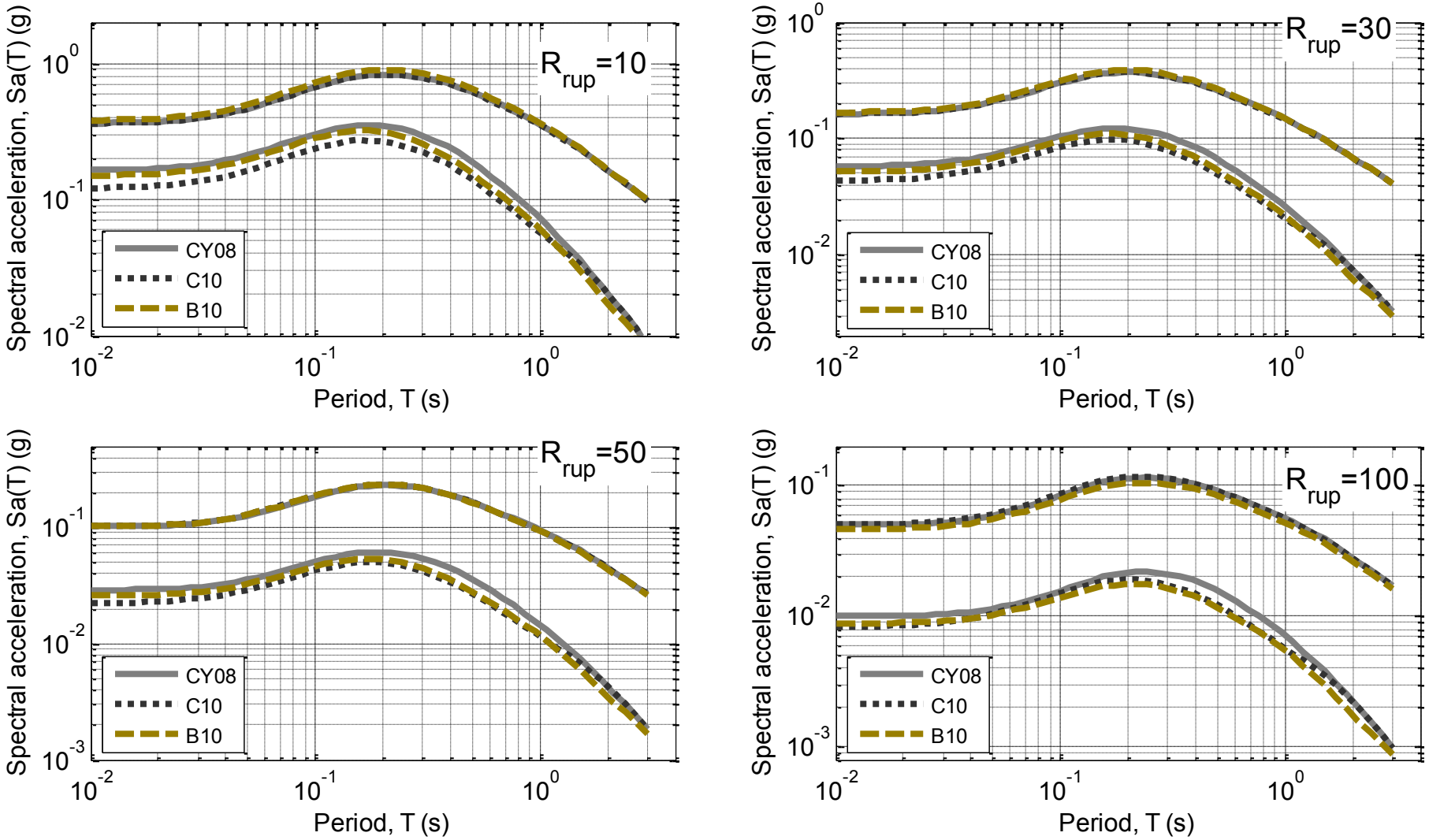

Figure F-3: Vibration period scaling of the median of crustal ground motion prediction equations for magnitudes of 5.5 and 7.5: (a) R_{rup} = 10km; (b) R_{rup} = 30km; (c) R_{rup} = 50km; and (d) R_{rup} = 100km. (predictions for site class C and strike-slip focal mechanism).

F.2. Parameter scaling of the median of slab prediction equations

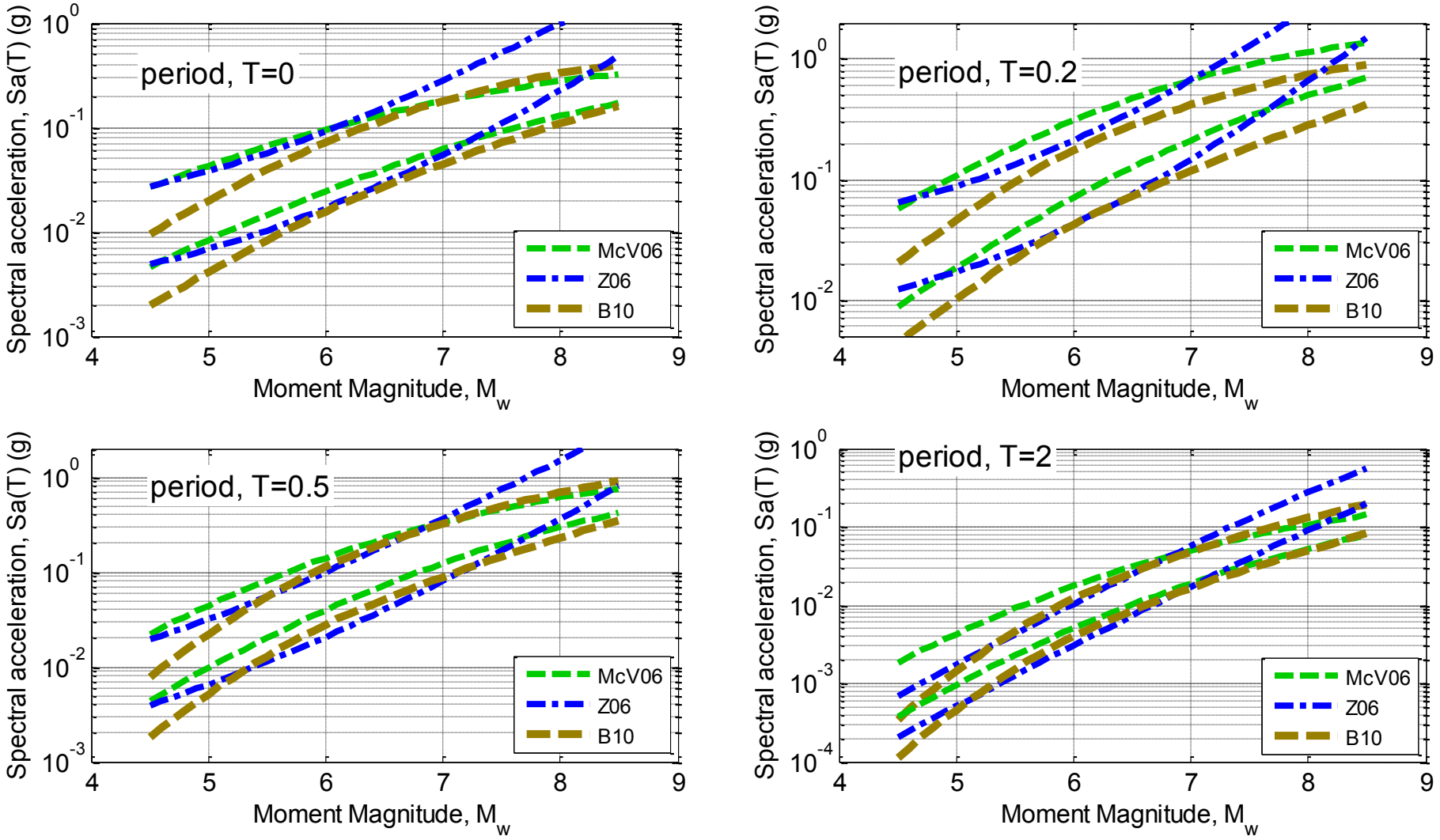

Figure F-4: Magnitude scaling of the median of slab ground motion prediction equations for distances of 50, and 120 km: (a) Sa(0.0); (b) Sa(0.2); (c) Sa(0.5); and (d) Sa(1.0). (predictions for site class C, depth 40km).

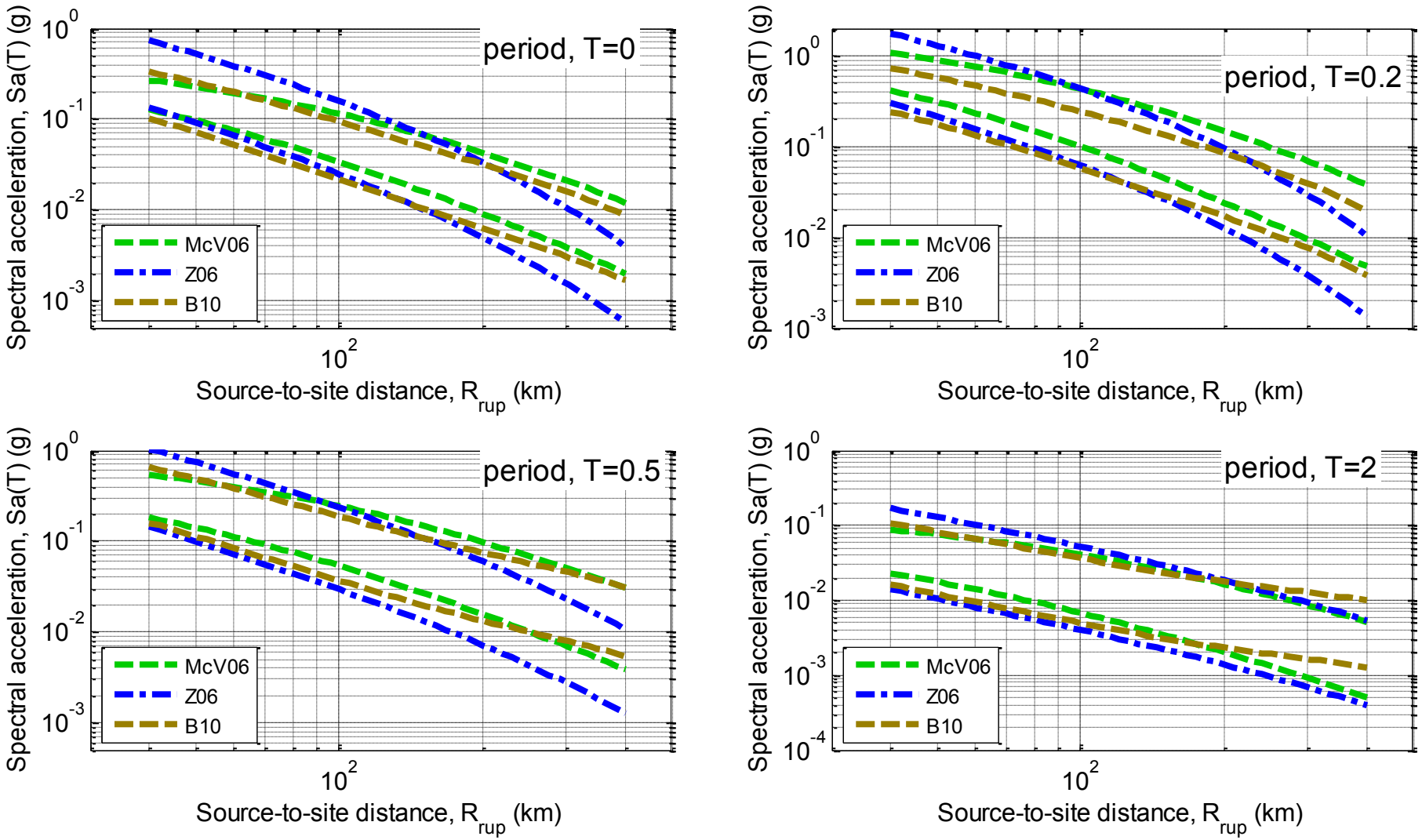

Figure F-5: Path distance scaling of the median of slab ground motion prediction equations for magnitudes of 6 and 7.5: (a) Sa(0.0); (b) Sa(0.2); (c) Sa(0.5); and (d) Sa(1.0). (predictions for site class C, depth 40km).

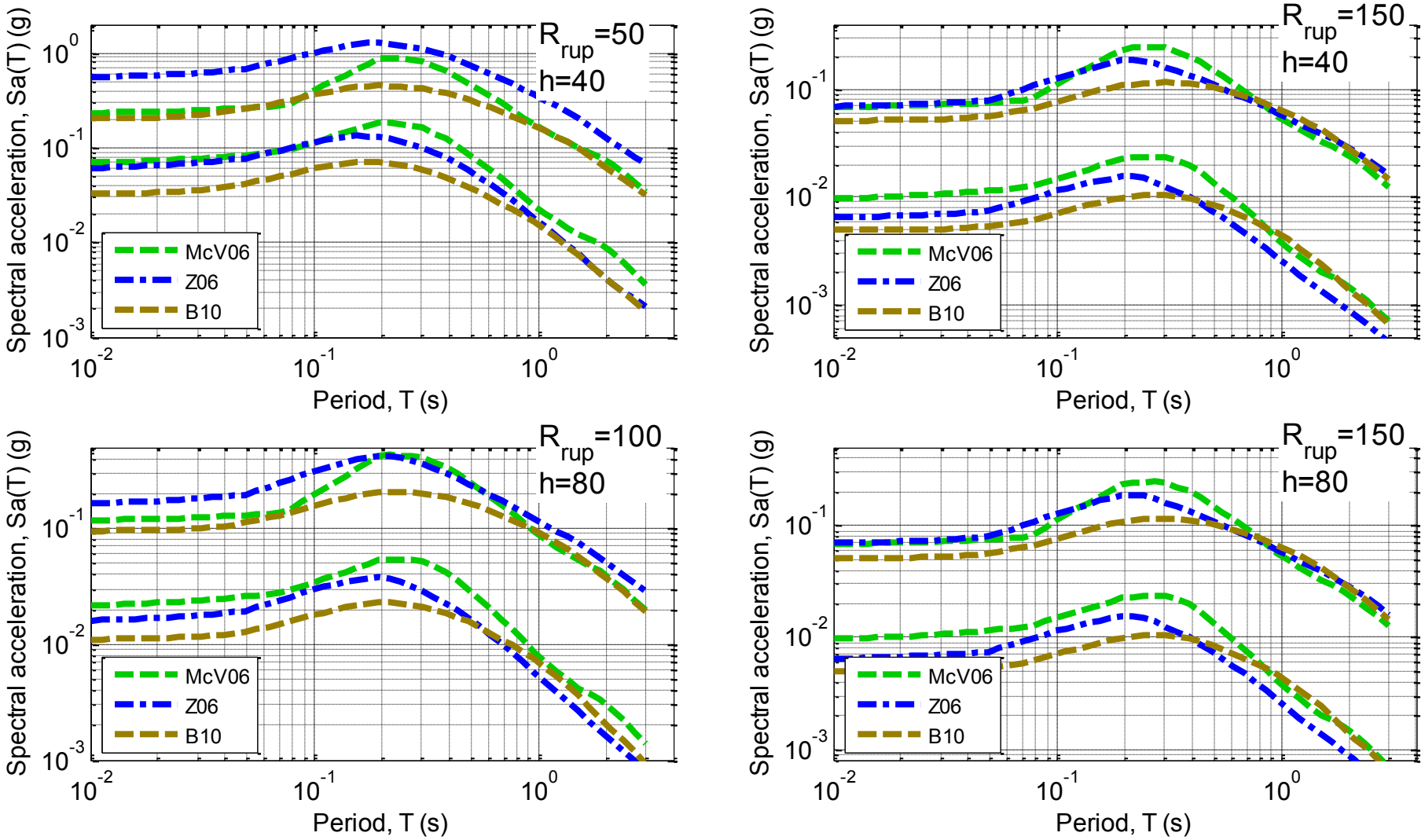

Figure F-6: Vibration period scaling of the median of slab ground motion prediction equations for magnitudes of 5.5 and 7.5: (a) R_{rup} = 50km, h=40km; (b) R_{rup} = 150km, h=40km; (c) R_{rup} = 100km, h=80km; and (d) R_{rup} = 150km, h=80km. (predictions for site class C).

F.3. Parameter scaling of the standard deviation of interface prediction equations

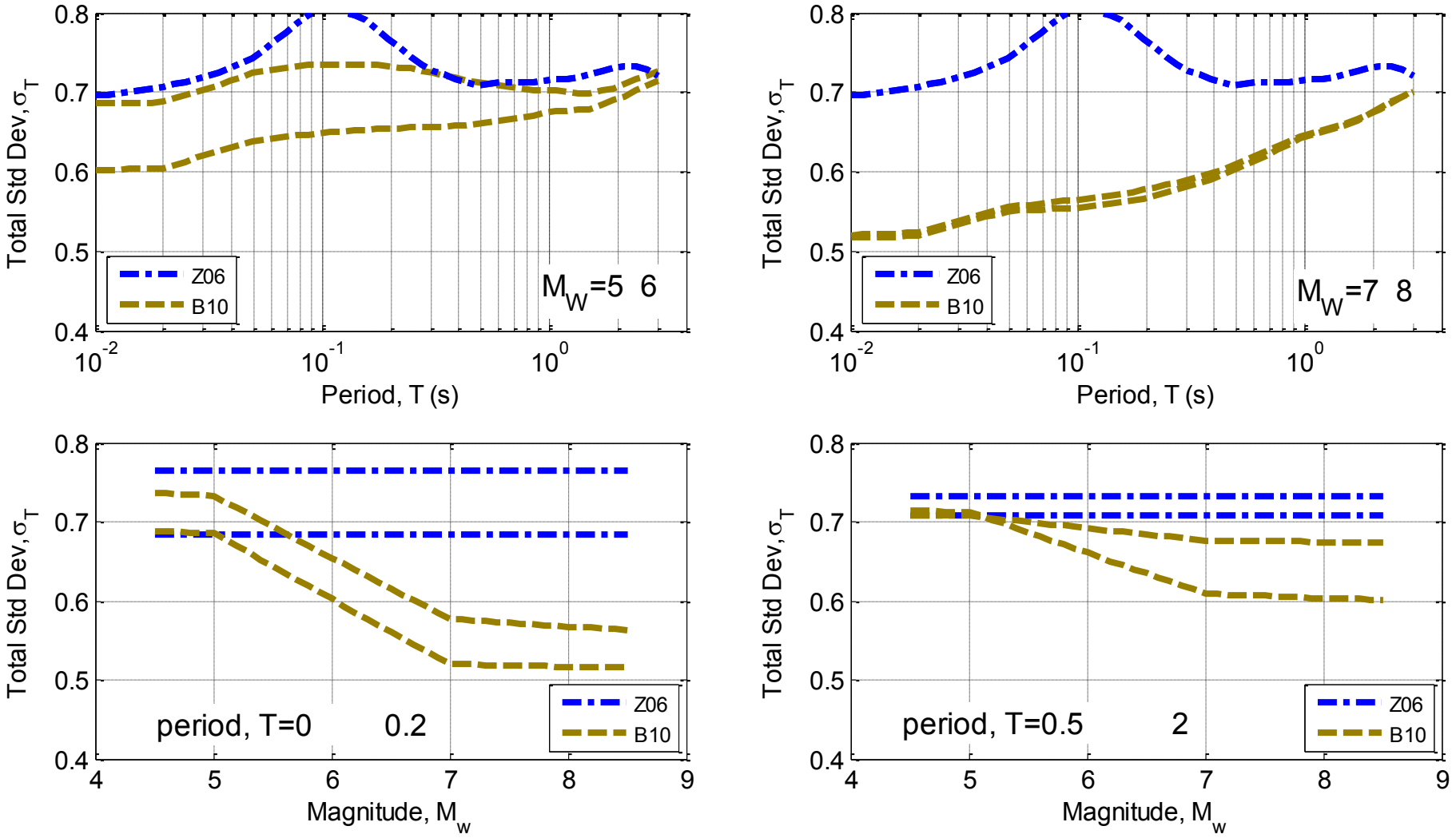

Figure F-7: Total standard deviation scaling of interface ground motion prediction equations with period and magnitude.

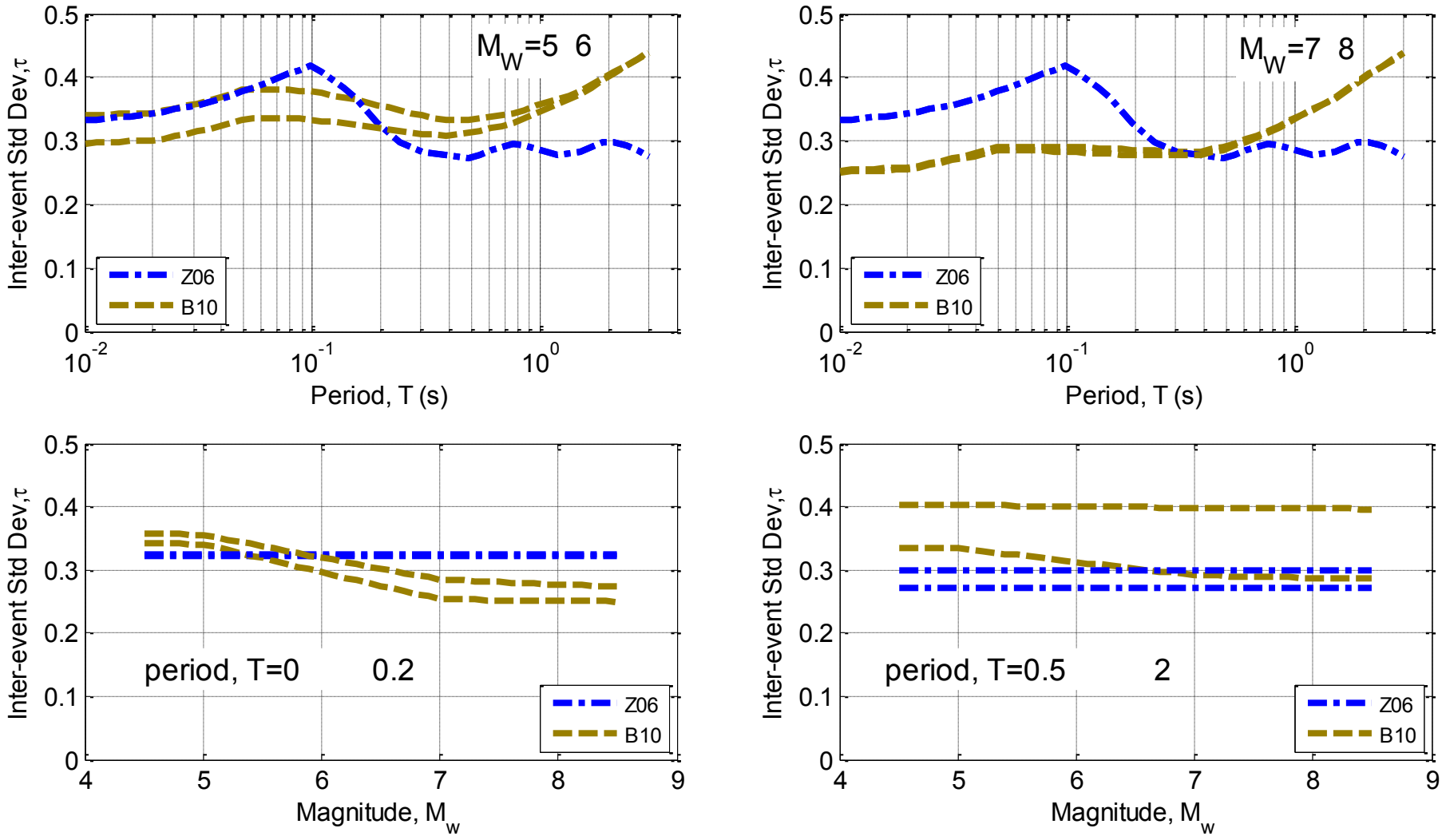

Figure F-8: Inter-event standard deviation scaling of interface ground motion prediction equations with period and magnitude.

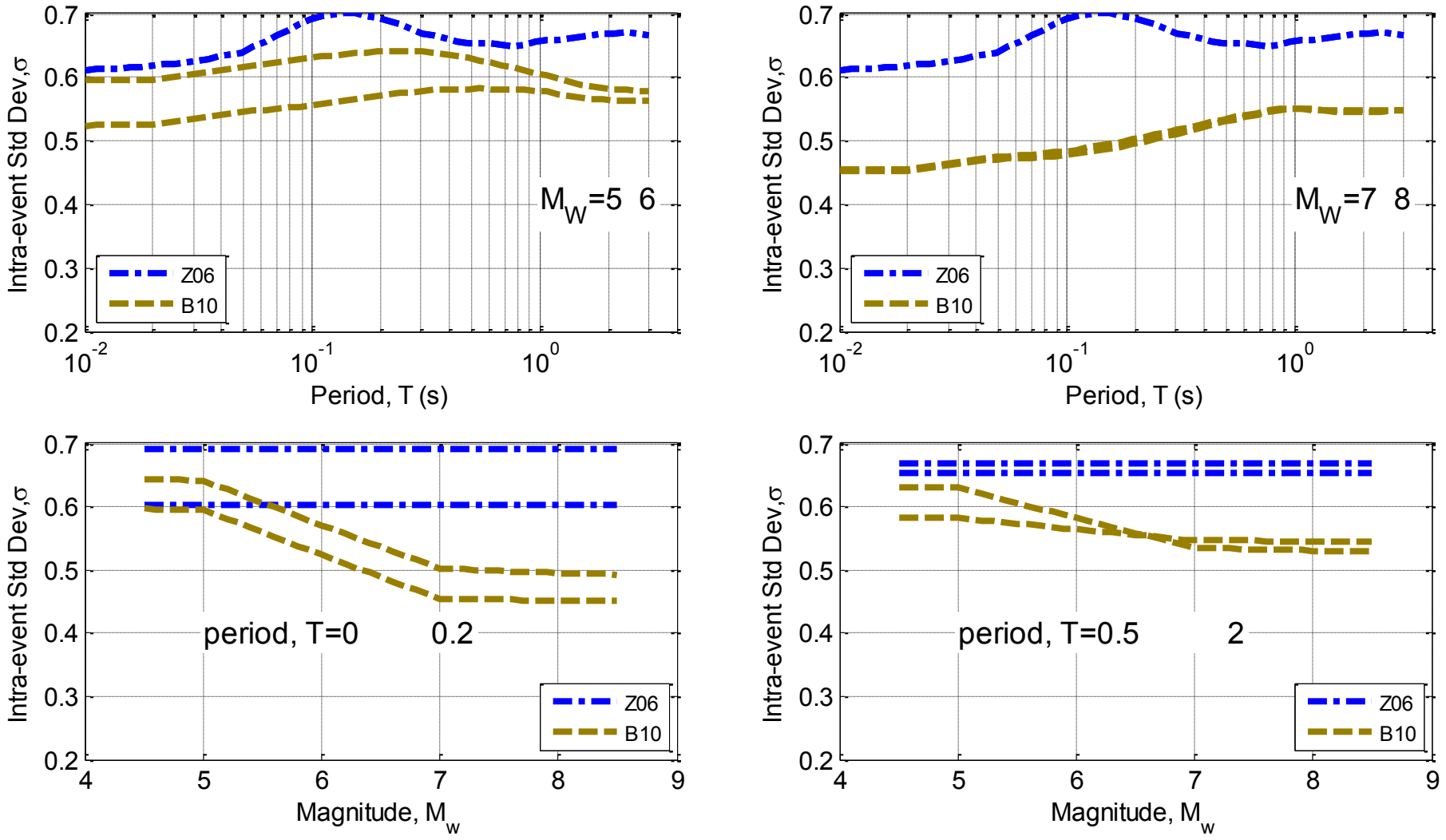

Figure F-9: Intra-event standard deviation scaling of interface ground motion prediction equations with period and magnitude.

F.4. Parameter scaling of the standard deviation of slab prediction equations

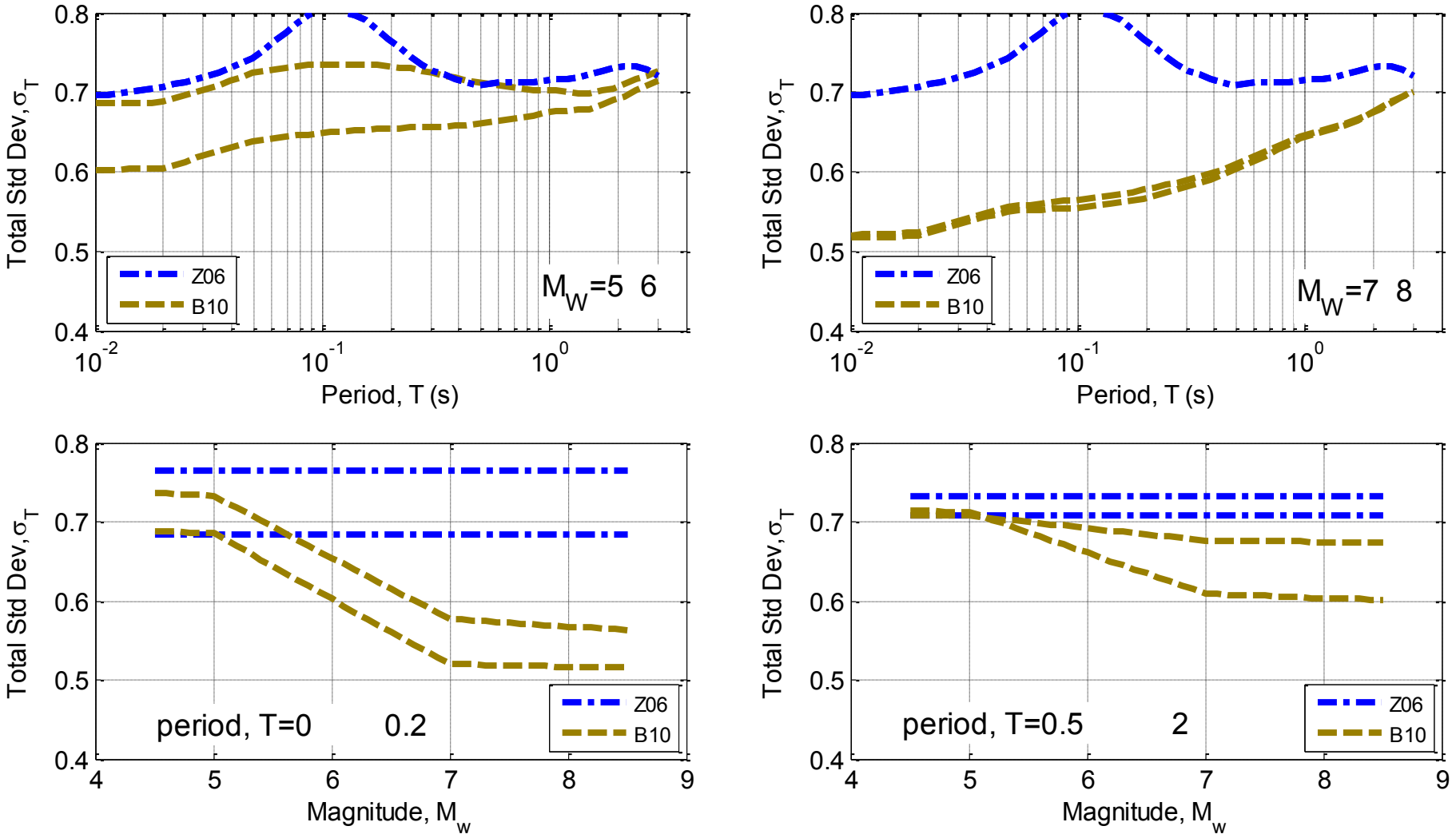

Figure F-10: Total standard deviation scaling of slab ground motion prediction equations with period and magnitude.

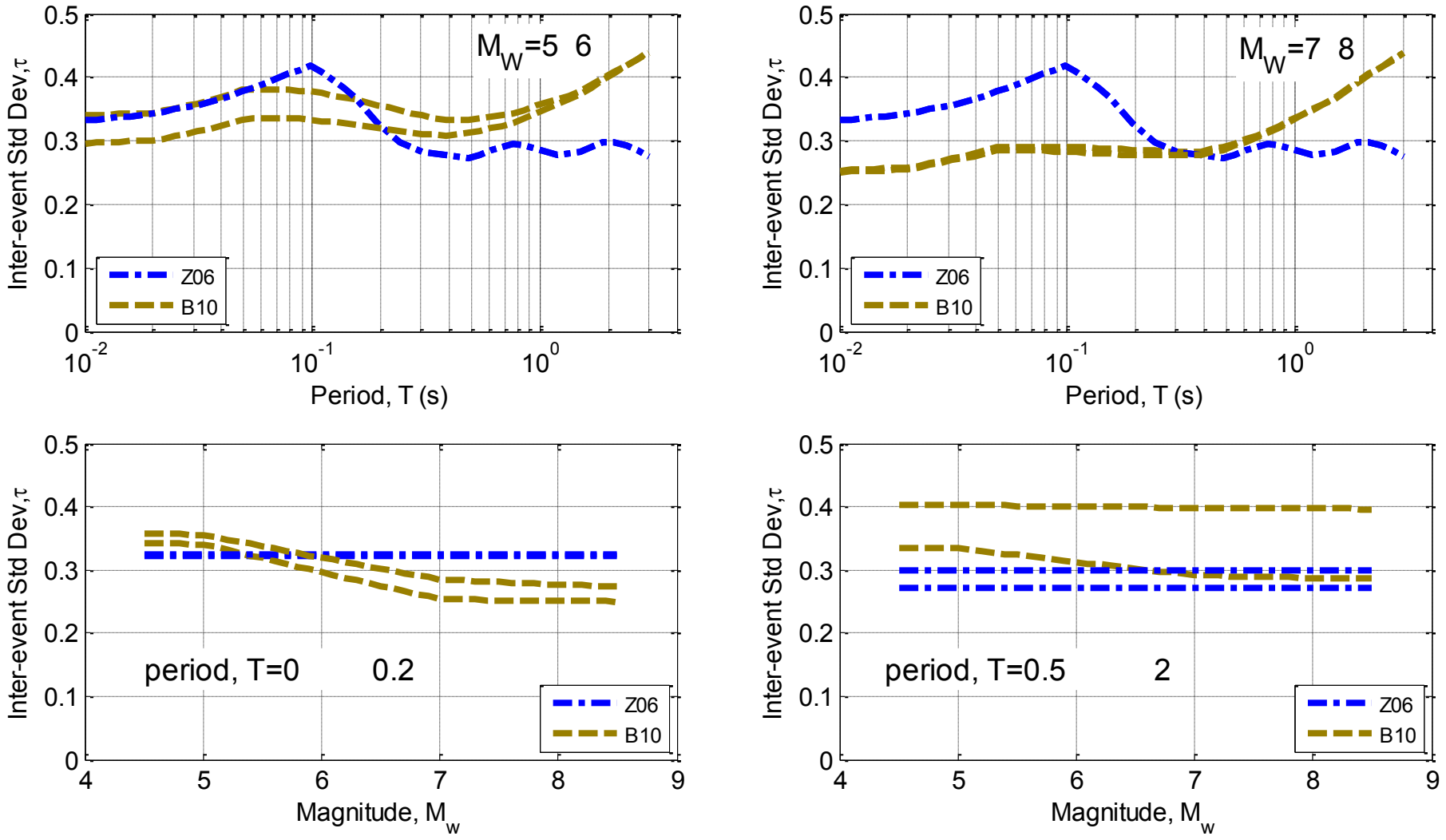

Figure F-11: Inter-event standard deviation scaling of slab ground motion prediction equations with period and magnitude.

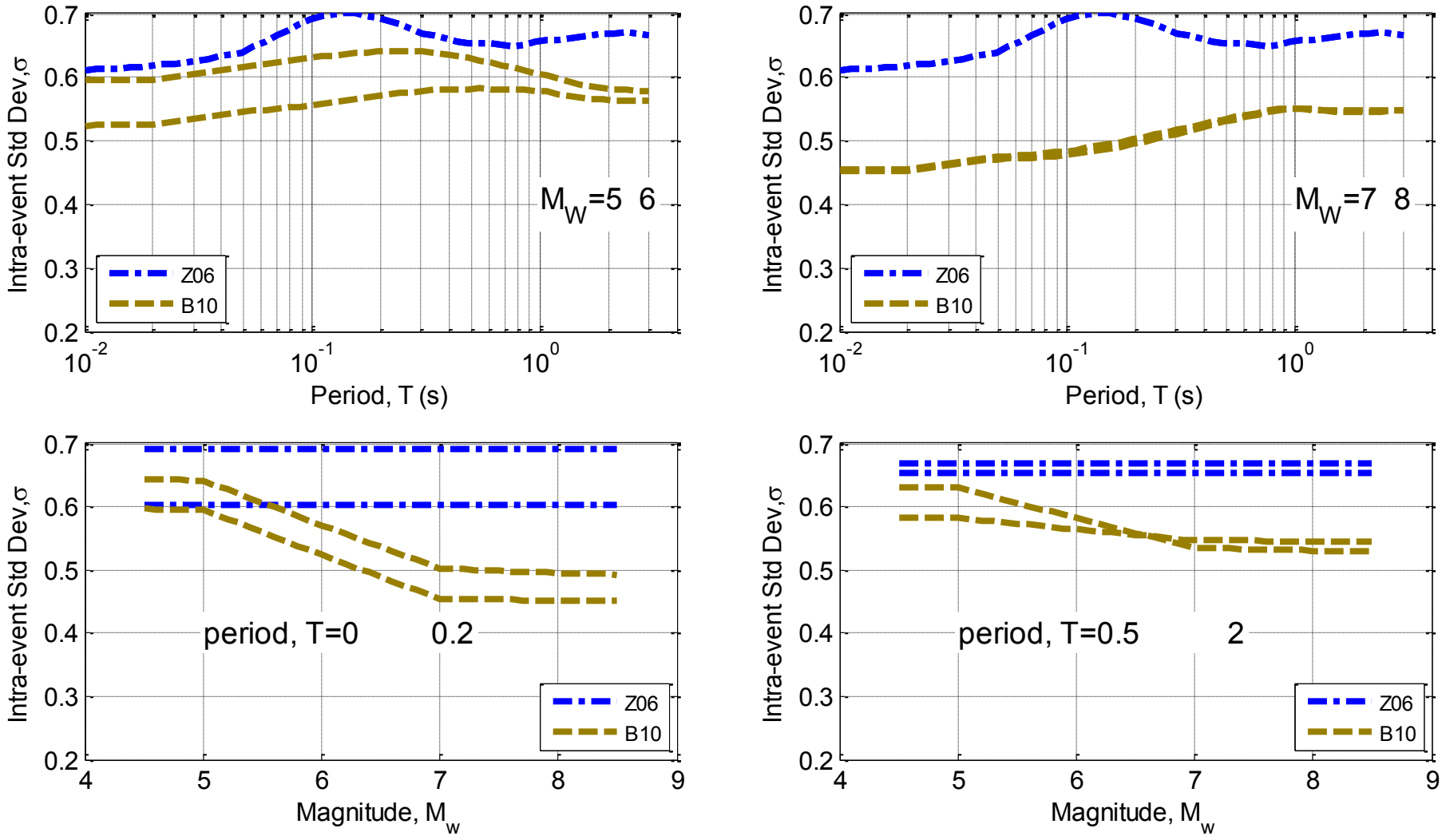

Figure F-12: Intra-event standard deviation scaling of slab ground motion prediction equations with period and magnitude.

F.5. Parameter scaling of the median of interface prediction equations

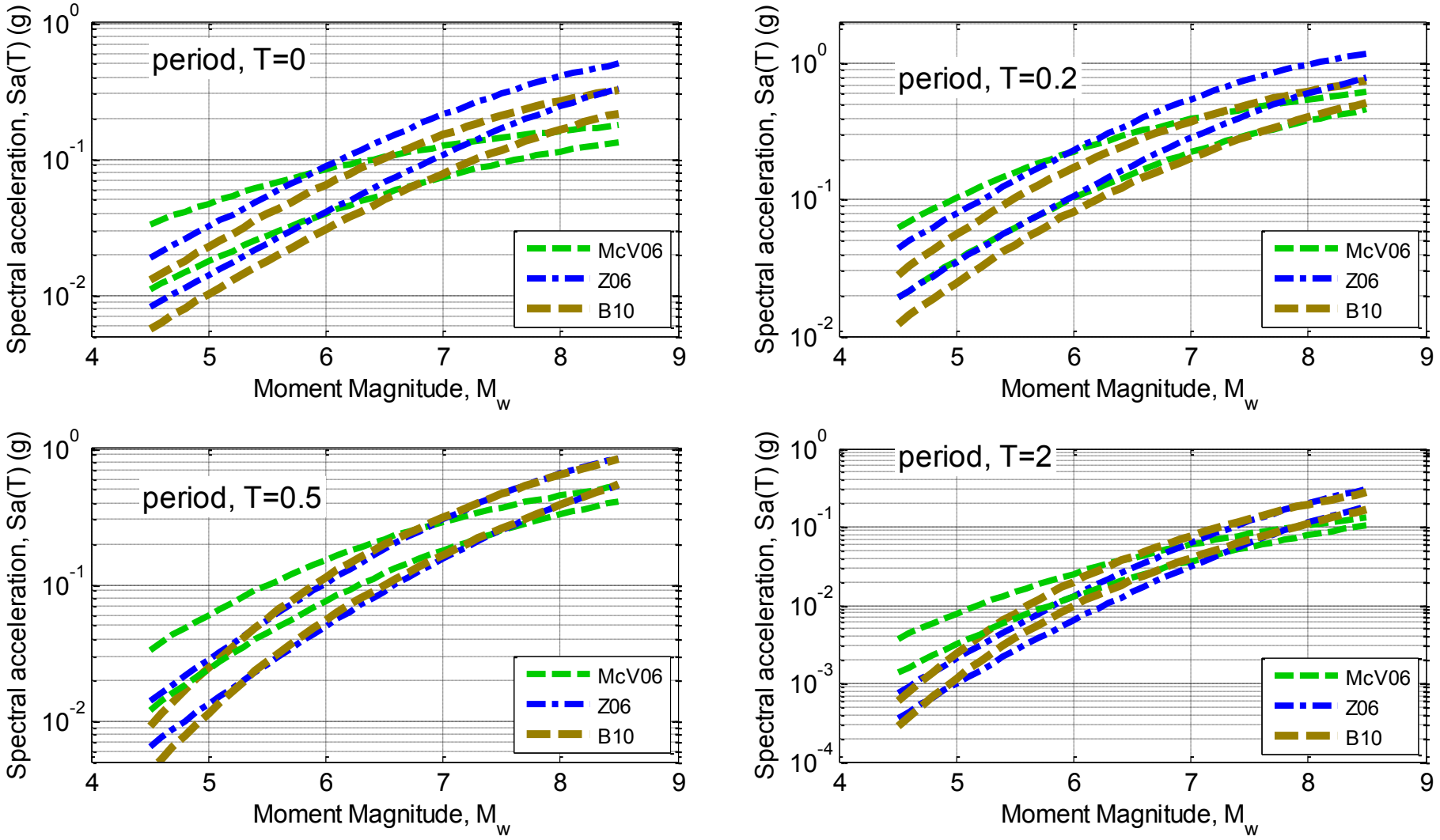

Figure F-13: Magnitude scaling of the median of interface ground motion prediction equations for distances of 15, and 25 km: (a) Sa(0.0); (b) Sa(0.2); (c) Sa(0.5); and (d) Sa(1.0). (predictions for site class C, depth 15km).

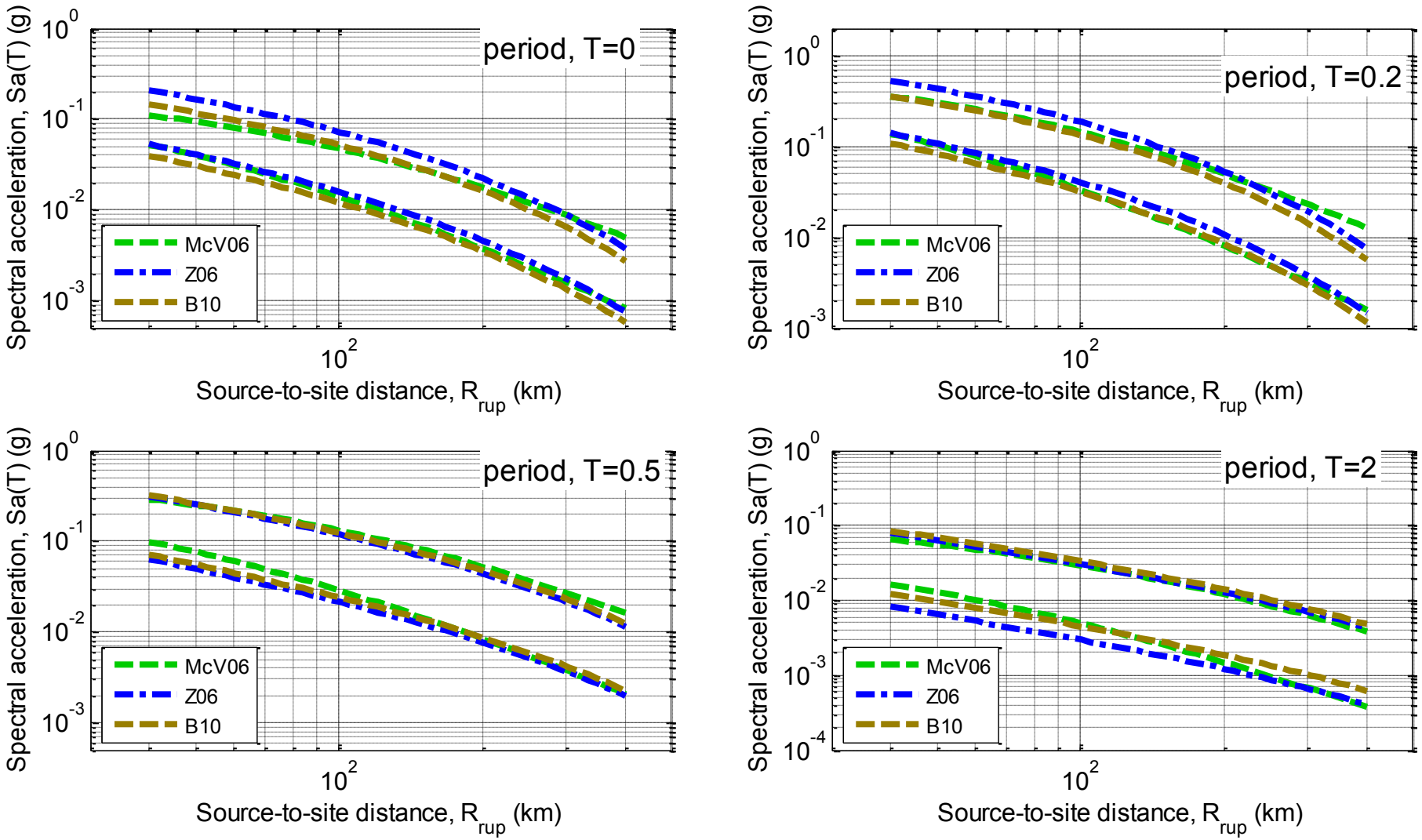

Figure F-14: Path distance scaling of the median of interface ground motion prediction equations for magnitudes of 6 and 7.5: (a) Sa(0.0); (b) Sa(0.2); (c) Sa(0.5); and (d) Sa(1.0). (predictions for site class C, depth 15km).

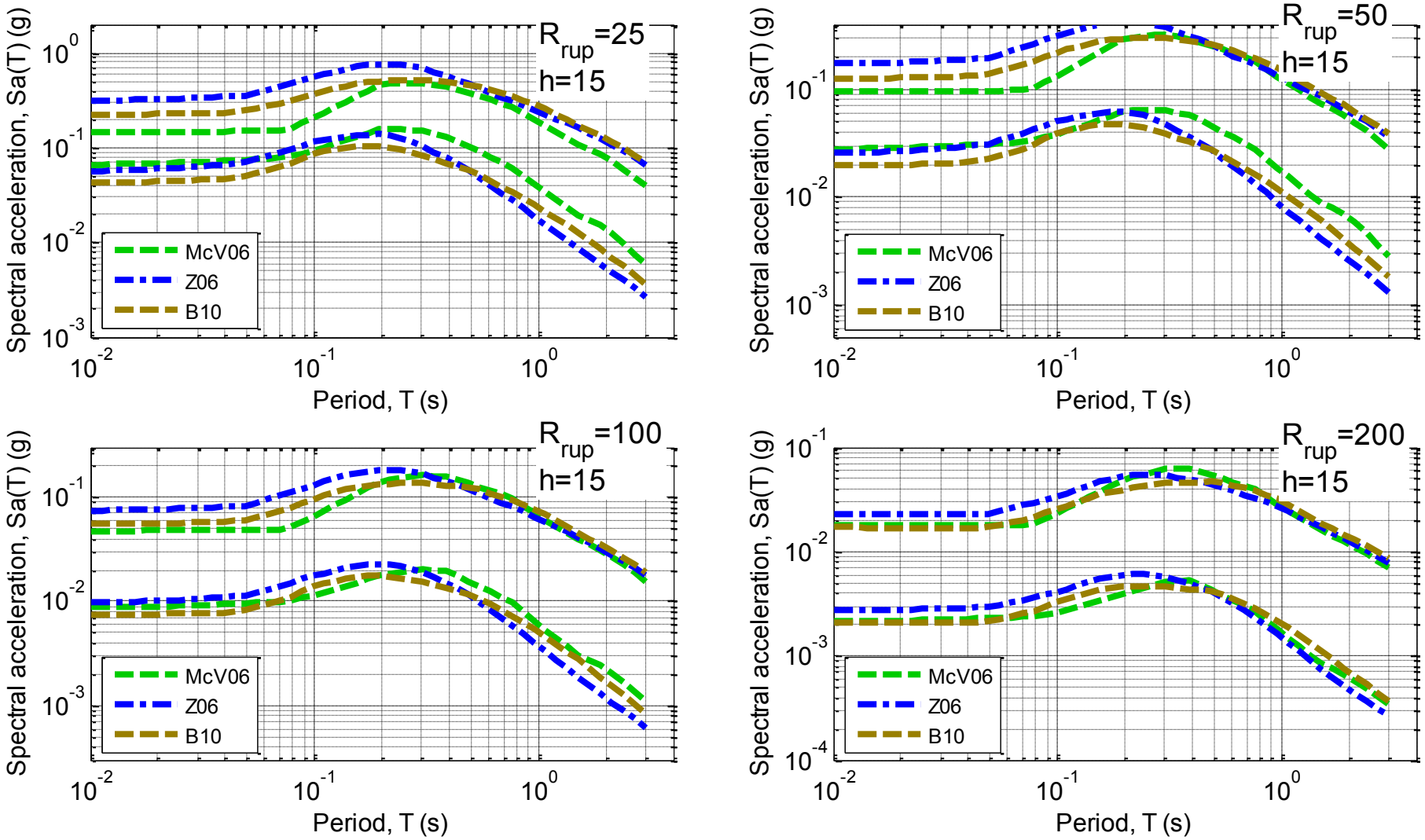

Figure F-15: Vibration period scaling of the median of interface ground motion prediction equations for magnitudes of 5.5 and 7.5: (a) R_{rup} = 25km; (b) R_{rup} = 50km; (c) R_{rup} = 100km; and (d) R_{rup} = 200km. (predictions for site class C and depth 15km).

F.6. Parameter scaling of the standard deviation of interface prediction equations

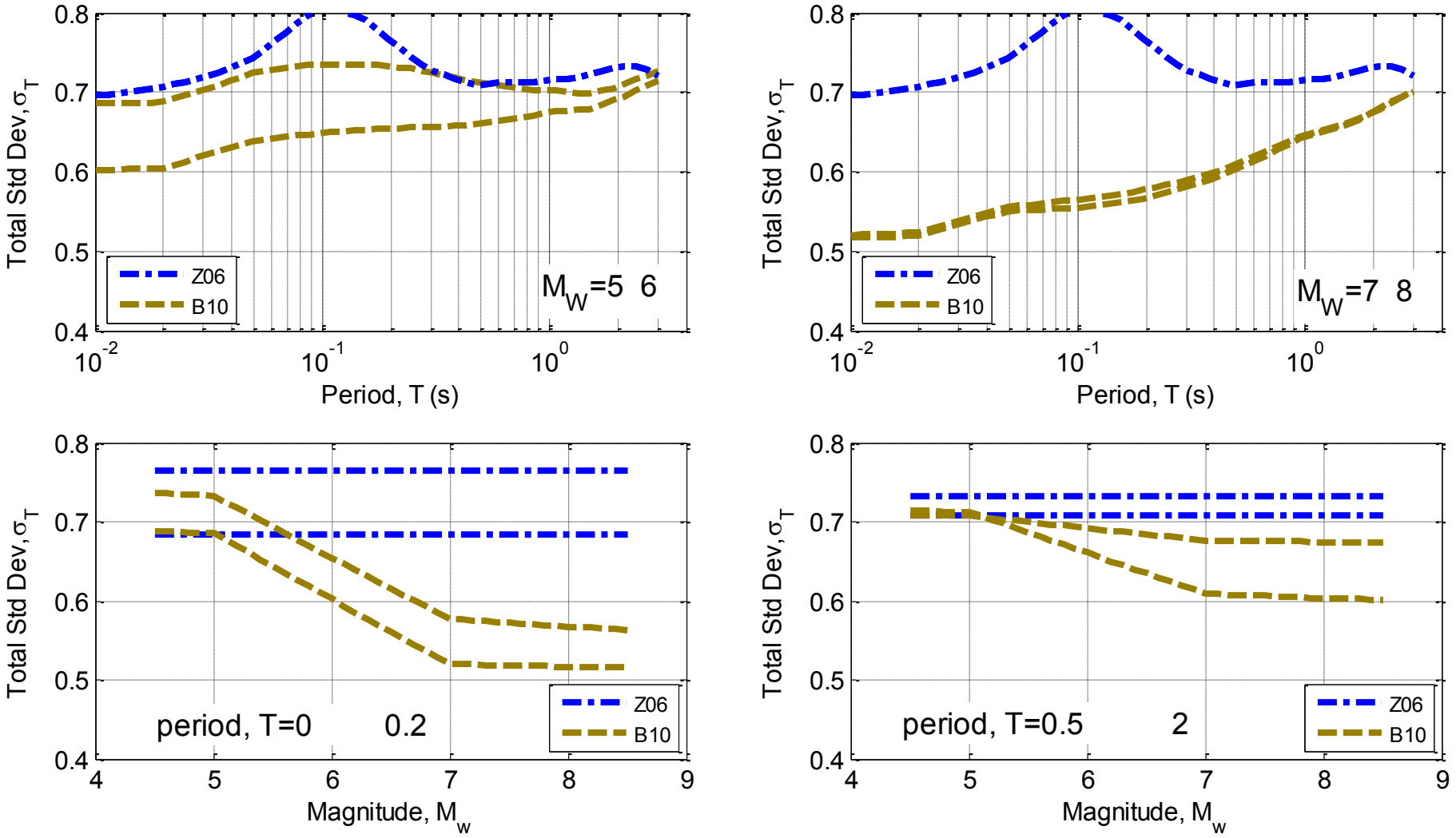

Figure F-16: Total standard deviation scaling of interface ground motion prediction equations with period and magnitude.

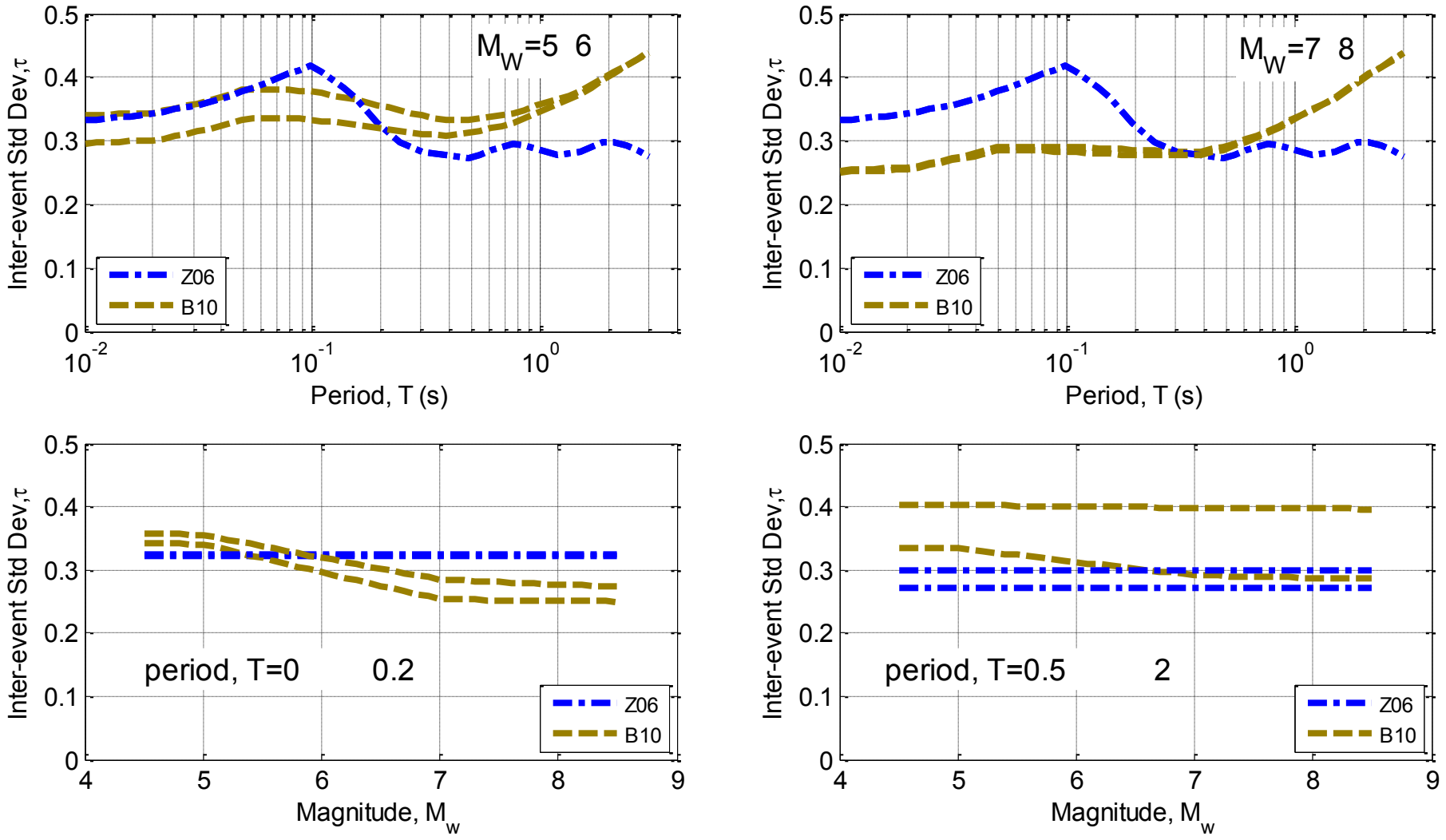

Figure F-17: Inter-event standard deviation scaling of interface ground motion prediction equations with period and magnitude.

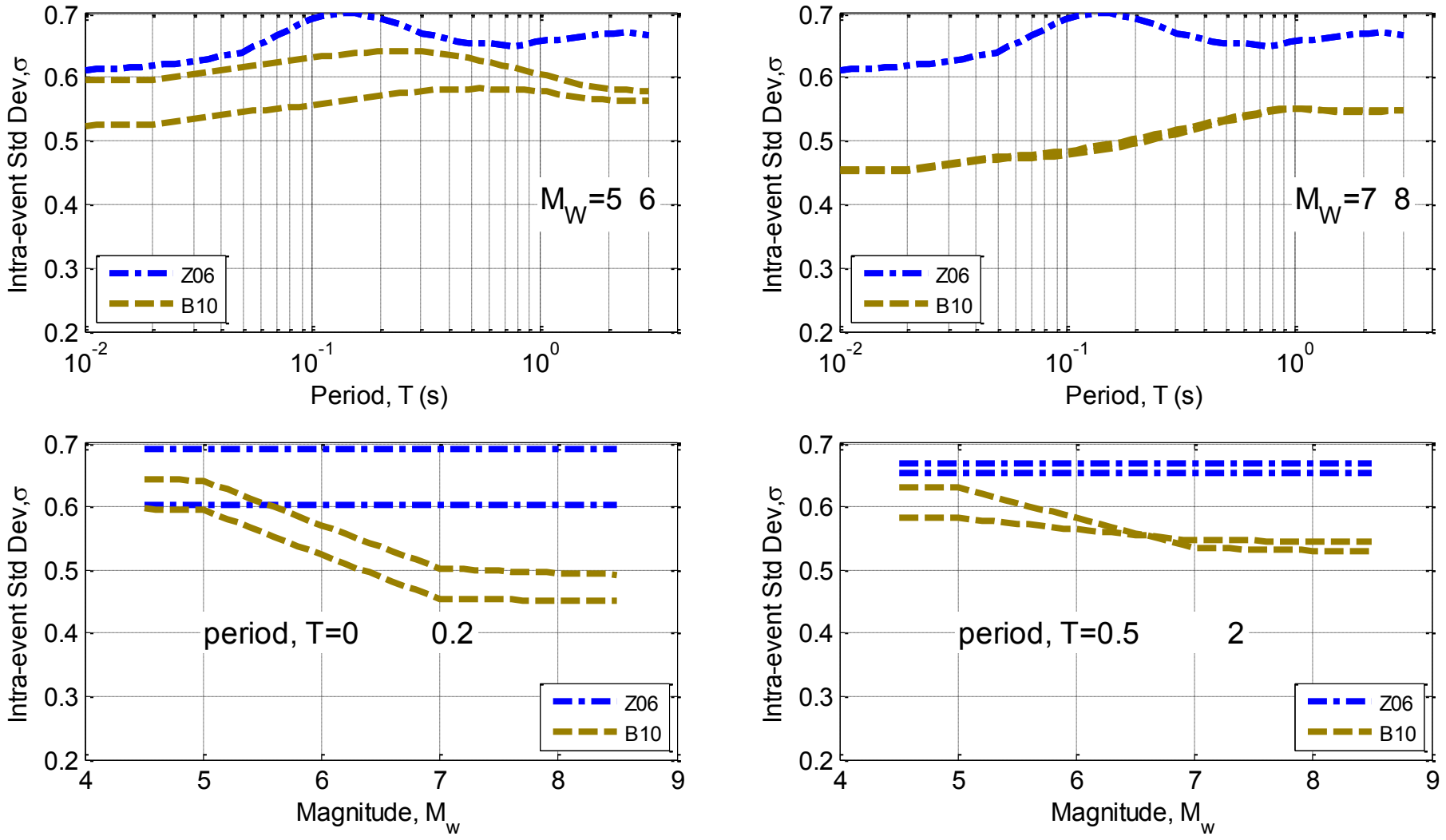

Figure F-18: Intra-event standard deviation scaling of interface ground motion prediction equations with period and magnitude.